EXPERIMENTAL STUDIES OF SCALE EFFECTS ON SHEAR STRENGTH, AND DEFORMATION OF ROCK JOINTS

by

S. Bandis, B.Sc., M.Sc.

Submitted in fulfilment of the requirements
for the degree of Doctor of Philosophy

Department of Earth Sciences,
The University of Leeds

January, 1980

To my parents and Jose

ABSTRACT

The effect of scale on shear strength is studied by performing direct shear tests on different sized samples of large joints. A rubber moulding system is used to obtain impressions of the roughness from a variety of natural joint surfaces. A brittle model material is developed and used to cast several sets of identical interlocking specimens, which are in turn subdivided into sets of equidimensional joint block samples, each of the sets representing a different average block size or joint length. All sample sizes are tested in the same relative direction of shearing and under precisely the same level of normal stress. A total of eleven joints displaying a large variety of surface roughness is included in the experimental programme.

The results from those tests show that peak shear strength is a strongly scale-dependent variable. Scale effects are most pronounced in cases of rough undulating joints, whereas they are virtually absent for relatively planar joints. The key factor behind the changing behaviour and strength with increasing scale is the involvement of different sizes of asperities in controlling the peak behaviour of different lengths of joints. An important consequence is a decrease in the value of roughness coefficient (JRC) and wall strength (JCS) operating at larger scale. Use of those indices may enable realistic allowance to be made for the scale effect in peak shear strength.

The normal deformability of rock joints is investigated by conducting loading/unloading and repeated load cycling tests on a wide ranging variety of fresh and weathered joints in five different rocks. The shear deformability is studied by performing direct shear tests at different levels of normal stress in a portable shear box. Several mismatched joints are also tested under compression.

In the present work the analytical representation of the stress-deformation curves is considered in detail.

Quantitative relationships between maximum closure, aperture, wall strength and roughness are defined.

TABLE OF CONTENTS

LIST OF FIGURES

LIST OF TABLES

ACKNOWLEDGMENTS

The author wishes to deeply thank his supervisor Mr. A.C. Lumsden for his unfailing interest and valuable contribution towards the completion of this thesis. He is also indebted to Dr. N.R. Barton of the Norwegian Geotechnical Institute for the help and constructive criticism that he offered during all the stages of this work.

He would further like to acknowledge with appreciation the contributions which have been made by:

Dr. R. Powell of the Department of Earth Sciences during the statistical processing of data;

Dr. W.E. Worrall of the Department of Ceramics on the selection of modelling materials;

Dr. J. Ergatoudis of the Department of Civil Engineering on the use of his finite element programme;

Professor R. Goodman of the University of California for his comments on some aspects of joint deformation.

A special word of thanks is to the technical staff of the Department of Earth Sciences; Messrs. J. Mott, M. Whitaker and L. Caddick fabricated expertly the large shear apparatus and helped to overcome various technical problems during the experimental stage. Thanks are also to Professor P.A. Young and Dr. N. Brook of the Mining Department for allowing free access to laboratory facilities.

The author is sincerely thankful to Miss S.H. Toon for her neat and patient typing, to Mr. F. Johnston and to Mr. I. Hatzinakos for their help in the preparation of the thesis.

Above all, most grateful acknowledgment has been reserved for the author's parents who offered him the opportunity to undertake these studies. Without their financial support and encouragement this work would never have been possible.

PART ONE

GENERAL INTRODUCTION

CHAPTER 1.1

SHEAR STRENGTH AND DEFORMATION OF ROCK JOINTS

1.1.1 Introduction

Rock encountered in engineering practice is in its general form an anisotropic discontinuum, which usually deforms and fails along pre-existing mechanical 'breaks' or discontinuities of geological origin, such as joints, bedding planes, faults, etc. Unless otherwise specified, the term joint will be used in the context of this thesis as a general term to describe all natural discontinuities in rock having zero tensile strength and no previous shear displacement history.

Early work in rock mechanics was based on the assumption that rock was a continuous, elastic, homogeneous, isotropic material. It was not until two decades ago that the discontinuous character of the rock mass and the implications on behaviour were emphasized in the works of Talobre (1957), John (1962) and Muller (1963). Under the low level of stresses associated with most civil engineering structures it is the geometrical arrangement and properties of joints which determine the mechanical behaviour of the rock mass. Unfavourably orientated jointing or individual features such as fault planes, persistent clay partings, etc., provide low energy paths along which shear failure may occur. In addition to the reduction in strength, jointing increases the deformability of the mass. In foundations, cuttings, and tunnels sited in hard rock, the closure and slippage of joints are the main contributors to the total amount of displacement.

Discontinuous rock masses can be analyzed in either of two ways (Goodman, 1976). The 'weakening' and 'softening' influence of the network of joints can be accounted for implicitly by reducing the mechanical properties assumed for a large body of rock by a selected amount. In that approach the rock mass is still treated as a continuum. Or, the actual properties of individual joints can be introduced explicitly in limiting equilibrium calculations, physical models, or numerical approximation techniques such as the explicit finite element or finite difference methods. Major steps have been made in the discipline of numerical modelling of jointed rock masses over the last

ten years (e.g. Goodman and St. John, 1977). However, there seems to exist an ever-widening gap between the methods of analysis and the quality of the input property values. Computer techniques although seemingly elegant and exact can only be as good as their input data which, at present, seems to be more or less guessed or extracted from the literature.

1.1.2 Objectives of this study

Explicit numerical or physical model methods of analysis of jointed rock masses require data on both the shear strength and deformation properties of joints.

The literature of the mechanical properties of jointed rock which has accumulated over the past two decades, reveals an impressive number of studies which have been devoted to the all-important aspect of shear strength along joints. However, the directly related question of scale effects seems to have attracted very little attention. In the majority of publications the potential existence or non-existence of a scale effect is acknowledged in passing or is ignored. There are also a limited number of studies where the shear strength-scale effects have been considered more seriously, but the interpretations and conclusions are different. The urgent need for high quality shear strength data and the uncertainties surrounding the question of a scale effect in joints warrants a systematic investigation of this important aspect. The experimental study reported in part two of the thesis represents an attempt to answer some of the questions. The main objectives of that work can be summarized under the following three headings:

(a) investigation of the existence or otherwise of a scale effect in the shear strength of joints

(b) clarification of the causes of a scale effect

(c) examination of potential solutions to the problem of allowing for a scale effect in a practical situation.

There is a large margin between the currently available literature on joint shear strength and the literature on joint deformability. This is probably because of the predominant use of limit equilibrium methods in

stability analyses of slopes and foundations. The experimental study described in the third part of the thesis deals with the analytical and quantitative aspects of joint deformability. The main objectives are summarized below:

(a) investigation of the stress-deformation relationships of a variety of natural, unfilled, fresh and weathered joint types, and their analytical representation

(b) study of the variables influencing joint deformability and derivation of quantitative relationships of possible practical use.

Reviews of the current literature directly related to each specific topic of investigation have been included in the corresponding parts of the thesis. In the following sections a review will be made of the fundamental characteristics of joint shear strength and deformation, as a general introduction to the contents of the subsequent parts.

1.1.3 Shear strength of joints

When a rock surface slides over another, the phenomenon of friction comes into play. Jaeger (1971) reviewed the various empirical laws of friction, which are based on research into materials other than rock - usually metals. The theories advanced in the past to explain the friction on metal surfaces are based on one of the four following concepts (Lama and Vutukuri, 1978): (a) lifting of microasperities over each other; (b) molecular attraction between the two surfaces; (c) a "ploughing" effect introduced by penetration on one solid by the asperity of the other solid; (d) interlocking of surface microroughness and lifting of asperities over each other. The mechanism of friction in brittle materials such as rocks is bound to be different. For instance the concepts of molecular attraction and plastic deformation at low stresses are not relevant to rock surfaces.

The basic criteria which have been adopted to describe rock friction are linear or non-linear:

1. If σ_n is the normal stress corresponding to a given shear strength τ, the coefficient of friction may be defined as:

$$\tan \phi = \frac{\tau}{\sigma_n} \quad \text{i.e.} \quad \tau = \sigma_n \tan \phi \qquad 1.1$$

2. In general, for soil and rock materials better experimental verification is achieved by assuming a shear strength component at zero normal stress. This is the term of cohesive resistance (c) in Coulomb's equation:

$$\tau = c + \sigma_n \tan \phi \qquad 1.2$$

The intercept 'c' has little relevance when dealing with rock joints unless the walls are bonded with 'bridges' of intact material. An "apparent cohesion" intercept is often used as equivalent to the shearing component of failure of intact asperities.

3. Both the above criteria are linear. This however is not the case for non-planar rock surfaces and various attempts have been made to fit non-linear relationships with mathematical laws in the form

$$\tau = f(\sigma_n) \qquad 1.3$$

In those cases the shear strength may be described by a variable coefficient of friction or in terms of a normal stress dependent "apparent cohesion" and a variable coefficient of friction (see text below and Figure 1.1).

In a simplistic model the shear strength of a rock joint may be considered to consist of two main components:

(i) A basic frictional component (ϕ_b) which represents the minimum resistance between two flat, unpolished rock surfaces. The basic friction angle depends on the mineralogy of the rock.

(ii) An additional resistance due to the presence of irregularities on the joint walls (roughness component, R_c). The effects of surface roughness may be recognized in the shear strength versus normal stress curve as an apparent cohesion or as an increase in the observed friction angle over the basic friction angle of the rock.

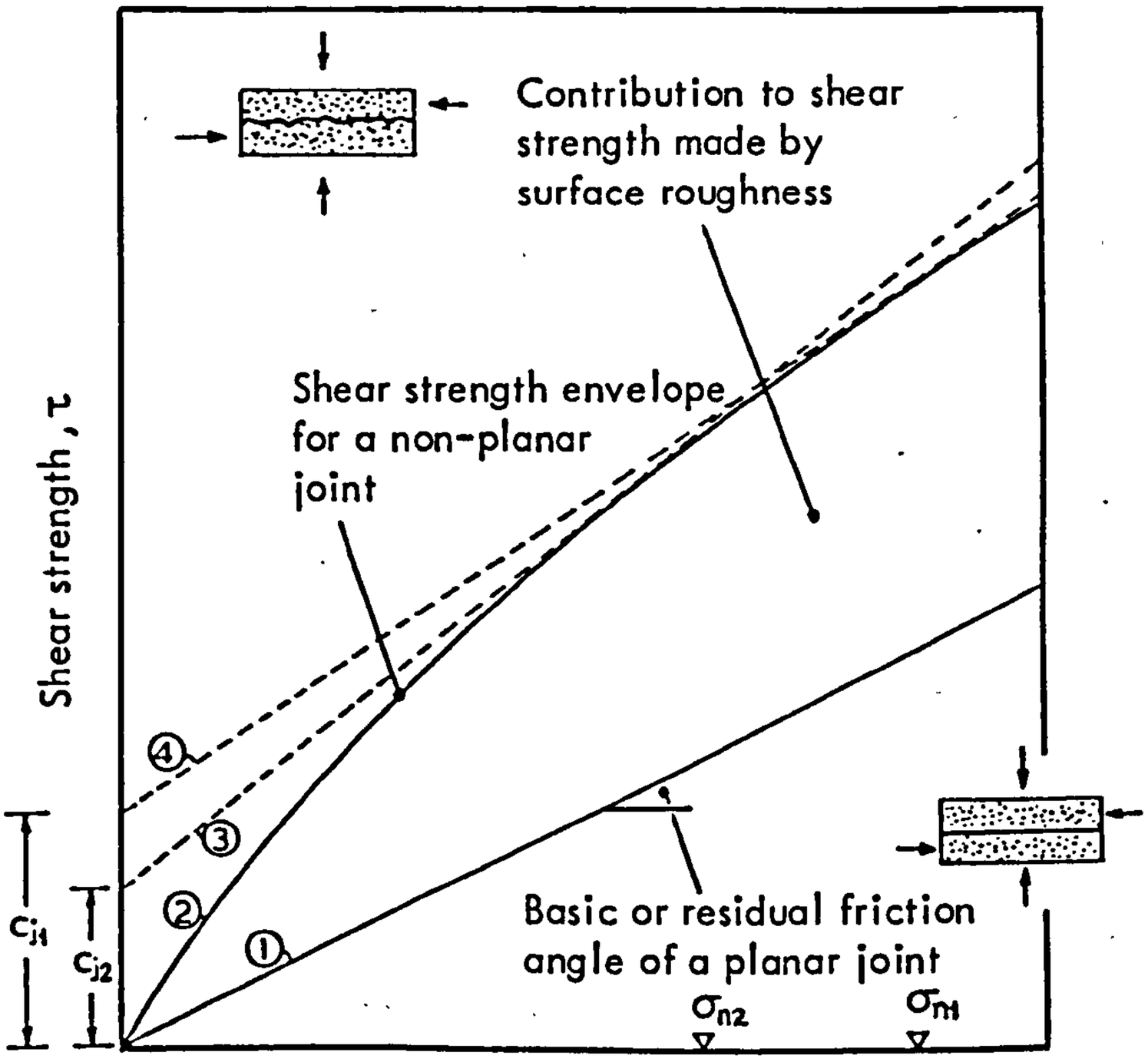

c_{j1} and c_{j2} are the apparent cohesions caused by surface roughness for an assumed linear shear strength envelope

Shear strength equations :

1. $\tau = \sigma_n \tan \emptyset$
2. $\tau = f(\sigma_n)$
3. $\tau = c_{j2} + \tan \emptyset_2 \sigma_{n2}$
4. $\tau = c_{j1} + \tan \emptyset_1 \sigma_{n1}$

FIGURE 1.1 Simple models of joint shear strength (from Richards, 1975)

The above models are illustrated diagrammatically in Figure 1.1.

1. The basic frictional component of joint shear strength

The frictional resistance (ϕ_b) developed between two flat rock surfaces is affected by the mineralogical composition of the material and the moisture conditions. Measurements of mineral friction by Horn and Deere (1962) showed that the crystal structure is related with adverse effects of the moisture condition. Oven-drying increased the friction of lattice-structure minerals (mica, chlorite, clay, talc, serpentine) but surprisingly lowered the friction of minerals with massive structure such as quartz, calcite and feldspar, from approximately 23° - 37° when tested wet to 6° - 8° when dried. Since tests on dry flat surfaces of rock with high mineral content of those types do not display the low friction values suggested in Horn and Deere's experiments, it may be concluded that the phenomenon is restricted to highly polished mineral surfaces.

In general, the friction coefficients of minerals range between 0.4 (~ 22°) and 0.8 (~ 39°), but for lattice minerals it can be as low as 0.2 (~ 11°) when wet. Consequently, rocks composed largely of such minerals can have quite low basic friction angles. For example, Brown et al. (1977) have reported angles of friction as low as 20.5° for wet smooth cleavage planes in Delabole slate, which was 9° lower than the values obtained from similar dry specimens.

Table 1.1 presents a summary of basic friction angles for unweathered flat rock surfaces. From the data it is seen that sedimentary and igneous rocks have generally higher ϕ_b values than metamorphic rocks. This is due to the relative proportions of massive and layer lattice minerals in the rock materials. Unweathered igneous rocks are little affected by the presence of water whereas fine-grained sedimentary rocks show large strength losses under saturated conditions.

For practical purposes the angle of basic friction can be determined from the residual shear strength of flat rock surfaces. The latter may result from residual shear tests on planar natural joints. Alternatively, the residual state may be simulated by preparing planar, rough-sawn or planar, sandblasted surfaces and conducting residual shear tests. It is

TABLE 1.1 BASIC FRICTION ANGLES OF VARIOUS UNWEATHERED ROCKS OBTAINED FROM FLAT AND RESIDUAL SURFACES

(from Barton and Choubey, 1977)

Rock type	Moisture condition	Basic friction angle ϕ_b	Reference
A. Sedimentary Rocks			
Sandstone	Dry	26—35	Patton, 1966
Sandstone	Wet	25—33	Patton, 1966
Sandstone	Wet	29	Ripley & Lee, 1962
Sandstone	Dry	31—33	Krsmanović, 1967
Sandstone	Dry	32—34	Coulson, 1972
Sandstone	Wet	31—34	Coulson, 1972
Sandstone	Wet	33	Richards, 1975
Shale	Wet	27	Ripley & Lee, 1962
Siltstone	Wet	31	Ripley & Lee, 1962
Siltstone	Dry	31—33	Coulson, 1972
Siltstone	Wet	27—31	Coulson, 1972
Conglomerate	Dry	35	Krsmanović, 1967
Chalk	Wet	30	Hutchinson, 1972
Limestone	Dry	31—37	Coulson, 1972
Limestone	Wet	27—35	Coulson, 1972
B. Igneous Rocks			
Basalt	Dry	35—38	Coulson, 1972
Basalt	Wet	31—36	Coulson, 1972
Fine-grained granite	Dry	31—35	Coulson, 1972
Fine-grained granite	Wet	29—31	Coulson, 1972
Coarse-grained granite	Dry	31—35	Coulson, 1972
Coarse-grained granite	Wet	31—33	Coulson, 1972
Porphyry	Dry	31	Barton, 1971b
Porphyry	Wet	31	Barton, 1971b
Dolerite	Dry	36	Richards, 1975
Dolerite	Wet	32	Richards, 1975
C. Metamorphic Rocks			
Amphibolite	Dry	32	Wallace et al.; 1970
Gneiss	Dry	26—29	Coulson, 1972
Gneiss	Wet	23—26	Coulson, 1972
Slate	Dry	25—30	Barton, 1971b
Slate	Dry	30	Richards, 1975
Slate	Wet	21	Richards, 1975

important that the granular texture of the rock is maintained as very smooth or too "coarse" (i.e. rough) surfaces due to sandblasting will give different than the true values. Coulson (1972) found that both the initial and residual friction of flat surfaces treated with different grades of carbide grit (from no. 80 to no. 600) increased with increasing 'roughness' under low normal stresses. A simple alternative method of measuring ϕ_b is by conducting tilt tests between pairs of sawn surfaces (Barton and Choubey, 1977). In that case at least ten samples should be tested to characterize a rock type.

The basic friction angle of a rock type is very close to the true residual friction (ϕ_r) of a non-planar unweathered joint and for all practical purposes they can be considered interchangeable. However, extreme care should be exercised when the joints of interest have weathered surfaces. Richards (1975) found from shear tests on weathered sandstone joints that it is possible to have residual friction angles as low as 12° if normal stress levels were low. Under high levels of normal stress the more resistant sandstone beneath the weathered skin came into effect and the mean ϕ_r value obtained from the same specimens was 28.5°. Barton and Choubey have suggested an empirical method for predicting the ϕ_r value for weathered joints based on the Schmidt hammer rebound numbers obtained from fresh and weathered surfaces and the angle of basic friction.

2. The roughness component of joint shear strength

The usual idealization for joint roughness is to consider sliding taking place up the slope of a wedge shaped asperity inclined at an angle i to the direction of shearing, as shown in Figure 1.2(a); N is the applied normal load and T is the shear resistance under that load. Resolving these forces normal and parallel to the inclined surface AB yields:

$$//AB: \quad T' = T\cos i - N\sin i \Rightarrow T = \frac{T' + N\sin i}{\cos i} \Rightarrow T = T'\cos i + N'\sin i \qquad 1.4$$

$$\perp AB: \quad N' = N\cos i + T\sin i \Rightarrow N = \frac{N' - T\sin i}{\cos i} \Rightarrow N = N'\cos i - S'\sin i \qquad 1.5$$

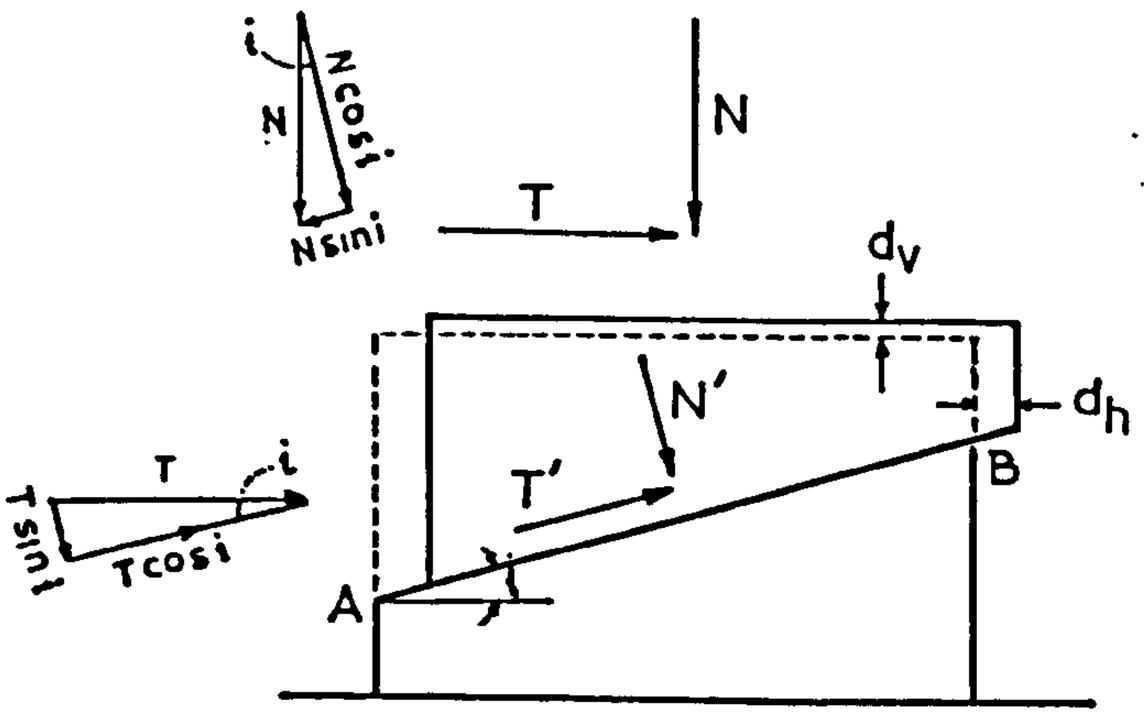

(a)

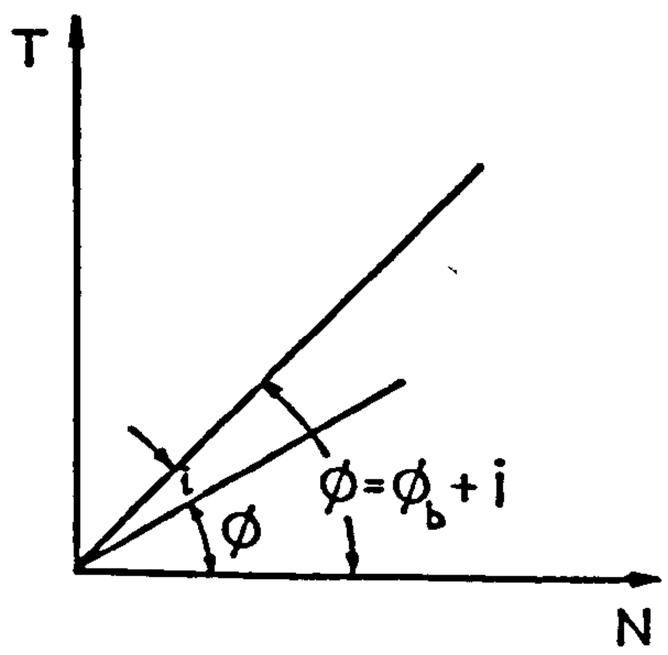

(b)

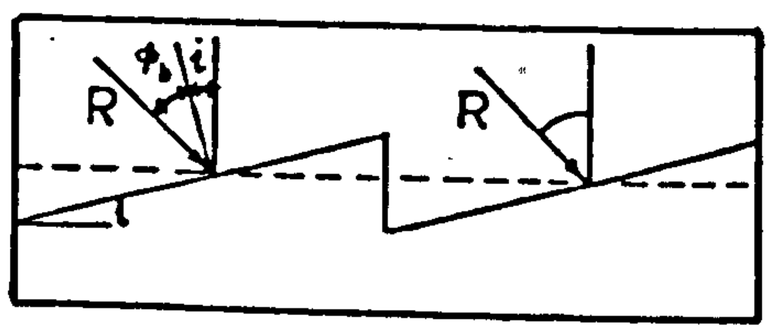

(c)

FIGURE 1.2 Sliding on inclined asperities

The friction angle on the smooth sliding surface is ϕ_b, i.e.

$$T' = N' \tan \phi_b \qquad 1.6$$

At the limit of sliding T and N are connected by:

$$\frac{T}{N} = \frac{T'\cos i + N'\sin i}{N'\cos i - T'\sin i} \qquad 1.7$$

Introducing 1.6 in 1.7:

$$\frac{T}{N} = \frac{N'\cos i \tan \phi_b + N'\sin i}{N'\cos i - N'\sin i} = \frac{\tan \phi_b + \tan i}{1 - \tan \phi_b \tan i}$$

thus

$$\boxed{\frac{T}{N} = \tan(\phi_b + i)} \qquad 1.8$$

The effect of regular asperities inclined at a uniform angle i is therefore to increase the friction angle by i (Figure 1.2b). This result is also apparent upon examining the inclination $(\phi_b + i)$ of the resultant force on the plane of sliding (Figure 1.2c). If a natural joint is idealized as a regular set of saw toothed asperities, the function 1.8 can be considered to be a crude approximation of real joint behaviour. At low normal stresses displacement results in overriding of the irregularities. Asperity overriding gives rise to changes in the value of the normal deformation (d_v) which has been termed dilation. The equation 1.8 implies that when there is no normal stress, asperities of inclination (i) less than $90° - \phi_b$ can be overriden. Under high normal stresses the work required to dilate against the normal force will exceed the work sufficient to shear through some asperities. Patton (1966) found that a bilinear relation (Figure 1.3) described his experimental data for shear of model joints with regular teeth. At low normal stresses the gradient of the steep primary portion was approximately equal to $\phi_b + i$ where i was the inclination of the "asperities", and hence the curve was described by 1.8. Beyond a certain level of normal stress the gradient changed rapidly as "asperity" failures occurred and the upper portions were fitted with Coulomb's equation.

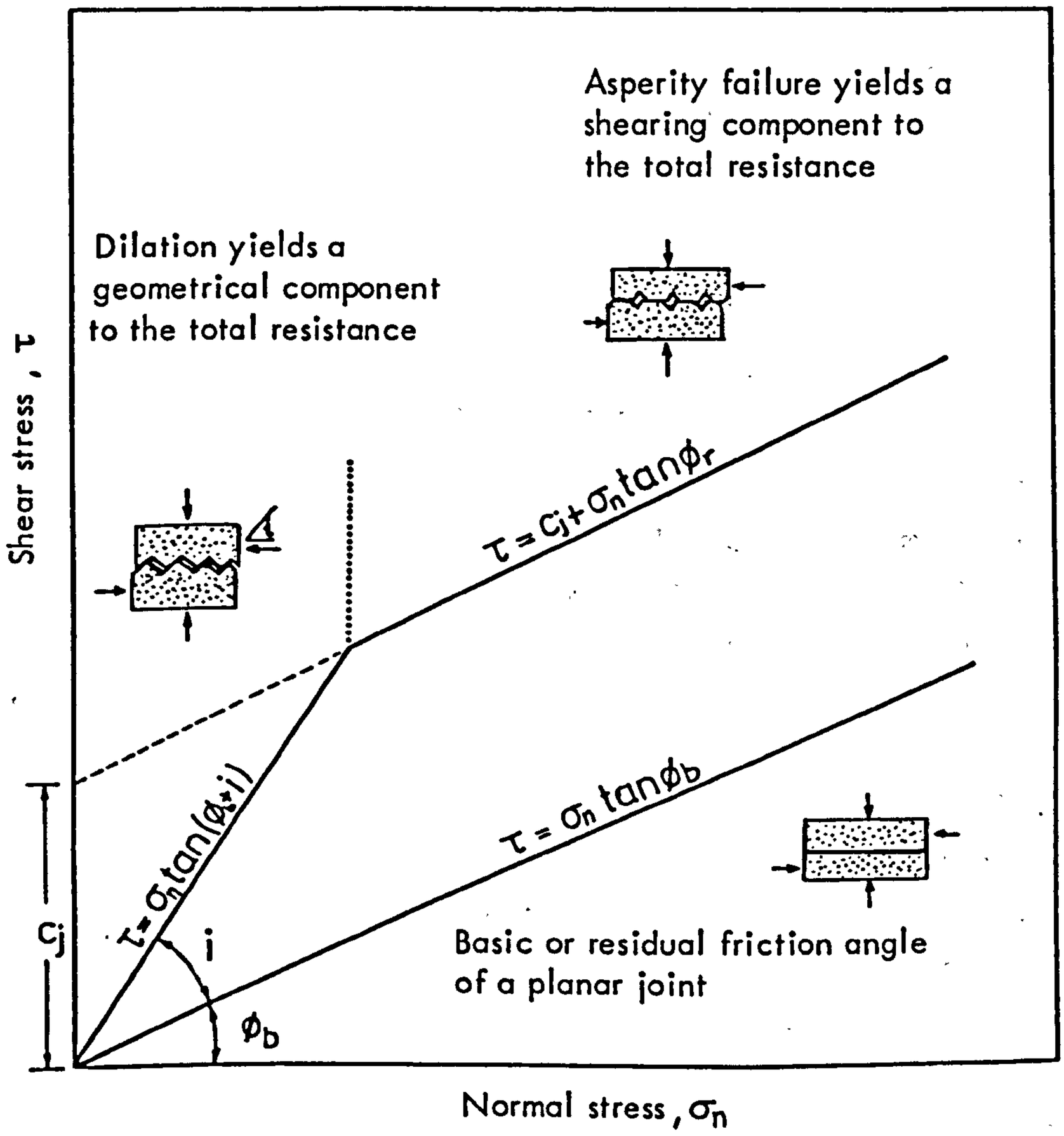

FIGURE 1.3 Patton's bilinear law of friction

In a real situation the transition from asperity overriding to shearing is not as abrupt as suggested in Figure 1.3 and the envelopes usually display a continuous curvature, which reflects a progressive transition from one mode of failure to the other. However, the original assumption of a bilinear friction law was a marked departure from the traditional concept of interpreting the shear strength of joints on the basis of Coulomb's "constants" c and ϕ. The normal stress dependency of the shear strength of non-planar joints has been demonstrated by many investigators over the years e.g. Jaeger (1959), Krsmanovic and Langof (1964), Drozd (1967), Byerlee (1967), Ruiz et al. (1968), Barton (1973) to mention just a few. A review of proposed non-linear criteria will be made in subsection 4.

3. Peak, ultimate and residual shear strength

The bilinear law relates to peak shear strength only. The peak shear strength of a joint is, as the term implies, the maximum resistance which usually develops after a very small amount of displacement. It is conventionally described as peak frictional resistance or peak total frictional resistance. An interlocked rough joint subjected to shearing under a given normal stress, initially behaves in a "stiff" fashion, i.e. there is a large increase in shear strength for small displacement. In general, small initial displacements produce a steep increase in shear resistance until a peak value is reached at a "peak shear displacement" $(d_h)_P$. Continuation of the movement after the peak results in progressive decrease in shear strength until a residual value is approached. Different joint types behave in different ways and a more detailed examination of the stress-displacement behaviour will be made in section 1.3.

As has been discussed in the previous subsection 1, the residual friction of a non-planar fresh joint may for practical purposes be considered equal to the basic friction angle, thus assuming that roughness is not influencial any more and hence dilation at the residual stage must be zero. Another practical rule proposed by the Commission on Standardization of Laboratory and Field Tests (ISRM 1974) regards the residual stage as reached when at least four consecutive sets of readings are obtained which show not more than 5% variation in shear stress over a

shear displacement of 10 mm. However, the Commission does recommend an independent check of the residual friction angle thus obtained, by testing two artificially prepared surfaces (saw-cut and ground flat with no. 80 silicon carbide grit).

Krahn and Morgenstern (1979) observed that "two rock joint samples of the same mineral composition and tested under the same stress state will not have the same 'large strain shearing resistance' if the structure or roughness along the shearing surfaces is not similar". They therefore suggested the use of the term ultimate frictional resistance in place of the word residual. This terminology was in fact also used some years ago by Krsmanovic (1967) who recognized the limits imposed by direct shear testing. The ultimate frictional resistance depends on the initial roughness of the joint by contrast to the 'theoretical' minimum of ϕ_{res}. ϕ_{ult} is probably the lowest value which may be obtained by shear testing a rough joint unless asperity strength is low and normal stresses high.

Use of the residual angle of friction for purposes of design is dictated when geological evidence suggests that displacements have occurred in the past or are anticipated during construction. The same applies when a high factor of safety is required for important structures of long life-span. When slopes are to be cut in a rock mass which has persistent clay filled joints, the adoption of ϕ_r for those 'weaknesses' is also justified. Barton (1973a) commends that for slopes cut in "cleanly"-jointed rock it is reasonable to design for peak strength along at least part of the potential failure surface. He also considers that it may be justifiable to adopt a global peak strength for designing the short term stability of working slopes in open cast mines, and the long term stability of bolted or anchored rock cuttings. Hoek and Londe (1974) also suggest that peak shear characteristics may be used for temporary rock structures provided that the design values are checked against values from back analysis of failures in similar materials.

The residual shear strength of joints is perhaps the least problematic parameter, at least in the form assumed in practice. It can be easily measured on small size samples, generally shows small variation, and weathering effects can readily be allowed for. Peak shear strength is

still an "uncertain" parameter to use Schneider's (1978) expression. It certainly is an extremely variable property which depends on the roughness of the surface, the asperity strength and the operating normal stress. Peak total friction angles may range from as low as 30° to as high as 80°. The wide spectrum revealed by literature data is illustrated in Figure 1.4. Barton (1973) noted the lack of any differences between joints in sedimentary, igneous or metamorphic rocks. This can be expected considering that for instance limestones may have high compressive strength and rough bedding joints. Conversely, the high compressive strength of many metamorphic rocks may have little effect on the shear strength of the relatively smooth and planar foliation planes.

On a simplified basis the geometry or roughness of joints is characterized by a waviness and by an uneveness (ISRM, 1978a). Waviness describes the large scale undulations which, if interlocked and in contact, cause dilation during shear displacement since they are too large to be sheared off. Uneveness describes small scale roughness that tends to be damaged during shear displacement unless the discontinuity walls are of high strength and/or the stress levels are low, so that these small features can also cause dilation. In the same context Patton (1966) described waviness and uneveness as first and second order irregularities. Patton's classical example showing the different orders of surface roughness is illustrated in Figure 1.5. The small scale roughness (uneveness) affects the shear strength of joint specimen sizes that would be sampled in a laboratory or small scale in-situ shear test. The large scale undulations (waviness) affect the initial direction of shearing relative to the mean joint plane. If the effects of uneveness are ignored, the angle of inclination of the undulations can be substituted for i in equation 1.8.

The interrelationship between roughness and dilation was introduced in the last section. Dilation increases the peak shear strength of a joint irrespective of the stiffness of the normal loading system. If normal deformation is unrestricted, dilation will increase the strength by forcing the joint to slide up at an angle to the mean shearing direction. If normal deformation is restricted due to fixed external boundaries the tendency of the joint to dilate will increase the normal stress exerted across the joint and shearing will be possible only if the asperities themselves fail.

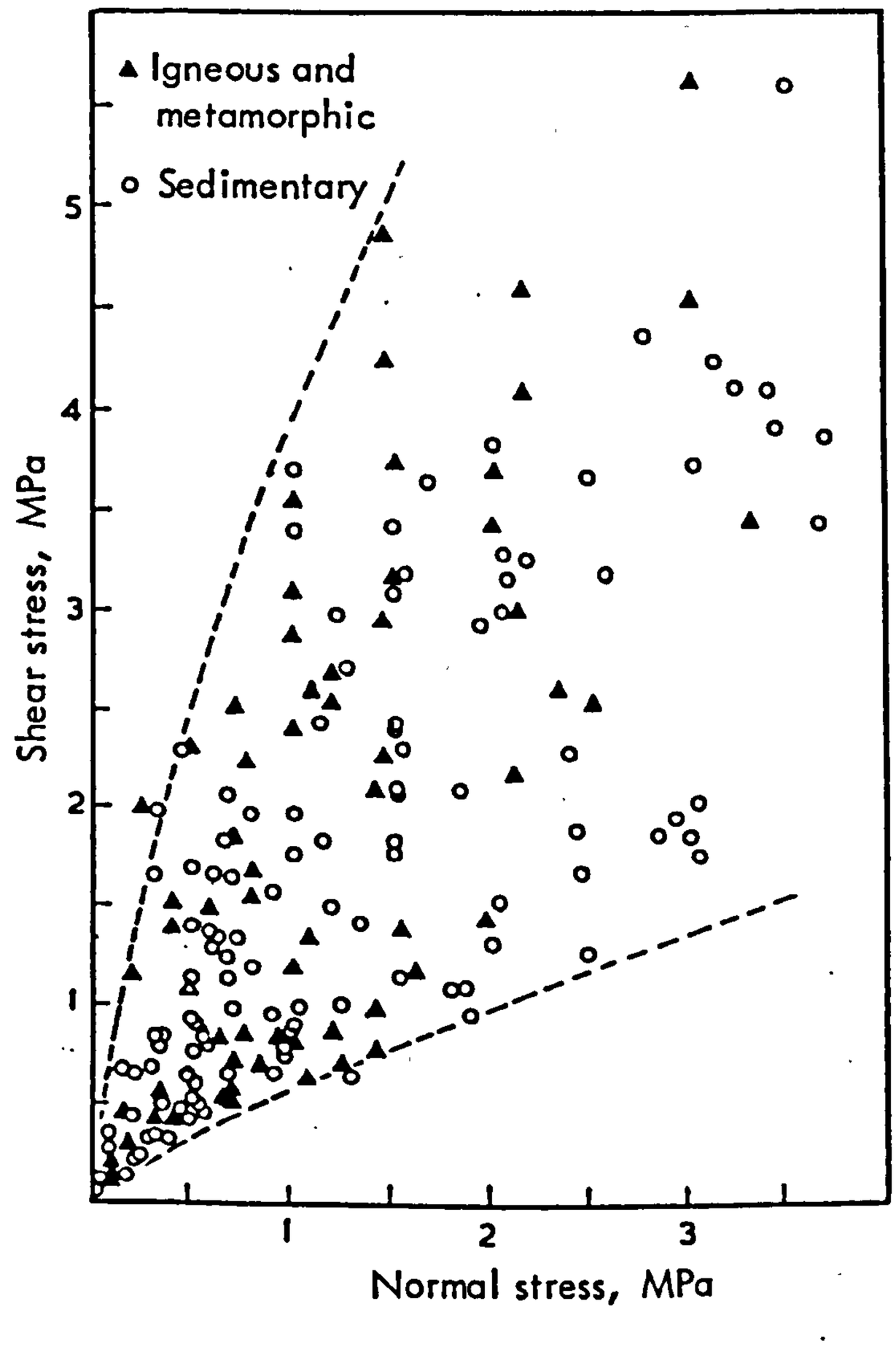

FIGURE 1.4 Range of peak shear strength of unfilled rock joints from laboratory and in situ tests. Rock types include : amphibolite, diabase, gneiss, granite, greywacke, hornfels, mylonite, porphyry, quartzite, schist, serpentine, chalk, limestone, marl, sandstone, shale, siltstone. (after Barton, 1973)

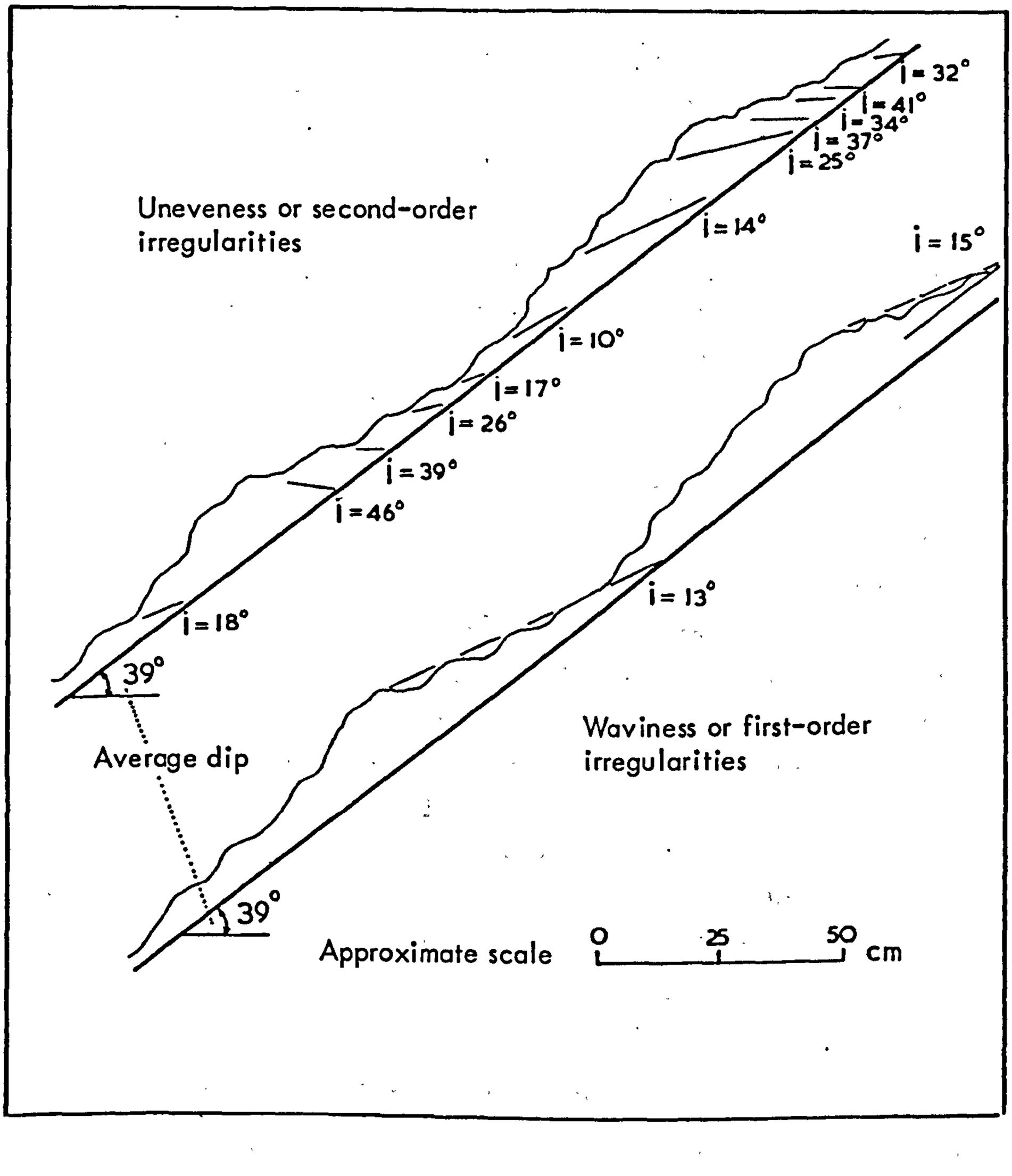

FIGURE 1.5 Illustration of the different roughness features found on natural joint surfaces (after Patton, 1966)

It is generally recognized that non-planar joints under shearing experience maximum dilation at or near the moment of mobilization of the peak shear strength. Under prolonged displacement a non-planar joint may continue to dilate (depending on σ_n) but at reduced rate. The above two characteristics are illustrated in Figure 1.6, where the top curve represents the total frictional resistance of the joint, comprising the frictional component "ϕ" (= basic friction + asperity failure) and the dilation angle (d_v/d_h).

Oversliding of asperities without rock breakage is unlikely, except at extremely low normal stress. The fluctuations observed along the "ϕ" curve in Fig. 1.6 are due to the very reason of failing asperities. This "shearing through" mode of failure normally occurs when the normal stress is high, but it can also occur at low stresses if the geometry of the remaining unsheared asperities allows shear failure to occur for a lower energy input than would be required for dilation. Whenever the shearing component rises as shown by sudden upward jumps in the "ϕ" curve, the dilation curve (d_v/d_h) is seen to fall. If both rose together, then the total strength component $\tan^{-1}(\tau/\sigma_n)$ shown in the upper curve would have to show an upward kick, signifying an increased energy input for continued shearing. Under very high normal stresses, and especially at levels approaching the unconfined compressive strength of asperities, dilation tends to become completely suppressed. An example of the mode of variation that could be shown by the peak dilation angle with increasing normal stress to asperity strength ratio is shown in Figure 1.7. The inverse relationship would have been obtained if the asperity failure component in each case had been similarly plotted.

4. Peak shear strength envelopes and related criteria

The bilinear law of friction represents an idealized expression of the effects of normal stress on the peak shear strength of non-planar joints. Shear tests on real joints demonstrate that the envelopes display a continuous curvature, and various approaches have been made in the past to yield a suitable peak shear strength criterion. Some workers have simply fitted their experimental data with appropriate functions, whereas others have attempted to derive constitutive relations by quantifying the variables other than σ_n which influence the peak shear strength.

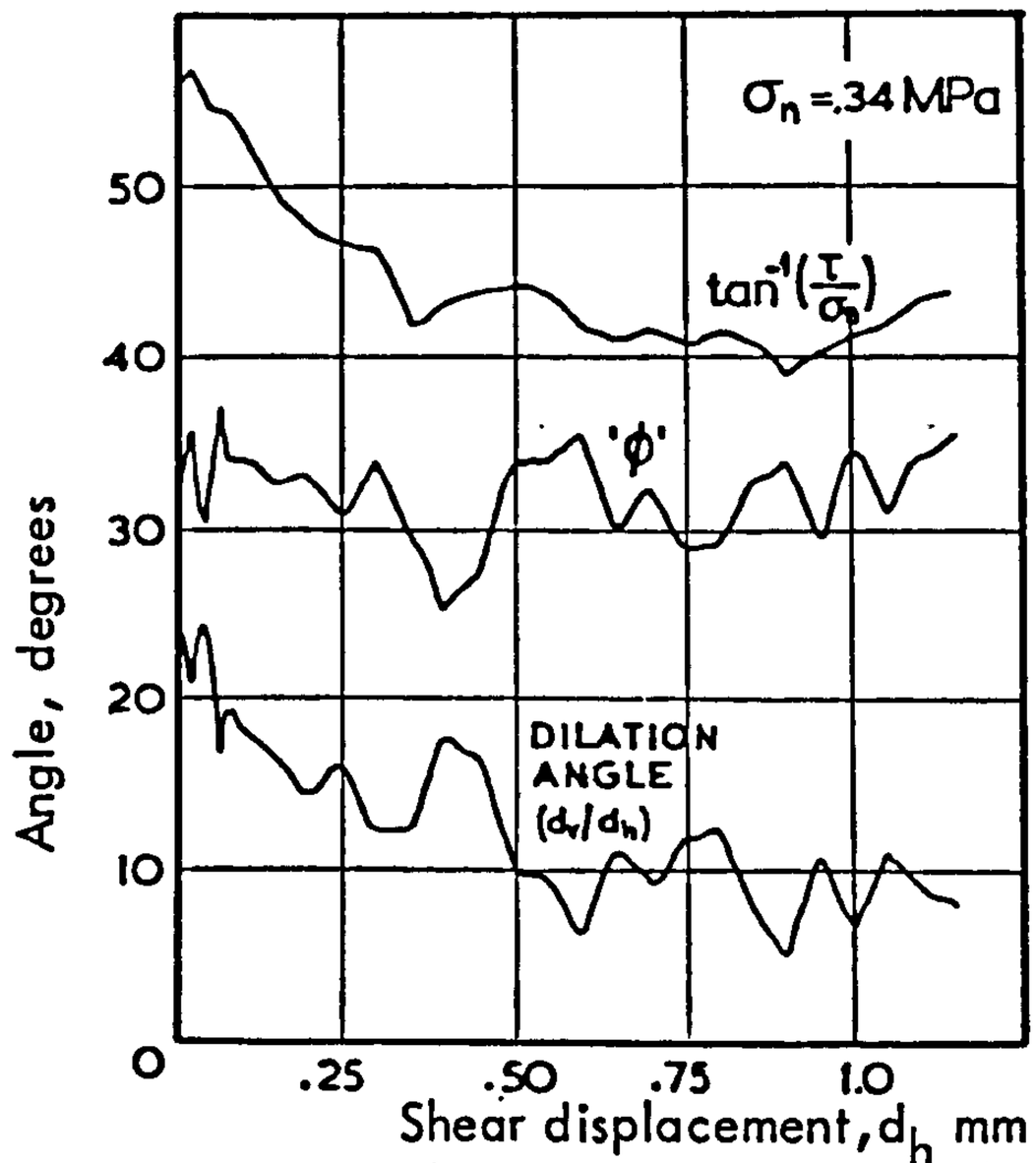

FIGURE 1.6 Variation of dilation and shear strength measured on a natural joint in coarse grained granite (after Coulson, 1970)

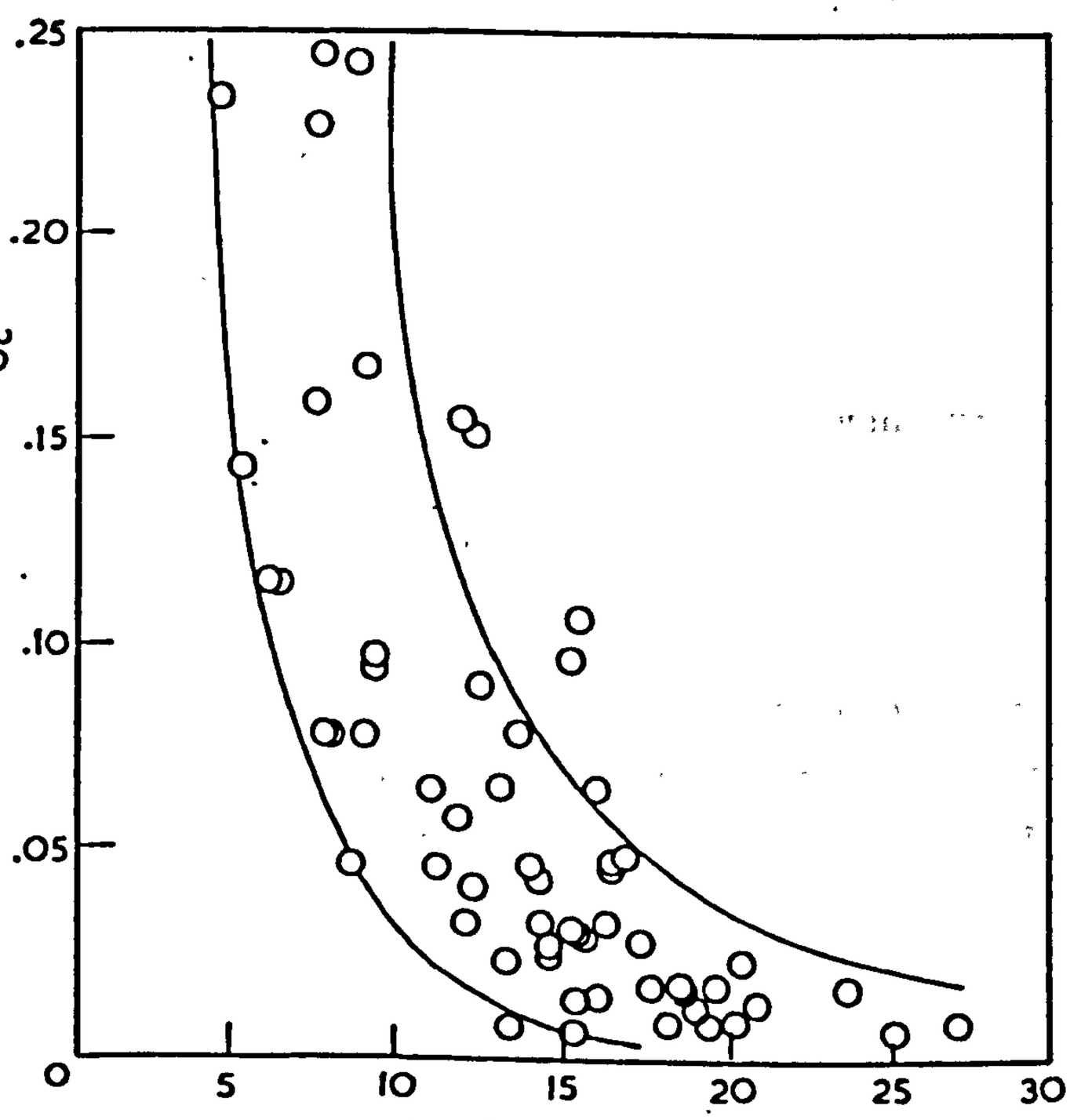

FIGURE 1.7 Peak dilation angle as a function of the ratio of normal stress to compressive strength for model extension joints (after Barton, 1971

Murrell (1965) found that the post-fracture shear strength of specimens failed under triaxial compression was best approximated by a power law. Similar conclusion was reached by Ruiz et al. (1968) when interpreting the results of in-situ sliding tests. In general, the most common relation used to describe curved peak shear strength envelopes are:

$$\tau_p = A \sigma_n^{\ a} \qquad 1.9$$

$$\tau_p = c + B \sigma_n^{\ b} \qquad 1.10$$

Jaeger (1971) gave another non-linear function:

$$\tau_p = a\left[1 - \exp(-b \sigma_n)\right] + \sigma_n \tan \phi_r \qquad 1.11$$

The latter gives an empirical "smoothing" of Patton's bilinear relationship (Figure 1.8). When σ_n tends to zero the slope of the curve is given by

$$\frac{\partial \tau_p}{\partial \sigma_n} = ab + \tan \phi_r \qquad 1.12$$

At large normal stresses the shear strength is given by:

$$\tau_p = a + \sigma_n \tan \phi_r \qquad 1.13$$

and therefore 'a' is equivalent to the apparent cohesion used for linear strength envelopes. If it is assumed that at low σ_n behaviour is primarily dependent on the asperity angle i, then $\tan(\phi + i) = ab + \tan \phi$ and thus:

$$b = \frac{\tan i \ \sec^2 \phi_r}{a(1 - \tan \phi_r \tan i)} \qquad 1.14$$

While Jaeger's empirical equation should be satisfactory for a wide range of conditions, it is helpful to have an equation derived from identifiable properties of the joint and wall rock. Ladanyi and Archambault (1970)

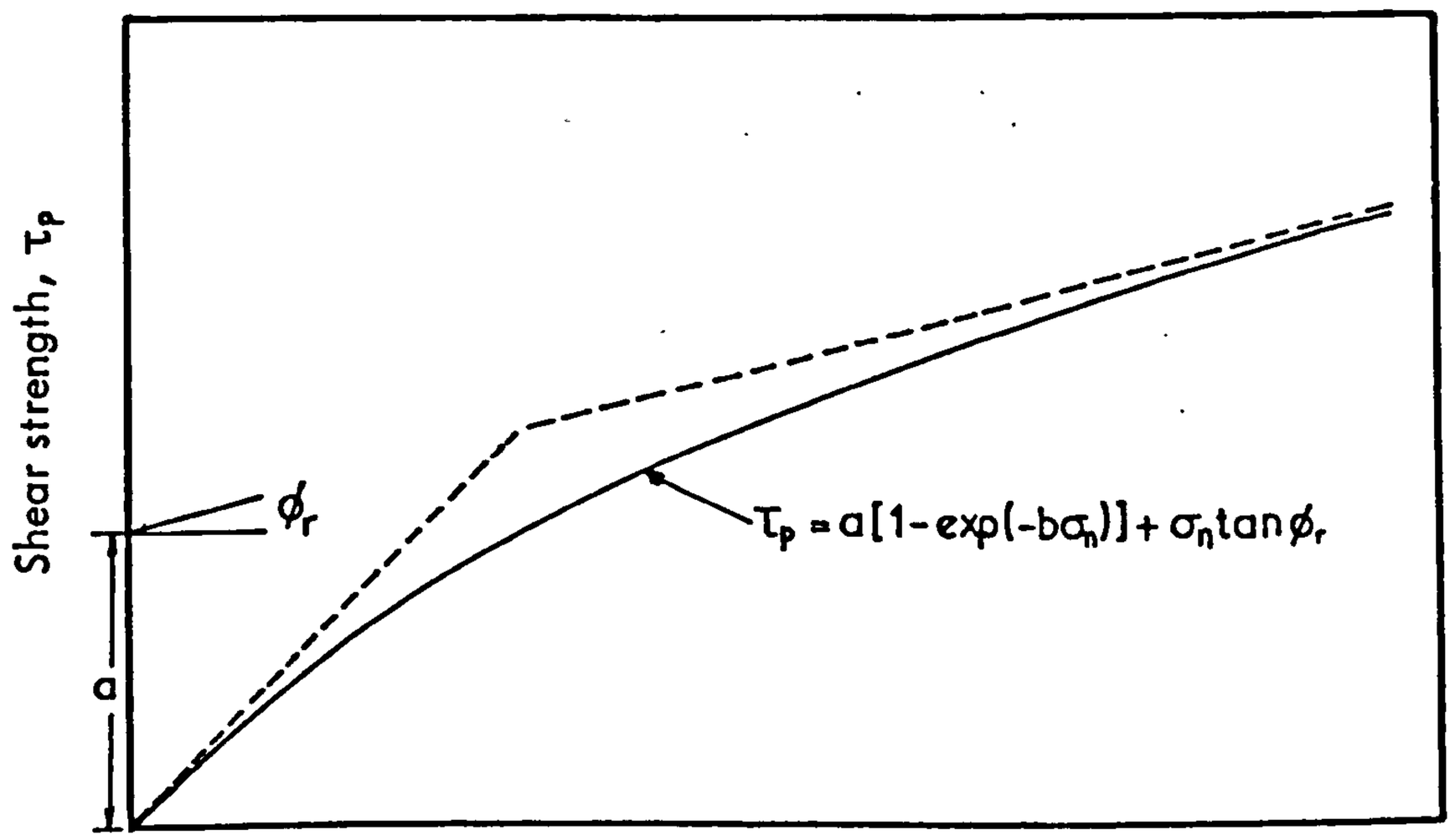

FIGURE 1.8 Continuous function approximating Patton's bilinear friction criterion (after Jaeger, 1971)

suggested a peak shear strength criterion related to the intact strength of the rock material, given by:

$$\tau_p = \frac{\sigma_n(1 - a_s)(\dot{V} + \tan \phi_b) + a_s S_r}{1 - (1 - a_s)\dot{V} \tan \phi_b} \qquad 1.15$$

where: a_s, termed the shear area ratio, is the ratio of the sum of areas of failed asperities to the total sample area

$\dot{V}$ is the rate of dilation at the instant of peak

S_r is the shear strength of the asperity rock.

At very low normal stresses when almost no asperity failure occurs, $a_s \rightarrow 0$ and $\dot{V} \rightarrow \tan i$ and therefore equation 1.15 reduces to $\tau_p = \sigma_n \tan(\phi_b + i)$. At extremely high stresses when $a_s \rightarrow 1$, then $\tau_p \rightarrow S_r$.

The authors suggested that S_r can be represented by the equation of a parabola attributed to Fairhurst:

$$S_r = \sigma_c \frac{\sqrt{1 + n} - 1}{n} \left(1 + n \frac{\sigma_n}{\sigma_c}\right)^{\frac{1}{2}} \qquad 1.16$$

where σ_c is the uniaxial compressive strength of the wall material

n is the ratio of the uniaxial compressive to the uniaxial tensile strength of the rock material.

S_r may also be expressed by any other shear strength criterion, e.g. Coulomb's. The functions a_s and $\dot{V}$ were described by the following empirical relations:

$$\dot{V} = \left(1 - \frac{\sigma_n}{\sigma_c}\right)^K \tan i \qquad 1.17$$

$$a_s = 1 - \left(1 - \frac{\sigma_n}{\sigma_c}\right)^L \qquad 1.18$$

where for rough rock surfaces, K = 4 and L = 1.5. Hoek and Bray (1977) integrated the various functional relationships 1.7 to 1.10 in the

following dimensionless form assuming n = 10 and K = 4, L = 1.5:

$$\frac{\tau_p}{\sigma_c} = \frac{\frac{\sigma_n}{\sigma_c}\left(1 - \frac{\sigma_n}{\sigma_c}\right)^{1.5}\left[\left(1-\frac{\sigma_n}{\sigma_c}\right)^4 \tan i + \tan \phi_b\right] + 0.232\left[1-\left(1 - \frac{\sigma_n}{\sigma_c}\right)^{1.5}\right]\left(1+10\frac{\sigma_n}{\sigma_c}\right)^{0.5}}{1 - \left[\left(1 - \frac{\sigma_n}{\sigma_c}\right)^{5.5} \tan i \tan \phi_b\right]} \qquad 1.19$$

The above equation relates the two dimensionless quantities τ_p/σ_c and σ_n/σ_c; the only unknowns are the roughness angle i and the basic friction angle ϕ_b. A hypothetical example of a predicted peak shear strength envelope by using 1.19 and assuming i = 20° and ϕ_b° = 30° is shown in Figure 1.9. The latter demonstrates that Ladanyi and Archambault's function 1.19 gives a smooth transition between Patton's equation at low σ_n levels to Fairhurst's equation for the intrinsic shear strength of the rock material adjacent to the joint when $\sigma_n \longrightarrow \sigma_c$.

An alternative approach to the problem of predicting the peak shear strength of non-planar joints was proposed by Barton (1973). Based upon experiments on model tension fractures, Barton determined the following relationship between i, normal stress and rock compressive strength:

$$i = JRC \log_{10}(JCS/\sigma_n) \qquad 1.20$$

where JRC is a joint roughness coefficient varying from 20 to 0 from the roughest to the smoothest surfaces

JCS is the joint wall compressive strength (= σ_c if the joint is unweathered).

Substituting 1.20 in the fundamental expression 1.8 yields:

$$\tau_p = \sigma_n \tan\left[JRC \log_{10}\left(\frac{JCS}{\sigma_n}\right) + \phi_b\right] \qquad 1.21$$

The unknowns in 1.21 are: ϕ_b which can be measured as already discussed (if the joint is weathered the value of ϕ_r should be used instead); JCS which can be obtained either indirectly from representative rock material or directly from the joint surfaces themselves by means of simple index tests, e.g. Schmidt hammer, scratch index, etc. (ISRM, 1978a); JRC can be either back-calculated from the results of sliding tests (shear or tilt)

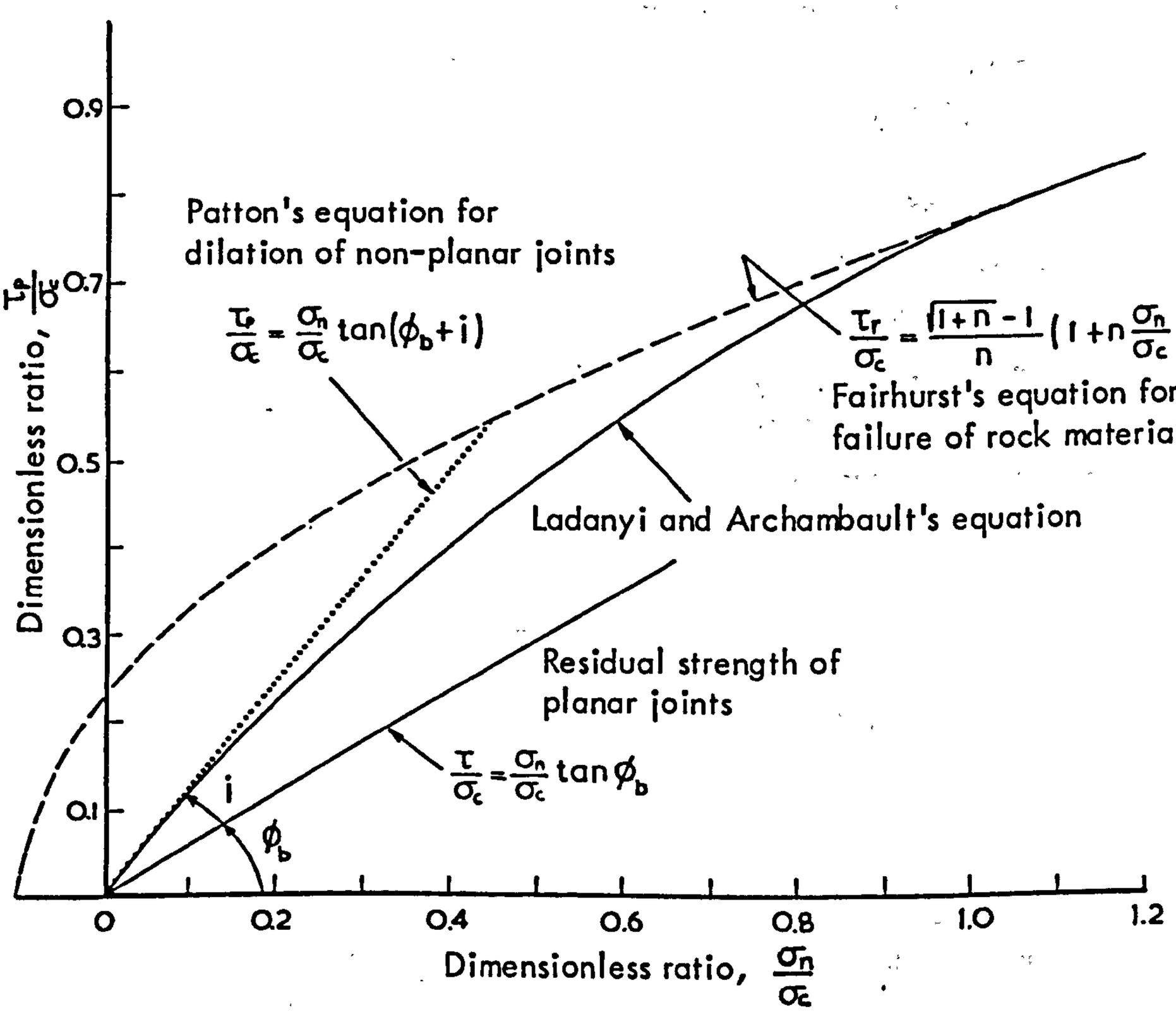

FIGURE 1.9 Transition from dilation to shearing of asperities predicted by Ladanyi and Archambault's equation (1.19) for $i = 20^\circ$ and $\phi_b = 30^\circ$ (from Hoek and Bray, 1977)

from 1.21 or an approximate value can be predicted by matching surface profiles from the joints of interest with typical profiles as illustrated in Figure 1.10. Once the values of the unknowns have been established equation 1.21 can be used for curve fitting or extrapolation of experimental peak shear strength data.

The families of curves presented in Figure 1.11 illustrate the practical nature of Barton's empirical law of friction. Values of JRC of 20, 10 and 5 are used to illustrate the effect of joint roughness, while the numbers 5, 10, 50, 100 assigned to the curves are the assumed values of joint wall strength (JCS in MPa units).

The criterion is valid within certain boundaries of the normal stress. At extremely low σ_n the slope of the envelope becomes unrealistically high, depending of course on JRC. By reviewing literature results Barton suggested a maximum peak arctan (τ/σ_n) of 70°. When $\sigma_n \rightarrow$ JCS then the logarithmic formulation of the dimensionless ratio predicts negative dilation. The following forms were suggested for the corresponding stress ranges:

1. $JCS/\sigma_n \geq 100$ ..... $\tau_p = \sigma_n \tan 70°$
2. $100 > JCS/\sigma_n \geq 1$ ..... $\tau_p = \sigma_n \tan[JRC \log_{10}(\frac{JCS}{\sigma_n}) + \phi_b]$
3. $1 > JCS/\sigma_n$ ..... $\tau_p = \sigma_n \tan \phi_b$

The upper boundary of the criterion is illustrated in Figure 1.11, where the envelopes predicted for the roughest joints have been truncated to a curvi-linear form.

If a comparison is made between Barton's and Ladanyi and Archambault's functions it is seen that the predicted envelopes are in close agreement under very low normal stresses, but they diverge as the normal stress increases. This is because in Barton's equation (1.21) as $\sigma_n/JCS \rightarrow 1$, $\tau_p = \sigma_n \tan \phi_b$, whereas Ladanyi and Archambault's equation (1.19) reduces to $\tau_p = S_r$ (shear strength of intact rock). Therefore, 1.21 tends to be more conservative than 1.19 at higher normal stress levels.

Schneider (1976) approximated the variation in peak dilation (i) with normal stress as observed in his experiments on model joint casts with

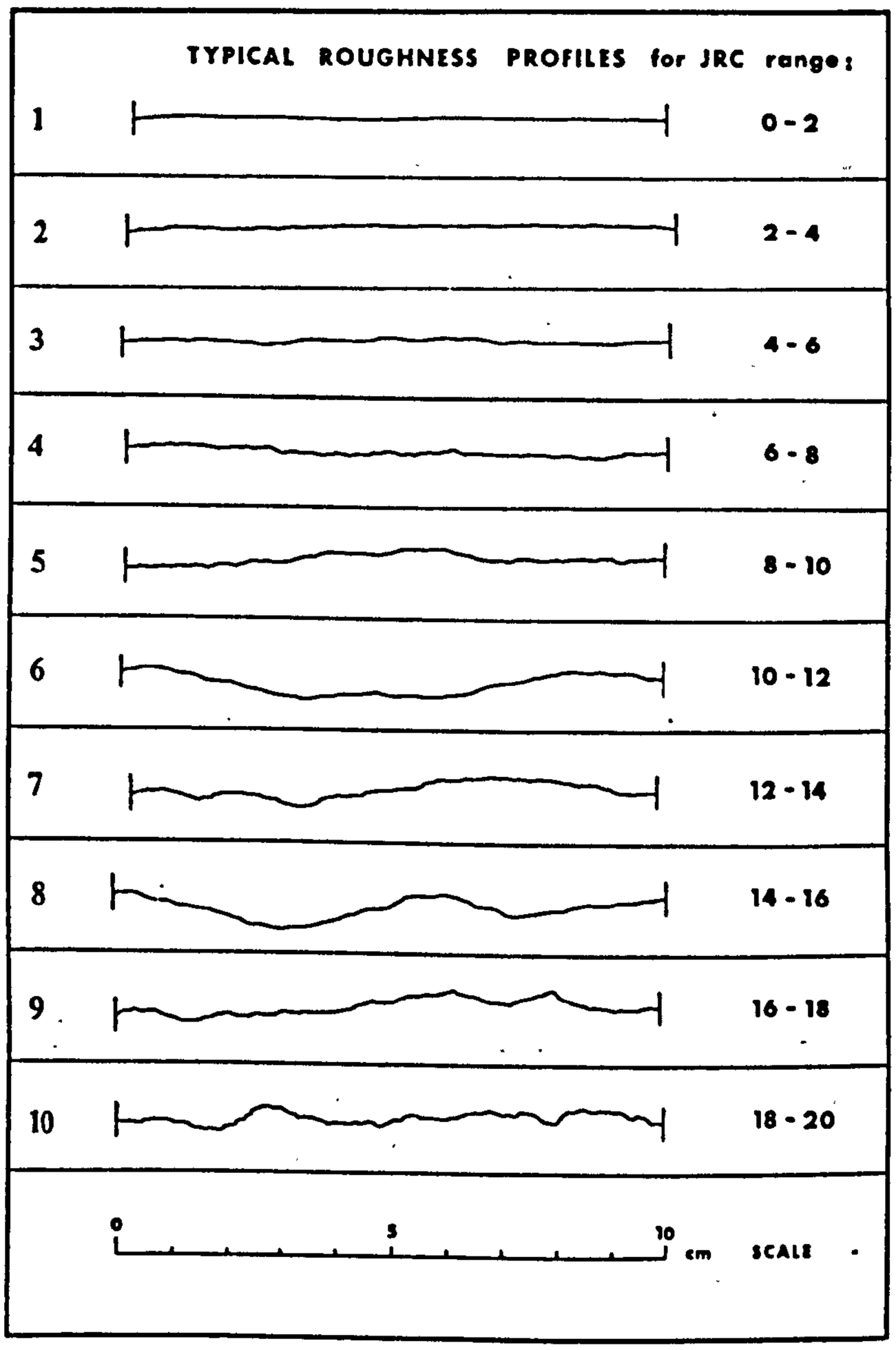

FIGURE 1.10 Profiles of joints with given range of JRC (after Barton & Choubey, 1977)

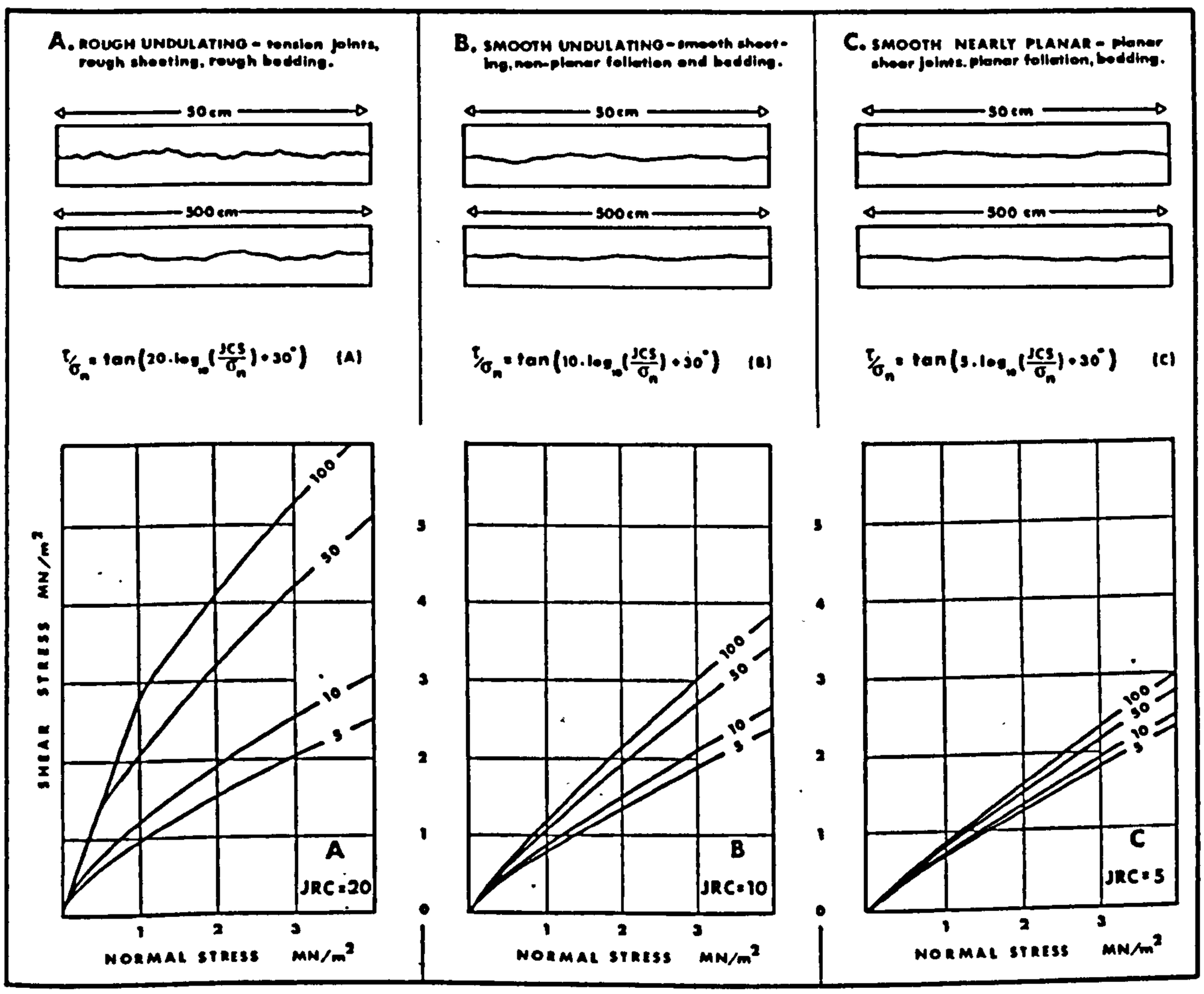

FIGURE 1.11 Illustration of Barton's empirical law of friction in graphical form. Each curve is numbered with the appropriate JCS value (MPa units). The roughness profiles give an approximate guide to the appropriate JRC values 20, 10 and 5. Completely smooth planar joints have JRC = 0.

(from Barton and Choubey, 1977)

an exponential relation which, if substituted in equation 1.8, yields

$$\tau_p = \sigma_n \tan(\phi_b + i_o e^{-k\sigma_n}) \qquad 1.22$$

where: i_o = peak dilation angle at zero normal stress
k = empirical reduction factor.

From a correlation with the tensile strength (σ_t) of the materials, Schneider found the following empirical function between k and σ_t:

$$k = a(\sigma_t d)^{-b} \qquad 1.23$$

where d simply serves the purpose of making the function dimensionless.

An inspection of all the peak shear strength criteria reviewed in this section shows that all except for Barton's rely on empirical constants. These constants can be obtained only by fitting the proposed curves to experimental data points. The relative advantage in Barton's criterion is that it is based on simple, measurable or at least estimable joint properties, JRC, JCS and ϕ_r. In a recent article, Tse and Cruden (1979) pointed out that small errors in estimating the value of JRC when visually comparing joint profiles with the "prototypes" in Fig. 1.10, could result in serious errors in estimating the peak shear strength from 1.21. They therefore recommended a numerical check of the value of JRC, based on a detailed profiling and analysis utilizing several of the mathematical techniques for describing surface characteristics used in mechanical engineering, to "avoid the subjectivity of estimates of JRC by comparison with typical profiles". Such errors could easily be avoided by actually "measuring" JRC from simple index tests as will be discussed later in part two.

In the preceding discussions the shear strength of joints without infilling material has been considered. If the joint walls are separated by a filling of clay, fault gauge, or weathered material, the shear strength will depend on the character and mechanical properties of infill, and its thickness in relation to the geometry of the joint walls. Comprehensive reviews of the behaviour of infilled joints have been presented by Barton (1973a,1974). The infilled class of joints have not been included in the present experimental study. Brief reference to their behaviour will be made in the literature reviews in parts two and three.

1.1.4 Shear deformation

Following an extensive review of in-situ and laboratory shear tests, Goodman (1970) classified the shear stress-shear deformation curves into four types, as illustrated in Figure 1.12.

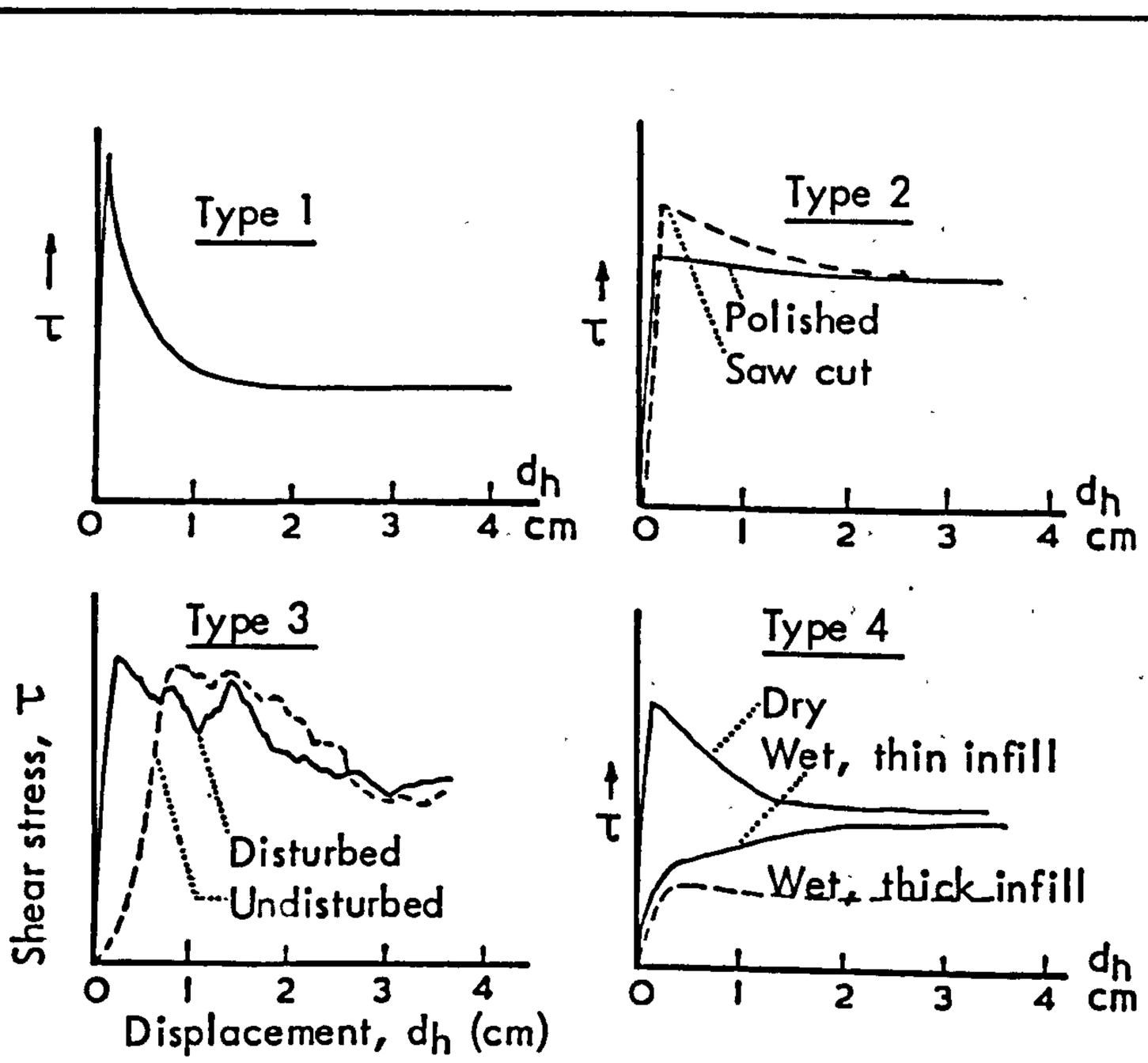

FIGURE 1.12 Typical shear stress - displacement relationships for various types of discontinuities (after Goodman, 1970)

Type (1) behaviour is typical of incipient joints and 'healed' types containing e.g. chlorite, calcite, pyrite or cemented gauge. The stress-deformation curve rises steeply to a peak shear stress at very low deformations and then falls quickly to a residual value that may be one-third or less of the peak.

Type (2) curves which are roughly simulated by artificial sawn, or polished planar surfaces, are also typical of joints with hard and fairly smooth surfaces, although the latter do not always show a distinct peak point. Differences between peak and residual strength are generally low.

Type (3) curves are typical of clean, rough, undulating joints. The relatively rapid rise in shear stress to a peak is usually followed by an irregular post-peak history from overriding of successive asperities, and

considerable loss in load carrying capacity. Jaeger & Rosengren (1969, quoted in Lama and Vutukuri, 1978) give a variation of this behaviour, showing somewhat smoother curves which they associate with undulating bedding planes such as those with cross ripple markings and also faults with cross slickensides or grooves.

Type (4) behaviour which is typical of joints containing infilling material is extremely dependent on the water content of the infill. Behaviour can range from 'brittle' to 'plastic' depending upon the moisture content and the thickness of the joint filling or seam.

In the context of this thesis it is the pre-peak portion of the shear stress-deformation curves that is of main interest. Goodman, Taylor and Brekke (1968) defined the slope of that part as the unit shear stiffness, K_s. In general terms the peak shear stiffness of a joint can be found by conducting a shear test and dividing the peak shear strength by the peak shear displacement. Joints may also exhibit non-linear behaviour; the exact shape of the pre-peak portion describes the dependency of the shear stiffness on the level of shear stress under a given normal stress. Inspection of the curve types in Figure 1.12 shows that types 1 and 2 display little, if any, nonlinearity, while types 3 and 4 display progressively more non-linearity.

For an initial appreciation of the variations in shear stiffness as dictated by the type of discontimuity some typical K_s values quoted by Goodman (1970) for the varieties in Figure 1.12 can be examined. As would be anticipated the highest K_s value corresponds to the healed and incipient joint type (K_s = 6.0 MPa/mm), and the lowest to joints containing thick wet infilling (K_s = .008 MPa/mm). The latter is approximately three times lower than the K_s value of joints with dry infill. Clean, smooth fractures such as those represented by type (2) behaviour have almost the same or slightly higher K_s values ($\sim$.01 - .06 MPa/mm) than the rough, undulating varieties (type 3, $K_s \sim$ .01 MPa/mm), because of the considerably smaller peak shear displacement. A more detailed review of K_s data from the literature will be made in part three.

Goodman (1970) noted that since K_s is a function of peak shear strength and displacement and the latter depend on the normal stress level, roughness, filling and other joint system variables, it follows that for a given type and condition of joint the shear stiffness is a function only of the normal stress.

John (1970) suggested that the variation of peak shear displacement and shear stiffness with changing normal stress can be simplified into two models of behaviour, that is a model of constant shear stiffness as illustrated in Figure 1.13(a) or a model of a constant peak displacement shown in Figure 1.13(b). Inspection of pre-peak shear stress-displacement records shows that neither of the two models is universally applicable to rock joints. Interchanging modes of behaviour can be seen in the collection of curves in Figure 1.14.

The plots in Fig. 1.14(a) by Jaeger (1971) correspond to a saw-cut ground trachyte sample (curve no. 1) and to a similar specimen after it had been subjected to 25 cm of cumulative displacement (curve no. 2). The former gave identical pre-peak curves thus matching the constant stiffness model. Conversely, the worn specimen revealed a marked dependency on σ_n resembling the constant displacement model. A similar observation can be made for the stress-displacement records by Chappell (1975) obtained from shear tests on graphite coated bedding planes in shale (Fig. 1.14(b)). For joint no. 1 the shear stiffness is a function of the normal load, while the stiffness of no. 2 seems to be independent of the normal load. The curves in Figs. 1.14(c) and 1.14(d) show varying degree of dependency of stiffness on σ_n. On the whole, experimental cases indicating an essential independence of K_s on σ_n seem to be the exception. The shear stiffness usually is normal stress dependent although the "constant peak displacement" model is not generally representative of the real behaviour, which seems to lie between the two extremes.

Since the shear deformation of joints in the pre-peak region is usually very small, the calculated values of shear stiffness are bound to be affected by the experimental technique, that is the method of "gripping" the specimen and the location of the displacement measuring devices. Rosso (1976) made an interesting comparison between shear stress-deformation curves and shear stiffness values as derived from triaxial and direct shear testing of joint samples by using different techniques for measuring the displacements. He found that the true shear stiffness can only be obtained if displacements are measured directly from the joint sample and as near to the shear plane as possible; errors in the displacement values can be quite high if the additional deformations of the loading system and the mounting material are not eliminated. Direct measurements of deformation of the joint specimen gave comparable shear stiffness values from both the triaxial and direct shear tests.

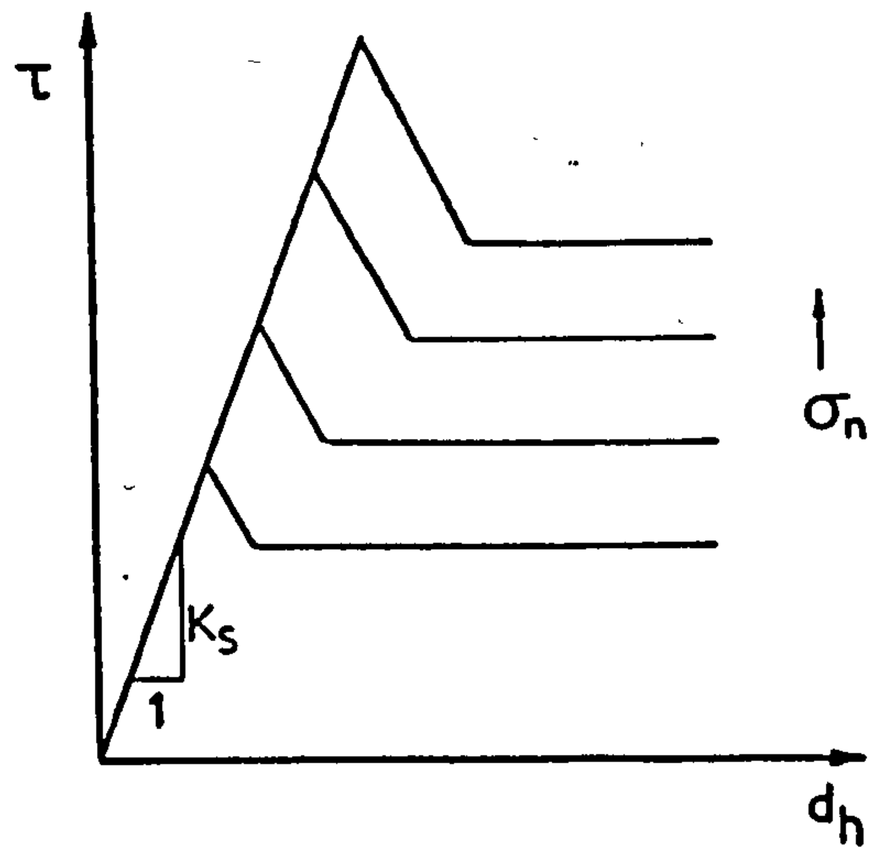

(a) constant stiffness model

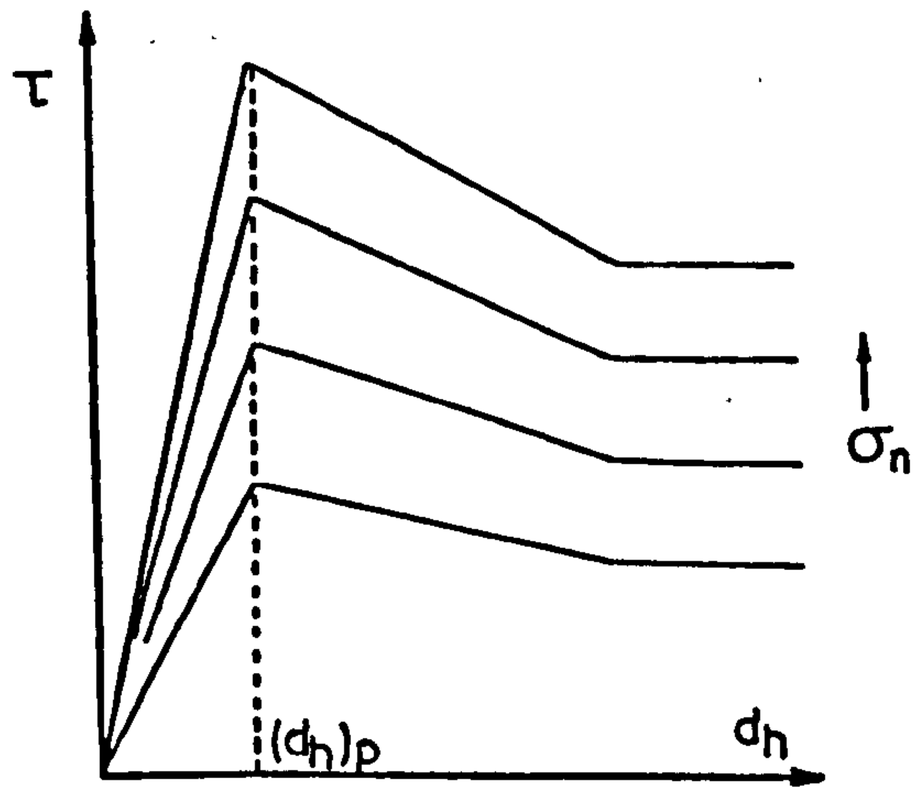

(b) constant peak displacement model

FIGURE 1.13 Simplified models of joint shear deformation under increasing normal stress

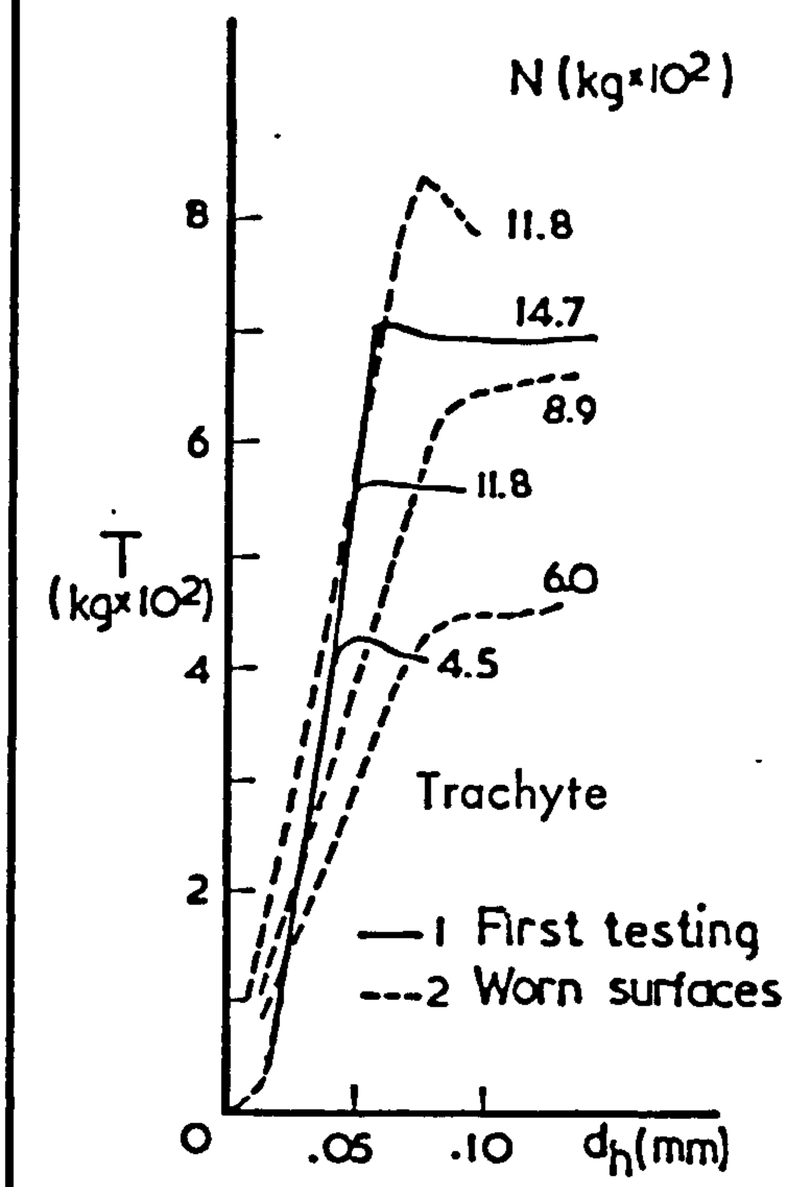

(a)
after Jaeger (1971)

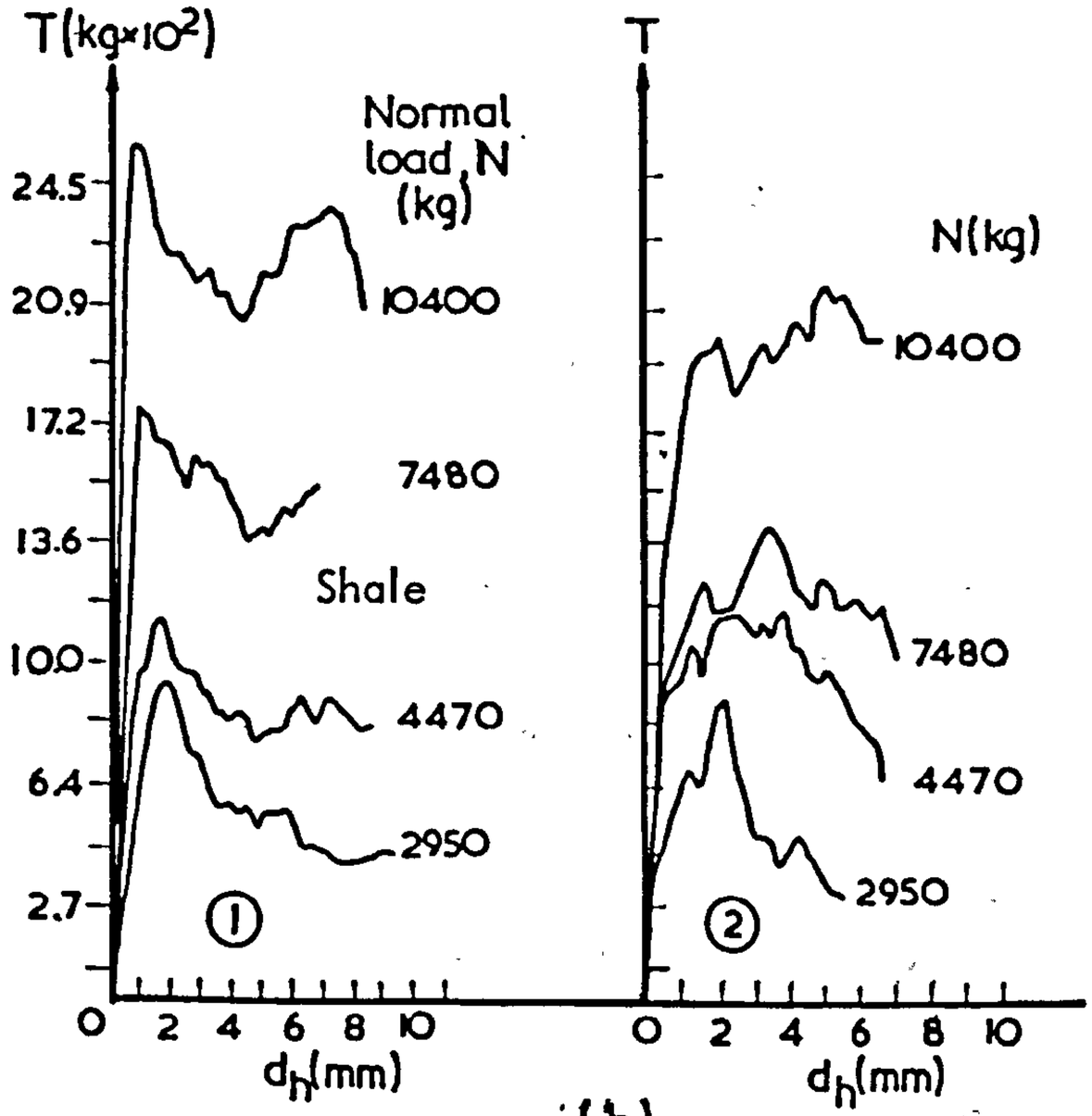

(b)
after Chappell (1975)

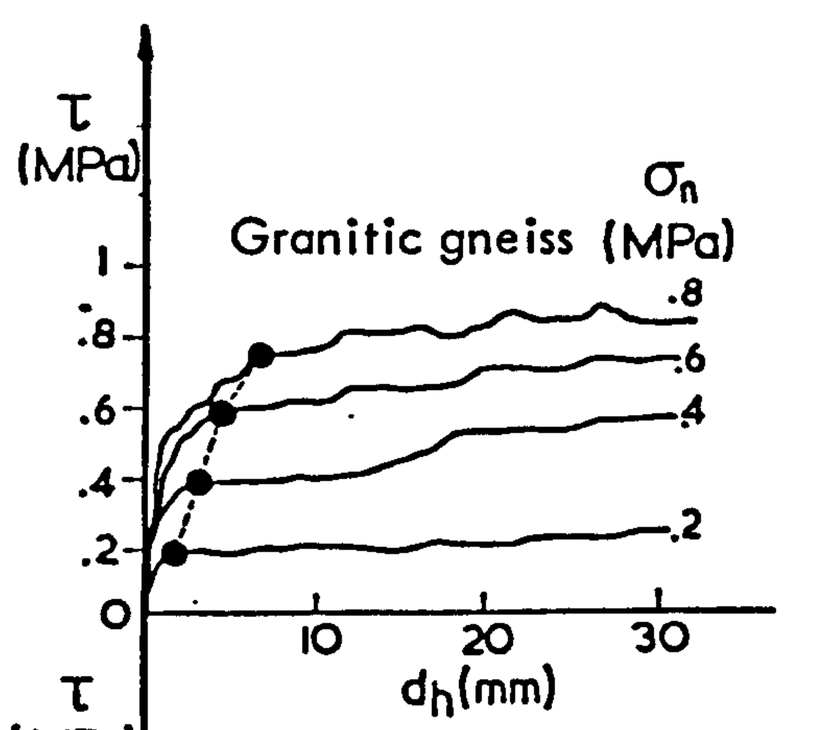

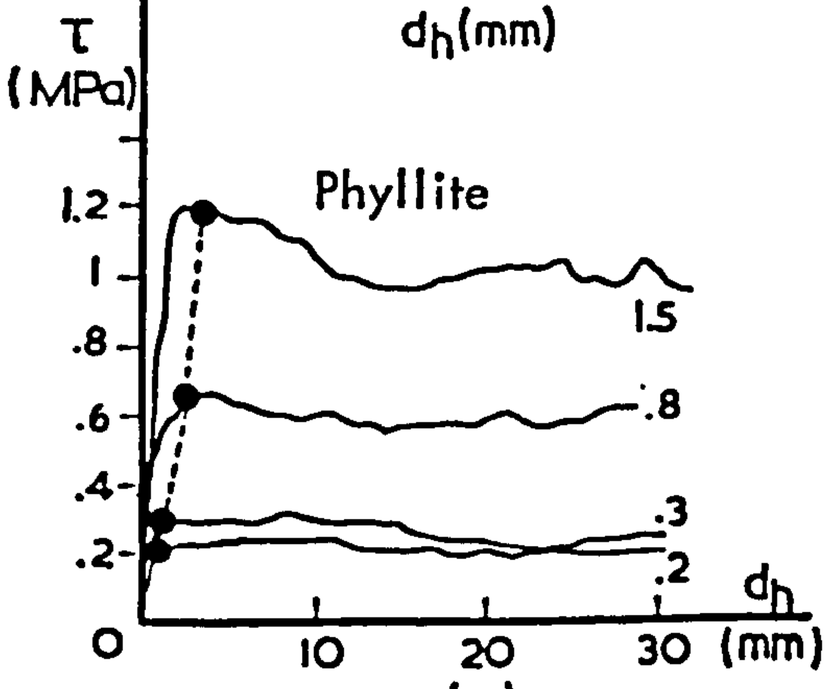

(c)
after Giuseppe (1970)

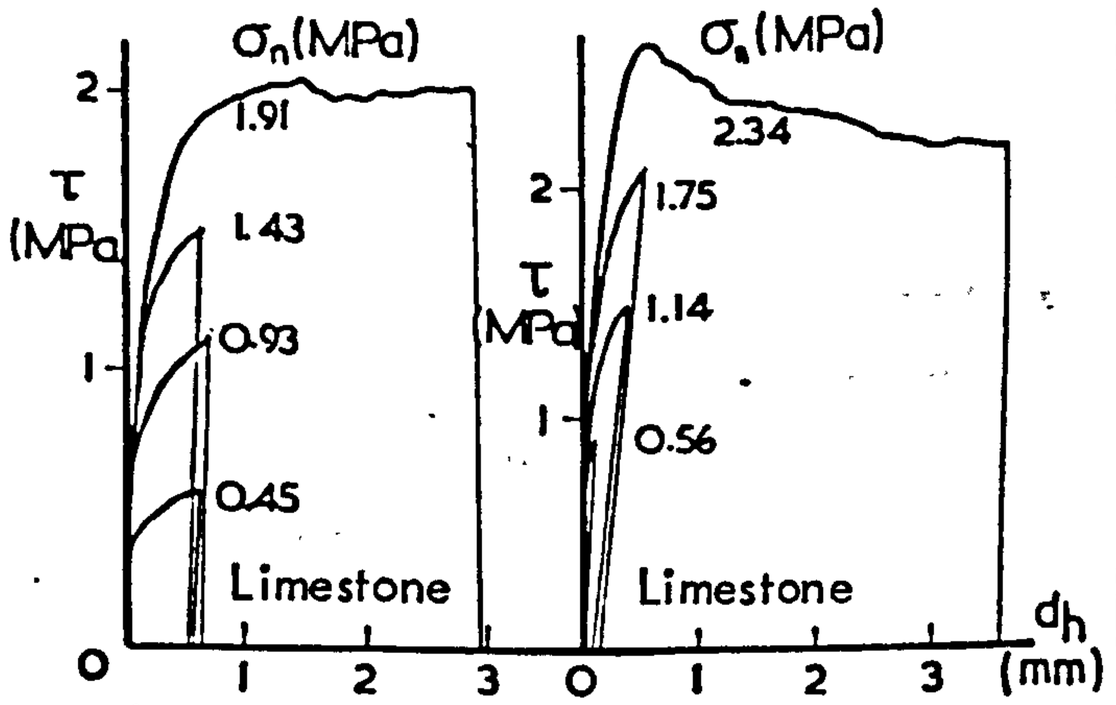

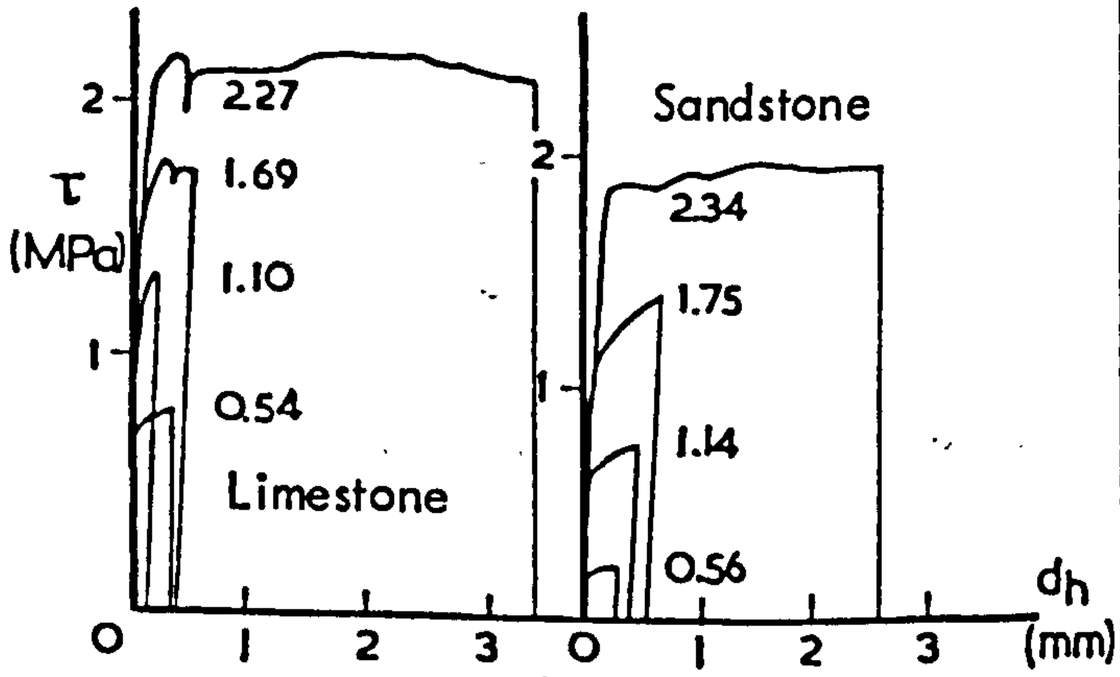

(d)
after Hungr and Coates (1978)

FIGURE 1.14 Shear stress (τ) - shear displacement (d_h) relationships of a variety of joint types illustrating the effect of normal stress on joint shear stiffness

Rosso also noted that ".. even after achieving repeatable results using two different techniques in the laboratory, it is often difficult to obtain data comparable to that derived from large scale tests in the field". By comparing his results with a set of K_s values from in-situ tests he found that overall the in-situ K_s data was 1.5 - 4.0 times lower than the K_s values obtained from the laboratory specimens tested in direct shear. Those differences were thought to be due to the different stress paths followed in the laboratory tests (σ_n held constant as τ increased) and in the field tests (σ_n increased along with τ until slip occurred), as well as due to the physical differences between the joint samples. However, experimental evidence from the literature suggests that a scale effect on K_s may be a key factor in such discrepancies. There appears to be an inverse proportionality between test dimension and shear stiffness, for a given normal stress (Barton, 1972). Shear joint stiffness in relation to scale will be considered in part three.

1.1.5 Normal deformation

Numerous in-situ plate loading tests have indicated that the deformation modulus of a jointed rock mass may be as much as an order of magnitude less than the Young's modulus measured from tests on intact laboratory specimens. This is because the normal deformability of joints is generally much higher than the deformation of the solid rock separating the joints. Goodman et al. (1968) introduced the term normal stiffness K_n to describe the stress-deformation character of joints under normal loading condition. Normal joint stiffness is defined as the normal stress per unit closure.

Goodman (1974) described the basic mechanics of normal deformation of joints by assuming a block resting lightly on a rough surface. In that situation, the proportion of the surface area in actual contact is extremely small and the entire contact force is sustained at a few (probably three) point contacts. Under increasing normal load a progressively larger contact area develops as the point contacts enlarge from elastic or plastic deformation, crushing, and indirect tensile cracking, whilst deformation is bringing new regions into contact. It is possible to pursue these mechanisms mathematically

and develop a theory of normal deformation under increasing normal load, as was done for metals by Bowden and Tabor (1964); however, as Goodman points out, the joint system is so poorly defined that an empirical approach is more useful.

In his description of the normal stress-joint closure relationship Goodman considered two physical constraints:

(i) there is a limit to the amount of joint closure possible; the maximum closure (V_m) must be less than the aperture thickness (a_j) defined as the maximum gap anywhere across two mated joint walls (Figure 1.15a).

(ii) the joint is assumed to exhibit negligible tensile strength, hence on complete removal of the normal load there will be no further resistance to motion, i.e. the normal stiffness will be equal to zero.

Combining these two conditions Goodman proposed that the normal stress-closure relationship can be fitted to a quarter space (Fig. 1.15b) and the following empirical hyperbolic relationship was advanced:

$$\sigma_n = \frac{\Delta V_j}{V_m - \Delta V_j} \sigma_{ni} + \sigma_{ni}, \qquad \Delta V_j < V_m \qquad 1.24$$

where ΔV_j is the amount of joint closure corresponding to an increase of normal stress from an initial level σ_{ni} to σ_n, and V_m is the maximum closure. The suggested hyperbolic variation between normal stress and joint closure implies that normal stiffness K_n is not a constant (as originally assumed by Goodman et al., 1968) but varies continuously from 0 to ∞. Hence for given σ_{ni} and V_m, the value of K_n can be found from the derivative of 1.24:

$$K_n = \frac{\sigma_n^2}{\sigma_{ni} V_m} \qquad 1.25$$

The non-linearity in the stress-closure relationship had been recognized in earlier studies by Shehata (1971, quoted in Sharp and Maini 1972) who described the relationship as semi-logarithmic, thus implying that complete joint closure in the sense assumed by Goodman's hyperbola never occurs.

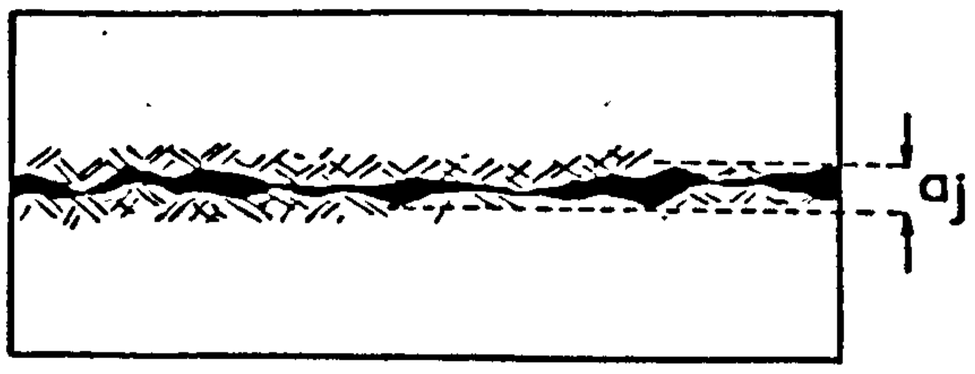

(a)

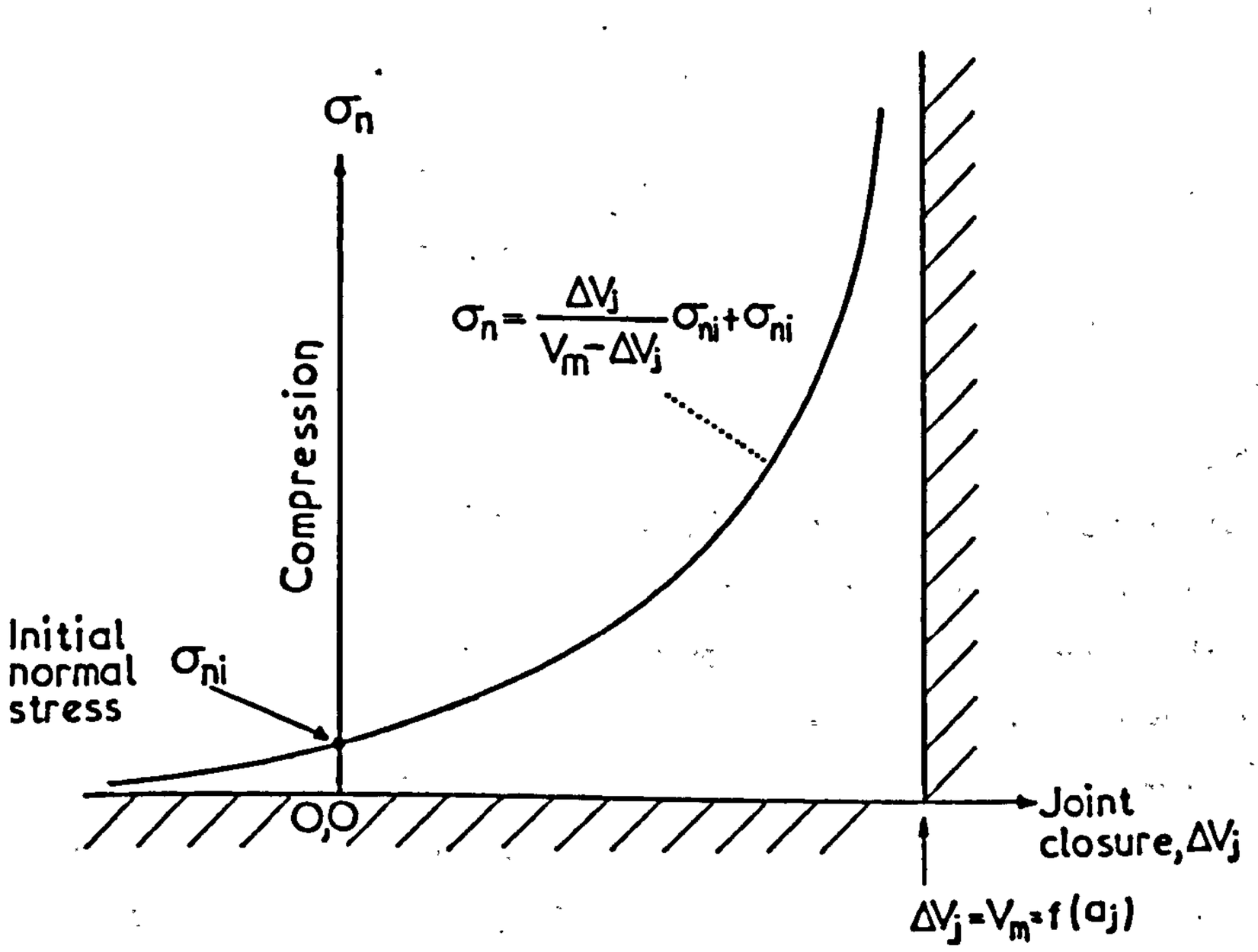

(b)

FIGURE 1.15 (a) Definition of joint aperture thickness
(b) Hyperbolic model of joint normal deformation
(after Goodman, 1974)

Witherspoon and Gale (1977) referred to two cases of large scale compression tests conducted by Pratt et al. (1974) on a large block (3 m x 3 m x 3 m) of naturally fractured granitic rock, and by Gale (1975) on a stiff saw-cut fracture in a large diameter (approximately 1 meter) granite core. The type of non-linear behaviour observed in those tests is shown in Figures 1.16 and 1.17. The stress-strain data from the field test show the relative contribution to the total deformation of the joint, microcracks and the intact rock, as well as the non-linear nature of the normal force-displacement curve. Similarly, Gale's data plotted in Fig. 1.17 show the elastic curve of the solid rock (A), the total deformation curve (B) representing both the elastic compression of the rock and the closure of the artificial saw-cut fracture, and the net closure curve (C) = (A) - (B). Gale found that non-linear behaviour persisted with repeated loadings.

Another experimental example by Goodman (1976) is shown in Figure 1.18. Curve (A) represents the deformation of an intact cylindrical specimen of granodiorite (91.4 mm length, 44.4 mm diameter) during its third loading cycle in uniaxial compression. Curve (B) shows the deformation of the same specimen with an interlocked extension fracture running parallel to its ends. Finally, curve (C) gives the deformation of the split cylinder after the two halves had been rotated to create a mismatched fracture with a mean aperture of 1.27 mm. The dotted line is an extrapolation of the experimental curve due to specimen failure at point F. The net joint closure curves shown in the lower half of Fig. 1.18 were derived by subtraction of (A) from (B) and (C). It is interesting to note the large difference in the maximum closure of the interlocked and mismatched fracture (0.119 mm and 0.386 mm respectively), which emphasises the fundamental significance of the initial seating condition in joint deformation. Goodman pointed out that unloading of the jointed specimens followed practically the same path as the unloading of the intact rock, signifying that the elastic portion of the normal deformation in a rock with a joint is entirely derived from the rock, hence joint closure is essentially irrecoverable.

Similar observations to the above have been reported by Iwai (1976) who found that uniaxial compression of three artificially fractured cylindrical specimens of granite, marble and basalt gave highly non-linear stress-deformation curves throughout repeated loadings up to

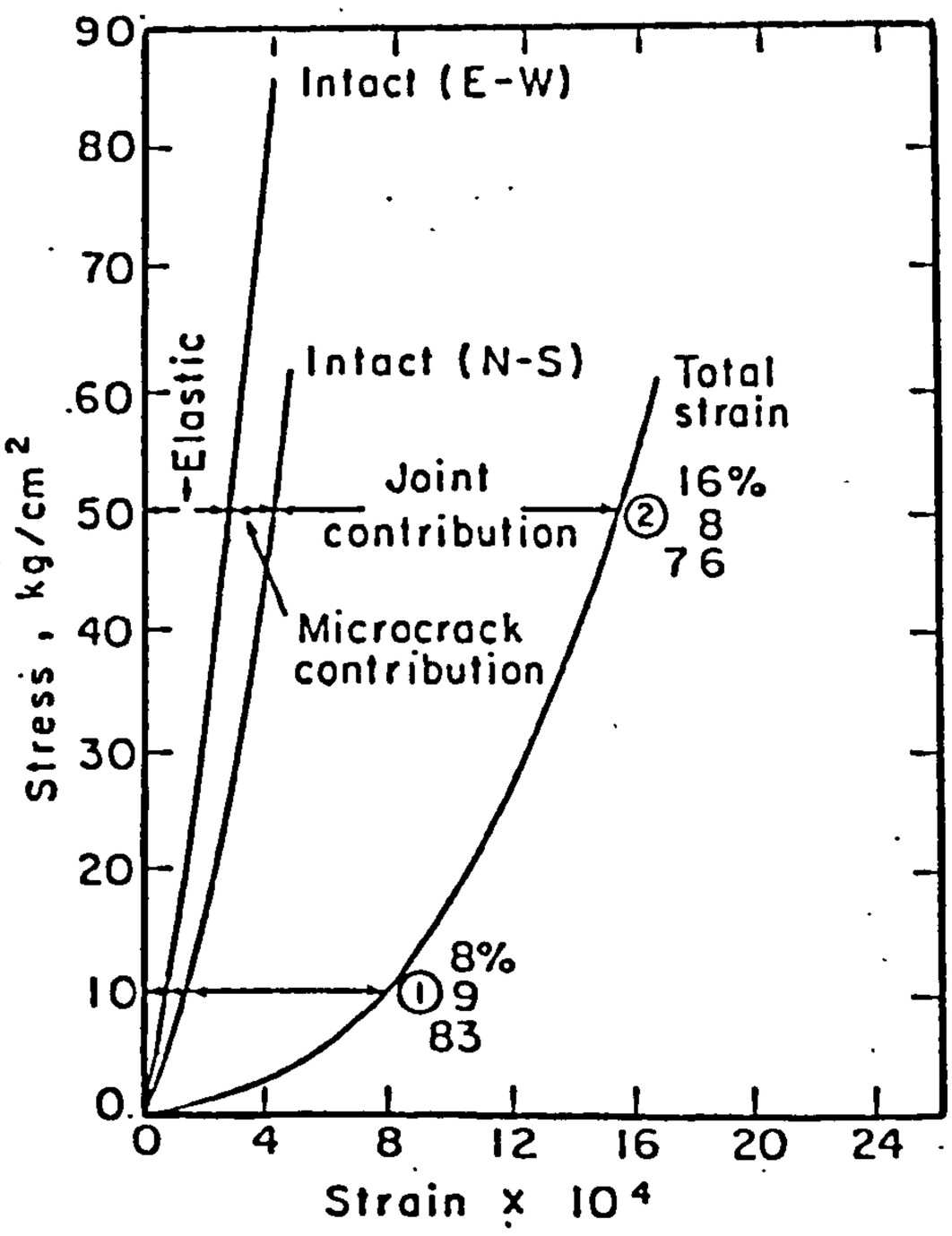

FIGURE 1.16 Stress-strain relationships from in situ compression tests on a naturally fractured granite block 3m x 3m x 3m .
(after Pratt et.al. 1974 , quoted in Witherspoon & Gale, 1977)

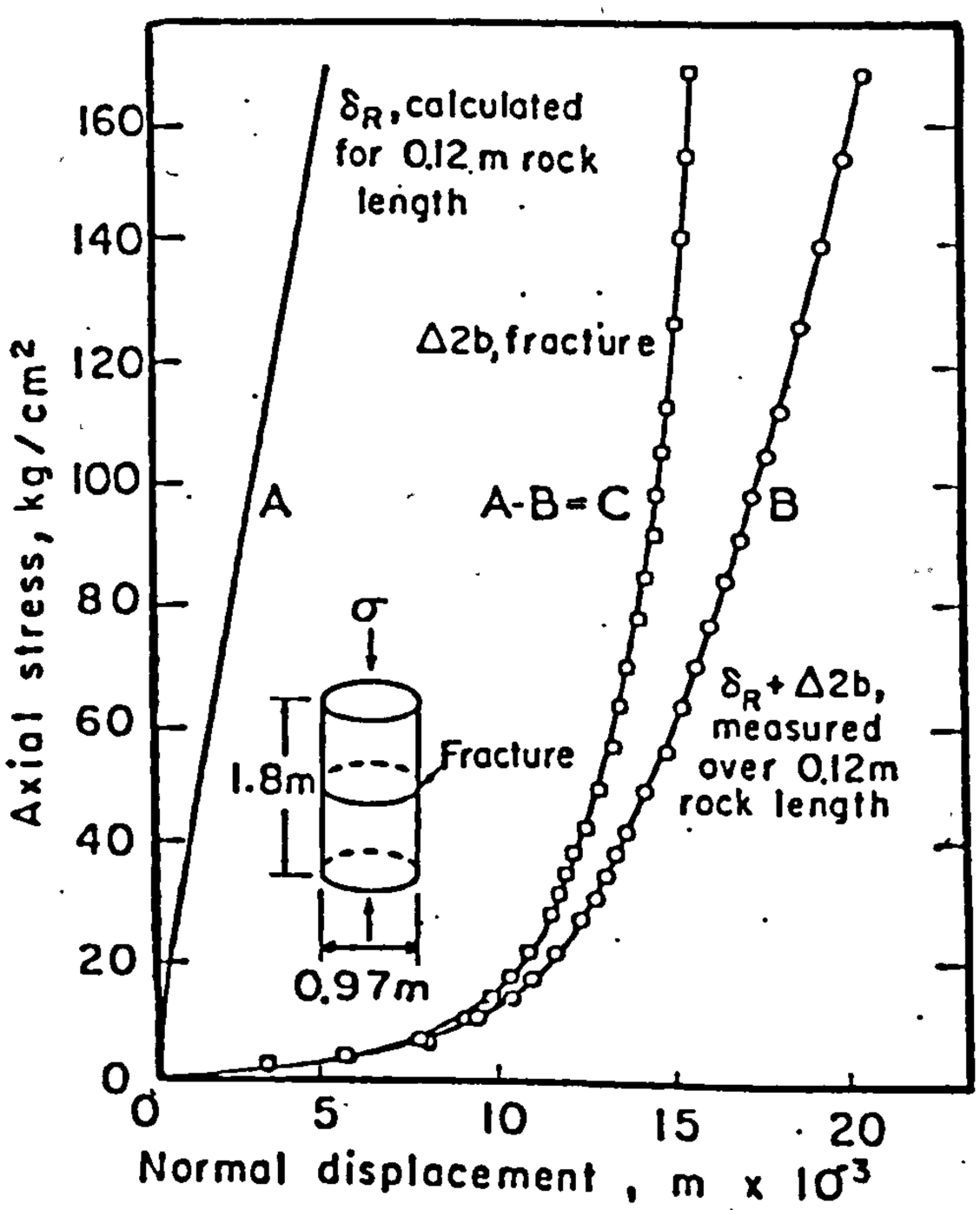

FIGURE 1.17 Axial stress - displacement relationships of a granite cylinder containing a saw cut fracture
(after Gale 1975, quoted in Witherspoon & Gale 1977)

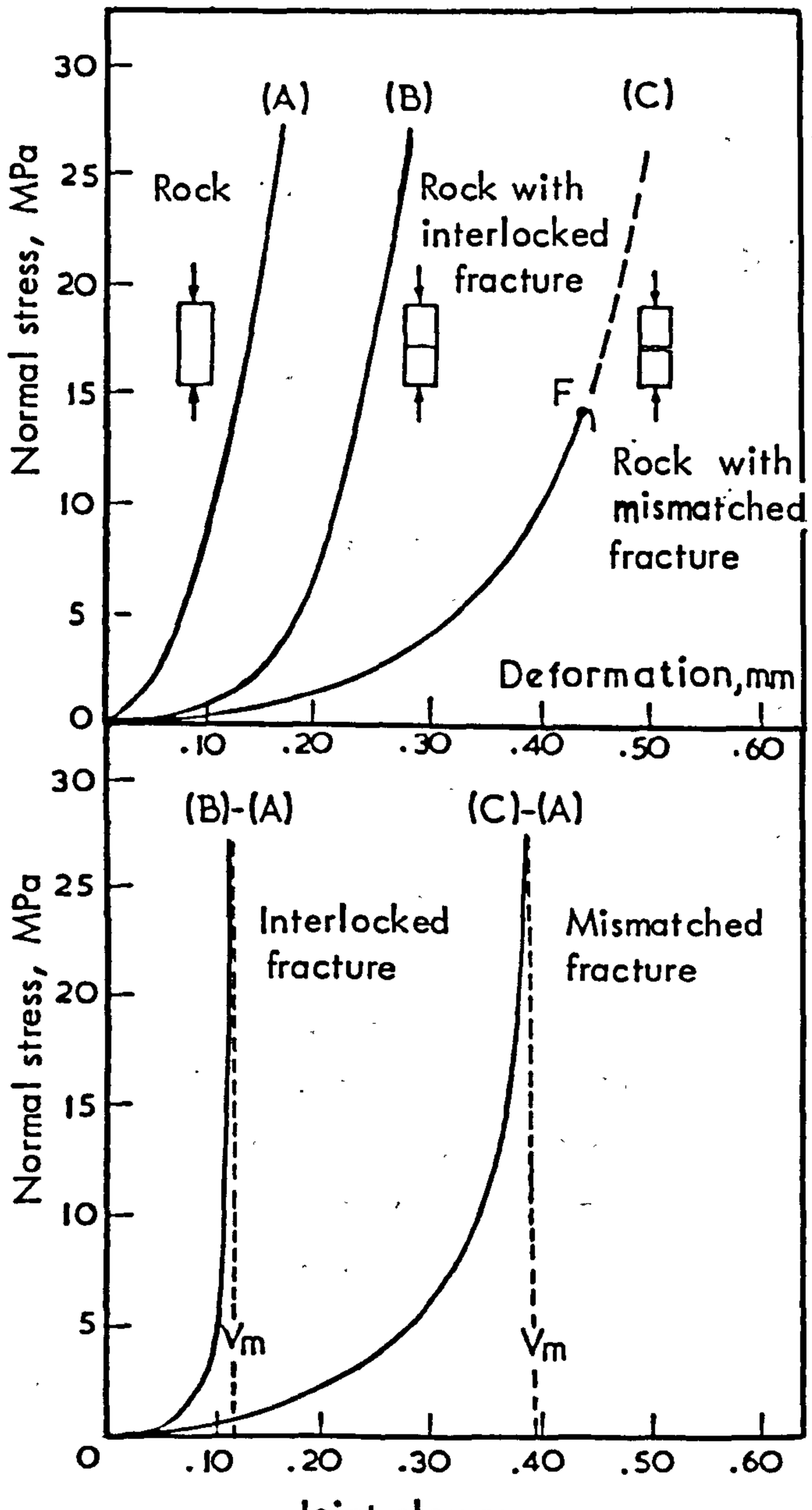

FIGURE 1.18 Normal stress – deformation relationships of intact and fractured cylindrical specimen of granodiorite (after Goodman, 1976)

20 MPa. An example of the stress-deformation relationships obtained in that study is shown in Figure 1.19. The three dotted curves represent the total deformation (rock + fracture) at three measuring points around the circumference; the difference in measurements was attributed to eccentric application of the axial stress. The net fracture closure curve (C) was derived by subtraction of the intact rock compression curve (B) from the average total deformation curve (A). It should be noted that the axial stress (σ_e) represents the applied effective normal stress, as these tests were conducted under simultaneous water injection in the fracture. Iwai found that the loading paths during each load cycling were best approximated by a hyperbolic fit. Upon unloading significant hysteresis and permanent sets were observed in all cycles.

Hungr and Coates (1978) conducted a series of compression tests on natural joints in limestone and sandstone. The normal stress-deformation curves obtained from those experiments did not exhibit non-linear behaviour, and in fact as illustrated in Figure 1.20(a), if minor irregularities were neglected all the curves were close to linear. The authors explained those relationships on the basis of a "joint precompression" effect. Specifically, they suggested that those joints had probably been compressed in the past by pressures much greater than those applied in the tests (maximum applied σ_n was in the order of 2.5 to 3.0 MPa). A large part of the original deformations was irrecoverable and hence unloading and recompression of the same joints followed a relatively steep path, as shown in the diagrammatic illustration in Figure 1.20(b). The recompression curves could be expected to possess a relatively low degree of curvature, since the contact of a pre-compressed joint would not change as rapidly as in the case of a normally loaded joint with a large proportion of asperity area intact.

The same views had been expressed earlier by Snow (1972) who noted that precompressed joints exhibit linear deformability. The author referred to unpublished data by Shehata, which apparently indicated linear variation in joint closure under repeated loading below some previously attained maximum load (value not quoted). In conclusion, Snow suggested that non-linear behaviour may be appropriate for "virgin" fractures that have never closed before. No other evidence on the normal stress-closure relationship of natural joints was found in the literature.

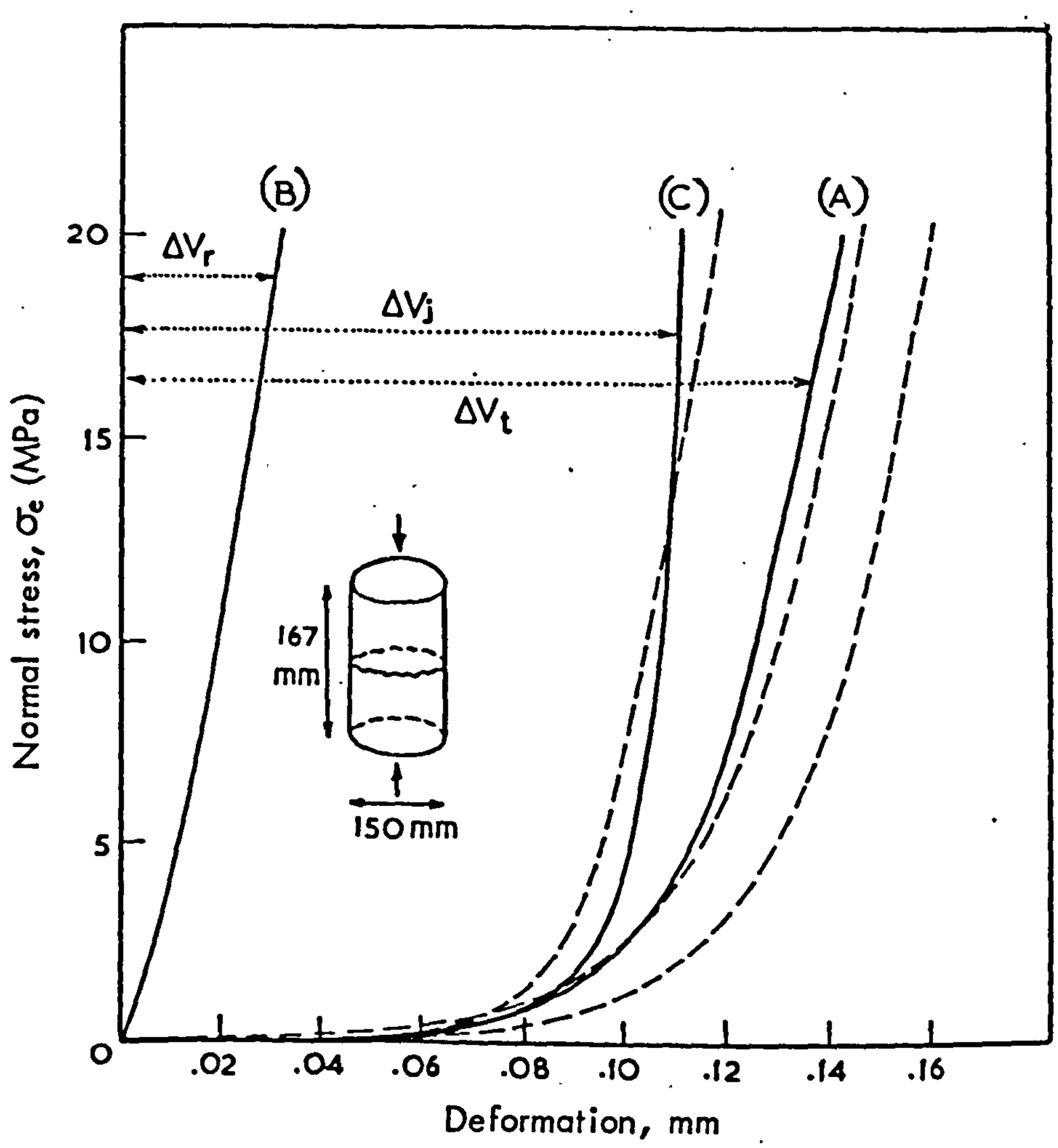

FIGURE 1.19 Normal stress - deformation relationships of an artificially fractured granite cylinder under the first loading
(after Iwai, 1976)

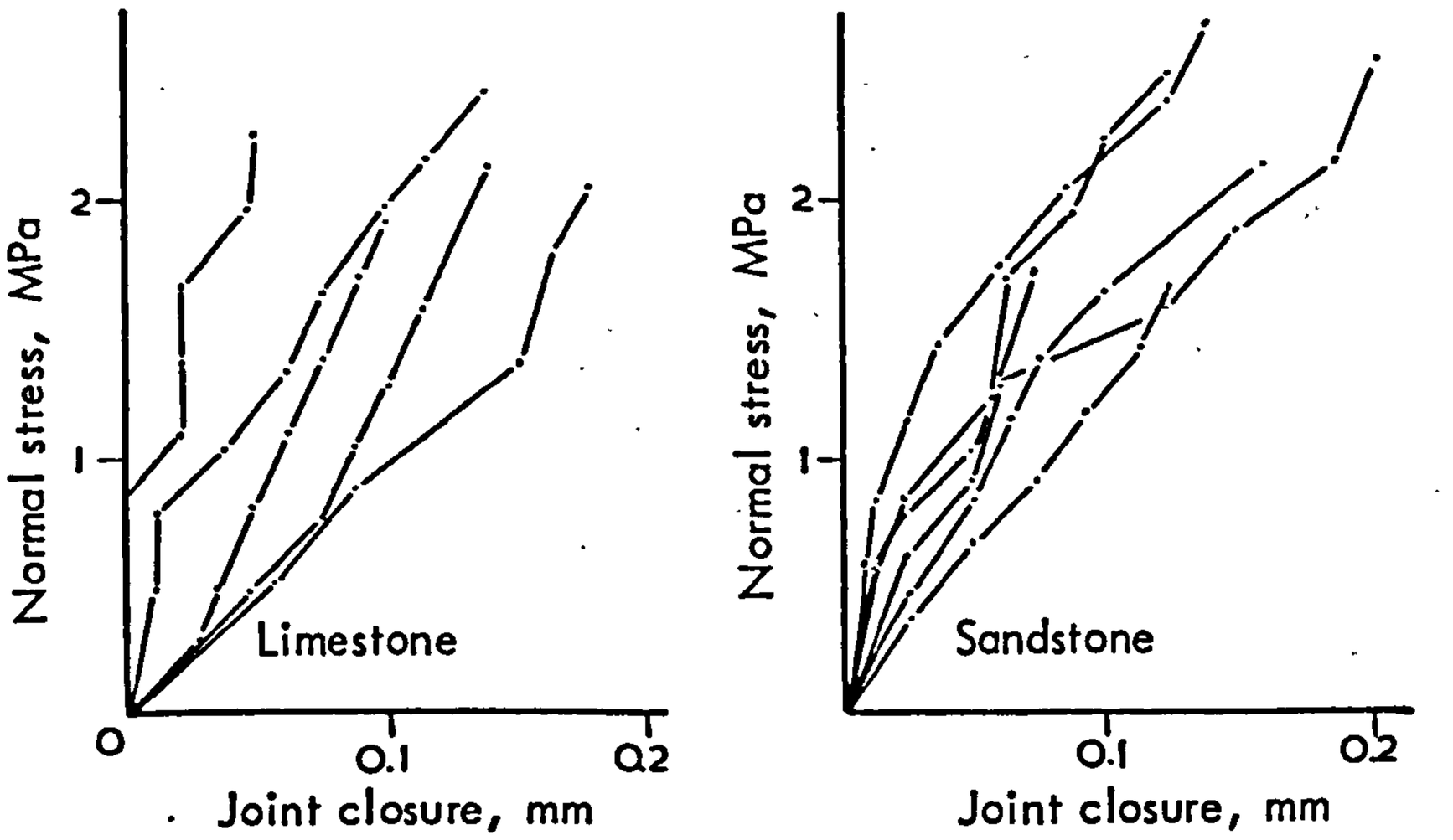

(a) Normal stress – closure curves from compression tests on natural joints in limestone and sandstone

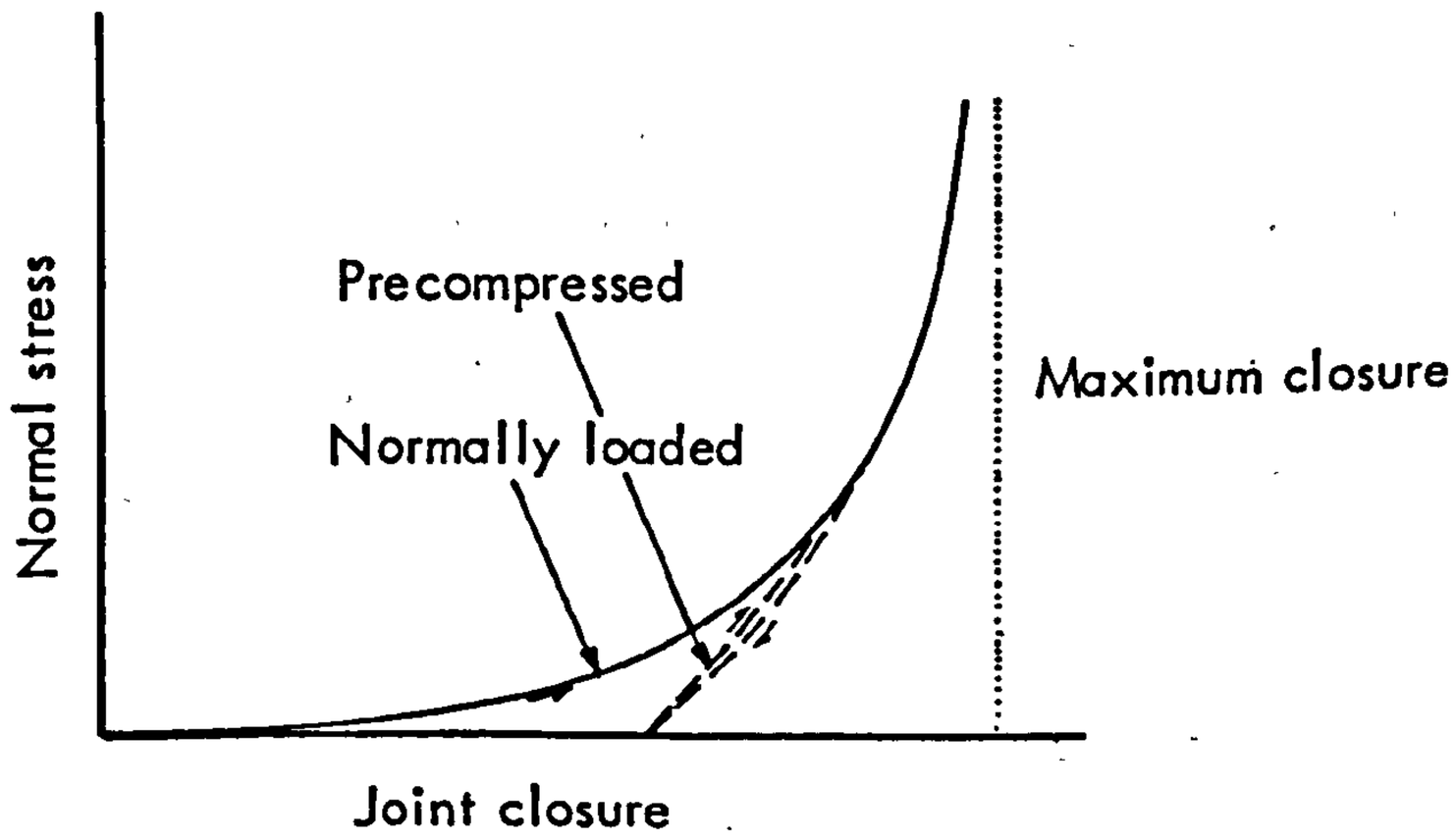

(b) Effect of precompression on the normal stress – displacement behaviour of unfilled joints

FIGURE 1.20 (after Hungr and Coates, 1978)

1.1.6 Concluding remarks

It is general knowledge that the engineering behaviour of the majority of rock masses at or near the earth's surface is largely determined by the geometrical structure of the network of intersecting discontinuities and their strength and deformation properties. The inherent limitation in attempting to quantify the influence of joints is that they are 'sampleable' only as individuals, or in small numbers when tested in-situ. Implicit analysis of a jointed rock mass, for example allowing for the "softening" effect of joints by using an 'effective' modulus of deformation, has the disadvantage that the mass is treated as a continuum. Joints introduce non-linear, low symmetry properties into the rock mass behaviour. In the 'discontinuum' approach joints are considered as discrete elements of the mass and their properties can be input into an explicit physical model study or numerical analysis. The review presented in this part gives a summary of the fundamental shear strength and deformation characteristics of joints as individual rock mass components.

It has long been recognized that the peak frictional resistance of joints depends on the physical characteristics of the surfaces, i.e. roughness and asperity strength,and the operating level of normal stress. The basic friction angle of planar surfaces depends on the mineralogical composition of the rock material and the moisture condition and in general is equal to the residual friction of non-planar, unweathered joints. Various empirical functions have been presented to describe the peak shear strength envelopes of non-planar joints. These range from simple mathematical expressions fitted to specific sets of experimental data to functions of more general application based on identifiable joint properties. Barton's criterion for peak shear strength is based on measurable indices of joint wall strength and roughness; other criteria largely rely on empirical constants which can only be defined by fitting the proposed equations to experimental data.

The term 'stiffness' of a rock joint is used to describe the overall stress-deformation characteristics in both the normal and tangential senses. The tangential or shear joint stiffness K_s describes the rate of change of the shear stress with respect to shear displacement. The shear stiffness of a given joint type depends on the level of normal

stress. K_s values may be affected by the experimental technique and the scale of the test specimen. The normal stiffness K_n describes the rate of change of normal stress with respect to normal displacement. Present experimental evidence, mostly from compression tests on artificial fractures, indicates non-linear variation. A small number of tests on natural joints have shown an almost linear variation between compression load and closure. Non-linear models imply that the normal stiffness K_n will increase to a very large number as the joint will be approaching a fully closed condition. Intuitively, the maximum joint closure will be some function of the initial aperture thickness, and the joint wall strength and roughness.

PART TWO

EXPERIMENTAL STUDY OF SCALE EFFECTS ON THE SHEAR STRENGTH OF JOINTS

CHAPTER 2.1

INTRODUCTION

2.1.1 General

One of the most argueable aspects in applied rock mechanics concerns the extent to which the strength characteristics of intact or jointed samples of conventional size can be confidently relied upon to predict the response of the entire rock mass to changes of the existing stress conditions.

It is of vital practical importance that the existence or otherwise of size-effects be established. A structure designed assuming a size-strength effect will be overly conservative should no such effect exist, while a design assuming no scale effect would be unsafe should the rock mass properties be, in fact, size dependent.

The size-strength relationships in intact rock material have received considerable attention in the past and an appreciable volume of experimental data exists. By contrast, a very limited amount of information is available on the sensitivity of the shear properties of discontinuities to scale effects.

The strength properties of the intact rock constitute an essential parameter (viz. joint compressive strength, JCS) in the evaluation of the frictional resistance along joints. It has been suggested that a scale effect in the shear strength of discontinuities may be induced by the size-dependency of the strength properties of the intact material.

In the following sections a brief review of the literature on the strength-size effects in intact rock is followed by a detailed reference to the available information regarding similar effects along discontinuities.

2.1.2 Effects of scale upon the strength of intact rock

The influence of size upon the strength properties and in particular the uniaxial compressive strength of rock materials has attracted the interest of a number of investigators.

Laboratory and in-situ compression tests on specimens (mostly of coal) with sample volumes differing by several orders of magnitude have revealed significant scale effects.

The effect of size upon the tensile strength (σ_t) has been studied in connection with the standardization of indirect methods for evaluation of σ_t (Brazilian disc test, point load test). Although restricted mostly to comparisons of specimen sizes in the laboratory range, tensile strength appears to be scale dependent. Furthermore, the intrinsic cohesion of intact rock ruptured in shear has been reported to decrease with increasing size of the test specimen.

1. Uniaxial Compressive Strength

It is well known in the field of materials testing that the strength values of specimens of a given material decrease as specimen size increases. The majority of the investigations on the size-strength relationships in rock have revealed similar trends, with laboratory to in-situ strength ratios generally ranging between 2 and 10 (Bieniawski and Van Heerden, 1975).

The changes in the compressive strength of rock materials with increasing specimen size have been attributed to the action or interaction of the following factors:

- a purely statistical "volume effect" arising from the existence of internal structural flaws
- a "surface effect" due to external imperfections induced either during specimen preparation or by the natural reaction of the rock minerals to the free surface
- "mechanical" effects related to the amount of strain energy stored during compression.

The "volume effect" is based on the assumption that any material contains a number of flaws which affect the strength by their geometry, orientation and location. As the volume increases so does the probability of flaws in the specimen and therefore the probability of failure (Weibull's statistical volume effect).

Weibull's theory has been applied in size effects investigations in the form of:

$$\frac{\sigma_{c1}}{\sigma_{c2}} = \left(\frac{V_2}{V_1}\right)^{1/m} \qquad 2.1$$

where σ_{c1} and σ_{c2} are the strength of samples with volumes V_1 and V_2 respectively and m is a constant of the material.

Ludborg (1967) used the above expression to quantify the decrease in compressive strength of cylindrical specimens of granite with increasing volume and quoted a value of 6 for the constant m.

Lama and Gonano (1976) collected various strength-volume relationships that have been found in different rock types, which are presented in Figure 2.1. For all types of materials the strength showed a decrease with increasing specimen volume at least in the initial stage. The apparently linear normal-log plot of some of the strength-volume relationships was assigned the following empirical expression:

$$\sigma_c = a + b \log V \qquad 2.2$$

where σ_c is the compressive strength and V the specimen volume.

The last authors quoted the following values of b for the various types of rocks: sapropolite = -.3443; durain = -.0699; "bedded coal" = -.0877; Barnsley Hard = -.1316; Deep Dufryn = -.0524.

As clearly shown in Figure 2.1 for some of the rocks the strength in the earlier stages seems to be independent of the volume while the drop in strength starts at a point when the volume increases beyond a certain limit. In saprolite, there is a drop in strength until the specimen volume increases to 100. cm^3, then the strength remains constant until the volume increases further to about 10000 cm^3. For volume increases beyond 10^5 cm^3 the strength values appear to approach an asymptotic value.

The cases presented in Figure 2.1 are a good example of the variability of the strength-size relationships which inhibit the establishment of a universal law. They are also indicative of the fact that the changes in strength with size probably cannot be explained by indiscriminate adaptation of Weibull's theory.

The theoretical statistical relationships between size and strength are based on the assumption that only the distribution of flaws influences the strength. Implicitly, the assumption is also made that the process

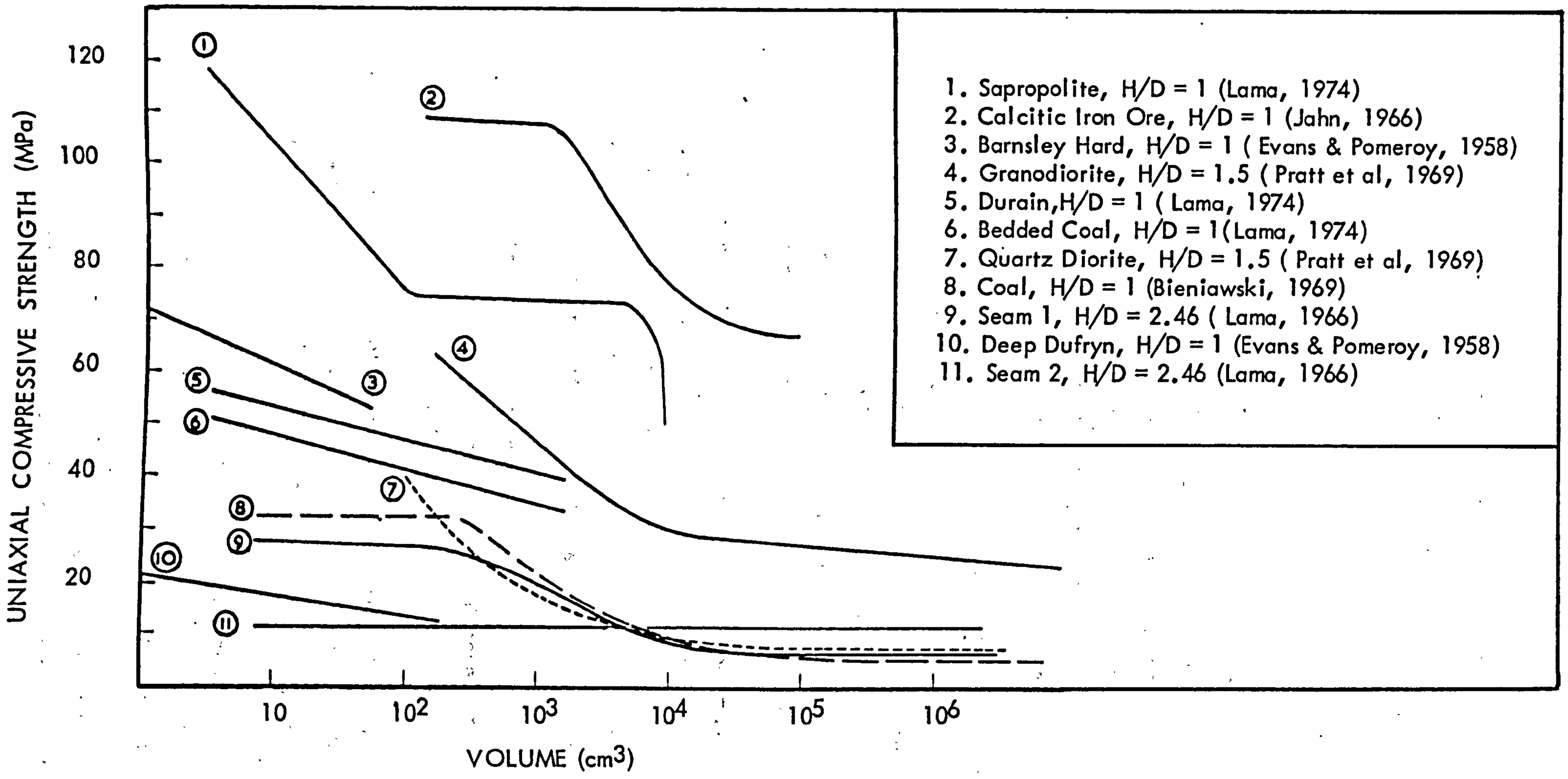

FIGURE 2.1 Effects of specimen volume on the uniaxial compressive strength of different rock types.
(from Lama & Gonano, 1976)

of specimen deformation and fracture initiation is not influenced by size (Einstein et al., 1970). Experimental studies by the last authors have shown the opposite effect.

The amount of strain energy that is stored in a specimen under compression increases with its volume and tends to accelerate crack propagation (Bernaix, 1974). A study of the "energy effects" has been reported by Einstein et al. (1970) who tested a range of sizes of cylindrical (D = 2.52 - 5.04 cm, $^{L}/D = 2$) and prismatic (width = 1.26 - 5.04 cm, length/width = 2, height/width = 4) specimens made of a brittle model material. In the course of each test the stress levels corresponding to initiation of stable and unstable crack development were monitored and related to the respective specimen volume.

On the basis of those results Einstein et al. were able to conclude that stable crack development was affected only by the statistical volume effect, the stress range over which propagation of stable cracks occurred being apparently independent of size. The unstable crack growth and propagation was significantly accelerated by stored strain energy, the latter being correlative with specimen volume.

As a further demonstration of the effects of strain energy, Einstein et al. tested a number of model cylinders in series with a "spring", which was a hollow plexiglass cylinder able to store a considerable amount of additional strain energy. Characteristically, those specimens failed at lower stress levels than similar ones tested without the "spring".

The influence of surface flaws has been suggested as a possible explanation for the lower strength values obtained occasionally from small specimens as compared to larger ones.

Hoskins and Horino, 1969 (quoted in Vutukuri, Lama & Saluja, 1974) tested cylindrical specimens (L/D = 2, D = 2.5 - 15 cm) of limestone, marble, sandstone and granite. The last authors found that for all rock types (except granite) the 2.5 cm diameter specimens had lower compressive strength than the 5 cm specimens of the same rock type. Maximum strength was obtained either from the 5 cm or the 7.5 cm diameter specimens, while further increase in diameter resulted in decrease of specimen strength.

Stephenson and Triantafilidis (1974) found that the strength of limestone and granite specimens showed a small increase in strength with larger specimen sizes.

In both of the above cases "surface effects" were held responsible for the lower strength of the smaller specimens. Since the specific surface is inversely proportional to the volume, the smaller the specimen the larger its specific surface area and the weaker the specimen when the surface flaws are the dominant characteristic of the test specimen.

Although the majority of the reported experimental studies indicate the existence of size effects, other investigators argue that the phenomenon is not necessarily an inherent material property.

Brown (1971) pointed out that general comparisons of test results between different specimen sizes are not valid because of the variable stress-gradients resulting from specimen size and geometry and testing conditions. He further suggested that the size effect can only be studied as an intrinsic material property if the tests are designed to apply as nearly uniform a loading to the specimen as possible. As an experimental confirmation of the above views, Brown called upon the results obtained by Hodgson and Cook (1970). The last authors tested cylindrical specimens of quartzite and quartzitic shale (L/D = 3, D = .56 - 45.7 cm) under uniform stress condition. No "gross" scale effect was found in that size range.

On the other hand, an approximately ten-fold reduction in strength of a weathered quartz-diorite reported by Pratt et al. (1972) was obtained from tests on specimens with comparable stress gradients and uniform loading in the central portion of the specimens. The experimental studies of the last authors revealed an apparent "shelf" in the strength-specimen size curve, beyond which there was no further decrease in strength with increasing size. The asymptotic value of the strength was attained at specimen size (length of equilateral triangular prism) of 0.9 meters.

Similar findings have been reported by Bieniawski and Van Heerden (1975) from tests by the first author on cubical specimens of coal. In that case, the "critical" specimen size (side of cube) was approximately 1.5 meters. Strength reductions by up to a factor of 7 had been recorded for specimen sizes below 1.5 m.

However, such comprehensive testing programmes as the above two are the exception rather than the rule, and additional testing is required over

similar ranges of specimen sizes of other rock types, before the relationship between strength and specimen size can be finalized. As Bernaix (1974) pointed out, "... any laws defining scale effect derived from experimental test programmes or theoretical calculations must be approached with considerable caution".

2. Tensile strength

Various investigators have reported reduction of the tensile strength of materials with increasing specimen size. As already pointed out, most of the relevant studies were conducted in connection with the standardization of various indirect methods of assessment of tensile strength.

Figure 2.2a and b shows the effect of specimen size in the Brazilian (a) and point load (b) methods. An apparent decline in the scale effect beyond a certain specimen size is evident in most of the relationships illustrated.

3. Shear strength

Experimental studies on the effects of scale upon the shear strength characteristics of intact rocks have shown that the important property of cohesion (c) may also be size dependent.

Il'Nitskaya, 1969 (quoted in Vutukuri, Lama & Saluja, 1974) investigated the influence of specimen size on the shear strength of gabbro and marble. A number of cylindrical samples with diameters ranging from 1.0 to 7.0 cm were tested with the method of single shear with compression between bevelled dies. All specimens were tested for shear at two different angles of the shearing plane to the horizontal, viz. 50° and 70°. The results - illustrated in Figure 2.3a - showed that for both rock types the cohesion decreased with increasing size to an asymptotic value, which was characteristic for each rock type. For an increase of the specimen cross-section by a factor exceeding 110 the obtained reduction in cohesion was 29% for the marble and 26% for the gabbro.

Barroso (1966) presented some results of in-situ direct shear tests on intact rock blocks of different sizes. The scale effects are shown in Figure 2.3(b) where cohesion has been plotted against test surface area.

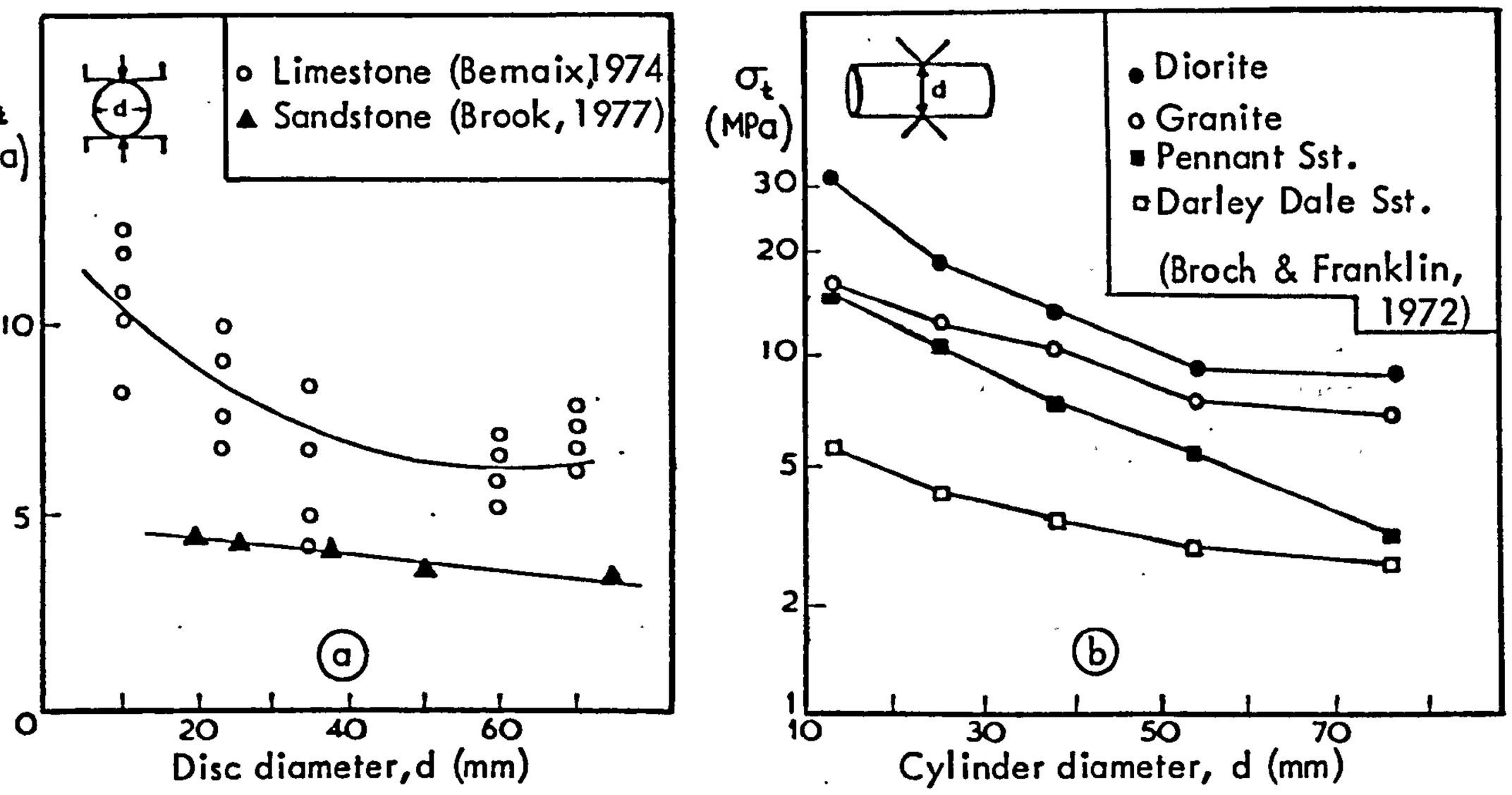

FIGURE 2.2. The effect of specimen size on the indirect tensile strength (σ_t) of rock materials as determined by the Brazilian (a) and Point Load (b) tests.

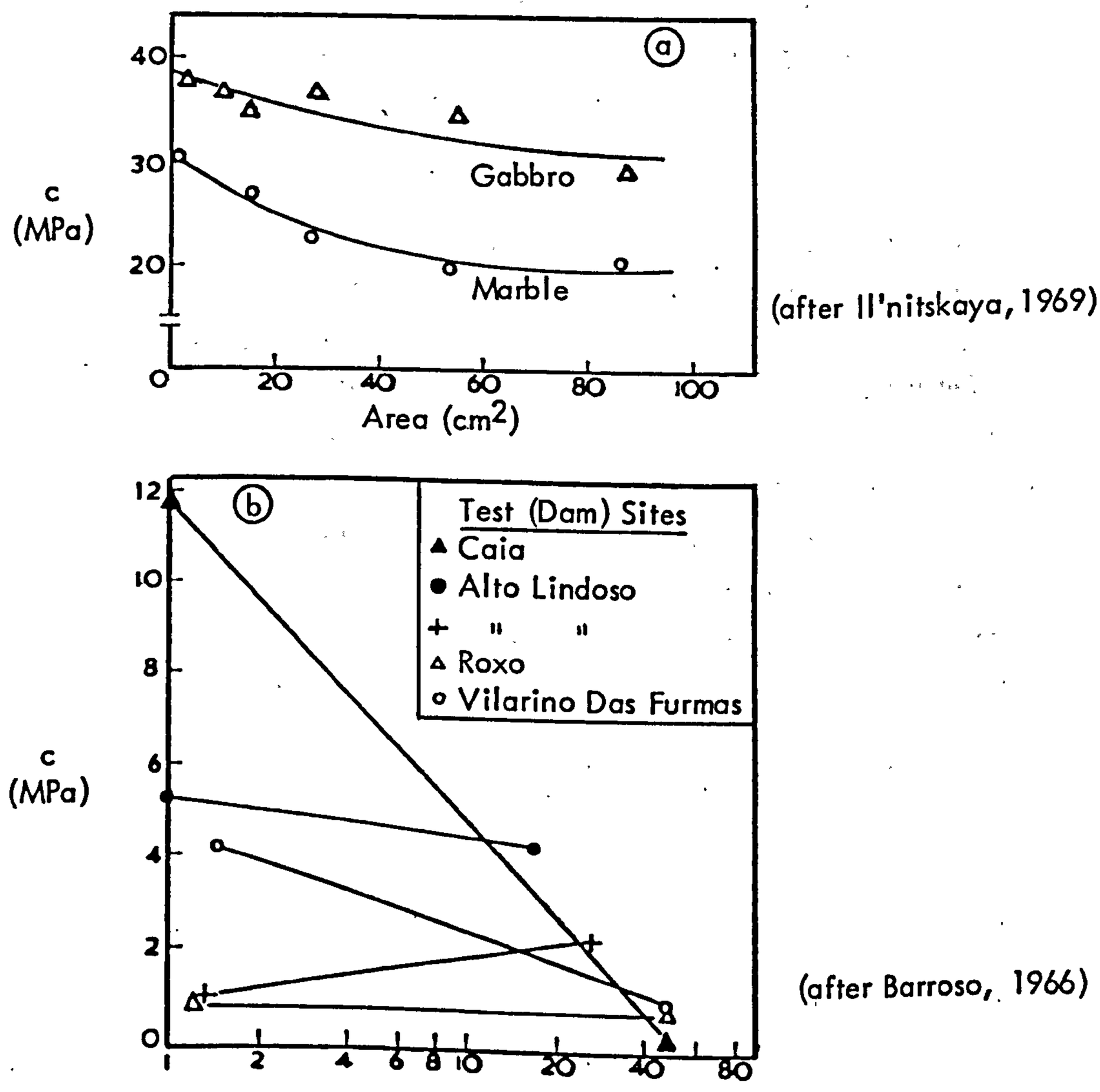

FIGURE 2.3 Effect of specimen size on the inherent cohesion (c) of intact rocks from laboratory (a) and in-situ (b) shear tests.

In the light of the experimental evidence presently available one could accept, at least in a qualitative sense, that some form of an inverse relationship between size and strength properties of intact rock may exist. However, because of the uncertainties involved with regard to the exact mechanism that causes this strength reduction with increasing size, reliable extrapolation of laboratory values to field dimensions still remains a matter for speculation. Knowledge of the maximum amount of strength loss of the intact rock with increasing size can prove very important in the quantitative evaluation of the scale effects upon the shear strength of joints.

2.1.3 General considerations regarding the effect of scale upon the shear strength of joints

The methods of determination of the shear properties relevant to stability analyses may vary from a full scale "test" involving back-analysis of a known failure to small scale laboratory tests on specimen sizes representing an extremely small portion of the field joint exposures Whenever economically and technically possible, in-situ shear tests are conducted on larger samples.

One could justifiably argue that estimation of the mobilized "cohesion" (c) and friction (ϕ) from the back-analysis of a well documented case history would provide parameters most relevant to the real field conditions. However, indiscriminate use of numerical values derived in this way for general design purposes has been cautioned by Hoek and Bray (1977). Back analysis of a failed slope will yield values of c and ϕ valid only for the normal stress level in that particular slope at the moment of failure. One could assume that such values could be taken into consideration in the design of other slopes where the same normal loads and similarly orientated critical set(s) of discontinuities exist.

In the majority of cases joint shear strength estimates are obtained from laboratory and/or small scale in-situ tests. The relevance of such numerical values to full scale field exposures has been questioned in the past.

Deere et al. (1967) outlined the significance of full appreciation of the likely effects of scale upon the shear strength of different types of joint surfaces. They considered some hypothetical examples of shear

tests on joint specimens of different sizes sampled from large exposures, as shown in Figure 2.4 (the smooth planar joint example was added by the present author). If A, B and C denote the sizes of a laboratory specimen (say 15 cm), an in-situ block (1 meter) and the full scale discontinuity (3 to 30 meters or even more) respectively, then the surface morphology would probably dictate the difference in strength (s).

Salas (1968) stressed the need for large scale joint testing because of the variable and complex morphology of the in-situ exposures. He noted that a test carried out on a small surface cannot show the influence of surface roughness.

Jaeger (1970) pointed out that "... a question of great importance is that of how values of friction measured on small specimens in triaxial apparatus or on larger specimens in direct shear can be extrapolated to the practical scale". He drew attention to the possible anisotropy of frictional values and sliding behaviour with increasing joint size as for instance in cases of prominent current ripple marks frequently characteristic of bedding planes.

Although there is a very large volume of published in-situ shear test results, and the sizes of joints that have been tested in the laboratory and field cover an appreciable range, it is very rare that any well documented work regarding the strength-size relationships in joints can be found. There are a number of reasons for this lack of information.

Because of the high costs involved, large scale in-situ tests are usually only employed to investigate the most critical discontinuity types such as infilled joints, shear zones, contacts of materials with strikingly different mechanical properties, etc., where scale effects may well be irrelevant.

Tests on different sizes of those joint types which could be susceptible to size effects (e.g. clean, rough bedding planes) have shown inconclusive results. Some tests have indicated no size effects, whereas in other cases the variations were either on the positive or negative side. In view of the well documented effects of surface roughness upon the shear strength of joints, it is readily understandable that unless surfaces

1. SMOOTH, ALMOST PLANAR

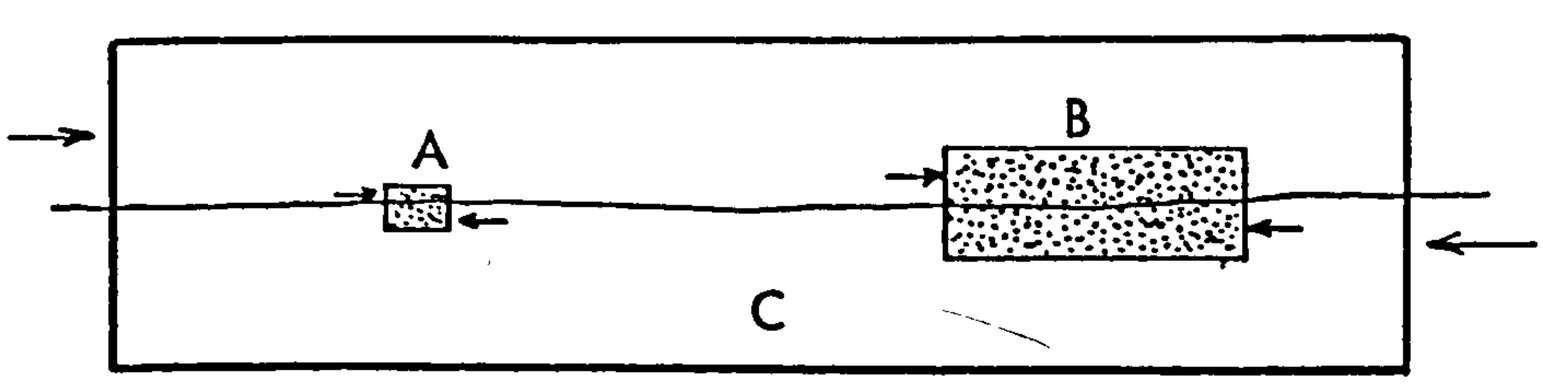

2. SMOOTH, UNDULATING

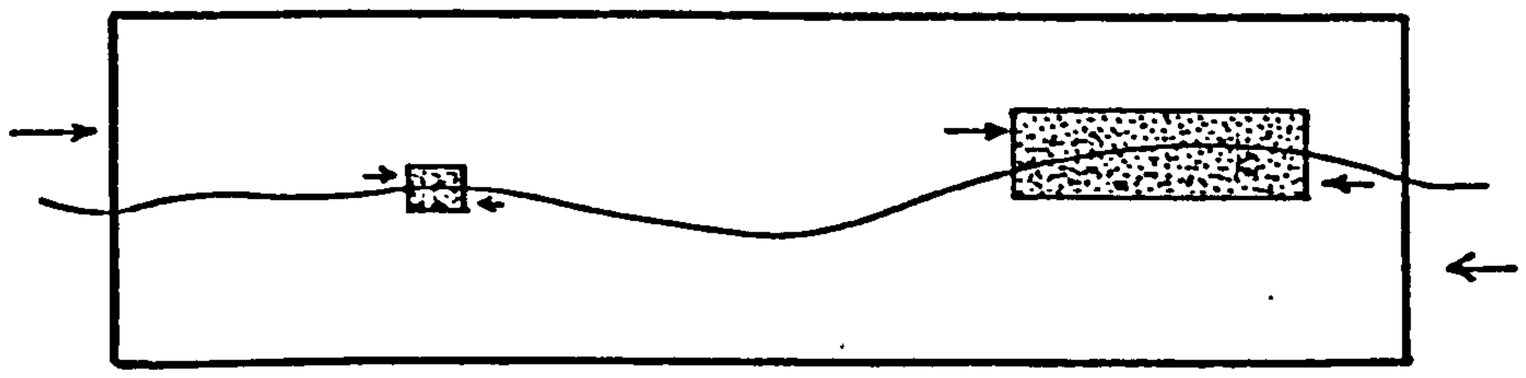

3. ROUGH, UNDULATING

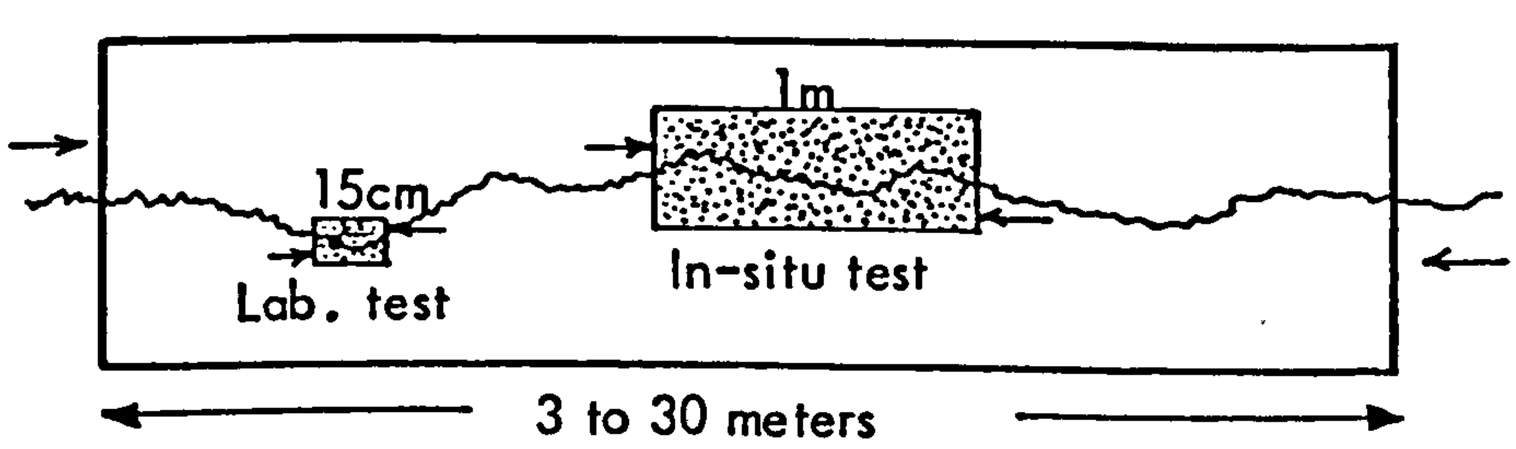

Size of actual failure surface in field problem

1. $S_A \approx S_B \approx S_C$
2. $S_A \approx S_B \neq S_C$
3. $S_A \neq S_B \neq S_C$

FIGURE 2.4. Examples of the probable effects of different specimen sizes in shear testing of joints and the relevance of the measured shear strength (S) to that of full scale failure planes.

(after Deere et al , 1967)

Note: Example No.1 has been added by the present author.

with related morphologies are tested, i.e. with the small joints sampled from the same or at least very similar surfaces as those tested in-situ, then comparisons would be anything but conclusive.

In addition, the practical problems frequently involved with large scale testing make the interpretation of the results very difficult. It has been reported that sliding tests of large blocks often result in differential displacements between the loaded and free ends of the specimen, because of the non-uniform shear stress distribution along the sheared surface area (e.g. see Krsmanovic and Popovic, 1966, and Evdokimov and Sapegin, 1970). Deformations of the rock block overlying the discontinuity may induce a progressive type of failure due to the displacement gradient. In such cases the portion of the joint surface adjacent to the point of shear load application may reach its peak resistance while displacements have not even started at the other end. The problem is obviously all the more serious when the block contains large numbers of fissures and open cracks.

The limited number of experimental studies where the effects of size upon the shear strength of joints have been coincidentally or intentionally considered are reviewed in the following section.

2.1.4 Review of experimental evidence on size-strength effects in joints

The literature search has revealed a small amount of experimental data from tests on joint specimens of different sizes. The range of the joint types tested has been broadly divided into two groups based on the presence or absence of infilling material, and the relevant information will be presented in that order. Joints without infilling have been sub-divided into "discontinuous" and "continuous" types, depending upon the presence or absence of intact bridges between the walls.

1. Infilled joints

Salas (1968) reported on a series of shear tests conducted in-situ at Mequinenza Dam on joints of three different sizes, viz. 0.5 x 0.5 meters, 1 x 1 meters and 4 x 4 meters. As shown in Figure 2.5(a), no apparent size effect was found as the results of the large scale tests corresponded perfectly, within the scatter, to the smaller size tests. That behaviour was attributed to the regular surface morphology of those joint types and

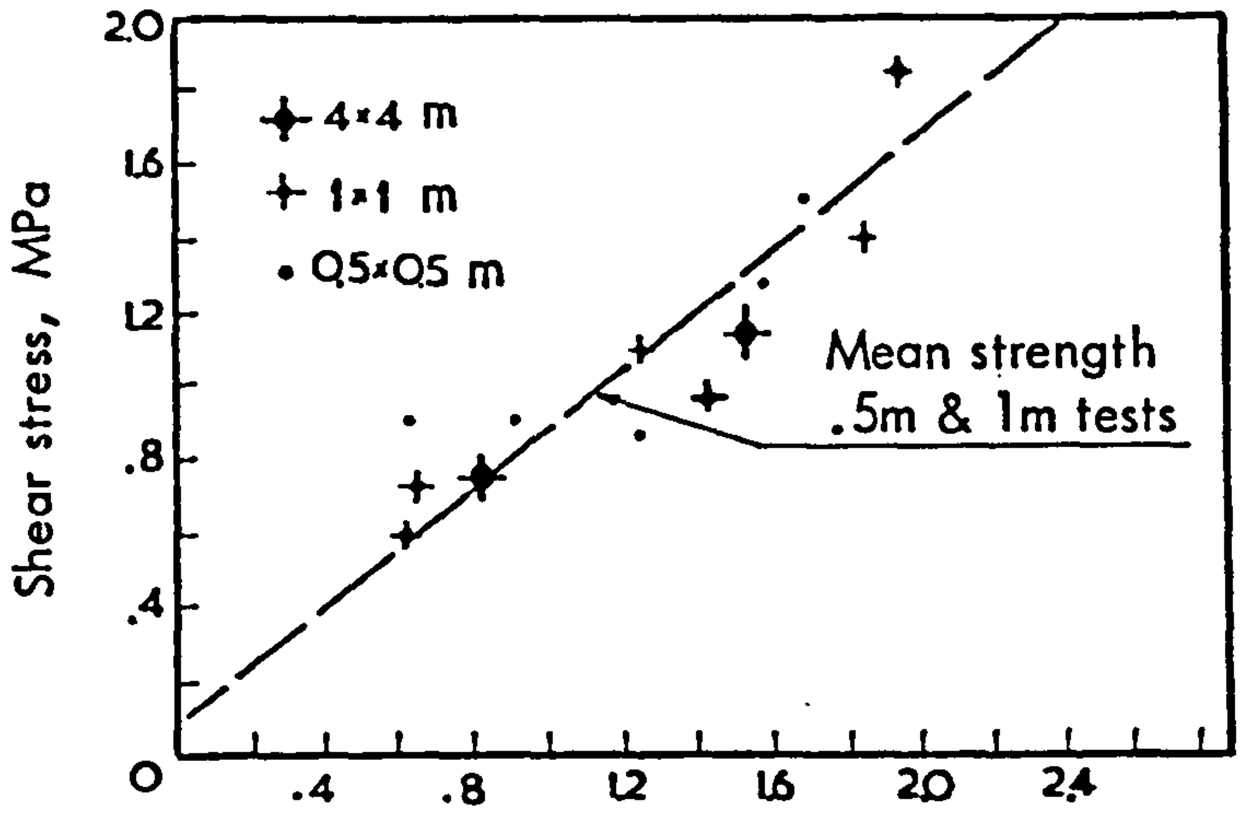

(after Salas, 1968)

(a)

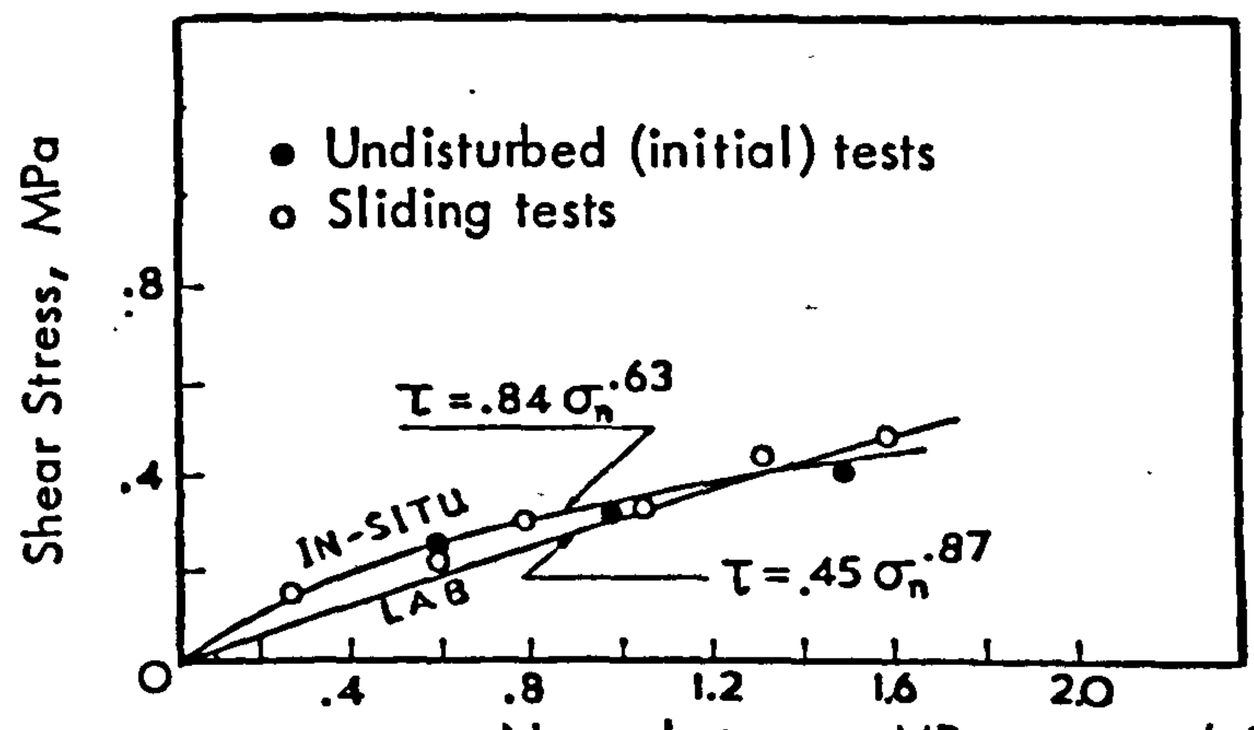

(after Infanti & Kanji, 1978)

(b)

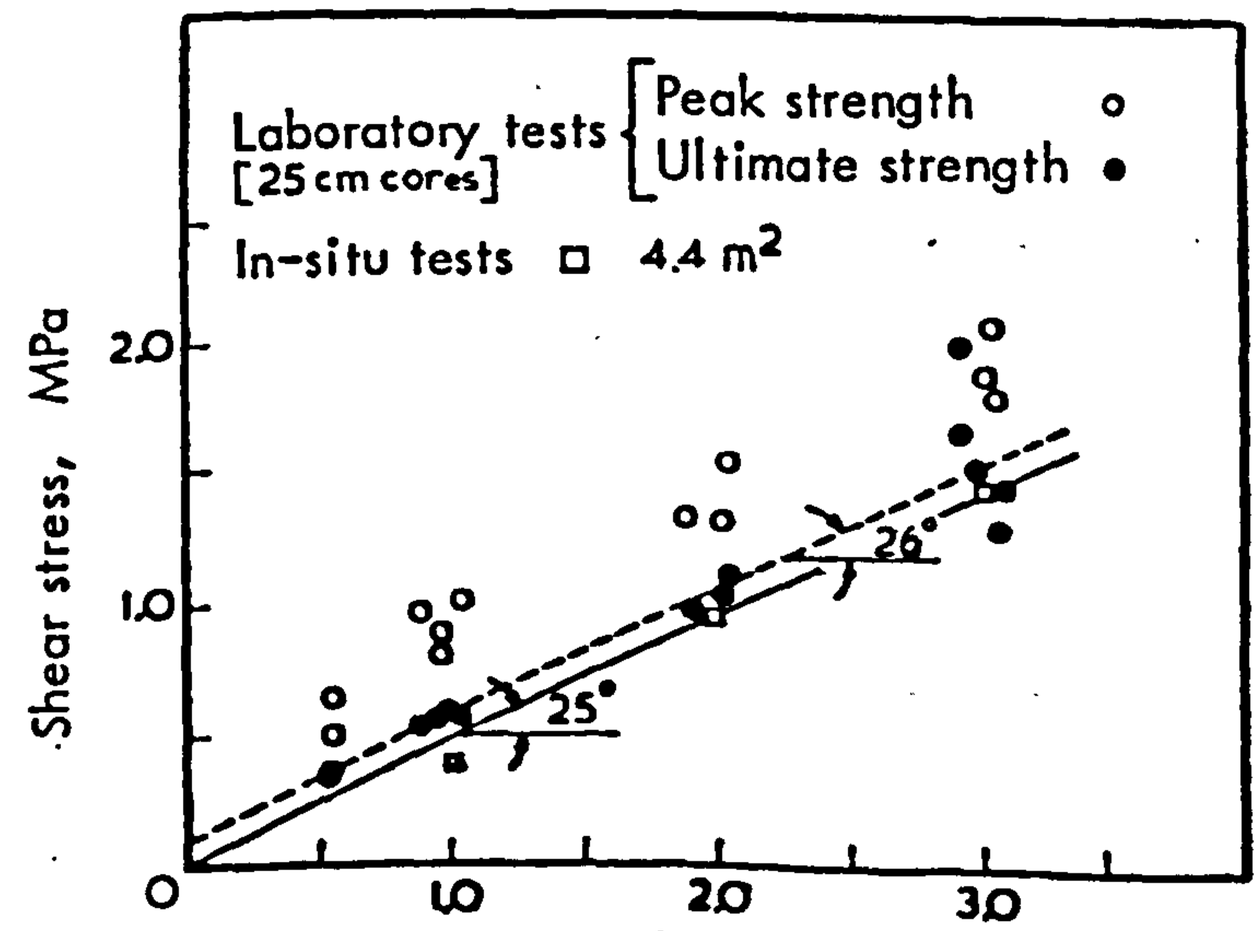

(after Londe, 1973)

(c)

FIGURE 2.5 Shear strength envelopes from tests on infilled joints of different sizes.

the existence of a soft infilling material of thickness sufficient to prohibit any contact between the existing irregularities. In other words, the tests merely measured the shear strength of the infill.

Findings similar to the above have recently been reported by Infanti and Kanji (1978), from a laboratory and in-situ testing program on joints in basalt infilled with montmorillonite (Agua Vermelha hydroelectric power plant in Brazil). In that investigation joint sizes ranged between 400 cm^2 (laboratory) and 10,000 - 40,000 cm^2 (in-situ). All the tests were run after saturation for 48 hours. The results showed that, irrespective of size, the shear strength of those joints was dominated by the type (clayey, sandy, etc.) and thickness of infilling. The maximum shear stress envelopes obtained from the smallest (20 x 20 cm) and largest (200 x 200 cm) test sizes are shown in Figure 2.5(b). As seen, the in-situ joints appeared to exhibit slightly higher shear strength than the small ones tested in the laboratory. The equations fitted to the experimental data are given in Figure 2.5(b). One of the large joints showed lower strength at $\sigma_n \approx 1.5$ MPa than smaller joints tested in the laboratory under the same normal stress. Overall, no significant size effects were apparent and the minor differences were presumably due to small variations in the thickness and properties of the infilling.

Londe (1973) presented the results from direct shear tests on clayey joints in limestone conducted on 25 cm diameter cores and on an in-situ joint of an area of 4.4 m^2. The shear stress-normal stress curves are shown in Figure 2.5(c). As clearly seen, the ultimate frictional resistance of the laboratory specimens agreed very well with that measured in the in-situ test.

2. Discontinuous joints

The term is used for those joint types which exhibit a certain amount of cohesion under a theoretically zero normal stress as a result of existing "bridges" of intact material bonding the two joint walls together. The peak shear strength of those joint types develops at the moment of rupture of those bonds. The sliding movement which follows is resisted by frictional forces only.

The random pattern of the intact bridges may produce an apparent scale effect when an experimental determination is attempted of the peak shear strength of those joint types.

Londe (1973) presented the results from shear tests on discontinuous limestone joints of two different sizes, viz. 8 cm and 30 cm diameter cores. The shear vs. normal stress plots of the data are shown in Figure 2.6.

The peak shear strength (cohesion mainly) of the larger samples (30 cm) was overall found to be lower than that of the smaller (8 cm) ones, while a good agreement was observed between the ultimate strength (friction only) values from both sizes, with the larger ones apparently being slightly stronger. The explanation offered for this size-effect will be discussed later.

3. Continuous joints

In this type of discontinuity no wall intact bonding exists and the peak shear resistance is fundamentally linked with the morphology of the joint surfaces and the strength of asperities.

Krsmanovic and Popovic (1966) reported a series of large scale in-situ shear tests on "clean" and infilled bedding planes in limestone. The peak shear strength of a large, unfilled bedding joint (2.8 x 1.8 m) was compared to the results from laboratory tests on large specimens 40 x 40 cm, which have been published by Krsmanovic, Tufo and Langof(1966). The derived peak shear strength envelopes for the in-situ fissure and the 40 cm joints (Fig.6a) showed a good agreement for normal stresses up to 1.5 MPa. The apparent size effect at higher normal stresses could be related to the multistage testing method which was employed for the large joint. In absolute terms all the results obtained after the initial shearing under higher normal stresses did not truly represent peak strength conditions.

Locher and Rieder (1970) published the results (Table 2.1) from large scale laboratory (200 cm^2) and in-situ tests (~ 3 m^2) on bedding planes in limestone. The two large scale field tests yielded a friction angle higher by 5° than the average laboratory equivalent. The authors attributed the difference to a scale effect but no further explanation was given in that publication.

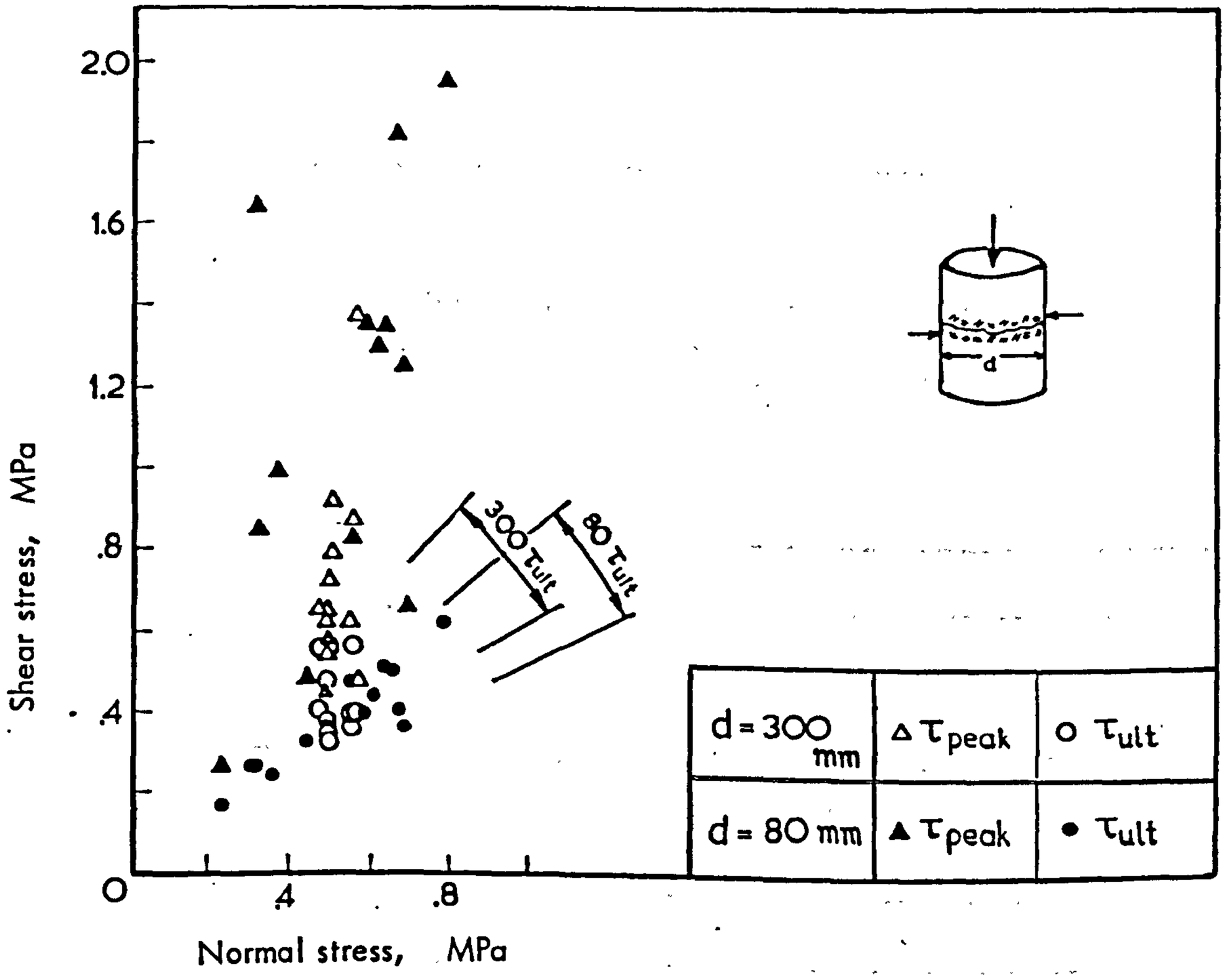

FIGURE 2.6 Scale effects in the shear strength of discontinuous limestone joints.

(after Londe, 1973)

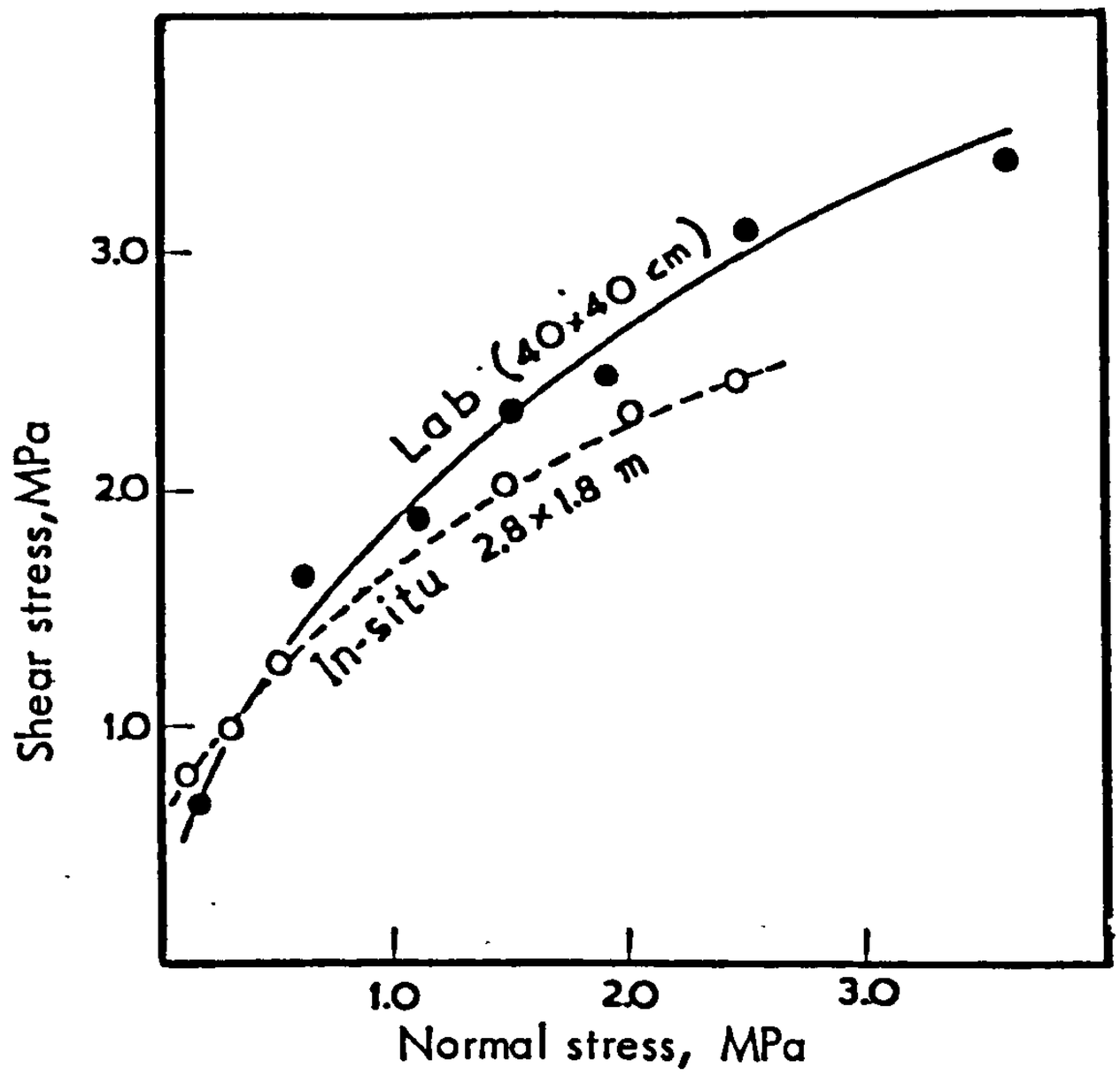

FIGURE 2.6a Comparison of peak shear strength envelopes from laboratory and in-situ multistage testing on limestone bedding planes. Data reported by Krsmanovic et. al. (1966) and Krsmanovic and Popovic (1966)

TABLE 2.1

Results from laboratory (200 cm^2) and in-situ ($\sim 3\ m^2$) shear tests on beddin.: planes in limestone rock. (From Locher and Rieder, 1970).

A. LABORATORY TESTS			B. IN-SITU TESTS			
Specimen	Peak friction angles		Block	Range of friction angles		Average
	Minimum	Maximum		Lower limit	Upper limit	
H	36°	40°	I	50°	54°	52°
M	42°	48°	II	48°	54°	50°
N	45°	51°				
Average H,M,N	41°	(46°)	Average I,II			(51°)

Note: The min. ϕ_{peak} values in laboratory tests correspond to the point of "bending" of the shear stress-shear displacement diagram at the beginning of any movement.

However, on the basis of other information given by Locher and Rieder one could infer that the morphology of the walls of the different joints was responsible for that size effect. In particular, the authors described the laboratory joints samples as "smooth", in which case even small undulations present on the large test surfaces could have well offered the additional resistance. Indeed, it was reported that post-test measurements on the in-situ surfaces showed deviations from the assumed sliding planes to be up to $\pm$ 2 cm.

Jaeger (1970) referred to some triaxial tests by Rosengren on graphite coated joints in cores of two different diameters, viz. 5 and 15 cm. Two of the joints were described as smooth and another two as rough. The mean angles of friction for the 5 cm smooth and rough joints were 11° and 24° respectively. Two other smooth joints in 15 cm core gave an angle of friction of 8.5° and a rough one of similar dimensions gave of ϕ_{peak} value of 39° and residual friction of 17°. On the basis of those results Jaeger commented that on that scale size-effects might not be important but outlined the need for much further work.

Pratt et al. (1974) conducted a series of laboratory and in-situ tests on diorite joints of various sizes. Field testing covered a range of areas between 142 and 5130 cm^2 with joints up to 2 meters long. The laboratory tests were carried out on 60 cm^2 joint specimens cored from the same natural surfaces which were tested in-situ.

The testing programme revealed a remarkable size-effect upon the peak shear strength. The largest in-situ joint ($\sim$ 5000 cm^2) showed an approximately 40% drop in strength compared to the 140 cm^2 specimens. Figure 2.7(a) shows the shear stress-shear displacement diagrams for different joint areas. The variation of peak shear strength with joint area is given by the semi-log plot in Figure 2.7(b).

Barton and Choubey (1977) reported the results from a combination of tests conducted on a 45 x 50 cm joint in granite. The full-size specimen was originally tilt-tested and was then sawn into 18 samples with dimensions of 9.8 x 4.9 cm. Six of the latter were tilt tested and the remaining 12 were "push"-tested. The roughness of the surfaces dictated the choice of the index testing method. Finally, all eighteen samples were sheared in a conventional shear box under low normal stress level (the average ratio of Joint Compressive Strength to normal stress was $\sim$ 182). All types of tests were conducted in the same direction.

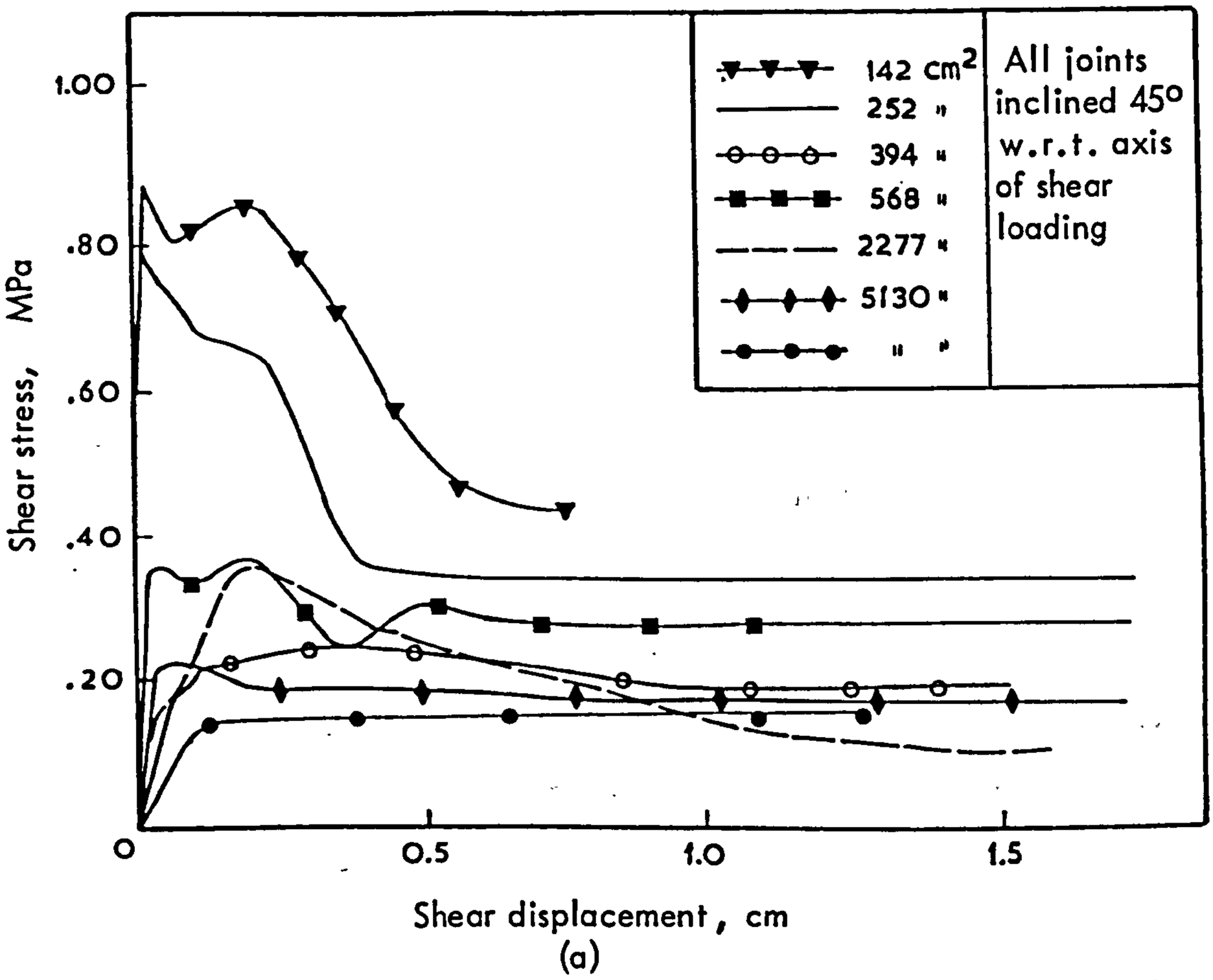

FIGURE 2.7. Scale effects in the shear strength of joints in quartz diorite

(after Pratt et al., 1974)

The Joint Roughness Coefficient for each of the specimens tilt-tested was found from:

$$JRC = \frac{a° - \phi_r}{\log(^{JCS}/\sigma_n)} \qquad 2.3$$

where a° was the tilt angle at sliding and ϕ_r was the angle of residual friction (= 29° for that type of granite). The normal stress was calculated from

$$\sigma_n = \gamma h \cos^2 a \qquad 2.4$$

where h was the thickness of the top half of block (m) and γ was the rock density (KN/m^3).

Because of the large length/thickness ratio of the full size joint (~20) the normal stress was calculated from $\sigma_n = \gamma h \cos a$. Had the expression (2.4) been used the back-calculated JRC value would have been lower by 0.3. The average results from all tests are given in Table 2.2.

TABLE 2.2

Average results of tilt, push and shear box tests on different sizes of the same joint

(after Barton and Choubey, 1977)

Type of test	Joint length (cm)	No. of specimens	Angle of sliding under "tilting" or "pushing"	Arctan (τ/σ_n)	Back-calculated value of JRC
Tilt	45	1	59°	-	5.5
Tilt	10	6	67.2°	-	8.8
Push		12	70.5°	-	
Shear box	10	18	-	48.5°	8.7

As shown by the results in Table 2.2, a decrease of the joint length resulted in an increase of the JRC value from 5.5, corresponding to the 45 cm joint, to 8.8 which is the average of 18 specimens from the same original surface, irrespective of the testing method. On the basis of those results, Barton and Choubey suggested that there must be a size-effect in the relative contribution of surface roughness to sliding resistance with increasing joint size.

On the basis of the available experimental information, various views regarding the size-strength effects in joints have been expressed in the past and different practical approaches to the problem have been suggested, as reviewed in the following section.

2.1.5 Current state-of-art

The experimental evidence presented in the last section has shown that the shear strength of joints infilled with soft materials must be independent of the joint sample length, particularly in the cases where the thickness of the infilling is larger than the amplitude of the wall roughness. The fact that in those cases failure takes place inside the infilling material without any involvement of the actual joint surfaces is the obvious explanation.

Discontinuous joints with "bridged" walls appear to be sensitive to size as far as peak strength is concerned but apparently scale free when they reach a "steady-sliding" stage (ultimate strength). Continuous joints have been reported to suffer a strength-loss with increasing size, whereas in other cases no such effects seem to exist. If one accepted the existence of size-effects two questions of fundamental significance arise:

(a) which are the factors responsible for the scale effects?
(b) in quantitative terms, how can we allow for them?

Londe (1973) argued that if one analyzed the strength of a discontinuous joint in terms of cohesion (c) and friction (ϕ), then both reasoning and experiment lead to the following conclusions: (a) strength due to cohesion decreases with increasing size; (b) strength relying on friction only (i.e. after the collapse of the sound rock bridges) is more or less insensitive to scale effects.

In order to prove the reasoning behind his statements, Londe gave as an example the hypothetical case of a joint with intact bridges randomly distributed across the interface. He pointed out that test specimens sampled from such an occurrence could be any of the types shown by the diagrammatic illustration in Figure 2.8. Sample (A) would obviously show the highest peak strength (equal to the shear strength of the intact rock) and sample C would be the "weakest". In general the value of peak shear strength would depend upon the relative location of the tested specimen.

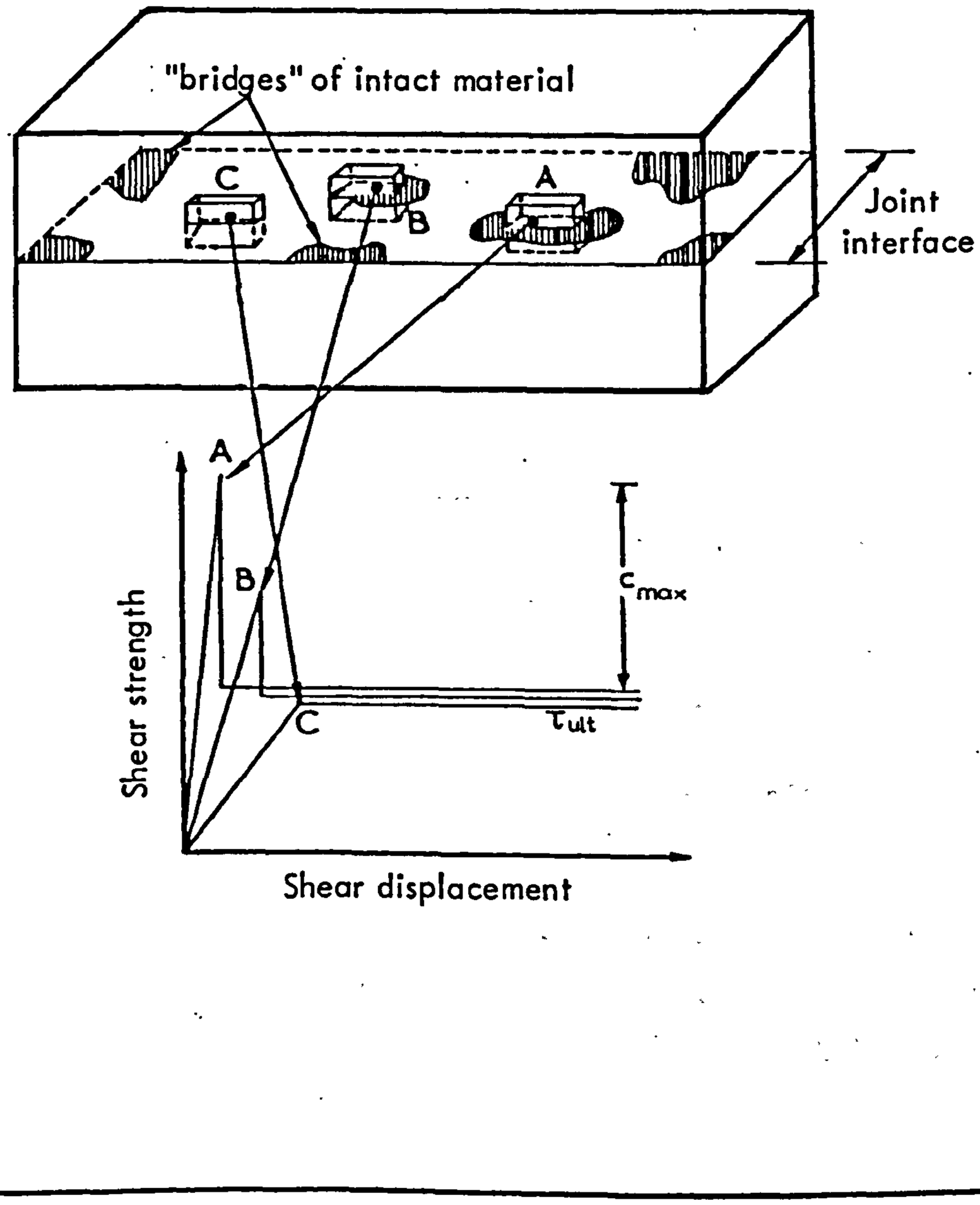

FIGURE 2.8. Diagrammatic illustration of the sampling "risks" in small scale testing for the determination of the shear strength of discontinuous joints.

(after Londe, 1973)

In a general comment concerning the size-effects in rock mechanics testing, Londe stated that "... a characteristic property of discontinuous bodies is the decrease in the arithmetic mean of measured strengths and the scatter of the results as the size of the sample increases". In accordance with that concept Londe pointed out that the scale effect on the peak shear strength of discontinuous joints becomes more significant as the scatter of the experimental values determined on small specimens increases.

Londe further suggested that "... where failure depends only on friction, the scale effect can only increase the strength of the larger samples because, if it is assumed that the normal stress distribution is more or less uniform over the whole area sheared, the strength will be governed by those 'elements' of the surface where the friction angle is highest".

As an experimental confirmation of his views, Londe referred to the experimental data which has been presented in Figure 2.6. In conclusion he suggested that in view of the size-effects associated with the peak strength of discontinuous joints, it is preferable to use for design purposes the average ultimate strength values obtained in the laboratory which by contrast show much lower scatter (Figure 2.6) and are comparable with those obtained from large scale tests.

Let us now consider the existing views about the scale effects associated with unfilled, continuous joints.

The test results on diorite joints of different sizes by Pratt et al. (1974) have been presented in Figure 2.7 of the last section. The authors attributed the drop in strength with increasing size to decrease of the actual contact area. From observations of the joint surfaces after completion of tests, Pratt and co-workers found that the actual contact areas between the walls were sometimes as low as 10 to 20% of the total surface area, depending upon the wavelength and amplitude of the joint irregularities. Consequently, the actual shear stresses must have been considerably higher than the average stress values calculated from the apparent surface areas. This led to the size-effect for larger joints with lower contact areas. Pratt et al. presumed that "... there would probably be no size effect if the contact areas of large and small joints were the same". They suggested that such might be the case of unweathered, perfectly mating discontinuities under high normal stresses.

Barton (1976) made an empirical approach to the problem. He suggested that the effects of scale upon the uniaxial compressive strength of intact rock would potentially affect the value of Joint Compressive Strength (JCS) operating along a joint interface. By referring to the diagrams presented in Figure 1.11(section 1.1.3(4), in part one), he pointed out that a scale effect on the joint compressive strength (JCS) would have a marked effect on the shear strength predicted for rough undulating joints (Joint roughness coefficient, JRC = 20), but a minimal effect on smooth, nearly planar joints (JRC = 5). By analogy, there would be minimal or zero scale effect on residual strength and maximum scale effect on the peak strength of very rough joints.

Based on the above assumptions, Barton attempted an alternative interpretation of the experimental results on diorite joints by Pratt et al. An investigation of the size-effects upon the uniaxial compressive strength of the same diorite rock has also been reported by Pratt et al. (1972), and has been referred to briefly in section 2.1.2.

As has been shown in Figure 2.7, the increasing size of diorite joints resulted in roughly 40% drop in peak shear strength. Three distinct peak strength envelopes corresponding to mean joint areas of 200, 1500 and 5000 cm^2 are shown in Figure 2.9(a). By assuming square test surfaces those areas represent joint lengths of approximately 14 ($\approx\sqrt{200}$), 39 ($\approx\sqrt{1500}$) and 71 ($\approx\sqrt{5000}$) cm respectively.

Barton (1976) derived the theoretical counterparts of those experimental envelopes by using the following input data in his criterion (eqn. 1.21, part one):

(i) he assumed a Joint Roughness Coefficient (JRC) of 20 and a basic friction angle (ϕ_b) of 30°.

(ii) a peak arctan (τ/σ_n) value was derived from a middle point from each of the experimental envelopes shown in Figure 2.9(a).

He was then able to back-calculate the JCS value in each case from

$$\log_{*}(^{JCS}/_{\sigma_n}) = \frac{\text{Peak arctan } (\tau/\sigma_n) - \phi_b}{JRC} \qquad 2.5$$

The derived JCS values were: 54 MPa (14 cm joint); 23 MPa (39 cm joint); 13 MPa (71 cm joint).

By using the above JCS values and the other data defined in (i) and (ii) Barton predicted the peak strength envelopes of the three joints (Fig. 2.9(b)).

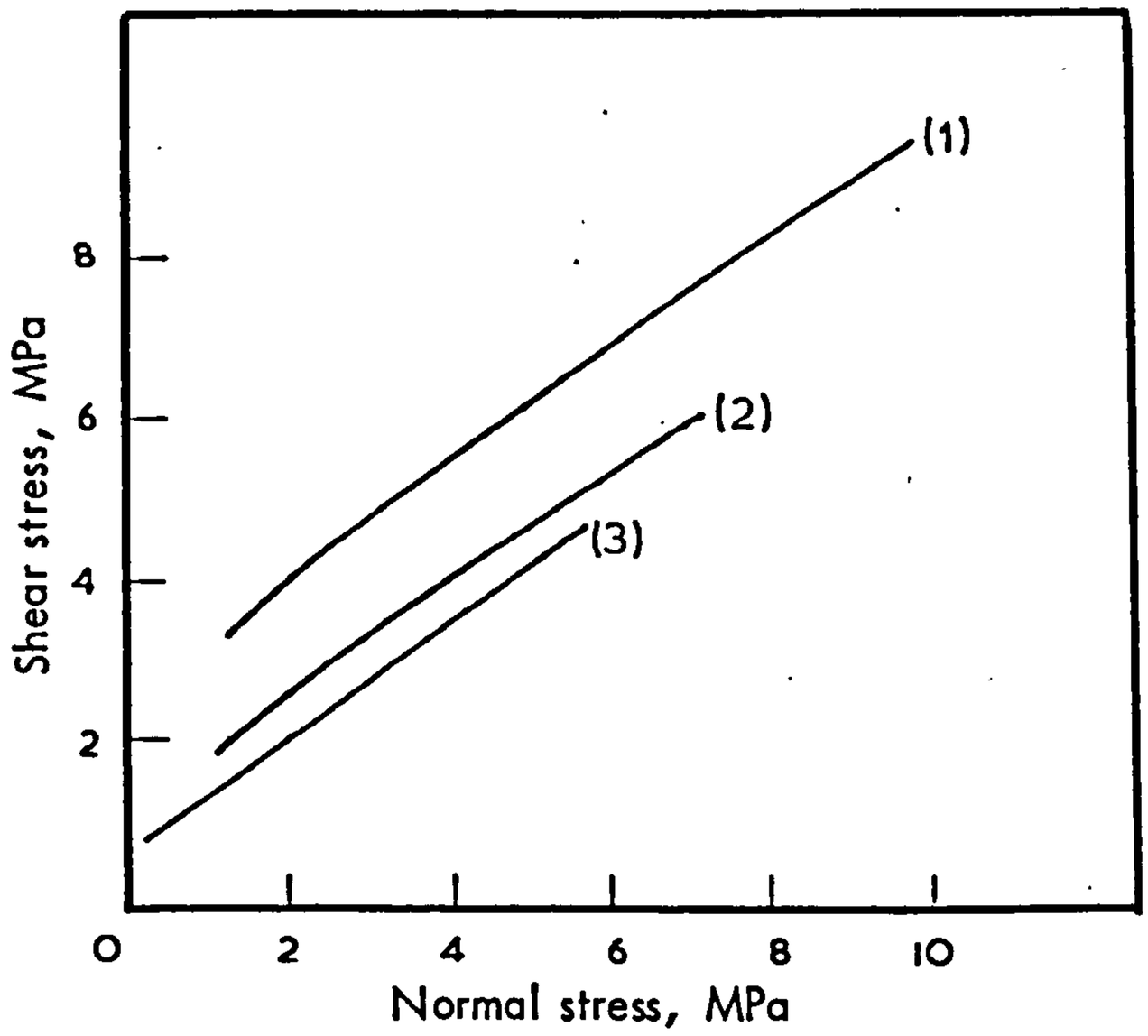

(a) Peak shear strength envelopes from in situ shear tests on joints in quartz diorite. Envelope (1) represents specimens with an average area of approximately 200 cm^2, (2) an average area of 1500 cm^2, and (3) an average area of 5000 cm^2 (after Pratt et. al. 1974)

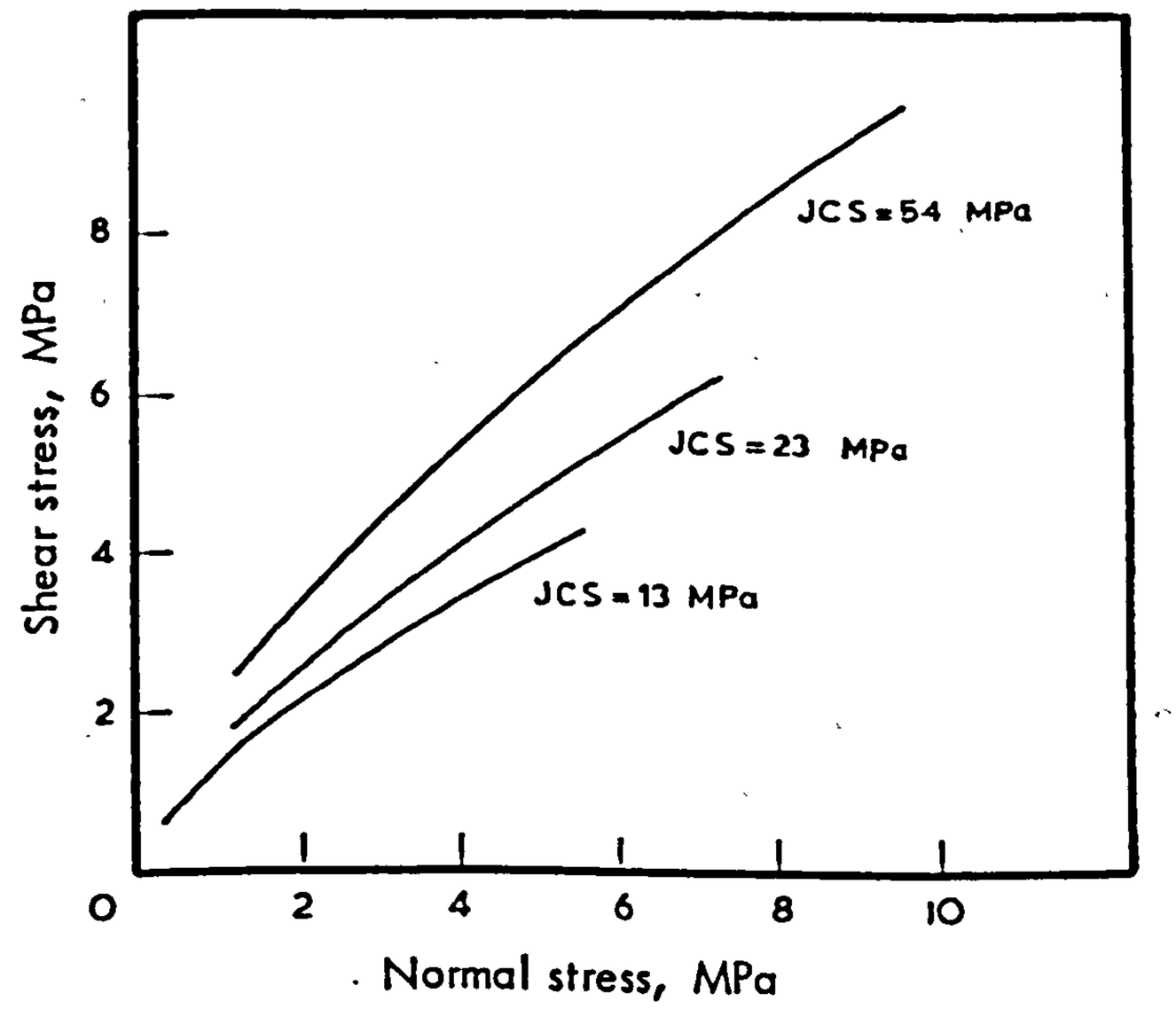

(b) Theoretical peak shear strength envelopes obtained from $\tau_p = \sigma_n \tan[JRC \log_{10}(\frac{JCS}{\sigma_n}) + \phi_b]$ with values of JCS as shown, and assumed values of $\phi_b = 30^o$, and JSC = 20 (after Barton, 1976)

FIGURE 2.9

As can easily be seen, the theoretical envelopes had a very similar to almost identical trend with the experimental ones.

The apparent four-fold reduction in the back-calculated JCS values corresponded roughly to the decrease in unconfined compression strength (σ_c) in intact specimens of the same rock as has been reported by Pratt et al. (1972). The back-calculated JCS and measured σ_c values are given below for comparison.

Equivalent joint length, $L = \sqrt{A}$ cm	Back-calculated JCS, MPa	Measured σ_c of intact rock	
		Specimen size (cm)	σ_c (MPa)
14	54	5	60-70
71	13	30-45	15-20
		100	7
		>100	No further reduction in σ_c.

It is interesting to note that the back-calculated JCS = 54 MPa for the 14 cm joint was approximately the same as the σ_c of the 5 cm specimens of intact rock. Similarly, the JCS = 13 MPa of the 71 cm joint corresponded to the strength of the 30-45 cm intact specimens. In those two cases the ratio of intact specimen length/joint length was 5/14 ($\approx$1/3) and 35/71 ($\approx$1/2). Barton's hypothesis was that should that ratio (1/2 - 1/3) hold good for larger specimens, then the shear strength-scale effect might die out when the representative joint lengths were 2 to 3 times that of the largest compression specimen which was just sensitive to the size effect. As the compressive strength of the intact diorite specimens ceased to be size-dependent for specimen sizes in excess of 100 cm, it could then be assumed that the shear strength scale effect might die out for joint lengths larger than two to three meters.

In a subsequent publication Barton and Choubey (1977) related the envisaged size-dependency of Joint Compressive Strength (JCS) with the scale effect on the Joint Roughness Coefficient (JRC) revealed by their tilt-tests on the granite joints (Table 2.2 in section 2.1.4). Specifically, they suggested that as the joint length is increased, the

inherent stiffness of the surrounding rock will result in joint wall contact being transferred to the major irregularities as peak strength is approached. Therefore, they concluded, on a larger scale there are larger individual contact areas with correspondingly lower JCS values. As those irregularities are less steeply inclined in relation to the mean plane of the joint than the small steep asperities, they will give correspondingly reduced JRC values.

The last authors further suggested that the scale effects in the peak shear strength of a rock mass could be closely related with the joint spacing, which potentially controls the mass stiffness. Scale effects might die out earlier if joint spacing and block size was small. The rock mass might not be stiff enough for the large irregularities to provide the only effective rock wall contacts, as could be the case if the rock mass was very massive with widely spaced joints.

As a schematic illustration of their ideas, Barton and Choubey presented the diagram shown in Figure 2.10. In the case of the joint BB' the scale effect on JRC would be less marked (or perhaps non-existent) than in the case of AA'. The small individual blocks would move somewhat independently along BB' thus maintaining contact across the smaller and steeper asperities. On the other hand, the inherent stiffness of the large blocks overlying AA' would allow larger voids to open up and peak strength would not be reached until after a larger displacement when the major flatter undulations were in contact.

The above speculations led Barton and Choubey to the tentative suggestion that the size of the in-situ blocks as defined by the spacing of the cross-joints might represent a "critical joint length" just sensitive to scale effects and by implication the most relevant "specimen" size for testing. Further reference to the problem of practical allowance for scale effects in joints will be made in Chapter 2.5.

2.1.6 Conclusions and present experimental work

The review of the literature on shear strength-scale effects in unfilled joint types has shown that very little attention has been focussed on this all-important matter.

Londe (1973) considers that scale-effects in the peak shear strength of discontinuous joint types arise from the inherent limitations of small scale

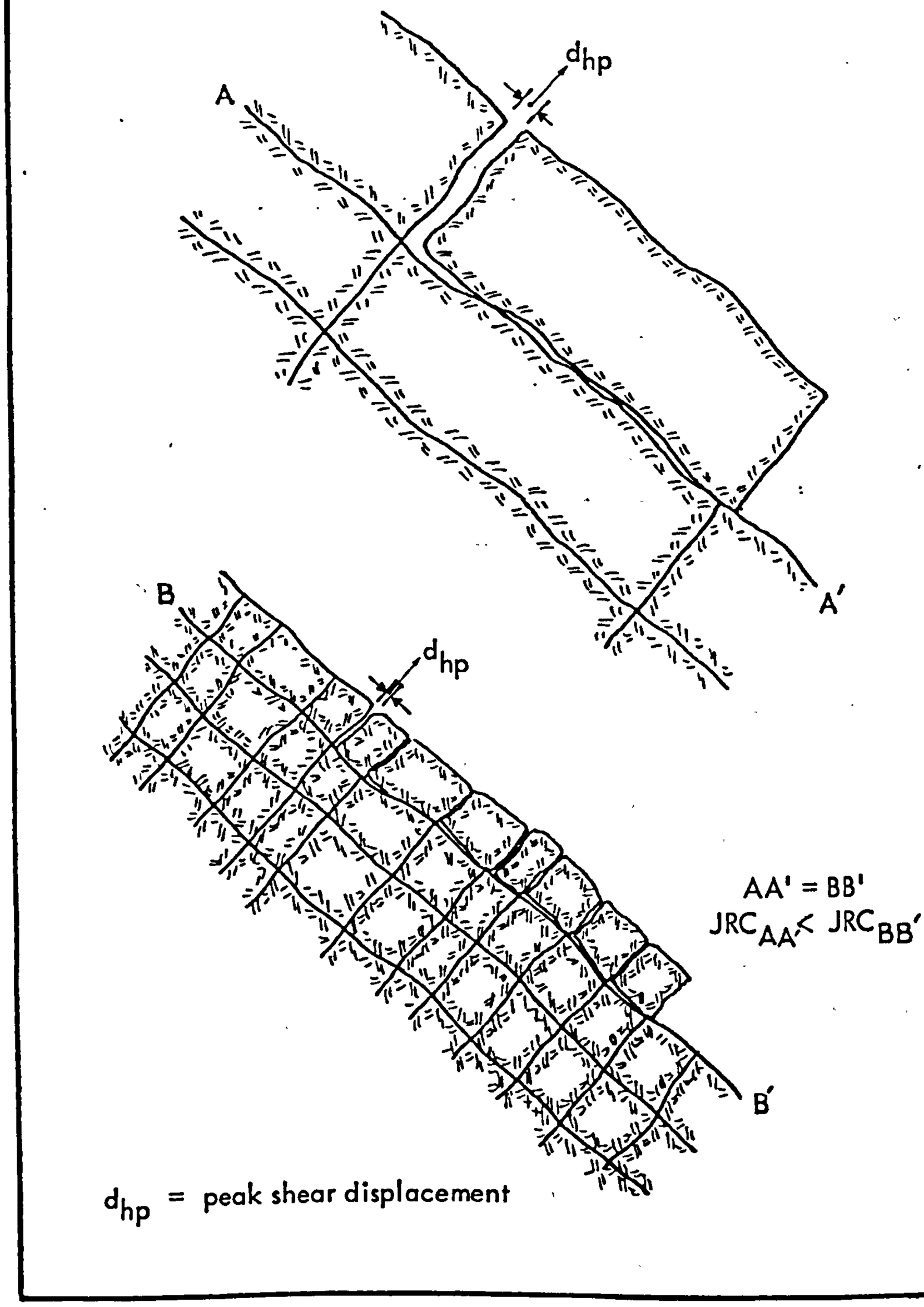

FIGURE 2.10 Schematic illustration of the probable effect of different cross-joint spacings on the shear behaviour of a rock mass

(after Barton & Choubey, 1977)

testing. From the practical point of view, this type of joint is probably the least critical and in any case the shear strength is most frequently described in terms of the ultimate(frictional)resistance which is probably not susceptible to scale effects.

It is the effect of scale on the peak shear properties of joints with no tensile strength which requires further attention. The limited amount of the experimental evidence currently available indicates that peak shear strength is probably related to joint size. However very little factual information exists as to the variables responsible for that effect and essentially different views have been expressed in the past.

Pratt et al. (1974) interpreted the reductions in the peak shear strength with increasing size of joints in a weathered quartz-diorite as a "circumstantial" phenomenon rather than as an inherent joint property. As has been reviewed in the last section the experimentally observed scale-effects were thought to be induced by differences in the actual contact areas between small and large specimens. On that basis they arrived at the tentative conclusion that scale effects in fully interlocked un-weathered joint types would probably be absent.

Barton and Choubey (1977) advanced a number of new concepts by attributing such scale effects to corresponding reductions in JRC and JCS, hence setting the problem on a different basis. However, those concepts are in urgent need of experimental verification before their practical potential can be fully appreciated.

In absolute terms, the effect of scale on the shear strength of a long joint can be studied quantitatively, only if the results from tests on small specimens sampled from the large joint can be compared to those obtained by testing the <u>same</u> joint at full scale.

An attempt was made to reproduce such a condition in the laboratory. A rubber moulding system was used to take precise impressions of natural joint surfaces. A carefully designed model material was used to cast at least four sets of identical interlocking specimens from each pair of moulds. Three of the full scale specimens were then cut into smaller blocks, each set having a different average block size or joint length. The component blocks of the subdivided models and the corresponding full size counterparts were individually tested in direct shear under constant normal load. All tests were conducted in the same shearing direction and under precisely the same level of normal stress.

The lengths of the full size joints were between 36 and 40 cm, while those of the smaller blocks were 18 or 20 cm, 10 or 12 cm and 5 or 6 cm. When converted into prototype scale those model sizes represented joints of 10.8 or 12.0, 5.4 or 6.0, 3.0 or 3.6, and 1.5 or 1.8 meters length respectively.

A total of eleven types of surfaces were included in the experimental study, with morphologies ranging from rough/undulating to almost smooth/planar. The "prototype" joints were collected from exposures of sandstone, siltstone, limestone and a fine-grained lightly metamorphosed sandstone.

The primary objective of the present study has been to investigate the potential existence or otherwise of scale effects in the peak shear behaviour and properties of joints. An appropriate level of normal stress was adopted to ensure that the total frictional resistance would comprise both a geometrical (dilation) and an asperity failure component, so that any scale effects on either or both variables could be analyzed. The present study also offered the opportunity to examine the effects of scale on the joint property of peak shear stiffness. That aspect will be referred to in part three of the thesis.

The development of a suitable model material is presented in Chapter 2.2 and Appendix I, followed by description of the method of preparation of the model joints (Chapter 2.3). The experimental results are presented and analyzed in Chapter 2.4 and some practical considerations are discussed in Chapter 2.5.

CHAPTER 2.2

DEVELOPMENT OF A MODEL MATERIAL

2.2.1 Introduction

Two important prerequisites of the present study were the development of:

(i) an artificial material with rock-like characteristics, and
(ii) model joints which would exhibit a behaviour comparable to that of real rock joints.

The model material which was found to satisfy the specified requirements was made from a mixture of "silver" sand, calcined alumina, barytes, plaster of Paris,and water.

2.2.2 Basic principles of model material design

Detailed discussions on the derivation of the laws of model-prototype simulation have extensively been reported in the literature (e.g. Obert and Duvall, 1967, Fumagalli, 1974) and only a brief reference will be made here.

The laws of model material design can be established by application of the principles of dimensional analysis. Dimensional analysis enables expression of the variables entering a problem, in the particular case the strength and deformation properties of a prototype intact rock, in terms of dimensionless products (π-terms).

A list of some basic rock material parameters and their dimensions (expressed in terms of the three primary dimensions of mass [M], length [L] and time [T]) is given below:

Compressive strength	(σ_c)	$ML^{-1}T^{2}$
Tensile strength	(σ_t)	$ML^{-1}T^{-2}$
Young's Modulus	(E)	$ML^{-1}T^{-2}$
Poisson's ratio	(ν)	1
Density	(ϱ)	ML^{-3}
Acceleration due to gravity	(g)	LT^{-2}

Angle of internal fraction	(ϕ)	1
Cohesion	(c)	$ML^{-1}T^{-2}$
Any linear dimension	(L)	L

The set of dimensionless products which can be obtained from these is as follows:

$$\frac{\sigma_c}{g\,L'}, \quad \frac{\sigma_t}{g\,L'}, \quad \frac{c}{g\,L'}, \quad \frac{\varrho gL}{E}, \quad \nu\ , \quad \phi$$

For similitude to be achieved between the model material (m) and the prototype rock (p), it is necessary that these dimensionless products be equal in model and prototype. For instance:

$$\left(\frac{\sigma_c}{g\varrho L}\right)_m = \left(\frac{\sigma_c}{g\varrho L}\right)_p$$

$$\left(\frac{g\varrho L}{E}\right)_m = \left(\frac{g\varrho L}{E}\right)_p$$

$$\phi_m = \phi_p$$

The first of the above equalities can be re-written as

$$\frac{\sigma_{cp}}{\sigma_{cm}} = \frac{L_p}{L_m}\cdot\frac{g\cdot\varrho_p}{g\cdot\varrho_m}$$

or

$$\boxed{\zeta = \lambda \times \frac{\varrho_p}{\varrho_m}} \qquad 2.7$$

where $\zeta = \sigma_{cp}/\sigma_{cm}$ is the <u>stress scale factor</u> and $\lambda = L_p/L_m$ is the <u>geometric scale factor</u>.

Equation 2.7 is a fundamental relationship which defines all the stress-displacement properties of the model. <u>Once the geometric scale factor (λ) is chosen, all the prototype properties with specific force dimensions must be reduced by $\lambda \times \varrho_p/\varrho_m$ in the model</u>. For example:

$$E_m = \frac{E_p}{\lambda \times \varrho_p/\varrho_m}\ , \qquad c_m = \frac{c_p}{\lambda \times \varrho_p/\varrho_m}\ , \quad \sigma_{tm} = \frac{\sigma_{tp}}{\lambda \times \varrho_p/\varrho_m}$$

Dimensionless quantities such as strain, Poisson's ratio and angle of internal friction should be the same for both prototype rock and model

material. The same applies to other dimensionless quantities such as the ratio of compressive to tensile strength (σ_c/σ_t), modulus ratio (E_r/σ_c), etc.

In addition to the above similitude requirements, Fumagalli (1974) drew attention to the need for geometrical similarity of the stress-strain curves and Mohr failure envelopes of the model and prototype materials.

The laws of similitude which have been referred to above in connection with the design of a model material can also be applied for scaling the properties of a prototype discontinuity and vice versa. A discussion on that matter is made later in section 2.3.4.

2.2.3 Specification of the model material properties

The nature of the study did not require simulation of any specific type of rock. A range of prototype properties was established such that it would represent medium strength rock type(s) falling in the upper half of the average modulus ratio zone in the DEERE and MILLER's scheme of intact rock classification.

A geometric scale factor (λ) of 30 was adopted. The choice of that value was made by considering the range of sizes of the model joints to be tested and their equivalent prototype dimensions. The minimum length (L_m) of the model blocks was approximately 5 cm and the maximum 40.0 cm. At prototype scales those dimensions represented joints of lengths ($L_p = \lambda \times L_m$) ranging between 1.5 and 12.0 meters. By using a relatively small λ value, the surface roughness for most of the model joints gave a fairly realistic picture when extrapolated to prototype scale considering the length (L_p) of the prototype joints.

Prior to the development of the model material, a ratio value of $\varrho_p/\varrho_m = 3/2 = 1.5$ was envisaged. By substituting $\lambda = 30$ and $\varrho_p/\varrho_m = 1.5$ in equation 2.7, a stress scale factor (ζ) of 45 was derived.
The final material had a higher density than originally anticipated ($\varrho = 1.85$ gr/cm^3) and by considering an average prototype rock density of 2.5 gr/cm^3, the ratio's ϱ_p/ϱ_m value was 1.35. Using the latter in equation 2.7, the value of ζ became 40 for the same geometric scale factor.

The range of prototype rock properties originally specified were:

- uniaxial compressive strength (σ_c) = 50 - 80 MPa
- compressive to tensile strength ratio (σ_c/σ_t) = 10
- modulus ratio (E_T/σ_c) = 300 - 400
- axial strain at uniaxial failure (ε_f) = 0.15 - 0.40%

Considering the value of the stress scale factor of 40 it was evident that the model material should have a relatively high compressive strength of the order of 1.5 to 2.0 MPa.

Achieving a material of high strength was an easy task. The main problems concerned the high deformability of the various mixes originally tried. Consequently, improvement of the "brittleness" of the material was the chief objective of the extensive experimental search that followed.

2.2.4 Experimental work

An extensive experimental programme was undertaken in the attempt to develop a brittle model material with properties resembling those of real rocks as closely as possible.

The two basic components normally used in the development of granular model materials are:

(i) a filler to provide the frictional properties
(ii) an agent to cement the frictional filler.

Initially the experimental study was directed towards the understanding of the simple sand-plaster-water system, which formed the basis of all subsequent combinations.

1. Composite materials, specimen preparation and testing

The development of the final model material was preceded by an extensive testing of a large number of trial mixes prepared from combinations of various substances.

The various components which were tried included: five types of sand with different grain sizes and degrees of sorting; three types of plaster (dental, pink and plaster of Paris); three different additives (barytes,

kaolinite, alumina). The physical properties of the above materials are presented in section 1 in Appendix I.

Test specimen preparation involved three stages, namely mixing, casting and curing. The procedures were standardized and faithfully followed for all materials.

In brief, the "dry" components (excluding plaster) were initially mixed for a standard period of five minutes. Next, water was added and the saturated mix was blended for another five minutes. Finally, the plaster was added and the stirring was continued until the mixture attained a creamy consistency.

Once the material had reached that state it was poured into plastic cylindrical moulds. A fine longitudinal slit cut on the cylinder walls enabled easy removal of the specimens after they had set, by pulling the sides of the slits apart and at the same time carefully pushing the specimen out of the mould.

The quantity of components used in each combination was sufficient to enable preparation of eight to ten specimens. Those with visible defects, for instance large surface pores etc., were discarded.

The curing of the various trial mixes consisted of drying at room temperature for 24 hours and then at 85°C for 36 hours. Curing temperature is critical for the strength of plaster cemented model materials as it controls the amount of dehydration of gypsum. Details on the curing of the trial mixes are given in section 2 in Appendix I. Lower oven temperature (50°-55°C) was used for the final model material.

The testing program included uniaxial compression of 25 mm diameter/50 mm length cylinders with simultaneous recording of the axial deformation. The tensile strength was indirectly measured by axial point load testing of 25 mm diameter/20 mm length cylinders, and diametral point loading of standard compression specimens. Also, at later stages the Brazilian test was applied on 25 mm diameter/8 mm thickness discs. Detailed notes on the procedures of test specimen preparation and testing are given in sections 2 and 3 in Appendix I.

During the early stages of the search it was evident that the relatively high strength (~ 2 MPa) specified for the model material could very easily

be achieved. The main problem faced was the high deformability of the various mixtures and improvement of the latter was the basic aim of the investigation.

A detailed description of the behaviour of the 'unsuccessful' materials is given in section 4 in Appendix I, together with analytical tables of the experimental results.

In the present context, a very brief summary of the successive experimental stages that led to the development of the final model material will be given.

2. Brief review of the properties of the trial mixes

(i) Sand/Plaster/Water

Five types of sand with different grain sizes and degrees of sorting were tried. Sands with uniform grain size were found to give weaker and more deformable materials than graded ones because of the reduced mechanical interlocking of the grains, particularly in cases of coarse types. "Silver" sand was chosen as the most suitable type.

The densities of the mixes were generally low - 1.5 to 1.6 gr/cm^3 - and the porosities were of the order of 38 to 42%. The axial strain at failure ranged between 0.9 and 2.1% depending upon the sand type and amount of water.

Compressive strengths up to 1.2 MPa were obtained under high temperature curing conditions (24 hrs at 20°C and 36 hrs at 85°C) and the σ_c/T_{500} ratio was generally low (~ 5 on average).

Use of pink and dental plaster revealed the unsuitability of the former because of its very slow setting, whereas dental plaster behaved similarly to plaster of Paris.

(ii) Sand/Barytes/Plaster/Water

Addition of barytes improved the properties of the sand/plaster/water system by increasing the density (ρ) and decreasing the strain at failure (ε_f). Furthermore, the inclusion of barytes appreciably reduced the water requirements of the mixes. A similar observation had been made by Barton (1971) who used red lead as a dense filler for his model material. The explanation offered was that the saturated red lead acted as a

lubricant on the sand particles and hence maintained the "pourable state" of the mix at a water content lower than would otherwise be required.

From the various combinations between sand and barytes tested, a B:S proportion of 1:2 appeared to show the most promising behaviour. One part of water was mixed with four parts of (B+S) and by adding various amounts of plaster (PP:(B+S) = 1:7 to 1:4) the following range of properties was obtained:

σ_c = 347 - 1112.5 kPa; T_{500} = 66.4 - 194.3 kPa; % ε_f = 0.79 - 0.90;

ρ = 1.85 gr/cm^3; E_T/σ_c = 256 - 285.

It should be noted that all specimens were cured at 85°C for 1½ days.

(iii) Sand/Alumina/Plaster/Water

Use of alumina instead of barytes produced mixtures with somewhat higher water requirements. However, two combinations of alumina with sand - A:S = 1:4 and 1:8 - gave materials with comparatively high σ_c/T_{500} ratios of 6.6 and 7.1. Furthermore, the recorded strain at failure was 0.6 and 0.74% which was the lowest in comparison with the other materials tested.

Presumably the interference of the chemically inert silt-sized grains of alumina amongst the gypsum crystals reduced the effective bonding of the latter and hence reduced their resistance to tension. In addition, they probably offered a "reinforcement" to the sand structure by occupying part of the intergranular space that would be otherwise filled solely by plaster, and therefore improved the mechanical interlocking of the granular skeleton. The latter could explain the comparatively low deformation of the test specimens.

Since both barytes and alumina as individual fillers improved the performance of the basic sand-plaster-water system, their combined effect was studied on a series of materials prepared from different proportions of sand-to-(Barytes + Alumina), varying at the same time the relative quantities of the latter two. That led to the development of a multi-component material whose properties fulfilled to an acceptable degree the model design specifications. The properties of the final model material are discussed in detail in the following section.

2.2.5 Properties of the final model material

1. General information

The model material adopted in this study consisted of sand, alumina, barytes, plaster and water, combined in the following proportions:

(Barytes+Alumina):Sand = 1:2
Alumina:Barytes = 1:3
Water:(Barytes+Alumina+Sand) = 1:4

The grain-size distribution of silver sand and alumina is shown in Figure 2.11 where the specific gravities of all components have also been included.

During preparation of test specimens the standardized mixing procedure that has been described in section 2.2.4 was followed.

The temperature of curing was set at 50° to 55°C. At first, the specimens were allowed to dry at room temperature for 8 hours and then placed in the oven and left for 48 hours. Measurements of the weight loss at regular time intervals showed that all free water had evaporated within 30 hours. A characteristic curing curve is presented in Figure 2.12.

An attempt was made to evaluate the "moisture content" of the fully cured specimens. A mixture was prepared using 400 grms sand, 150 grms barytes, 50 grms alumina, 150 grms water and 80 grms plaster.
If the various components are expressed in percentages by weight, then: sand = 48.193%, barytes = 18.072%, alumina = 6.024%, water = 18.072%, and plaster = 9.639%.

A set of five specimens was prepared from the above mix; their average weight was recorded and they were left to cure for the prescribed period. After 56 hours their average weight was measured again and the average moisture loss was found:

average weight of uncured specimens	:	57.980 grms
" " " cured "	:	48.584 grms
moisture loss	:	9.396 grms of water

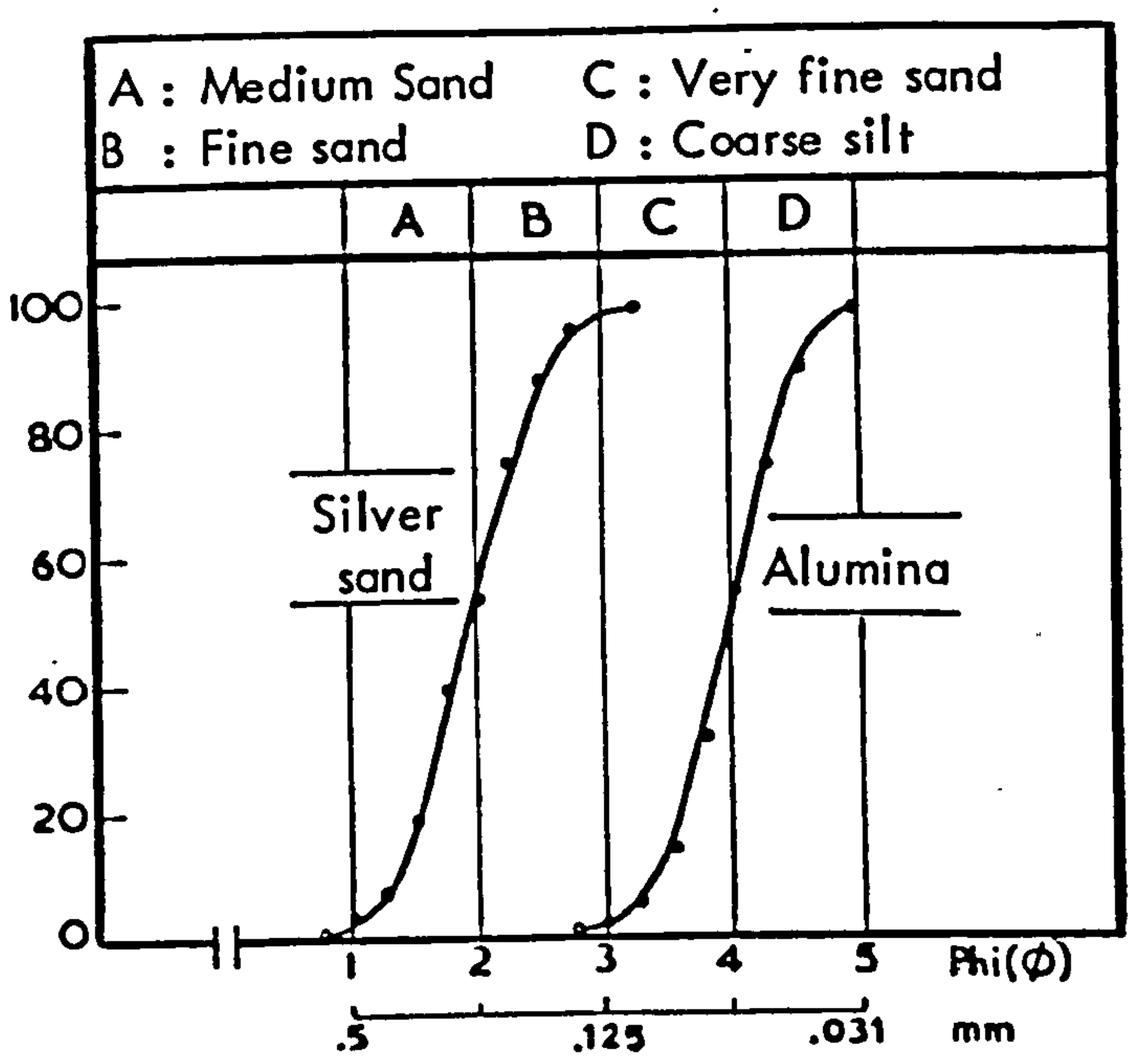

Specific gravities of materials

Silver sand	: 2.609
Barytes	: 4.349
Alumina	: 3.800
Plaster of Paris	: 2.995

FIGURE 2.11 Grain size distribution and specific gravities of modelling materials.

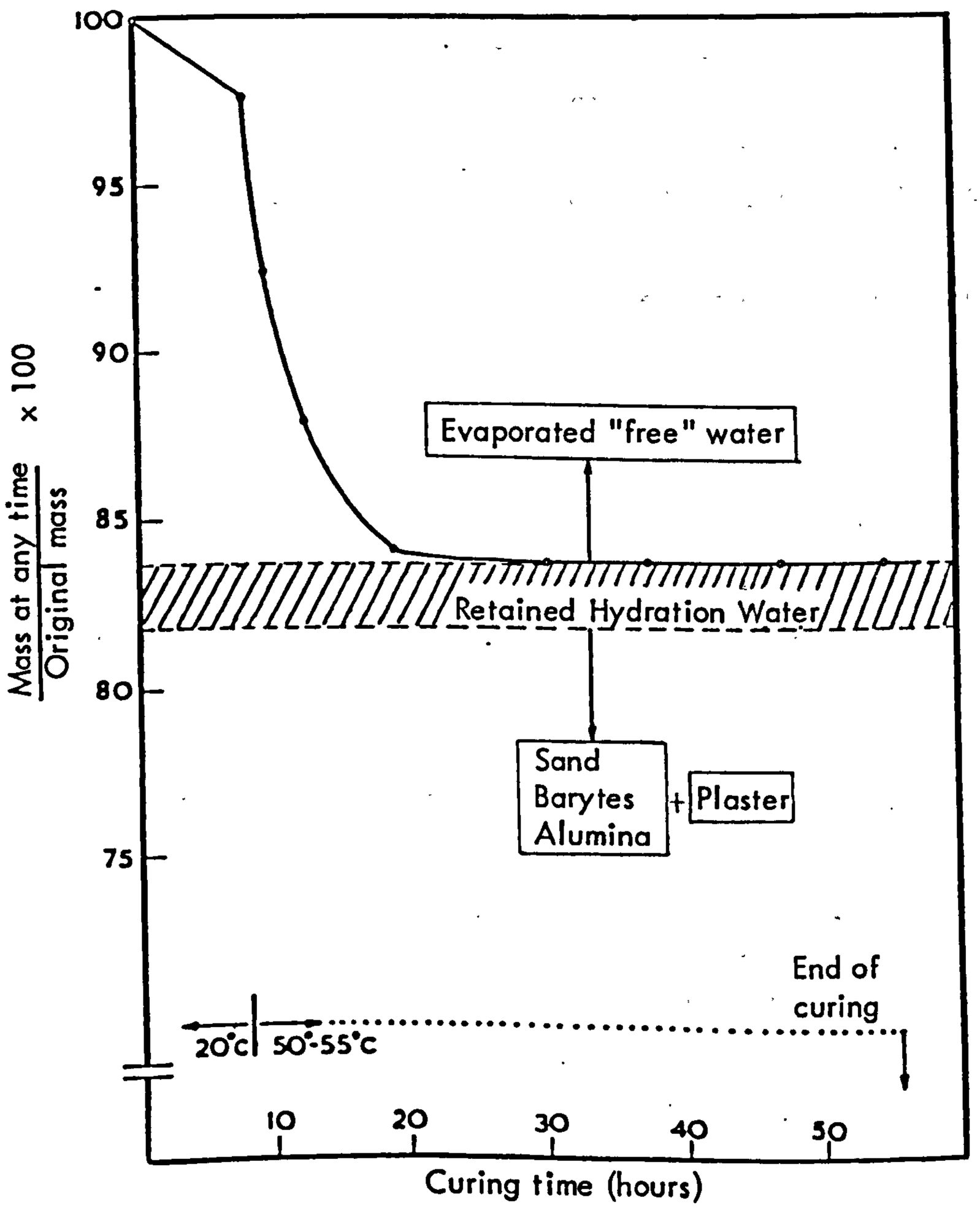

FIGURE 2.12 Curing curve of model cylindrical specimens 25mmD / 50mmL

Assuming perfectly uniform distribution of the components in the mixture, each specimen should consist of 48.193% sand, 18.072% barytes, 6.024% alumina, 18.082% water and 9.639% plaster.

As mentioned, the average mass of the uncured specimens was 57.98 grms. Combining the latter with the percentage by weight of plaster and water means that the average uncured specimen should contain 10.478 grms of water and 5.589 grms of plaster. Since 100 grms of plaster require 18.6 cm^3 of water for complete hydration, the 5.589 grms of plaster would need 1.039 grms of water. Therefore:

Free water in uncured specimen = Total amount of water - Water for hydration of plaster =

10.478 grms - 1.039 grms = 9.438 grms.

The "theoretical" amount of free water (= 9.438 grms) agreed very well with the estimated water loss through evaporation (= 9.396 grms), which meant that no breakdown of the gypsum commenced under the present curing conditions, while all free water had escaped. Holdridge and Walker (1964) concluded from D.T.A. studies that the dehydration of gypsum starts above 70°C. The fully hydrated form of gypsum was reflected in the high strength values of the materials.

2. Density and porosity of the material

The density (ϱ) of the material was found by dividing the weight (mass) of a number of cured specimens by their average volume (26.52 cm^3). The average density values for mixes with different plaster quantities are tabulated below.

PP: :(B+A+S)	No. of spec.	Density, ϱ (gr/cm^3)	
		Mean	Std. dev.
1:705	13	1.86	0.0246
1:7.5	14	1.85	0.0232
1:8.0	15	1.84	0.0223
1:8.57	15	1.84	0.0200
1:9.23	14	1.84	0.0205

The average density of all mixes was approximately 1.85 grms/cm^3.

An approximation of the material porosity (P) could be obtained if it was assumed that the pore space of the cured material was occupied by the evaporated water. Then:

$$\% P = \frac{\text{Volume of voids}}{\text{Bulk volume}} \times 100 \qquad 2.8$$

where: volume of voids (V_v) ≈ volume of free water, and
bulk volume (V_b) = weight/density.

Considering a typical mix of 400-150-50-80-150 by weight of sand-barytes-alumina-plaster-water, then the 150 cm^3 of water minus the amount retained for the hydration of plaster (~ 15 cm^3) would form the free water phase which after evaporation would create an equivalent volume of voids (V_v). The bulk volume (V_b) would be equal to 695/1.85 = 375.7 cm^3. According to 2.8 the porosity could be calculated from:

$$P = \frac{V_v}{V_b} = \frac{135 \text{ cm}^3}{375.7 \text{ cm}^3} \approx 36\%$$

Two factors that could affect the above estimate should be pointed out. Entrappment of microscopic air-bubbles may cause an unaccounted increase of the actual porosity. On the other hand, the above value may be slightly higher than the actual one, as the amount of water loss by bleeding and surface evaporation has been ignored. Provided that the method of evaluation is valid, the porosity value of 36% is quite acceptable compared with the range of plaster-water systems (40% to 80%).

3. Uniaxial compressive strength of material

The uniaxial compressive strength range (σ_c) of the model material was determined by testing mixtures prepared with constant amounts of sand/barytes/alumina/water and variable plaster quantities. The proportions of PP:(B+A+S) ranged between an arbitrary minimum of 1:15 and a maximum of 1:7.06. The latter brought the mixture very close to its workability limit.

Under the employed curing procedure the above quantities of plaster gave uniaxial compressive strength values ranging between .747 MPa and 3.455 MPa.

Separate sets of compositionally similar specimens were prepared and tested in order to examine the reproducibility of the material.

The analytical results from all tests are presented in Table 9 in Appendix I, and the average values are given below together with the number of separately prepared sets of specimens.

Table 2.3

Range of average uniaxial compressive strength (σ_c) values of model material

PP:(B+A+W)	No. of specimen sets	Total no. of spec.	σ_c (MPa)	
			Mean	Std. dev.
1:15	1	9	0.747	0.0542
1:12	1	8	1.251	0.0832
1:10.91	2	11	1.316	0.0901
1:9.65	1	10	2.030	0.0807
1:9.23	2	10	2.050	0.1405
1:8.57	2	10	2.456	0.1866
1:8	2	10	2.757	0.0991
1:7.5	3	17	3.129	0.1691
1:7.06	3	16	3.455	0.1794

The compressive strength of the material was found to be reproducible to an acceptable degree, as indicated by the relatively low values of standard deviation of the σ_c values obtained from specimens prepared from more than one mixtures of the same composition. The calculated relative dispersion (% variation = [std. dev./mean] x 100) of the σ_c values determined for each of the eight mixtures ranged between 3.6 and 7.6%.

A variety of failure modes was observed during specimen testing, and some characteristic examples are shown by the photograph in Figure 2.13, which also includes some similarly tested cores of a massive siltstone for comparison. The majority of failures of the model cylinders occurred

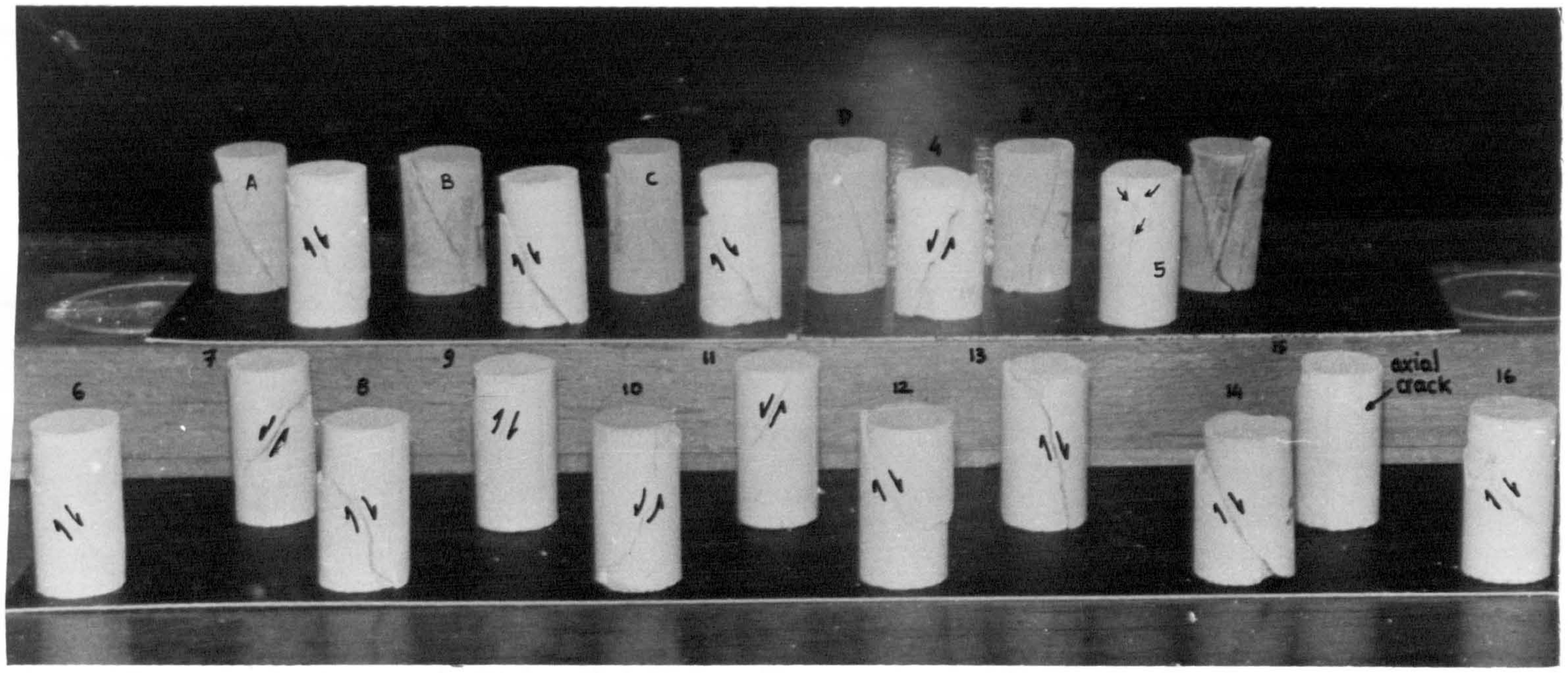

FIGURE 2.13 Photograph showing a collection of cylindrical specimens (25mm diameter / 50mm length) of the model material loaded to failure under uniaxial compression. A, B, C, D and E in the second row are similarly tested specimens of a siltstone rock.

by development of shear fracture running diagonally at an angle of approximately 45° with respect to the longitudinal axis. The length of the fracture was variable - for example compare specimens 2, 4, 7 and 11 - and occasionally had a strongly curved shape, e.g. see specimens no. 8 and 10. In some cases, the failure was induced by axial splitting along one or more longitudinal cracks (e.g. specimen nos. 5 and 15).

4. Indirect tensile strength (σ_t) of material

Three methods of indirect determination of tensile strength were applied to the model material, namely axial and diametral point loading (on 25 mm D/ 20 mm L and 25 mm D/50 mm L cylindrical specimens respectively) and the Brazilian solid disc (25 mm D/8 mm thickness) method. The detailed results from the tests are given in Table 10 in Appendix I, and the average values are included here in Table 2.4.

Table 2.4

Range of indirect tensile strength values of model material

PP: (B+A+W)	Indirect tensile strength ($_t$), MPa								
	Axial point loading			Diametral point loading			Brazilian Test		
	No.	$\bar{T}_{500}$	std.dev.	No.	$\bar{T}_o$	std.dev.	No.	$\bar{\sigma}_{tb}$	std.dev.
1:15	-	-	-	6	0.103	0.009	5	0.127	.009
1:12	-	-	-	8	0.184	.007	-	-	-
1:10.91	6	.284	.0188	-	-	-	-	-	-
1:9.23	6	.349	.0266	6	0.371	.0353	9	.288	.0354
1:8.57	7	.450	.0199	9	.419	.0195	7	.353	.0261
1:8	7	.488	.0207	6	.469	.0221	5	.403	.049
1:7.5	7	.573	.0197	7	.488	.0371	8	.421	.0298
1:7.06	6	.612	.0216	6	.566	.0089	12	.473	.0418

Depending upon the proportion of plaster to filler and the type of test, the tensile strength ranged between 0.284 - 0.612 MPa (axial point loading, PP:(B+A+S) = 1:10.91 to 1:7.06), 0.103 - 0.566 MPa (diametral point loading,

PP:(B+A+S) = 1:15 to 1:7.06) and 0.127 - 0.473 MPa (Brazilian method, PP:(B+A+S) = 1:15 to 1:7.06).

Comparatively the T_{500} values were the highest and the σ_{tb} from the disc tests were the lowest.
With regard to the Brazilian method, care was exercized to select meaningful results, due to the problems associated with that type of test. Hobbs (1966) described the modes of failure associated with diametral compression of solid discs. Some of the tested model specimens developed wedge-shaped fractures at the loaded ends due to local concentration of compression stresses, which according to Hobbs (1966) may form prior to failure along the loaded diameter. The results in those cases were discarded.

The photograph in Figure 2.14 shows some failed specimens under axial point loading (a) and diametral compression (b). The latter include two examples of the aforementioned wedge-shaped fractures (bottom row).

5. Deformation of the model material under uniaxial compression

The axial deformation of the model material under uniaxial compression was studied by measuring the "shortening" of the test specimens at various load increments, according to the method described in section 3 in Appendix I.

The material exhibited a satisfactory brittle behaviour under compression. The axial strain at failure ranged between 0.33 and 0.4%. The calculated tangent values of Young's Modulus at 50% of ultimate compressive stress were between 316 and 1305 MPa for materials with minimum (PP:B+A+S = 1:15) and maximum (PP:B+A+S = 1:7.06) plaster quantities respectively.
The estimated modulus ratio ($E_{T_{50}}/\sigma_c$) was between 350 and 445.

A family of axial stress-axial strain curves corresponding to materials prepared with various plaster quantities are presented in Figure 2.15. All relevant property values are also included.

(a)

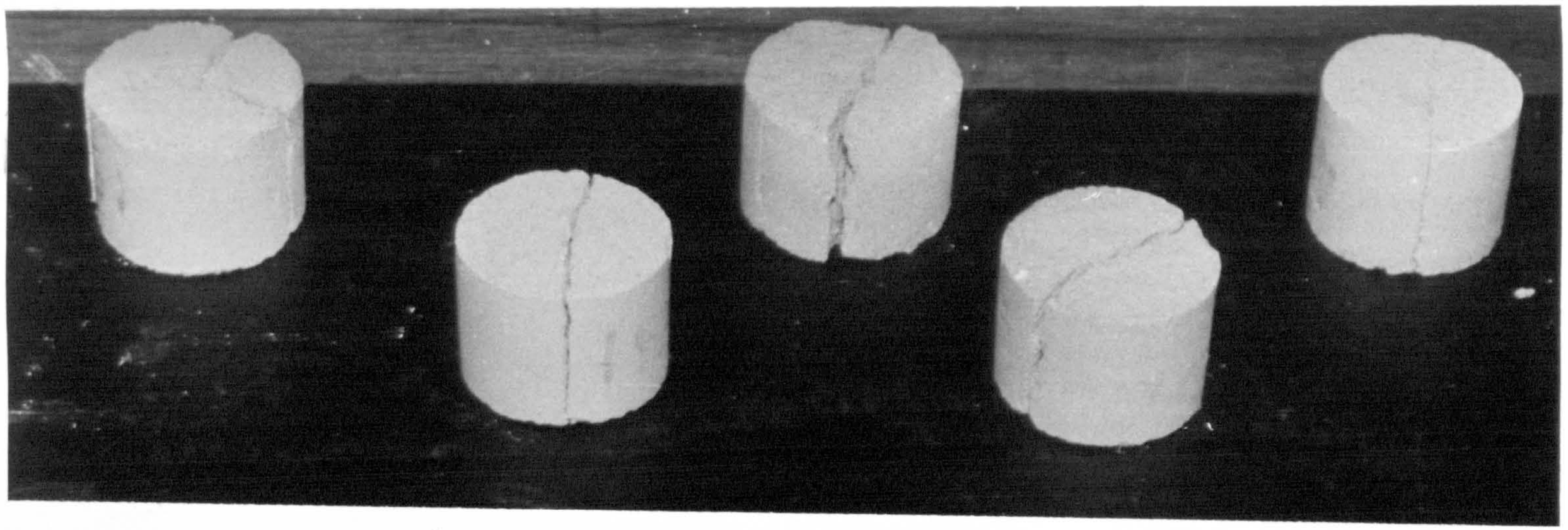

(b)

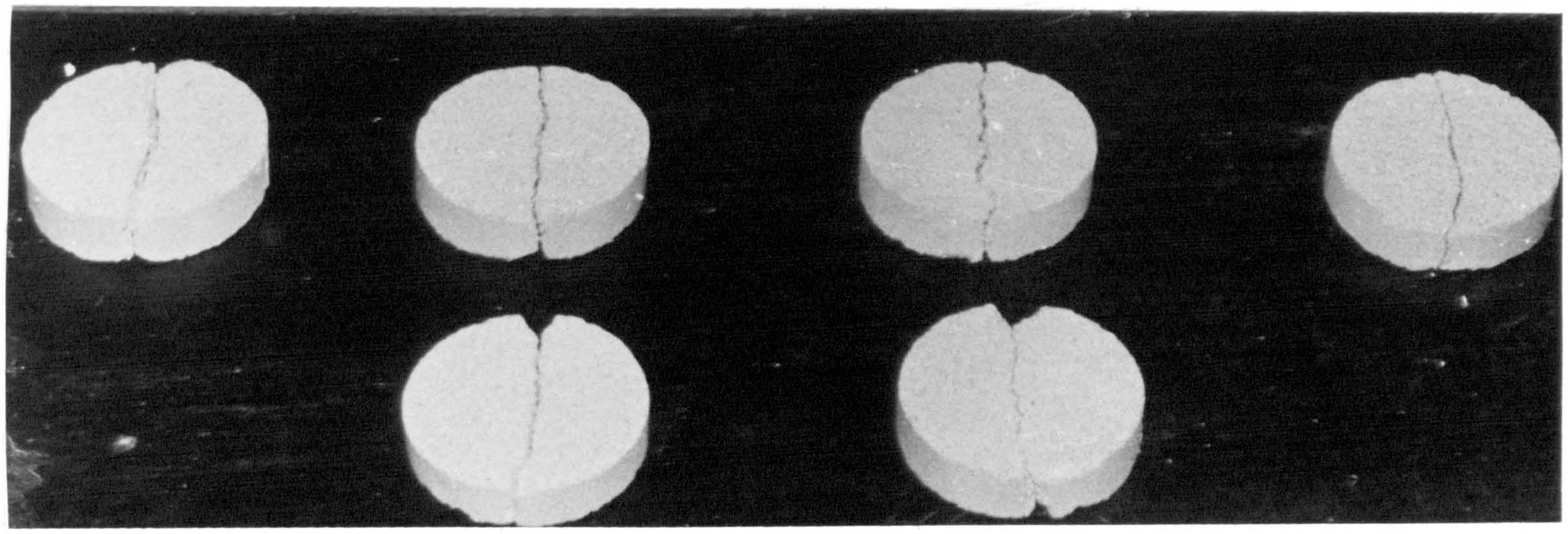

FIGURE 2.14 Photograph showing some model specimens loaded to failure under (a) axial point loading (25mm diameter / 20mm length) and (b) diametral compression (disc diameter = 25mm, thickness = 8mm)

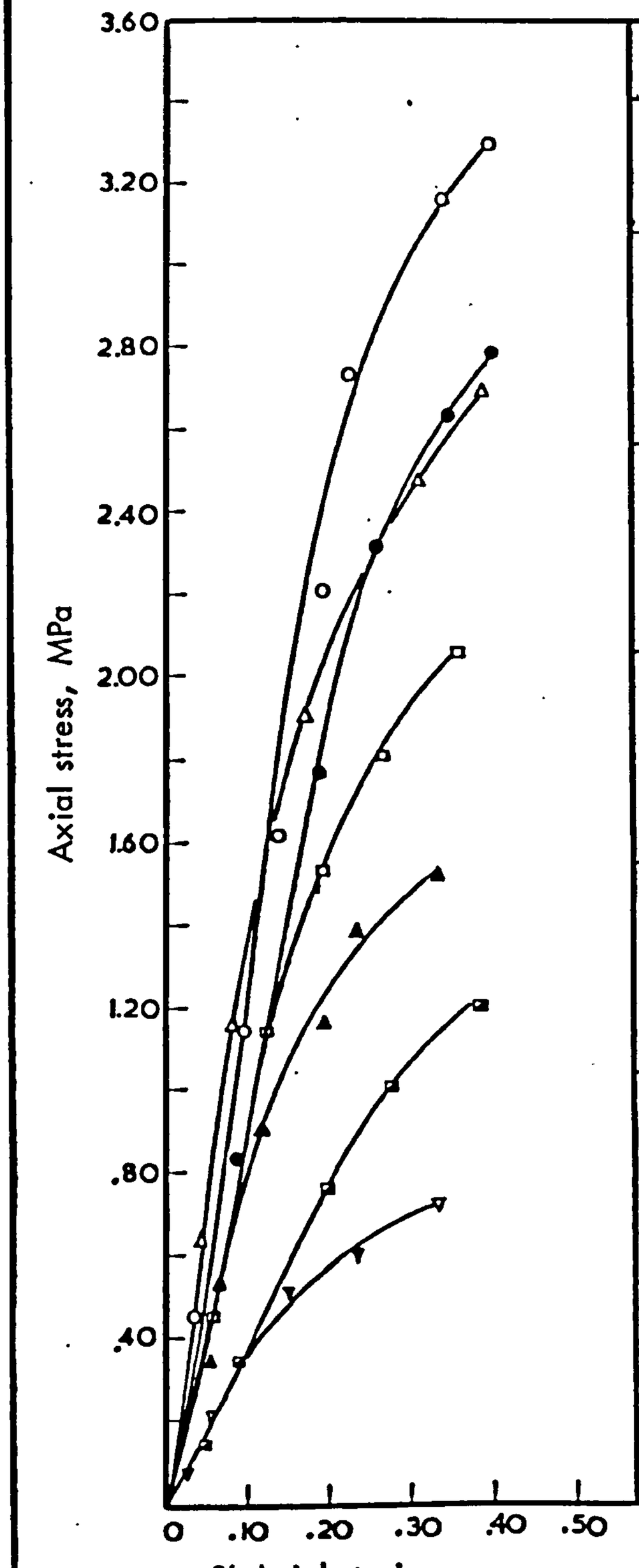

PP : [B•A•W]	σ_c MPa	E_T MPa	E_T/σ_c	% ε_f
1 : 7.5 ○—○	3.305	1305	395	0.39
1 : 8 ●—●	2.784	980	352	0.40
1:8.45 △—△	2.701	1136	421	0.38
1:9.45 □—□	2.059	867	421	0.36
1:10.91 ▲—▲	1.506	668	444	0.32
1:12 ■—■	1.202	425	353	0.39
1:15 ▽—▽	0.710	316	445	0.34

FIGURE 2.15 Axial stress–strain relationships of the model material for different plaster : filler proportions and relevant property values.

2.2.6 Summary and critical evaluation of the behaviour of the model material

The specifications for the design of the model material required in the present study were discussed in section 2.2.3. The tedious experimentation with a variety of components and mixtures resulted in the development of a model material which fulfilled to a satisfactory degree those requirements.

In composition, the final material consisted of silver sand as the frictional filler, barytes as the dense filler, and calcined alumina which played an intermediate role since its grain size and specific gravity were between those of sand and barytes. Plaster of Paris was used as the cementing agent and the quantity of the added water was kept to as low levels as possible.

By appropriate variation of the quantity of plaster and by employing a relatively low curing temperature (50°-55°C) the specified compressive strength for the model material was comfortably achieved, with maximum possible σ_c being 3.455 MPa.

The other two material properties which were thoroughly investigated were the tensile strength and the axial deformation.

The tensile strength (σ_t) of the model material was somewhat higher than that exhibited by many rock types. Despite the improvement that was achieved in the course of the experimental search, the compressive to tensile strength ratio of the final model material ranged between 6 and 7.5, which was below the "target" average value of 10.

However, the above range is not too low to be considered unrealistic, as one can deduce by studying the $\sigma c/\sigma_t$ ratio values of various prototype rocks. From typical compressive and tensile strength data presented by Attewell and Farmer (1976), the ranges of $\sigma c/\sigma_t$ values were derived for some rock types and are given in Table 2.5.

The $\sigma c/\sigma_t$ ratio for the model material appears to agree in general with that corresponding to sedimentary rock types.

Table 2.5

Typical ranges of σ_c/σ_t ratio values for various rock types

IGNEOUS	σ_c/σ_t	SEDIMENTARY	σ_c/σ_t	METAMORPHIC	σ_c/σ_t
Granite	10-14	Sandstone	5-7	Quartzite	10-15
Diorite	10	Shale	2.5-10	Gneiss	10
Dolerite	6.5-10	Limestone	6-10	Marble	12-14
Gabbro	10	Dolomite	2-10	Slate	10-14
Basalt	10-15				

The deformability of the material under uniaxial compression was within the specifications. The % axial strain at failure ranged between .33 and .4 compared to .15 - .40% which is considered as representative for the majority of rock types.

An interesting feature of the uniaxial stress-strain curves (Figure 2.15) was the absence of excessive non-linearity at relatively low stresses, which one might expect in view of the high material porosity (~ 36%). In general the curves showed a more or less linear shape up to approximately $\frac{3}{4}$ of the ultimate stress, from then onwards exhibiting a "strain-softening" behaviour until failure.

In order to relate the deformation characteristics of the model material with those of prototype intact rock types, the values of compressive strength and tangent Young's Modulus were scaled up and plotted in a log-log graph, in accordance to the DEERE and MILLER's system of intact rock classification (Deere, 1974), as shown in Figure 2.16. The regions on the graph enclosed by lines represent data from various prototype rocks. As can be seen, the final model material data fell within the upper half of the average modulus ratio zone ($E_T/\sigma_c \sim 400$), being comparable to those for sandstone and weaker limestone rock types.

The design chart for the model material was produced by plotting the average compressive strength values determined from each set of specimens tested against the respective proportion of plaster-to-(barytes+alumina+sand). The σ_c values showed a linear variation with increasing plaster proportion as shown in Figure 2.17.

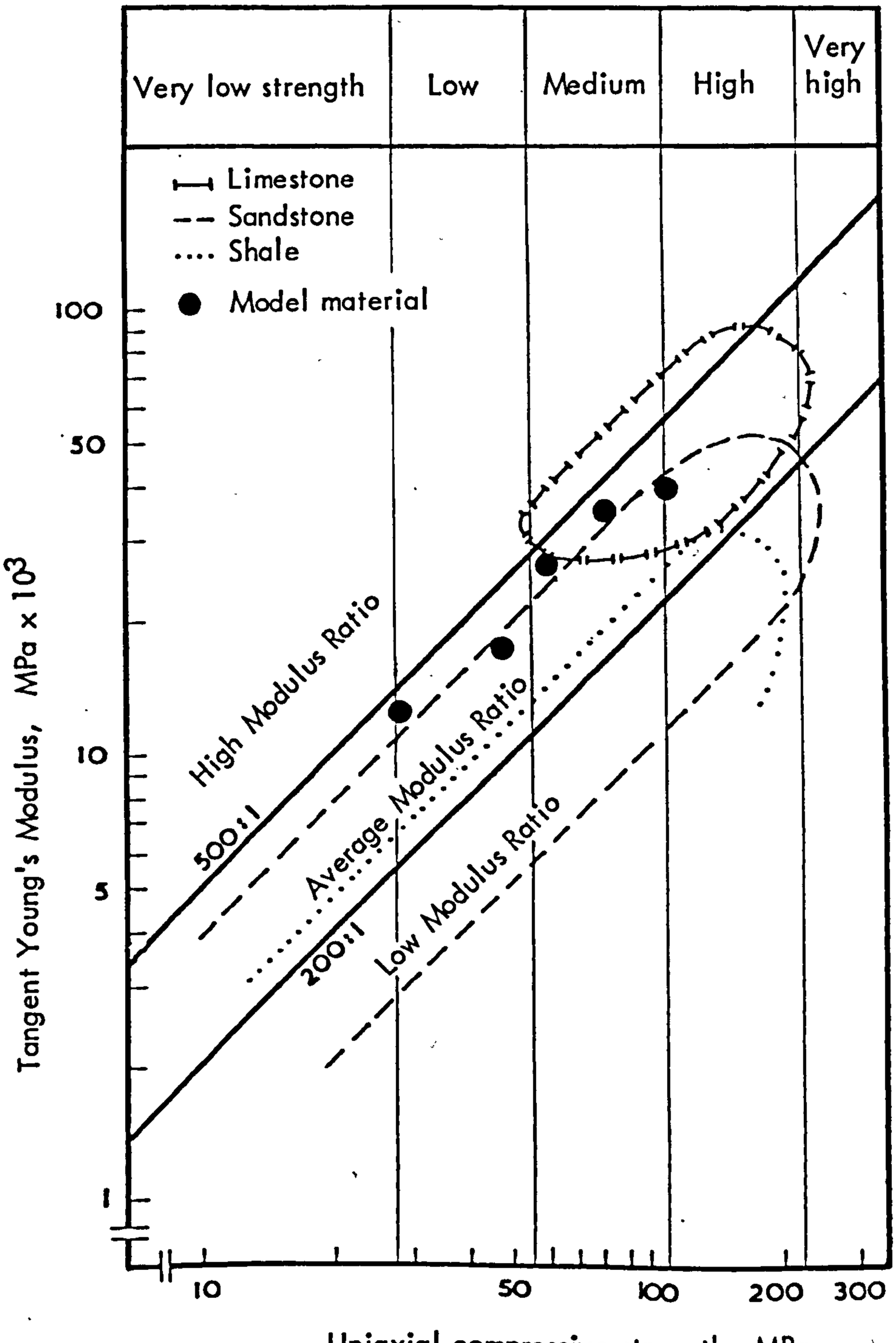

FIGURE 2.16 Relative position of the model materials in DEERE & MILLER'S system of intact rock classification. The rock envelopes were taken from Deere (1974).

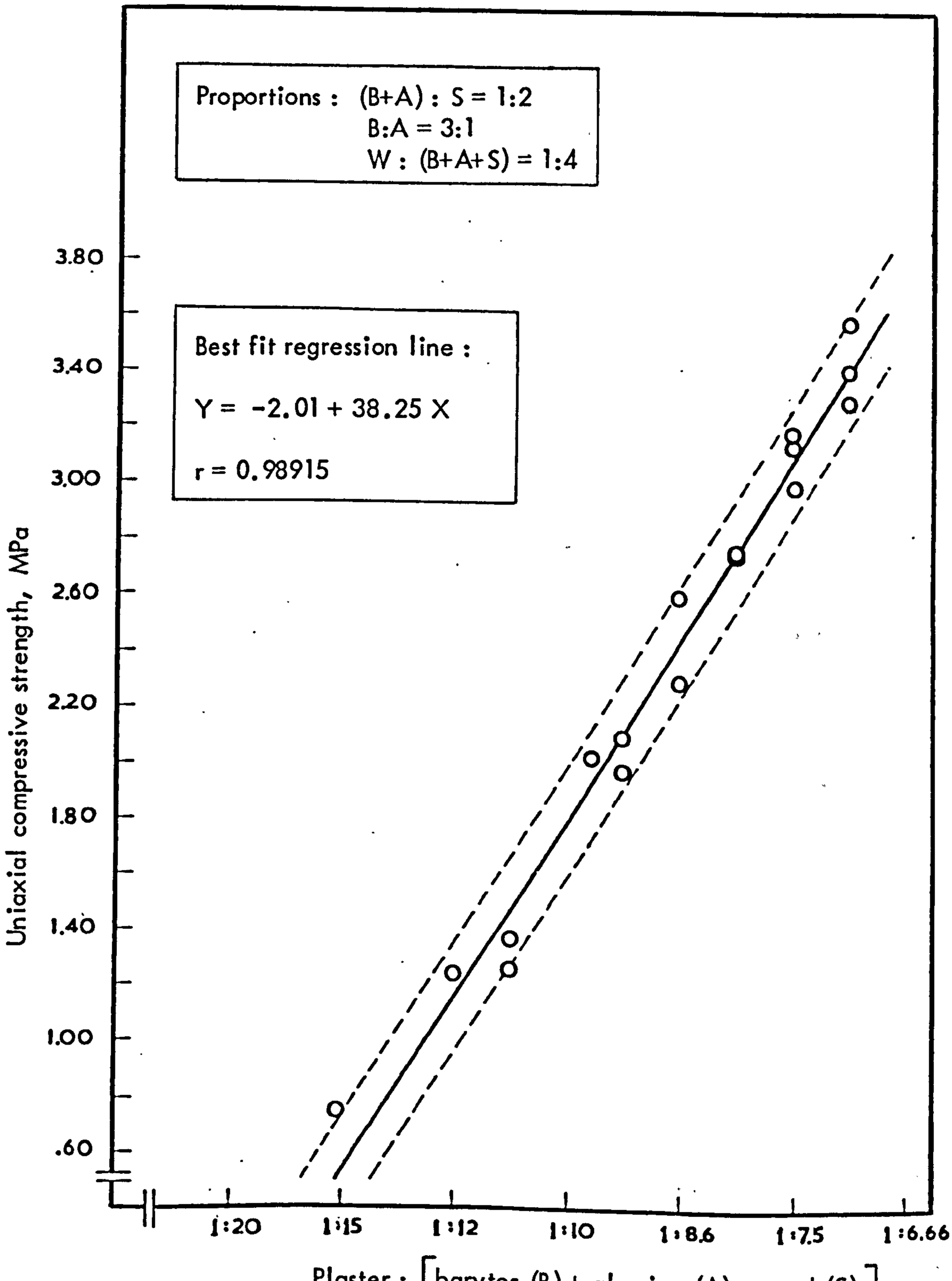

FIGURE 2.17 Design curve for the model material

Linear regression analysis of the plotted data gave the design equation for the model material, which was found to be:

$$\boxed{Y = -2.01 + 38.25\ X\ ,\quad r = +0.98915} \qquad 2.9$$

where: Y = uniaxial compressive strength σ_c , and
X = proportion of PP:(B+A+S).

The above formula 2.9 can be used to estimate the proportion of plaster required for the material to exhibit a desired strength. If, for example, a σ_c of 3 MPa is required, then according to 2.9 the proportion of PP:(B+A+S) should be:

$$X = \frac{3 + 2.01}{38.25} = 0.131 \quad \text{or} \quad 1{:}7.63$$

Therefore, for an amount of 2000 grms of B+A+S the appropriate quantity of plaster would be 262.12 grms. Obviously, the amount of water should also be varied according to the W:(B+A+S) = 1:4 proportional ratio.

The error in σ_{cm} by using the "prediction" formula 2.9 was estimated from:

$$S_{y,x} = \sqrt{\frac{\sum(Y_a - Y_e)^2}{n-2}} \qquad 2.10$$

where $S_{y,x}$ = standard error of regression estimate
Y_a = actual (experimental) Y-value
Y_e = estimated (from 2.9) Y-value, and
n = number of data.

The uncertainty in the value of σ_c by using the predicted amount of plaster is illustrated by the two bands on either side of the best-fit line in Figure 2.17 drawn at a distance equal to 1 S_{yx}. The latter was found to be $\pm$ .130 MPa.

CHAPTER 2.3

PREPARATION AND TESTING OF MODEL JOINTS

2.3.1 Introduction

A brittle model material with realistic rock-like characteristics has been described in Chapter 2.2. That material was utilized to produce model joints by a casting technique.

The nature of the present study dictated that the method of preparation of model joint samples should enable:

(i) production of joints with different surface geometries, and
(ii) exact reproduction of the same surface as many times as required.

Those fundamental requirements were fulfilled by casting the model material against perfect moulds of natural joint surfaces prepared from a high resolution moulding compound. Preliminary shear tests on model joints with various surface geometries revealed that their properties were acceptably comparable, at least in a qualitative sense, with those expected from real rock joints.

A large direct shear apparatus had to be designed and built to accommodate joint specimens of lengths up to 40 cm.

2.3.2 Method of preparation of model joints

A number of techniques have been used in the past to represent joint surfaces with different "morphologies". These include: insertion of various fillers between the planar faces of model bricks (Fumagalli, 1974); use of interlocking teeth joints of different tooth height and baselength (Patton, 1966); use of imbricated surfaces by arranging model bricks at various angles and heights of step (Krsmanovic et al., 1966). In view of the requirements of the present study, the above methods had only an academic interest rather than any practical potential.

A casting technique has been described by Boyd (1975) who used a rubber material to obtain moulds of natural joint exposures. A similar procedure has also been reported by Schneider (1976). Such a technique fitted perfectly with the requirements of the present investigation.

A rubber hot melt moulding compound called VINAMOLD 9525 ("Hard" variety) was used to prepare moulds with negative impressions of natural joint surfaces. The moulding material was chosen for its very high resolution which extended to clear reproduction of very fine scratches on a smooth aluminium sheet. The quality of reproduction of the natural joint surfaces achieved with that moulding compound can be seen in Figure 2.18 where some model specimens are compared with the natural originals. The procedure of mould preparation is described below.

The joint surface to be moulded was at first thoroughly cleaned and was then placed on the bench facing upwards, ensuring that the average joint plane was horizontal along both length and width with the aid of perspex strips and spirit levels. Once the horizontal levelling had been achieved, plaster was used to "fill-in" the gaps between the joint block and the bench, thus ensuring a permanent horizontal orientation, which was necessary for drawing the profiles of the respective surfaces, as will be discussed later in section 2.3.6.

As the selected natural joint specimens had usually a width larger than that required for the model joints, an outline of the selected portion of the surface was drawn. A two-piece rectangular aluminium frame of 4 cm height was carefully fitted over the outline of the relevant area, also ensuring that the four top edges were all horizontal. If the joint surface to be moulded was very rough, the gaps along the contact line of the frame with the surface were carefully "built up" with plaster. For the less rough types plaster was used only externally to "bind" the base of the frame, which formed an outwards facing right angle with the frame wall, with the rock surface.

Once that rigorous procedure of joint positioning and frame installation had been completed, the whole system was transferred onto a hot-plate and warmed to 50^{o} - $60^{o}C$ to avoid rapid cooling of the melted compound (manufacturer's recommendation).

The melting of the Vinamold material was carried out in a progressive sequence as instructed by the manufacturer. The material was firstly cut into small pieces and a small amount was placed in a vessel and allowed to melt at a temperature of $\sim 100^{o}C$. As melting progressed, small quantities were added at a time, and the temperature was eventually increased to $\sim 140^{o}C$. The melting was considered completed when the

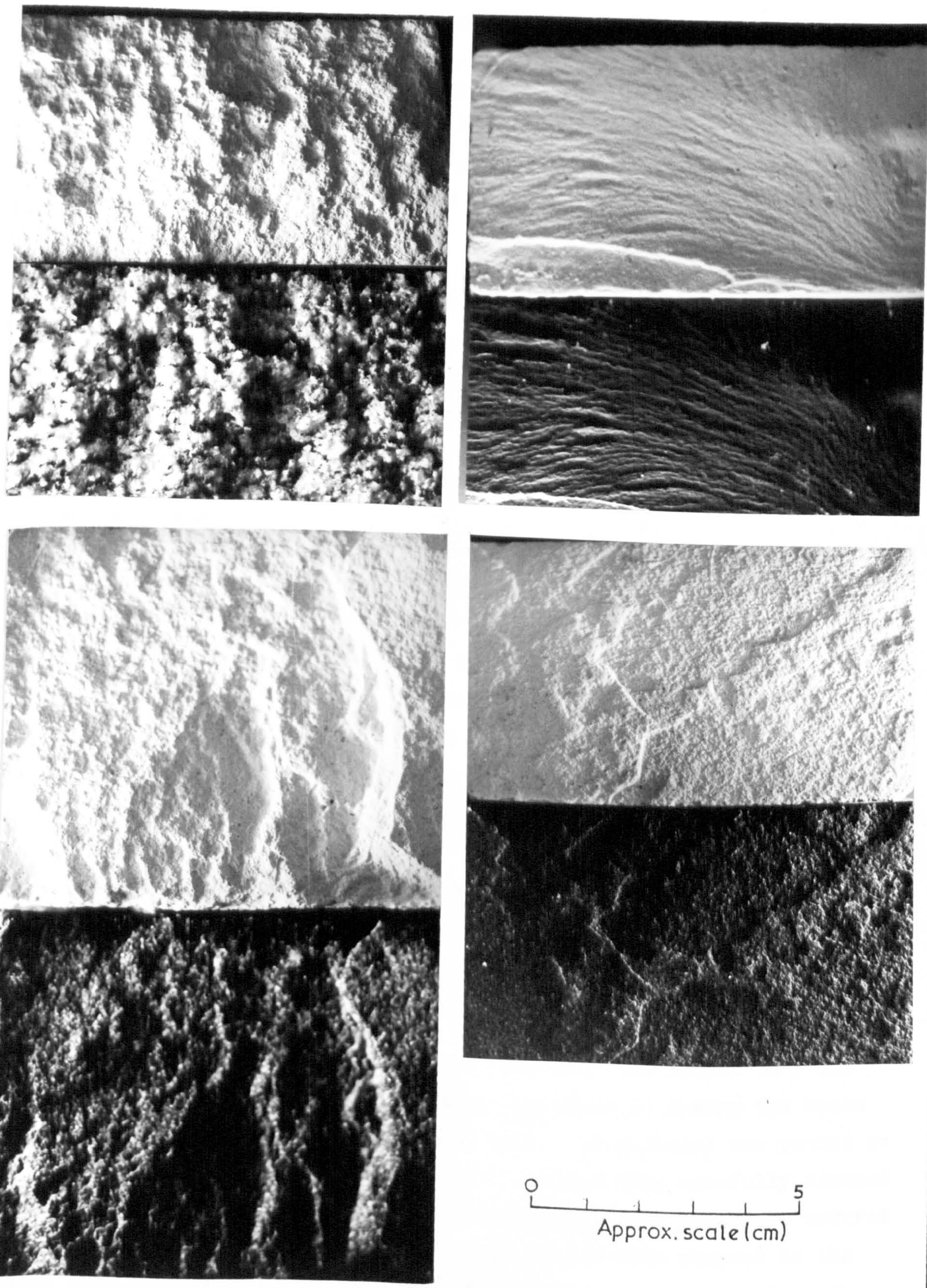

FIGURE 2.18 Photograph illustrating model joint surfaces obtained by casting the model material against rubber moulds of natural joint surfaces.

rubber was a viscous, creamy substance. It was then removed from the hot-plate and left to cool down to 120°C.

The warmed-up joint and frame were then placed precisely on to the same original position, and once the melt had reached the temperature of 120°C it was slowly poured onto the rock surface, until the melt reached the top edge of the frame. The mould was left in place for 8-12 hours before removal.

In order to define precisely the area of the other joint half that should be moulded (as mentioned earlier, in most cases only part of the total joint plane was reproduced), a cast of the first mould was carefully placed on to the corresponding portion of the second half to find the exact interlocked position. An outline of the mating portion on that joint plane was then drawn and the second mould was prepared in the manner already described.

Once the moulds were ready, casting of the model joints was a simple matter. The moulds were placed on a horizontal glass plate and were enclosed in accurately cut aluminium frames whose base also rested on the glass plate. The top edges of the frames defined a horizontal plane parallel to the base of the mould and the average plane of the joint surface and offered a constant reference for the preparation of different sets of model specimens. The height of the walls of the frames which were used for specimen casting was from 6.5 to 10 cm and the choice was based on the intended use of the casts. For example, when the cast was to be cut into 6 cm length specimens a thickness of 2 cm for each joint half was sufficient, while for the full scale tests the thickness of each of the halves was 5 to 6 cm.

The model material was poured very carefully onto the moulds to avoid entrappment of air near the joint plane. In order to ensure the bases of all recasts were horizontal, a small amount of material was poured in excess to that required to fill the mould and was then carefully scraped off to the level of the top edges of the frames. That procedure ensured that the relative orientation of the joint planes with respect to the shear force was the same for all specimens from each recast. Once the material had set hard the surrounding frame was removed, and the model specimen could be easily detached from the mould.

Due to the practical difficulties of the collection of large natural joint specimens, two of the collected surfaces did not have a mating second half. In those cases only one rubber mould was prepared while the other half was obtained by direct casting of the model material against the rock surface. In this case an oil release agent had to be used to ease the specimen removal.

The design equation (2.9) for the model material (section 2.2.6 in Chapter 2.2) was used to determine the proportion of plaster-to-filler (= sand+barytes+alumina) required for a material of uniaxial compressive strength of 2.0 MPa. Considering the stress scale factor (ζ) value of 40, the model material represented a prototype rock of σ_c equal to 80 MPa.

A convenient total quantity of components of approximately 4 kgms was mixed each time, according to the standardized blending sequence described in subsection 2.2.4(1) in Chapter 2.2. The "dry" and "wet" mixing period of the components was increased to 8 minutes. Addition of plaster was followed by 1 min and 15 seconds of blending, by which time the mixture had attained the familiar "creamy" consistency.
The quantities of the individual components were: 2000 grms of sand; 750 grms of barytes; 250 grms of alumina; 750 cm^3 of water; 314.4 grms of plaster.
The above quantities gave sufficient material to cast two specimens of 2 cm thickness. An additional quantity of material had to be prepared to "top up" the moulds when specimens intended for full scale testing were being cast (5-6 cm thickness).

Upon removal from the moulds the specimens were placed on a glass plate and left for ~ 8 hours to set at room temperature. At the end of that period they were transferred to the oven (50° - $55^{\circ}C$). After 10 to 12 hours of drying the specimens intended to provide the small joint blocks were removed and cut by using a fine-blade saw. At that stage, the partially cured specimens were hard enough, and hence the risk of accidental damage to any small asperities was minimized.

After cutting, the specimens were put back in the oven and left to dry completely.

In order to standardize the curing procedure in accordance with the specifications set for the model material, a set of block specimens of

dimensions equal to those of the actual models were prepared and cured. The rate of loss of free water was regularly recorded until evaporation apparently stopped. Termination of the free water evaporation was ascertained by performing the simple calculations discussed in sub-section 2.2.5(1) of Chapter 2.2. It was found that both the 6 x 4 x 2 cm and the 12 x 6 x 2.5 cm specimens were completely "dry" after 2 days of oven curing. A drying period of $2\frac{1}{2}$ to 3 days was necessary for the 18 x 6 x 4 cm specimens, while for the largest block (36 x 12 x 5 cm) the curing time was 4 days. At the end of those trials rectangular prismatic specimens cut from each of the cured blocks were point-load tested. The T_{500} values calculated for each set were almost identical ($\overline{T}_{500} = 268 \pm 15$ kPa) and very near to those which had been obtained from the original tests on the model material. The above curing periods were faithfully followed in the preparation of all model joints.

2.3.3 General shear characteristics of model joints

Prior to initiation of the major testing programme, the basic frictional characteristics of the model surfaces were established and a number of direct shear tests were conducted on model joints with a variety of surface morphologies. The purpose of that preliminary investigation was to examine the suitability of the model material and that of the method of specimen preparation for producing joints displaying shear behaviour comparable to that of real rock joints.

1. Basic friction of flat model surfaces

Basic friction represents the minimum (residual) frictional resistance available during sliding of two flat, non-dilatant surfaces. A total of 12 joint blocks were prepared in two separate sets of six by direct casting of the model material against a glass plate on which square frames 6 x 6 x 2 cm were firmly fixed with plasticine.

The specimens were cured in the standard way and then tested in direct shear under normal stresses (σ_n) ranging between 6.8 and 98 kPa (equivalent to 0.2 - 3.5 MPa at prototype scale). The shearing was continued until residual conditions had evidently been reached. The latter required 4 to 5 mm of relative shear displacement. Two tests were conducted under the same normal stress (σ_n) and the average residual shear stresses were plotted against the corresponding σ_n, as shown in Figure 2.19.

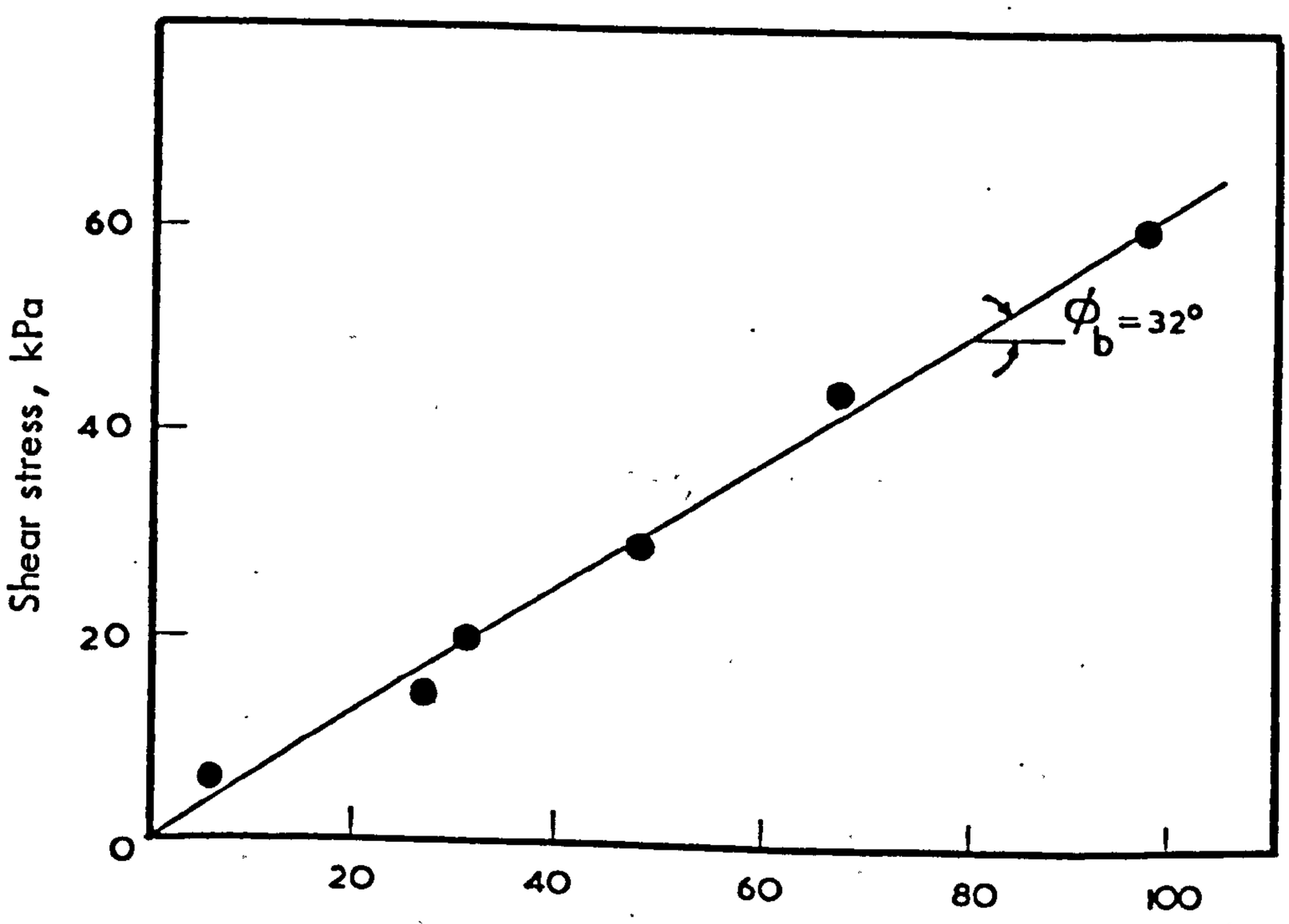

FIGURE 2.19 Residual friction envelope of flat model surfaces

The slope of the average straight line envelope gave an angle of basic friction (ϕ_b) of 32°, which was perfectly acceptable in view of the 25° to 35° range quoted to represent the majority of rock types.

2. Shear strength characteristics of rough model surfaces

Four natural joint specimens with interlocked faces and distinctly different roughness characteristics were selected and their respective rubber moulds prepared. A number of recasts were taken from each mould to prepare four sets of model joints. The size of those specimens was on average 9 x 5 cm, which when interpreted at prototype scale ($\lambda = 30$) represented joints of 2.7 x 1.5 meters. A characteristic profile from each of the four types of model joints is shown in Figure 2.20. The strength of the model "intact" material was 2.0 MPa, which was equivalent to a prototype rock of σ_c = 80 MPa. The various specimens of the same surface recast were tested under normal stresses ranging from approximately 1 to 100 kPa. That range corresponded to prototype σ_n between 0.04 to 4.0 MPa.

The various shear strength characteristics displayed by the model joints are discussed below.

(a) Shear stress (τ) - shear displacement (d_h) relationships

The τ vs d_h diagrams obtained from the four types of model joints showed clearly the sought after "unstable" mode of failure which is characteristic of interlocked natural joints. A sharp increase in the shear stress preceded mobilization of the peak shear strength, which occurred after displacements of approximately 0.5 to 0.8 mm, was followed by considerable strength loss, particularly in the cases of the rough joints.

Some characteristic examples of the τ -d_h relationships displayed by the four models are presented in Figure 2.20, where each family of four curves corresponds to the four model surfaces tested under the same normal stress.

The basic features of rock joint behaviour are qualitatively expressed by the diagrams in Figure 2.20. Under the same level of normal stress the shear strength of the model joints was clearly a function of the surface roughness, while an appreciable increase in the shear strength (τ) of each joint type was the result of application of higher normal stress.

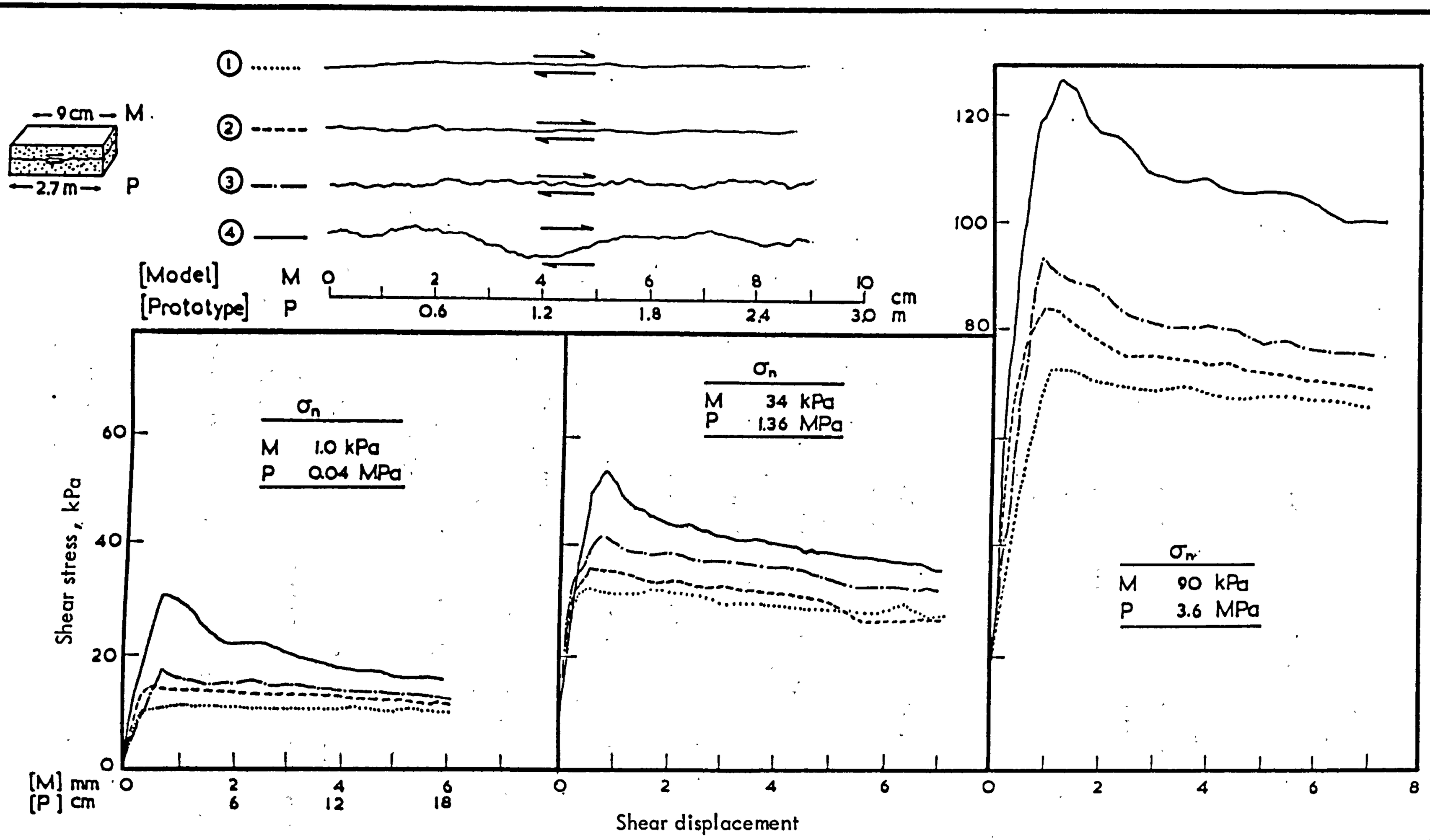

104

FIGURE 2.20 Shear stress–shear displacement diagrams of model joints with different surface roughness at three levels of normal stress(σ_n)

(b) Dilation characteristics of the model joints

The amount of dilation of a rock joint sheared under normal stress σ_n depends upon the roughness of its surface, and the value of the dimensionless ratio JCS/σ_n, where JCS is the joint compressive strength.

The distinct differences in the surface morphology of the above four types of model joints offered an ideal opportunity to examine the dilation effect. From measurements of vertical displacements taken during the tests the vertical vs horizontal displacement diagrams were drawn for each type of model joint under various levels of normal stress. The dilational behaviour of the model joints resembled very realistically the pattern one would expect from real joints, as illustrated by the two diagrams in Figure 2.21 .

Figure 2.21(a) illustrates a family of dilation curves (i.e. vertical (d_v) vs horizontal (d_h) displacement) corresponding to the four types of joints tested under the same normal stress (σ_n = 24 kPa). In that case, the dilation was a function of the geometry of the surface, as for example described by Barton's joint roughness coefficient (JRC). The derivation of the JRC values will be described in the following subsection. The important feature of the curves in Figure 2.21(a) is the distinct increase in the dilation of the joints with rougher surfaces.

A better illustration of the realistic behaviour of the model joints is presented in Figure 2.21(b). The peak dilation angles $(i)^o_p$ were derived from the slope of the appropriate portion of the dilation curves (i.e. corresponding to peak shear displacement) and were plotted against $\log \sigma_n$ for each of the four types of model joints. The expected inverse proportionality between $(i)^o_p$ and σ_n is clearly demonstrated together with the obvious effect of surface roughness.

(c) Peak shear stress (τ_p) - normal stress (σ_n) relationship

The non-linearity of the peak shear strength envelopes of rock joints has been discussed in Chapter 1.1.

Plots of the peak shear strength (τ_p) data from the tests on the model joints against normal stress (σ_n) revealed a realistic deviation from a linear relationship.

The peak shear strength criterion of Barton (1973) was found to fit the plotted data very well, allowing for experimental scatter.

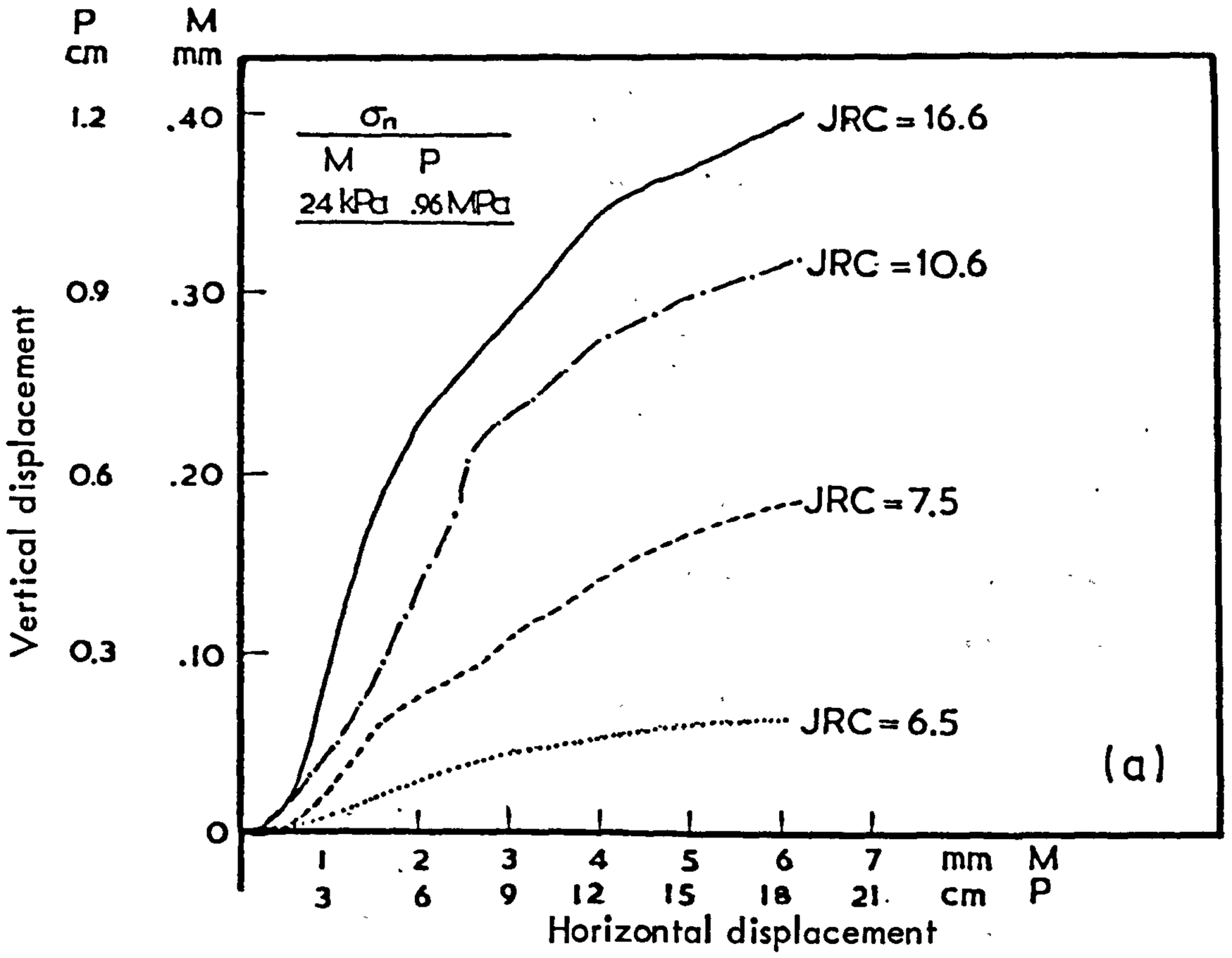

Dilation curves of model joints with different surface roughness sheared under the same normal stress

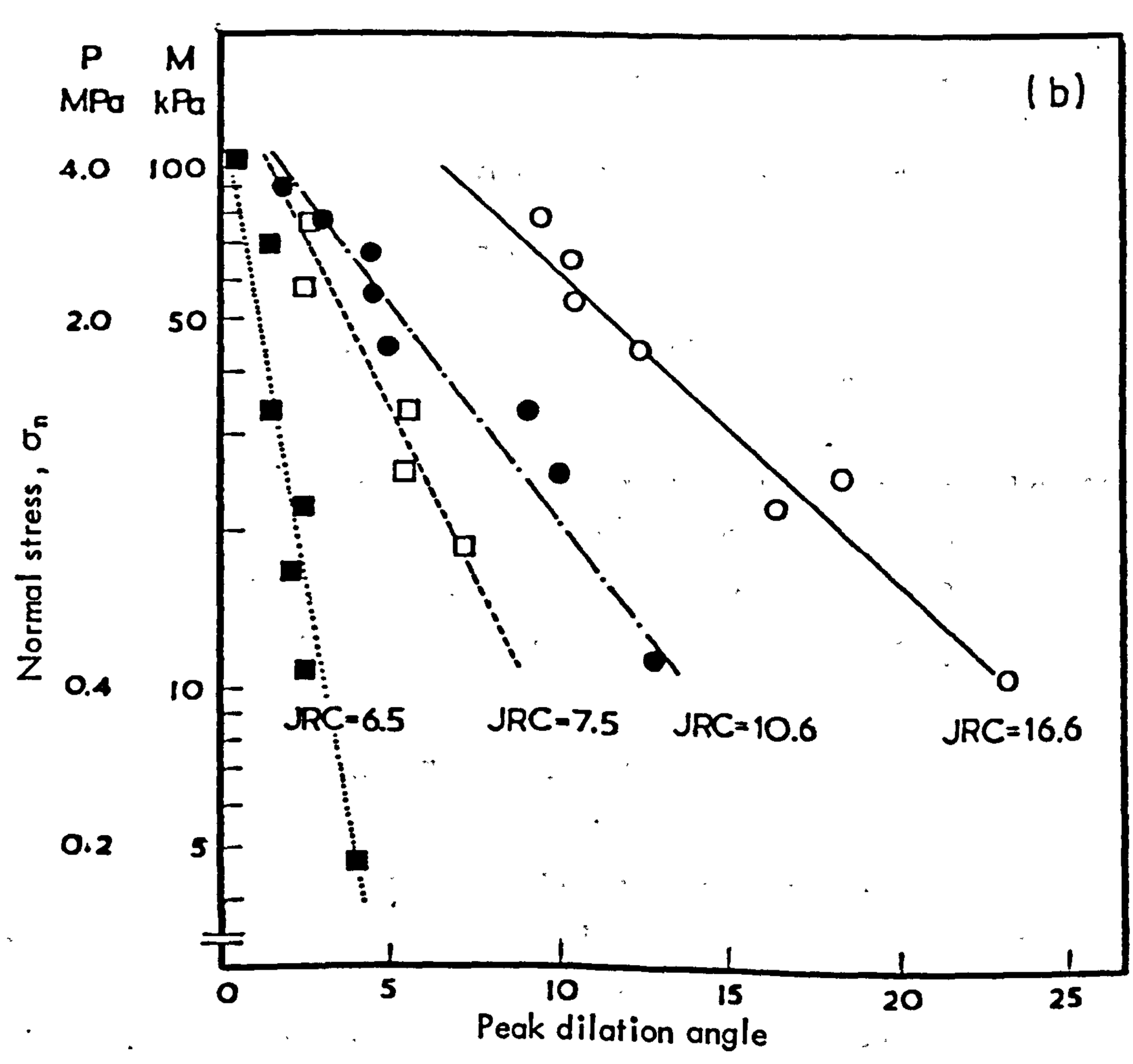

Relationships between normal stress and peak dilation angles of model joints with different surface roughness

FIGURE 2.21

The Joint Roughness Coefficient (JRC) corresponding to each of the four model types was found by solving Barton's equation (2.12) for JRC:

$$JRC = \frac{\text{peak arctan } (\tau/\sigma_n) - \phi_b}{\log_{10}(JCS/\sigma_n)} \qquad 2.11$$

The following input data was used in equation 2.11:

peak arctan (τ/σ_n) = average of the values measured from two shear tests under two different levels of normal stress

$\phi_b = 32^o$

JCS = 2000 kPa

σ_n = mean value applied in the two shear tests.

By substituting the data in 2.11 the following values were back calculated for each type of joint:

$JRC_1 = 6.5$, $JRC_2 = 7.5$, $JRC_3 = 10.6$ and $JRC_4 = 16.6$

Note that the subscripts correspond to the joint numbers in Figure 2.19.

By using the relevant values of the three constants JRC, JCS and ϕ_b in

$$\tau = \sigma_n \tan \left[JRC \log_{10}\left(\frac{JCS}{\sigma_n}\right) + \phi_b \right] \qquad 2.12$$

the corresponding peak shear strength envelopes were established for the appropriate range of normal stress, as has been recommended by Barton and Choubey (1977). The realistic agreement between the envelopes fitted by using 2.12 and the experimental data is shown in Figure 2.22.

2.3.4 The quantitative relevance of model joints to prototype rock joints . . .

The preliminary investigation on the shear properties of the model joints revealed a realistic performance at least from a qualitative standpoint. It is pertinent, however, to consider what might the quantitative relevance be between the shear properties of model joints and those of natural joints.

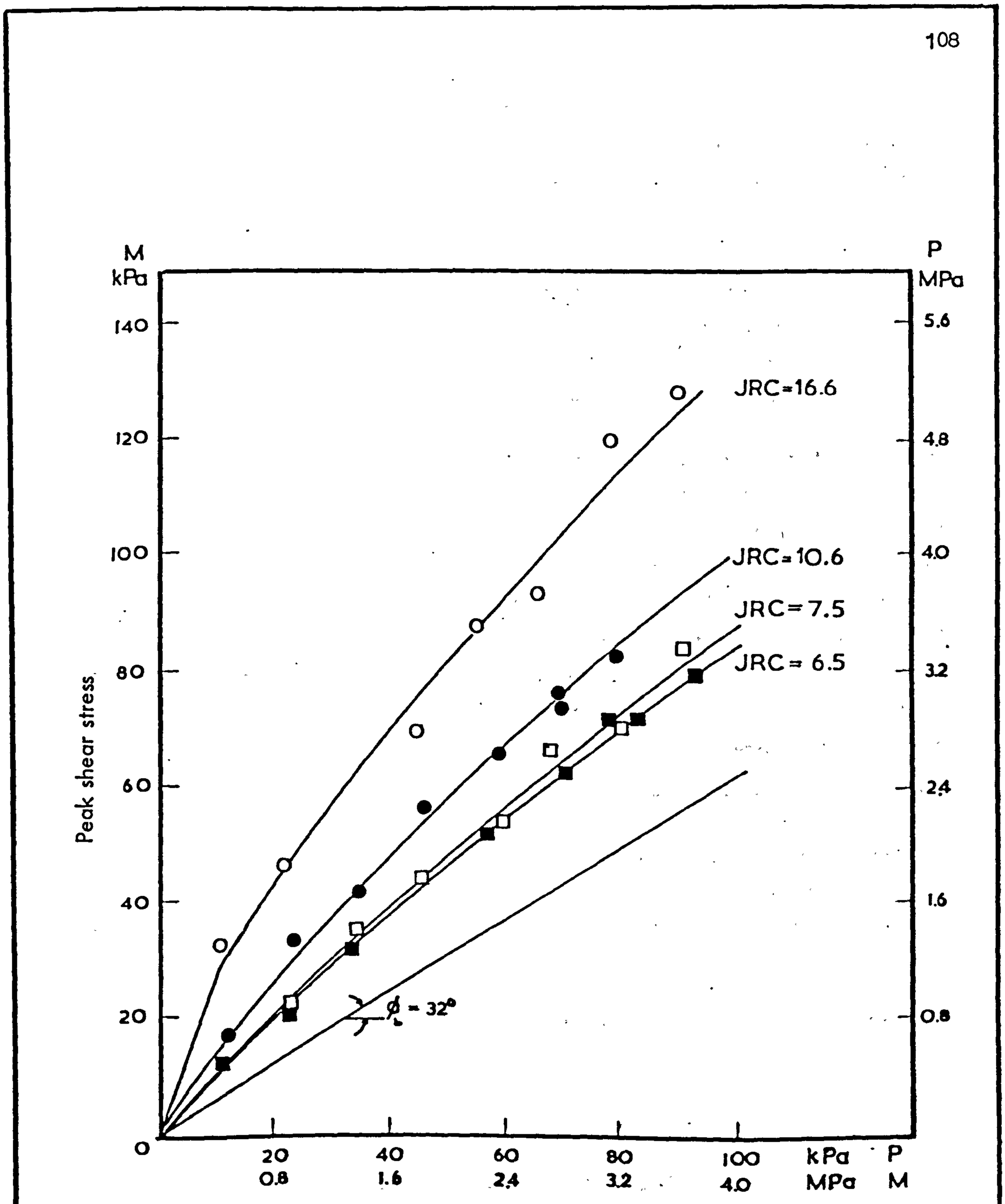

FIGURE 2.22 Peak shear stress – normal stress relationships of model joints. The envelopes were fitted using Barton's criterion

As has been referred to in section 2.2.2, the basic laws of model-prototype simulation can in principle be extended to relate the properties of a prototype joint and those of a model. The geometric scale factor (λ) can be used to convert all model characteristics with dimensions L at prototype scale, whilst the stress scale factor (ζ) can be used similarly to extrapolate all model properties with specific force dimensions. According to the same principles all dimensionless quantities such as peak and residual angles of friction, peak dilation angle etc. should be the same for both the model and prototype.

The inherent "weakness" of model discontinuities arises from the problem of geometrical simulation of the surfaces of prototype joints. It can be seen that in most model studies of jointed rock masses that are found in the literature, blocks with flat faces are being adopted for an over-simplified simulation of the prototype joints (e.g. Reik and Teutsch, 1974). In other cases extension fractures have been used (Barton, 1971) and despite the more positive nature of such an approach (i.e. inclusion of the important effect of joint roughness upon the performance of the rock mass), the problem immediately posed is that <u>conversion of the model roughness into prototype dimensions may lead to an exaggerated surface morphology</u>. Consequently, one might expect that the various shear property values derived from model joints would be <u>higher</u> than those of the same properties of a natural discontinuity. Such an effect would obviously be enhanced in cases of very rough model joints and high geometric scale factors.

The resemblance of the surface morphology of the eleven joint types included in the present study to that found in large natural joint exposures is considered later in section 2.3.6.

2.3.5 <u>Experimental procedure and instrumentation</u>

Each of the eleven types of natural joint surfaces chosen to be tested was reproduced in four models, three of which were subsequently cut into a number of smaller interlocked block elements to obtain "jointed" models with different "joint spacing" or average block size. An example of a complete set of specimens is shown in the photograph in <u>Figure 2.23</u>.

Each joint block was individually tested in direct shear under constant normal load , i.e. "unrestrained" dilation. The conventional testing

FIGURE 2.23 Photograph showing subdivided and full size samples of the same model joint (No.7 in Fig. 2.28)

facilities available could not accommodate specimen sizes larger than 10 to 12 cm long and consequently a large shear apparatus had to be designed and built for testing joints up to 40 cm long. Reference to the testing arrangements will be made after a brief discussion on the principles of direct shear testing.

The direct shear test constitutes the most commonly used method for the determination of peak and residual shear strength along rock discontinuities. The conventional test set-up involves alignment of the joint plane, as closely as possible, with the line of action of an externally transmitted tangential force and applying a normal load at the centre and vertical to the shear plane.

Despite the apparent simplicity of the method a careful insight will reveal that the above testing arrangement induces a complex stress distribution within the sample. On a strict theoretical basis such complexity apparently produces uncertainty as to the validity of the concept of average stress distribution along the shear plane assumed for all intents and practical purposes. Discussions on the patterns of distribution of the normal and shear stresses along the shear plane in both laboratory and in-situ testing have often appeared in the rock mechanics literature (cf. Ruiz et al., 1968; Lajtai, E.Z., 1969; Goodman, R.E., 1970; Jaeger, J.C., 1971; Kutter, H.K., 1971; Rocha, M., 1974; Schneider, H.J., 1978).

Schneider (1978) described the basic concepts regarding the force transmission in direct shear test samples and his relevant schematic illustration is shown below, where the sample has a longer lower portion as compared to the upper portion.

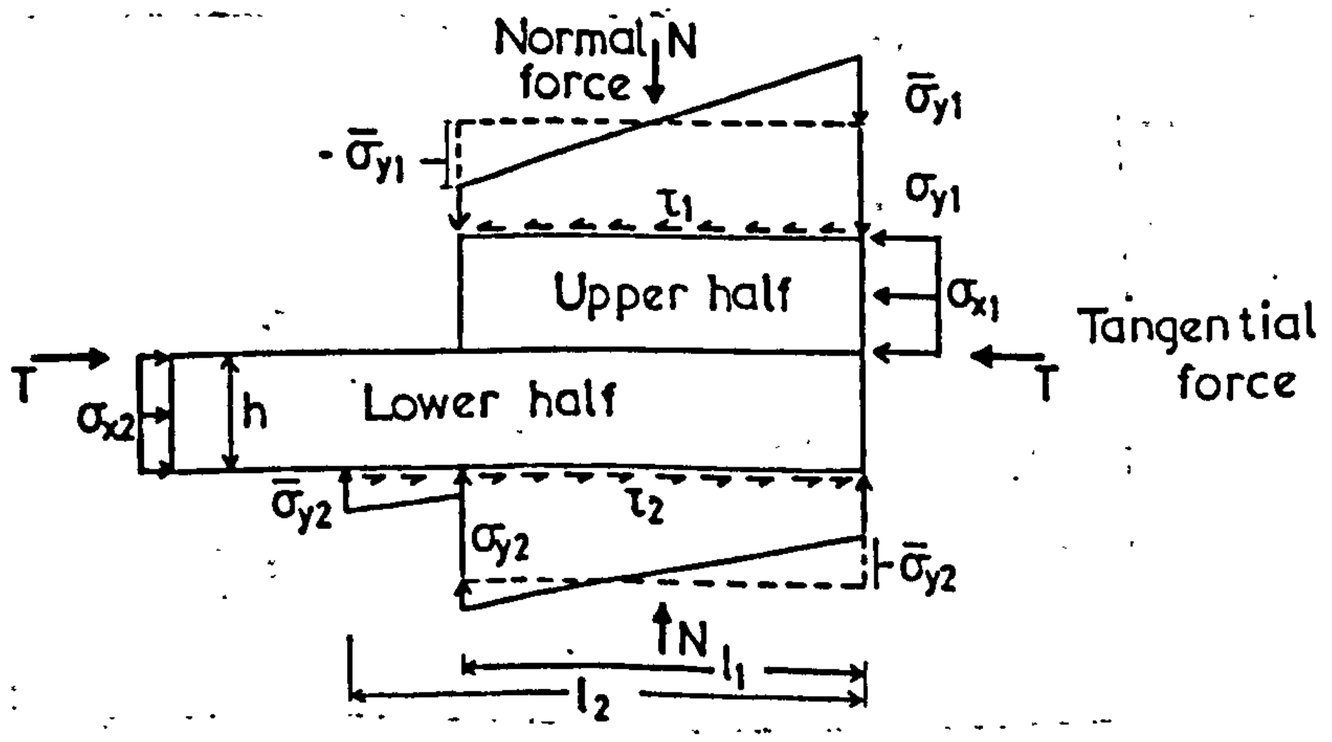

The normal force N produces an average normal stress σ_{Y1} (or σ_{Y2}). The shear force T induces a compressive stress σ_{X1} (or σ_{X2}) on the side walls of the frame, while the remaining part of T is transmitted through the upper and lower frames as τ_1 (or τ_2). Both σ_X and τ contribute to the development of overturning moments which should be balanced by $\pm \overline{\sigma_Y}$. On the basis of the above concepts, Schneider concludes, large stress concentrations would be anticipated near the side boundaries of the sample.

The results from stress analysis by the finite element method conducted by Schneider and others (e.g. Kutter, H.K., 1971, on the 100 ton direct shear apparatus at Imperial College) have shown that the above concepts are essentially correct. Kutter found that the distribution of the shear and normal stresses along a hypothetical shear plane presented with a σ_n peak at either end, whereas the stresses were uniformly distributed over the central 70% of the total plane.

To check the above observations a stress analysis by the F.E. method was attempted on a test set-up resembling the one used in the present study. The element in the two-dimensional F.E. programme used was of the cubic type with two extra nodes per side. The finite element mesh consisted of a total of 140 elements and is shown in Figure 2.24(a) together with the assumed boundary conditions. The relevant input property values for both the reaction frame and the isotropic homogeneous "sample" are also given in Fig. 2.24(a). Normal (N) and shear (T) loads of equal magnitude (= 100) were assumed. The normal (σ_Y) and shear (τ_{XY}) stress distributions along the shear plane (AB) as derived by that analysis are shown in Figure 2.24(b).

A pattern similar to the one mentioned earlier is clearly discernible. The stresses in the central portion are uniformly distributed and compare favourably with those calculated from the external forces and the nominal contact area. On the basis of similar results, Kutter (1971) concluded that use of average normal and shear stresses in the determination of shear strength is a valid procedure. However, one should always bear in mind that any form of analysis that assumes a continuous, isotropic, homogeneous material offers only a crude approximation of the actual conditions which prevail in the complex discontinuous joint system.

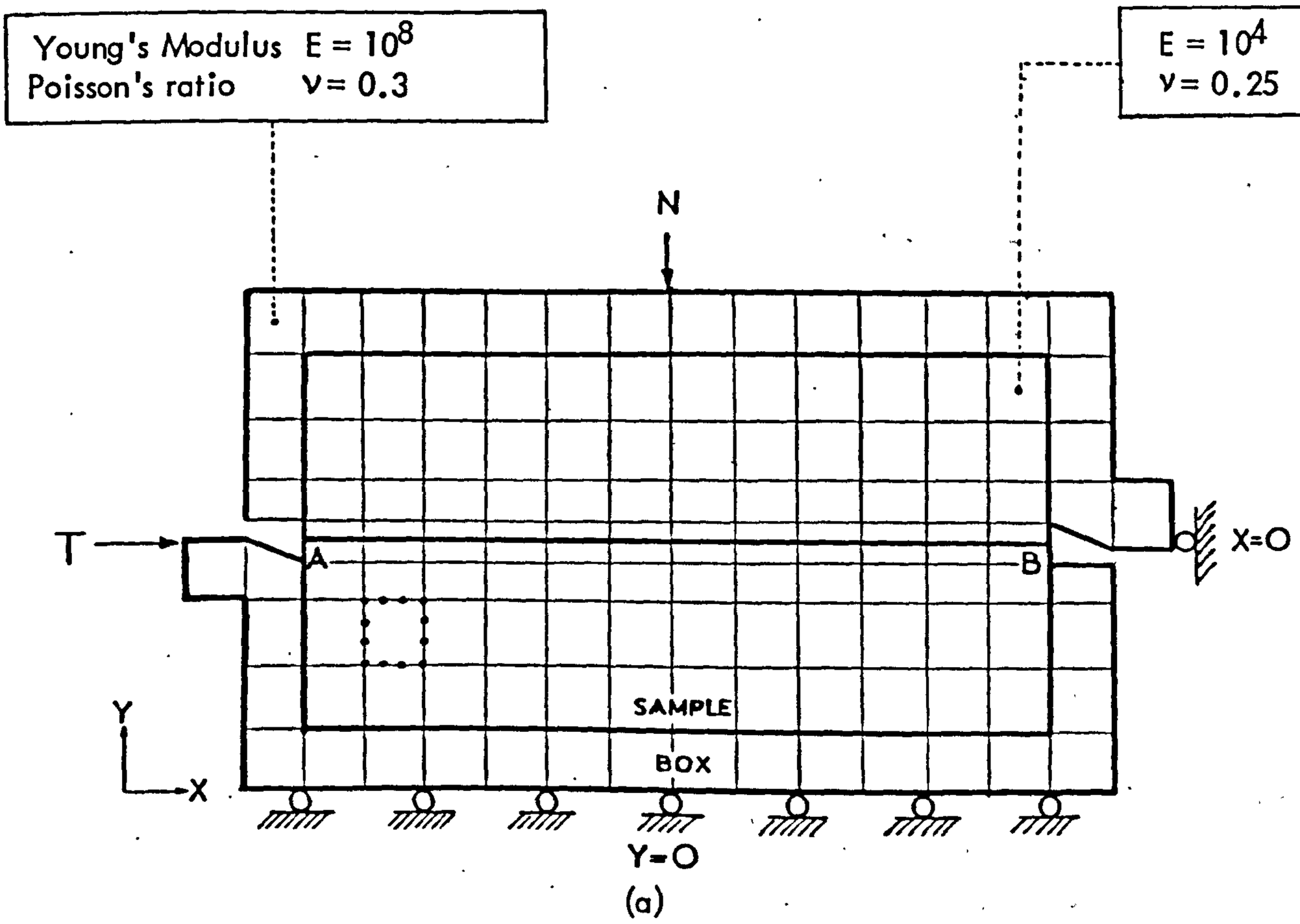

(a)

Two-dimensional finite element mesh and boundary conditions for the stress analysis.

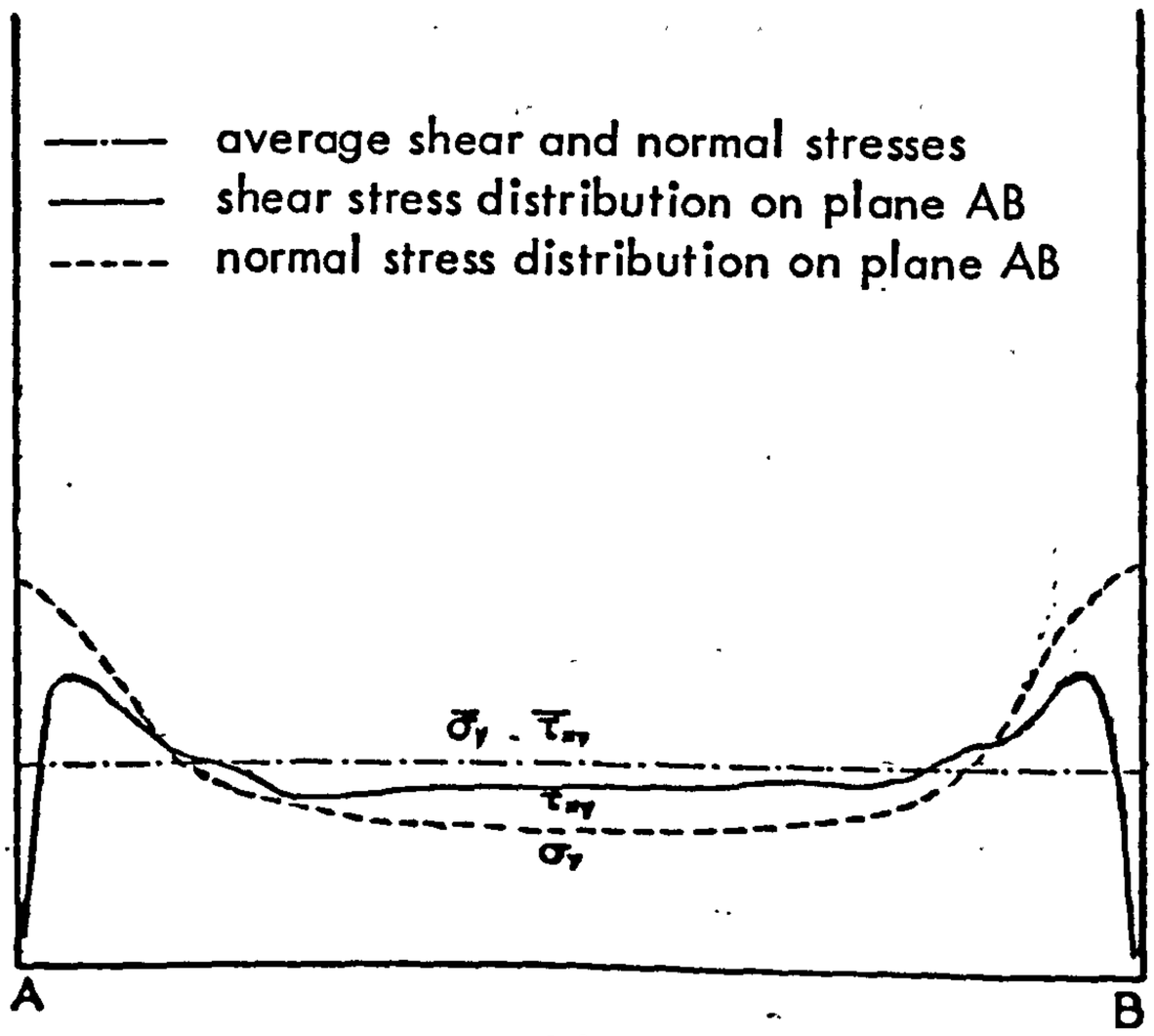

(b)

Shear and normal stress distributions along a shear plane in a continuous isotropic and homogeneous sample. The assumed normal (N) and shear (T) forces are of equal magnitude (= 100)

FIGURE 2.24

From a practical point of view the best precaution that can be taken during testing is to ensure that the shear force is transmitted as near to the shear plane as possible, so as to minimize the risk of excessive overturning moments. That precaution was ensured throughout the testing programme.

Joint blocks with lengths 5 to 12 cm were tested on a Wykeham Farrance WF 25 300 Direct Shear Box apparatus. Use of the conventional boxes for mounting the specimens proved impractical because of the variability of the joint sizes. A range of simple adjustable clamping devices consisting of two rectangular plates of metal connected by threaded rods was prepared. The width of those metal plates was from 18 to 25 mm to allow for the variation in thickness of the joint halves in the length range of 5 to 12 cm. The plates were firmly positioned against the front and back vertical walls of each joint half by tightening the screws of the connecting rods at either side of the specimen. The lower joint half was firmly fixed in place by means of two horizontally aligned bolts passing through the front carriage wall.

The normal load was applied at the centre of the specimen via a pin connected to a x10 lever arm. The shear load was applied by a 300 kgms proving ring. Shear displacements were monitored by a 0.01 mm dial gauge. Vertical displacements were measured by either one dial gauge resting on to the normal load pin (5 and 6 cm specimens) or two gauges positioned symmetrically on either side of the pin and resting on the loading platen (10 and 12 cm specimens). An example of the test set-up is shown by the photograph in Figure 2.25(a).

A large shear apparatus was designed for testing the 36-40 cm long specimens. A minor modification also enabled accommodation of the 18-20 cm long joints.

The machine is basically a large version of the conventional direct shear apparatus , and its design was based on the simple principle of applying a shear force at constant rate under constant normal load. The various parts are bolted or welded onto a rigid 2.0 x 0.3 meters base. The shear motionis transmitted by a horizontal shaft powered by an electric motor via a worm and wheel arrangement; the force (T) is applied by a proving ring. The sliding table (56 x 30 cm) rests on low-friction ball bearings and has a free movement of approximately 4 cm. The normal load is applied either directly by a vertical hanger or by using a x5 lever arm.

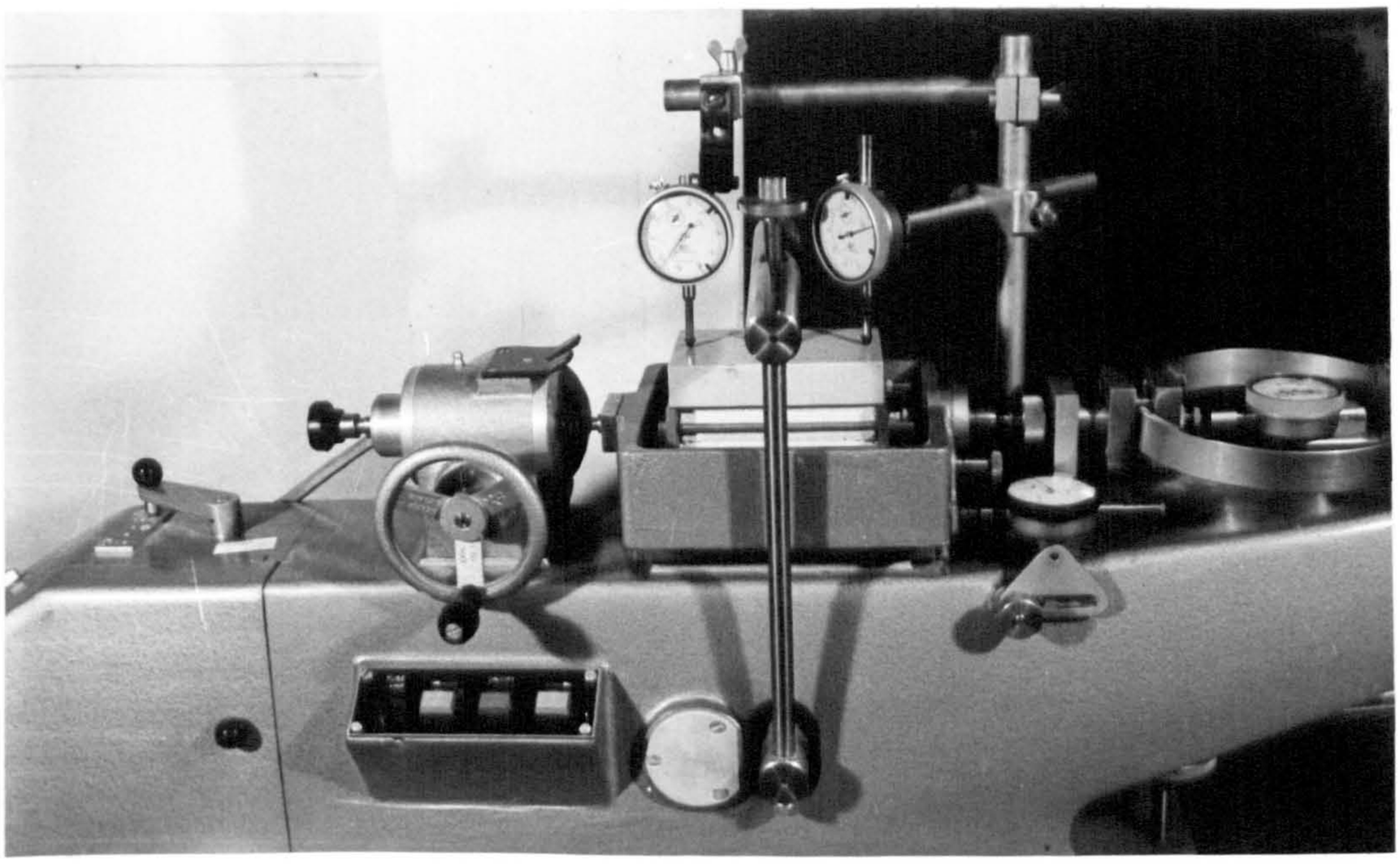

FIGURE 2.25 (a) Direct shear test arrangement for model joints 5-12 cm long

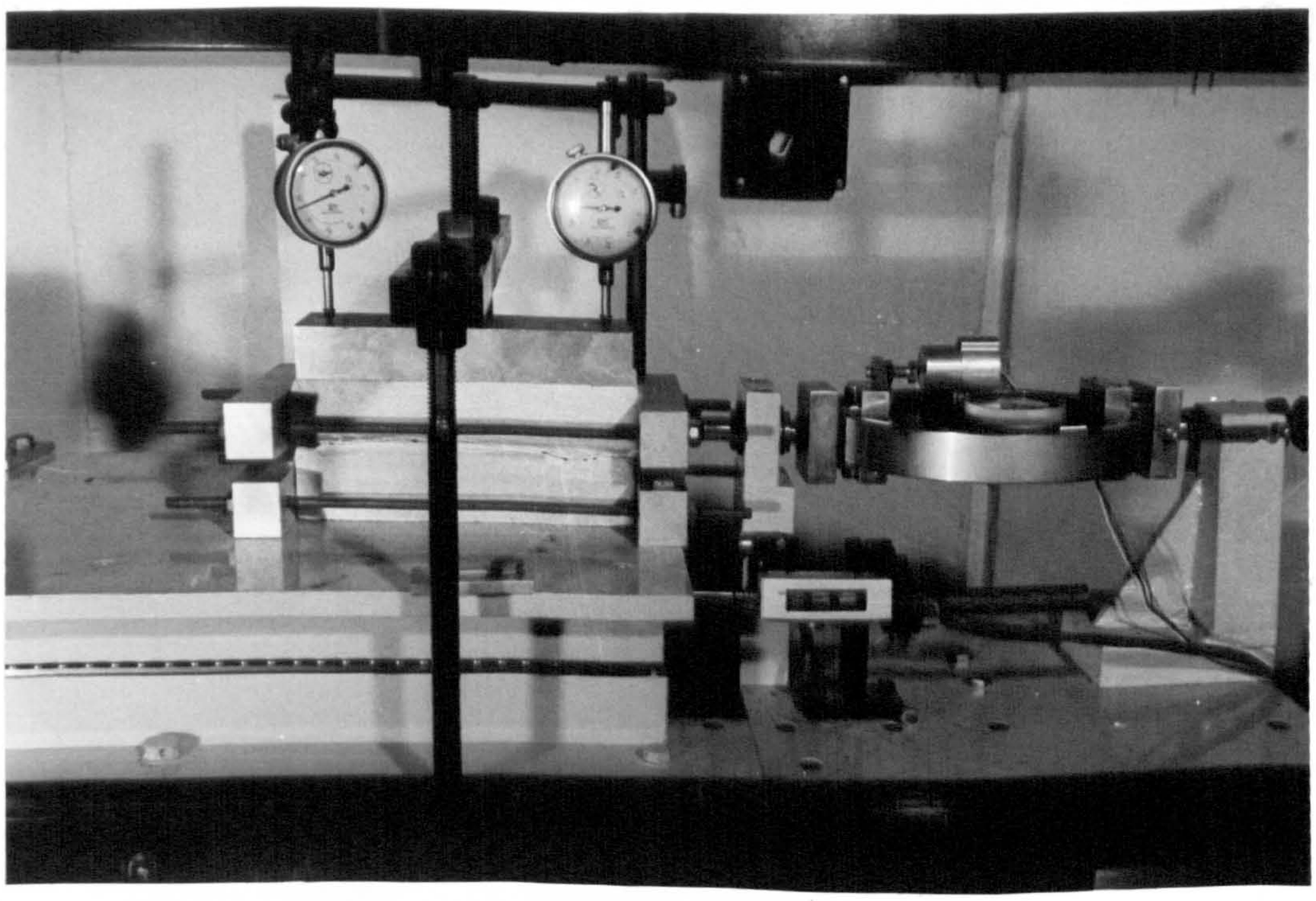

FIGURE 2.25 (b) Direct shear test arrangement for model joints 18-20cm long

Adjustable reaction frames consisting of four interbolted sides were used to enclose the two joint halves. The vertical distance between the sliding plane and the spindle of the proving ring was adjusted to 5 cm to coincide with the thickness of the bottom joint half. Dilation measurements were taken from two dial gauges positioned symmetrically near the two ends of the specimen. Provision was also made to accommodate transducers for electronic recording of the shear displacement and shear force on a Hewlett-Packard X-Y recorder.

In order to enable testing of the 18 to 20 cm specimens a clamping device similar to the one already described was bolted onto the sliding table near the proving ring. The experimental set-up for the 18-20 cm and 36-40 cm joints testing can be seen in the photographs in Figures 2.25(b) and 2.26 respectively.

The rate of shearing of all joint sizes was standardized to 0.4-0.45 mm/min. At an early stage three tests on 10 cm long specimens with identical surfaces sheared at rates of 0.048 mm/min, 0.4 mm/min and 0.6 mm/min produced practically identical results.

The shear load and vertical displacements were recorded at 0.1 mm "gross" shear displacement interval until peak strength had been passed. That interval was then increased to 0.20 mm and later to 0.50 mm. The "gross" shear displacements were afterwards corrected for proving ring deflection to obtain the true relative displacement between the joint halves.

All joint sizes were tested in the same relative direction and under precisely the same level of normal stress of 24.5 kPa, which corresponds to 0.98 MPa when interpreted at prototype scale.

Repeat tests on separately prepared full size joint specimens were conducted for all the types of surfaces to check on the reproduction of the results. The new specimens gave consistently similar values of peak shear strength but more significantly they displayed almost identical deformation characteristics, i.e. peak shear displacement and dilation. Whenever a discrepancy was observed, a third specimen was tested for comparison and matching with the previous results.

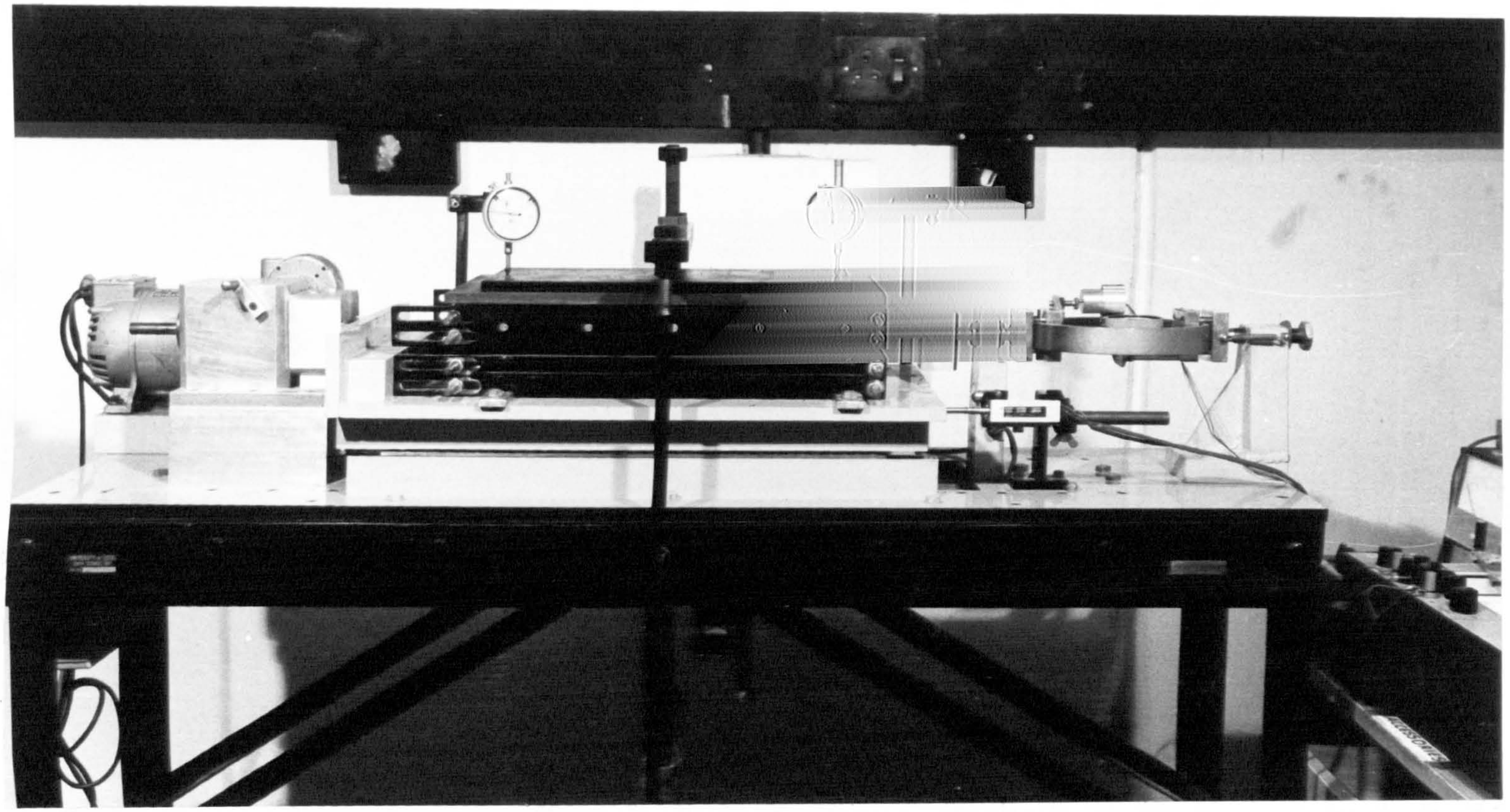

FIGURE 2.26 Direct shear apparatus used for testing large model joints up to 40 cm in length

2.3.6 Description of the types of joints

A total of eleven natural joint specimens were finally selected so that a wide spectrum of surface geometries could be studied, ranging from rough undulating to almost smooth and planar. The "prototype" joints were collected from natural exposures of coarse-grained sandstone, siltstone limestone and a lightly metamorphosed fine grained sandstone. The genetic type of those discontinuities ranged from tension and shear joints to bedding planes. Longitudinal profiles were drawn for each of the joints by the method described below.

The bottom half of the joint was positioned on a horizontal table. As has already been discussed in section 2.3.2 a permanent horizontal reference for the average joint plane was ensured during the moulding procedure. Consequently, the relative orientation of the profiles with respect to an arbitrary horizontal reference was identical (within the range of human error) with that of the model joint specimens when placed on the sliding table of the appropriate shear apparatus.

A set of lines was drawn lengthwise on each joint surface as shown by sketch (a) in Figure 2.27. A 15 cm long Vitrex profile gauge was matched over consecutive sections of the profile lines and the outline was transferred on to tracing paper placed on a perspex slab (sketches b and c in Figure 2.27). A levelling bubble fixed on the Vitrex gauge provided a standard horizontal reference during the profile matching. A line on the tracing paper drawn parallel to the edge of the slab provided a horizontal reference (see line XY in sketch c). The edge of the gauge was aligned with the top end of the perspex slab and the outline was traced using a fine technical pen. All the profiles which are presented later have been normalized to the same horizontal plane. It should also be noted that the wire strands in the profile gauge had an approximately 0.7 mm diameter and hence some very fine details may have not been "picked up".

The variable geometry of the eleven types of surfaces can be seen in Figure 2.28 where a characteristic profile for each of those is shown. The figure also includes information about the type of the "prototype" joints. Model nos. 5 and 6 are the ones for which a mating half had to be prepared by direct casting of the model material against the joint face.

In a brief discussion in section 2.3.4 about the similarity of the scaled-up roughness of model joints to that found on natural joint exposures it was

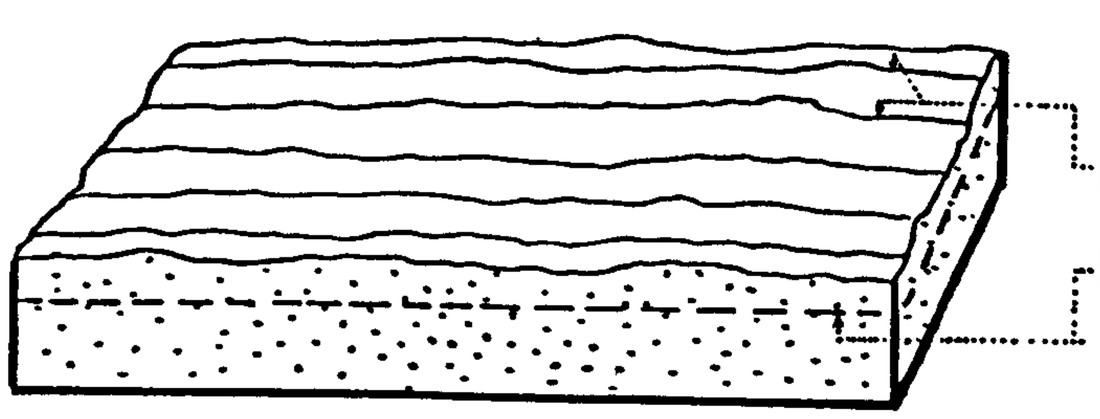

(a)

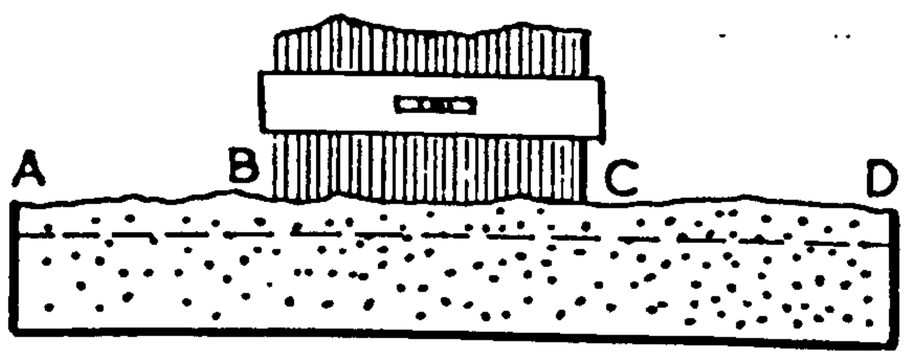

Gauge positioned horizontally over consecutive sections with the aid of a levelling bubble

(b)

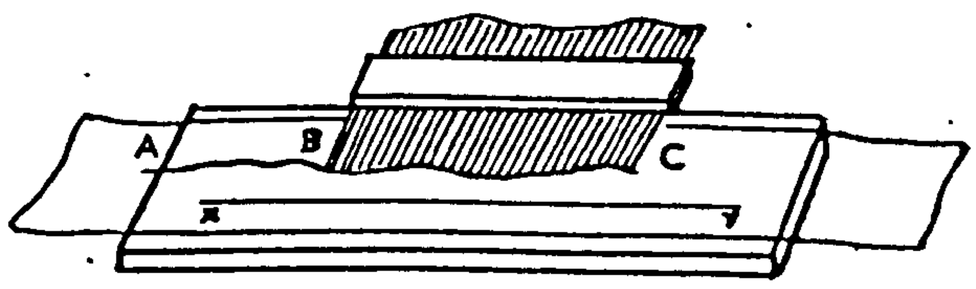

Gauge aligned with edge of the perspex slab

(c)

FIGURE 2.27 Diagrammatic illustration of profile drawing procedure

No.	Surface profiles	Description of "prototype" joint types
1		Bedding planes in limestone
2		
3		Vertical tension joints in siltstone
4	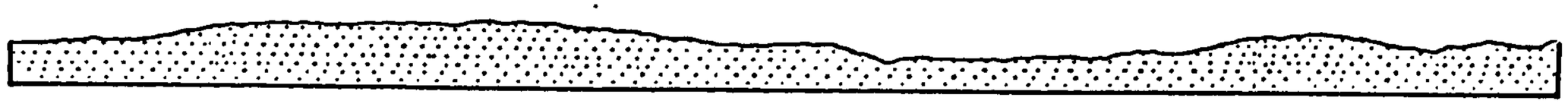	
5	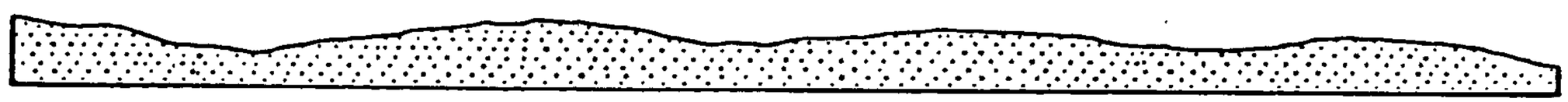	Bedding plane in slightly metamorphosed fine-grained sandstone
6	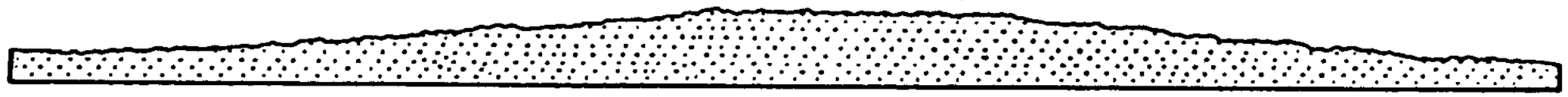	Bedding plane in limestone
7	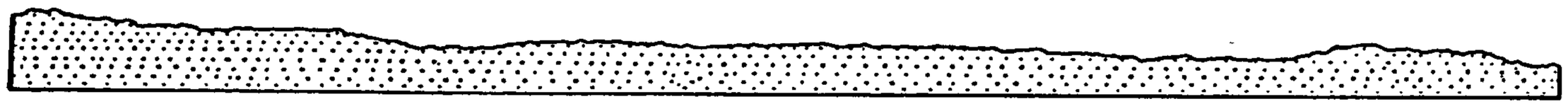	Bedding planes in coarse-grained sandstone
8		
9		Bedding planes in slightly metamorphosed fine-grained sandstone
10		
11	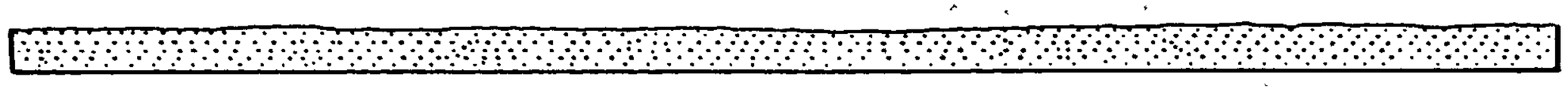	Shear joint in slightly metamorphosed fine-grained sandstone

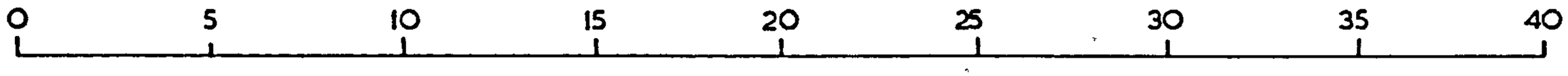

FIGURE 2.28

pointed out that an exaggerating effect might be inevitable, particularly when the model surfaces are very rough and the geometrical scale factor (λ) is large. A similar condition is probably relevant with some of the present rough, undulating joint types (e.g. model nos. 1, 2, 3). Of course, such uncertainties do not involve only the relevance of the vertical roughness amplitude but also the overall roughness when considered in relation to joint length.

In the case of model no. 1 a scaled-up ($\lambda = 30$) average wavelength of approximately 3.5 meters produced an average vertical amplitude of approximately 25 cm. Likewise, the wavelengths on the surface of model no. 2 were between 1 and 3 meters and the corresponding amplitudes ranged between 12 and 20 cm. These ranges are realistic when compared with similar data from the literature. For instance, Mogilevskaya (1974) has reported vertical amplitudes in the order of 9 to 22 cm for wavelengths between 1.45 and 2.40 meters found on joint exposures in limestone and granite. However, the overall geometry of the nos. 1 and 2 joint surfaces is perhaps "too rough" considering their prototype length (~11 meters). A more realistic overall picture is probably presented by joint types such as nos. 6 to 11. In general, the aforementioned uncertainties should always be borne in mind in any form of quantitative extrapolation from model to prototype scales.

CHAPTER 2.4

PRESENTATION AND ANALYSIS OF THE EXPERIMENTAL RESULTS

2.4.1 Introduction

In this chapter the results of the extensive direct shear testing programme are presented and analyzed. The "component" blocks of each subdivided full size joint were tested individually and the results from all specimens within each set were interpreted in a cumulative form.

Increasing size of the individual jointed blocks was found to induce marked changes in the shear behaviour of surfaces with identical roughness. Significant scale effects were revealed in both the strength and deformation characteristics.

2.4.2 Presentation of the results

As stated in section 2.3.5, the direct shear tests on all joint block sizes were conducted under precisely the same level of normal stress (σ_n). The surface area of each individual joint specimen was accurately measured to allow for any minor variations from the expected average joint area which might have been accidentally induced during the block cutting procedure. The individual surface areas were then used to calculate the load required to produce a normal stress of 24.5 kPa which was equivalent to approximately 1 MPa at prototype scale.

The model joint compressive strength (JCS_m = uniaxial compressive strength of model material) was set at 2 MPa for all the types of surfaces tested. Extrapolation of JCS_m in prototype scale ($JCS_p = JCS_m \times \zeta$) gives a value of 80 MPa. The JCS/σ_n ratio value was thus maintained at a constant level of approximately 80 for all joint block sizes.

The results from nearly 400 shear tests have been summarized in Tables 2.6 to 2.16. Each table includes a set of three profiles illustrating the full scale surface geometry of the bottom half of the respective joint type. A plan of the pattern of subdivision of the original joint plane into sets of successively smaller equidimensional samples is shown beneath the profiles.

TABLE 2.6

MODEL No. 1

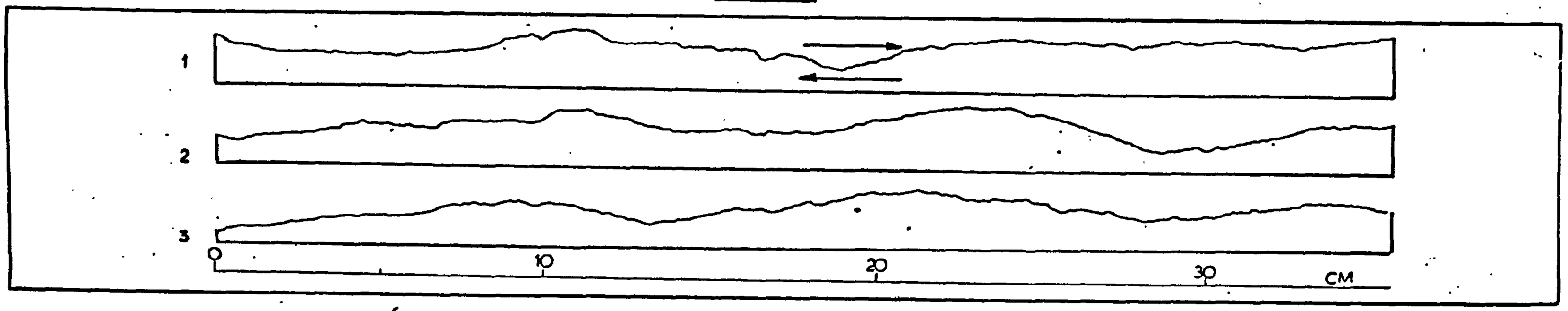

6 cm

1	2	3	4	5	6	4.8cm
7	8	9	10	11	12	
13	14	15	16	17	18	29cm²

12 cm

1	2	3	7.2cm
4	5	6	86cm²

18 cm

1	2	7.2cm
3	4	130cm²

36 cm

1	14.4cm
2	
3	1504cm²

Block No.	d_h (mm)	τ_p (kPa)	$\phi_p°$	Cont. No.	d_h (mm)	τ_p (kPa)	$\phi_p°$	Cont. No.	d_h (mm)	τ_p (kPa)	$\phi_p°$	No.	d_h (mm)	τ_p (kPa)	$\phi_p°$	No.	d_h (mm)	τ_p (kPa)	$\phi_p°$	d_h (mm)	τ_p (kPa)	$\phi_p°$
1	.55	37.8	57.1	7	1.20	43.8	60.8	13	.58	40.5	58.8	1	.88	51.6	64.6	1	1.20	47.1	62.5	2.72	36.2	55.9
2	.84	63.5	68.9	8	.56	57.3	66.8	14	.62	68.1	70.2	2	.63	46.4	62.3	2	.72	44.7	61.3			
3	.61	93.6	75.3	9	.35	33.2	53.6	15	.63	49.8	63.8	3	.72	56.5	66.6	3	1.90	37.5	56.8			
4	.34	38.5	57.5	10	.67	86.7	74.2	16	.33	44.2	61.0	4	.90	49.6	63.7	4	1.10	38.8	57.7			
5	.52	47.6	62.8	11	.94	101.1	76.4	17	.70	141.1	80.1	5	.90	72.3	71.3							
6	.45	37.1	56.6	12	.80	24.7	45.2	18	.44	40.5	58.8	6	.61	48.9	63.4							
MAXIMUM :					1.20	141.1	80.1						.90	72.3	71.3		1.90	47.1	62.5			
MINIMUM :					0.33	33.2	45.2						.61	46.4	62.3		0.72	37.5	56.8			
AVERAGE :					0.62	59.1	65.7°						.77	54.2	65.3°		1.23	42.0	59.6°	2.72	36.2	55.9°
% V :						49.9	13.7							17.5	5.1			11.0	4.7			

TABLE 2.7

MODEL No. 2

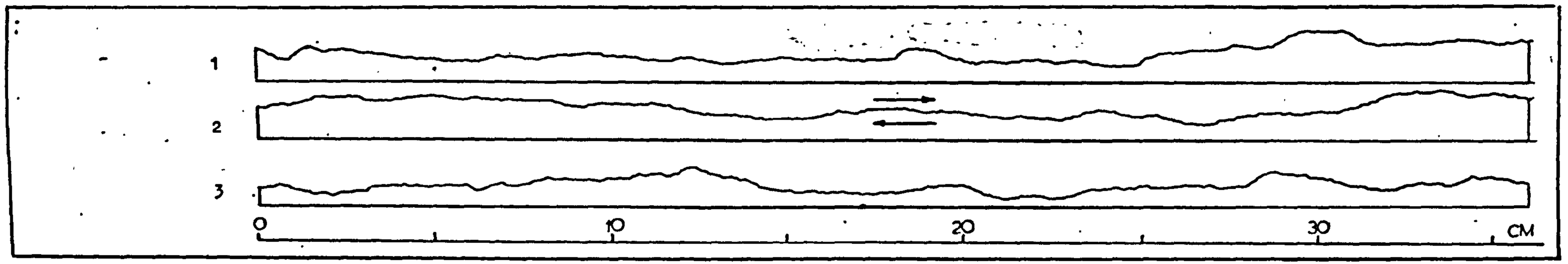

6

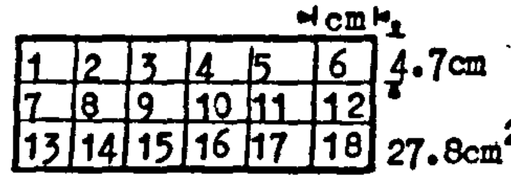

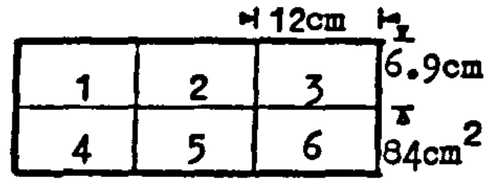

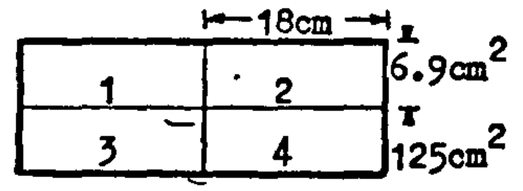

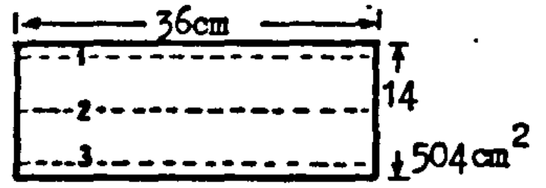

Block No.	d_h (mm)	τ_p (kPa)	$\phi_p°$	Cont. No.	d_h (mm)	τ_p (kPa)	$\phi_p°$	Cont. No.	d_h (mm)	τ_p (kPa)	$\phi_p°$
1	.60	54.2	65.7	7	.97	34.7	54.8	13	1.11	51.2	64.4
2	.63	47.1	62.5	8	.70	47.6	62.8	14	.32	43.5	60.6
3	1.23	49.4	63.6	9	1.00	61.1	68.2	15	.47	56.8	66.7
4	.57	65.8	69.6	10	.50	51.4	64.5	16	.66	64.7	69.3
5	.83	88.0	74.4	11	.72	43.2	60.4	17	.82	45.0	61.4
6	.56	39.3	58.1	12	.90	52.5	65.0	18	.76	60.7	68.0

	No.	d_h (mm)	τ_p (kPa)	$\phi_p°$	No.	d_h (mm)	τ_p (kPa)	$\phi_p°$	d_h (mm)	τ_p (kPa)	$\phi_p°$
MAXIMUM :	1	.90	32.0	52.6	1	2.80	32.8	53.2	2.20	31.3	51.9
MINIMUM :	2	.97	30.0	50.8	2	1.85	33.3	53.7			
AVERAGE :	3	1.20	32.9	53.3	3	1.90	41.2	59.3			
% V :	4	.60	64.3	69.1	4	1.15	35.0	55			
	5	.92	51.1	64.4							
	6	1.03	32.4	52.9							

MAXIMUM :	1.23	88.0	74.4	1.20	64.3	69.1	2.80	41.2	59.3		
MINIMUM :	.32	39.3	54.8	.60	30.0	50.8	1.15	32.8	53.2		
AVERAGE :	.74	53.1	64.4°	.94	40.5	57.2°	1.92	35.6	55.3°	2.20	31.3	51.9°
% V :		23.0	7.2		34.6	2.2		10.9	5.0		

TABLE 2.8

MODEL No. 3

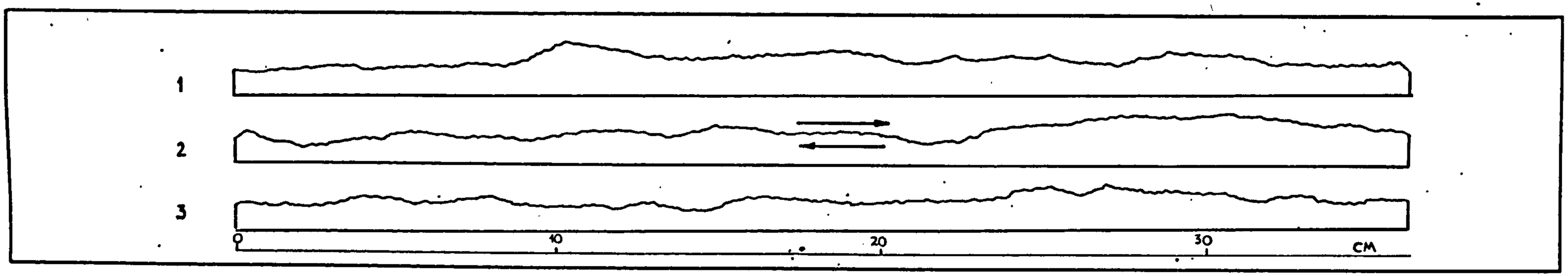

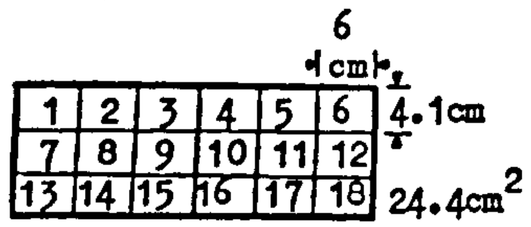

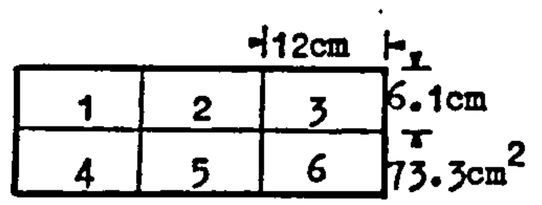

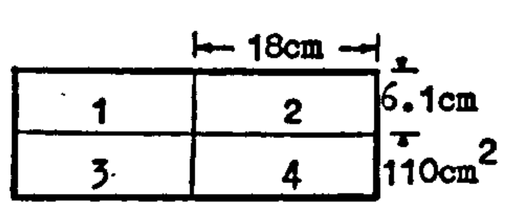

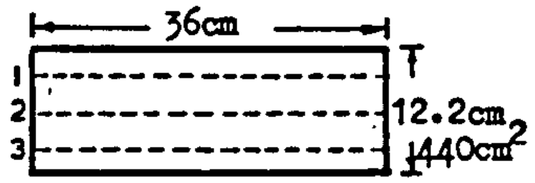

Block No.	d_h (mm)	τ_p (kPa)	$\phi_p°$	Cont. No.	(mm)	(kPa)	(°)	Cont. No.	(mm)	(kPa)	(°)
1	1.0	44.9	61.4	7	1.10	34.4	54.5	13	1.20	35.2	69.4
2	1.17	39.6	58.3	8	1.40	39.4	58.3	14	.90	62.4	68.6
3	.94	48.8	63.3	9	.60	44.4	61.1	15	1.13	52.6	65.0
4	1.00	48.5	63.2	10	1.10	59.0	67.4	16	1.30	91.8	75.1
5	1.00	84.4	73.8	11	.62	22.7	42.8	17	1.39	35.2	55.2
6	1.26	95.5	75.6	12	1.70	59.1	67.5	18	1.81	60.1	67.8

No.	d_h (mm)	τ_p (kPa)	$\phi_p°$
1	1.74	26.2	46.9
2	1.80	39.4	58.1
3	1.34	43.5	60.6
4	2.10	30.6	51.3
5	1.80	66.3	69.7
6	1.53	26.3	47.0

No.	d_h (mm)	τ_p (kPa)	$\phi_p°$
1	1.88	30.8	51.5
2	1.20	31.6	52.2
3	2.98	31.3	51.9
4	2.2	41.3	59.3

d_h (mm)	τ_p (kPa)	$\phi_p°$
3.50	27.0	47.8

MAXIMUM :	1.81	95.5	75.6	2.10	66.3	69.7
MINIMUM :	.60	34.4	54.5	1.34	26.2	46.9
AVERAGE :	1.15	53.2	63.8°	1.72	38.7	55.6°
% V :		38.0	12.9		39.4	16.0

MAXIMUM :	2.98	41.3	59.3			
MINIMUM :	1.20	30.8	51.5			
AVERAGE :	2.14	33.8	53.7°	3.50	27.0	47.8°
% V :		14.9	6.9			

TABLE 2.9

MODEL No.4

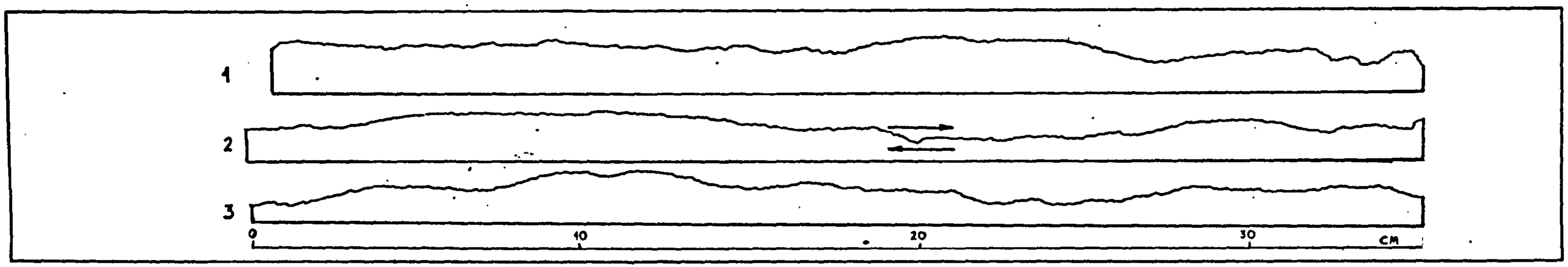

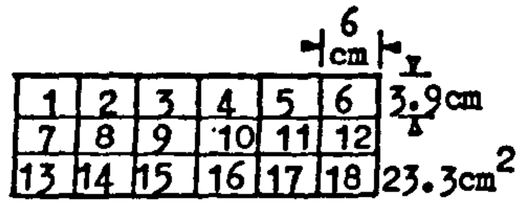

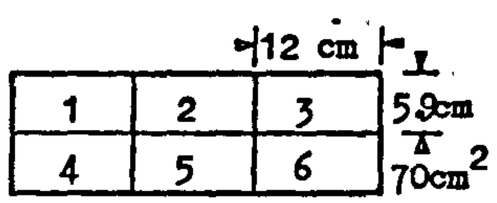

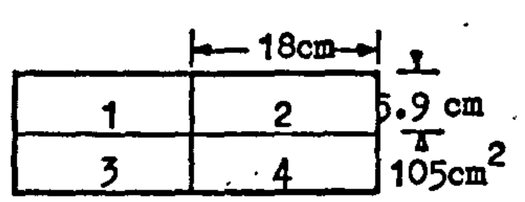

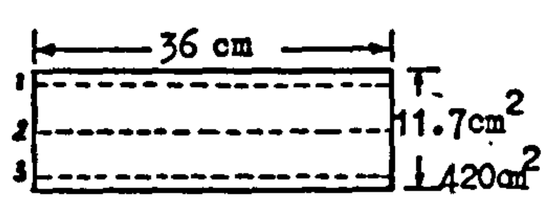

Block No.	d_h (mm)	τ_p (kPa)	$\phi_p°$	Cont. No.	d_h (mm)	τ_p (kPa)	$\phi_p°$	Cont. No.	d_h (mm)	τ_p (kPa)	$\phi_p°$	No.	d_h (mm)	τ_p (kPa)	$\phi_p°$	No.	d_h (mm)	τ_p (kPa)	$\phi_p°$	d_h (mm)	τ_p (kPa)	$\phi_p°$
1	1.00	50.1	63.9	7	.99	32.8	53.2	13	1.20	37.9	57.1	1	1.14	36.6	56.2	1	1.16	35.6	55.5	2.20	25.7	46.4
2	.85	42.9	60.3	8	1.30	46.3	62.1	14	.90	62.1	68.5	2	.75	45.5	61.7	2	1.80	32.4	52.9			
3	.92	24.2	44.6	9	.83	54.2	65.7	15	.90	32.2	52.7	3	1.13	48.2	63.1	3	1.48	32.9	53.3			
4	.72	52.4	64.9	10	1.00	46.7	62.3	16	1.70	35.7	55.5	4	1.32	45.6	61.8	4	1.26	35.3	55.2			
5	.95	35.4	55.3	11	.88	38.2	57.3	17	1.50	43.0	60.3	5	1.64	37.1	56.6							
6	1.10	62.9	68.7	12	.90	31.3	51.9	18	1.33	54.7	65.9	6	1.65	42.3	59.9							
				MAXIMUM :					1.70	62.2	68.7		1.65	48.2	63.1		1.80	35.6	55.5			
				MINIMUM :					0.72	24.2	44.6		.75	36.6	56.2		1.16	32.4	52.9			
				AVERAGE :					1.10	43.5	59.5°		1.27	42.5	59.9°		1.43	34.1	54.2°	2.20	25.7	46.4°
				% V						25.3	10.9			11.2	4.8			4.8	2.4			

TABLE 2.10

MODEL No. 5

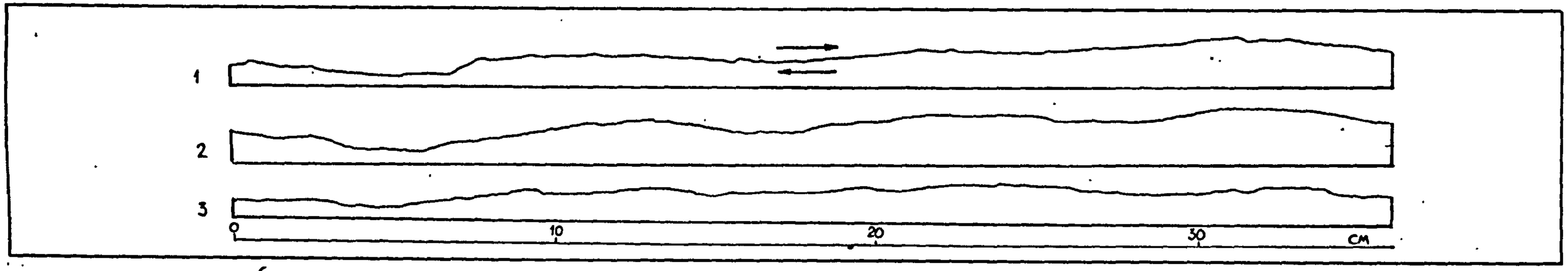

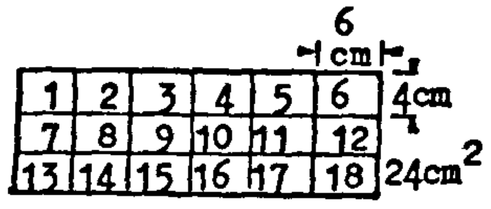

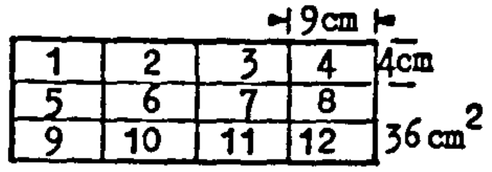

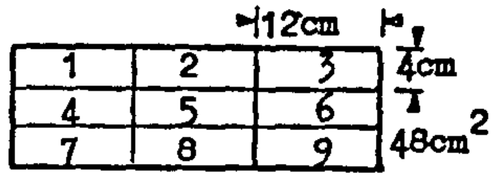

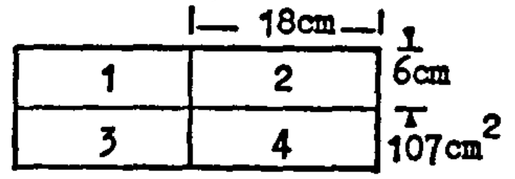

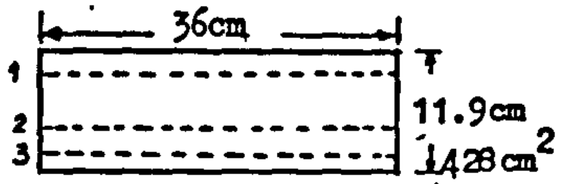

Block No.	d_h (mm)	τ_p (kPa)	ϕ_p°	Cont. No.	d_h (mm)	τ_p (kPa)	ϕ_p° (°)
1	1.24	51.4	69.5	10	1.10	30.4	51.1
2	.73	49.0	63.4	11	1.11	27.1	47.9
3	.90	32.8	53.2	12	.63	50.8	64.3
4	1.19	33.3	53.7	13	1.46	75.4	72.0
• 5	1.28	24.2	44.6	14	.99	32.0	52.6
6	1.10	37.9	57.1	15	1.35	25.0	45.6
7	.66	73.2	71.5	16	1.18	36.1	55.8
8	.44	20.4	39.8	17	1.10	35.2	55.2
9	.90	64.9	69.3	18	1.34	69.0	70.5

No.	d_h (mm)	τ_p (kPa)	ϕ_p°
1	1.30	36.5	56.1
2	1.44	50.6	64.2
3	1.35	30.2	50.9
4	2.0	38.8	57.7
5	1.21	52.8	65.1
6	.74	49.8	63.8
7	1.14	45.2	61.5
8	1.19	42.0	59.7
9	1.30	41.1	59.2
10	1.19	38.9	57.8
11	.97	42.2	59.9
12	1.50	57.5	66.9

No.	d_h (mm)	τ_p (kPa)	ϕ_p°
1	.32	26.0	46.7
2	1.20	34.2	54.4
3	1.46	36.4	56.1
4	1.26	37.4	56.8
5	1.44	42.8	60.2
6	.89	63.6	68.9

No.	d_h (mm)	τ_p (kPa)	ϕ_p°
1	1.35	35.0	55.0
2	1.63	26.2	46.9
3	1.56	38.0	57.2
4	2.00	30.1	50.9

d_h (mm)	τ_p (kPa)	ϕ_p°
2.90	29.0	49.8

MAXIMUM :	1.46	75.4	72.0	2.00	57.5	66.9	1.46 63.6 68.9	2.00 38.0 57.2	2.90 29.0 49.8
MINIMUM :	.44	25	45.6	0.74	30.2	50.9	0.32 26.0 46.7	1.35 30.1 46.9	
AVERAGE :	1.10	42.7	57.3°	1.28	43.5	60.2°	1.10 41.2 58.0°	1.64 32.3 52.5°	2.90 29.0 49.8°
% V :		41.7	17.3		17.7	7.3	28.5 12	16.2 8.6	

TABLE 2.11

MODEL No.6

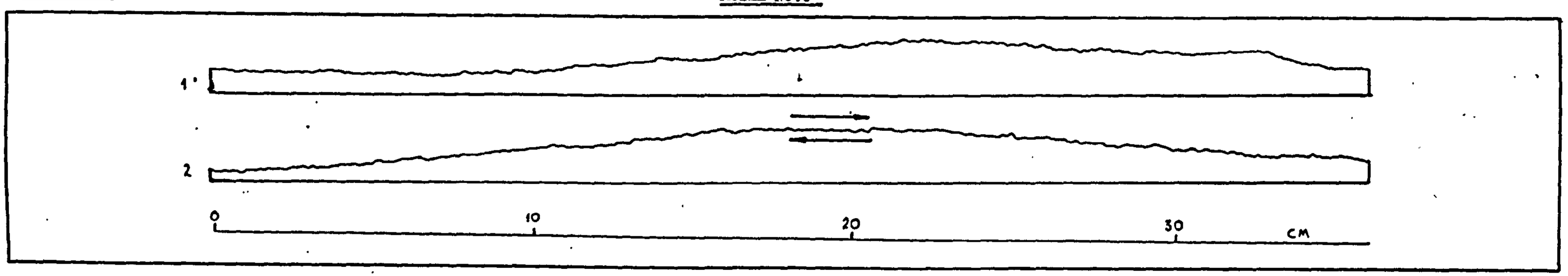

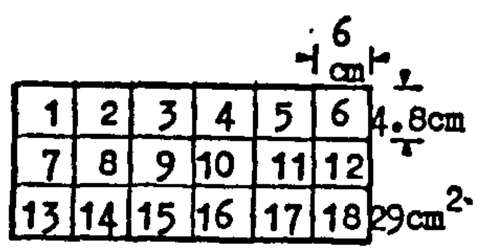

Block No.	d_h (mm)	τ_p (kPa)	$\phi_p°$
1	.40	52.0	64.8
2	.55	33.2	53.6
3	.65	35.7	95.5
4	.67	32.1	52.6
5	.70	26.0	46.7
6	.60	28.0	48.8
7	.36	31.7	52.3
8	.50	49.1	63.5
9	.68	50.4	64.1

Cont.

No.	d_h (mm)	τ_p (kPa)	$\phi_p°$ (°)
10	.43	62.4	68.6
11	.81	62.8	68.7
12	.65	60.0	67.8
13	.57	34.1	54.3
14	.66	35.9	55.7
15	.84	33.5	53.8
16	.72	39.6	58.3
17	.61	84.8	73.9
18	.32	76.8	72.3

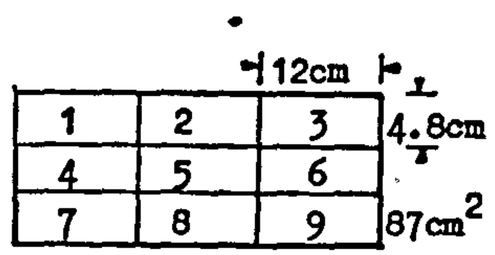

No.	d_h (mm)	τ_p (kPa)	$\phi_p°$
1	.53	43.4	60.6
2	.65	34.5	54.6
3	.72	29.0	49.8
4	1.14	26.7	47.5
5	.40	32.9	53.3
6	.75	61.2	68.2
7	.47	27.8	48.6
8	.45	42.0	59.7
9	.67	42.1	59.8

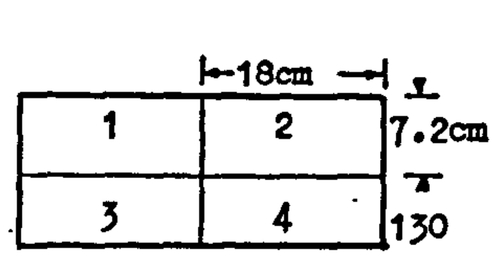

No.	d_h (mm)	τ_p (kPa)	$\phi_p°$
1	1.25	22.3	42.3
2	1.23	22.1	42.1
3	.44	28.9	49.7
4	.45	49.0	63.4

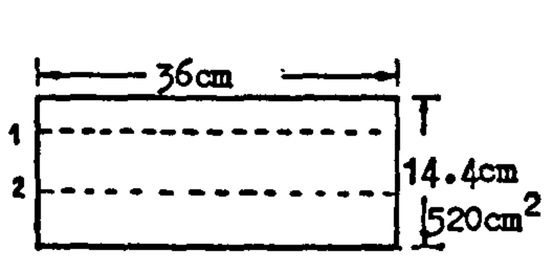

d_h (mm)	τ_p (kPa)	$\phi_p°$
1.80	23.3	43.6

	No.	d_h (mm)	τ_p (kPa)	$\phi_p°$ (°)
MAXIMUM :		.84	84.8	73.9
MINIMUM :		.32	26.0	46.7
AVERAGE :		.60	46.0	59.7°
% V :			37.7	13.9

No.	d_h (mm)	τ_p (kPa)	$\phi_p°$
	1.14	61.2	68.2
	.40	26.7	47.5
	.64	37.7	55.8°
		28.9	6.8

No.	d_h (mm)	τ_p (kPa)	$\phi_p°$
	1.25	49.0	63.4
	.45	22.1	42.1
	.84	30.6	49.4°
		41.4	20.2

d_h (mm)	τ_p (kPa)	$\phi_p°$
1.80	23.3	43.6°

TABLE 2.12

MODEL No. 7

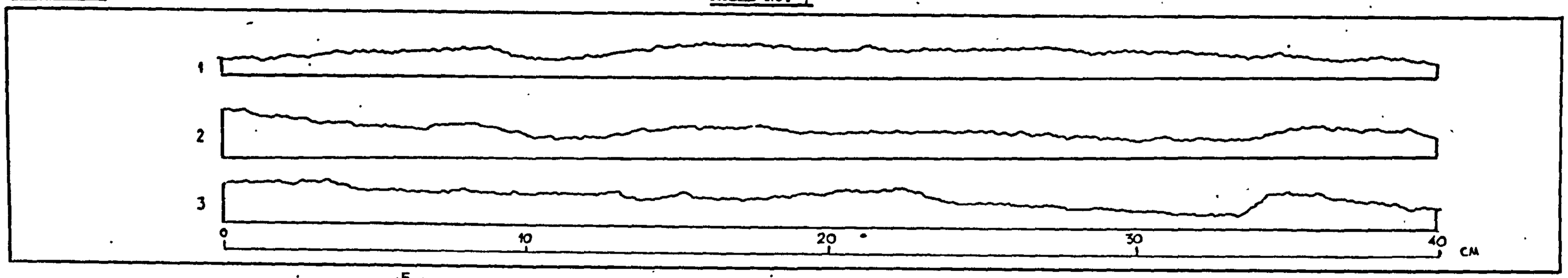

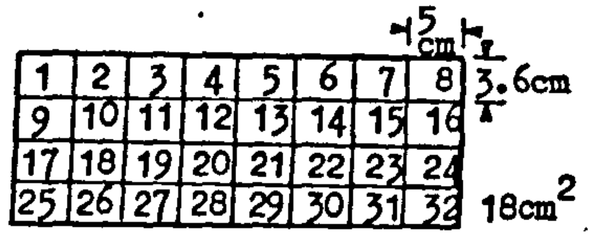

Block No.	d_h (mm)	τ_p (kPa)	$\phi_p°$	Cont. No.	(mm)	(kPa)	(°)	Cont. No.	(mm)	(kPa)	(°)
1	.65	70.9	70.9	13	.41	42.5	60.0	25	.62	69.3	70.5
2	.55	67.4	70.0	14	.99	48.7	63.3	26	.79	46.0	62.0
3	.42	37.1	56.5	15	.87	51.2	64.4	27	1.00	42.7	60.2
4	.56	63.5	68.9	16	.55	64.9	69.3	28	1.00	44.5	61.2
5	.55	60.8	68.1	17	.73	77.0	72.3	29	.67	57.6	67.0
6	.60	42.8	60.2	18	.55	68.9	70.4	30	.88	53.6	65.4
7	.80	85.9	74.0	19	.67	58.1	67.1	31	.84	73.8	71.6
8	.93	65.0	69.3	20	.67	62.1	68.5	32	.76	98.7	76.1
9	.64	69.4	70.6	21	.67	55.4	66.1				
10	.85	69	70.6	22	.36	65.9	69.6				
11	.58	57.4	66.9	23	1.00	40.7	59.0				
12	.57	61.6	68.3	24	.49	84.8	73.9				
MAXIMUM :					1.00	98.7	74.0				
MINIMUM :					.42	37.1	56.5				
AVERAGE :					.69	61.2	67.3°				
% V :						23.4	7.0				

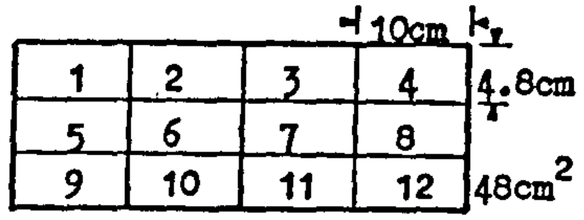

No.	d_h (mm)	τ_p (kPa)	$\phi_p°$
1	1.15	59.5	67.6
2	1.15	61.5	68.3
3	1.22	45.4	61.6
4	.78	49.7	63.8
5	1.16	36.8	56.3
6	.46	39.2	58.0
7	.52	41.9	59.7
8	.45	55.1	66.0
9	.80	62.9	68.7
10	1.00	36.5	56.1
11	.68	32.9	53.4
12	.40	59.5	67.6
MAXIMUM :	1.16	62.9	68.7
MINIMUM :	.40	32.9	53.4
AVERAGE :	.81	48.4	62.3°
% V :		22.7	8.8

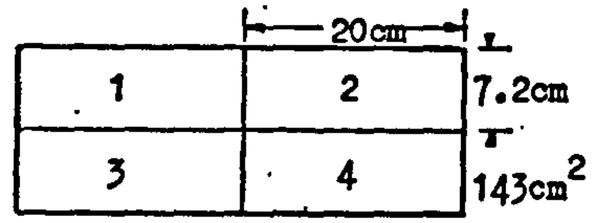

No.	d_h (mm)	τ_p (kPa)	$\phi_p°$
1	.85	30.7	51.4
2	1.35	31.1	51.8
3	.73	30.8	51.5
4	1.38	37.1	56.6
MAXIMUM :	1.38	37.1	56.6
MINIMUM :	.73	30.8	51.4
AVERAGE :	1.10	32.4	52.8°
% V :		9.6	4.7

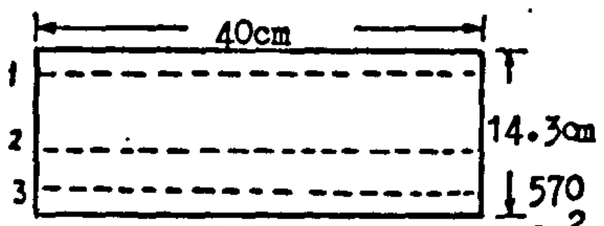

d_h (mm)	τ_p (kPa)	$\phi_p°$
2.0	25.7	46.4
2.0	25.7	46.4°

TABLE 2.13

MODEL No. 8

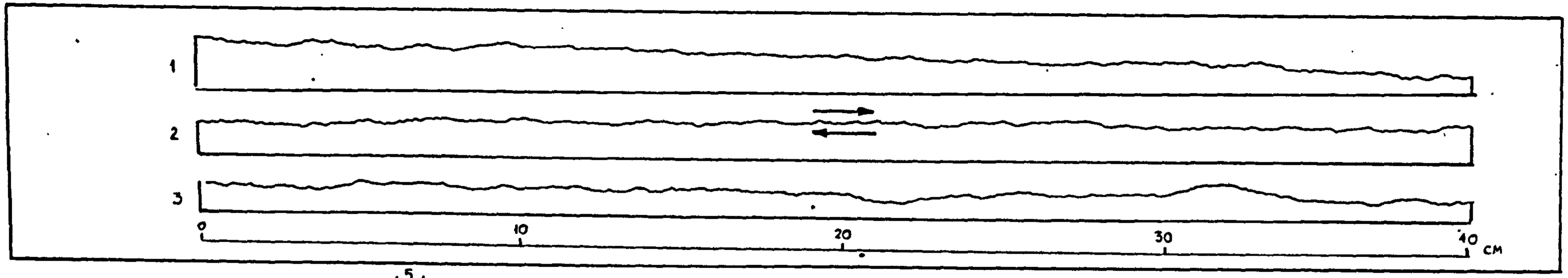

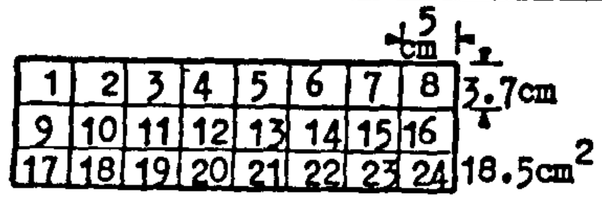

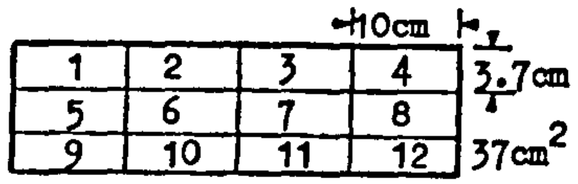

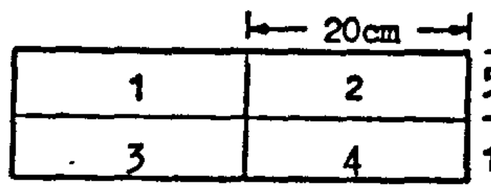

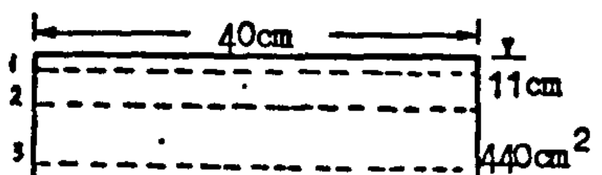

Block No.	d_h (mm)	τ_p (kPa)	$\phi_p°$	Cont. No.	d_h (mm)	τ_p (kPa)	$\phi_p°$	Cont. No.	d_h (mm)	τ_p (kPa)	$\phi_p°$	No.	d_h (mm)	τ_p (kPa)	$\phi_p°$	No.	d_h (mm)	τ_p (kPa)	$\phi_p°$
1	.36	58.5	67.3	9	1.1	38.8	57.7	17	.70	41.6	59.5	1	1.0	60.4	67.9	1	.89	32.8	53.2				
2	1.1	55.4	66.1	10	.89	46.2	62.1	18	.64	58.1	67.1	2	1.46	45.7	61.8	2	.95	37.7	57.0				
3	1.1	35.0	55.0	11	.56	54.2	65.7	19	.46	53.0	65.2	3	.89	41.8	59.6	3	.67	32.8	53.2				
4	.73	66.8	69.9	12	.44	61.0	68.1	20	.59	38.1	57.3	4	.93	49.5	63.7	4	1.77	32.2	52.7				
5	.35	58.5	67.3	13	.58	48.4	63.2	21	.57	47.7	62.8	5	.86	43.9	60.8								
6	.65	51.5	64.6	14	.69	41.7	59.6	22	.67	50.9	64.3	6	.59	34.7	54.8								
7	.56	54.2	65.7	15	.59	42.3	59.9	23	.86	51.4	64.5	7	.50	57.2	66.8								
8	.39	49.8	63.8	16	.63	68.3	70.3	24	.57	54.8	65.9	8	.60	61.9	68.4								
												9	.49	61.1	68.2								
												10	1.0	37.3	56.7								
												11	.89	37.5	56.8								
												12	.77	62.1	68.5								
				MAXIMUM :	1.10	68.3	70.3		1.46	62.1	68.5		1.77	37.2	57.0								
				MINIMUM :	.35	38.1	55.0		.49	34.7	54.8		.67	32.2	52.7								
				AVERAGE :	.66	51.1	63.9°		.83	49.4	62.8°		1.10	33.90	54°		1.70	25.7	46.4°				
				% V :		17.2	6.3			21.5	8.1			7.6	3.7								

TABLE 2.14

MODEL No. 9

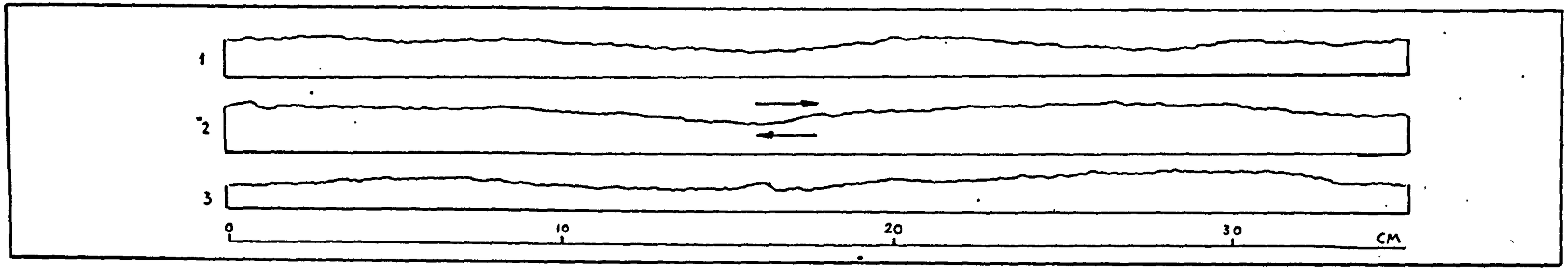

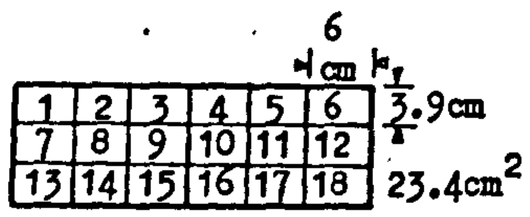

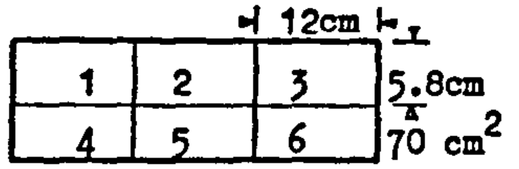

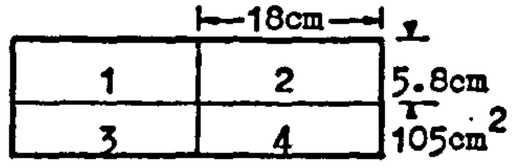

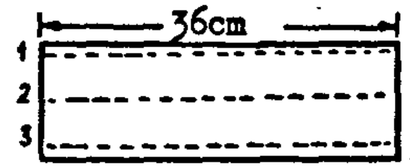

Block No.	d_h (mm)	τ_p (kPa)	ϕ_p°	Cont. No.	d_h (mm)	τ_p (kPa)	ϕ_p°	Cont. No.	d_h (mm)	τ_p (kPa)	ϕ_p°	No.	d_h (mm)	τ_p (kPa)	ϕ_p°	No.	d_h (mm)	τ_p (kPa)	ϕ_p°
1	1.1	35.6	55.5	7	1.20	29.0	49.8	13	1.40	48.1	63.0	1	1.30	35.0	52.6	1	1.65	24.7	45.2	1.40	24.0	44.4
2	.85	40.7	59.0	8	.61	31.2	51.9	14	.73	29.9	50.7	2	1.00	37.1	56.6	2	.75	24.9	45.5			
3	.90	31.3	51.9	9	.51	27.4	48.2	15	1.00	26.9	47.7	3	.67	24.4	44.9	3	1.25	26.1	46.8			
4	.84	48.9	63.4	10	.83	45.9	61.9	16	.83	48.2	63.1	4	1.15	25.8	46.5	4	.80	33.4	53.7			
5	.82	29.7	50.5	11	.88	40.3	58.7	17	.88	40.7	59.0	5	.97	38.8	57.7							
6	.89	28.4	49.2	12	.89	35.8	55.6	18	.38	41.0	59.6	6	1.13	28.7	49.5							
				MAXIMUM :					1.10	58.2	63.1		1.15	43.8	57.7		1.65	33.4	53.7			
				MINIMUM :					.38	18.4	49.2		.67	18.7	44.9		.75	24.7	45.2			
				AVERAGE :					.86	36.7	55.5°		1.04	31.6	51.3°		1.11	27.3	47.8°	1.40	24.0	44.4°
				% V :						21.3	10			19.4	10.3			15.1	8.4			

TABLE 2.15

MODEL No. 10

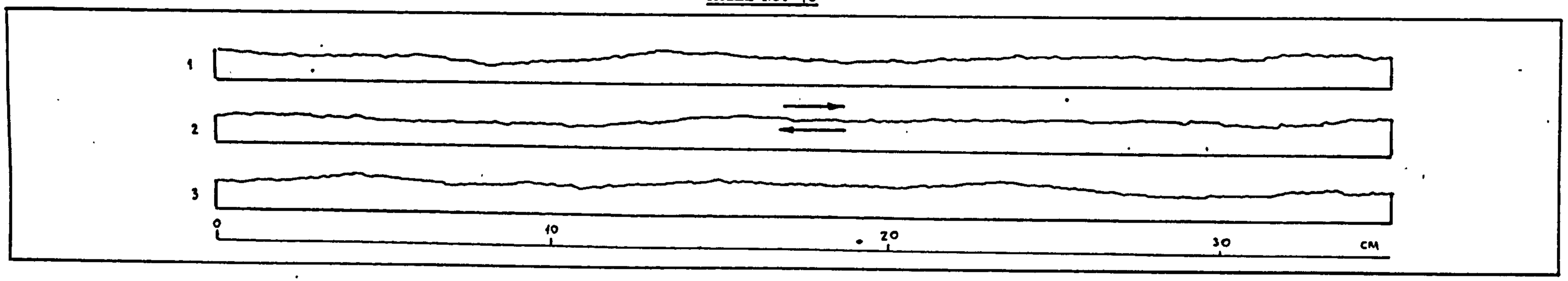

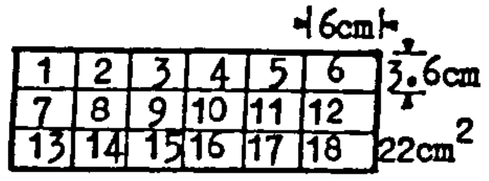

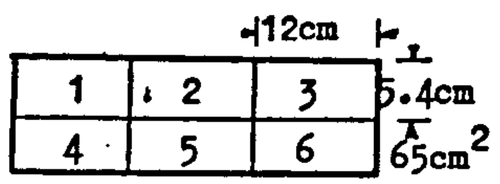

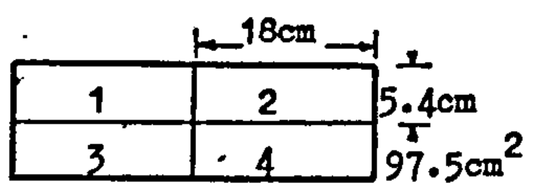

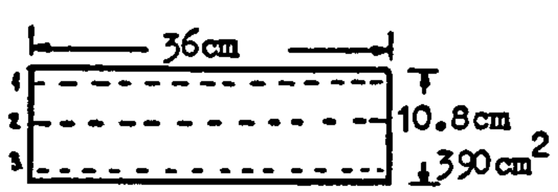

Block No.	d_h (mm)	τ_p (kPa)	$\phi_p°$	Cont. No.	d_h (mm)	τ_p (kPa)	$\phi_p°$	Cont. No.	d_h (mm)	τ_p (kPa)	$\phi_p°$	No.	d_h (mm)	τ_p (kPa)	$\phi_p°$	No.	d_h (mm)	τ_p (kPa)	$\phi_p°$
1	.13	26.6	47.4	7	1.20	32.6	53.1	13	.64	21.6	41.4	1	.64	21.3	41.0	1	.76	22.7	42.8	1.20	21.0	40.6
2	.43	22.4	42.4	8	.63	26.0	46.7	14	.52	24.4	44.9	2	1.36	24.4	44.9	2	1.26	23.1	43.3			
3	.74	23.5	43.8	9	.88	35.2	55.2	15	.70	28.0	48.8	3	1.20	26.4	47.1	3	1.37	22.4	42.4			
4	.72	24.1	44.5	10	.62	23.7	44.0	16	.70	27.4	48.2	4	1.15	35.2	55.2	4	.75	24.5	45.0			
5	1.10	32.0	52.6	11	.55	22.1	42.1	17	.66	37.0	56.5	5	1.29	21.6	41.4							
6	1.10	30.9	51.6	12	.58	36.4	56.1	18	.64	22.6	42.7	6	1.10	22.6	42.7							
				MAXIMUM :	1.20	42.0	56.5		1.36	39.2	55.2		1.37	24.5	45.0							
				MINIMUM :	.13	16.1	41.4		.64	17.3	41.0		.75	22.4	42.4							
				AVERAGE :	.70	27.6	47.9°		1.12	25.3	45.4°		1.04	23.2	43.4°					1.20	21.0	40.6°
				% V:		18.7	10.6			20.7	11.7			4.1	2.6							

TABLE 2.16

MODEL No. 11

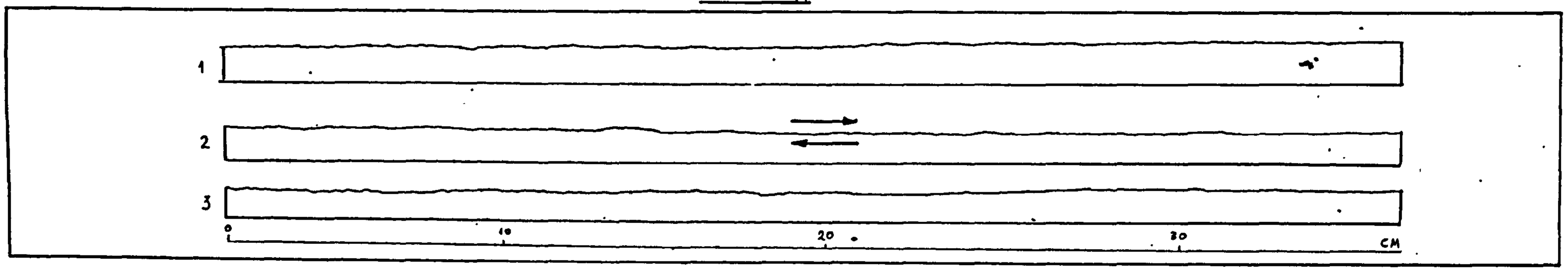

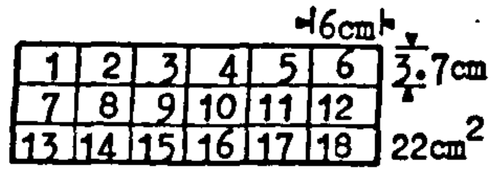

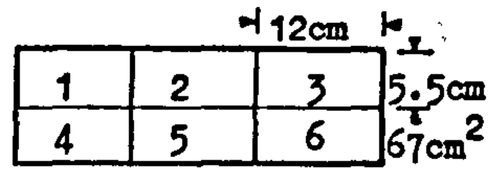

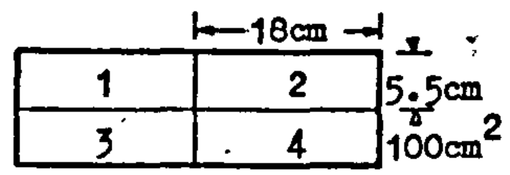

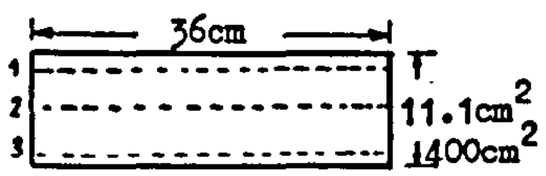

Block No.	d_h (mm)	τ_p (kPa)	$\phi_p°$	Cont. No.	d_h (mm)	τ_p (kPa)	$\phi_p°$	Cont. No.	d_h (mm)	τ_p (kPa)	$\phi_p°$	No.	d_h (mm)	τ_p (kPa)	$\phi_p°$	No.	d_h (mm)	τ_p (kPa)	$\phi_p°$	d_h (mm)	τ_p (kPa)	$\phi_p°$
1	.64	20.0	39.2	7	.90	29	49.8	13	.14	21.0	40.6	1	1.12	18.7	37.4	1	1.0	17.4	35.4	1.30	20.2	39.5
2	.53	22.7	42.8	8	1.0	32.2	52.7	14	.70	33.9	54.1	2	1.00	20.5	39.9	2	1.12	19.8	38.9			
3	.53	22.6	42.7	9	.73	26.9	47.7	15	.30	32.9	53.3	3	.95	21.4	41.1	3	1.25	22.0	41.9			
4	.53	23.8	44.2	10	1.10	27.6	48.9	16	.82	24.7	45.2	4	.82	25.9	46.6	4	.80	17.5	35.5			
5	.53	23.4	43.7	11	.73	23.1	43.3	17	.52	25.1	45.7	5	1.30	24.8	45.3							
6	.92	27.5	48.3	12	.42	24.7	45.2	18	.34	23.8	44.2	6	1.00	19.7	38.8							
MAXIMUM :					1.10	33.9	54.1		.14	33.9	54.1		1.30	25.9	46.6		1.25	22.0	41.9			
MINIMUM :					.14	19.8	39.2		.14	21.0	40.6		.82	18.7	37.4		.80	17.4	35.4			
AVERAGE :					.67	25.8	46.2°		.67	25.8	46.2°		1.03	21.8	41.5°		1.09	19.2	37.9°	1.30	20.2	39.5°
% V :						16.3	9.3			16.3	9.3			13.2	8.9			11.4	3.1			

The numbers on each block have been assigned to denote the relative position of each "element" onto the full size joint. As an example, block no. 1 in Table 2.6 should be imagined as positioned at the farthest left hand side of section no. 1, block no. 2 is adjacent and so on. The locations of the profile lines are given by the dotted lines drawn on the large joint.

The dimensions of the full size model joint and those of the smaller specimens are given as the average length (cm) and width (cm), as well as average joint surface area (cm^2).

The values of three shear parameters have been included for each individual joint specimen tested, namely:

(i) peak shear stress (τ_p)
(ii) angle of peak total friction ($\emptyset_p$)
(iii) peak shear displacement (d_{hp}).

The <u>peak shear stress</u> (τ_p) was calculated by dividing maximum shear force (F_{max}) by total joint area (A_T)

$$\tau_p \ (kPa) = \frac{F_{max}}{A_T} \times 98.07 \qquad 2.13$$

where F_{max} is in kgms and A_T in cm^2.

It should be noted that maximum force values were used only in the cases where a clearly discernible peak was present in the shear force (F) - shear displacement (d_h) diagram. In the event of absence of such a peak point, it was assumed that the joint had reached its peak resistance at the level of maximum inversion of the F-d_h line (GUISEPPE, 1970). To avoid any subjectivity in the choice of the F value, the relatively steepest portion of the dilation curve - which is well known to correspond to mobilization of peak strength - was used as a control. Ill-defined peak conditions were more frequently met during testing of the larger joints, irrespective of surface roughness, as well as in smaller joints which had relatively smooth and planar surfaces.

The <u>peak total friction angle</u> was derived as the arc of tangent τ_p/σ_n. From simple geometrical considerations (section 1.1.3 in part one), the total friction angle is equal at least to the sum of the basic angle of friction ($\emptyset_b$) and peak dilation angle $(i)^o_p$;

$$\arctan\left(\tau_p/\sigma_n\right) \geqslant (i)_p + \phi_b \qquad 2.14$$

Under the present JCS/σ_n ratio value of ~ 80 the total friction angle was larger than the sum of i_p^o and ϕ_b^o due to failure of intact asperities.

The peak shear displacement (d_{hp}) values correspond, as the term implies, to the instance of mobilization of peak shear strength and are given in mm units. All d_{hp} values have been corrected for the deflection of the proving ring and hence represent the net relative displacement between the two joint halves.

At the bottom of each table the range and mean value of each of the three shear parameters is given for each block size, together with the % scatter of the τ_p and arctan (τ_p/σ_n) values as expressed by the coefficient of variation V (%V = [std. dev./mean] x 100).

A detailed analysis of the experimental results will be presented in the following sections.

2.4.3 Peak shear strength in relation to joint block size

It is a well documented fact that the peak frictional resistance of unfilled interlocked joints depends upon the geometrical and strength characteristics of the surface and the effective normal stress operating across the sliding interface. The stringent techniques employed for the preparation of recasts of the same original joint ensured identical surface geometry and the composition of the model material was carefully controlled to give a uniaxial compressive strength of 2.0 MPa according to the design curve in Figure 2.17.

Even a cursory glance at the individual and average shear strength data presented in Tables 2.6 - 2.16 gives an appreciation of the effects of the new variable introduced, i.e. the length of the joint. An obvious inverse proportionality between the peak shear stress and the average joint block size persists, to a greater or lesser extent, in all the types of surfaces which were included in the present testing programme.

As an introduction to the size effect in the peak shear strength, an overall summary of the experimental results is presented in Table 2.17

TABLE 2.17

Summary of mean peak arctan (τ/σ_n) values obtained from model joints with comparable surface morphology by varying the average joint length.

Joint length (L)		Description of joints according to visual appearance							
Model (cm) M	Prototype (m) P	STRONGLY UNDULATING, ROUGH (1,2,3) TO MODERATELY ROUGH (4,5)		MODERATELY UNDULATING, VERY ROUGH		MODERATELY UNDULATING TO ALMOST PLANAR, MODERATELY ROUGH TO ALMOST SMOOTH	
		Model nos.					
		1, 2, 3	4, 5	6, 7, 8		9, 10, 11	
5,6	1.5,1.8	$64.5^\circ \pm 6.8^\circ$	(54)	$58.4^\circ \pm 8.3^\circ$	(36)	$64.3^\circ \pm 6.3^\circ$	(74)	$49.8^\circ \pm 6.4^\circ$	(54)
10,12	3.0,3.6	$59.4^\circ \pm 7.9^\circ$	(18)	$58.7^\circ \pm 5.6^\circ$	(12)	$60.7^\circ \pm 6.3^\circ$	(33)	$46.1^\circ \pm 6.1^\circ$	(18)
18,20	5.4,6.0	$56.2^\circ \pm 3.8^\circ$	(12)	$53.4^\circ \pm 3.2^\circ$	(8)	$52.1^\circ \pm 5.9^\circ$	(12)	$43.0^\circ \pm 5.0^\circ$	(12)
36,40	10.8,12.0	$51.9^\circ \pm 4.1^\circ$	(3)	48.1°	(2)	$45.5^\circ \pm 1.6^\circ$	(3)	$41.5^\circ \pm 2.6^\circ$	(3)

Notes: The $\pm$ values correspond to one standard deviation.

Numbers in brackets give the corresponding total number of specimens from all joint types in that group.

to give an initial idea of the range of values obtained by varying the size of the individual joint blocks.

The eleven types of model joints were broadly divided, on a purely descriptive basis, into three classes according to the visual intensity of the surface undulations and the roughness features of order lower than 1st. Model nos. 1, 2, 3, 4 and 5 were grouped together as "strongly undulating, rough (1,2,3) to moderately rough (4,5)". The "moderately undulating, very rough" group comprised model nos. 6, 7 and 8, and finally model nos. 9, 10 and 11 were characterized as "gently undulating, moderately rough (nos. 9 and 10) to relatively planar and smooth (no. 11)". A visual clarification of the above descriptions can be obtained from the profiles in Figure 2.28 and those presented in Tables 2.6 to 2.16.

The peak arctan $(\tau / \sigma_n)^\circ$ values for each group in Table 2.17 represent the mean values from all tests on joint blocks of similar size. Comparisons of the mean data within each of the four columns show in each case a decrease in the average total friction angle associated with the gradual increase of the joint length. The maximum average reduction ranged from $\sim 8^\circ$ to $\sim 20^\circ$ as the joint length increased from 5 or 6 cm (equivalent prototype, P = 1.5 or 1.8 meters) to 36 or 40 cm (P = 10.8 or 12 meters).

A characteristic of the overall average values presented in Table 2.17 is the decrease in the value of standard deviation about the mean with increasing joint block size. A more clear picture is given by the coefficients of variation (V) which have been calculated for each set of specimens (see Tables 2.6 - 2.16). The fluctuations in the strength of the small individual joints are the expected result of two geometrical characteristics of the full scale surfaces, namely, the large undulations and the random distribution and variable size of the asperities smaller than the major waves.

With regard to the variable of surface waviness, it is readily understandable that the shear strength of a joint whose length is appreciably smaller than the wavelength of an undulation would depend upon its relative position on the limbs of the latter. If it fell on the negative or positive side with respect to the direction of shearing, it would show minimum and maximum respectively resistance to sliding. Accordingly, a block situated on the peak of that undulation or in the trough between two

successive ones would exhibit strength between the upper and lower limits.

Those differences would obviously be enhanced by the variable geometry and location of the smaller irregularities, and would accordingly be minimal in the case of joints with planar surface geometry. The scatter (%V) in the peak shear stress (τ_p) values corresponding to 6 cm long specimens of the rough undulating joint types (nos. 1 to 5) ranged between 23% and 49%. For similar joint block sizes of model nos. 6 to 8 (moderately undulating very rough) the %V was between 17.2% and 37.7%. Finally, the scatter in τ_p of the 6 cm long samples from the least irregular surfaces (model nos. 9 to 11) was between 16.3 and 21.3%.

The scale effect in the peak shear stress (τ_p) is illustrated in Figure 2.29 where the average τ_p values corresponding to each set of specimens tested have been plotted against the average joint area (A_T). A characteristic feature of those average trends is the non-linear variation in τ_p evidently tending to reach an asymptotic value with increasing A_T. Furthermore, it is shown that size effects become much less pronounced with increasing regularity of surface geometry, as in the cases of model nos. 9, 10 and 11.

A summary of the percentage reductions in joint strength with increasing block size is presented in Table 2.18. For each of the models the ratios of the average length (L) and area (A) of the individual blocks to the corresponding length (L_F) and area (A_F) of the full scale joint are included. The % reductions in peak shear stress (τ_p) and total friction angle $\tan^{-1}(\tau_p/\sigma_n)$ have been calculated with respect to the maximum experimental values which are also included in the table for reference.

In most cases the joints of 5 or 6 cm length showed maximum peak shear strength as compared to the larger sizes. The 6 cm blocks of model nos. 1 and 4 showed virtually the same strength as the 12 cm ones, while in the case of model no. 5 an intermediate size of 9 cm displayed higher strength than both the 6 and 12 cm joints. The explanation for those deviations lies in the preceding arguments regarding the scatter of the results with decreasing joint size, which can be supplemented here with the introduction of another factor, namely the symmetry of the undulation. A small amount of asymmetry was present in the case of model no. 5, where the "negative" limbs of the large undulations were overall longer than the "positive" ones (see corresponding profiles in Table 2.10). In combination with the

TABLE 2.18

Summary of the percentage reductions in peak shear strength with increasing joint block size.

Size relationships between individual joint blocks and full scale model		% REDUCTION		Size relationships between individual joint blocks and full scale model		% REDUCTION	
L:L_F*	A:A_F**	Peak shear stress (τ_p)	Angle of total friction (ϕ_p) = $\tan^{-1}(\tau_p/\sigma_n)^\circ$	L:L_F	A:A_F	Peak shear stress (τ_p)	Angle of total friction(ϕ_p) $=\tan^{-1}(\tau_p/\sigma_n)^\circ$
		MODEL No. 1				MODEL No. 6	
1:6	1:18	(6) 59.1 kPa	65.7°	1:6	1:18	(6) 46 kPa	59.7°
1:3	1:6	(12) 8.3%	0.6%	1:3	1:6	(12) 18%	6.5%
1:2	1:4	(18) 28.9%	9.3%	1:2	1:4	(18) 33.5%	17.3%
1	1	(36) 38.7%	14.9%	1	1	(36) 49.3%	26.7%
		MODEL No. 2				MODEL No. 7	
1:6	1:18	(6) 53.1 kPa	64.4°	1:8	1:32	(5) 61.2 kPa	67.3°
1:3	1:6	(12) 23.7%	11.2%	1:4	1:12	(10) 20.9%	7.4%
1:2	1:4	(18) 33:0%	14.1%	1:2	1:4	(20) 47.1%	21.5%
1	1	(36) 41.1%	19.4%	1	1	(40) 58.0%	31.1%
		MODEL No. 3				MODEL No. 8	
1:6	1:18	(6) 53.2 kPa	63.8°	1:8	1:22	(5) 51.1 kPa	63.9°
1:3	1:6	(12) 27.3%	12.9%	1:4	1:12	(10) 3.3%	1.7%
1:2	1:4	(18) 36.5%	15.8%	1:2	1:4	(20) 33.7%	15.5%
1	1	(36) 49.2%	25.1%	1	1	(40) 49.7%	27.4%
		MODEL No. 4				MODEL No. 9	
1:6	1:18	(6)		1:6	1:18	(6) 36.5 kPa	55.5°
1:3	1:6	(12)	43 kPa ..... 59.7°	1:3	1:6	(12) 13.9%	7.6%
1:2	1:4	(18) 20.7%	9.2%	1:2	1:4	(18) 25.6%	13.9%
1	1	(36) 40.2%	22.3%	1	1	(36) 34.6%	20.0%
		MODEL No. 5				MODEL No. 10	
1:6	1:18	(6) 1.8%	4.8%	1:6	1:18	(6) 27.6 kPa	47.9°
1:4	1:12	(9) 43.5 kPa	60.2°	1:3	1:6	(12) 8.3%	5.3%
1:3	1:9	(12) 5.3%	3.7%	1:2	1:4	(18) 15.9%	9.4%
1:2	1:4	(18) 25.7%	12.8%	1	1	(36) 23.9%	15.2%
1	1	(36) 33.3%	17.3%				
						MODEL No. 11	
				1:6	1:18	(6) 25.8 kPa	46.2°
				1:3	1:6	(12) 15.5%	10.0%
				1:2	1:4	(18) 25.5%	18.0%
				1	1	(36) 21.7%	14.5%

* L = length of individual joint block
L_F = length of full scale joint

** A = area of individual joint block
A_F = area of full scale joint

Numbers in brackets give the average model joint length in cm.

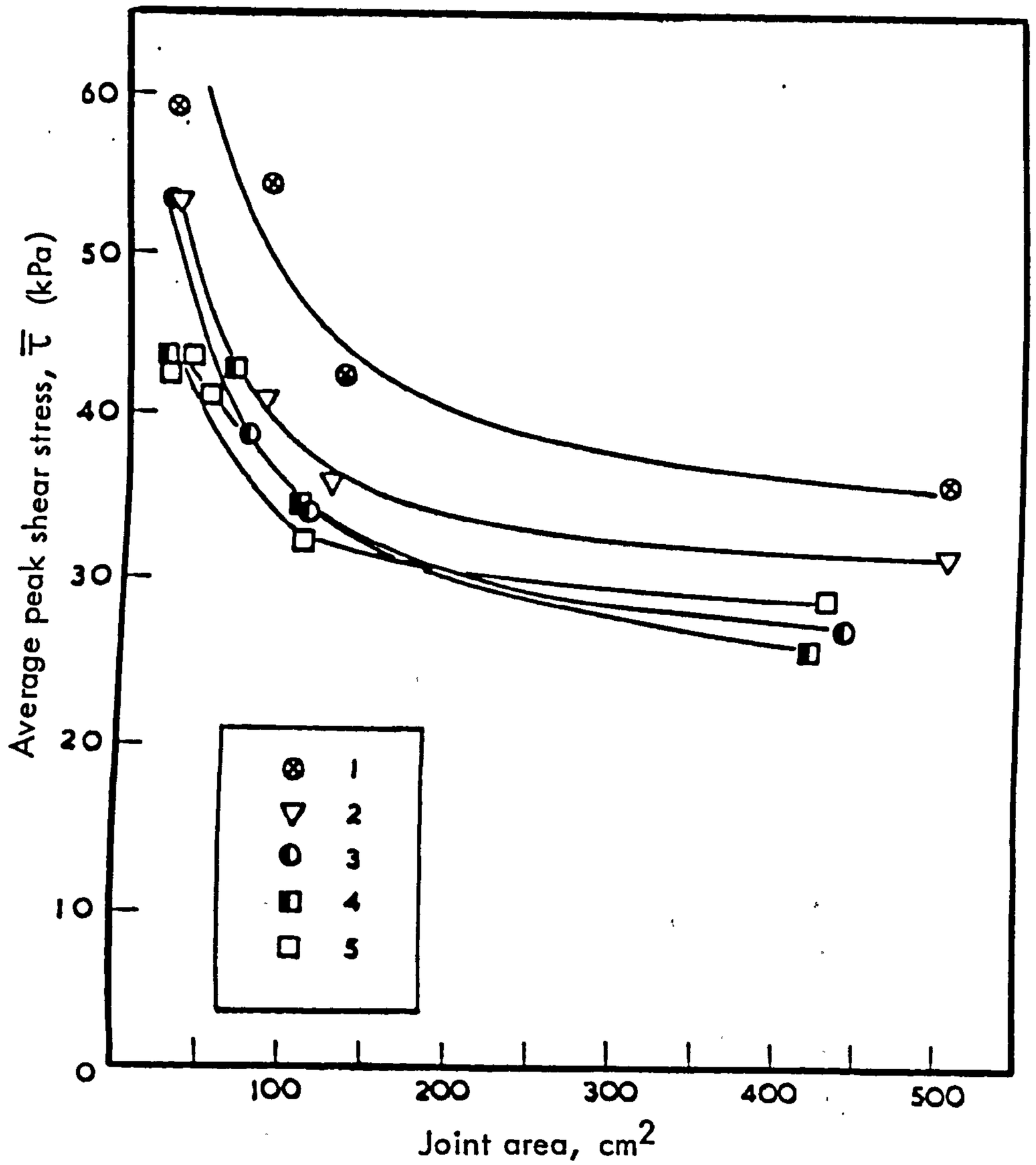

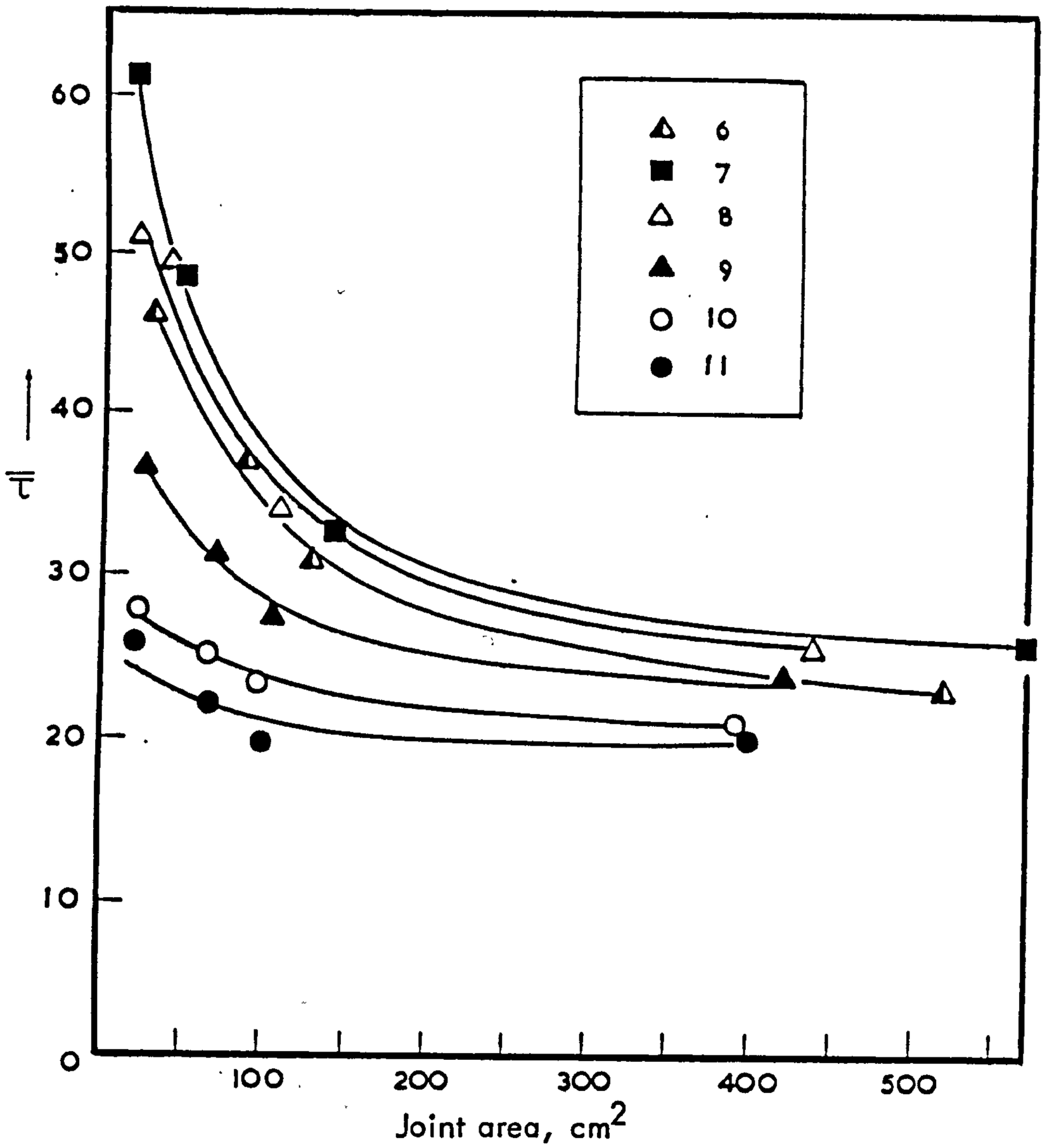

FIGURE 2.29 Variation of average peak shear stress with joint specimen area

moderate small scale roughness, that type of surface geometry resulted in more 6 cm joints to be sheared "downslope" and hence show somewhat lower average strength than expected.

For all joint types except no. 11 the full scale models exhibited the lowest peak shear strength. In case no. 11 the 36 cm joint showed slightly higher strength than the 18 cm ones, but lower than the 6 and 12 cm blocks.

The maximum loss in strength was displayed by model no. 7, in which case an increase in joint area by a factor of 32 resulted in almost 60% reduction in peak shear stress (31% reduction in peak total friction angle). For the other rough/undulating joints the maximum reductions in peak shear stress ranged between 33 and 50% as the area increased by a factor of 18 to 22. The equivalent reductions in the total friction angle ranged between 17 and 27%. In the cases of the relatively planar joints nos. 10 and 11, the maximum reduction in τ_p was 24 and 22% respectively (14-15% in $\tan^{-1} \tau_p/\sigma_n$).

2.4.4 Analysis of the shear stress-horizontal displacement relationships

1. Derivation of the stress-displacement curves

The shear stress (τ)-horizontal displacement (d_h) diagrams for each sub-divided model were derived by summing up the shear forces (T) which acted upon each of the component blocks for the same amount of shear displacement. The total shear force ($\sum_{i=1}^{n} T_i$) was then converted into stress units by dividing with the total joint area ($\sum_{i=1}^{n} A_i$). An example of that cumulative process is given below where a full size joint is assumed to have been divided into 18 jointed blocks which were tested separately:

Shear displacement (mm)	SHEAR FORCE (T)				CUMULATIVE SHEAR FORCE $\sum_{i=1}^{18} T_i$
	Block no.1	Block no.2	.....	Block no.18	
0.10	21	18	.....	10	21 + 18 + ... + 10
0.20	32	26		22	32 + 26 + ... + 22
0.30	37	25		30	37 + 25 + ... + 30
⋮	⋮	⋮		⋮	⋮
1.00	24	21		19	24 + 21 + ... + 19
⋮	⋮	⋮			⋮

Tables with the cumulative results for all types of models and block sizes are included in Appendix II.

The shear stress-shear displacement diagrams are presented in Figures 2.30 - 2.40. Each of those figures also includes the corresponding dilation curves, to which reference will be made in the next section.

The τ-d_h curves demonstrate clearly the scale effects on the shear strength and deformation properties of joints. Study of the diagrams obtained for each of the eleven types of surfaces reveals, in addition to the already discussed size-dependency of peak shear strength, two further scale effects:

(i) a gradual increase in the peak shear displacement (d_{hp}) with increasing joint block size,

(ii) an apparent transition from "brittle" to "plastic" mode of shear failure.

2. Shear displacement-size effects

The displacement-size effect is illustrated in Figure 2.41 where the average d_{hp} values given in Tables 2.6 - 2.16 have been plotted against the respective joint length (L).

As shown by the three groups of data in Figure 2.41, the geometry of the surfaces played a decisive role in the variation of d_{hp} with increasing joint length. In general, the rough undulating joint types (nos. 1, 2, 3, 4, 5) underwent larger horizontal displacements before peak strength was reached than those with rough but less wavy surfaces (nos. 6, 7, 8), while the joint types with the least irregular wall geometry (nos. 9, 10, 11) occupied the lowest end of the d_{hp} range.

The differences in the magnitude of displacements as related to surface roughness were more pronounced between the larger block sizes and in particular those of length 18 or 20 cm and 36 or 40 cm. The above size-roughness-displacement effects are summarized in Table 2.19, where the mean d_{hp} values corresponding to each group of data in Figure 2.41 are presented, together with the equivalent prototype values.

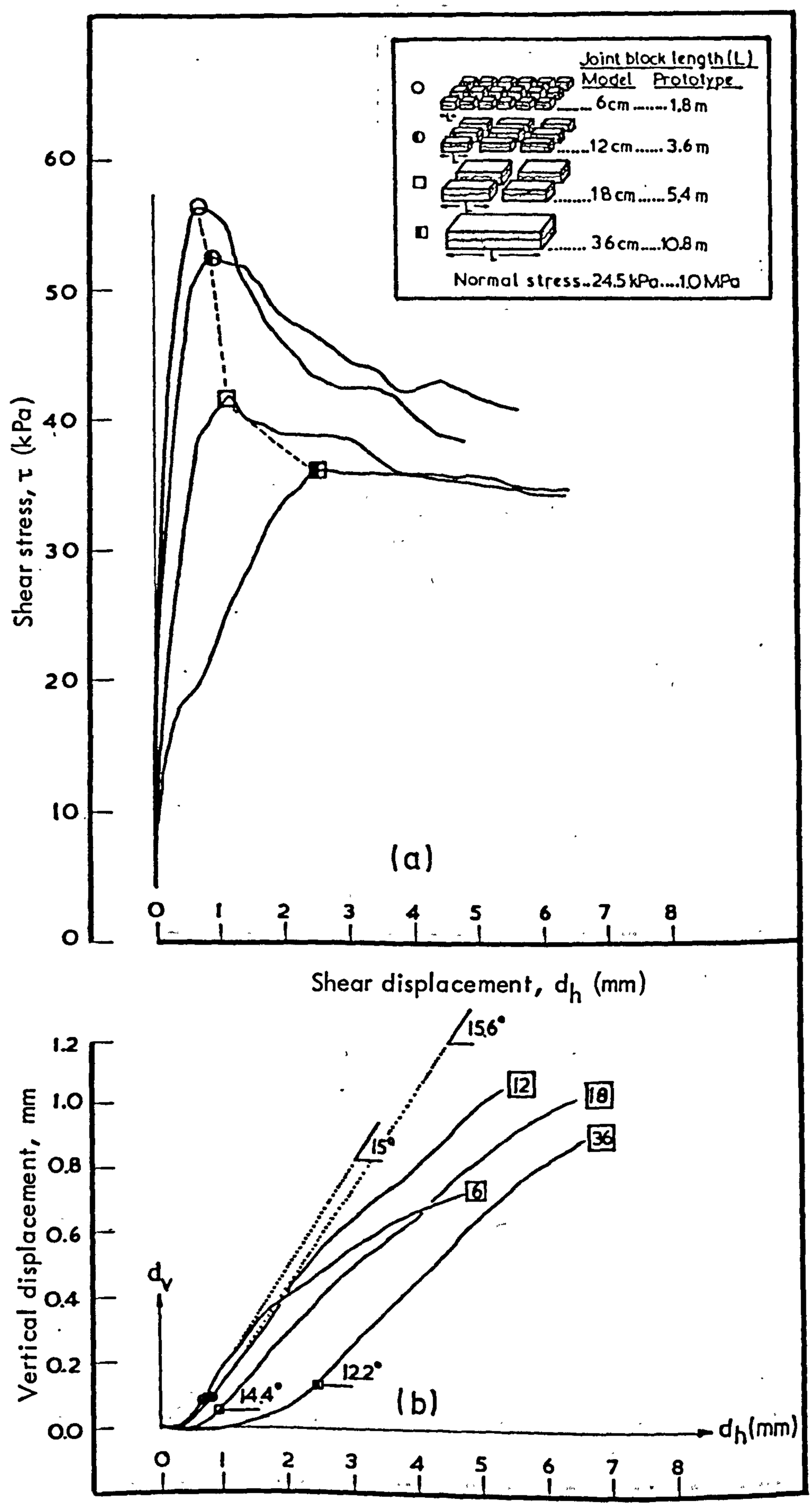

FIGURE 2.30 Cumulative mean shear stress – shear displacement (a) and dilation (b) curves of MODEL No. 1

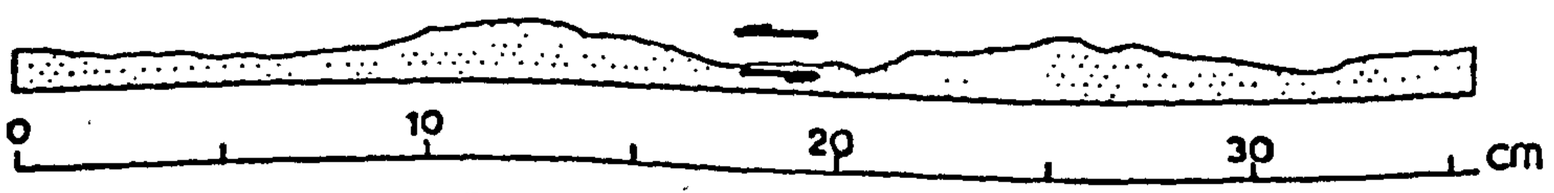

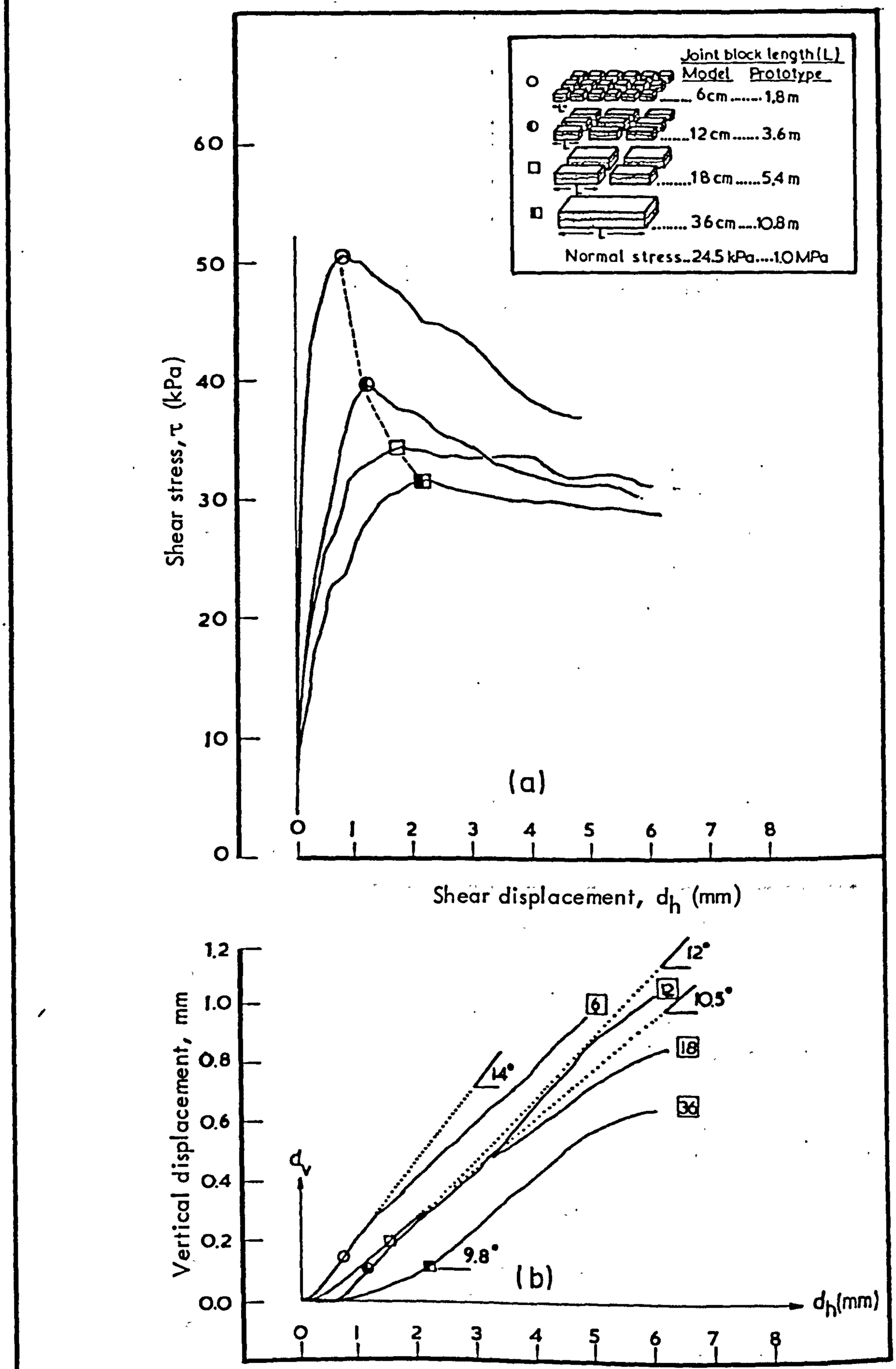

FIGURE 2.31 Cumulative mean shear stress – shear displacement (a) and dilation (b) curves of MODEL No.2

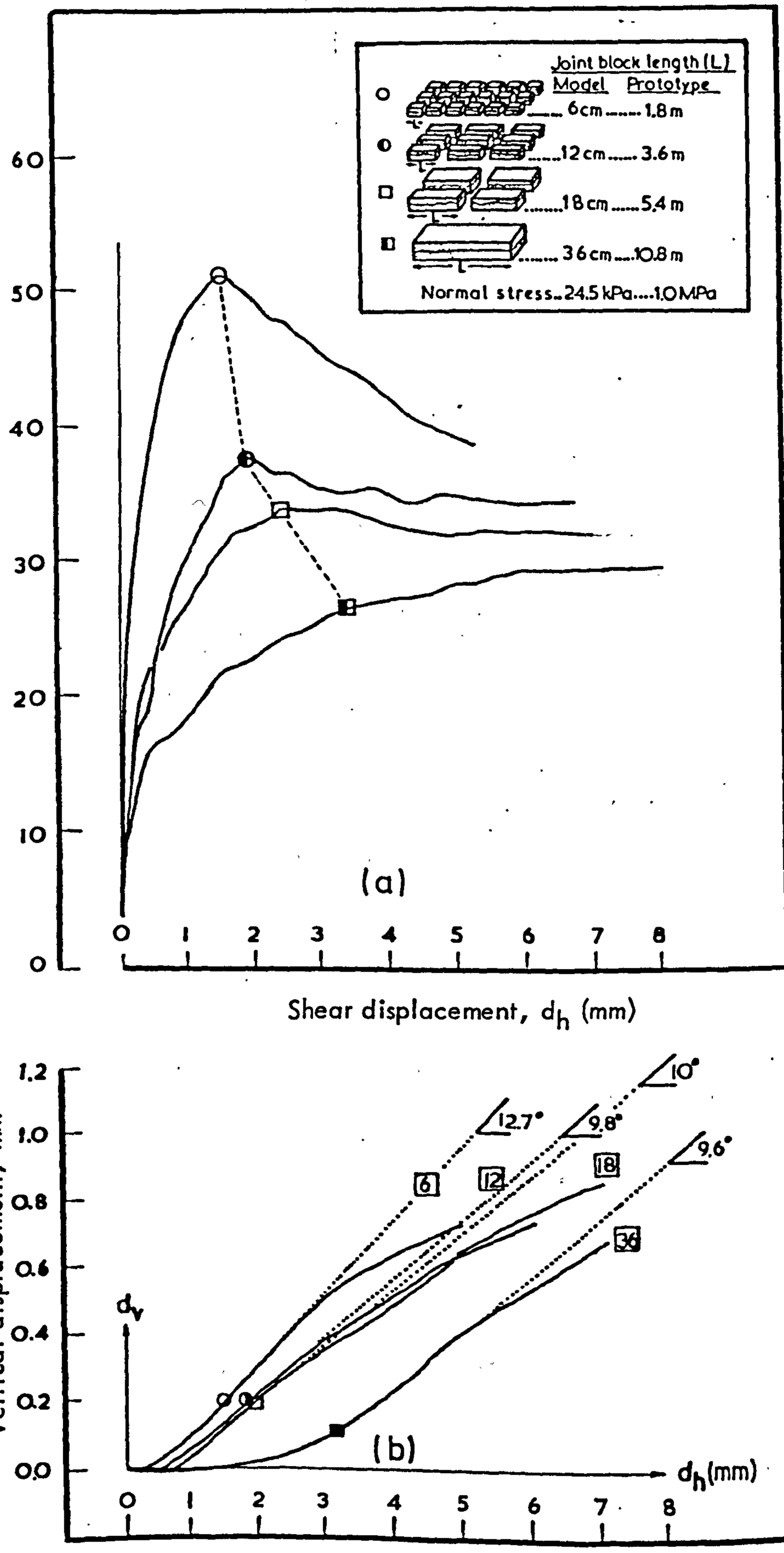

FIGURE 2.32 Cumulative mean shear stress – shear displacement (a) and dilation (b) curves of MODEL No.3

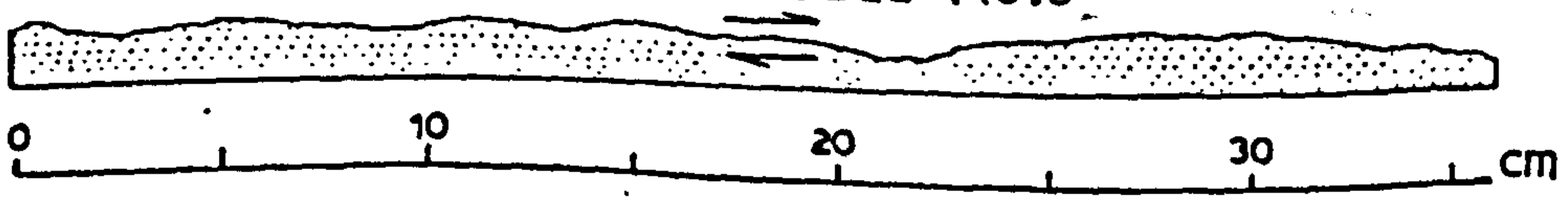

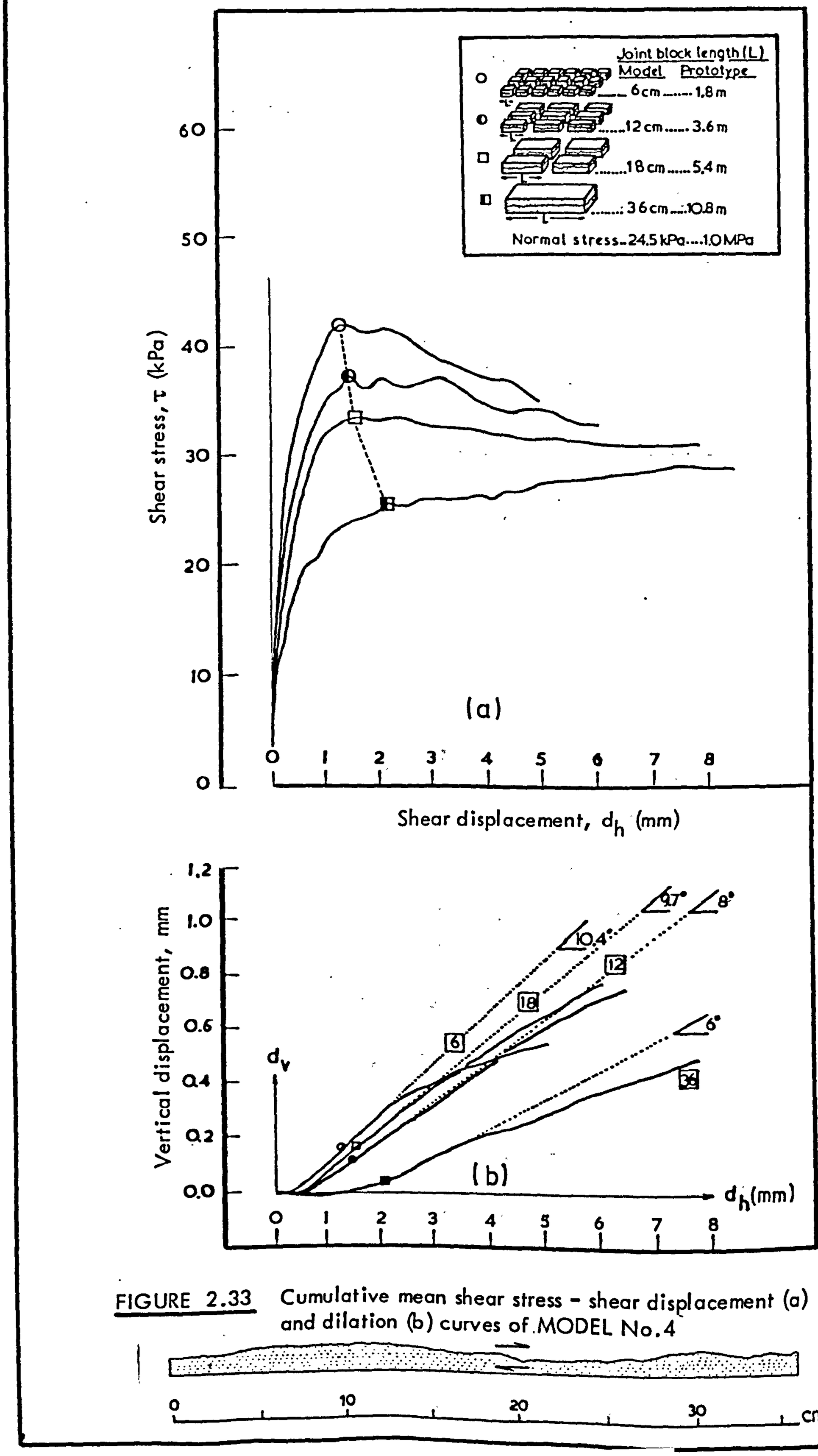

FIGURE 2.33 Cumulative mean shear stress - shear displacement (a) and dilation (b) curves of MODEL No.4

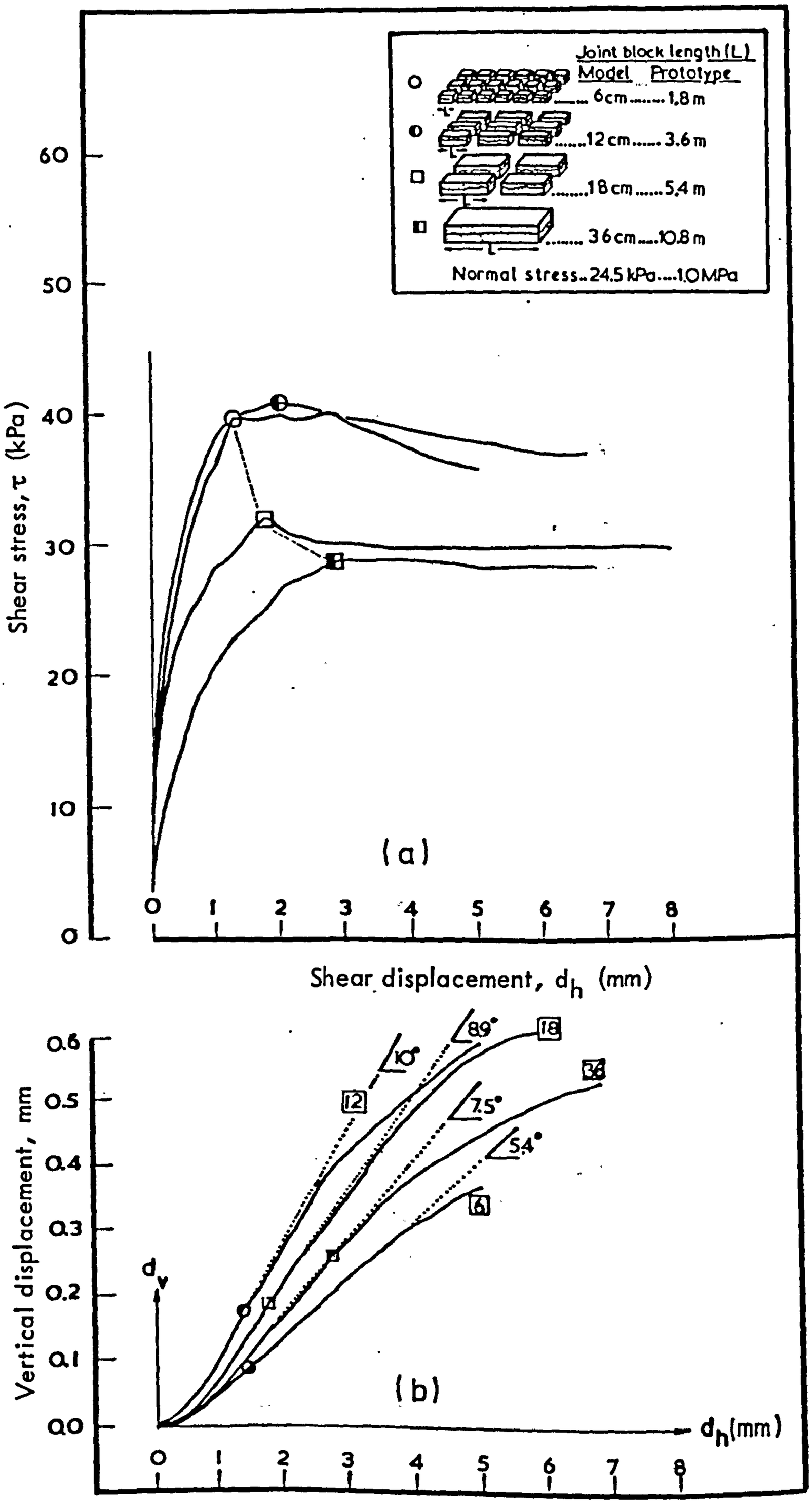

FIGURE 2.34 Cumulative mean shear stress – shear displacement (a) and dilation (b) curves of MODEL No.5

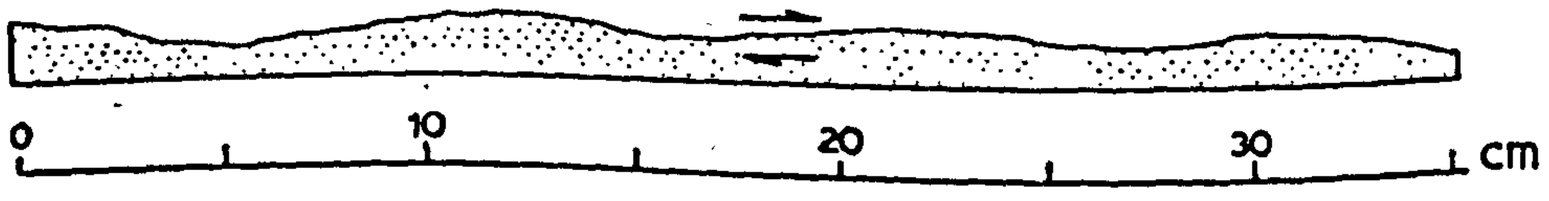

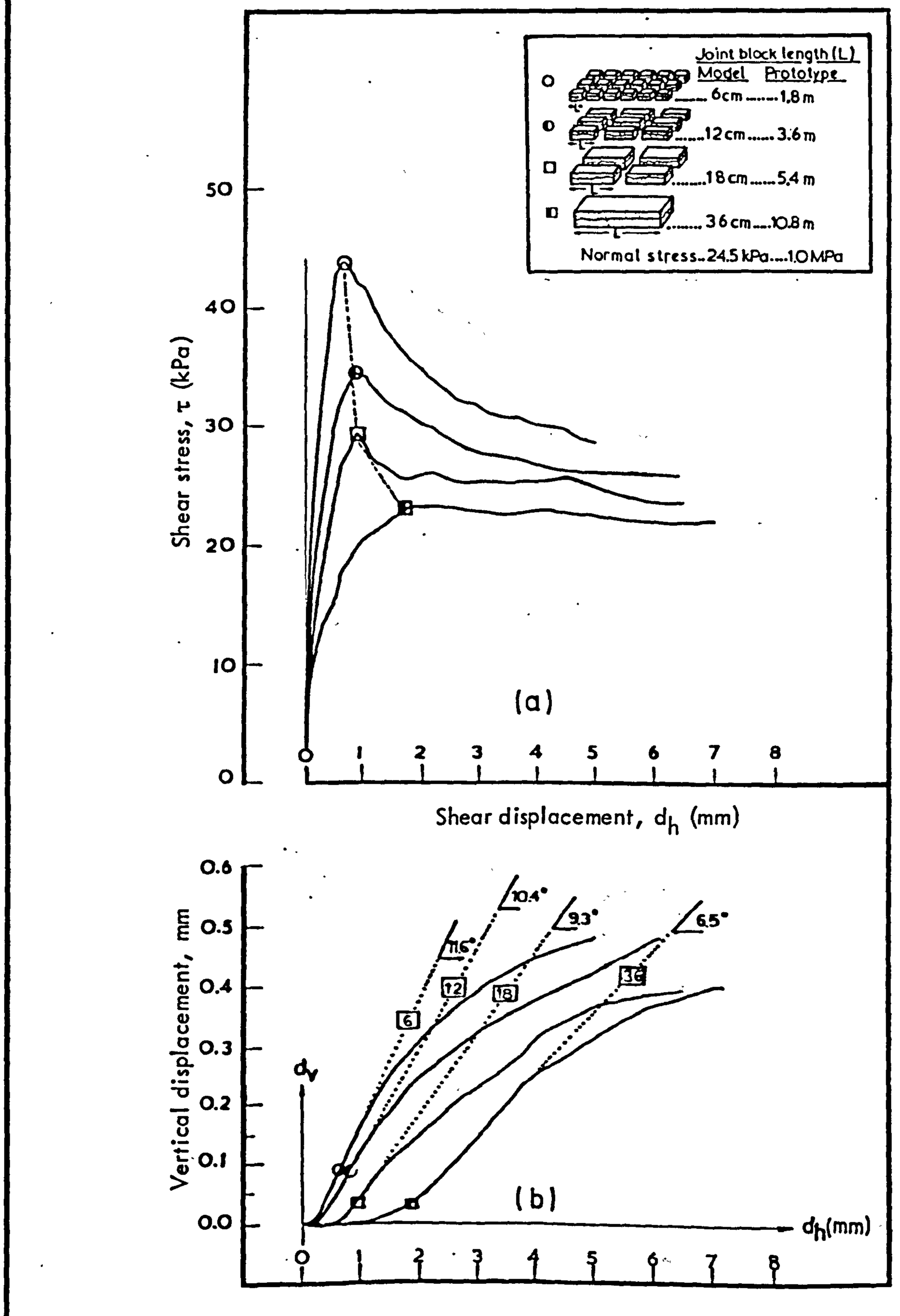

FIGURE 2.35 Cumulative mean shear stress – shear displacement (a) and dilation (b) curves of MODEL No.6

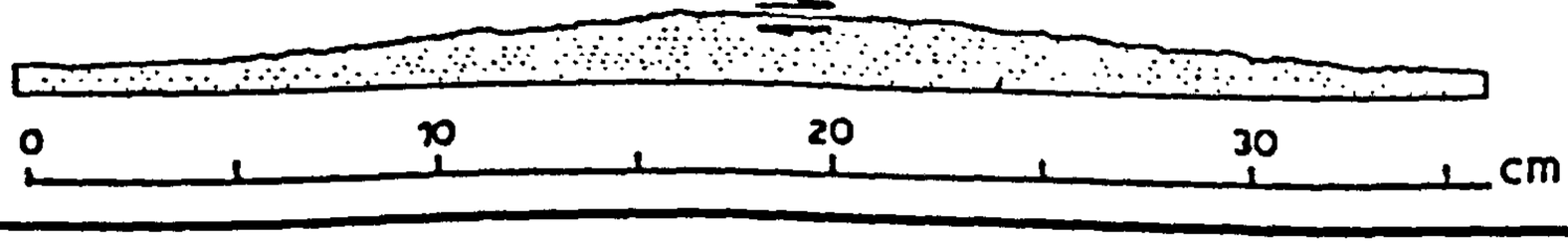

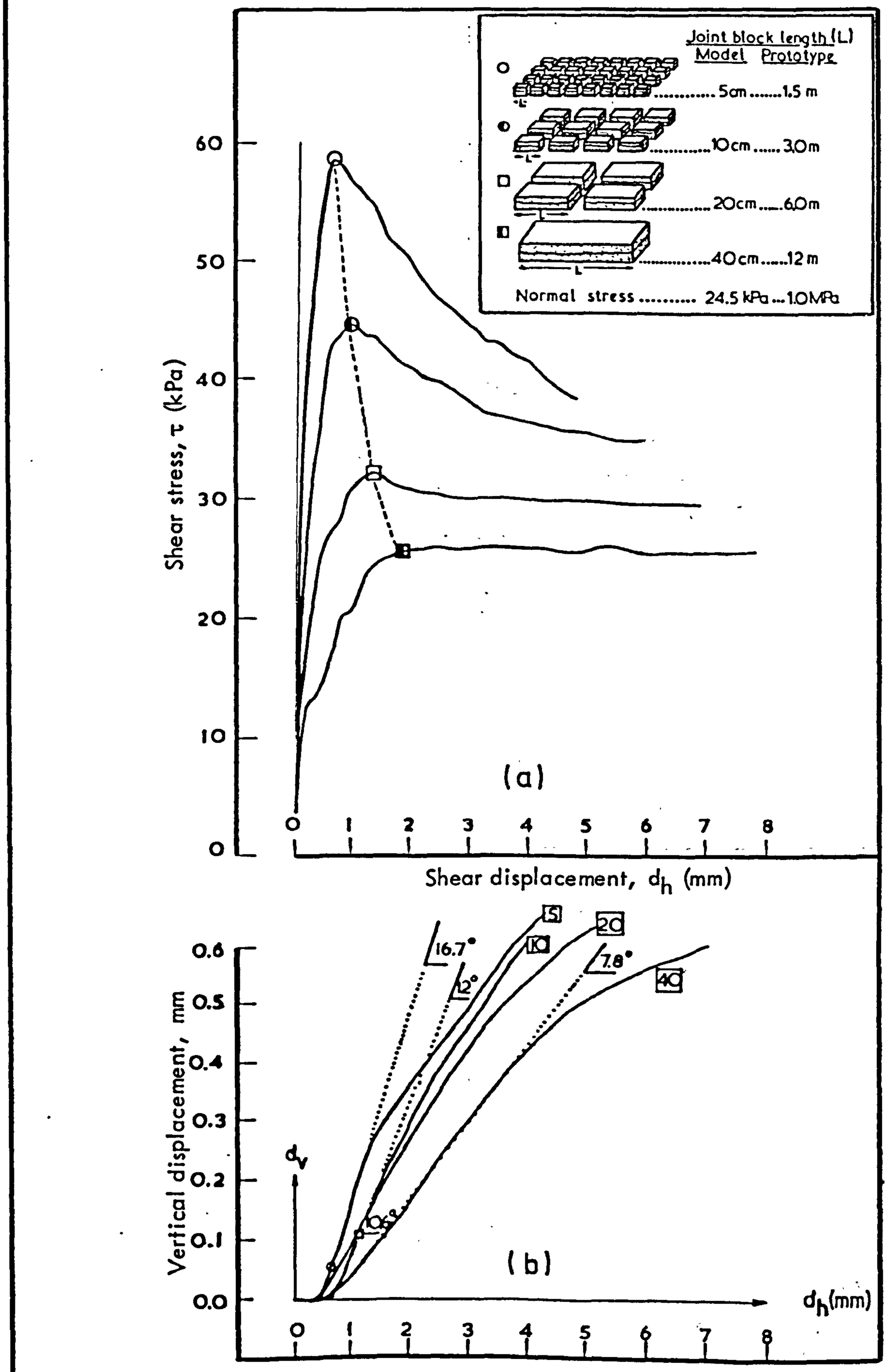

FIGURE 2.36 Cumulative mean shear stress – shear displacement (a) and dilation (b) curves of MODEL No.7

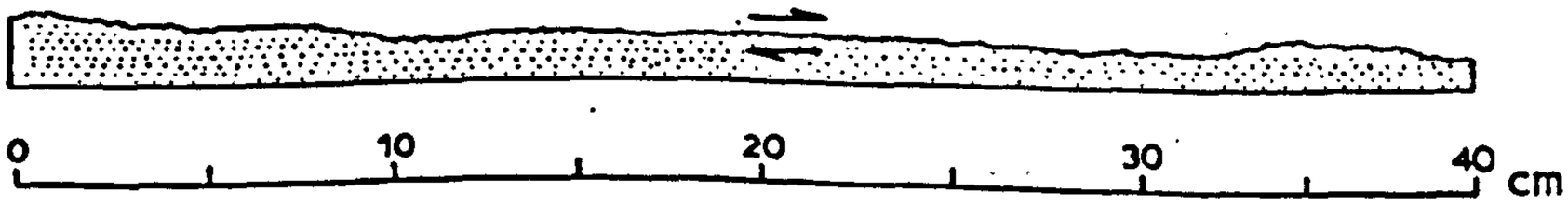

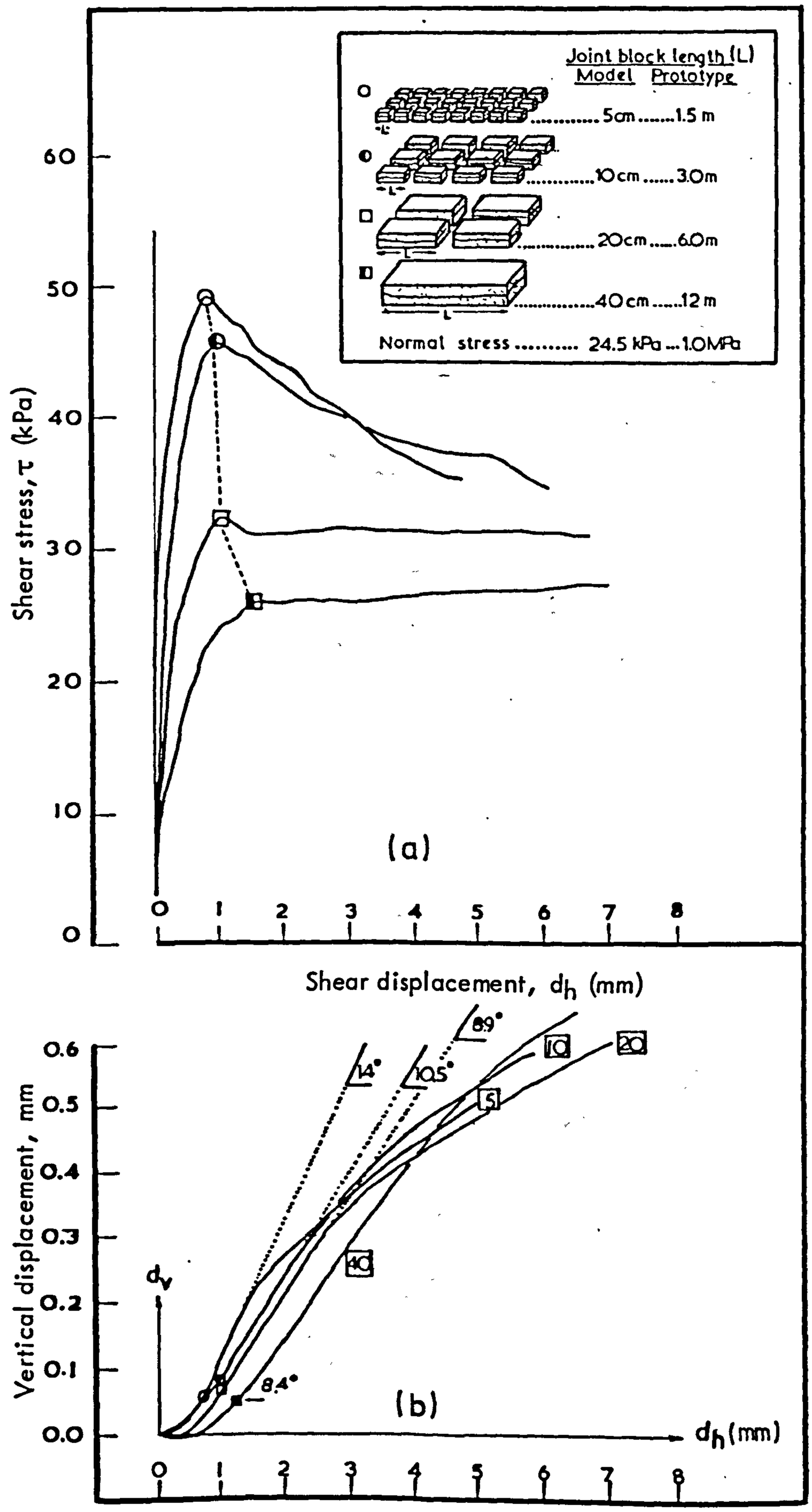

FIGURE 2.37 Cumulative mean shear stress – shear displacement (a) and dilation (b) curves of MODEL No.8

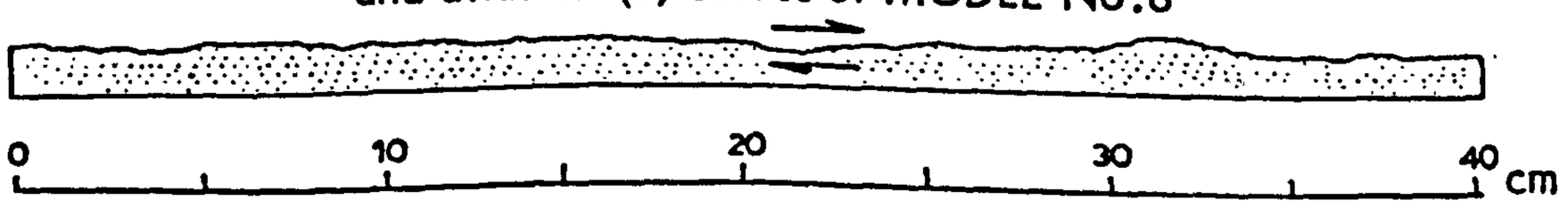

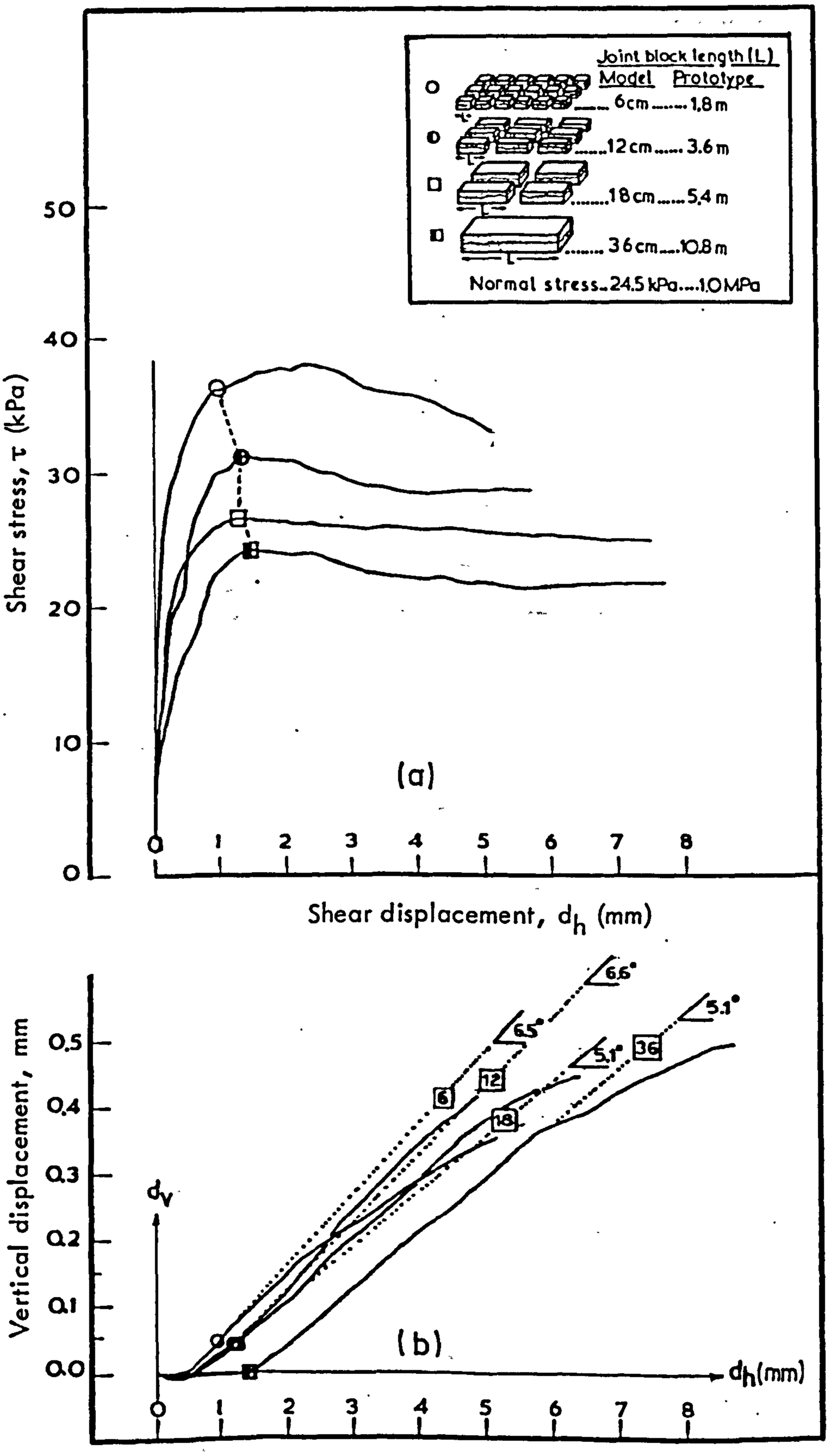

FIGURE. 2.38 Cumulative mean shear stress – shear displacement (a) and dilation (b) curves of MODEL No.9

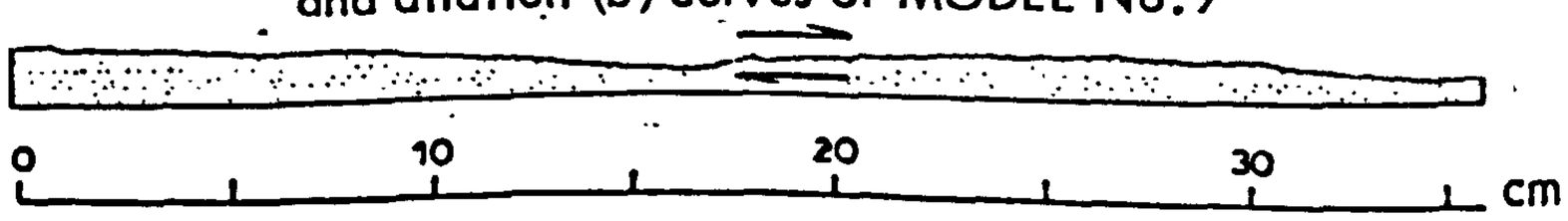

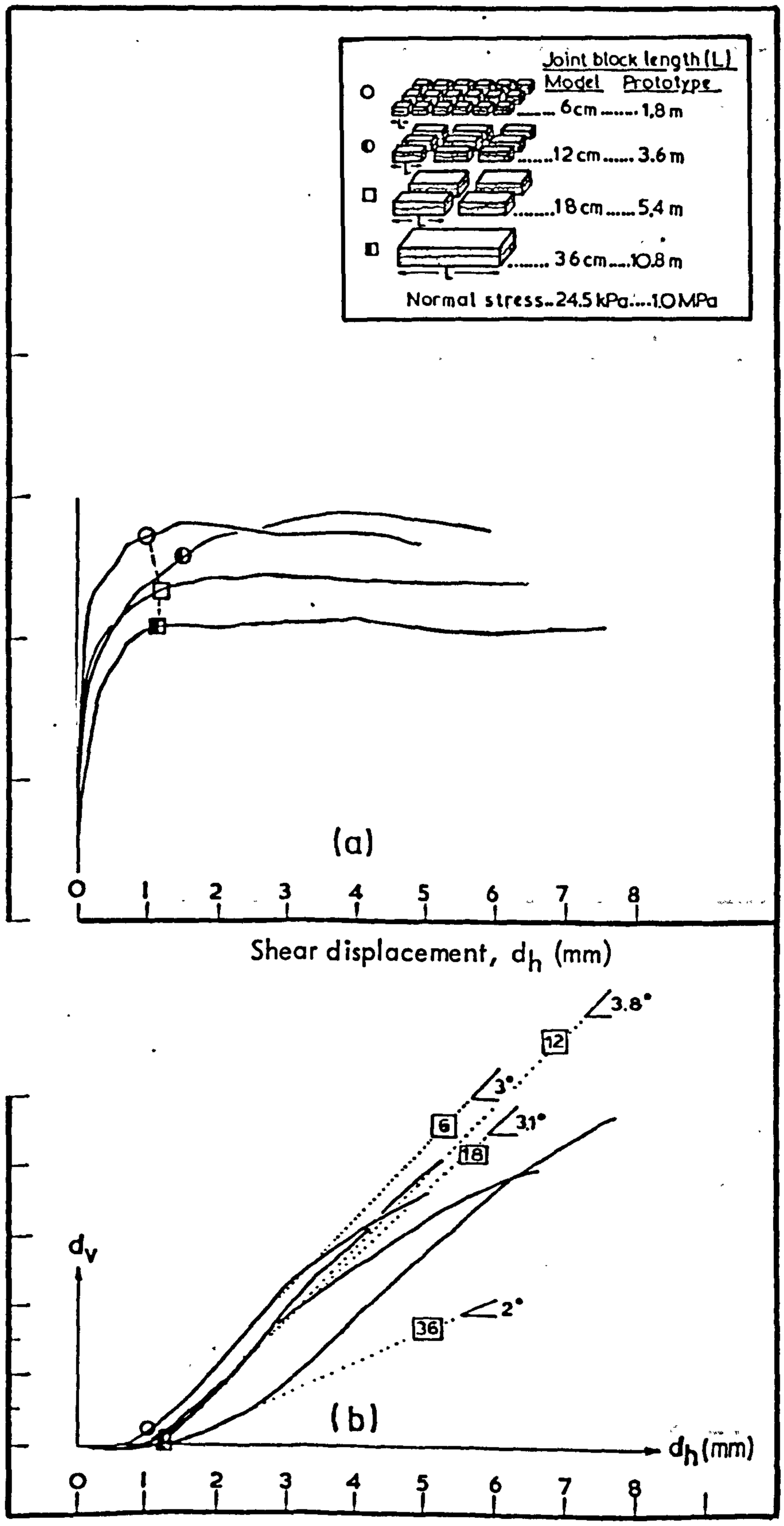

FIGURE 2.39 Cumulative mean shear stress – shear displacement (a) and dilation (b) curves of MODEL No. 10

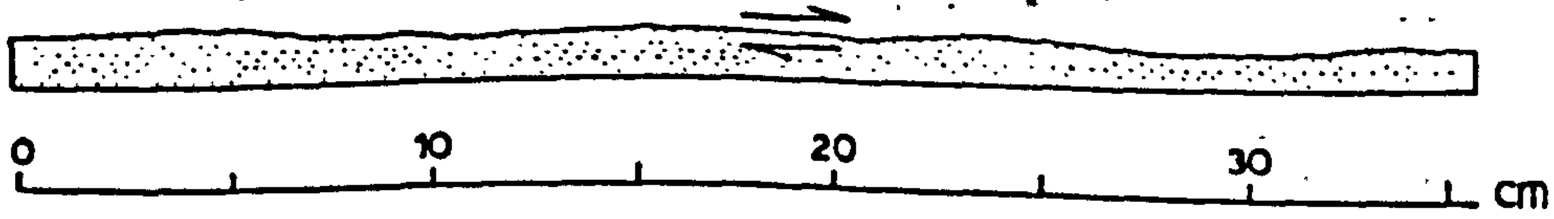

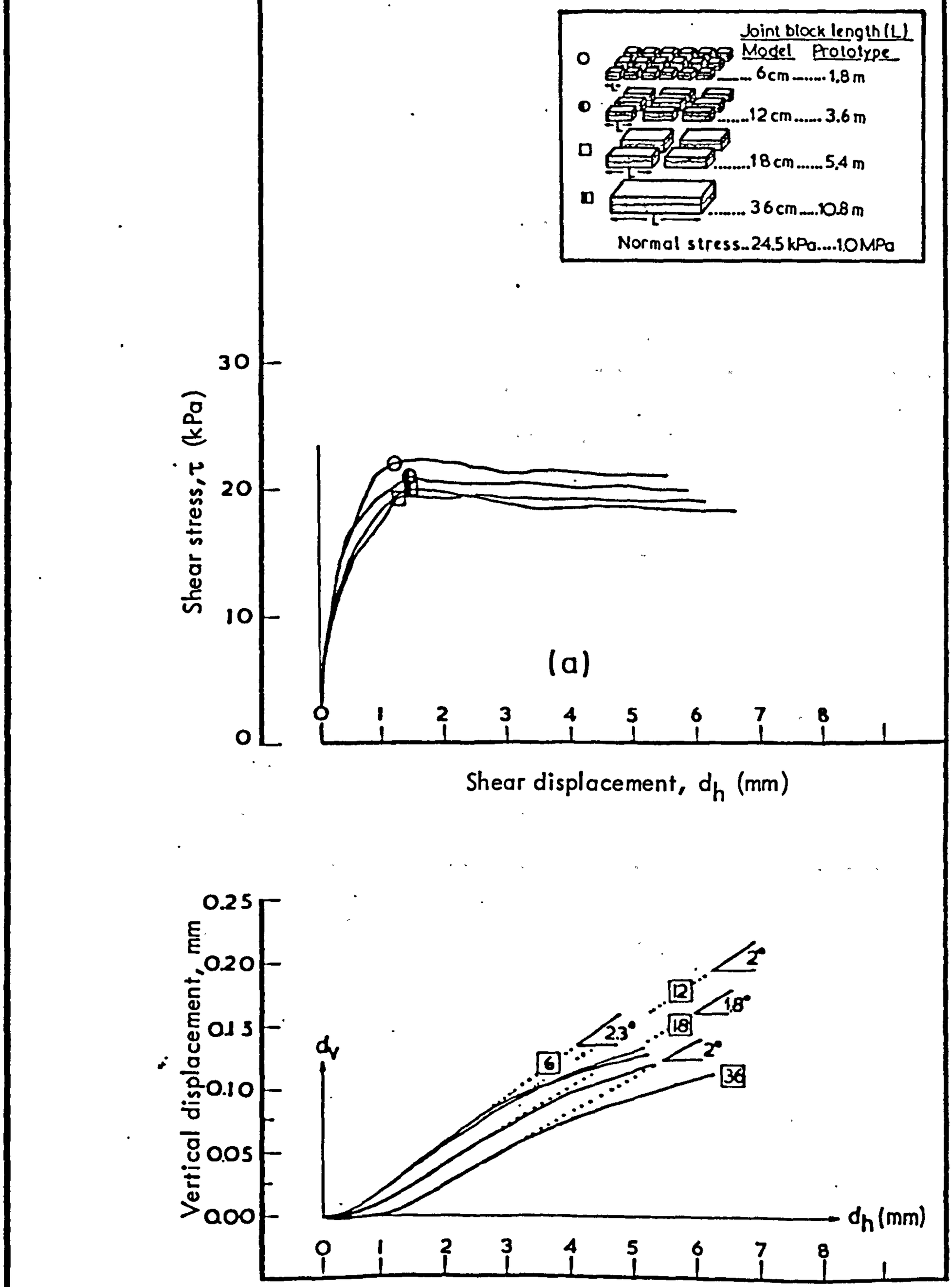

FIGURE 2.40 Cumulative mean shear stress – shear displacement (a) and dilation (b) curves of MODEL No. 11

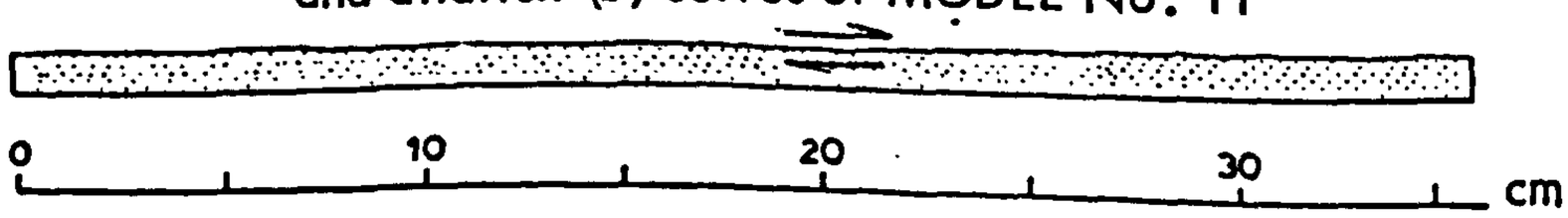

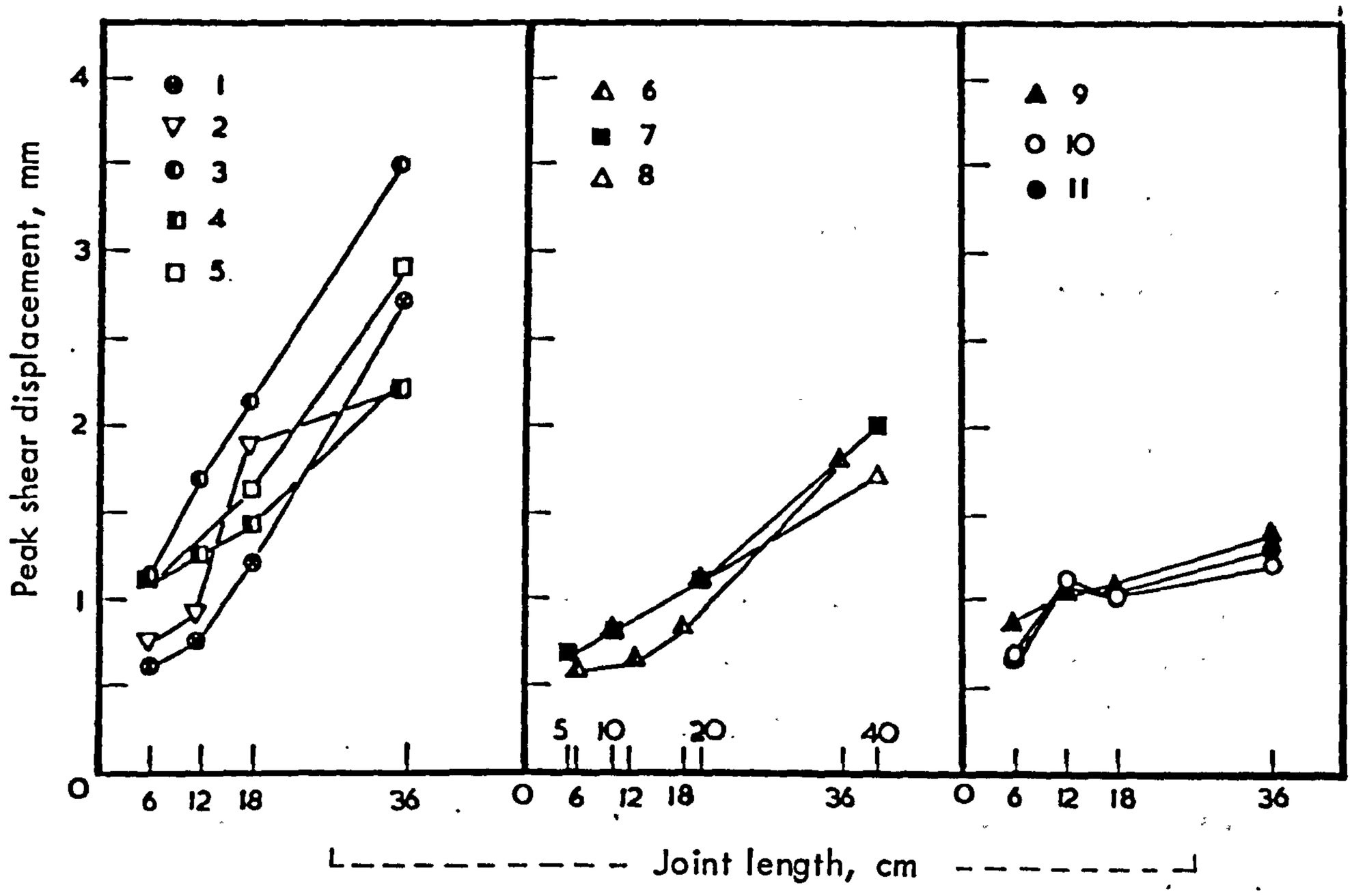

FIGURE 2.41 Variation of peak shear displacement with increasing length of joint specimen.

TABLE 2.19

Summary of the peak displacement-size effect

JOINT LENGTH (L)		MODEL Nos.					
Model M (cm)	Prototype P (m)	1, 2, 3, 4, 5		6, 7, 8		9, 10, 11	
		M(mm)	P(cm)	M(mm)	P(cm)	M(mm)	P(cm)
5,6	1.5,1.8	0.90	2.91	0.65	1.95	0.74	2.22
10,12	3.0,3.6	1.20	3.60	0.76	2.28	1.06	3.18
18,20	5.4,6.0	1.64	4.92	1.01	3.03	1.06	3.18
36,40	10.8,12	2.67	8.01	1.83	5.49	1.30	3.90

Overall, a maximum increase in joint length by a factor of 6 to 8 resulted in an increase in d_{hp} by a factor of 1.8 to 2.8. The effect of surface roughness upon the peak displacement of equidimensional blocks agrees, at least in a qualitative sense, with the behaviour expected from natural joints. Peak displacements of 0.1 to 0.2 mm were quoted by Goodman (1970) as typical of smooth fractures, compared to d_{hp} values of the order of 2 to 8 mm normally obtained from rough joints.

A certain amount of quantitative exaggeration probably exists in some of the equivalent prototype d_{hp} values included in Table 2.19, if the peak displacements usually measured from in-situ shear tests (rarely exceeding 2 centimeters) were used as a basis for comparison. Peak displacements in the order of 5.5 to 8.0 cm associated with joints approximately 11 to 12 meters long might not appear too unrealistic, although "specimen" sizes in that range are well beyond the usual reach of in-situ tests and obviously no valid comparisons can be made.

On the basis of results from tests on model fractures, Barton (1972) suggested that an empirical relationship of "d_{hp} equal to 1% of joint length" offers a reasonable compromise for a practical allowance of the size-displacement effect. The "1% rule-of-thumb" was tested against the mean data in Table 2.19 and the findings are summarized below:

JOINT LENGTH (L) Model (cm)	Prototype (meters)	Mean $\frac{d_{hp}}{\text{Joint length (L)}}$ x 100		
		1, 2, 3, 4, 5	6, 7, 8	9, 10, 11
5,6	1.5,1.8	1.5%	1.2%	1.2%
10,12	3.0,3.6	1.0%	0.7%	0.9%
18,20	5.4,6.0	0.9%	0.5%	0.6%
36,40	10.8,12.0	0.7%	0.5%	0.4%

In general, the empirical rule appears to agree reasonably well with the experimental data with the exception of the large joints (18-40 cm long) of model nos. 6 to 11. The overall mean of the (d_{hp}/L) x 100 values derived for joint nos. 1 to 5 (full range of block sizes) is 1.025%, while for the 5 to 12 cm long joints of model nos. 6 to 11 the mean values are 0.95% and 1.05%.

Barton and Choubey (1977) pointed out that d_{hp} would be expected to reduce to less than 1% of the joint length as the latter increased to several meters. Distinction of a limiting joint length beyond which the 1% rule ceases to have any realistic correspondence to the actual behaviour is a difficult task when the combined effect of both size and roughness effects on peak displacement is considered.

On the basis of the present experimental results it would appear that such a limit could be represented by the 18 cm long joints of the undulating joint types (nos. 1 to 5) and probably the 10 to 12 cm long joints representing less wavy to relatively planar surfaces (nos. 6 to 11). Those sizes interpreted at prototype scale correspond to joints 5.4 and 3.0-3.6 meters long respectively. It is perhaps unwise to quantify these observations further in view of the uncertainties surrounding the relevance of model joint roughness to that of natural exposures.

Peak shear displacement is actually a measure of the distance a joint has to travel from an initial "at rest" position until effective contact is made between the irregularities controlling its peak resistance. The displacement-size effect revealed in the present series of joint types implies a potential involvement of different orders of asperities in defining the optimum shear path of joints of different length. Conclusive evidence to that effect will soon be given.

The scale-dependency of peak shear strength (τ_p) and peak horizontal displacement (d_{hp}) combined produces a strong scale effect upon the property of shear stiffness (K_s), which is expressed as

$$K_s = \frac{\tau_p}{d_{hp}} \qquad 2.15$$

i.e. as the average slope of the pre-peak portion of the τ-d_h curve. The effects of scale upon the shear stiffness of joints have been considered by Barton (1972), Barton and Choubey (1977) and Barton and Hansteen (1979). That aspect will be discussed in part three of the thesis.

An interesting feature of the pre-peak part of a number of τ-d_h curves representing joint blocks 18 and 36 cm long was the occurrence of one or more inflection points normally followed by a discernible decrease in the slope of the line. Such slope changes can be seen in some of the curves of

model nos. 1 (36 cm), 2 (18 and 36 cm), 3 (36 cm) and 7 (36 cm) in Figures 2.30, 2.31, 2.32 and 2.36 respectively.

Similar interruptions of the continuity of the pre-peak portion of the shear stress-horizontal displacement curves are frequently observed in shear testing of rock joints. They are generally attributed to a small preliminary displacement occurring at some shear stress level, which brings the two halves of an undisturbed joint into a fully interlocked position.

The present model joints were fully interlocked prior to the application of shear force. Furthermore, it would appear that those inflection points and accompanying slope changes occurred after horizontal displacements corresponding roughly to the average peak displacements of the 6 cm and sometimes 12 cm long joints. A plausible explanation relating the above features with a probable "progressive" joint failure will be given in Section 2.4.8.

3. Modes of failure with increasing joint block size

The apparent change in the mode of shear failure from "brittle" to "plastic" as the joint length increased can be seen to persist, to a greater or lesser extent, in all the highly irregular types of surfaces tested. Rough joints 5 or 6 cm long displayed a marked drop in shear strength almost immediately after mobilization of peak resistance to levels rapidly approaching ultimate conditions ("brittle" mode of failure) as shown by the corresponding τ-d_h curves of model nos. 1, 2, 3, 4, 6, 7, 8 in Figures 2.30 - 2.33 and 2.35 - 2.37. Similar behaviour but somewhat less pronounced was shown also by the 10-12 cm long joints of the same 1 to 8 surface types.

As the size of the individual blocks was increased further to 18 or 20 cm, a much more "stable" failure was observed. Mobilization of peak shear strength was followed by only small changes in the shear resistance with increasing horizontal displacement (quasi-"plastic" mode of failure). Such a pattern was characteristically shown by almost all the largest specimens (full scale models 36 or 40 cm long) tested. Two exceptional cases of "strain-hardening" behaviour should be noted (36 cm long joints in Figures 2.32 and 2.33). In those cases prolonged sliding was associated with small increase in the shear strength, until an apparently stable state

was approached after 7-8 mm of displacement. The relevance of the above patterns of behaviour to that expected from a jointed rock mass is discussed in Section 2.4.8.

Ultimate strength is reached after horizontal displacements of a scale larger than the size of the irregularities of the joint walls (Krahn and Morgenstern, 1979); in other words, when the joint halves have displaced by an amount sufficient to result in loss of the effective contact between the asperities at the moment of peak shear resistance.

In that context, the contrast in the post-peak behaviour of small and large specimens representing identical sliding planes indirectly implies that asperities of different baselength effectively control the shear strength of joints of different lengths. Evidently, the shear displacement of joint specimens 18 cm and in particular 36 cm long was not adequately large in relation to the size of the "important" irregularities to enable substantial overriding of the latter, unlike the cases of the smaller joint block sizes.

As would be expected, the "flat" geometry of the roughness features of all scales on the relatively planar and smooth types of surfaces (model nos. 10 and 11) resulted in a more or less "plastic" behaviour irrespective of joint block size.

The analysis so far of the shear characteristics of joint blocks of various sizes indicates the probable involvement of asperities of different order, which potentially control the shear behaviour of joints of correspondingly different lengths. The effects of surface roughness are reflected in the all-important property of joint dilation. The variations in the latter associated with increasing joint lengths are discussed in the next section.

2.4.5 Dilation-size effects in joints

The dilation curve for each "jointed" model was derived by averaging the vertical displacements (d_v) of all component blocks for the same increment of shear displacement (d_h). The average vertical displacement data for each joint type and block size are included in the Tables of Appendix II. The d_v vs d_h graphs have been presented together with the τ-d_h diagrams in Figures 2.30 to 2.40.

The peak dilation angle (i_p^o) was calculated in each case from the slope of the portion of the dilation curve corresponding to peak shear displacement. The so derived average i_p^o values are given in Table 2.20 and their variation with length of joint is illustrated in Figure 2.42.

As can be seen from the tabulated and plotted data the average peak dilation angle dropped appreciably with increasing joint length. The maximum difference in the i_p^o values between the largest and smallest block sizes representing non-planar surfaces ranged approximately between 2.5^o and 9.0^o, although in majority the maximum drops in i_p were below 5^o. The surfaces with regular geometry showed an extremely small (no. 10) to practically non-existent (no. 11) variation in i_p^o with increasing joint length, as would obviously be expected.

The differences between the average i_p^o values displayed by the same joint when variable profile lengths were sheared under the same normal stress signify that the peak shearing path of short and long joint profiles was defined by asperities of different baselength. Under a given σ_n the peak dilation angle represents the inclination of the contacts between the 'effective' asperities with respect to the mean joint plane at the instant of peak strength. Analyses of joint profiles have shown that the longer the baselength considered, the less steep the asperities (Patton 1966, Barton 1971 and Rengers 1971/ quoted in Goodman 1976). Combining the scale effects in the shear displacement required to mobilize the peak strength and in the peak dilation angle it becomes clear that as the length of joint samples increased peak resistance was not reached until effective contact had been developed between asperities of longer baselength and correspondingly 'flatter' slopes. That was confirmed from post-test observations of the sheared surfaces (see next section). The reducing dilation of longer joint samples accounts for part of the strength loss displayed by the latter. Partial or complete damage of effective asperities under the experimental σ_n contributed a shearing component to the peak total frictional resistance as will be discussed in section 2.4.7.

An extremely significant implication of the involvement of asperities of different baselength in controlling the shear strength of different joint lengths is that the value of the joint roughness coefficient (JRC) determined for a particular joint exposure will depend upon the size of specimen tested. A joint length whose peak behaviour was controlled by small steep asperities would give a higher JRC value than a longer profile (of the same joint) whose behaviour was dominated by larger and more gently inclined irregularities.

TABLE 2.20

Average peak dilation angles (i_p^o) of different joint lengths.

JOINT LENGTH (L)		MODEL Nos.										
Model (cm)	Prototype (m)	1	2	3	4	5	6	7	8	9	10	11
5,6	1.5,1.8	15.0°	14.0°	12.7°	10.4°	5.4°	11.6°	16.7°	14.0°	6.5°	3.0°	2.3°
10,12	3.0,3.6	15.6°	12.0°	9.8°	8.0°	10.0°	10.4°	12.0°	10.5°	6.6°	3.8°	2.0°
18,20	5.4,6.0	14.4°	10.5°	10.0°	9.7°	8.9°	9.6°	10.6°	8.9°	5.1°	3.1°	1.8°
36,40	10.8,12.0	12.2°	9.8°	9.6°	6.0°	7.5°	6.5°	7.8°	8.4°	5.1°	2.0°	2.0°

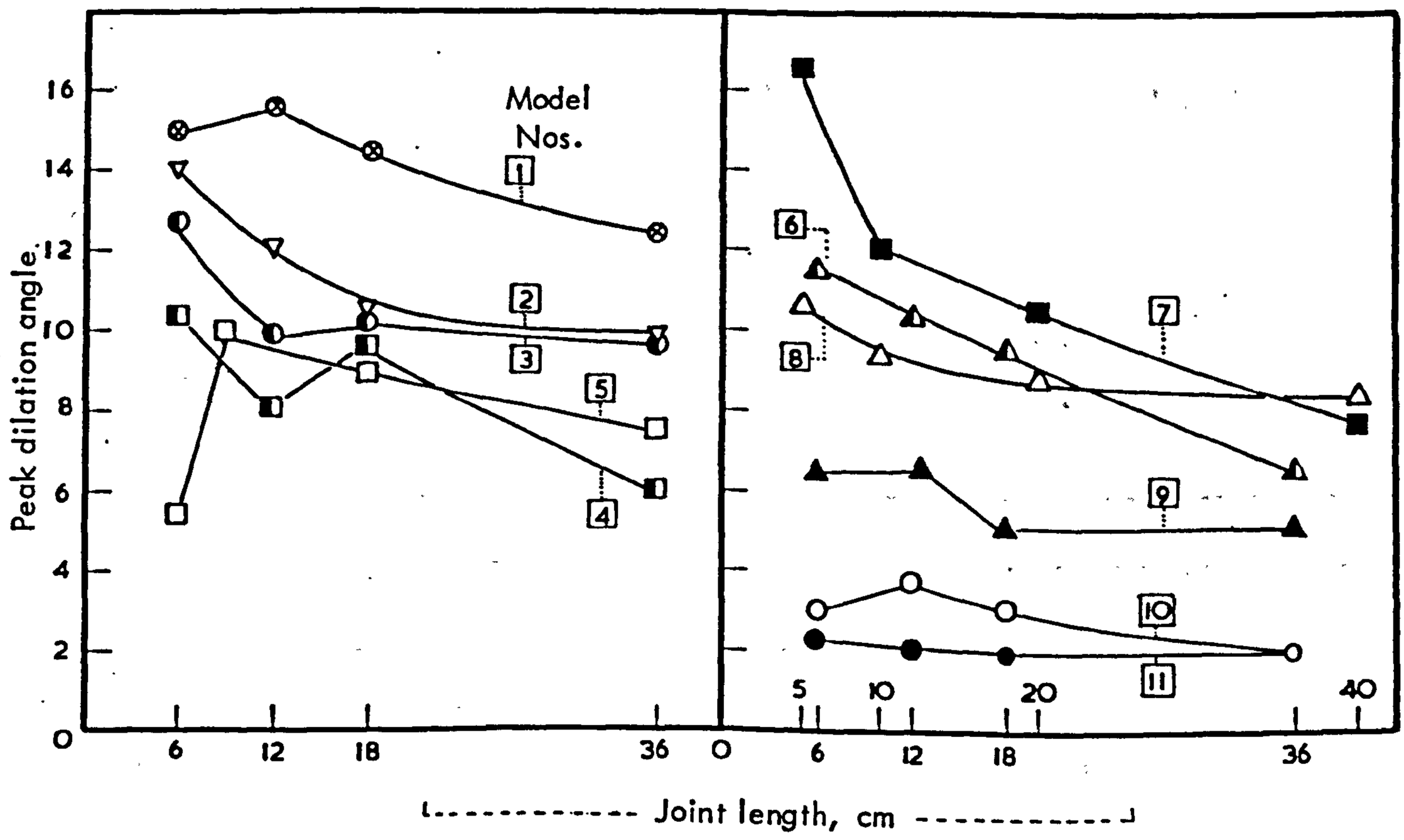

FIGURE 2.42 Variation of peak dilation angles with increasing length of joint specimen

2.4.6 The scale dependency of Joint Roughness Coefficients

The values of JRC corresponding to the full size surfaces and the cumulative mean JRC's for each set of individually tested joint specimens have been back-calculated from Barton's equation:

$$JRC = \frac{\arctan(\tau_p/\sigma_n) - \phi_b}{\log_{10}(JCS/\sigma_n)}$$

where: τ_p = cumulative mean peak shear stress (kPa)
σ_n = normal stress equal to 24.5 kPa
ϕ_b = basic angle of friction (= 32°)
JCS = joint compressive strength equal to 2000 kPa.

The back-analyzed values are presented in Table 2.22 and the variation in JRC with increasing length of joint is illustrated in Figure 2.43. The tabulated and plotted data show very distinctly the reduction in the effective JRC value representing the same joint surface as the length of profile of the individual block components increased. The JRC values dropped by a maximum of 1.3 to 11.2. As is to be expected the minimum reductions were associated with the relatively smooth and planar joint types (nos. 10 and 11).

TABLE 2.22

Cumulative mean JRC values for different types of surfaces and joint lengths.

JOINT LENGTH (L)		MODEL Nos.										
Model (cm)	Prototype (m)	1	2	3	4	5	6	7	8	9	10	11
5,6	1.5,1.8	18.1	16.8	17.0	14.5	13.8	15.0	18.5	16.7	11.9	8.4	5.1
10,12	3.0,3.6	17.3	13.6	13.1	13.0	13.7	11.8	15.3	15.7	10.3	7.2	4.4
18,20	5.4,6.0	14.4	11.8	11.7	11.4	10.9	9.6	10.8	11.1	7.8	6.2	3.5
36,40	10.8,12.0	12.5	10.4	7.8	7.5	9.0	6.0	7.3	7.5	6.5	4.5	3.8

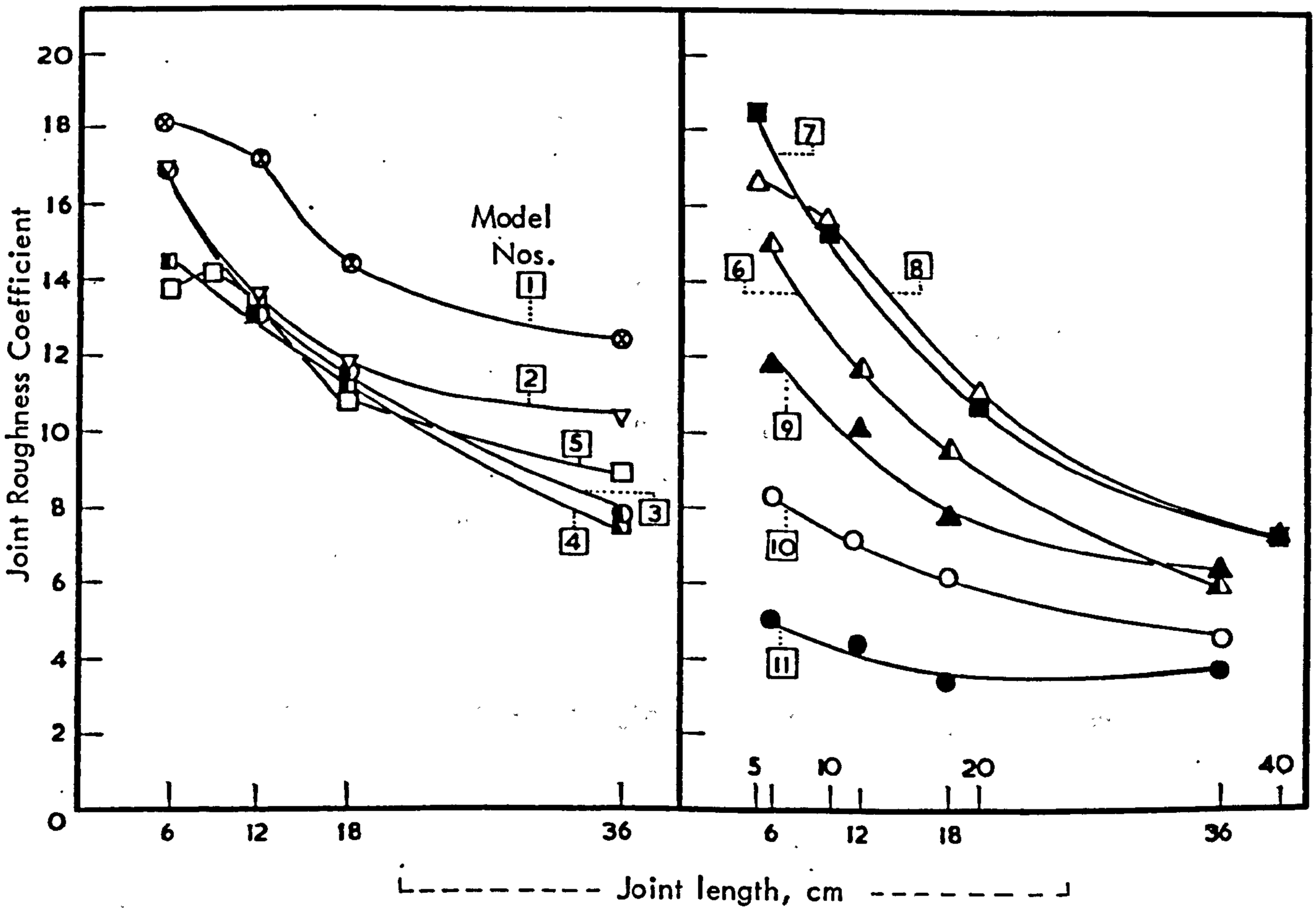

FIGURE 2.43 Variation of Joint Roughness Coefficients with increasing length of joint specimens.

The scale-dependency of JRC manifests the potential decline in the effective contribution of surface roughness to the total frictional resistance of a non-planar joint as its length increases. Barton and Choubey (1977) drew attention to the probable size-effects in the joint compressive strength (JCS) as a consequence of similar effects in the uniaxial compressive strength of intact rock.

A constant JCS value (= 2000 kPa) was used in the derivation of the JRC estimates in Table 2.22. Had the JCS been assumed as size-dependent and the original value of 2000 kPa been reduced, the back-calculated JRC's for joint lengths larger than 5 or 6 cm would have been somewhat larger than those given in Table 2.22. Some characteristic examples will be presented in the next section.

The probability of scale effects in both JRC and JCS implies that the lower shear strength of longer joints could result partly from a reduced geometrical contribution of the surface roughness (lower JRC) and partly from a reduced resistance to failure of larger asperities due to the inherent strength-size effect of the intact material. Analysis of the present experimental results showed that the asperity failure or intact strength component represents a potential source of size effects in the shear strength of joints.

2.4.7 Asperity failure components in relation to joint block size

The total frictional resistance of a non-planar joint sheared under normal load comprises three angular components as shown diagrammatically in Figure 2.44:

(i) the basic frictional component (ϕ_b) which is generally accepted as a constant material property

(ii) the inclined plane or geometrical component (i_p^o) from asperity overriding

(iii) the intact strength or asperity failure component (S_A^o) arising from intact failure of some irregularities.

As has already been discussed in Section 2.4.5, the dependency of dilation on scale is one of the reasons for the lower shear strength of longer joints. However the reductions in the peak dilation angle

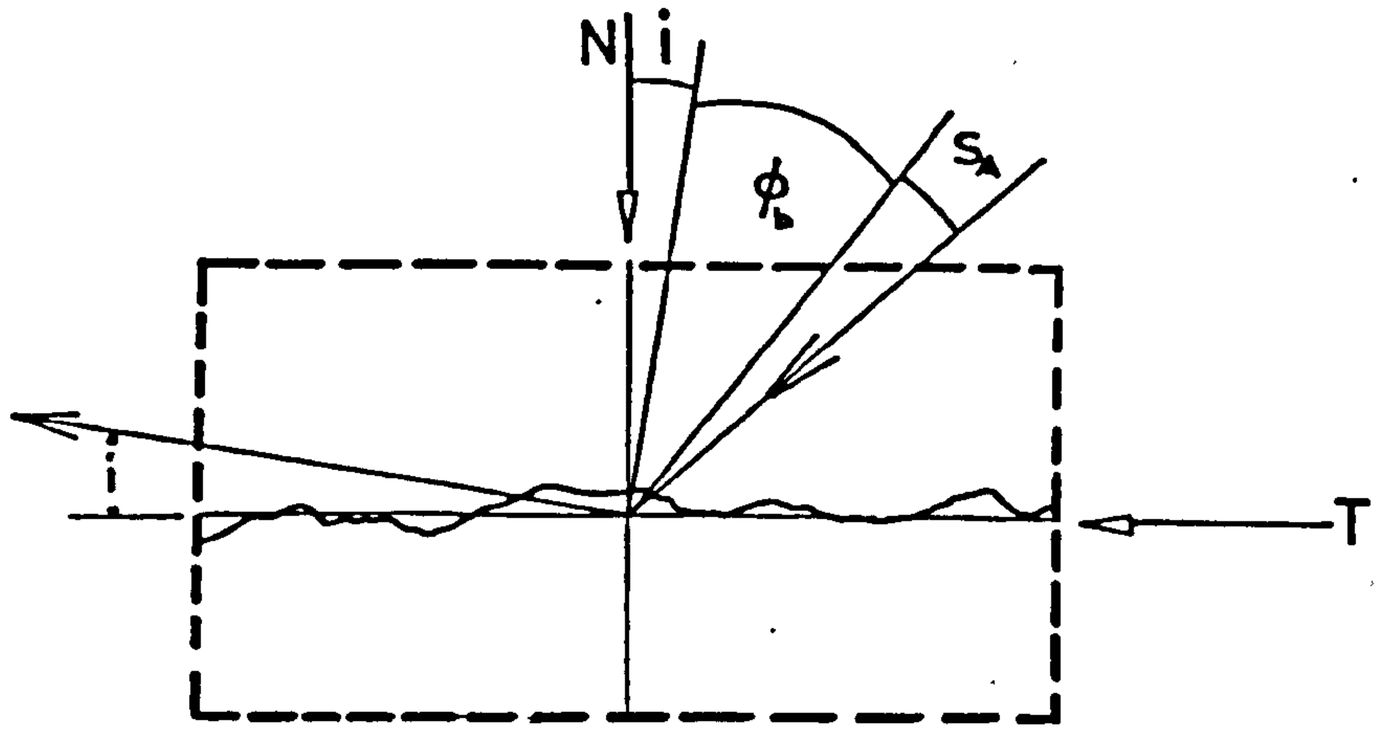

FIGURE 2.44 The angular components of shear strength for an undulating joint (after Barton, 1971)

TABLE 2.23

Variation of the asperity failure component (S_A^o) with increasing joint length (L)

JOINT LENGTH (L)		MODEL Nos.										
Model (cm)	Prototype (m)	1	2	3	4	5	6	7	8	9	10	11
5,6	1.5,1.8	19.6°	18.1°	19.9°	17.3°	21.1°	17.3°	18.7°	17.9°	16.3°	13.1°	7.5°
10,12	3.0,3.6	17.4°	14.2°	15.4°	16.8°	17.1°	12.2°	17.2°	19.5°	12.7°	9.6°	6.6°
18,20	5.4,6.0	13.2°	12.4°	12.2°	12.1°	12.1°	8.7°	10.4°	12.1°	10.7°	8.3°	4.9°
36,40	10.8,12.0	11.7°	10.1°	5.3°	8.4°	10.3°	5.1°	6.2°	6.0°	7.3°	6.6°	5.3°

cannot account for the full scale effect in the total friction angle ($\tan^{-1} \tau_p/\sigma_n$) which is represented by:

$$\tan^{-1}(\tau_p/\sigma_n)^\circ = [i_p^\circ + S_A^\circ + \phi_b^\circ] \qquad 2.16$$

Had i_p° been the only scale dependent variable one would expect S_A° to be constant irrespective of joint length. The values of the asperity failure component estimated from

$$S_A^\circ = \tan^{-1}(\tau_p/\sigma_n)^\circ - [i_p^\circ + \phi_b^\circ] \qquad 2.17$$

revealed a strong scale effect in S_A° as shown by the data in Table 2.23. A comparison of the percentage reductions in S_A° with those of the peak dilation angles (i_p°) in Table 2.20 shows that in fact the intact strength component was apparently more dependent on scale than was the dilation. For example, in model no. 1 the maximum reduction in S_A° was 41% while i_p° decreased by 18.4%. In the case of model no. 2, S_A° dropped by 45% compared to a 30% reduction in i_p°. The largest joint size of model no. 3 showed a 50.8% reduction in S_A° while i_p° decreased by 24.4%. Similar observations can be made for all types of joints tested.

The apparently different "sensitivity" of the geometrical and intact strength components to size effects can be readily appreciated if each of them is expressed as a percentage of their sum, which in effect represents the total contribution of surface roughness to the frictional resistance of a joint sheared under a certain level of normal stress:

$$[i_p^\circ + S_A^\circ] = \text{ROUGHNESS COMPONENT, } R_c^\circ = \tan^{-1}(\tau_p/\sigma_n)^\circ - \phi_b^\circ \qquad 2.18$$

Under the present level of normal stress (σ_n = 24.5 kPa, JCS/σ_n = 80), the results showed that the intact strength component was somewhat larger than the dilation component of all the small joint block sizes (5 or 6 cm). The disproportional reduction in i_p° and S_A° with increasing joint length eventually led to an inversion of that original analogy, as shown with a few characteristic examples in the next page.

Joint Length (L)		i_p^o and S_A^o as % of R_c		
Prototype (m)	Model (cm)	Roughness Component, R_c	Geometrical Component (i_p^o)	Intact Strength Component (S_A^o)
		MODEL No. 1		
1.8	6	34.6°	43.4%	56.6%
3.6	12	33.1°	47.1%	52.3%
5.4	18	27.5°	52.4%	47.6%
10.8	36	23.9°	51.0%	49.0%
		MODEL No. 2		
	6	32.1°	43.6%	56.4%
	12	26.0°	46.2%	53.8%
"	18	22.6°	46.5%	53.5%
	36	19.9°	49.2%	50.8%
		MODEL No. 6		
	6	28.7°	40.4%	59.6%
	12	22.6°	46.0%	53.4%
"	18	18.4°	52.2%	47.8%
	36	11.5°	56.5%	43.5%

For instance, in the case of model no. 1, 43.4% of the roughness component (R_c) in the total shear resistance of the 6 cm long joints was contributed by the overridden irregularities (geometrical component, i_p^o) and the remaining 56.6% by the strength of the failed asperities (intact strength component, S_A^o). Similar analysis of the roughness component of the 36 cm long specimens showed that i_p^o represented 51% of the R_c value and S_A^o was 49%.

The difficult question is that of how can this size-effect in the asperity failure component be explained. A probable source of that phenomenon could be a large quantitative difference in the actual contact area between joint surfaces of different sizes.

As has been discussed in Section 2.1.5, Pratt et al. (1974) attributed a 40% reduction in the shear strength of diorite joints to the fact that "larger" specimens (~ 5000 cm^2) had lower actual contact area than "smaller" (~ 250 cm^2) ones. Post test observations of the large sheared surfaces had shown that the shear load had been applied over 10 to 20%

of the total area. However, no quantitative information was given in that publication about the contacts of the smaller size specimens.

If in the present case the contact area of the large joints was indeed much lower than that of the smaller ones, the peak shear stress values (τ_p), which in each case were calculated with reference to total joint areas, would be accordingly affected. By implication, the asperity failure components (S_A^o) would also "appear" as size-dependent, since they were calculated from τ_p (see equation 2.17).

Post-test observations were made on the actual contact areas (A_{actual}) of different joint block sizes in an attempt to clarify the above hypothesis. The areas on the surfaces of the bottom half of joint specimens over which asperities were visibly damaged or scratched were carefully contoured and then traced onto transparent graph paper.

Comparisons were mainly concentrated between the 6 cm long joints and their full size counterparts (36 cm). In each case, the areas of contact on all component joints of the subdivided model were added up and the average value of the A_{actual}/A_{total} ratio was estimated, where A_{total} was the apparent total area of the full size joint.

From measurements on different types of surfaces, the average A_{actual}/A_{total} ratio values corresponding to the subdivided models were found to range between 5.3% and 9.6%. The contact ratio values of the corresponding full size joints were between 8 and 10.5%. Overall, the sum of the actual contact areas which were found on the component joints of the subdivided models were somewhat smaller than the total contact area of their full size counterparts. Some examples are given below:

	Individual Joint Length	Sum of actual Contact Areas A_{actual} (cm^2)	Total Surface Area A_{total} (cm^2)	$(\frac{A_{actual}}{A_{total}}) \times 100$
Model No. 1	6 cm	48	504	9.5%
	36 cm	53	504	10.5%
Model No. 2	6 cm	41	504	8.1%
	36 cm	49	504	9.7%
Model No. 11	6 cm	30.6	400	7.7%
	18 cm	37.5	400	9.4%

It is important to note that those contacts corresponded to 5-6 mm of joint displacement and hence were accordingly larger than those expected at the moment of mobilization of peak shear strength (2 to 3% at the most).

The effect of the continued displacement must have been an enlargement of the "peak" contacts and development of some new contact areas. Considering the size and geometry of the asperities which controlled the peak strength of joints of different length, it is reasonable to expect that the "enlargement effect" would be more pronounced in the cases of the full size joints, where the effective irregularities maintained a substantial contact after peak strength was reached, evidently unlike the smaller specimens (see Section 2.4.4). That may explain the apparent "negative" size effect in contact areas of small and large joints.

It is probable that the A_{actual}/A_{total} ratio value for both specimen sizes was reasonably comparable at the moment of peak strength. At any rate, it would appear as a rather remote likelihood that post-peak displacements of a few millimeters masked the originally suspected size-effect of substantially decreasing contact area with increasing specimen size. In conclusion, it would seem that as far as the present types of joints is concerned, the scale effects in the asperity failure components cannot be related to a size-contact effect in the context considered above.

Three characteristic examples of the contact areas found on different specimen sizes of three joint types (nos. 1, 4 and 11) are shown by the photographs in Figures 2.45, 2.46 and 2.47. A cursory glance at the two rough undulating surfaces (model nos. 1 and 4, Figs. 2.45 and 2.46 respectively) reveals some very distinct features regarding the pattern of distribution and size of the contact areas: a larger number of smaller individual contacts can be seen on the subdivided surfaces (individual joint length L = 6 cm) by contrast to the full size specimens (L = 36 cm) which were characteristically marked by fewer but larger contacts.

For instance, a total of 230 individual contacts were counted on the subdivided (L = 6 cm) model no. 1 compared to 75 found on the corresponding full size specimen. Similarly, 156 areas of contact were traced on the subdivided model no. 4 compared to a total of 55 on the 36 cm joint. Similar differences were also observed on other non-planar joint types. A less contrasting pattern was found on the nearly planar joint no. 11. The contacts on the 6 cm/ and 18 cm /subdivided models were 215 and 175 respectively, while the size of the individual areas was only slightly larger in the case of the 18 cm joint specimens.

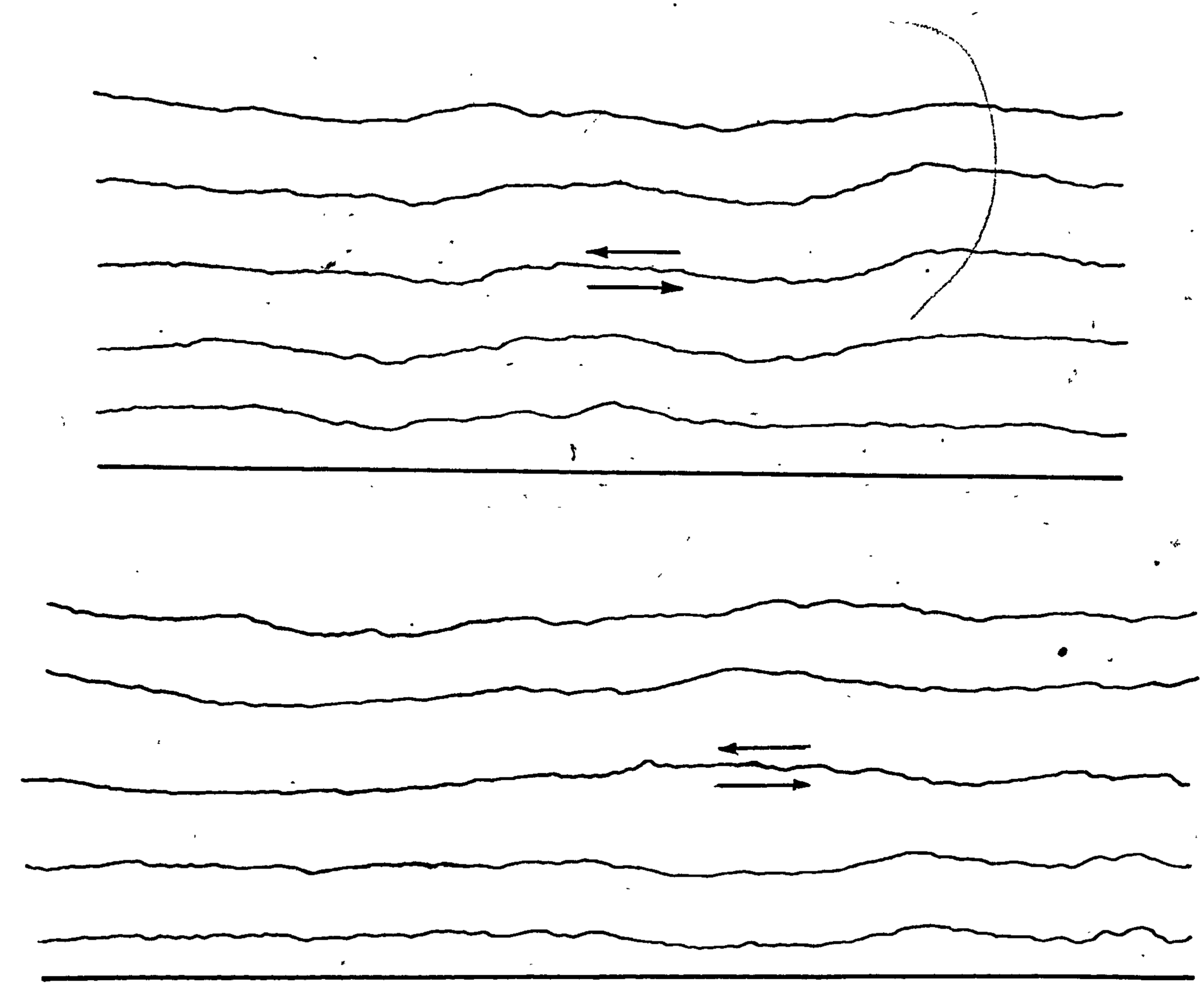

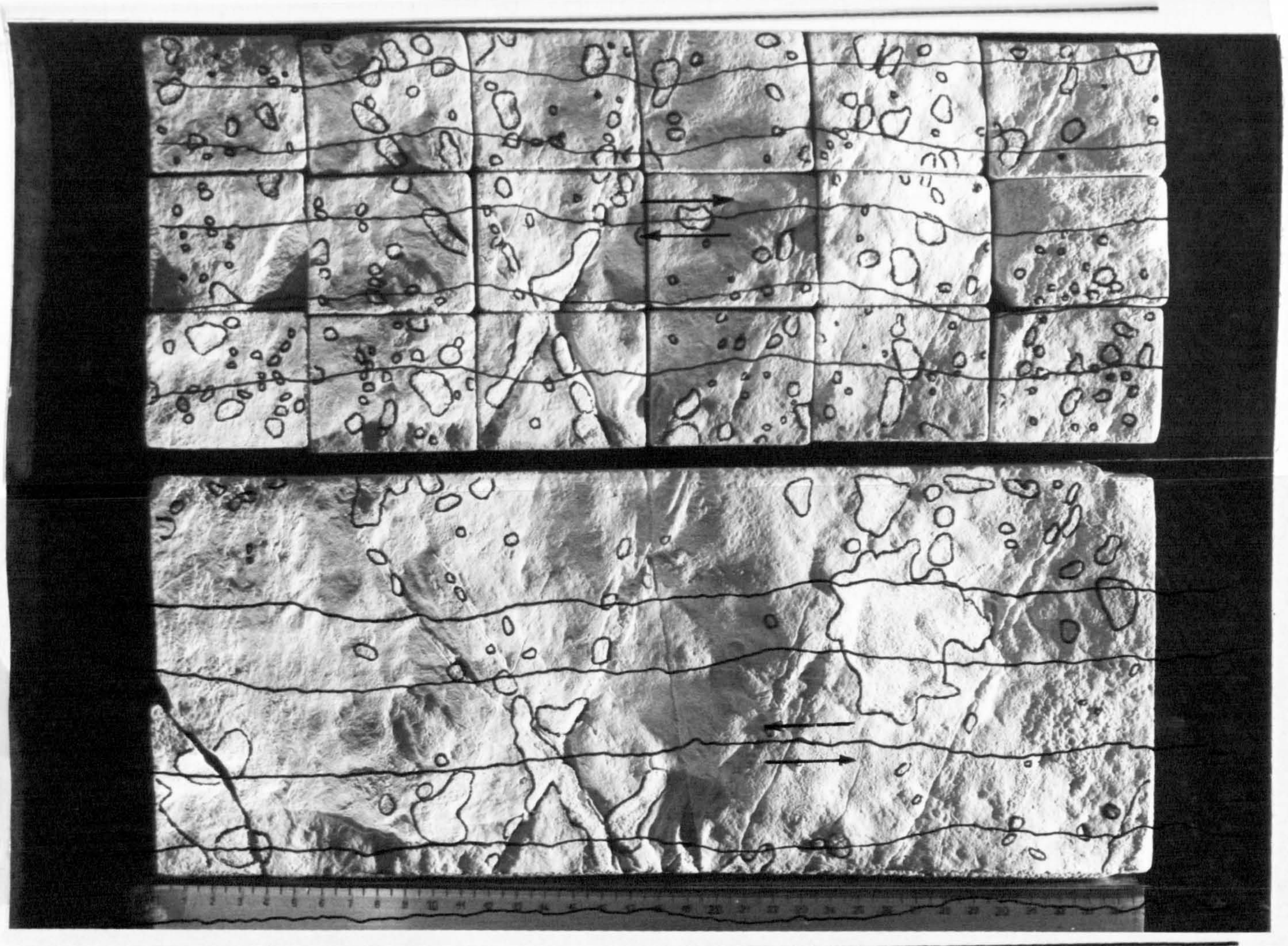

FIGURE 2.45 Photograph illustrating the distribution, number, and sizes of post-test contact areas on small and large joint samples of model No.1

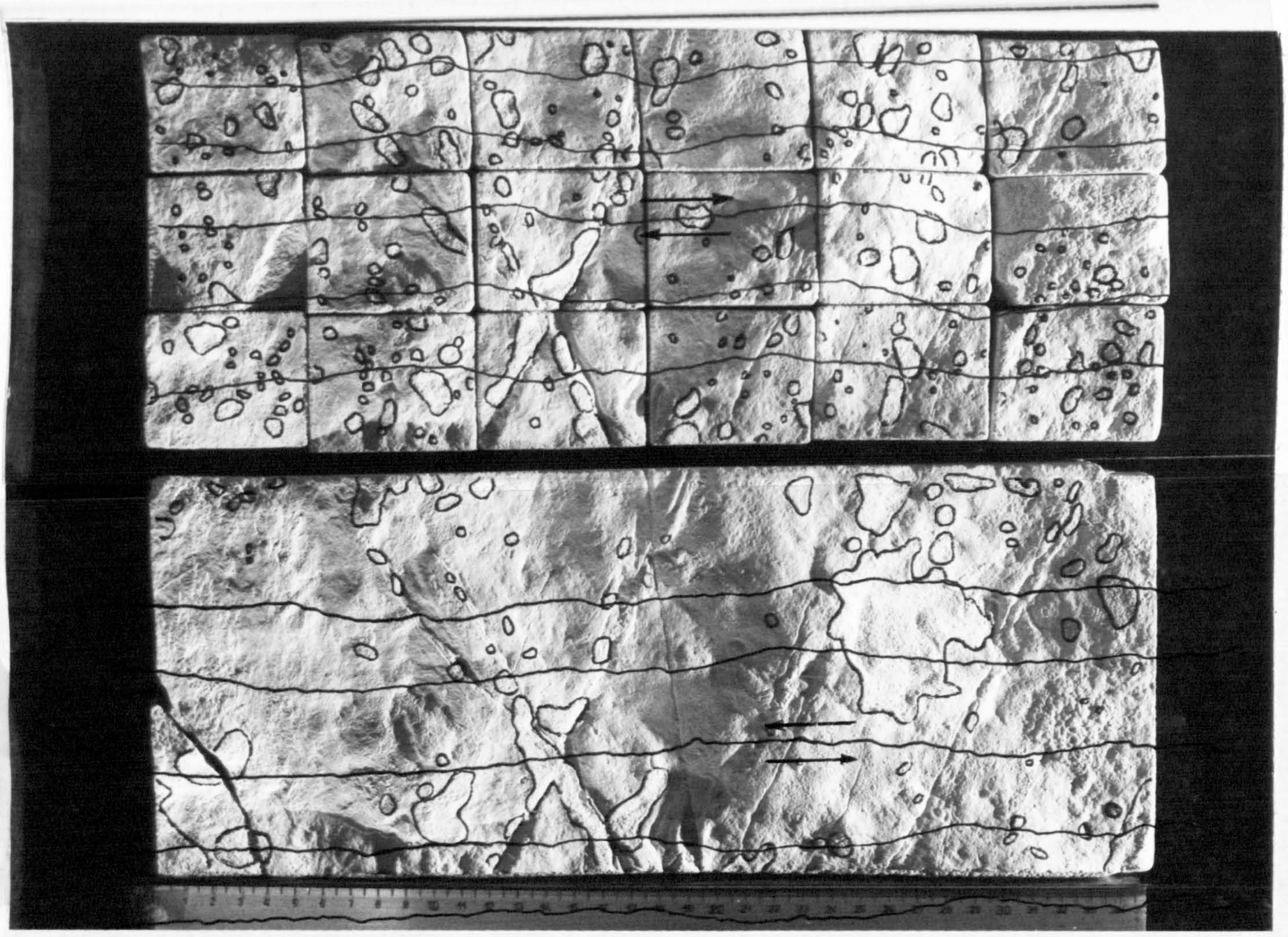

FIGURE 2.45 Photograph illustrating the distribution, number, and sizes of post-test contact areas on small and large joint samples of model No.1

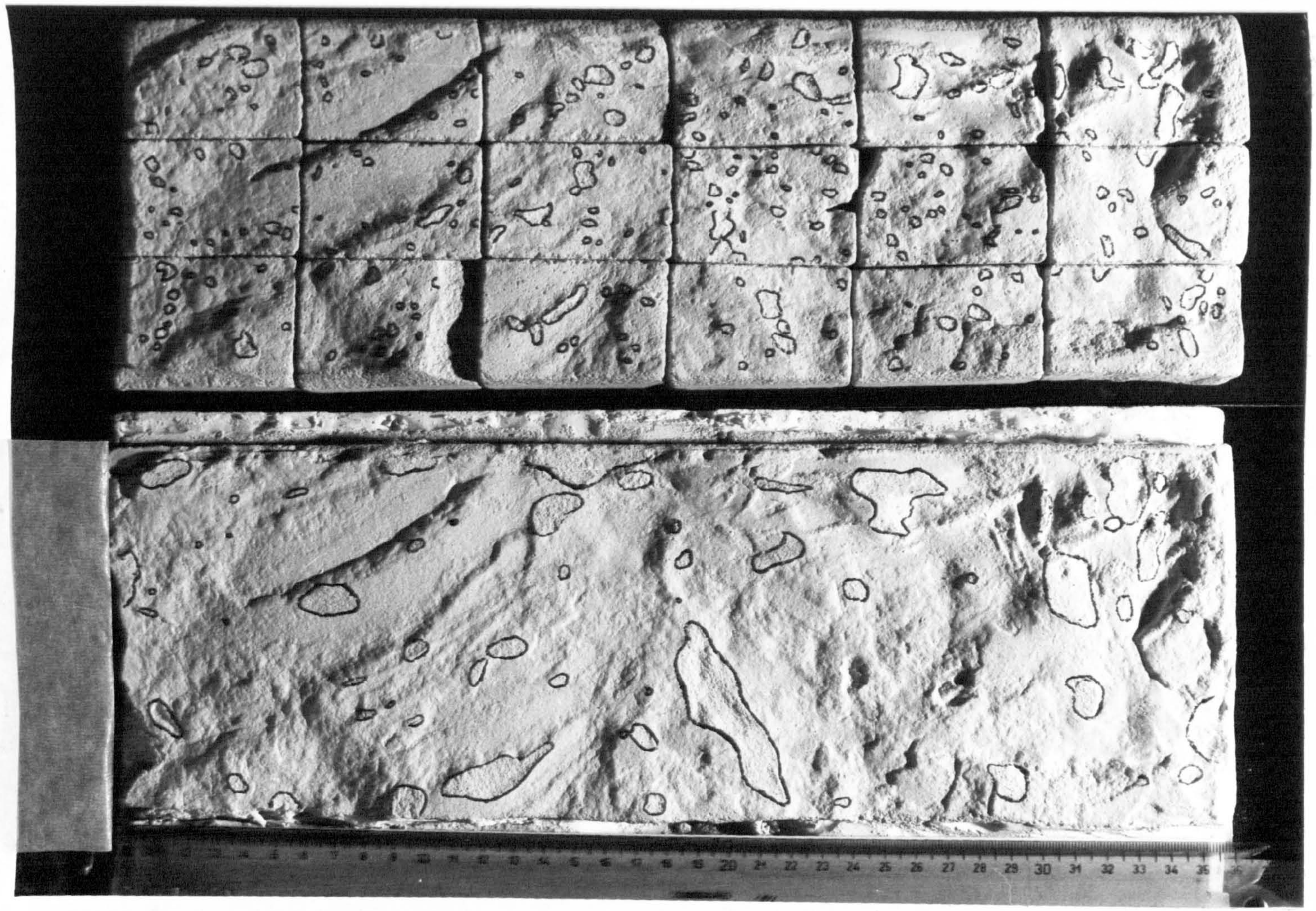

FIGURE 2.46 Photograph illustrating the distribution, number and sizes of post-test contact areas on small and large joint samples of model No.4.

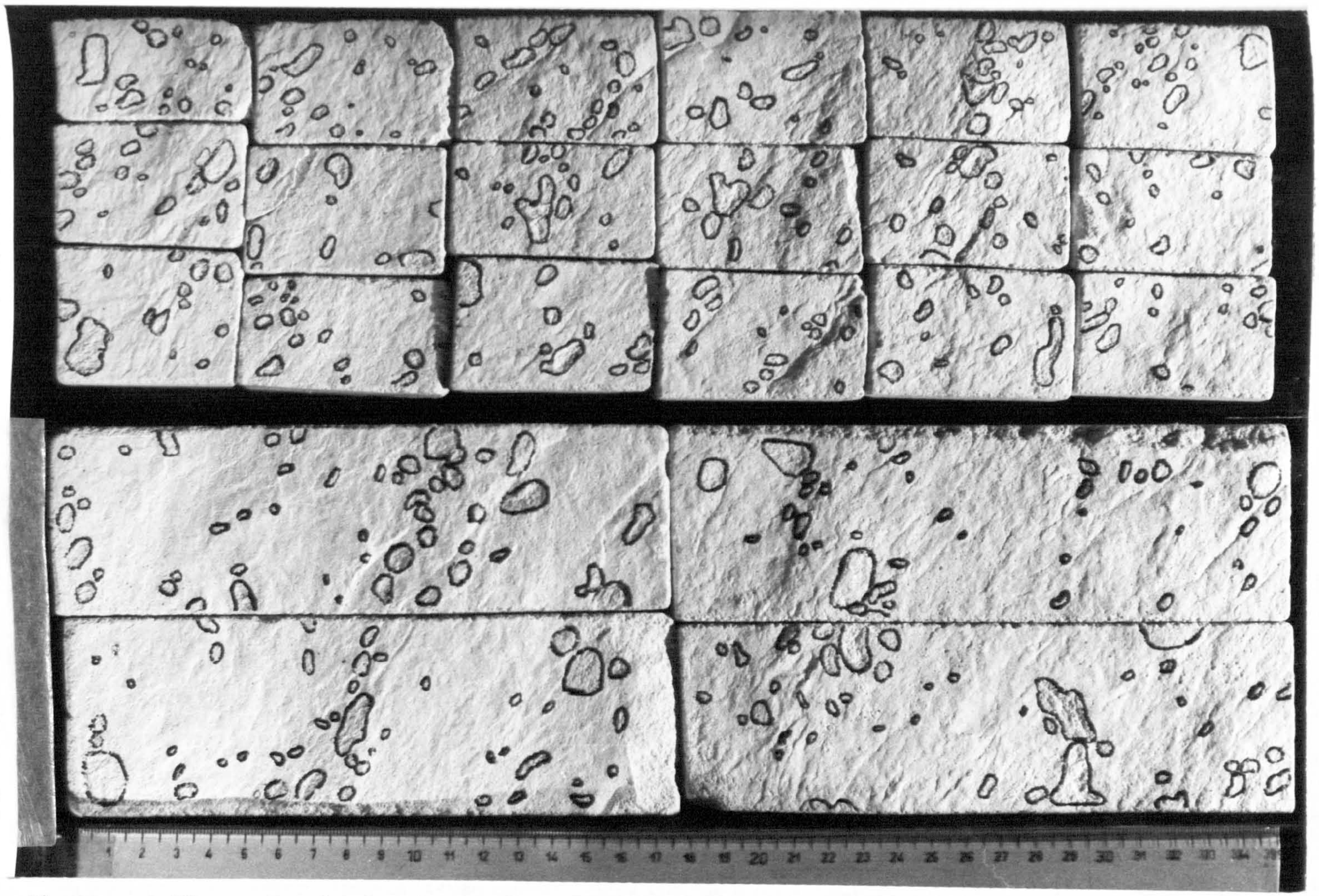

FIGURE 2.47 Photograph illustrating the distribution, number and sizes of post-test contact areas on small and large joint samples of Model No. 11.

There is a clear interrelationship between the size of the individual contacts and the dimensions of the asperities responsible for the contrasting behaviour of joints of different lengths. Large areas of contact developed between the slopes of the few large irregularities, which dominated the behaviour of the long joints. On the other hand, smaller contacts were created between the sides of the small asperities, which controlled the strength of the shorter specimens.

Such a contact area-size effect is linked with the hypothesis of Barton and Choubey (1977) regarding the probable existence of a scale effect in the joint compressive strength (JCS).

As reviewed in Section 2.1.2, the strength properties of intact materials are inversely related - to a greater or lesser extent - with specimen size. Consequently, it is not unreasonable to consider the probability of large irregularities "resisting" lower stresses than small asperities due to the inherent strength-size effect coupled with the aforementioned contact area-scale effect. In that context, Barton and Choubey proposed that the effective JCS - which actually represents a measure of the uniaxial compressive strength of asperities - during shearing of large joints (visualize large irregularities thrusting against each other across their large areas of contact) would probably be lower than the effective JCS mobilized upon failure of a shorter joint with the critical asperities "touching" one another over correspondingly smaller individual contacts.

Size-effects in the uniaxial compressive strength (σ_c) of plaster/sand based model materials have been reported in the past (e.g. Einstein et al. 1970, Lama and Gonano 1976) and it is not unlikely that a similar effect did exist in the case of the present material. The probable scale effects in σ_c, and potentially in JCS, could have been a key factor in the apparent reductions of the estimated asperity failure components (S_A^o) with increasing specimen size.

It should be carefully noted that the relatively small scale effect in S_A^o of joint no. 11 (a drop of 2.6^o as specimen length increased from 6 to 18 cm) agrees qualitatively with the small difference in the size of the respective actual contacts (Figure 2.47). Large reductions in S_A^o were found to be associated with more prominent differences in the areas of contact. For instance, in the case of model no. 4 (Fig. 2.46) S_A^o dropped by 9^o as joint length increased from 6 to 36 cm. For the same range of specimen sizes the estimated reduction in S_A^o for model no. 1 (Fig. 2.45)

was $\underline{7.9^{o}}$. It is interesting to note that the differences in the size of the individual contact areas between the 6 and 36 cm joints were more pronounced in model no. 4 (hence larger scale effect in S_A^o) than in model no. 1 (smaller scale effect in S_A^o as compared to no. 4).

However, it would be unwise to pursue the above observations any further because of the complicating factor of post-peak displacement. In any case the obvious uncertainties involved in a realistic assessment of the scale effects in JCS, should their existence be accepted, do not represent a serious limitation in a practical situation.

Use of "scale-dependent" values of JCS would result in back-calculation of somewhat larger values for JRC. A range of JCS scale reduction factors was tentatively derived from the ratios of the maximum S_A^o values, corresponding to the presumably "scale-free" 5 or 6 cm long specimens, to those derived for the longer joints. Those factors were then used to reduce accordingly the JCS value of 2000 kPa.

Characteristic examples of the new Joint Roughness Coefficients calculated by using the "corrected" JCS values are shown in Table 2.24. The original JRC's derived on the assumption of a constant JCS are also included in each case for comparison. The errors involved in the estimates of $\tan^{-1}(\tau_p/\sigma_n)^o$ at higher normal stress levels by using over- or under-estimated values for JRC and JCS are considered in the next chapter.

2.4.8 Critical evaluation of the scale effects in joints

The direct shear tests conducted on sets of joint specimens differing in size and representing sliding planes of identical geometry have shown the existence of significant scale effects in the shear strength and deformation characteristics. Size effects in joints are fundamentally linked with a proportional interrelationship between the length of the sheared surface and the size of the irregularities which potentially control its frictional resistance.

An idealized model of the scale effects in the strength and deformation properties of non-planar joints is presented in Figure 2.48. On the left-hand side of the diagram the shear stress – horizontal displacement relationships of four hypothetical joint sizes are given. The columnar drawings represent the relative variation in the geometrical and asperity failure components with increasing length of joint profile.

TABLE 2.24

Comparison of Joint Roughness Coefficients (JRC) back-calculated by using scale-dependent and constant values of Joint Compressive Strength (JCS).

JOINT LENGTH, L		Joint Compressive Strength (kPa)	JRC		Joint Compressive Strength (kPa)	JRC		Joint Compressive Strength (kPa)	JRC	
Model (cm)	Prototype (m)		JCS scale-dependent	JCS constant		JCS scale-dependent	JCS constant		JCS scale-dependent	JCS constant
		MODEL No. 1			MODEL No. 2			MODEL No. 3		
6	1.8	JCS =2000		18.1	JCS =2000		16.8	JCS =2000		17.0
12	3.6	JCS/1.12=1785	17.8	17.3	JCS/1.29=1550	14.4	13.6	JCS/1.29=1550	13.9	13.1
18	5.4	JCS/1.48=1354	14.8	14.4	JCS/1.50=1333	13.0	11.8	JCS/1.60=1250	13.1	11.7
36	10.8	JCS/1.67=1198	14.1	12.5	JCS/1.79=1116	12.0	10.4	JCS/3.73= 536	11.1	7.8
		MODEL No. 4			MODEL No. 7			MODEL No. 9		
5,6	1.5,1.8	JCS =2000		14.5	JCS =2000		18.5	JCS =2000		11.9
10,12	3.0,3.6	JCS/1.02=1960	13.1	13.0	JCS/1.08=1852	15.6	15.3	JCS/1.24=1607	10.8	10.3
18,20	5.4,6.0	JCS/1.43=1399	12.4	11.7	JCS/1.87=1070	12.6	10.8	JCS/1.66=1205	8.8	7.8
36,40	10.8,12.0	JCS/2.08= 962	9.0	7.5	JCS/3.02= 662	9.7	7.3	JCS/2.23= 897	7.9	6.5
		MODEL No. 10			MODEL No. 11					
6	1.8	JCS =2000		8.4	JCS =2000		5.1			
12	3.6	JCS/1.35=1481	7.7	7.2	JCS/1.17=1709	4.6	4.4			
18	5.4	JCS/1.64=1220	7.0	6.2	JCS/1.53=1307	4.2	3.5			
36	10.8	JCS/1.98=1010	5.3	4.5	JCS/1.42=1408	4.1	3.8			

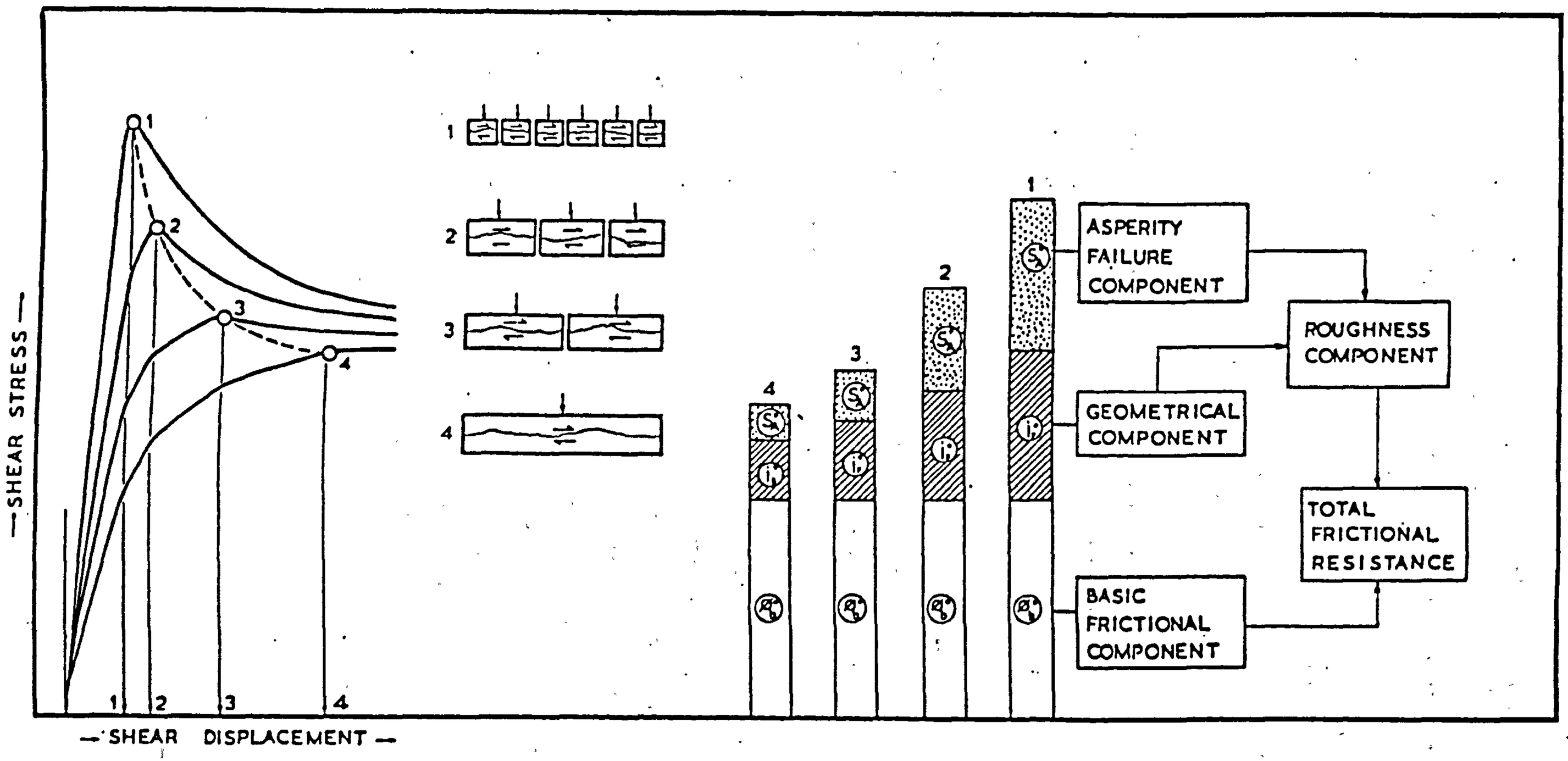

FIGURE 2.48 An idealised model of the scale effects on the shear behaviour and properties of non-planar joints

A few remarks had been made in Section 2.2.4 with regard to changes in the slope of the pre-peak portions observed in some of the τ-d_h curves (also illustrated by the no. 3 and no. 4 hypothetical curves in Fig. 2.48). It is probable that those slope changes are signs of a "progressive" joint failure. It is envisaged that during the course of the pre-peak displacement, the joint will have to overcome the resistance of "interfering" asperities of size smaller than the effective one for the particular case. If that is true, the joint will "feel" progressively larger asperities until its walls develop a firm contact between the effective irregularities. An interesting coincidence was that the inflection points occurred after horizontal movement roughly equal to the peak displacement of smaller joints (see relevant text in Section 2.4.4). That could mean that the inflection of the curve happened as the joint overcame the resistance of asperities which represented the effective size at the scale of the smaller specimens (6 to 12 cm long).

The experimental results have shown an expected decline of the scale effects in the properties of the relatively smooth and planar types of joints. Technically insignificant effects were also associated with the ultimate strength of most rough undulating joint types.

It is important at this stage to assess the relevance of the experimental findings and related interpretations to the probable response of a jointed rock mass. The inherent "weakness" in direct shear testing of individual jointed blocks is that the response of the surrounding rock mass is absent, a simplification which may sometimes lead to erroneous extrapolations. For instance, shear tests on joints as individual mass components have shown an apparent transition from "brittle" to "plastic" behaviour, as has been discussed in Section 2.4.4. Although <u>on an individual basis</u> small jointed blocks are likely to behave in a more "brittle" manner than large jointed blocks, <u>collectively</u> the much greater number of blocks in a heavily jointed rock mass will tend to cause more "plastic" behaviour.

In all the preceding analysis of size-effects in joints it was implicitly assumed that the small jointed blocks are capable of an independent movement, which is obviously essential to maintain contact between the small asperities. The only restraint imposed during testing was the constant normal load. The important question is that of whether the stiffness of the rock mass overlying an inferred sliding plane would allow

the small blocks to follow the individual shear paths they require for their higher strength. That important aspect is considered further later in this section, after the results from some recent experiments by Barton (1979) made available to the author have been discussed.

Barton tested a series of two-dimensional plane-stress jointed models in a biaxial loading frame. The dimensions of the jointed slabs were 40 x 40 x 2.5 cm and were prepared from a low strength model material consisting of a mixture of red lead-sand-ballotini-plaster cured at 105°C. The method of producing sets of rough interlocking tension fractures by the use of a double-bladed guillotine has been described by Barton (1971).

Two different joint orientations were produced, namely 18° and 45°, with respect to the vertical direction, and four different spacings of joints viz. 6.2 mm, 11 mm, 21 mm and 41 mm were simulated. Each model consisted of 4000, 1000 or 250 blocks, depending on the joint spacing chosen. The various details of the geometry of the jointed models are shown below.

Model Nos.

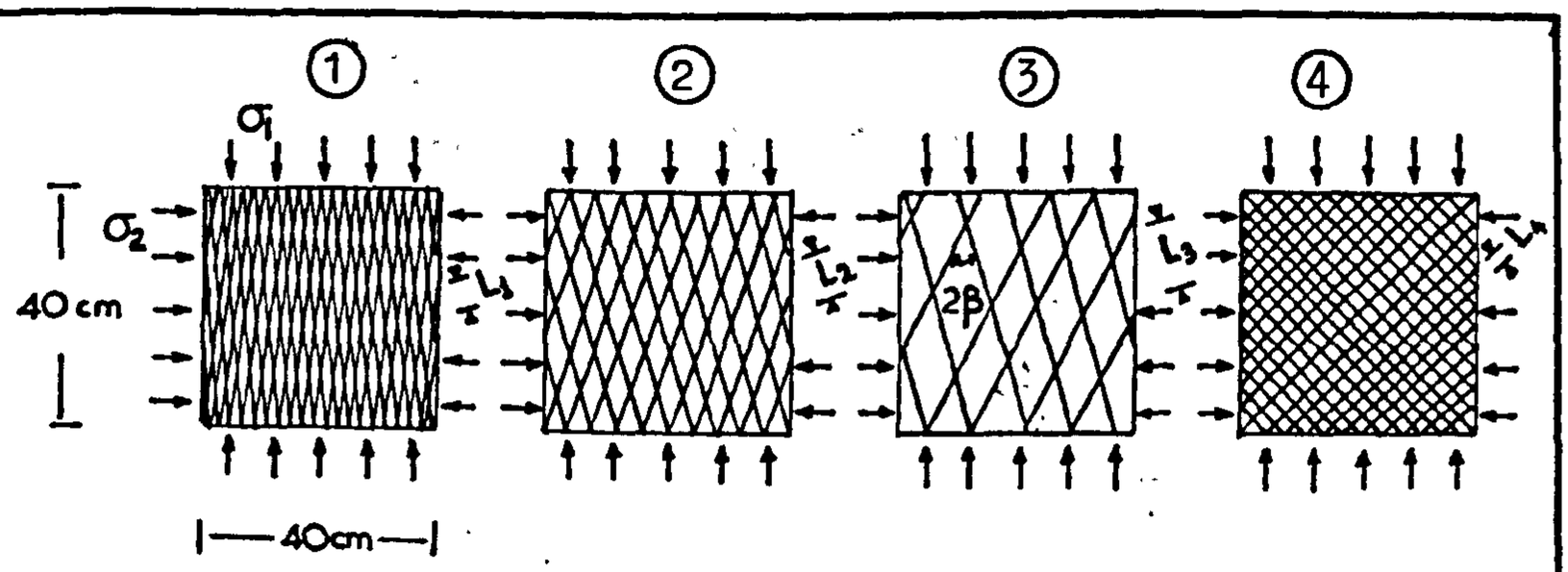

No. of Blocks		4000	1000	250	4000
β°		18°	18°	18°	45°
Joint Block Length (L)	Model, L_m (mm)	11	21	41	6.2
	Prototype, L_p (m)	3.3	6.4	12.3	1.8

The edges of the jointed slabs were loaded with compressed air filled rubber tubes to ensure a uniform stress distribution. The models were firstly loaded with an equal σ_1 and σ_2 value of 0.02 MPa (8.0 MPa at prototype scale) and σ_1 was increased to failure while σ_2 was maintained constant. The loading paths followed for model nos. 1, 2 and 3 ($2\beta = 36^\circ$ in each case) were identical and are shown by the σ_2/σ_1 values included in Figure 2.49. A different path was employed in the case of model no. 4 ($2\beta = 90^\circ$).

The theoretical peak shear strength envelopes in Figure 2.49 were drawn from the results of shear tests on model tension fractures 6 and 10 cm long, representing prototype joints 18 and 30 meters long respectively. The upper (JRC = 23) and lower (JRC = 17) envelopes represent the scatter of results from the tests on the single joints whose average JRC was approximately 20.

The solid squares plotted in Fig. 2.49 show the different levels in shear stress at which failure of the jointed materials with the same β angle took place. The lowest stress corresponded to the model with the most widely spaced joints (no. 3, L_m = 41 mm, L_p = 12.3 meters) and the highest to the most closely jointed one (no. 1, L_m = 11 mm, L_p = 3.3 meters). All three models failed at higher stress than the individually tested fractures representing prototype joints 18 and 30 meters long.

During the course of loading, displacements were measured by using a photogrammetric method, which has been described by Barton and Hansteen (1979). In Figure 2.50 the plots of the differential stress ($\sigma_1 - \sigma_2$) vs strain (axial ε_1 and lateral ε_2) representing three jointed models (nos. 1, 2 and 3) is shown. The corresponding estimates of the modulus of deformation (E_m) of the model jointed masses are also included. Depending upon the spacing of the joints the E_m values ranged between 19 and 46 MPa (7500 MPa to 18460 MPa at prototype scale), the lowest obviously corresponding to the most densely jointed model.

It is important to note the relationship between the values of the deformation modulus (E_m), the effective joint block sizes and the stress levels at which failure took place within the models. Reduced block size was found to increase the shear strength of the model jointed mass. The correspondingly reduced stiffness of the latter must have increased the degree of freedom of the individual joint blocks and enabled them to "follow" and "feel" all scales of roughness (viz. individual shear paths)

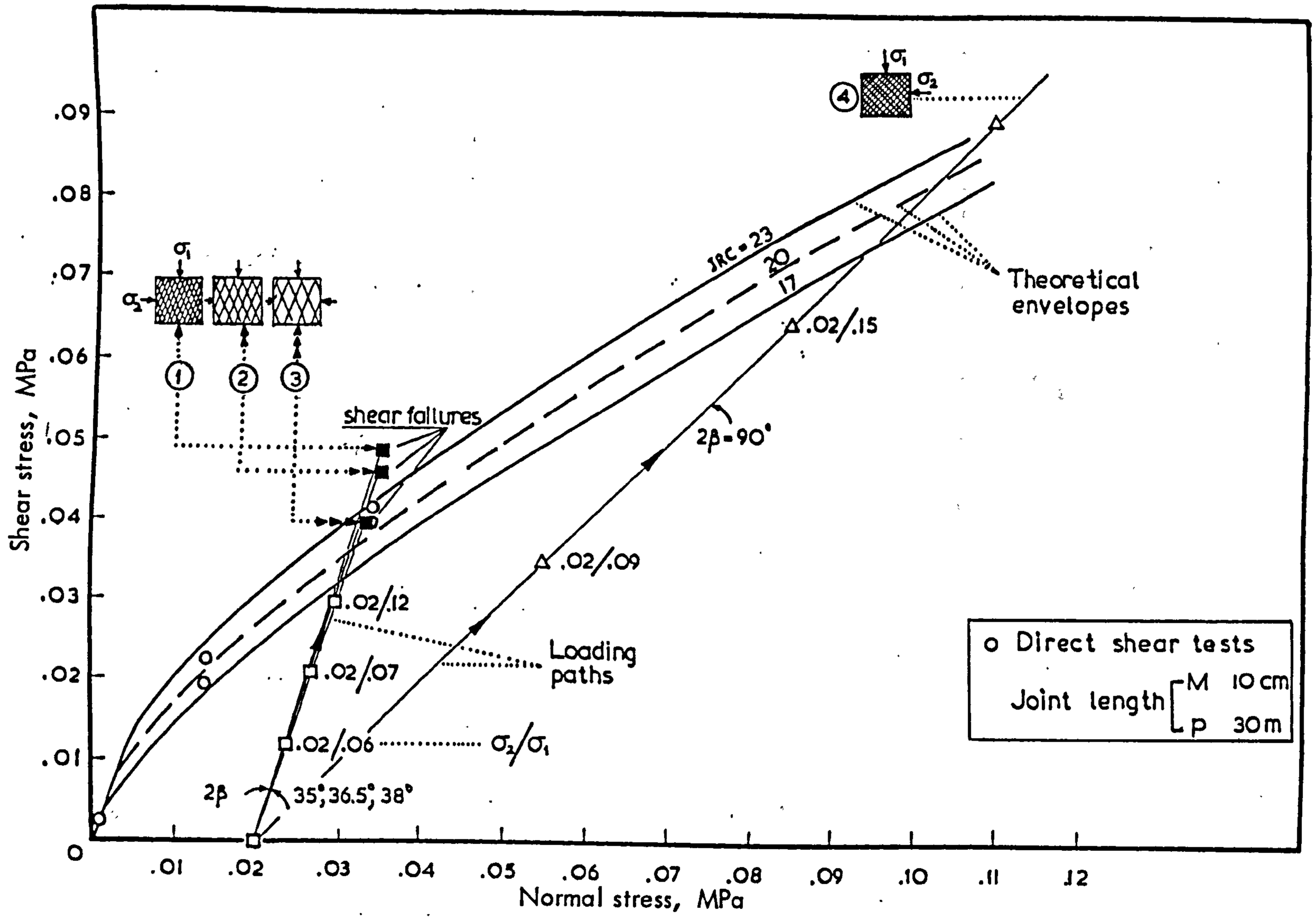

FIGURE 2.49 Results from biaxial tests on jointed model slabs demonstrating the effect of block size or joint length (L) on the shear strength of the model rock mass (after Barton, 1979)

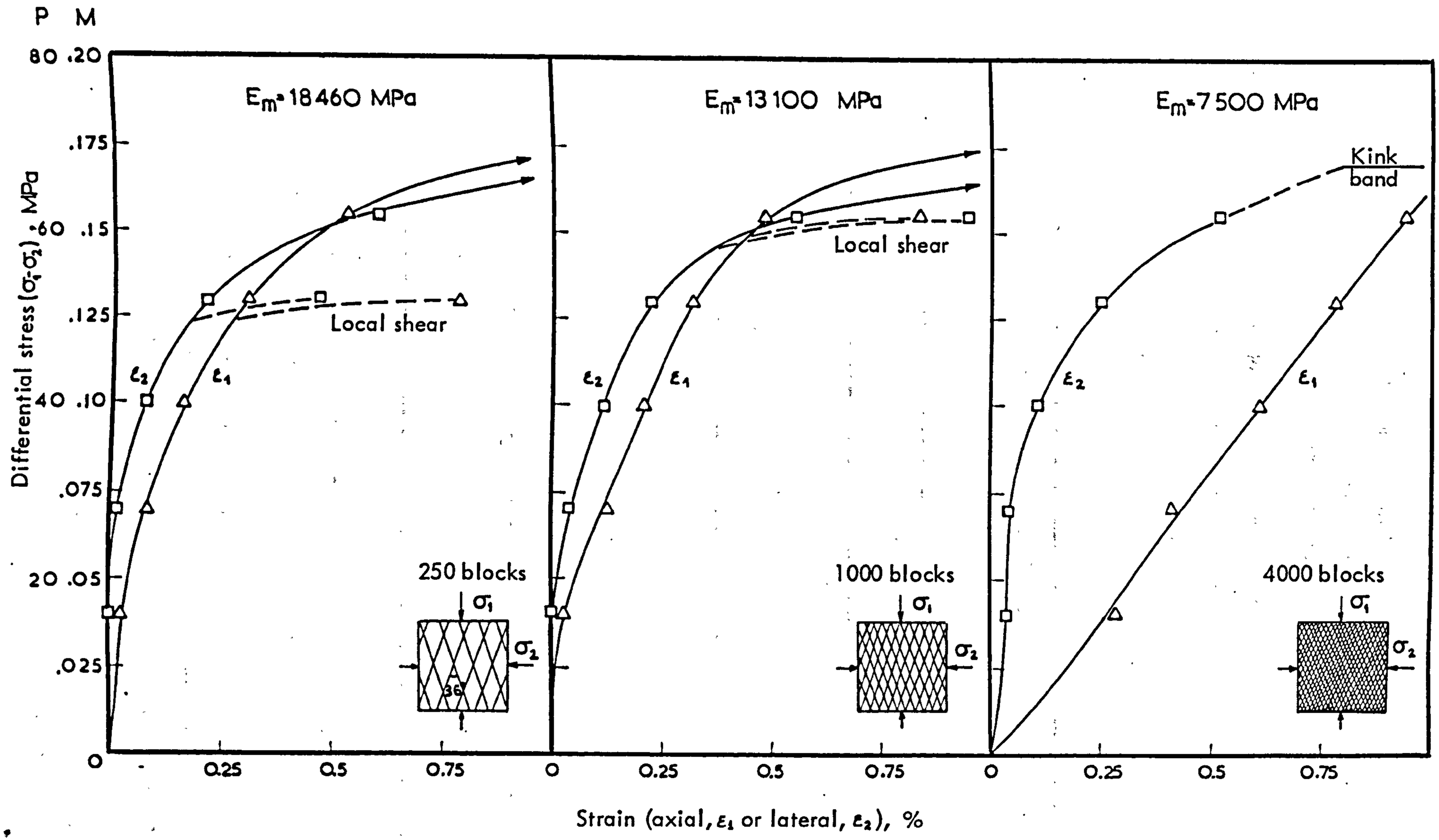

FIGURE 2.50 Differential stress – strain relationships of jointed model rock masses (after Barton, 1979) Note the changes in the deformation modulus (E_m) value with decreasing block size and the associated scale effect

more readily. As a result, the model rock masses composed of differently spaced joints had different JRC values, despite the almost identical surface roughness, and hence different shear strengths.

A tabulation of the Joint Roughness Coefficients which were back-calculated from the values of σ_1 and σ_2 required to cause shear failure in the biaxial tests is presented below. The results from the individually tested specimens are also included.

Type of Test	Joint length or cross joint spacing 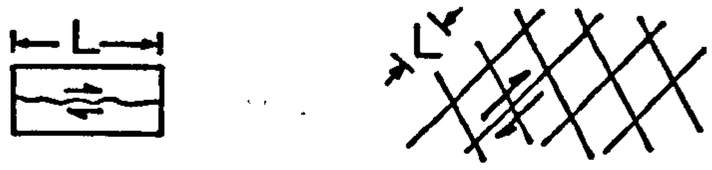		Joint Roughness Coefficient (JRC)
	Model Scale (mm)	Prototype Scale (m)	
Direct shear tests on individual jointed blocks	10	30	Mean of 20 >100 tests
	6	18	
Biaxial tests on jointed models, $\beta = 18°$	41 (250 blocks)	12.3	21.6
	21 (1000 blocks)	6.4	25.1
	11 (4000 blocks)	3.3	26.7
$\beta = 45°$	6.2 (4000 blocks)	1.8	>26 (failure did not occur)

The result of an approximately four-fold increase in cross-joint spacing (or block size) was a decrease in the JRC value by ~ 5.

A series of shear tests was conducted on a complete set of joint sizes, i.e. 6 cm, 12 cm, 18 cm and 36 cm of model no. 2 (rough, undulating) under normal stresses of up to 61.25 kPa. That level corresponded to 2.45 MPa in prototype scale. The object of those tests was to examine the scale effect in shear strength in relation to σ_n and the possibility of any changes in the conventional shape of the peak strength envelopes associated with increasing size of joint.

The results of those tests are summarized in Table 2.25, which includes the values of peak shear stress (τ_p), peak total friction angle $\tan^{-1}(\tau_p/\sigma_n)$, peak dilation angle (or geometrical component) i_p^o and the asperity failure component S_A^o as estimated from equation 2.17.

Shearing under different levels of normal stress revealed a "normal" behaviour irrespective of the size of the joints. Increasing σ_n resulted in lower dilation, increased asperity failure component in relation to joint dilation and of course a steady decrease in the peak total friction angle.

The peak shear stress data were plotted against the respective level of normal stress (Figure 2.51) and the theoretical peak strength envelopes were derived by utilizing Barton's criterion. It should be noted that the JRC values used in the derivation of the envelopes for the 12 cm, 18 cm and 36 cm joints are the ones presented in Table 2.24 derived on the assumption of a reduced JCS. As can easily be seen, the experimental data and the fitted envelopes showed a good agreement within that range of normal stress.

Observation of the data in Table 2.25 revealed an interesting point. The asperity failure component (S_A^o) of the 36 cm joint when tested under σ_n = 24.5 and 61.25 kPa was 10.1° and 9.8° respectively, that is it decreased by an amount of 0.3°. On the other hand, the estimated S_A^o of the 6 cm joint specimens decreased by an amount of 3.1° within the same range of σ_n. Under increasing σ_n it is expected that the dilation (i_p^o) of a joint will decrease and the asperity failure component will increase in relation to i_p^o. Those effects can be clearly seen in the test results from both the 6 cm and 36 cm joints.

A plausible explanation of the different values of S_A^o estimated for the 6 cm joints as σ_n increased may be offered on the basis of the earlier hypothesis relating the scale effects in S_A^o with the size of the individual contact areas and the "operating" value of JCS (viz. uniaxial compressive strength of asperities). It is probable that the increase in the contact area of the 6 cm joints under higher σ_n "reduced" the JCS value which was operating under lower σ_n (smaller contact areas). The question is why was there not a similar effect in the case of the 36 cm joint, since there must have been a corresponding increase in the contact areas.

Table 2.25

Summary of results from direct shear tests of joint specimens of various lengths under different levels of normal stress.

Joint Length L (cm)	Normal stress, σ_n P (MPa)	M (kPa)	Peak shear stress τ_p(kPa)	Peak total friction angle $\tan^{-1}(\tau_p/\sigma_n)$	Geometrical component i_p^o	Asperity failure component S_A^o
36	0.98	24.50	31.3	51.9°	9.8°	10.1°
	1.47	36.75	42.9	49.4°	8.2°	9.2°
	2.45	61.25	68.5	48.2°	6.4°	9.8°
18		24.50	34.2	54.4°	10.5°	11.9°
	"	36.75	49.8	53.6°	9.4°	12.2°
		61.25	73.9	50.3°	7.0°	11.3°
12		24.50	39.2	58.0°	12.0°	14.0°
	"	61.25	78.4	52.0°	7.5°	12.5°
6		24.50	50.5	64.1°	14.0°	18.1°
	"	61.25	90.5	55.9°	8.9°	15.0°

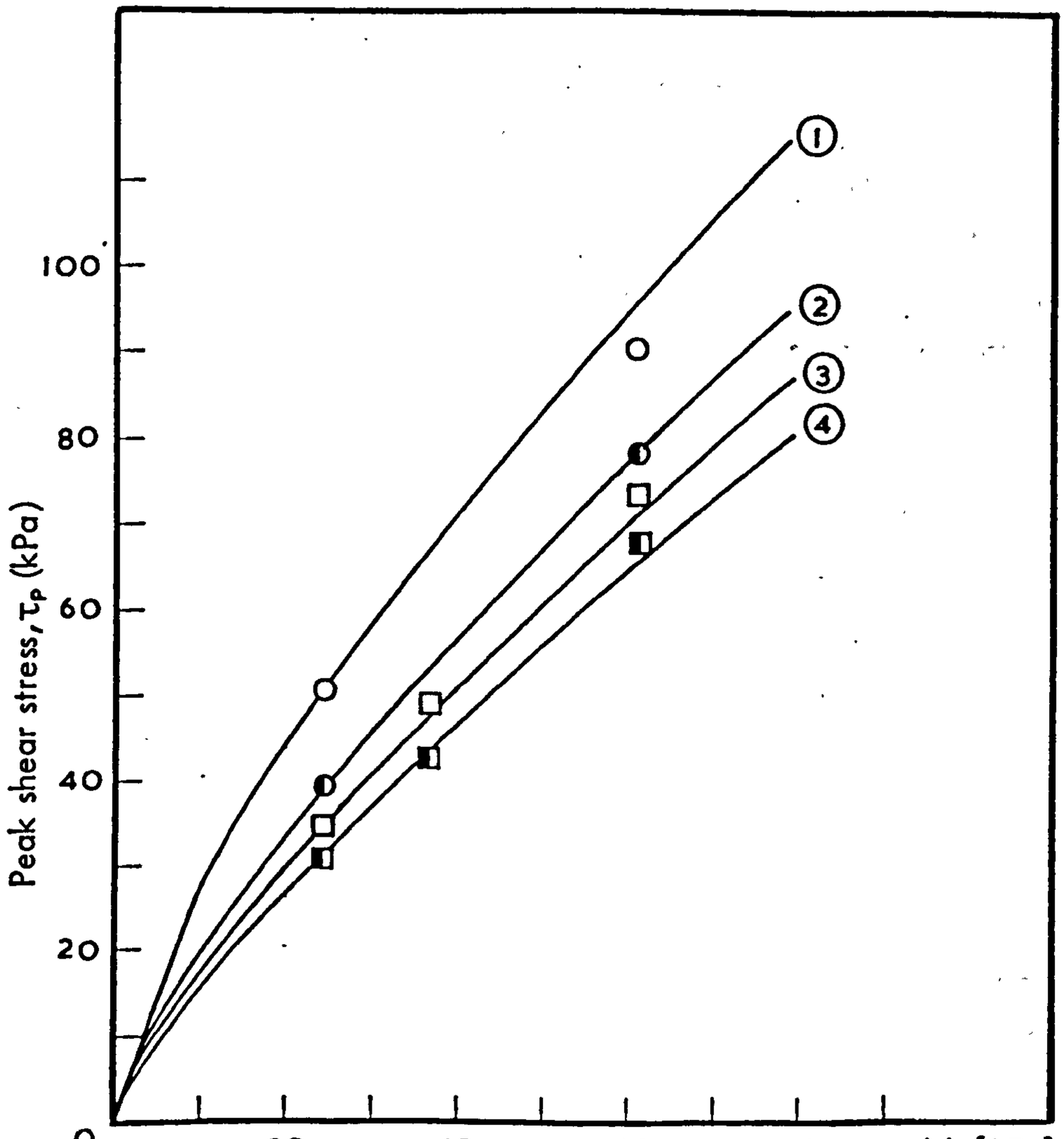

	L M(cm)	L P(m)	
○	6	1.8	① $\tau_p = \sigma_n \tan\left[16.8 \log_{10}\left(\frac{2000}{\sigma_n}\right) + 32\right]$
●	12	3.6	② $\tau_p = \sigma_n \tan\left[14.4 \log_{10}\left(\frac{1550}{\sigma_n}\right) + 32\right]$
□	18	5.4	③ $\tau_p = \sigma_n \tan\left[13 \log_{10}\left(\frac{1330}{\sigma_n}\right) + 32\right]$
■	36	10.8	④ $\tau_p = \sigma_n \tan\left[12 \log_{10}\left(\frac{1120}{\sigma_n}\right) + 32\right]$

FIGURE 2.51 Theoretical peak shear strength envelopes and experimental data from shear tests on joint specimens of different length (L) under different levels of normal stress. The envelopes were fitted assuming scale-reduced values for both JRC and JCS (see equations above)

It has often been found that the decrease in the uniaxial compressive strength (σ_c) of materials with increasing specimen size reaches a limiting level beyond which there is no further reduction in σ_c (e.g. see Pratt et al. 1974, Bieniawski and Van Heerden 1975, a[illegible] also Figure 2.1). It is probable that an analogous variation occur[illegible]n the case of the JCS/contact area size effect. Despite the increase [illegible]n the size of the individual contacts on the 36 cm joint, the effective JCS value had already reached a "reduction limit", hence the practically non-existent difference in the S_A^o values. The envisaged JCS-scale effect limit coupled with the more or less exponential variation in the angle of slope inclination with increasing baselength of asperity may explain the "flattening" of the shear strength-joint size (length or area) relationships (e.g. see Figure 2.29).

2.4.9 Concluding remarks

Direct shear tests on joint block specimens of different length representing surfaces with identical roughness have demonstrated that peak shear strength is a strongly scale-dependent variable. In general, short joint profiles exhibit higher peak strength than longer profiles of the same joint surface. The inverse relationship between shear strength and length of joint appears as non-linear, with a tendency to reach an asymptotic level. Maximum scale effects are associated with rough, undulating joint types; the shear strength of relatively smooth and planar joints is almost independent of the length of joint.

Analysis of the experimental results leads to the conclusion that both the geometrical and strength characteristics of surface roughness present potential sources of the scale effects. The peak shearing path of short joint profiles is regulated by the small and steep asperities, whereas that of longer joints is controlled by irregularities of larger baselength and correspondingly flatter slopes. Under a given normal stress the peak dilation angle is inversely proportional to joint length. There exists a strong scale effect in the peak shear displacement, which seems to be a measure of the distance a joint has to displace for contact to be made between those asperities which are effective for that particular joint. That distance increases with increasing joint length.

The different inclination with respect to the mean joint plane of the contacts between small and large asperities at the instant of peak strength introduces a scale effect in the value of the joint roughness coefficient (JRC) operating along two different profile lengths of the same joint. It has been found that the JRC value decreases with increasing joint length.

In addition to the contact inclination-scale effect, there is a relationship between the size of the individual contact areas and the joint length. Mobilization of peak shear strength along short joints is associated with development of small individual contacts between the small effective asperities. By contrast, larger areas of contact are created between the larger irregularities controlling the shear strength of longer joints. It has been tentatively concluded that the scale effect in the asperity failure components estimated for the present joints may be connected with a reduction in the effective value of joint compressive strength (JCS) operating along longer samples due to the increasing contact areas, as assumed by Barton and Choubey. There will probably exist a limit to the scale effect in JCS beyond which any further increase in the size of the individual contact areas will not affect the value of JCS, in compliance with the variation in the uniaxial compressive strength with specimen size found for intact rock materials. The latter effect coupled with a similar variation in the angle of slope inclination with increasing effective asperity baselength, and hence in the value of JRC, may explain the experimental non-linear trends between the peak shear strength and the joint block size.

In cases of relatively smooth and planar joints the actual contact area-scale effect is virtually absent and hence scale effects on JCS will be minimal. The joint roughness coefficient is also practically independent of the length of profile considered. Consequently, the peak shear strength of those joint types is unaffected by scale.

The shear stress-shear displacement relationships of rough undulating joints reveal significant changes in behaviour with increasing scale. The pre-peak region becomes gradually more non-linear and behaviour changes from 'brittle' to 'plastic'. The changing shape of the curves may be the result of a 'progressive' joint failure with increasing scale. The 'brittle' and 'plastic' behaviour exhibited by respectively

small and large joint blocks may be a characteristic of individual joints but not of composite rock masses with analogous joint spacing.

Comparison of experimental peak shear displacement data with Barton's suggestion of 'peak displacement equal to 1% of joint length' showed good agreement in the lower range of sizes (model lengths up to 18 cm). For the larger specimens, in particular the types without large undulations, peak displacements were smaller than those predicted from the "1%" rule. The present joint types indicate that the length range within which the "1%" assumption may be applicable, could be narrower in cases of joints with relatively planar full scale surface geometry. Interpretation of the model results at prototype scale shows that for moderately undulating to planar surfaces the "1%" rule may apply for joint lengths up to approximately 3-4 meters. For strongly undulating joints that limit is represented by 5-6 meters. However, the quality of such deductions is questionable due to the uncertainties with regard to the relevance of model joint roughness when extrapolated at prototype scale to that of natural exposures.

An implicit assumption in the interpretation of the results from this study has been that small joint blocks in a closely jointed rock mass would be capable of a more or less independent movement, which would obviously be necessary for the joint walls to maintain contact between the small asperities and hence develop higher peak shear strength. Some recent experimental results by Barton from biaxial tests on jointed model rock masses composed of different joint block sizes show that the shear strength of a rock mass increases with decreasing block size or joint spacing. It could therefore be concluded that the reduced stiffness of a closely jointed mass will increase the degree of freedom of the small blocks and allow them to rotate and 'feel' the smaller scale and steeper asperities of the component joints. Intuitively, the freedom for individual block movement will be limited at high stress levels.

CHAPTER 2.5

PRACTICAL CONSIDERATIONS

2.5.1 Introduction

The scale effect on shear strength implies that there will be a minimum test specimen size which should be regarded as technically acceptable for a shear surface of particular morphological characteristics.

Joint sizes which can be tested in the laboratory by using commercially available (e.g. standard soil mechanics shear box) or specially constructed apparatus (Krsmanovic 1967, Rengers 1970, Goodman 1970, Kutter 1971 describe some notable ones) are between approximately 5 and 40 cm in length. However, the technical size-limit in most laboratories rarely exceeds 10-15 cm. Those joint sample sizes represent fractional portions of the natural exposures and may yield unrealistic data. Schneider (1978) notes the reluctance of practicing engineers to apply friction values which have been determined in the laboratory, a situation which often leads to the use of more or less arbitrary reduction factors whereby friction values are reduced to one-half to two-thirds of their measured values.

The limited laboratory-size range can be extended substantially by in-situ testing. A large number of field shear tests have been reported in the literature with joint block sizes usually ranging from approximately 50 to 200 or 300 cm in length (e.g. Krsmanovic and Popovic 1966, Drozd 1967, Serafim and Guerreiro 1968, Locher and Rieder 1970, Pratt et al. 1974, Franklin et al. 1974, Infanti and Kanji 1978). In-situ shear tests are very costly and hence are used mainly on large scale projects such as dam foundations, major stability problems and complex underground openings, and even then are usually reserved for the worst conditions, e.g. faults, shear zones, infilled joints etc.

Predictions of the shear strength of large unfilled joint exposures, where scale effects may be potentially significant, are frequently based on laboratory-size specimens. Knowledge of the full scale joint morphology would then be essential for the interpretation of experimental data in order to make some allowance for a scale factor. Barton and Choubey (1977) have suggested an 'experimental' approach to the problem of derivation of full-scale shear strength estimates via inexpensive large scale index testing.

2.5.2 Choice of an appropriate joint test size

For each shear strength investigation a decision must be made on the size of joint specimens which will be tested. The choice is generally based on both economic and technical considerations. However, the dramatic increase in the cost of conventional shear tests with increasing specimen size (e.g. see Franklin et al., 1974) may lead to a decision based solely on a cost-benefit evaluation; that is, cost of testing larger joints versus possible excavation savings and maintenance costs such as disruption from and removal of a slipped mass. Wareham and Sherwood (1974) note that in some cases the test size which can be justified from economic considerations can only be regarded as an index test in the problem.

From the technical point of view the size of test specimen will depend upon the intended use of peak or residual parameters and the type of joints involved in the particular problem. Measurements of residual friction angles are independent of the test scale, and laboratory-size joints will be the immediate choice. The peak shear strength of the relatively planar joint types also seems to be little affected by scale and hence small joint samples may yield technically acceptable data..

In situations where irregular surfaces, e.g. rough undulating bedding planes, are the suspected failure paths, the scale factor becomes significant. According to Wareham and Sherwood (1974) the asperities controlling peak behaviour will probably have a minimum wavelength of about 1-10% of the total length of the potential sliding plane, and therefore the appropriate joint specimen size should be chosen accordingly. Barton and Choubey (1977) suggested that the correct joint test size might, as a first approximation, be given by the natural block size or more specifically the spacing of cross-joints. They envisage that the scale effect in a closely jointed mass may 'die-out' earlier, as the reduced stiffness might not allow the large scale irregularities to be mobilized as the only rock wall contacts, as might be the case in a rock mass with very widely-spaced joints and correspondingly high stiffness. Hence, the natural block size (or similar) may represent a 'critical joint length' still just sensitive to scale effects on τ and d_h and thus be the most relevant joint size for testing. The last authors point out that in the presence of tightly interlocked non-planar cross-joints the rock mass would remain quite

stiff due to the high peak shear stiffness of these joints, especially when under confined conditions within the mass. They further observe, however, that this complication might not arise often since closer spaced joints generally appear to be smoother and more planar than widely spaced joints.

The interconnection between cross-joint spacing, mass stiffness, freedom of block movement and the related scale effects have been discussed in the last chapter. Rock masses with widely spaced joints have less freedom for block rotation than rock masses with small block sizes. The greater freedom of smaller blocks for individual rotation enable them to maintain contact with the smaller scale and steeper asperities of the component joints. In effect the spacing of cross-joints (or block size) is the minimum 'hinge' length in the rock mass, hence its potential as a scale-effect size limit.

Under present considerations, therefore, Barton and Choubey's concept of a 'critical joint length' may be acceptable. The latter implies that if the maximum spacing of cross-joints was 50 cm, then joints of minimum 50 cm length should ideally be tested. If the maximum spacing of cross-joints was 200 cm correspondingly larger blocks should be tested, if technically and economically possible. It is also implied that the natural block size will represent the most relevant joint length for roughness analysis and related interpretation of laboratory-size joint test results.

2.5.3 Prediction of shear strength from laboratory-size joints

1. General considerations

The presence of different scales of roughness on large joint surfaces means that there may be a built-in 'scale' effect when using laboratory-size specimens to predict the shear strength of large exposures. Joint specimens are aligned in the shear box horizontally and parallel to the enforced direction of shear. In the field exposure the same joints may not be so aligned due to the presence of gently inclined large scale undulations and an inclined plane component (waviness angle i) may need to be added. This correction is most appropriate when residual friction angles (ϕ_r) are assumed in the general shear strength equation (Patton 1966):

$$\tau = \sigma_n \tan (\phi_r + i) \qquad 2.19$$

ϕ_r is not mobilized until after large displacements have occurred which generally makes the waviness angle (i) a realistic addition to shear strength.

In the "Suggested Methods" report of the ISRM (1978a) it is recommended that the value of the peak friction angle (ϕ_p) for use in 2.19 can be estimated from:

$$\phi_p = \text{JRC} \log_{10} \left(\frac{\text{JCS}}{\sigma_n}\right) + \phi_r \qquad 2.20$$

It is also noted that "since peak shear strength is mobilized after relatively small displacements it may not be realistic to add the large scale waviness angle (i) to the above estimate of ϕ_p".

As demonstrated from this study, the index of JRC can only be regarded as a constant for a fixed joint length, or when joints are of the relatively planar type. Longer profiles of the same non-planar joint will have lower JRC values. There may also be a scale effect in the value of JCS. Consequently, unless the JRC and JCS values have been corrected for a scale factor, the estimates of ϕ_p based on index values relevant to laboratory-size joint samples will tend to be optimistic.

Different lengths of roughness profiles of the present joint types were analyzed to examine the existence or otherwise of some simple relation between joint length and 'effective' roughness, for the purpose of arriving at some quantitative form of extrapolation of the JRC values representing short profiles (viz. laboratory-size specimens) to much longer ones (viz. natural joint exposures).

2. Roughness analyses of joint surface profiles

Scale effects on JRC are associated with the changing geometry of the 'effective' roughness which defines the peak shearing path of different profile lengths of the same joint. As the 'sample' length increases, so does the peak shear displacement and the contacts at the instant of peak strength are transferred onto larger irregularities.

Those contacts are less steeply inclined with respect to the mean joint plane than the contacts between smaller asperities which control the peak behaviour of shorter joint profiles, and the value of JRC changes accordingly. The shearing mechanism of different joint lengths is shown in Figure 2.52, which is a reconstruction of the approximate peak shear conditions for two joint samples 6 cm and 18 cm long under the experimental normal stress ($JCS/\sigma_n = 80$). The JRC value back-analyzed for the 18 cm joint, assuming constant JCS, was 12.2, whereas a JRC value of 18.5 was obtained for the 6 cm joint. The involvement of larger asperities with increasing scale is illustrated quite clearly. Under the particular normal stress level the mean inclination of the contacts at the instant of peak ($\equiv$ peak dilation angle i_p^o) was 10.5° and 16.3° for the 18 cm and 6 cm joints respectively.

Measurements of joint roughness have demonstrated that the roughness angle depends on the closeness between the adjacent measuring points (e.g. Rengers 1970, Barton 1971). As the distance or 'step'-size increases the inclination of the 'step'-lines connecting each pair of points decreases. In effect, larger 'steps' linearize smaller steep asperities thereby 'sampling' longer and more gently inclined asperities. The changing 'effective' roughness with scale could therefore be accounted for by increasing the 'step'-size when profiling longer joints. With reference to the particular example in Figure 2.52, 'steps' of approximately 1 mm would be necessary to 'sample' the 'effective' asperities for the 6 cm long joint, whereas at least 3-4 times larger 'steps' would be relevant to the 18 cm joint. Since the reduction in JRC is related with the flatter geometry of larger 'effective' asperities, it is tempting to consider whether the difference in the measured roughness angles by varying the 'step'-size could give some indication of the anticipated change in JRC at larger scale.

In order to examine the validity of that hypothesis the roughness of several non-planar joints was analyzed in the manner shown in Figure 2.53 (the three profiles are from model joint no. 2). Firstly, a series of points was located on the profiles at a distance equal to the baselength of the smallest asperities. A minimum 'step'-size was then defined by connecting point no. 1 with no. 2, no. 2 with no. 3, and so on. The next 'step' was taken between points no. 1 and 3,

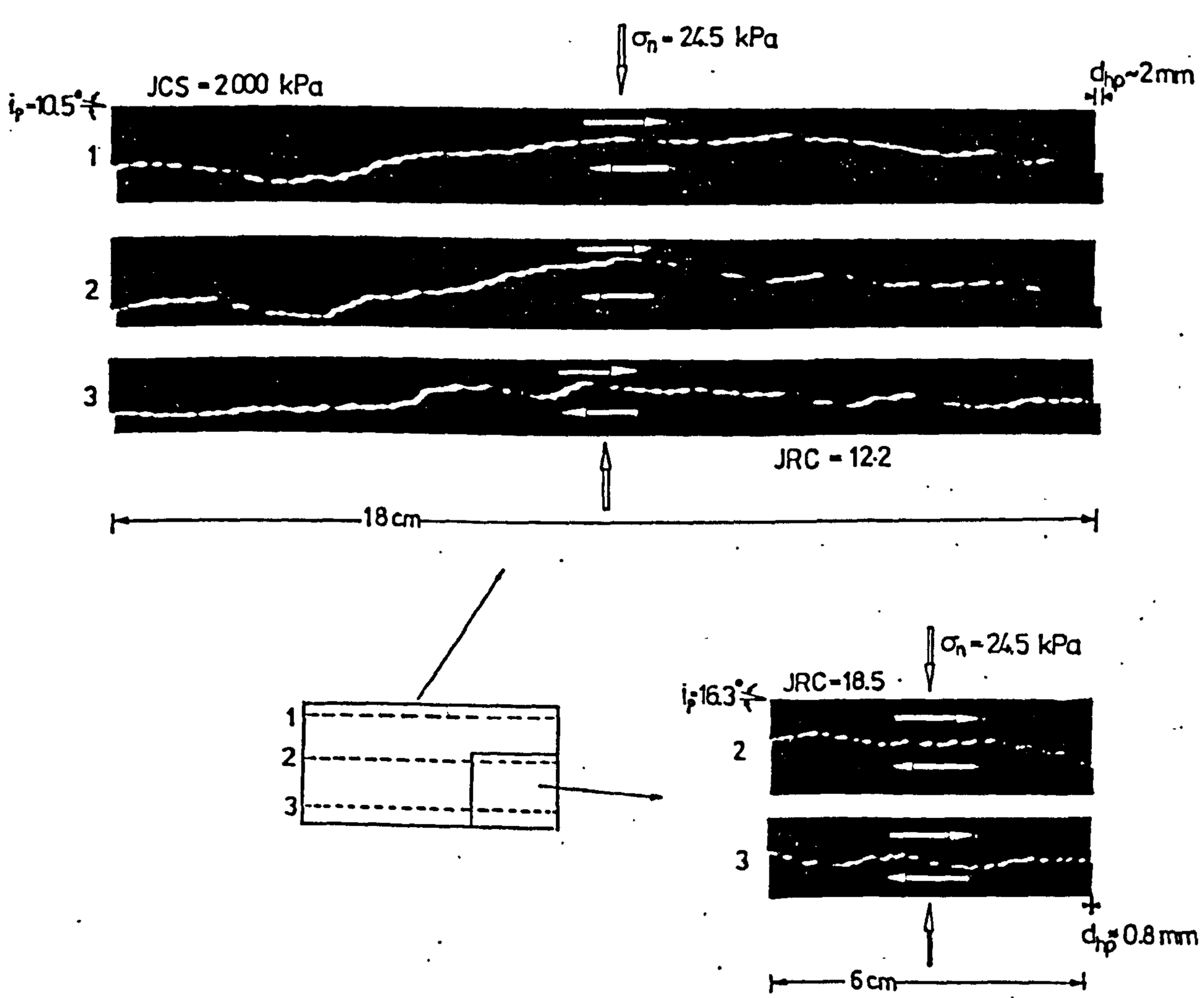

FIGURE 2.52 Reconstruction of the approximate peak shear condition of an 18 cm long joint and a 6 cm long "sample" illustrating the increase in the size of the asperities controlling the peak behaviour and hence the effective peak value of JRC. When profiling long joints the "critical" asperities can be sampled by increasing the step size (see following figure 2.53)

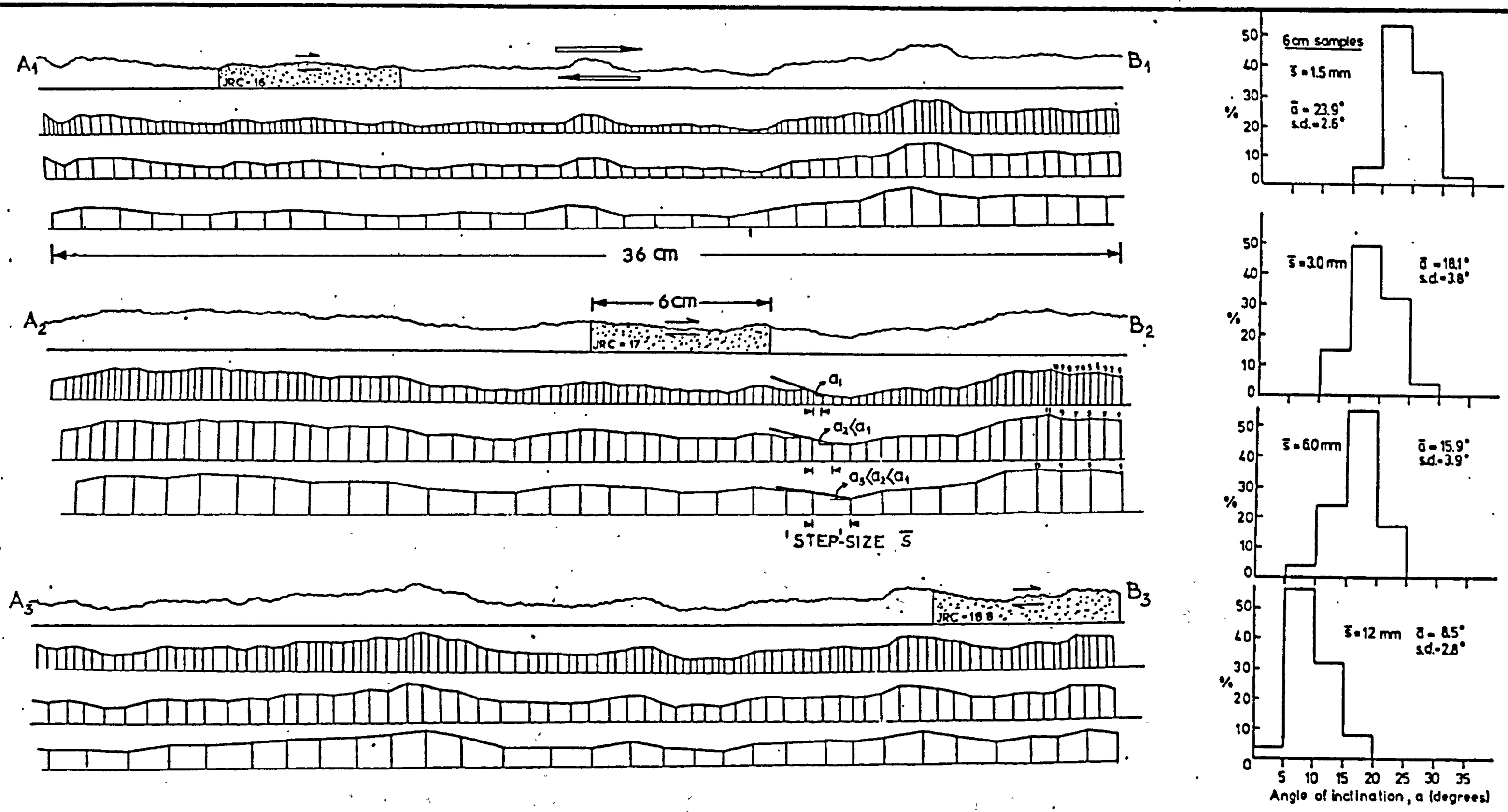

FIGURE 2.53 Typical example of the variations in the asperity inclination angle $\bar{a}$ with step size $\bar{s}$. The profiles analysed above are from Model No.1. Larger 'step'-sizes sample longer asperities with lower inclination angles. In practical terms, selection of a 'step'-size appropriate to the length of joint profiled will yield roughness data relevant to the peak behaviour of the particular joint length.

no. 3 and 5, etc., and the one after between points no. 1 and 5, no. 5 and 9 and so on. The range of 'step'-sizes for all joints was on average equivalent to 0.3-3.0% of the total length of the profiles and the baselengths of the asperities thus 'sampled' ranged between approximately 2 and 20 mm. The procedure was applied on three to five profiles of each joint surface. The inclination of the different 'steps' was measured with respect to a horizontal reference plane by using a combined protractor and parallel rule instrument of high accuracy. Only the positive angles with respect to the shearing direction were measured.

In addition to the roughness measurements on the large joints a similar procedure was applied on a few smaller 'samples' of the profiles. The 'step'-size for those joint sizes was equal to half the baselength of the small asperities. The roughness data for model no. 2 with increasing 'step'-size ($\bar{s}$) are shown in the form of block diagrams in Figure 2.53. If the 'effective' roughness for the 36 cm long joint was represented by asperities with average baselengths in the order of ~6 mm, the 'step'-size of ~3 mm would give the correct range of inclination angles (a) and so on.

The 'effective' roughness sampled by each of the 'steps' was expressed by the arithmetic mean of a° values. It should be noted that exceptionally small inclination angles were discarded from the averaging, hence the scatter about the mean values was generally small. In order to examine whether the difference in the $\bar{a}$ values representing the 'effective' roughness of the 6 cm samples and the 36 cm long joint was related quantitatively with the anticipated reduction in the JRC value measured from the 6 cm samples, a range of reduction factors was defined as $\bar{a}_6/\bar{a}_{36}$, where $\bar{a}_{36}$ was equal to the $\bar{a}$ values corresponding to each of the three 'step'-sizes considered. With reference to the particular case in Figure 2.53, if it was assumed that the 'effective' roughness for the 36 cm joint was represented by asperities with average baselength of ~ 6 mm, the corresponding reduction factor would be $\bar{a}_6/\bar{a}_{36} = 23.9°/18.1° = 1.32$. According to the hypothesis tested, the relevant JRC value for the 36 cm joint would be: $JRC_{36} = JRC_6/1.32$. If the 'effective' asperities were actually larger, a correspondingly larger reduction factor would be applicable, as shown over:

6 cm samples: $\bar{a}$ = 23.9°, JRC_6 (average of 3) = 17.7

Reduction factors (a_6/a_{36}): 23.9°/18.1° = 1.32
23.9°/15.9° = 1.50
23.9°/ 8.5° = 2.80

Predicted values of JRC_{36}: JRC_6/1.32 = 13.4
/1.50 = 11.8
/2.80 = 6.3

The experimental value of JRC_{36} was 10.4 (on the assumption of a 'constant' JCS value) or 12.0 (on the assumption of a scale-reduced JCS value, see Table 2.24 in p.174). It is interesting to note that the predicted JRC_{36} value of 11.8 is almost identical with that obtained on the assumption of a scale-dependent JCS. Another remarkable similarity exists in the predicted JRC value of 13.4 and the mean experimental value obtained for the 18 cm long samples of the same joint (= 13.0 on the assumption of a scale-dependent JCS). In this example, therefore, there is a quantitative relation between the 'effective' roughness for the 6 cm, 18 cm and 36 cm joints and their corresponding values of JRC when the 'step'-size is taken as approximately equal to 1.5% of the corresponding joint length. Similar observations were made for a range of joint types by considering approximately the same 'step'-sizes (~ 1-2% of joint length):

MODEL no. 3

6 cm samples (nos. 3, 14, 18): $\bar{a}_6$ = 25.8°, std. dev. = 4.1°
$\overline{JRC}_6$ (av. of 3) = 18

'Effective' roughness data: 18 cm joints $\bar{a}_{18}$ = 17.8°, std. dev. = 2.9°
36 cm joint $\bar{a}_{36}$ = 13.7°, std. dev. = 3.0°

Predicted JRC: $\overline{JRC}_{18} = \overline{JRC}_6/1.45 = 12.4$
$JRC_{36} = \overline{JRC}_6/1.88 = 9.6$

Experimental JRC: $\overline{JRC}_{18}$ = 11.7 (JCS = 2000 kPa) or 13.1 (JCS = 1250 kPa)
JRC_{36} = 7.8 (JCS = 2000 kPa) or 11.1 (JCS = 536 kPa).

MODEL no. 4

6 cm samples (nos. 2, 10, 18):	$\bar{a}_6$ = 25.1°, std. dev. = 4.5°
	$\overline{JRC}_6$ (av. of 3) = 16.1
'Effective' roughness data:	18 cm joints $\bar{a}_{18}$ = 19.9°, std. dev. = 2.8°
	36 cm joint $\bar{a}_{36}$ = 16.1°, std. dev. = 3.2°
Predicted JRC:	$\overline{JRC}_{18} = \overline{JRC}_6/1.26 = 12.8$
	$\overline{JRC}_{36} = \overline{JRC}_6/1.56 = 10.3$
Experimental JRC:	$\overline{JRC}_{18}$ = 11.7 (JCS = 2000 kPa) or 13.1 (JCS = 1400 kPa)
	JRC_{36} = 7.5 (JCS = 2000 kPa) or 9.0 (JCS = 960 kPa).

MODEL no. 7

5 cm samples (nos. 12, 17, 25):	$\bar{a}_5$ = 29.2°, std. dev. = 3.4°
	$\overline{JRC}_5$ (av. of 3) 20
'Effective' roughness data:	20 cm joints $\bar{a}_{10}$ = 16.0 std. dev. = 2.2°
	40 cm joint a_{40} = 14.7° std. dev. = 1.6°
Predicted JRC:	$\overline{JRC}_{20} = \overline{JRC}_5/1.82 = 11$
	$\overline{JRC}_{40} = \overline{JRC}_5/1.97 = 10.1$
Experimental JRC:	$\overline{JRC}_{20}$ = 10.8 (JCS = 2000 kPa) or 12.6 (JCS = 1070 kPa)
	JRC_{40} = 7.5 (JCS = 200 kPa) or 9.0 (JCS = 962 kPa).

The good agreement between the predicted and measured values of JRC implies that for the present type and size of joints and assuming that the baselength of asperities controlling peak behaviour is between 2 and 4% of the respective joint length, the hypothesis of a quantitative relation between 'effective' roughness angles and JRC at different scales may be a valid one. It is noted that for all the

joint surfaces analyzed the predicted JRC values were closer to the experimental ones derived by assuming scale-dependent JCS values. Those JRC values probably give a more realistic picture of the magnitude of scale effects on JRC than the somewhat exaggerated effect when JCS is kept constant. Should those relationships hold good for much larger joints, it would in principle be possible to derive a scale-corrected value for JRC from laboratory-size specimens. According to the concept of a 'critical joint length' the minimum joint size for roughness analysis would be defined by the maximum cross-joint spacing in-situ. Roughness measurements should be taken along several profiles of appropriate length for a minimum 'step'-size approximately equal to 1-2% of the joint length. A number of laboratory-size samples should also be collected for similar roughness analysis and determination of a statistically representative value of JRC for those sample sizes. Provided that the roughness data follow a more or less normal distribution it might be preferable to describe the 'effective' roughness by means of the arithmetic mean and standard deviation of the a° angles and derive a range of possible scale reduction factors for the 'laboratory' value of JRC.

3. Prediction errors

Prediction methods of the type considered in the last section may lead to significant errors if the data required are not statistically representative of the joint surfaces analyzed. Another inherent limitation in introducing independently 'corrected' JRC and JCS values is that the estimate of the peak friction angle ϕ_p at design stress levels could be seriously misleading, depending of course on the magnitude of error in the input JRC and JCS values. A hypothetical example will be given to demonstrate the range of errors in predicted ϕ_p values at different normal stress levels by using over- and under-estimated (with reference to hypothetical actual values) JRC and JCS data.

In the example it will be assumed that the 'true' JRC is equal to 8 and the 'true' JCS is equal to 40 MPa. Then the 'true' ϕ_p values at different σ_n levels would be:

Normal stress (MPa):	0.1	0.5	1.0	2.0
JRC = 8, JCS = 40 MPa) ϕ_p :	53°	47.2°	44.8°	42.4°

$\phi_r = 32°$

Assuming JRC values of 10 or 6, i.e. an over- and underestimate of the true JRC by 2, and JCS values of 60 and 40 MPa, i.e. an over- and underestimate of JCS by 50%, the following prediction errors could arise within the range of σ_n considered (the + and - values express the amount of over- and underestimation with respect to the 'true' ϕ_p values above):

JCS = 20(-50%)	JRC = 6 (-2) →	-7.2°	-5.6°	-5°	-4.4°
	JCS = 10 (+2) →	+2°	+0.8°	+0.2°	+0.9°
JCS = 60(+50%)	JRC = 6 (-2) →	-4.3°	-2.7°	-2.1°	-1.5°
	JCS = 10 (+2) →	+6.8°	+5.6°	+5°	+4.4°

From the various combinations considered above it is clear that the most serious error is introduced by an incorrect JRC value and that errors are higher when the JCS/σ_n ratio value is high. This type of analysis may be useful when deriving a range of possible full scale JRC values according to the procedures described earlier. Different scale reduction factors for JCS could also be considered depending on the rock type involved (e.g. see Barton and Choubey 1977), so that selection of a design ϕ_p value could be made in parallel with the knowledge of the likely margin of uncertainty.

The inevitable uncertainties in deriving the full scale values for JRC and JCS and the likely magnitude of errors in the predicted ϕ_p values could be largely reduced if, as Barton and Choubey suggested, the values of JRC were back-analyzed from the results of large scale tests. As the cheapest solution they suggested that tilt or pull tests could be conducted on naturally occurring block sizes.

2.5.4 Prediction of shear strength from large scale index tests

The potential of tilt testing in the determination of the angle of statical friction of rock joint surfaces has been considered by Cawsey and Farrar (1976) and Hencher (1976). Those studies concentrated on planar joint surfaces of laboratory dimensions.

Barton and Choubey (1977) considered the applicability of tilt-testing on rough joint surfaces. The higher angles of tilt (a°) associated with sliding of irregular planes imposes an obvious restriction to the range of surface roughness that can be tilt-tested. Steep angles a° may induce a tendency for joint opening and toppling depending upon the value of the length/height ratio, which defines the vertical line of action from the centre of gravity of the top block. As the angle of inclination increases, the uniform stress distribution across the originally horizontal basal

contact changes to the effect of producing higher stress concentrations towards the leaning edge of the block (Hencher, 1976).
Theoretically, the effective normal stress (σ_{no}) generated by the gravitational force acting on the upper half of an infinitely long block is given by

$$\sigma_{no} = \gamma h \cos a \qquad 2.21$$

where h = height of top half of block (m)
γ = unit weight of rock material (KN/m^3).

In a practical situation some allowance should be made in eqn. 2.21 for the uneven stress distribution. Barton and Choubey have proposed an empirical correction factor cos a and the modified version of 2.21 is given below:

$$\sigma_{no} = \gamma h \cos^2 a \qquad 2.22$$

The JRC value of a tilt-tested joint can be obtained from

$$JRC = \frac{a^o - \phi_r}{\log_{10}(JCS/\sigma_{no})} \qquad 2.23$$

σ_{no} = normal stress induced by self-weight of the block (calculated from 2.22)
γ, h = as defined above
ϕ_r = residual angle of friction
JCS = joint compressive strength.

Values of JCS can be estimated using the simple Schmidt hammer test (Miller 1965, ISRM 1978). Further information on Schmidt hammer testing is included in part three of the thesis. The value of ϕ_r can either be measured or estimated by a method described by Barton and Choubey. The estimate of ϕ_r is based on the ratio between the Schmidt hammer rebound (r) obtained on the weathered joint wall and the rebound (R) obtained on unweathered rock combined in the following form:

$$\phi_r = (\phi_b - 20^o) + 20(r/R) \qquad 2.24$$

where ϕ_b is the basic angle of friction of an unweathered flat surface (also measured from tilt tests). The key condition for the reliability of the parameters predicted by index testing lies in the large number of tests that can and should be made. Barton and Choubey recommend use of

the mean angle of tilt from three tests on the same joints and testing of as large a number of different specimens as practically possible. Comparisons of the friction angles measured by conventional testing methods and predicted by index testing of the same specimens representing eight different rock types (a total of ~140 joints) showed an agreement to within $\pm$ 1°.

The various principles referred to earlier can obviously be extended to in-situ tilt testing of large blocks. A worked out example of a hypothetical tilt test is presented in Figure 2.54. Tilt tests can safely be employed for a range of JRC values of up to 10.

Rougher joints can be pull-tested with the joint in a horizontal plane (or inclined as the case may be) and the top block pulled parallel to the joint plane. A diagrammatic illustration of the testing principle is presented in Figure 2.55.

The external "pulling" force T_2 (in addition to the tangential component T_1 of the self-weight W of the block) required to mobilize the peak value of JRC may be applied via a grouted bolt and hook. In many cases it would probably be necessary to "line-drill" at least one side of the block to remove the stabilizing effect of interlocking asperities from the surrounding blocks.

In this case the relevant value of JRC is given by the following relation:

$$JRC = \frac{\tan^{-1}\left(\frac{T_1 + T_2}{N}\right) - \phi_r}{\log_{10}\left(\frac{JCS \times A}{N}\right)} \qquad 2.25$$

where T_1 and T_2 are as defined in the text above

N = normal component of block weight (W)

A = joint area.

A hypothetical example is included in Figure 2.55.

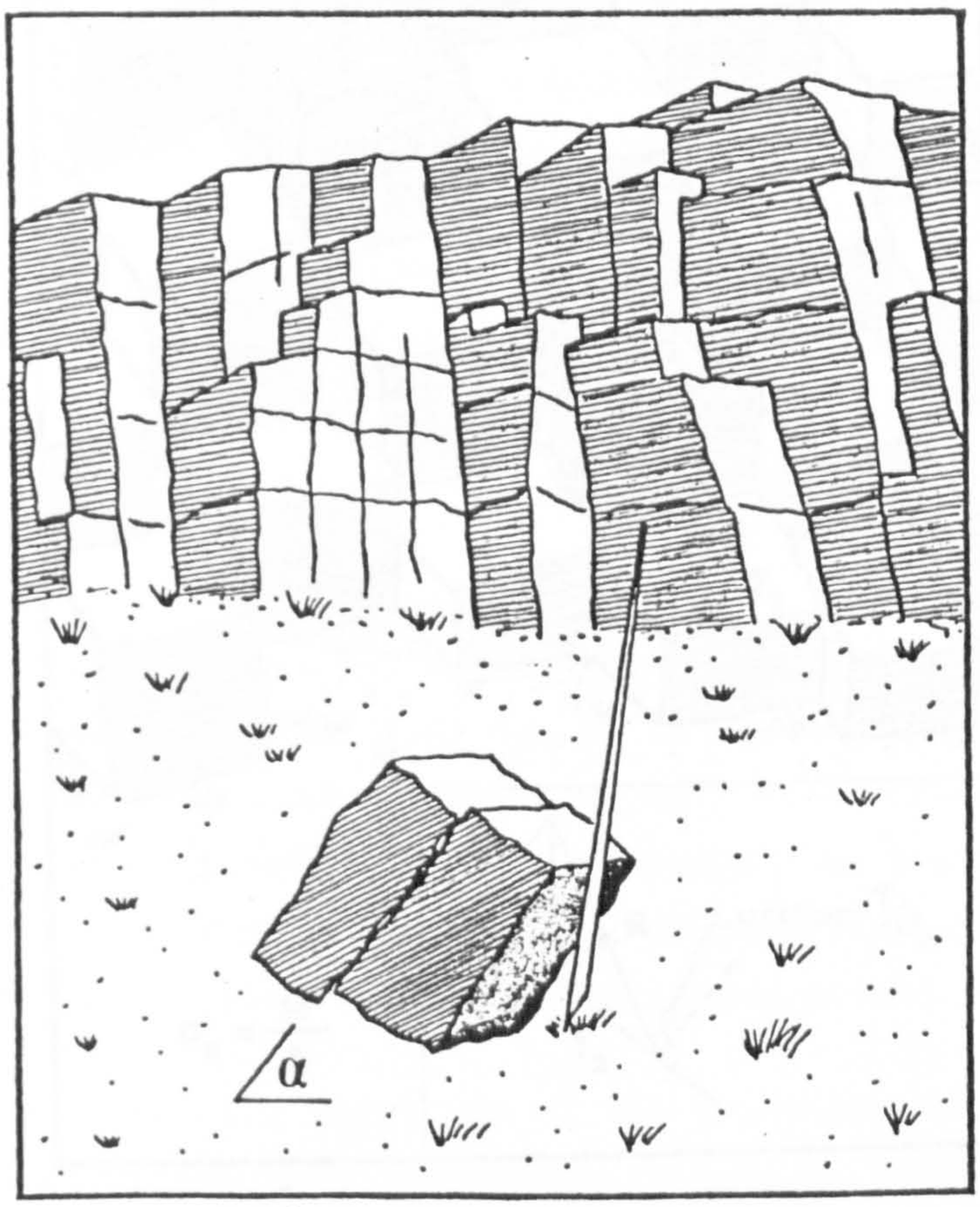

TILT TEST

Example:

Assume the following values have been measured:

$a = 51^{o}$ (tilt angle)
$h = .50$ m (block height)
$\gamma = 25$ KN/m^3 (unit weight)

} According to eqn. 2.22, $\sigma_n = 0.005$ MPa

JCS = 50 MPa Estimated using Schmidt hammer
$\phi_r = 23^{o}$ Estimated from eqn. 2.24

$$JRC = \frac{51^{o} - 23^{o}}{\log_{10}(\frac{50}{0.005})} = 7.0$$

FIGURE 2.54 (from Barton and Bandis, 1979).

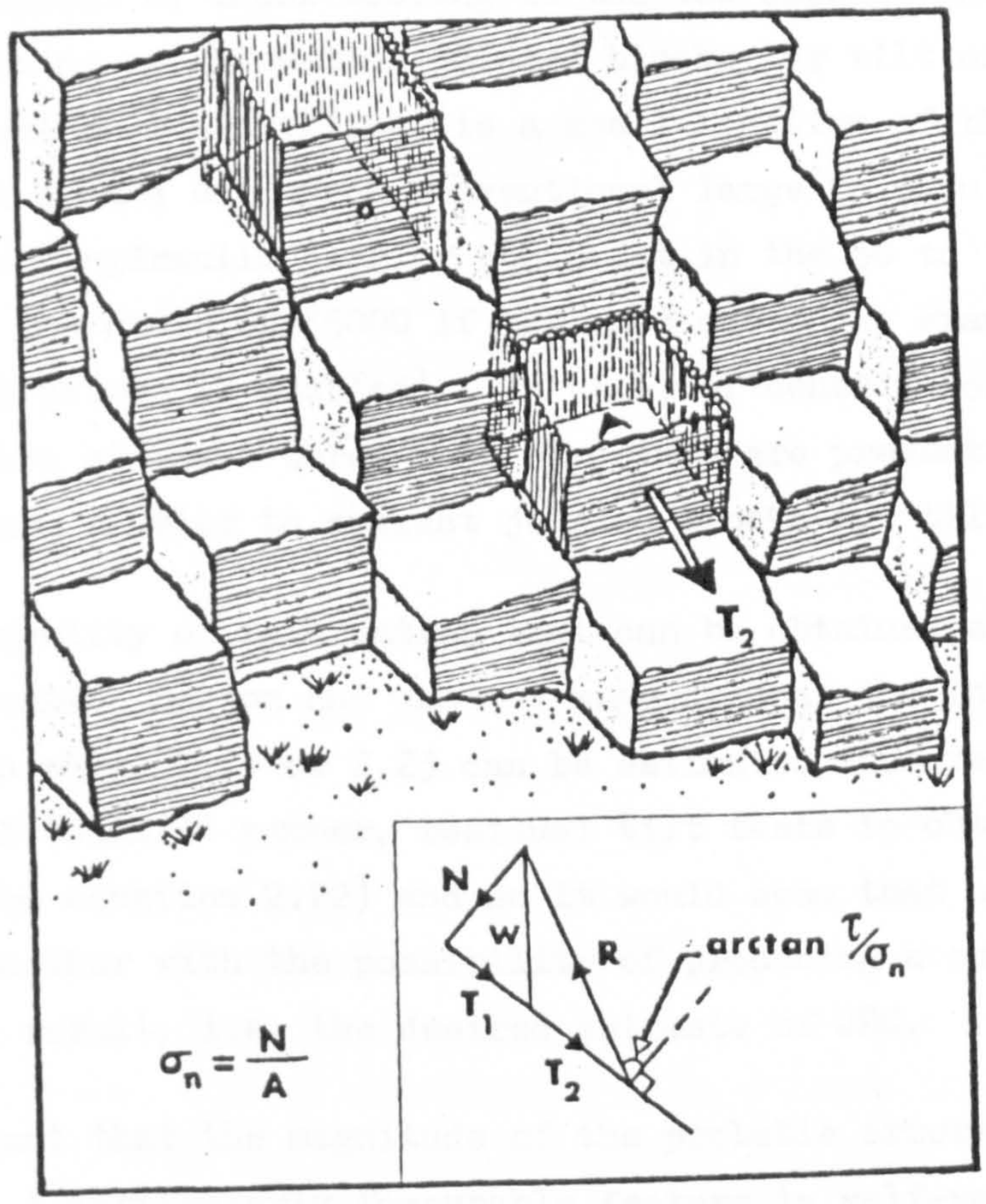

PULL TEST

Example:

$N = 2$ tons	Normal and tangential components of
$T_1 = 1$ ton	self-weight of upper block.
$T_2 = 1$ ton	External force
$A = 1\ m^2$	Area of test surface
JCS = 20 MPa	Estimated using S.H.
$\phi_r = 24^\circ$	Estimated from eqn. 2.24

$$JRC = \frac{\arctan(\frac{1+1}{2}) - 24^\circ}{\log_{10}(\frac{20}{.02})} = 7.0$$

FIGURE 2.55 (from Barton and Bandis, 1979).

The obvious appeal of index testing is the low expense involved. The cost of isolating or extracting jointed blocks for tilt or pull tests, for example using line drilling, is a small fraction of the amount needed to set up and execute a conventional large in situ test (e.g. 1 x 1 m) with associated hydraulic jacking equipment in the 50 to 100 tons range (probably in the order of £5000 if the cost quoted by Franklin et al., 1974, based on 1973 prices is doubled). In cases of densely jointed rock masses, especially when at least three sets of joints are present, it would be relatively much simpler to extract jointed blocks for tilt testing.

However the quality of information that can be obtained should be carefully considered. Barton and Choubey suggest that the input parameters JCS and ϕ_r in eqns. 2.21 or 2.23 can be estimated from relevant index tests as well (Schmidt hammer, residual tilt tests to obtain ϕ_b and then derive ϕ_r from equation 2.22) and so it would seem that one empiricism is built upon another with the possibility of producing a cumulative error upon the end result, i.e. the desired estimate of JRC.

It is important that the magnitude of the probable errors is carefully considered. A particularly favourable feature in self-weight tests is the high value of the ratio JCS/σ_n, which would probably be in the range of 1,000 to 100,000 in most conceivable cases. Thus errors in <u>estimating ϕ_r</u> would be reduced by a factor of 3 to 5 when those estimates are used in eqns. 2.23 or 2.25. Also, errors in <u>estimating JCS</u> would be relatively small due to the logarithmic formulation. At any rate, the formulation of eqns. 2.23 or 2.25 ensures an automatic compensation for overestimates or underestimates of ϕ_r and/or JCS by producing corresponding underestimation or overestimation of JRC (for instance refer to the data in Table 2.24 where JRC values for the same joint length have been derived by assuming two different values of JCS).

In order to test the effect of different values of JRC and JCS on the estimates of shear strength at levels of normal stress higher than the experimental, three pairs of "compensated" JRC and JCS values were derived for some of the 36 cm joint specimens by assuming:

(1) JCS to be equal to 2000 kPa (relevant JRC data already given in Table 2.22).
(2) JCS and JRC as both scale-dependent variables (see Table 2.24).
(3) JCS as equal to the value back-calculated by using the JRC corresponding to the 6 cm specimens of the particular model type.

As an example, in the case of the 36 cm specimen of model no. 1 the three respective sets of values would be

(1) JCS = 2000 kPa, JRC = 12.5 (2) JCS = 1198 kPa, JRC = 14.1 (3) JCS = 512 kPa, JRC = 18.1

with each pair expressing the $\tan^{-1}(\tau_p/\sigma_n)$ value as determined at the experimental σ_n. Some characteristic examples of the peak friction angles at higher σ_n estimated from

$$\tan^{-1}(\tau_p/\sigma_n) = JRC \log_{10}(JCS/\sigma_n) + \phi_b$$

by using each set of JRC and JCS values are given in Table 2.26.

As shown from those examples, "higher" JCS values combined with "lower" JRC resulted in estimation of larger peak friction angles and vice versa for the same σ_n. The magnitude of the differences depended upon the $JCS_1/JCS_{2,3}$ ratio value, the level of σ_n and the type of joint. Within the range of normal stress considered (up to 6 times the experimental σ_n of 24.5 kPa) and with the assumed JCS values differing by up to factor of 7.7, the maximum relative differences in $\tan^{-1}(\tau_p/\sigma_n)$ were between 3° and 5° for joint types ranging from very rough (no. 1) to nearly planar (no. 10).

Similar discrepancies should be expected when extrapolating the results from in-situ tilt or pull tests to design levels of normal stress, which would normally be at least one to two orders of magnitude higher than the test σ_n. In a relevant example given by Barton and Choubey (1977) an assumed extrapolation of the results from a hypothetical tilt test to σ_n = 1.0 MPa produced an overestimate of 6° by assuming a JCS value 10 times higher than the "true" scale-dependent JCS. They further commented that by making a reasonable allowance for size-effects in JCS the expected error from that source should be nearer 1° or 2° for that range of normal stress. It should also be noted that errors in extrapolated friction angles would be smaller in cases of less rough joints (low JRC) as shown by model no. 10 in Table 2.26. This is because the shear strength of planar joints is not seriously affected by the value of JCS, as demonstrated by the family of curves in the previous Figure 1.11 (p.26).

Regarding the problem of practical allowance for size effects in JCS, Barton and Choubey suggested a maximum two- to three-fold reduction to be adopted for dense, hard rocks and a maximum ten-fold reduction for more

Table 2.26

Comparisons between estimates of $\tan^{-1}(\tau_p/\sigma_n)^\circ$ at various σ_n levels using different JCS and JRC input values.

Normal stress σ_n × σ_n^* kPa	36 cm specimen (MODEL No. 1) JCS$_1$ = 2000, JRC$_1$ = 12.5	JCS$_2$ = 1198, JRC$_2$ = 14.1, JCS$_1$/JCS$_2$ = 1.7	JCS$_3$ = 512, JRC$_3$ = 18.1, JCS$_1$/JCS$_3$ = 3.9
1.0 *24.5	55.9°	55.9°	55.9°
2.0 49.0	51.2°	51.6°	50.4°
4.0 98.0	48.4°	47.3°	45.0°
6.0 147.0	46.2°	44.8°	41.8°

	36 cm specimen (MODEL No. 2) JCS$_1$ = 2000, JRC$_1$ = 10.4	JCS$_2$ = 1116, JRC$_2$ = 12.0, JCS$_1$/JCS$_2$ = 1.8	JCS$_3$ = 374, JRC$_3$ = 16.8, JCS$_1$/JCS$_3$ = 5.3
*24.5	51.9°	51.9°	51.9°
49.0	48.8°	48.3°	46.8°
" 98.0	45.6°	44.7°	41.8°
147.0	43.8°	42.6°	38.8°

	36 cm specimen (MODEL No. 10) JCS$_1$ = 2000, JRC$_1$ = 4.5	JCS$_2$ = 1010, JRC$_2$ = 5.3, JCS$_1$/JCS$_2$ 2.0	JCS$_3$ = 259, JRC$_3$ = 8.4, JCS$_1$/JCS$_3$ = 7.7
*24.5	40.6°	40.6°	40.6°
49.0	39.2°	39.0°	37.9°
" 98.0	37.9°	37.4°	35.5°
147.0	37.1°	36.4°	34.1°

*Experimental σ_n

Note: Subscripts 1, 2 and 3 correspond to assumptions 1, 2 and 3 as given in text.

porous and weathered rock types. Reductions in JCS of that magnitude are in compliance with the results from reported experimental studies on the size-effects upon the uniaxial compressive strength of intact rock materials (see Section 2.1.2).

2.5.5 Concluding remarks

It is of obvious practical implication that the determination of joint friction values during a shear strength investigation is based on sample sizes sufficiently large to allow for the scale factor. The current state-of-art with regard to the scale effect on the shear strength of rock masses leads to the conclusion that Barton and Choubey's concept of a 'critical joint length' controlled by the maximum spacing of cross-joints may be of potential practical value. The naturally occurring block size may effectively constitute a scale effect size limit thus being the most relevant joint size to test or analyze. This is of course considerably larger than the laboratory size specimens usually tested in rock mechanics. Use of conventional methods of testing at that scale would be impractical in most cases due to the very high cost involved. There is, therefore, great practical value in the use of empirical predictions via rationalized extrapolation procedures and inexpensive large scale testing methods.

Shear strength predictions demand that the scale effect on the input variables of JRC and JCS is realistically allowed for. According to the 'critical joint length' concept the nearest scale-free estimate of JRC could be measured on samples of minimum length equal to the maximum cross-joint spacing. The same minimum joint length should be considered when interpreting the results from tests on 'laboratory' size specimens.

Roughness analyses of joint surfaces revealed the existence of a potential relationship between the geometry of 'critical' asperities or 'effective' roughness for different lengths of joints and their respective values of JRC. Specifically, it has been found that the ratio between the average inclination angles of the 'critical' asperities for different joint lengths was approximately equal to the ratio between the respective JRC values. For the present range of joint sizes the wavelength of the 'critical' asperities was generally between 2 and 4% of the respective

joint lengths. If the above relation between 'effective' roughness and JRC at different scales holds good between joints with much larger difference in sizes, it may be possible to predict full scale estimates of JRC by correcting the values determined on laboratory samples according to reduction factors derived from roughness analysis of the respective profile lengths.

Allowance for a scale effect on JCS can only be made on the basis of experimental evidence of similar effects on the uniaxial compressive strength of intact rocks. The inherent uncertainty when using independently predicted estimates of JRC, JCS and ϕ_r in the calculation of the peak friction angle (ϕ_p) is that a cumulative error could be introduced if the variables had been over- or underestimated. This problem will be minimized if the JRC value is back-analyzed from the results of large scale tilt or pull tests (cf. Barton and Choubey). In that case the estimates of JCS and ϕ_r required for the derivation of JRC need not be very accurate. Underestimates and overestimates will be automatically compensated by corresponding overestimates or underestimates of JRC. Errors in the predicted ϕ_p values at higher normal stresses will then be relatively small, unless extrapolations are continued at very high stress levels.

PART THREE

EXPERIMENTAL STUDY OF ROCK JOINT DEFORMATION

CHAPTER 3.1

INTRODUCTION

3.1.1 General

The deformational behaviour of joints when stressed is a fundamental component of rock mass performance under load. At the relatively low stress levels encountered in near-surface excavations, it can be anticipated that joint behaviour will completely dominate the elastic deformations of the intact rock (Barton, 1971). Even under the higher levels of stress associated with heavy structures joint deformation often constitutes the major part of settlement on rock (Hungr and Coates, 1978).

The deformation modes of the joint system are considered to be made up primarily of direct compression or tension and tangential deformation. With the advances in the methods of numerical analysis, the deformation properties of joints have been explicitly introduced into the determination of the potential behaviour of the rock mass.

Joint deformability can be described by the character of the stress-deformation curves. Goodman et al. (1968) introduced the terms "normal stiffness" and "shear stiffness" to describe the rate of change of the normal stress with respect to normal displacements and of the shear stress with respect to shear displacements, respectively. Together with values for peak and residual shear displacement and maximum joint closure, these quantities allow computation of the contribution of joints to the total displacement of the rock mass.

The fundamental characteristics of joint behaviour under normal and shear loading conditions have been described in Part One of this thesis and the main points from the review of an extremely limited literature are summarized below:

(A) The normal stress-closure curves of certain joint types are highly non-linear. This mode of behaviour is mainly deduced from reported compression tests on artificial rock fractures. Non-linear deformation implies that the joint normal stiffness is not

a constant. According to a suggested hyperbolic model of behaviour (Goodman, 1974), the normal stiffness will increase to an extremely large number as the joint will approach its fully closed condition. The only published experimental study (Hungr and Coates, 1978) on the compression properties of natural joint specimens has indicated an essentially linear behaviour. The normal stresses applied in that case were extremely low. Quasi-linear behaviour has been attributed to "precompression effects", that is, past loading of the joints under pressures much higher than those applied in the tests. Similar views have been expressed in the past by Snow (1972) who stated that non-linearity is only relevant to "virgin" joints that have never closed before. The fundamental property of maximum joint closure depends on the loading history of the joint and the initial stress condition. Unloading of joints normally shows hysteresis and permanent set.

(B) The pre-peak portion of the shear stress-shear deformation curves obtained from direct shear testing indicate both linear and non-linear behaviour, which means that under a certain level of normal stress the joint shear stiffness may be independent of or dependent on the level of shear stresses. There is some uncertainty regarding the effects of normal stress and according to Goodman (1976), Chappell (1975) and others, neither a "constant stiffness" nor a "constant displacement" model as described by John (1970) are universally applicable. It is difficult to make strictly valid comparisons between various test cases, as shear stiffness values are affected by the experimental technique. Furthermore, joint peak shear stiffness seems to depend strongly on the size of the test specimen.

Despite their obvious practical significance the deformation properties of joints, and in particular the normal stiffness, have received very little attention over the past ten years. Although joint normal stiffness can relatively easily be measured from laboratory tests on single jointed blocks by applying loads normally to the joint plane and recording the vertical displacements, the literature review has shown that such data are extremely scarce. No systematic study has yet been reported regarding the variations in normal stiffness with joint type,

the effects of weathering, etc.

Although some uncertainties still exist, a relatively larger amount of information is available on the property of joint shear stiffness. Topics requiring further attention are standardization of laboratory techniques for measurement of the displacements, and more significantly, full appreciation of the potential effects of scale.

In the following two sections the factors affecting the joint deformability are discussed and some literature data are presented. Although reference will be made to the "infilled" class of joints, those types of discontimuities have not been included in the present experimental study. However, for the sake of a full discussion, it has been considered appropriate to review their behaviour.

3.1.2 Factors influencing the joint normal stiffness

Several workers have made qualitative reference to the factors affecting the normal stiffness of joints (Dunkan and Hancock, 1966, Goodman et al. 1968, Goodman 1970, Hungr and Coates 1978), which can be summed up as follows:

(i) initial actual contact area ratio; relative amplitude and vertical distribution of the aperture between the joint walls

(ii) joint wall roughness, strength and deformation properties of asperities

(iii) thickness, type, and physical properties of the infilling material, if present.

1. Infilled joints

The expected "softening" effect of infilling materials on the normal deformation of joints can be seen in the normal stiffness data by Infanti and Kanji (1978) listed in Table 3.1. The K_n values were obtained from in-situ normal loading tests on basaltic joints containing infilling materials of different thickness. As shown, under the range of applied normal stresses (<1 MPa), an average variation in filling thickness from 1 to 100 mm produced more than two orders of magnitude difference in the K_n values.

Table 3.1

Range of normal stiffness (K_n) in relation to thickness of infilling (t)

(after Infanti & Kanji, 1978)

t (mm)	K_n (MPa/mm)
50–100	0.01–0.50
10–20	0.50–2.00
<1 (1 case)	>5

The relative effects of a soft infilling on the deformability of a joint depend on the relationship between its average thickness and the roughness of the surface, that is the vertical amplitude of the wall asperities. Some experimental results by Goodman et al. 1972 (quoted in Kulhaway 1978) clearly demonstrate the interrelationship between the geometry of the joint system and the normal stiffness. Goodman et al. reported K_n values for four joints in granite and four joints in sandstone all filled with a soft, saturated clayey material (100% < 2μ, W_L = 57%, PI = 27) of variable thickness. The stiffness data and details of the geometry of the joint system (the "joint face roughness" was presumably expressing the average roughness amplitude) are given in Table 3.2 over.

Table 3.2

Normal stiffness data of joints with variable surface roughness and different thicknesses of infilling.

(after Goodman et al. 1972)

Rock type	Area (cm^2)	Thickness of infilling, t (mm)	Joint face roughness, r (mm)	$\frac{t}{r}$	Normal stiffness K_n(MPa/mm)
GRANITE	145	1.47	1.33	1.10	5.21
	"	1.37	1.51	0.91	16.91
	"	1.22	2.27	0.54	67.59
	"	1.07	0.06	17.83	7.22
SANDSTONE	145	2.26	1.91	1.18	5.59
	"	1.88	1.42	1.32	5.40
	"	0.53	0.21	2.52	5.43
	"	0.26	0.20	1.30	5.40

In the case of the granite joints, although the filling thickness did not vary substantially, the normal stiffness values differed by more than one order of magnitude. Assuming that all the joints had been compressed under the same level of normal stress, the large variation can easily be explained considering the ratio of filling thickness to surface roughness amplitude (t/r). For values of the ratio below unity (roughness amplitude > filling thickness) joint deformation is largely controlled by solid/solid contacts hence the large K_n values, as opposed to the cases where the filling thickness exceeds the height of asperities ($t > r$). Interestingly, the K_n values corresponding to the sandstone joints were virtually identical despite the considerable variations in the thickness of the infilling. However, it can be seen that in all cases the roughness of the joints varied in such a way that the t/r ratio values were comparable, and more significantly, larger than 1.

The expected amount of joint "stiffening" with increasing level of normal stress is obviously related to the geometrical variables referred to above. The variation in normal stiffness with increasing normal stress

is shown in the semi-logarithmic plot in Figure 3.1 for a suite of joints of comparable morphology but variable infilling thickness.

In the preceding discussion soft compressible infilling materials have been considered. However, as Goodman et al. (1968) have pointed out, a distinction should be made for cementing materials such as quartz, calcite, epidote etc., whose presence could result in high normal stiffness, unless weathering effects are involved, as for instance in cases of soluble calcite infillings.

2. Unfilled joints

Factual information regarding the effects of the variables referred to earlier on the normal deformability of unfilled contacting joints is virtually non-existent. This is largely because the majority of the relevant studies have been conducted on artificial fractures (extension or saw-cut), which resemble only certain types of natural joints and have a very restricted range of the variables in question.

The initial actual contact area (directly dependent upon the stress history of the joint) is the most important variable controlling the deformability of a joint. As an extreme case, a point-contacting mismatched fracture showed an approximately three-fold increase in maximum closure as compared to the closure achieved when the same fracture had been compressed in fully interlocked position (Goodman, 1976). Situations where natural joints may have such huge apertures and point contacts may arise from shear movement along undulating surfaces, dissolution and removal of wall material by migrating waters, etc.

Significant differences in the magnitude of deformations can also be traced in cases of interlocked joints with extremely small aperture and relatively larger actual contact area. Iwai (1976) found that the maximum closure (V_m) of a perfectly mating extension fracture in granite during first loading under maximum normal stresses of 20 MPa was 0.108 mm, whereas the V_m of a similar basaltic fracture was ~ 0.055 mm under the same stress level. Interestingly, the uniaxial compressive strength of the granite and basalt rocks was 135 MPa and 230 MPa respectively, and the Young's moduli were 44.4 and 74.4 GPa. The potential increase in joint deformability with decreasing rock strength has been pointed out

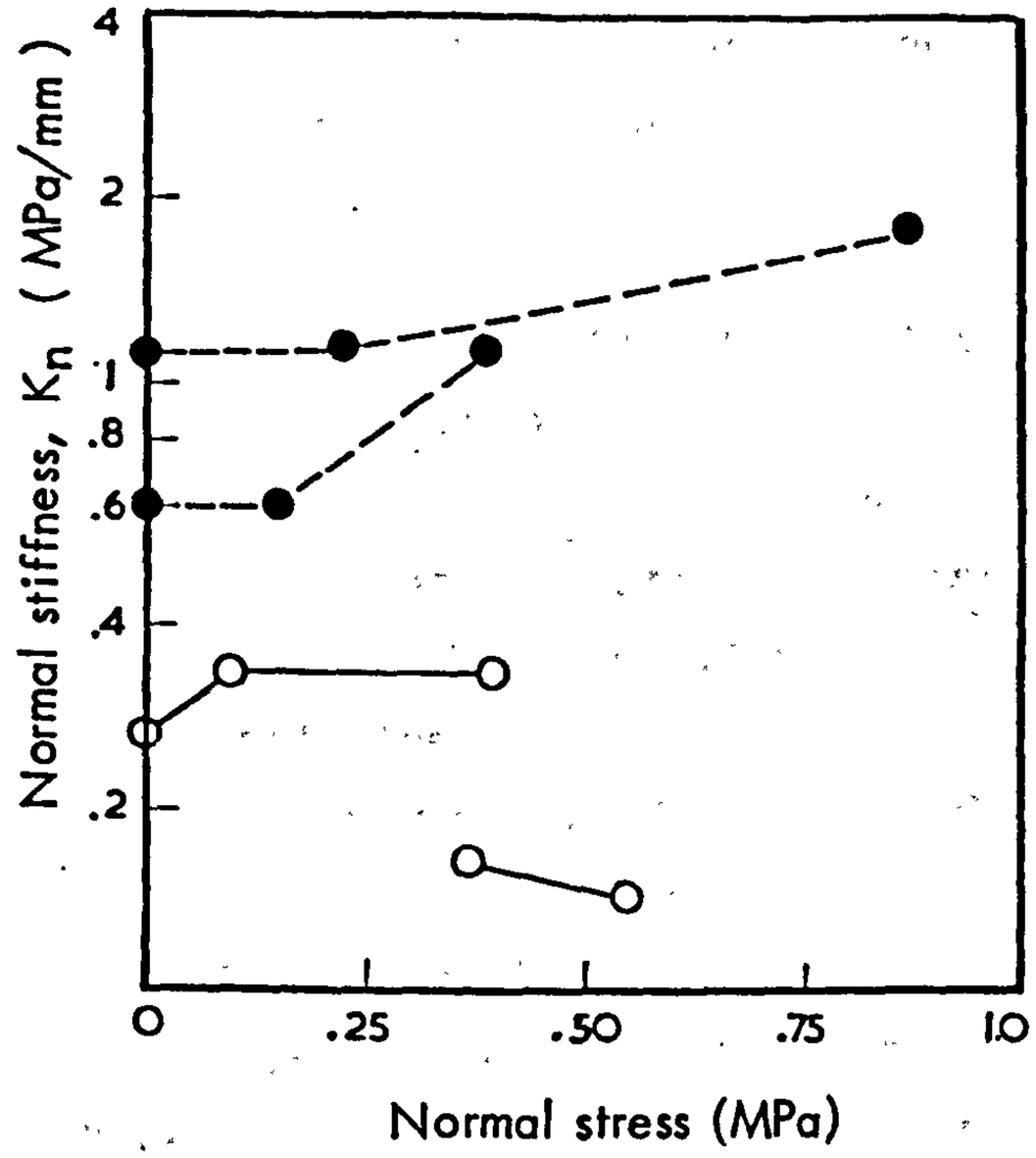

O—O Joints with very thick infilling.
Very low or no rock/rock contact.

●--● Considerable rock/rock contact. Joint "stiffening"

Note : Values plotted on the Y-axis indicate extremely low normal stress level (less than overburden pressure released during excavation of the in-situ test block).

FIGURE 3.1 Variation of K_n with normal stress for joints in basalt with different filling thicknesses

(after Infanti and Kanji, 1978)

by Duncan and Hancock (1966). From compression tests on natural joints the last authors concluded that an appreciable amount of joint closure may occur only when the intact wall material is deformable enough. Joints in rocks of strongly brittle nature would show minimum closure because the intact material would resist local failures, compaction of asperities or increase in actual contact area under compression. Unfortunately no experimental data were included in that publication.

It is of interest to note, however, that the difference in the uniaxial compressive strength of the rock material of the limestone (σ_c = 150-210 MPa) and sandstone (σ_c = 50-90 MPa) joints tested by Hungr and Coates (1978) was not reflected in the amount of joint closure, which seemed to range between 0.1 mm and 0.2 mm for both groups of joints. In fact, the average normal stiffness coefficient of the limestone joint group was 17.8 MPa/mm and of the sandstone group 18.5 MPa/mm. It is conceivable that the applied normal stresses were not high enough to mobilize the inherent differences in the strength and elastic properties of the asperities of the sandstone and limestone joints. On the other hand, a certain amount of variation was observed in the normal stiffness coefficients (calculated as maximum stress σ_n over maximum displacement ΔV) within each joint group. The K_n values of five limestone joints ranged between 11 MPa/mm and 46 MPa/mm; for eight sandstone joints K_n was between 13 MPa/mm and 25 MPa/mm. Incidentally, the upper bound K_n value of the limestone joints was obtained from a very tight, incipient fracture. Hungr and Coates attributed the scatter in the magnitudes of K_n to small differences in aperture opening. All joints were described as tight, and an average aperture thickness of less than 0.5 mm was quoted for the limestone joint specimens.

No attention seems to have been focussed on the weathering effects upon joint normal stiffness. Snow (1972) pointed out that the joint normal deformability coefficient may vary radically with degree of weathering, but no experimental evidence was given.

From the above review it becomes clear that the present state of knowledge leaves much to be learned about the normal stiffness property of natural joints, and in particular its variation under the influence

of joint system variables known to control joint behaviour under shear loading conditions. Joint normal stiffness is a very important parameter as it effectively determines the E_{mass}/E_{rock} ratio and representative data are much needed for both physical and numerical modelling of the rock mass. Furthermore, joint normal deformability is fundamentally related with the problem of water flow through jointed rock masses subjected to changes in the stress environment. Since it is known that the permeability of joints, which constitute the main water conduits in the mass, is a sensitive function of joint aperture, it is essential that the interaction of hydraulic and mechanical effects be considered.

3.1.3 Factors influencing the joint shear stiffness

Goodman et al. (1968) summarized the factors influencing the shear stiffness of joints as follows:

(1) the roughness of the joint walls determined by the distribution, amplitude, and inclination of asperities;

(2) the tangential aperture distribution and amplitude;

(3) the relevant properties of the infilling material, if present.

The effect of another variable has also to be considered, that is the length of the joint.

1. Infilled joints

The shear stiffness of infilled joints depends on the relevant properties of the intervening material and, of course, its thickness in relation to the geometry of the opposed joint walls. The behaviour of joints filled with a layer of uniformly graded and predominantly clayey or silty material of thickness several times that of the asperity amplitude will be governed by straight-forward soil mechanics principles. Complications arise due to fillings that consist of widely graded material, for instance rock breccia and clay mixtures, and for discontimuities which have a filling of thickness smaller than the amplitude of the wall roughness. In the latter case, "strain-

hardening" behaviour is usually observed due to increasing rock-rock interaction with shear displacement.

A carefully controlled experiment conducted by Goodman (1970) demonstrates the influence of an infilling material on the shear stiffness of joints. The effects of different thicknesses of a finely crushed mica filling on the K_s of regular saw-tooth surfaces cast in a plaster-celite model material were tested. The geometry of the "joints", the shear force vs. displacement curves and the variations in K_s with percentage joint infilling defined as

$$\% \text{ joint infilling} = \frac{t}{r} \times 100$$

where: t = thickness of infilling
r = vertical amplitude of asperities

are included in Figure 3.2. As shown, the stiffness showed a gradual decrease with the degree of joint filling until at 125% filling the shear stiffness of the infilled joint was less than one-third than that of the unfilled. At that stage the infilled joint was twice as stiff as the filling material alone. The experiment therefore demonstrates that sheared zones and filled joints may display shear deformability appreciably different from that of the filling material itself.

The expected significant reductions in peak shear stiffness with increasing thickness of filling has also been demonstrated by Infanti and Kanji (1978), who conducted in-situ shear tests on joints in basalt (the compression properties of these joints have already been discussed in section 3.1.2(1)). The infillings varied from silty sand to silty clay and their thickness ranged from discontinuous films of ~ 1 mm to continuous thick zones up to 100 mm. The authors listed the range of K_s values measured in relation to filling thickness, as shown in Table 3.3.

The peak shear stiffness of partially filled joints (i.e. when filling thickness < roughness amplitude) is directly related to the shear displacement required for contact to develop between the wall asperities. The variable size, shape and distribution of the irregularities on joint planes makes the establishment of any general empirical rules of practical reliability very difficult.

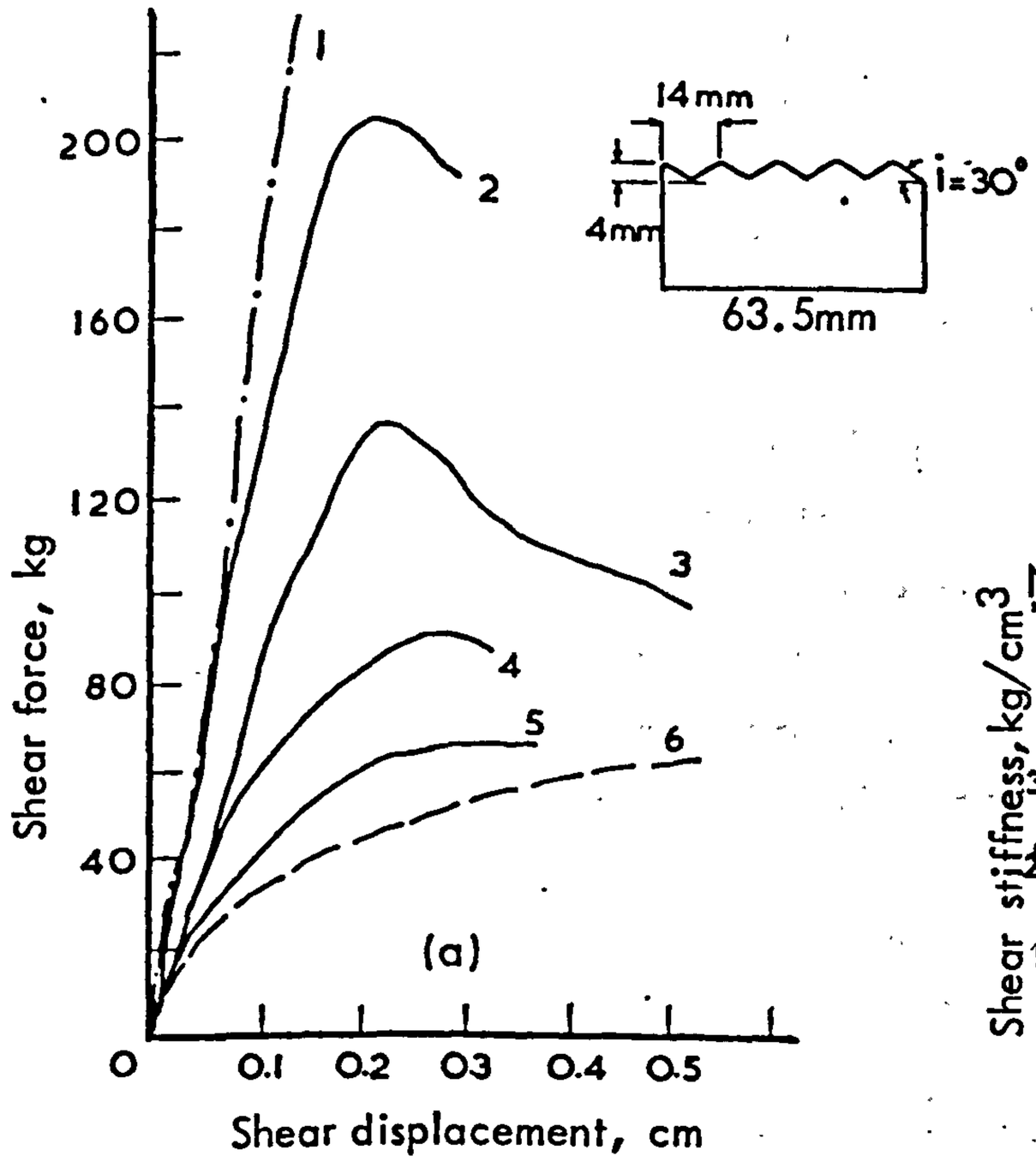

FIGURE 3.2 (a) Load - displacement curves from direct shear tests on mica-filled joints
(b) Effect of thickness of joint filling on shear stiffness
(after Goodman, 1970)

Table 3.3

Range of peak shear stiffness values of joints in basalt containing different thicknesses of infilling material.

(after Infanti & Kanji, 1978)

Joint infill thickness (mm)	Range of peak shear stiffness, MPa/mm
50–100	0.01–0.010
10–20	0.010–0.060
<1 (1 case)	> 0.100

The problems are further accentuated by additional complications such as development during shear of highly consolidated "pockets" of infilling forcing the advancing joint block to dilate and hence delaying actual contact. Moreover, the slight consolidation of normally-consolidated, and dilation of overconsolidated clayey materials during shearing, could be significant in cases of relatively smoother joint surfaces (Barton, 1973a). The complexity of the mechanics of shear deformation of infilled joints is usually reflected in poor correlations between peak displacements and filling thicknesses even under controlled laboratory conditions (for example, see Lama 1978). It seems therefore that actual shear testing of such discontinuities is the only reliable means of evaluation of the shear strength and deformation characteristics. As a result there exists a fair amount of shear stiffness data from laboratory and in-situ testing of different types of infilled joints. A collection of K_s values (both secant and yield) is presented in Table 3.4. Depending on the normal stress (range = 0.21 - 2.99 MPa), the thickness of infilling and dry or wet conditions, the peak shear stiffness data present a range from 0.32 to 23.55 MPa/mm, although maximum values rarely exceed 2 to 3 MPa/mm.

2. Unfilled joints

Since the roughness of the surface of unfilled joints effectively controls the peak shear strength and displacement, it will obviously influence the shear stiffness of a joint. The effect of surface roughness is clearly shown by the collection of peak shear stiffness data listed in Table 3.5. For instance, comparison of the K_s values for the limestone joints nos. 1 to 4, shows a substantial increase from an average value of 0.51 MPa/mm (σ_n = 0.88-2.40 MPa) to 3.06 MPa/mm (σ_n = 0.30-3.36 MPa/mm). The overall range of the average K_s values from laboratory size specimens is 0.51 to 3.06 MPa/mm under a range of normal stresses from 0.15 to 10.1 MPa.

Table 3.4

Summary of secant yield and peak shear stiffness values of infilled joints (data as compiled by Kulhawy, 1978).

Joint type	Area (cm^2)	Normal stress (MPa)	Thickness of filling (mm)	Secant Shear Stiffness (MPa/mm)			
				Yield		Peak	
				Range	Average	Range	Average
Marl layer in limestone (saturated)	605-730	.47-.56	1-3	2.16-3.73	2.84	0.51-3.73	2.13
Marly partings in limestone (saturated)	51-63	.24-.77	1-5	2.16-3.14	2.74	0.85-5.69	2.89
Marly joints in limestone (dry)	28-47	.49-1.47	.25-20	-	-	2.26-23.55	9.75
Foliated gneiss and mylonite	10.6-24.5	.39-2.94	40-50	1.46-4.71	2.55	0.69-3.69	2.36
Limestone bedding with mylonite	1500	.21-2.38	-	1.04-8.04	3.90	0.28-5.69	1.25
Marly joint in limestone (moist)	980-1243	.53-2.99	15-30	1.18-3.33	2.65	.41-4.71	1.70
Limestone bedding with thin shale seams	1500	1.23-2.80	-	1.55-13.90	5.96	.32-8.33	3.08
Joint filled with marly sand	44000	0.98	1-2	-	-	-	2.34
Marly joints in limestone (saturated)	20-40	.49-1.47	.25-2.0	-	1.47	.14-31.60	7.41
Vertical fault	-	.37-1.07	Thick, uneven	-	-	.17-0.23	0.20
Marly joint (saturated)	1030-1240	.49-2.94	1.3-3.2	0.09-2.74	2.41	.02-1.86	0.78

Table 3.5

Range of peak shear stiffness values (secant) for different types of unfilled joints.

No.	Rock and joint type	Area (cm^2)	Normal stress (MPa)	Peak shear stiffness, K_s (MPa/mm)	
				Range	Average
	LIMESTONE:				
1	- smooth joint	1600	0.88 - 2.40	0.20 - 1.28	0.51
2	- rough joint	1600	1.52 - 4.00	1.26 - 2.61	1.98
3	- slightly rough bedding	1500	0.15 - 3.63	0.20 - 1.37	0.84
4	- rough bedding	1600	0.30 - 3.36	0.25 - 7.35	3.06
	PORPHYRY:				
5	- dry, natural joint	500	3.24 - 10.10	0.26 - 1.94	1.02
	SLATE				
6	- natural cleavage plane	500	4.37	-	0.79
	GRANITE				
7	- rough joint	144-205	1.18 - 1.42	0.99 - 1.57	1.32
	AMPHIBOLITE				
8	- schistosity plane	$5x10^3$	0.12	-	0.59
	BASALT-SANDSTONE				
9	- contact plane (unbonded)	$308x10^3$	0.13	-	0.11

Notes: Data as compiled by Kulhawy (1978)
Nos. 1 to 7: laboratory tests
8 and 9: in-situ tests.

3. Scale effects

Direct shear tests on model tension fractures conducted by Barton (1972) revealed a potential scale effect on the peak shear stiffness of joints. In that study the joint test specimens were generated through the same size of block. By using a dimensionless relationship relating the stress and geometrical scale factors (equation 2.7 in section 2.2.2, Chapter 2.2 in Part Two), Barton simulated different prototype joint lengths (from 2.3 to 30 meters) by varying the compressive strength of his model material and assuming the same strength of prototype rock in each case. The results from that study showed no scale effects in the prototype peak shear strength but large increases in the prototype peak shear displacements with increasing length of the simulated prototype joints. Based on those observations Barton concluded that the peak shear stiffness is a strongly scale dependent parameter.

The experimental study on scale effects reported in part two of this thesis has demonstrated that profound scale effects exist in both the peak shear strength and peak shear displacement of physically increased lengths of joint specimens of identical morphology, which manifest the strong dependency of peak shear stiffness on joint length.

On the assumption that peak shear strength is reached after shearing approximately 1% of the joint length, Barton and Choubey (1977) suggested that for practical purposes the peak shear stiffness in relation to joint length can be found from:

$$K_s = \frac{100}{L}\ \sigma_n \tan \left[JRC \log_{10}\left(\frac{JCS}{\sigma_n}\right) + \phi_b \right] \qquad 3.1$$

where: K_s = peak shear stiffness ($MN/m^2/m$)
L = joint length (m).

In view of a potential existence of a critical joint length, L_c (defined as the length of joint still just sensitive to scale effects in peak shear strength and displacement) controlled by the average cross-joint spacing in the rock mass, the value of L in equation 3.1 should be replaced by L_c.

General trends of the variation in peak shear stiffness with increasing joint length are shown by the chart in Figure 3.3 as has been presented

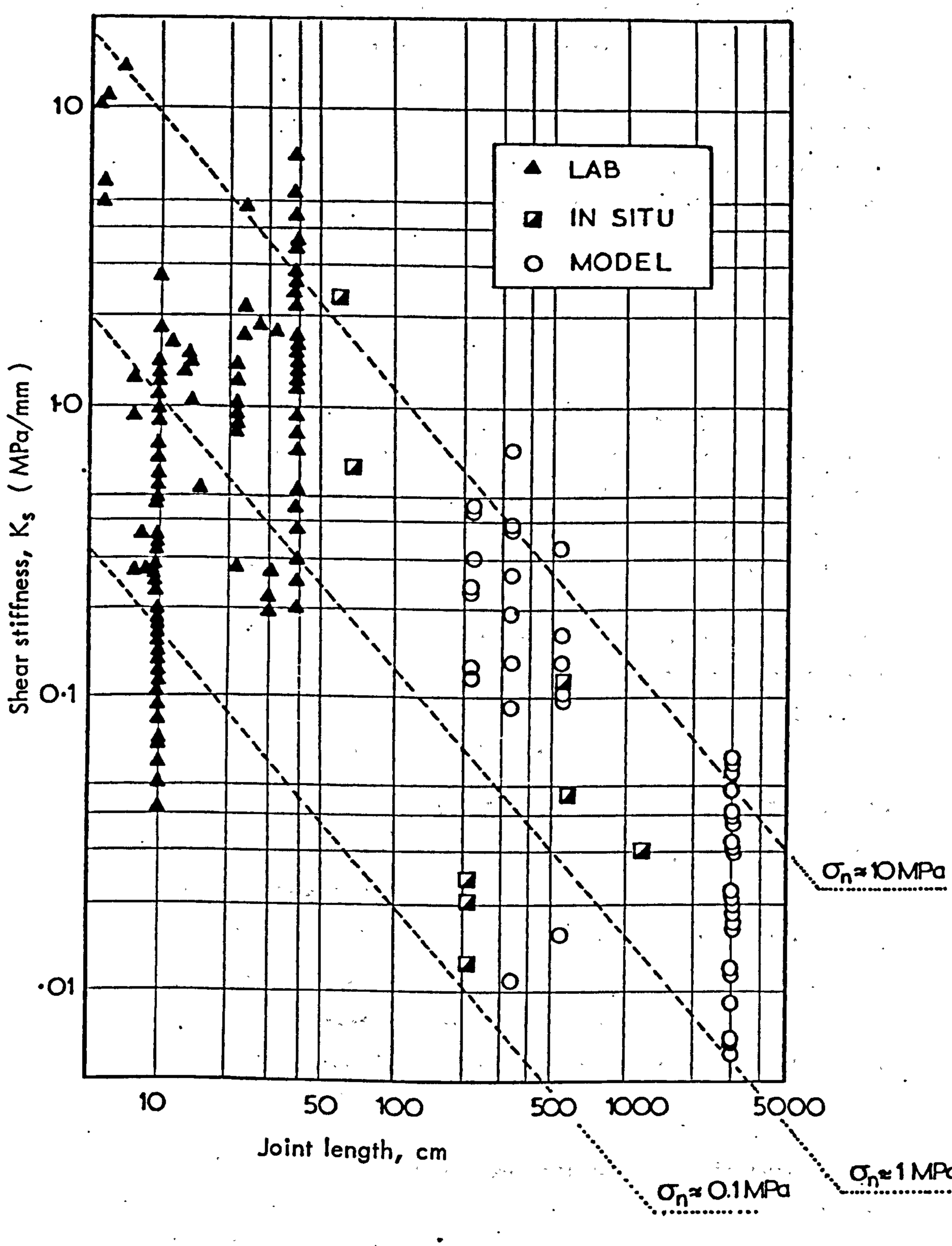

FIGURE 3.3. Shear stiffness data of rock joints showing stress and scale dependency

(from Barton and Hansteen, 1979)

by Barton and Hansteen (1979). The plotted data represent laboratory-size joints as well as larger joints tested in-situ (all clean, unfilled). Results from model fractures simulating different joint lengths according to the principles discussed earlier are also included. The set of parallellines represent approximate envelopes for equal normal stress (σ_n), demonstrating a dependency of K_s on σ_n. The peak shear stiffness of infilled joints is essentially independent of scale effects (Infanti and Kanji, 1978).

3.1.4 Present work

The experimental study to be reported in the next two chapters concentrates primarily on the property of joint normal stiffness. Normal loading tests have been conducted on a range of natural unfilled joints sampled from different rock types and displaying variable wall strength and roughness characteristics. The targets of those experiments are summarized below:

(1) Investigation of the complete stress-deformation relationship of different joint types - both fresh and weathered - under loading/unloading and repeated load cycling conditions, and definition of an analytical representation of the curves.

(2) Study of the effects of weathering on joint normal deformability.

(3) Derivation of empirical relationships of possible practical value between normal deformability parameters and fundamental joint variables, such as aperture, wall strength, and roughness.

(4) Comparative study of the deformational characteristics of point-contacting joints of variable aperture openings created by misfitting the joint halves in a manner approximately simulating the condition of joint surfaces displaced in shear.

A limited number of direct shear tests was conducted on different types of joints after the conventional configuration for measuring displacements had been refined in order to:

(1) study the exact shape of the pre-peak portion of the shear stress-displacement curves of different joints and compare the behaviour of fresh and weathered surfaces,

(2) examine the anisotropy in joint deformability in relation to joint type and weathering stage.

The test results from the model joints reported in part two have also been analysed further to investigate the scale effects on peak shear stiffness.

CHAPTER 3.2

EXPERIMENTAL STUDY OF JOINT DEFORMATION

3.2.1 Introduction

This chapter contains a review of the laboratory work undertaken to investigate the deformational behaviour under normal and shear loading conditions of a wide ranging variety of natural unfilled joint types, and a general analysis of the experimental results.

Fresh, interlocked joint samples with surfaces displaying an appreciable variety of roughness were collected from exposures of five different rocks, namely; limestone, sandstone, siltstone, dolerite, and slate. Each of the sampling locations yielded also a number of either surficially or throughout weathered joint blocks. For a quantitative indexing of the various joint types the surface roughness coefficients (JRC) and wall compressive strengths (JCS) were determined.

The normal deformability tests involved cyclic loading of carefully prepared single-jointed blocks and measurement of the vertical displacements. At first, all joints were compressed in fully locked position, and then a collection of different joint types was tested with artificially mismatched walls. Finally, a number of joints were tested in direct shear under different normal loads by adopting a multistage testing procedure.

The contents in this chapter have been divided into three main sections. The first contains descriptions of the different rock material and joint types together with their index properties, and a review of the joint testing procedures. In the second and third sections the stress-deformation relationships of the joints as derived from the experimental results are introduced and analysed.

3.2.2 Index properties of intact rock and joint types, and description of testing procedures

A series of index tests was conducted to examine the strength and deformation characteristics of the five rock materials. The joint wall strength and geometry were described in terms of the joint compressive strength (JCS) estimated from Schmidt hammer testing, and the joint roughness

coefficients (JRC) were back-calculated from the results of direct shear tests under extremely low normal stress. The various index properties of the intact rocks and joints will be presented after a brief geological description. The general descriptions have been based on the relevant terminology recommended in the reports by the Working Party of the Geological Society of London (GSL, 1977) and the Commission on Standardization of Laboratory and Field Tests of the International Society for Rock Mechanics (ISRM, 1978a).

1. Type of rock materials and weathering state

(a) SLATE : Ordovician from Skiddaw Slates, very fine-grained, finely laminated with micaceous partings, moderately well developed slatey cleavage, grey. Sampling location: disused quarry near Keswick, Lake District.

(b) DOLERITE : Permo-Carboniferous, medium-grained, grey-green. Sampling location: natural exposure at Horwick Crags, Middleton, Teesdale.

(c) LIMESTONE : Lower Carboniferous, medium-grained, dense, light grey. Sampling locations: Coldstones quarry (disused), Greenhow Hill, N. Yorks; Trollers Gill (old mine and natural exposure), N. Yorks.

(d) SILTSTONE : Upper Coal Measures, medium- to fine-grained, finely laminated with muddy partings, light grey. Sampling location: N.C.B. open cast pit at Snydale, W. Yorks.

(e) SANDSTONE : Lower Coal Measures, medium-grained, micaceous, light yellow. Sampling location: Mink Farm quarry, Shibden Dale, W. Yorks.

The constituent minerals of slates vary in their susceptibility to chemical weathering. Ferrous compounds are oxidized at an early stage and the subsequent changes are probably dominated by the alteration of mica to form new clay minerals, while the sericite and quartz of the rock remain unaltered (Greensmith, 1975). Some of the present slate samples were heavily oxidized and sections through cleavage blocks revealed penetration of weathering towards an apparently fresh corestone.

Weathering effects in the dolerite were visible along the joint planes which were frequently covered by a layer of limonite. Exposed block

faces showed a spalling effect with crusts of altered material of thickness 2 to 5 cm. Apart from those features the rock had a fresh appearance.

The non-porous, impermeable limestone rock was fresh and only the joint surfaces appeared discoloured to various shades of brown from deposition of iron oxides or into a dark grey-green colour due to algae growth.

The bedding and joint planes of the siltstone were heavily oxidized and had a rusty-coloured appearance. Chemical weathering in siltstones commonly involves oxidation of accessory minerals, e.g. pyrite (FeS_2), siderite ($FeCO_4$) to give limonite (Pettijohn, 1957). In this siltstone rock oxidation had penetrated most of the block to a depth of a few centimeters.

The basic weathering features of the sandstone included slight discolouration to darker yellow colour and iron deposition on the joint and bedding planes. Chemical weathering in sandstone consists of leaching or alteration of the cementing material surrounding the usually inert granular skeleton. The present rock was cemented by some ferruginous compound and hydration of the latter to hydroxides was probably the principal weathering agent. In some sections of the quarry highly weathered sandstone material of brown appearance was exposed.

2. Index properties of rock materials

An estimate of the uniaxial compressive strength (σ_c) of each material was obtained from point load tests on prismatic specimens of various sizes. The same specimens were also used for rock density determinations and evaluation of an alteration index of the weathered materials. Uniaxial compression tests were performed on cylindrical and prismatic rock specimens to measure the elastic modulus (E_r). The various property values obtained from each rock type are listed in Table 3.6.

The point load strength index T_{500} was determined according to a method described by Brook (1977). The load of failure of prismatic rock specimens of various sizes was plotted against the fracture cross-sectional areas in a log-log graph. The load (L) corresponding to the intersection of the average data curve with the 500 mm^2 line was used to calculate the T_{500} index from:

TABLE 3.6

Mechanical and physical properties of rock materials

Point load strength index T_{500} (MPa)	Estimated uniaxial compressive strength, MPa	Tangent Young's Modulus E_r(GPa)	at 50% σ_c *σ_c(MPa)	Unit Weight γ (kN/m^3)	Alteration index AI (%)	Description/Grade
SLATE						
14.9	186	66	159	27.7	-	FRESH / I
DOLERITE						
17.3	216	78	165	29.0	-	FRESH / I
LIMESTONE						
10.6	132	49	152	27.3	-	FRESH / I
SILTSTONE						
6.3	78	28.5	84	24.2	3.1	FRESH / I
4.7	59	20.5	50	24.3	3.7	SLIGHTLY WEATHERED / II
SANDSTONE						
5.1	64	24.0	78	24.1	3.0	FRESH / I
4.1	51	-	-	23.8	4.7	SLIGHTLY WEATHERED / II
0.8	10	4.8	14	19.9	8.6	HIGHLY WEATHERED / IV

*Values measured in uniaxial compression

Note: Weathering grades refer to the classification scheme as given in the ISRM (1978a) report.

$$T_{500} = \frac{L \text{ (kgms)} \times 9.807}{500} \quad \text{(in MPa units)} \qquad 3.2$$

Test specimens were prepared from solid blocks firstly tested in compression to determine the elastic behaviour of the rock materials, and from joint block sawing cut-offs. The point load testing apparatus was the ELE model. Typical relationships between failure load and fracture area for the fresh and weathered rock materials are shown in Figure 3.4. The calculated T_{500} values ranged from 17.3 MPa (fresh dolerite) to 0.8 MPa (highly weathered sandstone). An estimate of the uniaxial compressive strength (σ_c) was obtained from the relationship

$$\sigma_c = 12.5\ T_{500} \qquad 3.3$$

which Brook has found to represent a good approximation for a variety of rock types. The estimated σ_c ranged from 216 MPa to 10 MPa, and showed a reasonable agreement with the values of σ_c measured from a few conventional tests on cylindrical and prismatic rock specimens (* σ_c in Table 3.6).

The axial stress-axial strain behaviour of the various rock materials up to failure was studied by conducting uniaxial compression tests on prepared cylindrical and one prismatic specimens. Axial strain was recorded by means of electrical resistance strain gauges and measurements at regular load increments were taken from a Peeckel strain-meter. The cylindrical specimens had a diameter of 5.08 cm and a length to diameter ratio of approximately 2. No cores of satisfactory quality could be drilled from the heavily weathered sandstone and so a prismatic specimen was sawn and tested instead (the loading ends were ~ 5 cm square and the side length was 10 cm). One 10 mm strain gauge was mounted halfway along the length of each specimen after the area had been thoroughly cleaned using a low activity degreaser (Freon TF), a water based acidic (conditioner "A") and an alkaline (neutralizer 5) surface cleaners. The gauges were fixed on the rock surface using a mix of P-2 adhesive (Drug "A") and hardener (Drug "B").

The range of stress-strain relationships displayed by the various rock specimens is illustrated in Figure 3.5. All fresh rock materials failed in brittle fracture and exhibited different degrees of non-linear behaviour at low stress levels. No well defined point of failure could be distinguished for the highly weathered sandstone specimen. The elastic

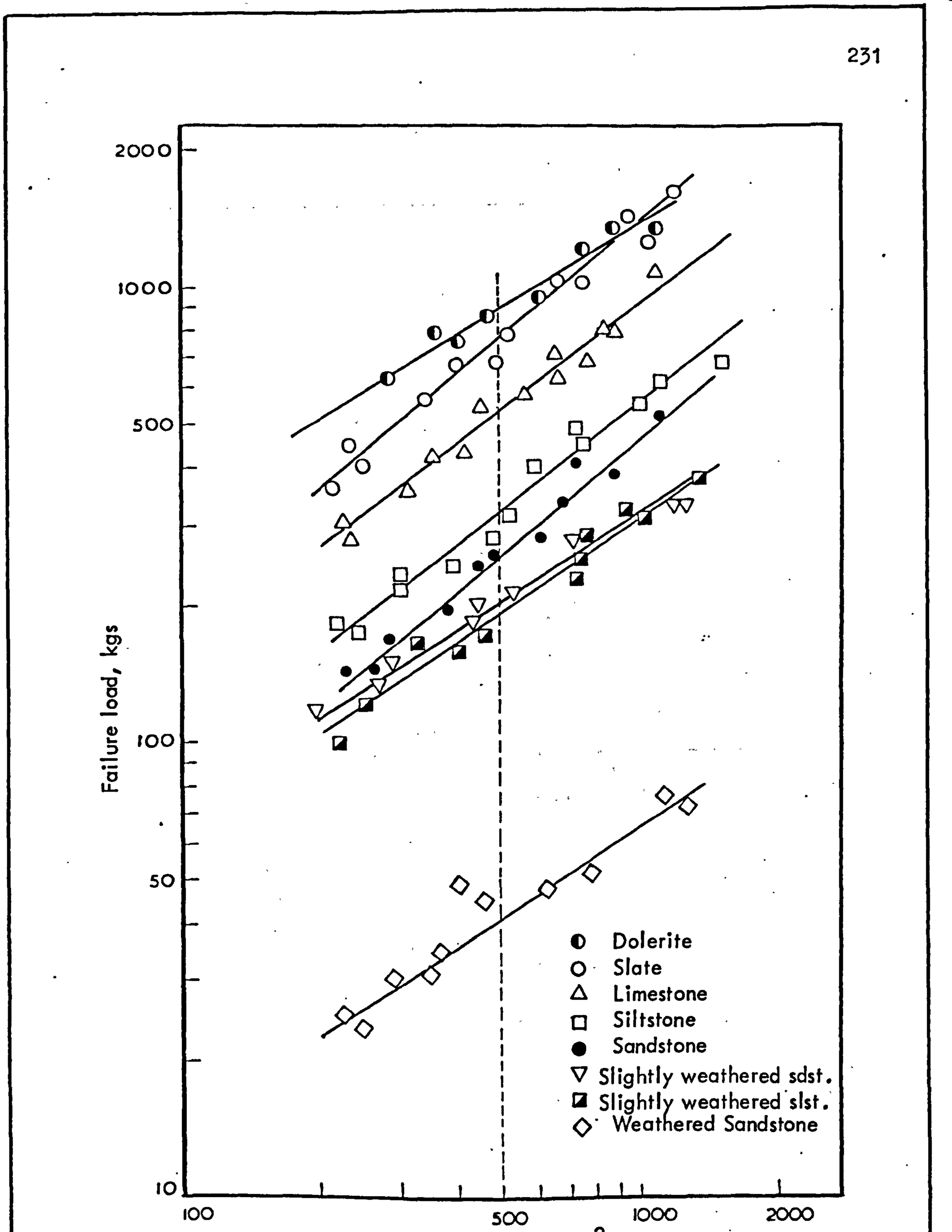

FIGURE 3.4. Log-log relationships between failure load and fracture area in point load testing of prismatic specimens from the various rock materials.

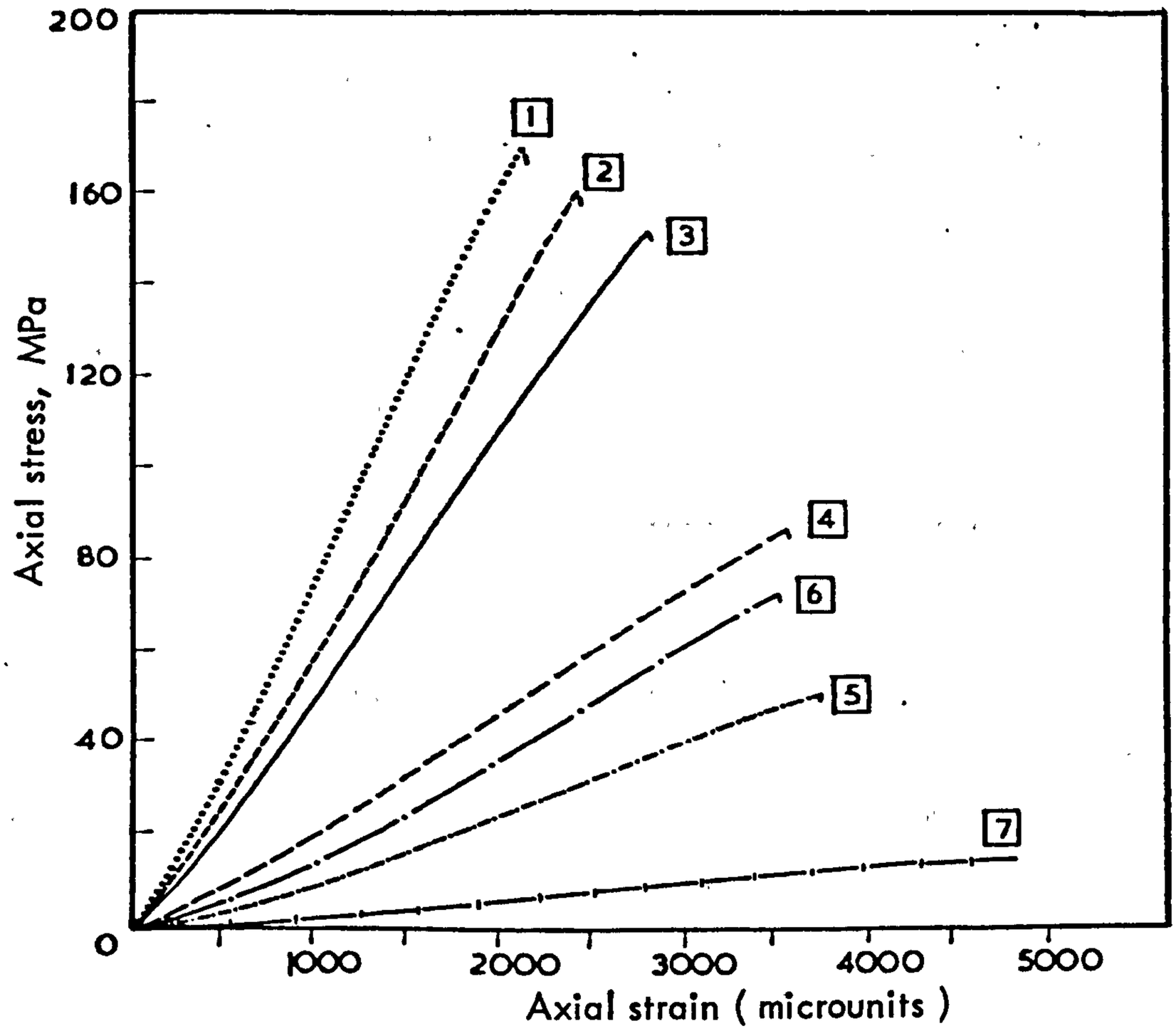

1. Dolerite, fresh
2. Slate, fresh ⊥ cleavage
3. Limestone, fresh
4. Siltstone, fresh // bedding
5. Siltstone, slightly weathered ⊥ bedding
6. Sandstone, fresh ⊥ bedding
7. Sandstone, weathered ⊥ bedding

FIGURE 3.5. Axial stress - strain relationships of the various rock materials

behaviour of the various rock types under cyclic loading will be considered in detail in section 3.2.3. The Young's modulus (E_r) of each rock type was calculated from the slope of the tangent to the stress-strain curve at 50% of the maximum axial stress. The values of E_r given in Table 3.6 represent the mean of two tests except for the slightly weathered siltstone and the highly weathered sandstone.

The moduli of the five fresh rock types ranged from 24 GPa (sandstone) to 78 GPa (dolerite). The significant effects of weathering on the strength and deformation of the sandstone can be seen in Figs. 3.4 and 3.5. The point load strength (T_{500}) and the Young's modulus (E_r) showed approximately six-fold and five-fold maximum reductions respectively. An alteration index (AI) defined by Hamrol (1961) as $AI(\%) = [(W_w - W_d)/W_d] \times 100$, where W_d and W_w are the dry and wet weights respectively of a rock piece after a quick ($\sim$ 2 hours) absorption test, was found to increase from an average value of 3% for the fresh sandstone to 8.6% for the highly weathered rock. The unit weight of the material decreased from 24.1 kN/m^3 to 19.9 kN/m^3.

3. Types of joints and weathering state

Single jointed blocks were extracted from the rock exposures manually with the aid of hammer and chisels. Maximum care was taken to ensure that no damage was caused on the joint walls especially in the cases of weathered surfaces. The differences in the physical and mineralogical properties of the rock materials were reflected in their variable susceptibility to weathering. In the cases of dense, impermeable rocks such as slate, dolerite and limestone, weathering was confined within a relatively thin band of joint wall material with rock in the immediate vicinity being fresh or slightly weathered. Advanced weathering effects were encountered only in the case of the sandstone exposure. A brief description of the weathering and geometrical characteristics of the joints included in the testing programme is given below. A representative selection of joints illustrating the range of surface roughness types is shown in the photographs of Figure 3.6.

(a) Slate cleavage planes : Surface geometry was variously rough, planar to slightly undulating. The sampled exposure yielded open cleavage planes with the surfaces covered by a film of limonite and weathered secondary

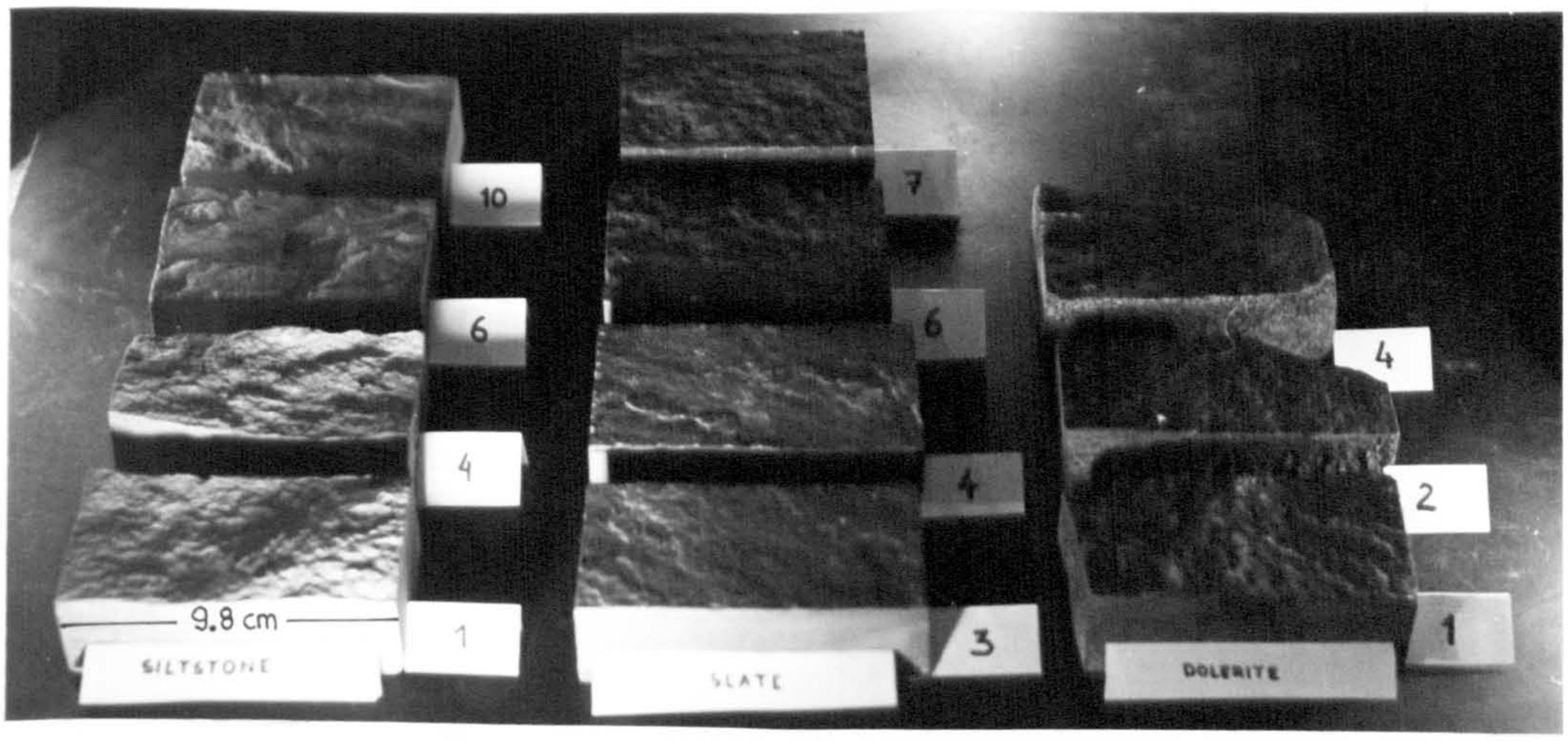

Slate , Dolerite , Siltstone

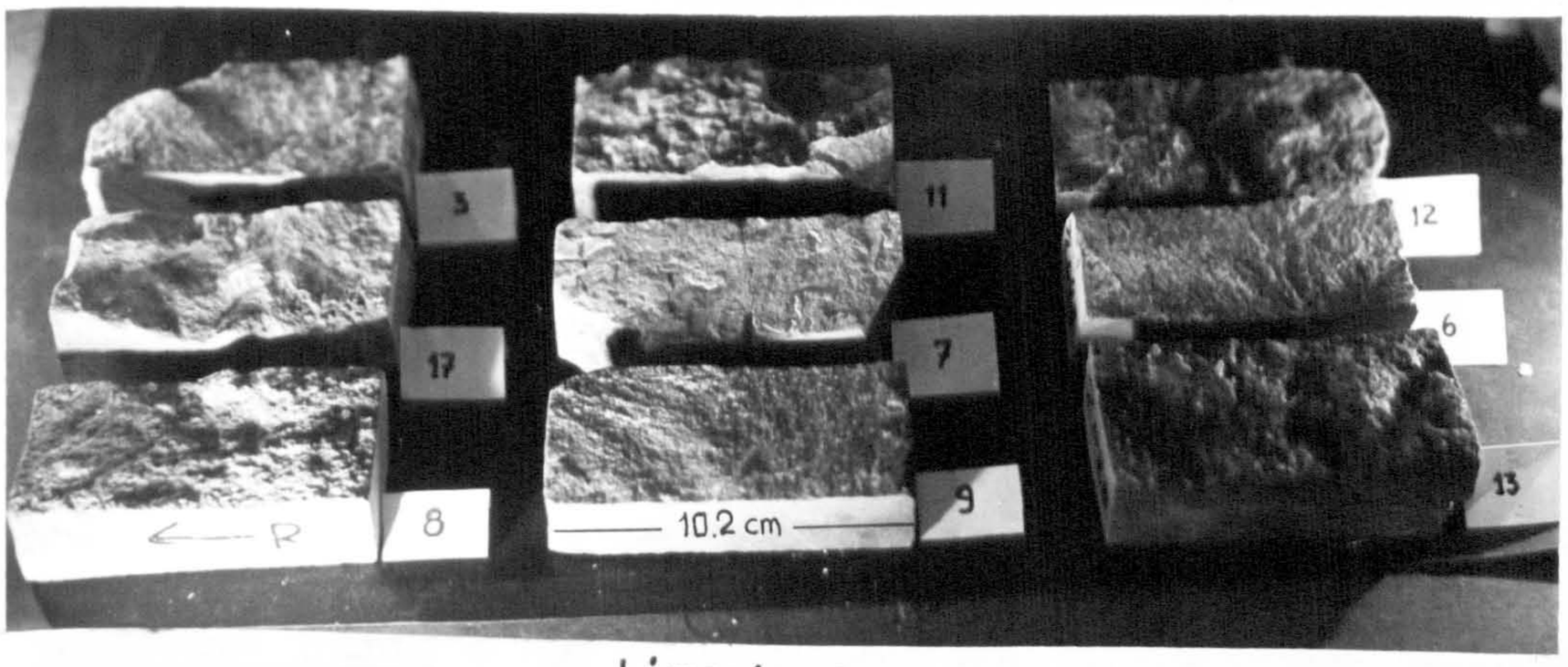

Limestone

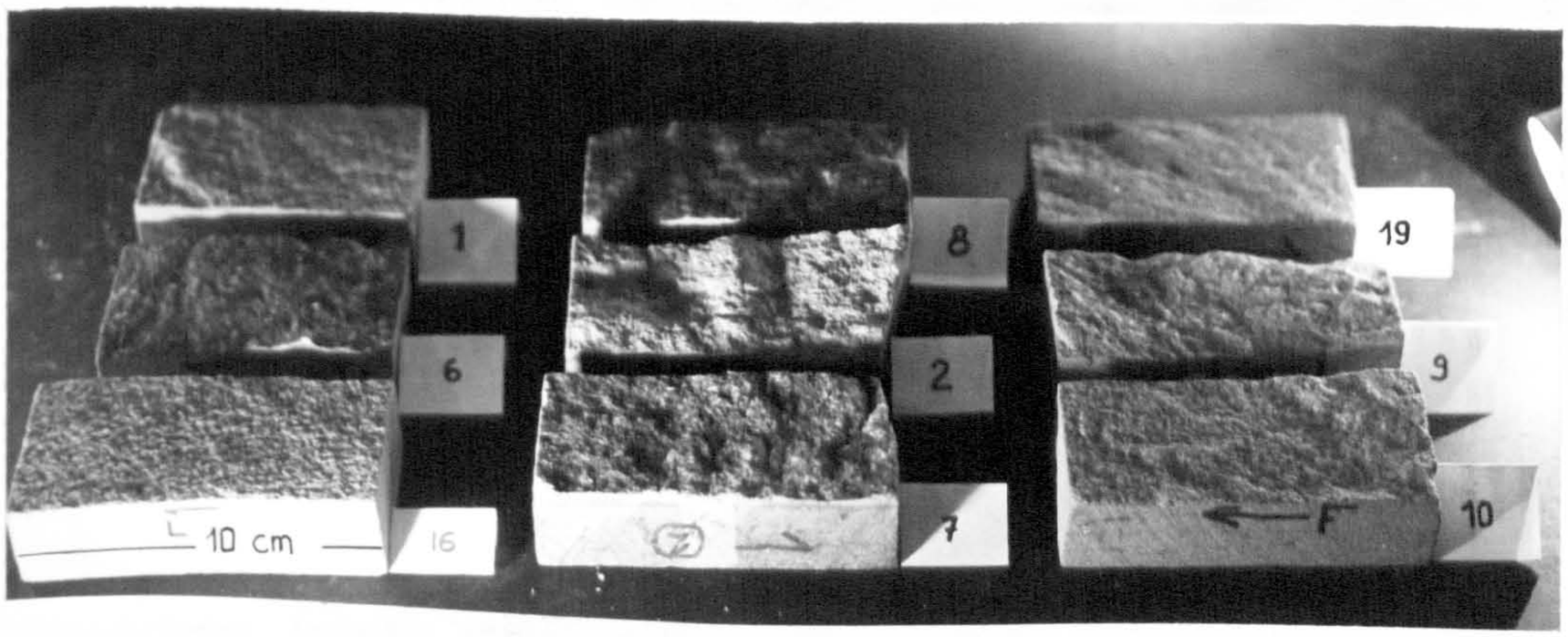

Sandstone

FIGURE 3.6 Photographs illustrating the range of surface roughness of joints from the different rock types.

crystalline calcite which had been dissolved in places. Fresh specimens were sawn from two incipient cleavage planes. A total of seven cleavage blocks were finally tested.

(b) Dolerite joints : These varied between planar to slightly undulating in roughness. Only five joint blocks could be prepared and tested because of sampling difficulties and breakages during saw-cutting, including: one fresh and one slightly weathered (lightly stained) joint and three surficially weathered samples. The surfaces of the latter were covered by a thin film of limonite and a 2-3 mm band of adjacent rock was discoloured to yellowish followed by perfectly fresh material.

(c) Limestone joints : The sampling locations yielded tension joints and bedding planes showing a considerable range of wall roughness from nearly smooth and planar to rough undulating. Most of the surfaces were partially or completely stained and some were discoloured to darker grey. Some joint planes were covered by a film ($\sim$ 0.50 mm) of a soft, yellow, porous material probably less soluble limestone and insoluble iron oxides. A total of twenty-one specimens were prepared for testing.

(d) Siltstone joints : The collected samples were all bedding planes of more or less similar rough, undulating surface geometry. Weathering effects included intense oxidation giving the surfaces a rusty colour, and "flakey" appearance presumably due to physical breakdown of the muddy partings in the rock. Fresh natural joint specimens could not be found in that particular exposure. For that reason, fresh core samples from an adjacent borehole were used to produce artificial extension fractures vertically to the bedding. Ten joints (five natural and five artificial) were finally tested.

(e) Sandstone joints : The samples were rough undulating vertical tension joints and rough, planar bedding planes. The surfaces of some bedding planes in slightly weathered rock had a light brown appearance due to iron staining. A number of vertical joints in fresh rock were covered by $\sim$ 0.1 mm dark brown crust of deposited iron oxides. Bedding planes collected from the highly weathered sections of the exposure were moderately rough, gently undulating. There was no visual difference between bedding surface and rock material. A total of twenty-one specimens were tested.

Based on an assessment of the relative differences in wall hardness the joints from each rock type were conveniently classed as "fresh" to "slightly weathered", "moderately weathered", and "weathered". Details on rock joint indexing are presented in the following subsection, where tables have also been included containing relevant quantitative information for each group of joints.

4. Index properties of joints

The variables of direct relevance to the deformational behaviour of joints are the aperture opening, and the wall strength and roughness.

(a) Measurements of joint wall strength

The mechanical strength of joint walls is the same as that of the surrounding rock only in cases where joints are running through perfectly fresh or uniformly weathered material. Water-conducting joints in impermeable rocks usually develop a thin layer of weathered material bounding an otherwise fresh rock block. Such weathering effects were present in some of the joint types described in the last section. It has frequently been emphasized that the shear strength and deformability of joints is crucially affected by the thin weathered "skin" of wall rock and various simple index tests have been recommended for direct assessment of its hardness (e.g. ISRM, 1978a).

In the present study, estimates of the wall compressive strength (JCS) were obtained by Schmidt hammer testing. The S.H. is a simple device for recording the rebound of a spring loaded plunger after its impact with a surface. A wide ranging assessment of the suitability of the hammer for indexing of rock materials was given by Miller (1965). The Commission on Laboratory and Field Testing of the ISRM has recently published recommended procedures for standardization of intact rock testing (ISRM, 1978) and the potential application of the method for a direct assessment of joint wall hardness has been described in another report (ISRM, 1978a). Further details on Schmidt hammer testing have been included in Appendix III (section 1).

An L-type hammer (impact energy = 0.075 mkg) was used in the present study. The tested blocks were securely clamped on a heavy concrete base to avoid any "drumminess" effects. In cases of irregularly shaped

blocks concrete moulds were built to ensure firm seating. Each joint surface was repeatedly tested by applying the hammer in a direction perpendicular to the joint (all tested in dry condition). A total of twenty tests was performed on each surface and the mean of the ten highest rebound numbers was assigned to each tested joint. It is known that in S.H. testing artificially low numbers often result from improper contact between the hammer plunger and the joint surface due to the presence of irregularities. A brief supplementary investigation into the effects of the surface roughness on the rebound numbers (see Appendix III) showed that rough surfaces give lower recordings than smooth ones. For three rock types tested (coarse-, medium- and fine-grained) the mean rebound number from twenty tests on saw-cut smooth surfaces and rough tension fractures showed a difference from approximately 4 to 8. The average values obtained from the ten highest readings from each rough fracture were very close to those measured on the flat surfaces, especially in the case of the medium- and fine-grained rocks.

The joint compressive strength (JCS) values were estimated in MPa units from a relationship given by Miller (1965):

$$\log_{10}(JCS) = 0.00088\ \gamma R + 1.01 \qquad 3.4$$

where: γ = dry unit weight (kN/m^3)
R = rebound number (mean of ten highest readings).

The dry unit weight (γ) values were measured either from rock pieces cut from intact material (for joints in fresh and uniformly weathered blocks) or from thinly sawn slices of joint wall material (for joints displaying visual difference between the surface and the surrounding rock). Significant differences were observed between the measured unit weights. Depending on the rock type, the extent, and the character of surface weathering, the γ values ranged: for the slate cleavage planes between 27.70 and 27.05 kN/m^3 (-2.4%); for the dolerite joints between 29.0 and 26.75 kN/m^3 (-8.4%); for the limestone joints between 27.27 and 25.68 kN/m^3 (-6.2%); for the siltstone joints between 24.20 and 23.62 kN/m^3 (-2.5%); and for the sandstone joints between 24.32 and 19.90 kN/m^3 (-22.2%).

The estimates of JCS obtained from equation 3.4 by using the mean R and appropriate Y values for each joint presented a clear pattern of the weathering effects on joint wall strength. The maximum variations in JCS values for the various types of joints are given below:

Slate	:	from 175 MPa	to	77 MPa
Dolerite	:	from 182 MPa	to	60 MPa
Limestone	:	from 170 MPa	to	35 MPa
Siltstone	:	from 105 MPa	to	42 MPa
Sandstone	:	from 95 MPa	to	22 MPa

A meaningful index describing the character of joint weathering is the ratio of the compressive strength (σ_c) of the rock in the interior of a joint block to the strength of the joint wall. Barton and Choubey (1977) have called that ratio the index of relative alteration (σ_c/JCS). In order to estimate the ratio values for the present range of joints, Schmidt hammer tests were conducted on the rock adjacent to the prepared blocks or on separate rock samples of the same weathering grade depending on the availability of pieces sufficiently large to be tested. The findings are summarized below:

i) Depending on the rock type, extent, and character of weathering the σ_c/JCS value for surficially weathered joints in fresh slate, dolerite and limestone rocks showed the following range: for the cleavage planes in slate it increased from 1.0 to 2.1; for the dolerite joints it increased from approximately 1.0 to 2.9; for the limestone joints it increased from approximately 1.0 to a maximum value of 4.7.

ii) For joints in slightly to highly weathered rock materials such as the siltstone and sandstone the σ_c/JCS values were slightly lower than the above. For the heavily stained siltstone joints the index was between 1.4 and 2.2. For the sandstone joints σ_c/JCS increased from approximately 1.0 (fresh blocks) to 1.2 - 1.6 (slightly weathered blocks) and then decreased again to approximately 1.0 for the joints in highly weathered material. If σ_c is taken as the strength of the freshest sandstone rock material (σ_c = 75 MPa) then the index value for the weathered joints becomes 3.4. A discrepancy was observed on a group of four sandstone joints whose surfaces were

covered by a film of iron oxides, in that the index value was below unity (= 0.8). The deposition of the iron oxides increased the strength of the rock surface from approximately 75 MPa to 95 MPa. A small increase was also observed in the unit weights from 24.32 kN/m^3 for the fresh rock to 24.75 kN/m^3 for the stained rock.

From a comparative evaluation of the Schmidt hammer test results it was deduced that the joint samples from each of the five rock types could be broadly divided into three main groups according to their relative weathering, as defined by the σ_c/JCS ratio values (where σ_c was the compressive strength of the freshest rock material):

$$\text{Fresh to slightly weathered} : \sigma_c/JCS \leqslant 1.2$$

$$\text{Moderately weathered} : 1.2 < \sigma_c/JCS \leqslant 2$$

$$\text{Weathered} : \sigma_c/JCS > 2$$

The above descriptive terms have been used for the sake of convenience in the subsequent discussions on joint behaviour. Reference to the specific weathering features of each group of joints will be made in Tables 3.7 to 3.11 seated at the end of this subsection.

(b) Measurements of joint aperture

Even in tightly mated joints the actual contact area is only a minute portion of the total surface area, thus creating a complex system of "gaps" between the walls. The aperture of contacting joints is defined as the maximum perpendicular distance of separation of the joint walls and effectively represents the distance that the joint walls have to close for perfect contact to be made over one hundred percent of the outline area of the sample (Duncan and Hancock, 1966). The aperture of joints is the most difficult parameter to measure with accuracy.

From visual examination of the field joint samples it was clear that fresh to moderately weathered joints from all rock types displayed very narrow range, if any at all, of aperture openings; whereas weathered joints had relatively larger apertures due to partial outwash of weathered surface material. The only technically feasible method of assessment of the average aperture value in the present case was to take measurements by using feeler gauges. This method is obviously not very

accurate since it only gives the width of the externally visible gaps which may have been widened by localized weathering. To avoid any such effects the measurements were taken after the joint blocks had been sawn and more representative sections across the joint planes were available.

Since the apertures for the majority of the joints (fresh to moderately weathered) were quite similar, it was decided to: (a) take measurements from all joints of each rock type, which belonged to the same group of relative weathering; (b) determine the most representative range and assign an average aperture value to the particular group of joints; and (c) note any striking deviations from the norm especially for weathered joint walls. A number of measurements were taken from each joint by inserting wedge-shaped feeler gauges in the visible gaps between the mated surfaces. The usual range of average apertures for fresh and moderately weathered joints from all rock types was between 0.10 to 0.30 mm. The range obtained from the weathered specimens was between 0.30-0.40 and 0.50-0.65 mm. The range and average aperture (a_j) values assigned to all joint groups are given below. Fresh, slightly weathered, moderately weathered and weathered joints are denoted as F, SW, MW and W respectively.

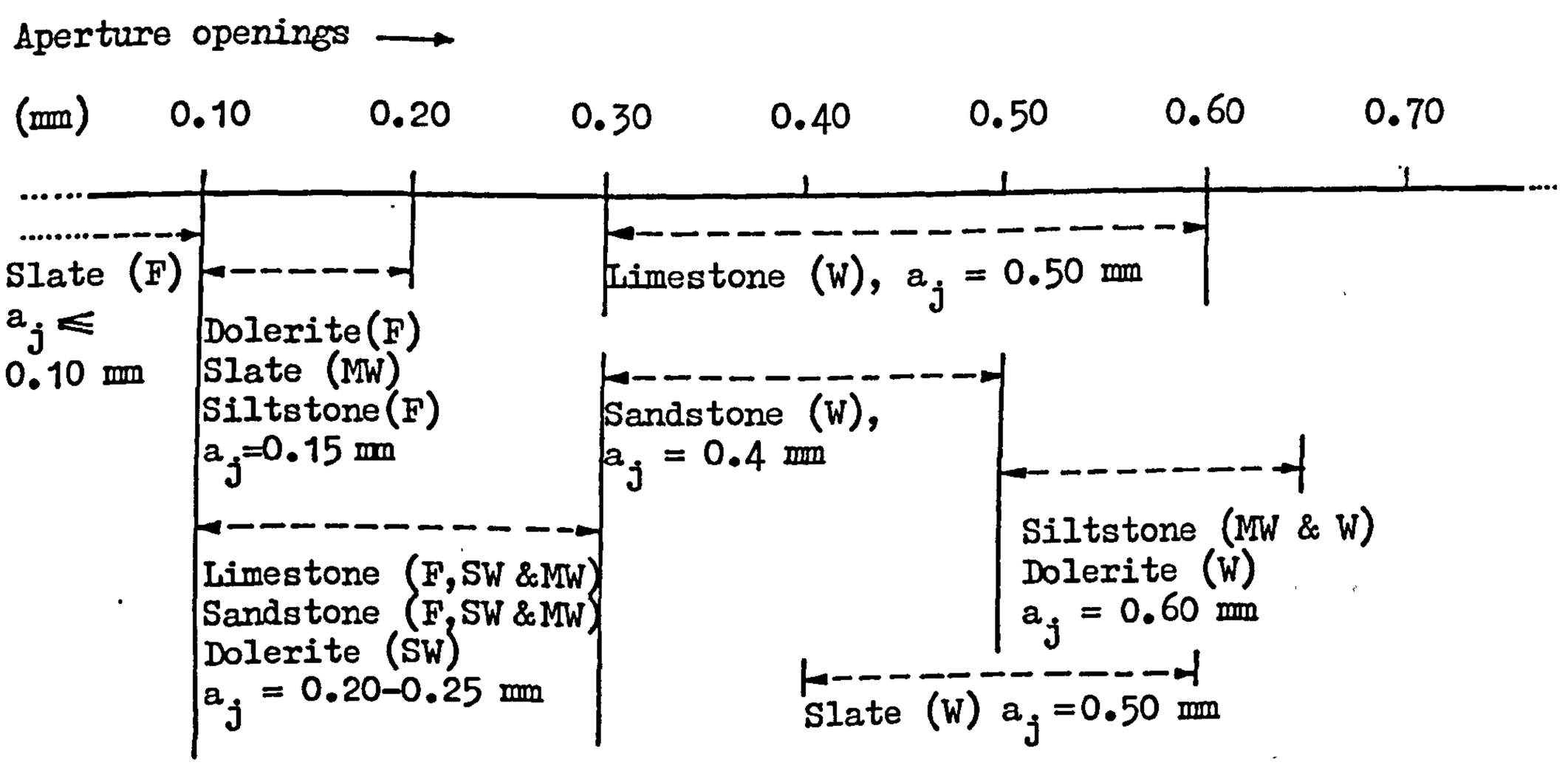

Some typical sections across various fresh and weathered joint types illustrating the differences in aperture thickness are shown by the photographs in Figure 3.7.

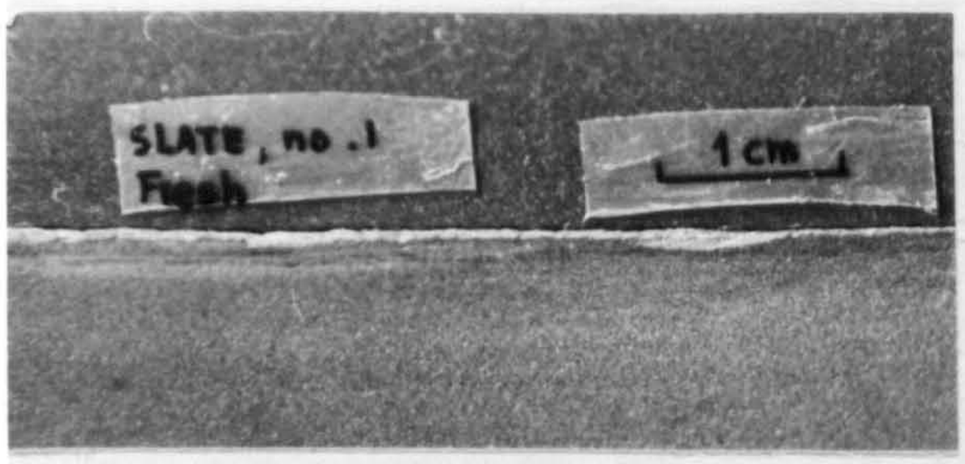

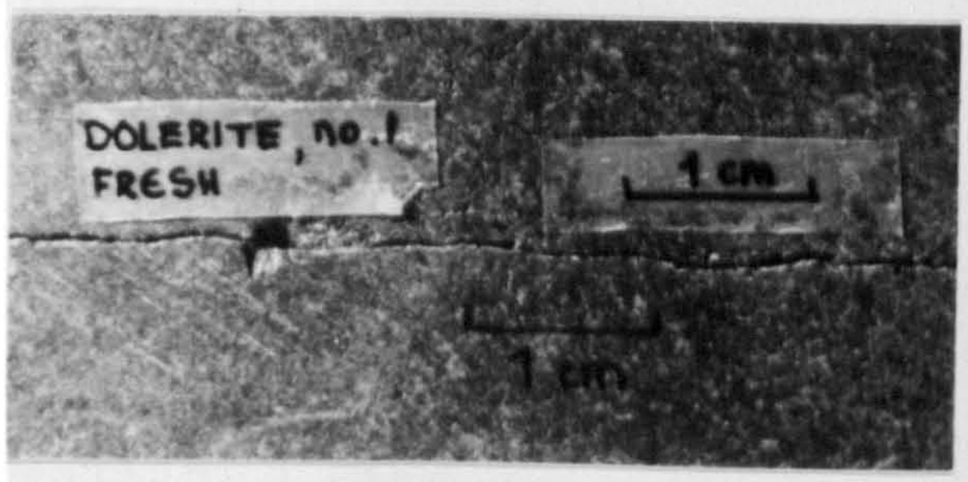

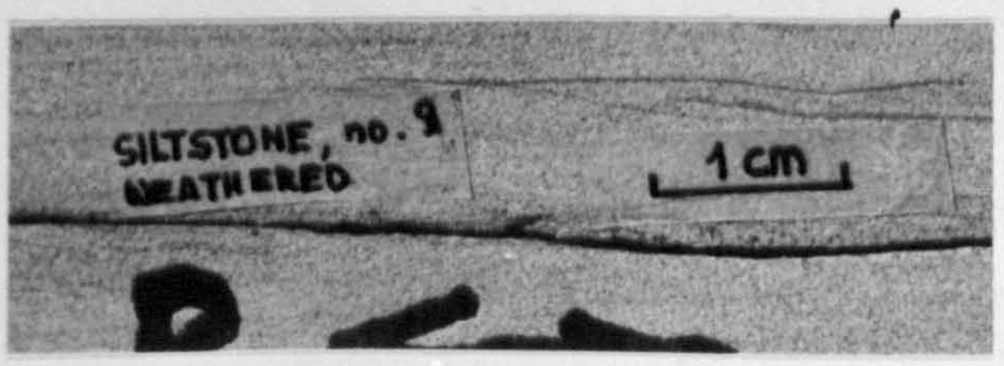

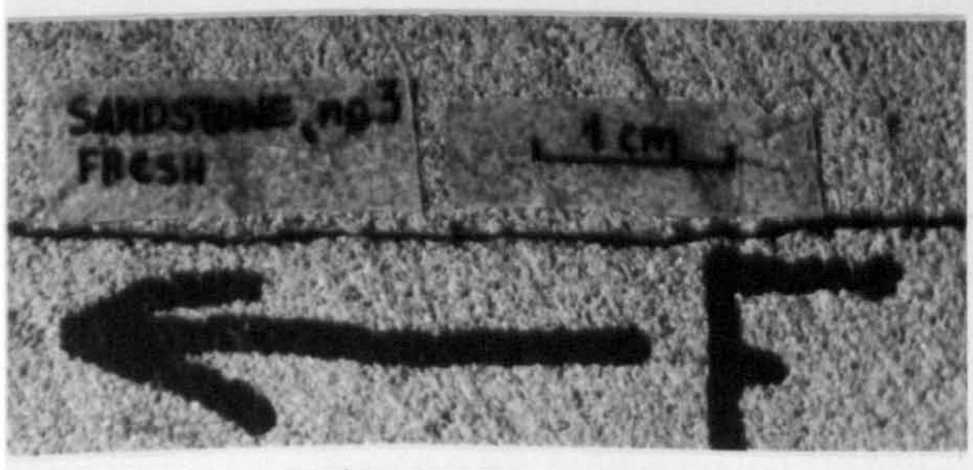

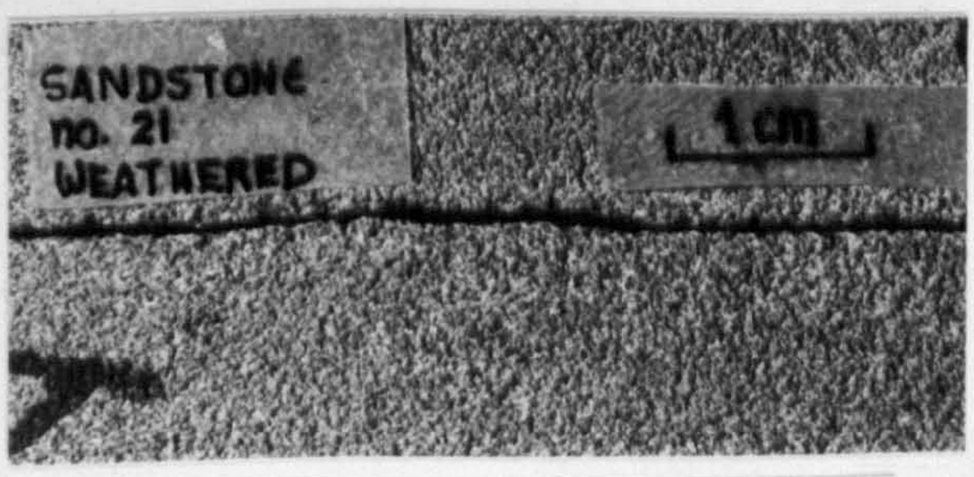

FIGURE 3.7. Photograph of sections across fresh and weathered joints illustrating the variations in aperture thickness

(c) Measurements of joint wall roughness

For quantitative description of the wall geometry the roughness coefficients (JRC) of the various joints were estimated from direct shear testing under extremely low normal load (the JCS/σ_n ratio was maintained at approximately 2000). A few cases were encountered where the shear tests yielded JRC values clearly unrepresentative of the geometry of the joint surfaces tested. This was observed in cases of overall planar surfaces with one or more "stepped" ridge(s) resisting sliding at the surfaces. For those joints, the direction of shearing was reversed and the test repeated. Residual angles of friction (ϕ_r) for joints in fresh and highly weathered rocks were measured from shear tests on saw-cut sandblasted surfaces. The ϕ_r values assigned to the surficially weathered joints were estimated according to the empirical method described by Barton and Choubey (1977). The ranges of JRC values for the various groups of joints are summarized below:

	FRESH TO SLIGHTLY WEATHERED		MODERATELY WEATHERED		WEATHERED	
	JRC range	($\phi_r°$)	JRC range	($\phi_r°$)	JRC range	($\phi_r°$)
Slate (ϕ_b=31°)	4.0-5.0	(31°)	5.3	(31°)	6.0-6.8	(25°*)
Dolerite (ϕ_b=34°)	7.1-8.8	(34°)	-		6.0-7.7	(27°*)
Limestone (ϕ_b=33°)	5.6-11.4	(33°)	5.8-16.9	(30°*)	5.0-15.0	(22°*)
Siltstone (ϕ_b=28°)	8.8-11.8	(28°)	7.0-7.5	(25°*)	6.1-6.7	(21°*)
Sandstone (ϕ_b=24°-30°)	5.4-10.7	(30°)	5.1-14.1	(26°*)	4.8-6.1	(24°)

ϕ_b^o = basic angle of friction (average data from 3 tests under σ_n = 0.25 - 0.75 MPa)

ϕ_r^o = residual angle of friction: (a) for fresh and uniformly weathered joints $\phi_b^o = \phi_r^o$

(b) for preferentially weathered joints

$$\phi_r^o = 10^o + {}^r/_R(\phi_b - 10^o)$$

where r = S.H. rebound on weathered joint surface

R = S.H. rebound on fresh rock surface

ϕ_r^o values thus derived are denoted by (*).

Detailed information on the strength and roughness characteristics of all the types of joints included in this study is presented in Tables 3.7 to 3.11.

A characteristic longitudinal surface profile for each joint has also been included.

The various symbols used in the tables are explained below:

- Joint types: IF = joint induced along a natural incipient fracture; CP = cleavage plane; VJ = vertical joints; BP = bedding planes; AF = artificial extension fracture.

- Strength of joint walls: R = mean rebound number from direct S.H. tests on joint surfaces; γ = unit weight of rock material or thin slices of wall rock as appropriate; JCS = joint compressive strength estimated from Miller's equation 3.4; σ_c/JCS = alteration index, where σ_c is uniaxial compressive strength of rock within the joint block as calculated from S.H. tests. Numbers in brackets give the ratio value when σ_c is equal to the strength of the freshest rock.

- Geometry of joint walls: A = joint surface area; profiles as drawn by using a Vitrex wire gauge; JRC = joint roughness coefficient as back-calculated from Barton's formula (equation 2.11, part two). In a few cases where the JRC values are marked with (*) it means that the particular joints have not been shear tested due to accidental failures during the compression tests. The JRC values in those cases have been assigned by matching the joint profiles with typical roughness profiles given by Barton and Choubey (1977); JRA = joint roughness amplitude describing the average vertical amplitude of the prominent surface protrusions. The aperture (a_j) values given with the general joint descriptions are the most representative average values assigned to the respective group of joints.

5. Joint block compression and direct shear testing procedures

The field samples were cut to a technically optimum size and shape using a diamond saw. The prepared joint blocks were rectangular prisms with side lengths ranging from approximately 80 to 100 mm, widths from 40 to 60 mm and heights from 50 to 70 mm. Specimens intersected by closed cracks were normally discarded from testing. During the saw-cutting, maximum care was taken to ensure that the average joint plane was aligned in a position parallel to the loading ends of the blocks. Parallelism between the three planes was subsequently improved by fine saw-trimming

TABLE 3.7

Description of type, wall strength, and geometry of SLATE cleavage planes

Joint no. and type	General description of joints	JOINT WALL STRENGTH Mean R	γ (kN/m^3)	JCS (MPa)	$\frac{\sigma_c}{JCS}$	GEOMETRY OF JOINT WALLS A (cm^2)	Profiles (0 — 5 — 10 cm)	JRC	JRA (mm)
	FRESH								
1 IF	Well interlocked planar cleavage fractures	50.6	27.70	175	1.0	45.6	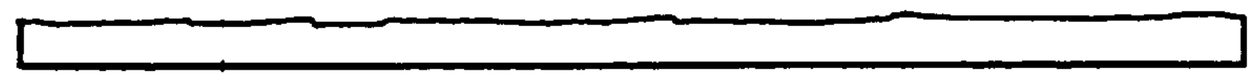	5.0	0.80
2 IF		50.6	27.70	175	1.0	45.0	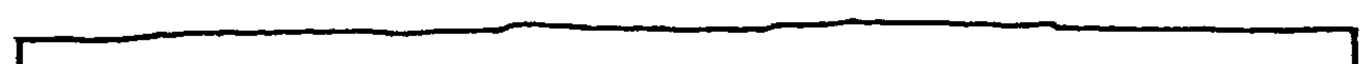	4.0	0.93
3 IF	$a_j \sim 0.1$ mm	50.6	27.70	175	1.0	48.0		4.5	0.85
4 CP	MODERATELY WEATHERED * $a_j \sim 0.15$ mm	42.5	27.82	122	1.3 (1.4)	56.0	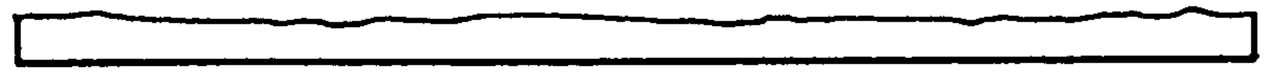	5.3	1.20
	WEATHERED								
5 CP	Walls covered by thin film of	36.8	27.05	77	2.1 (2.3)	53.8	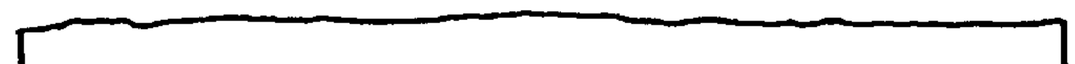	6.5	1.25
6 CP	limonite and weathered calcite. Poor interlocking.	36.8	27.05	77	"	69.0	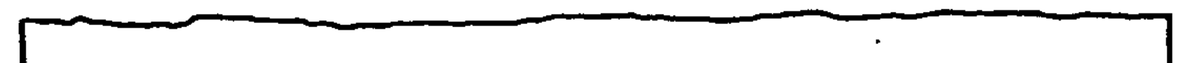	6.0	0.95
7 CP	$a_j \sim 0.5$ mm	36.8	27.05	77	"	53.3	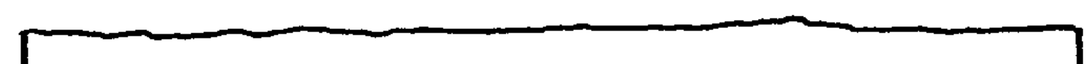	6.8	1.50

*Walls completely discoloured to yellow-brown.

TABLE 3.8

Description of type, wall strength, and geometry of DOLERITE joints.

Joint no. and type	General description of joints	JOINT WALL STRENGTH Mean R	γ (kN/m^3)	JCS (MPa)	$\frac{\sigma_c}{JCS}$	GEOMETRY OF JOINT WALLS A (cm^2)	Profiles	JRC	JRA (mm)
							0 5 10 cm		
1 VJ	FRESH TO SLIGHTLY WEATHERED No.2 lightly discoloured to yellow-brown. a_j ~ 0.15-0.20 mm	49.0	29.00	182	1.0	47.5		8.8	1.65
2 VJ		47.5	29.02	167	1.1	46.8		6.1	0.90
3 VJ	WEATHERED Surfaces covered by limonite. 2-3mm band of wall rock discoloured to yellowish. Poor interlocking. a_j ~ 0.5-0.6 mm	34.1	26.75	65	2.7 (2.8)	32.5		6.0	1.00
4 VJ		36.9	26.84	76	2.3 (2.4)	45.4		7.2	1.35
5 VJ		32.4	26.92	60	2.9 (3.0)	37.1		8.7	2.70

PAGE
NUMBERS
CUT OFF
IN
ORIGINAL

Text cut off in original

TABLE 3.9

Description of type, wall strength, and geometry of LIMESTONE joints.

Joint no. and type	General description of joints	JOINT WALL STRENGTH Mean R	γ (kN/m^3)	JCS (MPa)	$\frac{\sigma_c}{JCS}$	GEOMETRY OF JOINT WALLS A (cm^2)	Profiles	JRC	JRA (mm)
							0 5 10 cm		
1 BP	FRESH Nos. 2 & 3 lightly discoloured, no yellowish near the edges. Well locked. $a_j \sim 0.25$ mm	50.2	27.18	162	1	48.0		9.8	2.6
2 BP		51.0	27.18	170	1	52.5	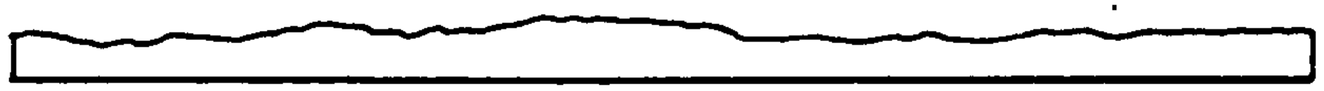	8.1	2.2
3 BP		50.2	27.18	162	1	52.4	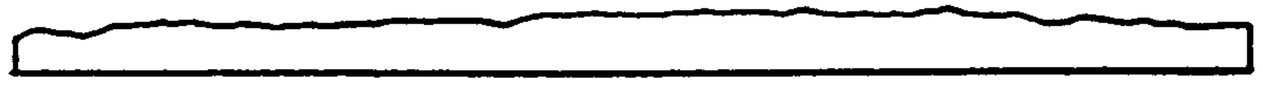	6.8	1.9
4 VJ	SLIGHTLY WEATHERED Surfaces partially (30-50%) discoloured to yellowish. Well locked except No. 6. $a_j \sim 0.25$ mm	49.1	27.27	154	1.1	48.5		11.4	2.5
5 VJ		49.1	27.27	154	1.1	49.5		8.9	2.0
6 VJ		49.8	27.27	160	1	48.5	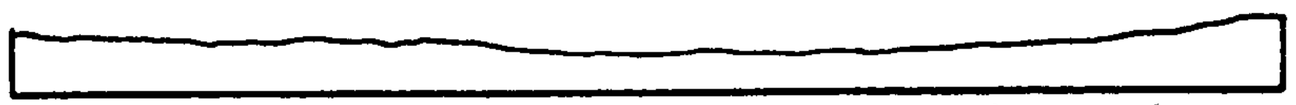	6.2	1.0
7 VJ		49.8	27.27	160	1	45.0		5.6	1.5
8 BP	SLIGHTLY WEATHERED Surfaces completely discoloured to yellowish. $a_j \sim 0.20$ mm	49.2	27.04	152	1.1	51.5		11.1	3.4
9 BP		49.8	27.04	157	1.05	49.0	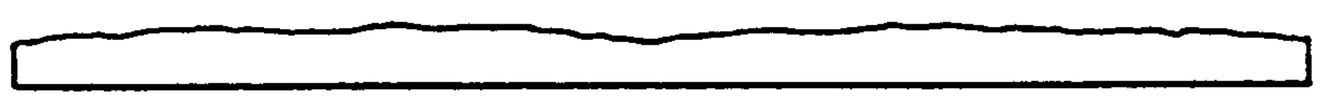	7.1	1.5
10 BP		50.0	26.95	157	1.05	51.0	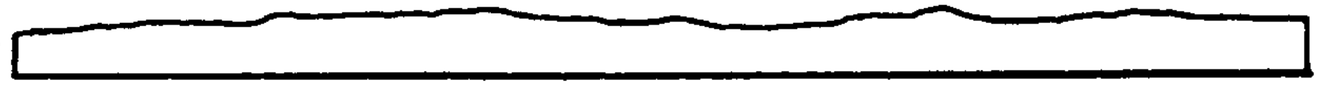	7.6	1.8
10a BP		50.9	26.95	165	1	51.0	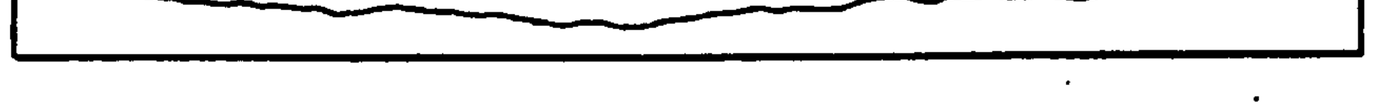	9.0*	2.0

(Continued)

TABLE 3.9 (Continued)

Joint no. and type	General description of joints	JOINT WALL STRENGTH Mean R	γ (kN/m³)	JCS (MPa)	$\frac{\sigma_c}{JCS}$	GEOMETRY OF JOINT WALLS A (cm²)	Profiles	JRC	JRA (mm)
							0 5 10 cm		
11 VJ	MODERATELY WEATHERED	45.0	26.80	118	1.4	53.0		14.8	4.0
12 VJ	Nos. 11, 12 & 13 discoloured to darker grey, and porous in places; nos. 14 & 15 heavily	44.7	26.80	116	1.4	49.0	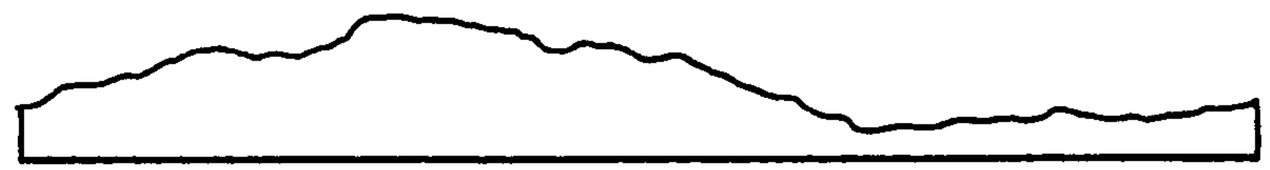	14.9	7.8
13 VJ	stained with soft porous patches. All	45.0	26.80	120	1.4	51.4		15.0	4.0
14 BP	well locked.	40.6	26.97	94	1.8	46.6	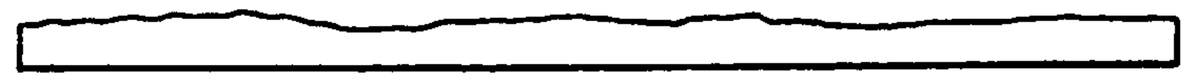	5.8	1.6
15 BP	a_j ~ 0.20 mm	43.9	26.97	113	1.5	36.4	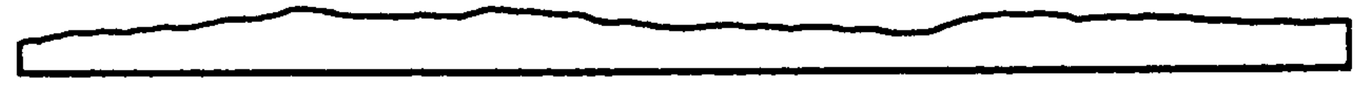	7.6	3.4
	WEATHERED								
16 VJ	All surfaces	30.5	25.68	50	3.3	39.4	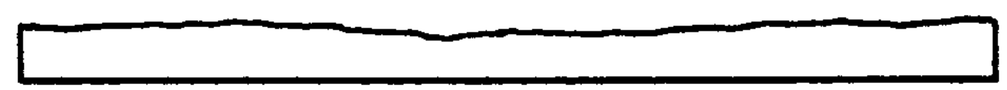	5.0*	1.1
17 VJ	covered by crust (~.5 mm) of yell-	28.0	25.68	44	3.8	48.6		15.0	5.5
18 VJ	owish, porous, weak weathered material. Nos. 16 & 20 poorly locked.	23.6	25.68	35	4.7	48.9	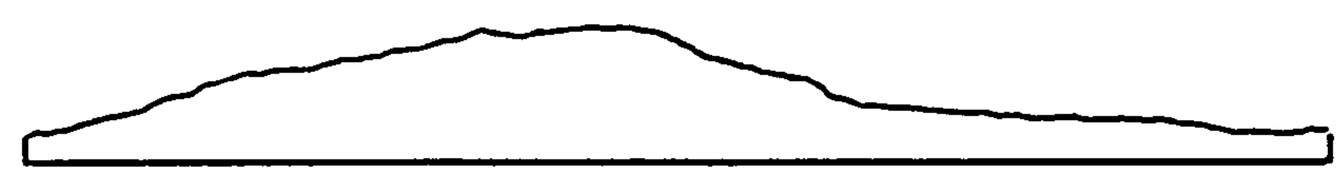	16.0	8.2
19 VJ	a_j ~ 0.40-0.50 mm	26.2	25.20	39	4.2	50.0		10.5	2.5
20 VJ		28.1	25.20	43	3.8	42.5		6.2	0.8

TABLE 3.10

Description of type, wall strength and geometry of SILTSTONE joints

Joint no. and type	General description of joints	JOINT WALL STRENGTH Mean R	γ (kN/m^3)	JCS (MPa)	$\frac{\sigma_c}{JCS}$	GEOMETRY OF JOINT WALLS A (cm^2)	Profiles	JRC	JRA (mm)
							0 5 10 cm		
1 AF	FRESH Rough extension fractures through fresh rock material. $a_j \sim 0.15$ mm	47.5	24.20	105	1	48.0		11.8	4.5
2 AF		47.5	24.20	105	1	45.2		10.2	3.9
3 AF		47.5	24.20	105	1	36.9	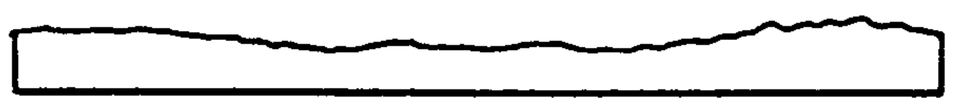	8.0	2.5
4 AF		47.5	24.20	105	1	39.6		11.0	4.3
5 AF		47.5	24.20	105	1	39.5	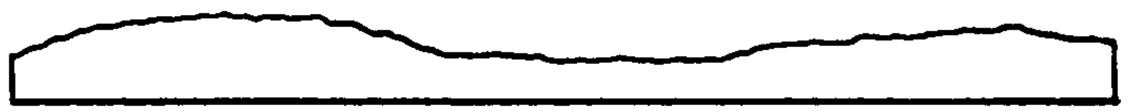	10.3	3.5
6 BP	MOD. WEATHERED Surfaces partially discoloured to yellow-brown, and "flakey". $a_j \sim 0.60$ mm	39.3	23.62	67	1.4 (1.6)	43.5	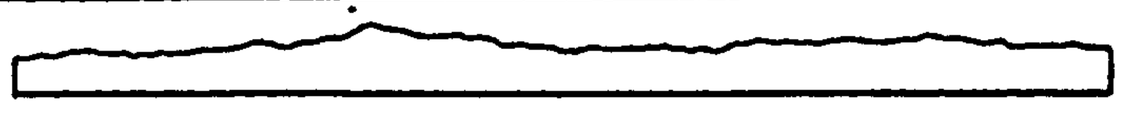	7.5	2.1
7 BP		39.3	23.62	67	1.4 (1.6)	46.0		7.0	1.6
8 BP	WEATHERED Completely discoloured to yellow-brown and "flakey". Poorly locked. $a_j \sim 0.60$ mm	30.7	23.80	45	2.1 (2.3)	44.6	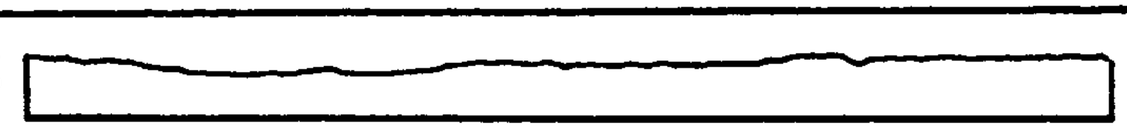	6.1	1.7
9 BP		29.3	23.80	42	2.2 (2.5)	47.8		6.7	1.9
10 BP		30.7	23.80	45	2.1 (2.3)	49.0	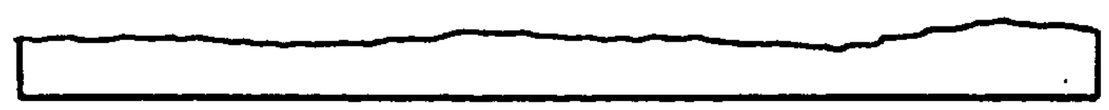	6.2	2.2

TABLE 3.11

Description of type, wall strength, and geometry of SANDSTONE joints.

Joint no. and type	General description of joints	JOINT WALL STRENGTH Mean R	γ (kN/m^3)	JCS (MPa)	$\frac{\sigma_c}{JCS}$	GEOMETRY OF JOINT WALLS A (cm^2)	Profiles	JRC	JRA (mm)
							0 5 10 cm		
1 BP	FRESH No visual difference between joint and rock. Well locked. $a_j \sim 0.25$ mm	40.5	24.10	74	1.0	47.0	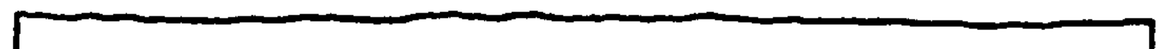	5.4	0.8
2 BP		38.8	24.10	68	1.1	49.0		11.9	3.7
3 BP		38.8	24.10	68	1.1	46.6	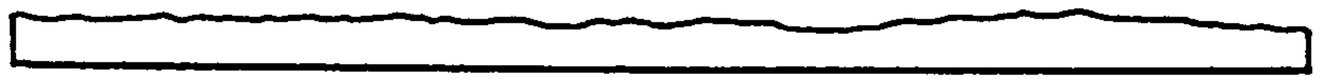	7.5	1.8
4 BP		38.7	24.32	69	1.1	41.5		8.6	2.5
5 VJ	SLIGHTLY WEATHERED Walls covered by a thin, dark brown, hard crust of iron oxides. Well locked. $a_j \sim 0.20$ mm	44.4	24.75	95	0.8	39.1		10.7	3.8
6 VJ		44.4	24.75	95	0.8	40.0		8.9	2.2
7 VJ		44.4	24.75	95	0.8	46.5		10.8	3.5
8 VJ		44.4	24.75	95	0.8	49.5	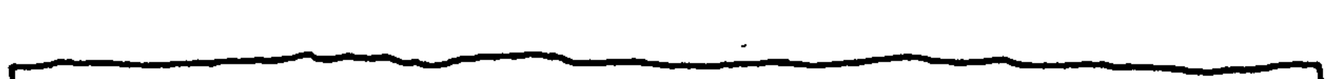	6.6	1.1

(Continued)

TABLE 3.11 (Continued)

Joint no. and type	General description of joints	JOINT WALL STRENGTH Mean R	γ (kN/m³)	JCS (MPa)	$\frac{\sigma_c}{JCS}$	GEOMETRY OF JOINT WALLS A (cm²)	Profiles	JRC	JRA (mm)
							0 5 10 cm		
	MOD. WEATHERED								
9 VJ	Rock material slightly weathered	36.0	23.80	58	1.2 (1.3)	52.8		10.8	3.2
10 VJ	(grade II). No visual difference	34.5	23.80	54	1.3 (1.4)	46.0		6.0	1.7
11 VJ	between joints and rock. Well locked.	30.7	23.80	45	1.5 (1.7)	50.0		14.1	5.4
12 VJ	$a_j \sim 0.25$ mm	33.7	23.80	52	1.3 (1.4)	50.6		7.5	3.5
	MOD. WEATHERED								
13 BP	Walls partially to	32.3	23.92	49	1.4 (1.5)	46.1		5.1	0.9
14 BP	completely stained. Rock material as	32.3	23.92	49	1.4 (1.5)	52.5		5.5	1.1
15 BP	above. Well locked. $a_j \sim 0.25$ mm	30.1	23.92	44	1.6 (1.7)	49.3		7.7	1.6
16 BP		30.1	23.92	44	1.6 (1.7)	50.5		7.4	1.8
17 BP		32.7	23.92	50	1.4 (1.5)	50.0		6.2	1.2
18 BP	WEATHERED Complete discolour-	22.2	19.9	25	1.0 (3.4)	50.0		6.1	1.8
19 BP	ation into brown. Rock highly weath-	22.2	19.9	25	1.0 (3.4)	49.9		5.0	0.9
20 BP	ered (grade IV). Poor locking.	19.0	19.9	22	1.0 (3.4)	53.0		5.1	1.5
21 BP	$a_j \sim 0.4$-0.6 mm	19.0	19.9	22	1.0 (3.4)	43.4		4.8	1.2

and grinding to within a tolerance of approximately ± 1° to 2°, although those specifications could only be approximated in cases of the very irregular joint surfaces.

(a) Joint block compression tests

The prepared joint blocks were compressed between two accurately machined hardened steel platens. The vertical displacements under normal loading or unloading were recorded by two sensitive dial gauges to an accuracy of ± 0.0005 mm. The vertical dimension for the majority of the joint blocks was insufficient for direct mounting of the gauges onto the block sides and therefore an alternative was to attach the gauges on independent stands and measure the relative displacement between the upper and lower platens. The problem in such an arrangement is that additional deformations may be introduced from improper preparation of the rock surfaces and hence poor quality rock/platen contacts. It was therefore necessary to ensure that such errors were reduced to a minimum.

The joint block compression tests were conducted on a 50 ton Dennison compression machine, which is shown together with the experimental set-up in the photographs in Figure 3.8. The dial gauges were connected to magnetic stands firmly seated on the basal plate. The spindles of the gauges were brought to rest vertically on two laterally projecting horizontal aluminium platelets. The latter were symmetrically fixed on two opposite sides of the upper block surface along a lengthwise central line. Two square grooves (20 mm long, 5 mm deep) were machined in the upper loading platen to accommodate the aluminium platelets. In that way the problem of upper platen/rock contact effect was eliminated. To minimize the effects for the basal contact of the block, a rigorous rock surface grinding and polishing procedure was applied. In order to examine the sensitivity and relative accuracy of the above experimental set-up a number of compression tests was conducted on solid rock samples and the axial strain measured directly by electrical resistance strain gauges was compared with the values calculated indirectly from the deformations recorded by the dial gauges. The two sets of measurements showed an overall good agreement. Details of those tests and of the surface preparation procedures have been included in Appendix III..

FIGURE 3.8 Joint block compression test arrangement and apparatus.

A problem which was encountered during a number of compression tests was that the dials gave dissimilar values of displacements at the two measuring points, the differences usually being in the order of 10 to 20%. This type of problem has been mentioned by other workers. Iwai (1976) described an extreme case of a fracture closing at one point and opening at another due to eccentric application of the normal load. Hungr and Coates (1978) referred to similar experiences involving rotation of the moveable half of the joint blocks, which they attributed to the design of their apparatus and application of the compression load by means of flexible air bellows.

Eccentric application of the normal load may have also been the cause of the differential deformations recorded in the present experiments. However, it would also seem that in some cases the geometry itself of the joint surfaces may have contributed to that effect. As an extreme example, during one test it was observed that under increasing load the initial difference between the deformation recordings of the two gauges (let us call them no. 1 and no. 2) progressively narrowed and at approximately 8 to 12 MPa the two gauges read very similar displacements. Then, for the following loading stages gauge no. 2 (which originally had given the lower readings) showed slightly larger displacement than no. 1 and the new discrepancy continued until the end of the test. The joint block in that case was limestone specimen no. 12. Gauge no. 1 was recording the deformation across the area of the joint occupied by a large undulation (see profile in Table 3.9). It is probable that stress concentrations on that large irregularity firstly caused larger deformation and then "closed" that region earlier than the rest of the surface. All experimental results were analysed by using the average of the displacement values recorded by the two dial gauges.

The normal deformations measured during compression of the joint blocks represented the sum of the elastic deformation of the solid rock and the closure of the intersecting joint (the term "total deformation" will be used hereafter). Therefore, the net joint closure at any stress level would have to be found by subtraction of the elastic deformation of the surrounding rock under the same normal stress from the experimental value of total deformation. When testing an artificial fracture the intact rock deformation can be measured on the same specimen prior to splitting, as for instance was done by Goodman (1976). Alternatively, a separate intact specimen can be used provided that it has precisely the same shape

and size as the jointed one. It is obviously essential to use a specimen from the same original sample and maintain the same relative orientation during cutting or coring particularly in cases of mechanically anisotropic materials.

During preparation of the test samples a number of intact rock blocks was also cut. It was impossible to obtain a "truly representative" solid rock block for each jointed block due to unavailability of sufficient quantity and/or good quality, uncracked material after the joint block had been sawn from the field sample. Eventually an alternative solution was adopted as will be discussed in the next chapter.

(b) Direct shear tests

Direct shear testing of a number of joints was performed on a portable shear apparatus. The latter was the model manufactured by Robertson Research International. The normal and shear loads are applied by means of wire ropes and hydraulic rams fitted onto the upper and lower boxes respectively. The loads exerted on the rams during testing are indicated by Bourton tube lead gauges which are worked independently by hand operated hydraulic rams. In the present model, the pump feeding the normal loading ram was fitted with an adjustable low friction pressure maintainer, thus allowing constant normal loading conditions during testing of dilatent surfaces. The joint samples were fitted in the machine after appropriate concrete moulds had been prepared (details included in Appendix III, section 3). The shear apparatus in assembled position and prepared specimen moulds are shown in the photograph of Figure 3.9.

The majority of joint types were sheared under different normal loads by following a positive (or incremental) multistage testing procedure. That is, the same joint was sheared repeatedly, each time applying a load higher than that of the previous test(s). The justification of such a practice lies in the practical impossibility of obtaining joint samples of identical surface geometry. That procedure suited the main purpose of these tests, which was to compare the normal and shear stiffness of different joint types at various normal stress levels. On the other hand, the disadvantages of multistage testing ought to be carefully considered. Martin and Millar (1974) derived peak shear strength envelopes from an incremental normal loading sequence applied on the same joints assuming that any surface irregularities which are damaged at a lower stress level

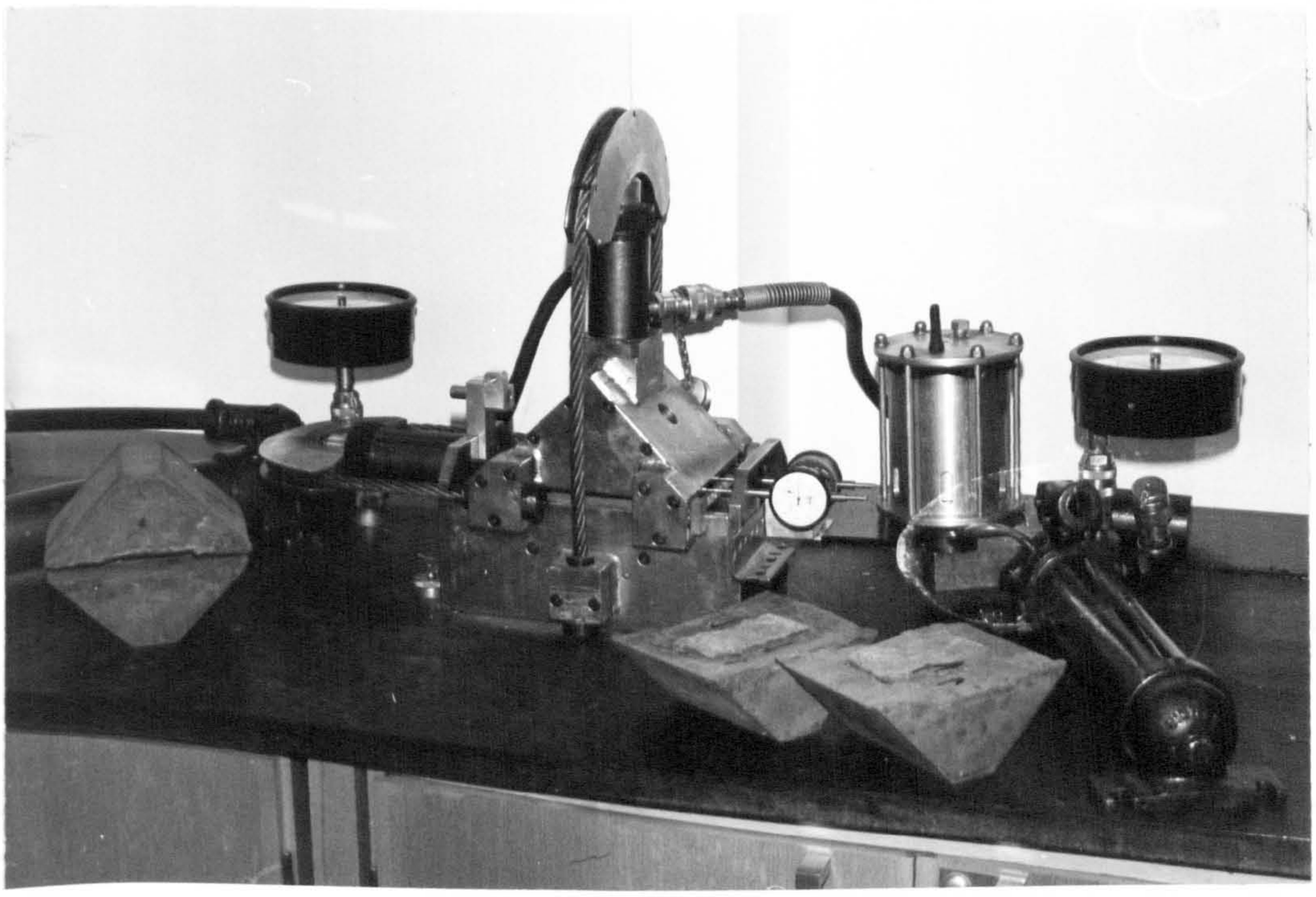

FIGURE 3.9 Photograph illustrating the portable shear box in assembled position with a modified dial arrangement for measuring shear displacements directly on the encased joint sample.

would not affect the strength at the higher stress level. However, after the first test it is logical to expect that the peak shear resistance will be affected to a certain extent by the previous stress-deformation history, depending of course on the level of normal stress applied in the preceding test(s).

There are various techniques which can be followed in peak strength determinations from multistage testing. For example, Ross-Brown and Walton (1975) describe a method in which after the peak shear strength under a certain normal load is reached the test is stopped and by maintaining the shear load the next normal load increment is applied. Alternatively, the shear load is released (thus causing some horizontal elastic rebound) before the normal load is increased to the next value. However, both those methods would obviously be unsuitable for the present purpose of multistage testing and hence the chosen procedure consisted of reassembling the sample to its original position before starting a new shear run under higher normal load. Some of the joint types had very similar surface geometry and a normal testing procedure was followed.

During early testing trials significant inconsistencies were observed in the recordings of the horizontal displacements by a dial gauge mounted on the lower box with the spindle resting on a position beneath the normal loading ram (standard manufacturer's design). Specifically, when testing strongly dilatant joints "negative" displacements or sudden large increases were obtained due to a small rotational movement of the box enhanced by the large vertical distance of the measuring point from the shear plane ($\sim$110 mm). Such anomalies were not observed in cases of relatively planar surfaces, but comparisons of the displacements recorded by the standard system with those recorded by two other gauges fitted at the level of the shear plane (spindles resting on the box) showed that overall the latter gave smaller average displacement values. It is generally advisable to record the displacements from points near to the shear plane, and preferably directly from the joint thus avoiding the additional deformations of the encasing components and the loading system (Rosso, 1976). A minor modification of the present apparatus enabled two dial gauges to be mounted on the lower box with their spindles resting directly on the upper joint block half at a distance of one or two millimeters above the shear plane. The positioning of the dials can be seen in

the photograph in Figure 3.9 and further details have been included in Appendix III (section 3). Comparisons between the displacement readings by using the standard and modified configurations showed that the original system could give up to three times larger displacements than the true ones. The latter were used for the calculation of the shear stiffness values for all the joints tested.

In the preceding sections the various preparatory stages of the experimental study have been reviewed. It has been shown that the joint specimens included in the testing programme represented a considerable range of the variables of potential influence on joint deformability. That was an imperative condition for the aims of this study.

The following two sections have been exclusively devoted to the analysis and preliminary qualitative interpretation of typical experimental results.

3.2.3 Fundamental aspects of joint normal deformation

As briefly stated in the introductory section of this chapter, normal loading tests were conducted on the joints by firstly assembling them into their fully interlocked position and subsequently by mismatching them to create point-contacting, "open" joints displaying variable aperture openings. The testing procedures were in both cases essentially the same. Interlocked joint blocks were subjected to a sequence of loading-unloading cycles and readings of the vertical displacements recorded by the two dial gauges were taken at regular increments or decrements of normal load. Misfitted joint testing presented various practical difficulties which will be discussed in the relevant section (3.2.3(3)).

The initial normal stress (σ_i) acting upon the joint planes was created by the weights of the upper loading platen, flexible coupling and upper joint block half, which created an average σ_i value of approximately 1×10^{-3} MPa. Depending on the rock type the interlocked joint blocks were loaded under maximum stresses ranging from approximately 5-10 to 50-55 MPa. Those levels of stress were applied to ensure that the solid rock deformation would be well within the elastic region and that maximum

closure of the joint could be achieved. The maximum normal stresses generally corresponded to approximately $\frac{1}{3}$ to $\frac{1}{2}$ of the uniaxial compressive strength (σ_c) of the rock material. The misfitted joint blocks were compressed under maximum stresses usually approaching $\frac{1}{3}$ of rock strength (σ_c); attempts to increase them further often resulted in specimen failures by tensile splitting.

The fundamental deformational characteristics of the interlocked and mismatched joints will be discussed in the two main subsections (2) and (3) to follow. The experimentally recorded displacements represented both the closure of the joints and deformation of the solid rock above and below the interface. It is, therefore, essential that the behaviour of the rock materials be fully appreciated and understood before proceeding to the analysis of joint behaviour.

1. Elastic deformation of the solid rock

The elastic deformational behaviour of the intact rock materials was studied by conducting a series of compression tests on saw-cut blocks. Those specimens represented the "solid counterparts" for a number of joint blocks and were cyclically loaded under the same levels of normal stress as the respective jointed blocks. The rock compression curves were subsequently used to derive the net closure of the joints.

Under compression the different materials displayed variable non-linear behaviour depending on the rock type and weathering state. On unloading all rock types underwent hysteresis and in some cases showed significant inelasticity. The loading/unloading curves from three cycles applied on fresh blocks of the five rock materials are presented in Figure 3.10. The applied maximum stresses were approximately equal to one-third of the uniaxial compressive strength. As shown the slate, dolerite and limestone rocks displayed essentially similar loading behaviour. The curves revealed a certain small amount of non-linear behaviour at low stress levels and then linearity. The elastic moduli (E_r) calculated as tangent values at the normal stress level of approximately 35 MPa (1st cycle loading curves) were very similar to those obtained from tests on cylindrical specimens with strain gauges, as reported earlier (section 3.2.1(2) and Fig. 3.5). On unloading, the limestone block displayed relatively more pronounced hysteresis than the slate and dolerite rocks, but all three materials were almost perfectly elastic. The fresh siltstone

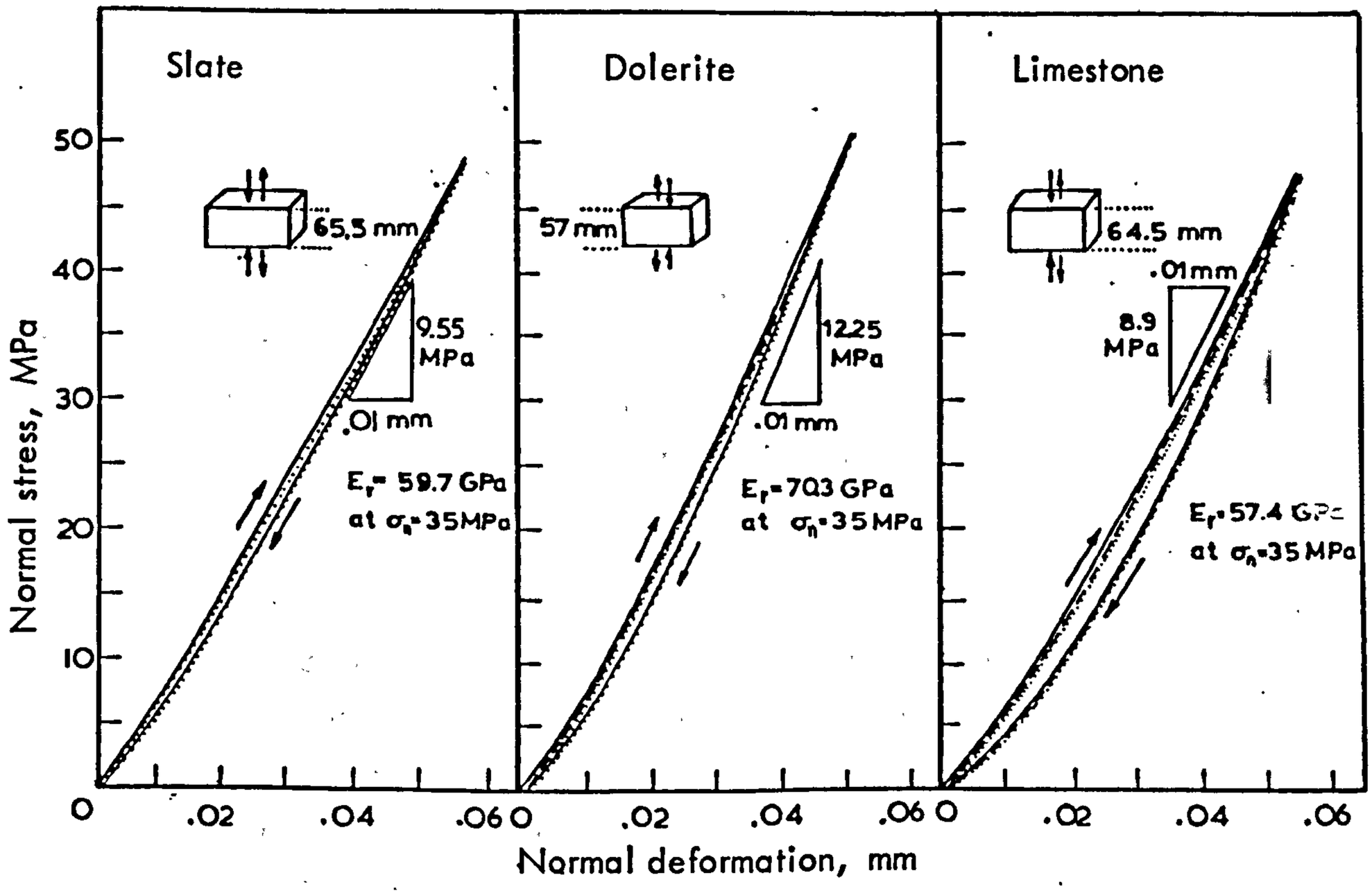

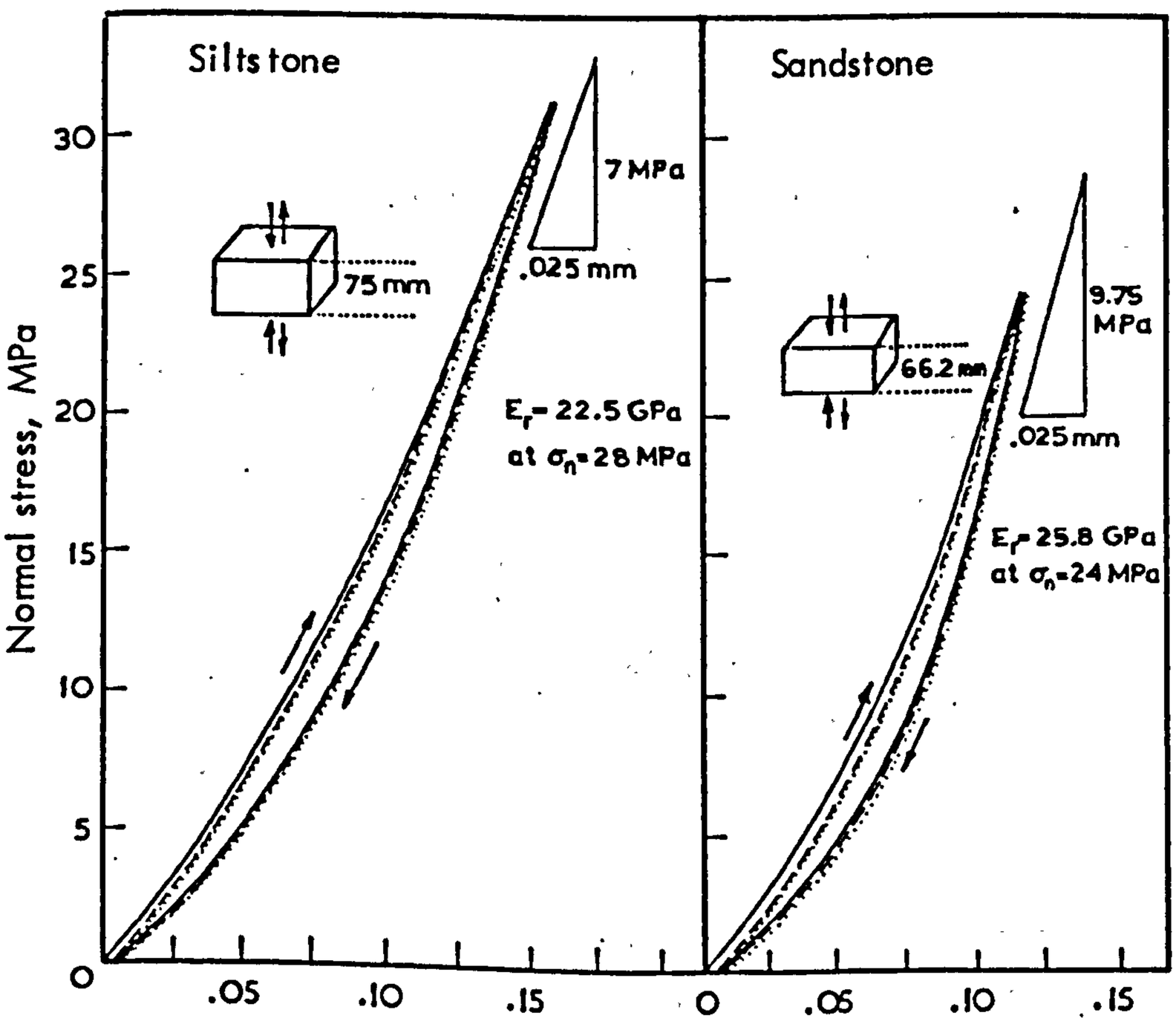

FIGURE 3.10 Normal stress – normal deformation relationships of solid rock blocks under repeated loading cycles

and sandstone samples showed markedly non-linear behaviour over a wider range of stresses, significant hysteresis and a small amount of permanent set at the end of the first loading cycle.

Non-linearity, hysteretic effects, and amount of permanent deformation all increased considerably with weathering. Load cycling curves on weathered materials are included with the respective experimental joint block compression curves in Figures 3.15 and 3.16 seated in the next subsection. Inelasticity was also observed in those materials after the first cycle, and especially in the case of the highly weathered sandstone, it persisted in all three cycles.

The non-linear stress-deformation behaviour of intact rock under uniaxial compression as well as the phenomenon of hysteresis in cyclic loading have been explained due to presence of structural flaws (Walsh, 1965). At low stresses cracks may be open; as the stress is raised the cracks begin to close (primarily those normal to the stress axis) and the rock becomes elastically stiffer, hence accounting for the non-linearity during initial loading. Walsh pointed out that in general, even if the cracks were closed, some sliding motion of opposing crack faces would still be possible. On unloading, a finite stress change is necessary such that it will allow the internal back stress to exceed the frictional resistance along the cracks and enable reversal of the crack sliding motion, and hence the hysteresis phenomenon appears. Favourably oriented cracks may remain interlocked and therefore on completion of unloading irrecoverable deformations are observed. Collapsing of pore spaces during loading would also add to the total permanent set.

Bearing in mind the above fundamental aspects of solid rock behaviour we can now embark on the description of the combined performance of jointed blocks and then proceed to extract the net joint behaviour.

2. Normal deformational behaviour of interlocked joints

(a) Normal stress (σ_n) - total deformation (ΔV_t) relationships

The experimentally obtained normal stress-total deformation curves of the various joint block types showed an invariably non-linear behaviour within a wide range of normal stresses. The type of relationships and the range of deformations as a function of the mechanical strength of the

intact rock and/or joint surface are illustrated by the family of curves presented in Figure 3.11. Each of those curves represents the loading path from the first loading cycle. Those denoted as A_1, B_1, C_1, D_1 and E_1 correspond to fresh joint blocks of slate, dolerite, limestone, siltstone and sandstone respectively. A_2, B_2 and C_2 are the lowest bound curves of slightly weathered slate and fresh dolerite and limestone blocks containing joints with weathered surfaces. Finally, D_2 and E_2 represent weathered joint blocks from siltstone and sandstone.

The behaviour of joint blocks under compression followed the general pattern outlined by Goodman and St. John (1977). At the initial stages of the first loading the deformability of each joint block was dominated by the displacements taking place across the joint interface. For example, at a normal stress level of approximately 1.0 MPa it was estimated that the average ratio values of joint block deformation to solid rock compression ranged between 5 and 30 depending on the rock type and the weathering of both joint walls and intact material. As would be expected, the lower ratio values were associated with joint blocks from uniformly weathered deformable material and the higher values corresponded to cases of weathered joint surfaces in fresh solid rock.

Under increasing normal stresses the curves became gradually steeper and in most cases developed into virtually straight lines, which were parallel or nearly so to the elastic compression curves of the solid rock (dotted lines in Fig. 3.11). Goodman and St. John consider that at this stage the joints have closely approached or reached a fully closed position and that any further increase in normal load is taken up by the solid rock above and below the joint, hence the similarity between the jointed and solid block compression curves in that stress range. It is noticeable that the total deformation curves of fresh blocks with weathered joints (e.g. A_2, B_2, C_2 which failed at ~ 28 MPa) began to approach the respective rock compression lines under higher stresses than those apparently required by the uniformly fresh joint blocks. That was because of the larger distance that the weathered walls had to cover due to the wider aperture, but other factors such as the wall strength and roughness were involved as will be discussed in detail in the next chapter.

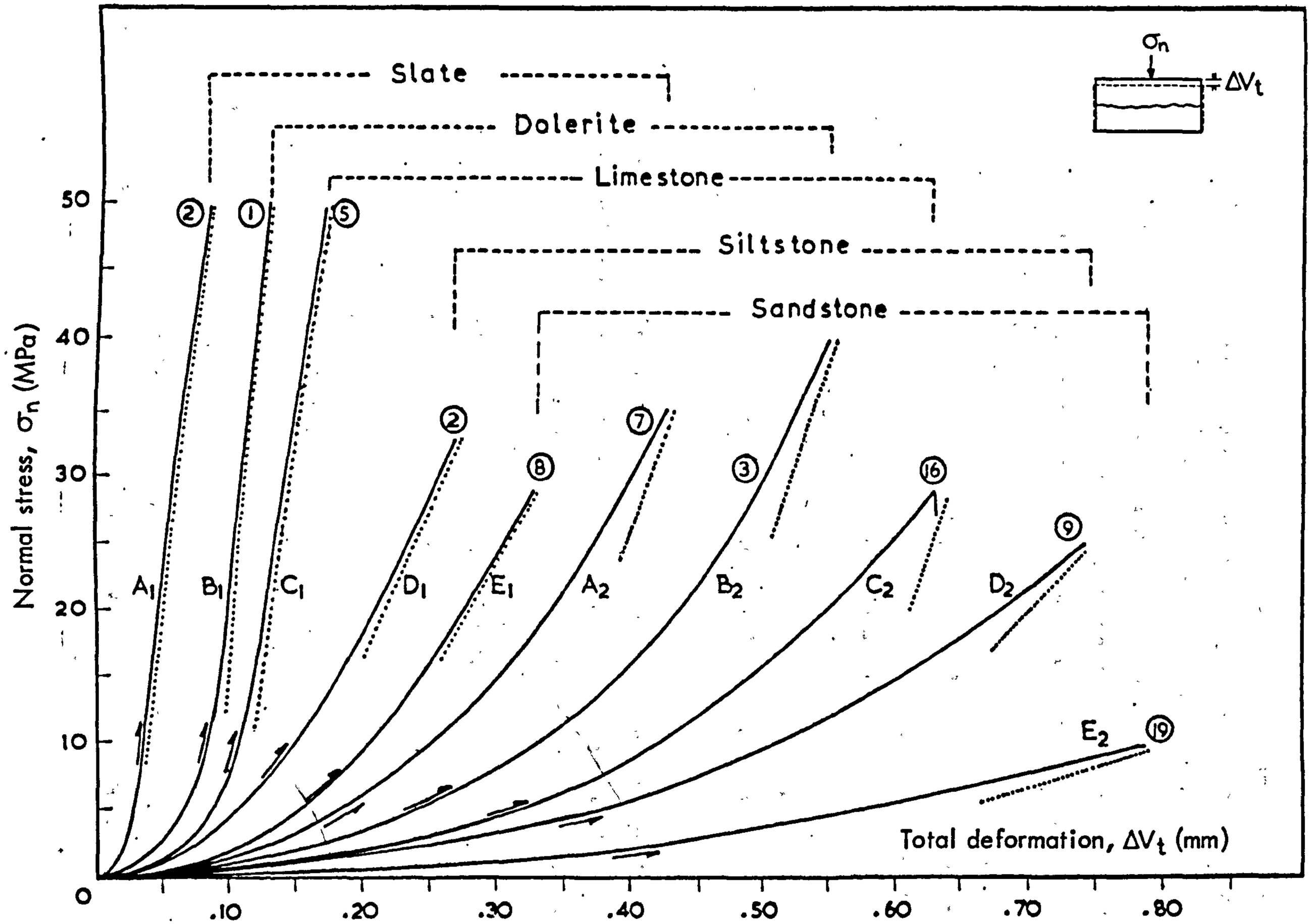

FIGURE 3.11. Range of normal stress – total deformation relationships of fresh and weathered joint blocks of different rock types as obtained from first loading. The dotted lines represent the elastic compression curves of the solid rock. Numbers in circles indicate the specimen number as indexed in Tables 3.8 to 3.12.

After the joint blocks had been compressed under the maximum stresses, the load was decrementally released and the rebound of the specimens recorded. Once the blocks were completely unloaded two further loading cycles were applied. Typical examples of the behaviour of fresh and weathered joint blocks from all five rock types under cyclic loading are shown in Figures 3.12 to 3.16. Each of the diagrams contains also the stress-deformation curves of a cyclically loaded solid rock specimen with the same dimensions and prepared from the same field sample as the corresponding joint block.

On decompression after first loading all joint blocks showed markedly hysteretic behaviour and upon return to zero normal stress a large amount of deformation remained irrecoverable. Reloading for the second and then third time produced much steeper curves, while each unloading persistently showed hysteresis and inelasticity. The permanent sets at the end of the second and third cycle were only a fraction of that obtained after the first.

Another typical feature also deserves attention, that is the similarity between the unloading paths of the solid and jointed blocks within a range representing over $\frac{3}{4}$ of the total applied stresses. That agrees with the observations by Goodman (1974) that the elastic portion of the normal deformation of a jointed block is derived from the solid rock. However, it should also be noticed that as the unloading approached very low levels of normal stress the jointed blocks displayed a much more rapid recuperation until completion of unloading in a mode similar to that frequently observed in plate-loading in-situ tests (e.g. Serafim, 1964, Guerreiro et al., 1968). That was due to some elastic recovery of the joint walls.

The basic qualitative characteristics of joint block deformation referred to above were invariably displayed by all the 64 specimens tested. Detailed tables with all experimental results have been included in Appendix IV.

(b) Normal stress (σ_n)-joint closure (ΔV_j) relationships

The net joint deformation or closure curves of the joint types in Figures 3.12 to 3.16 were derived by subtraction of the deformation lines of the intact rock samples from the experimental total deformation

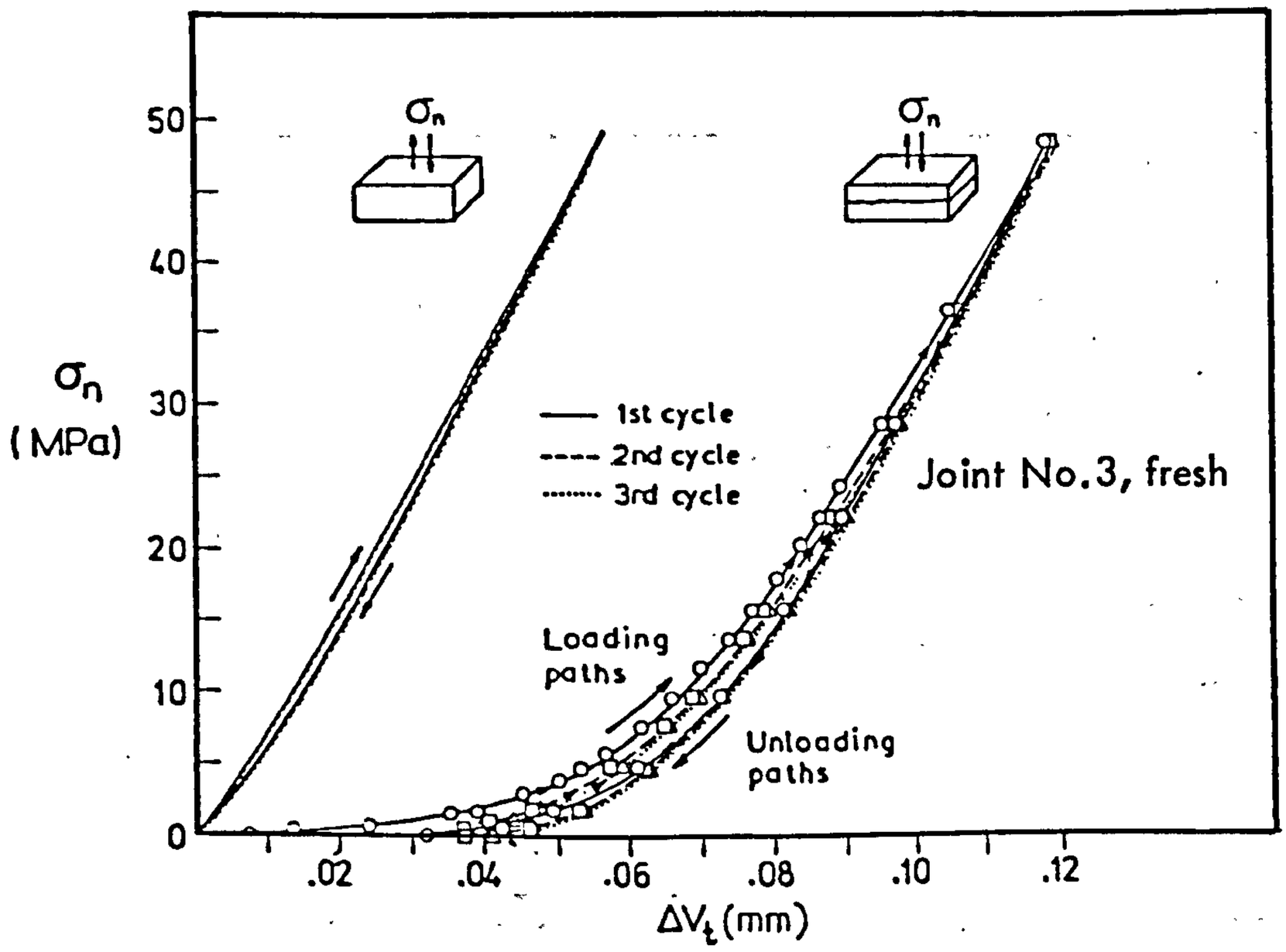

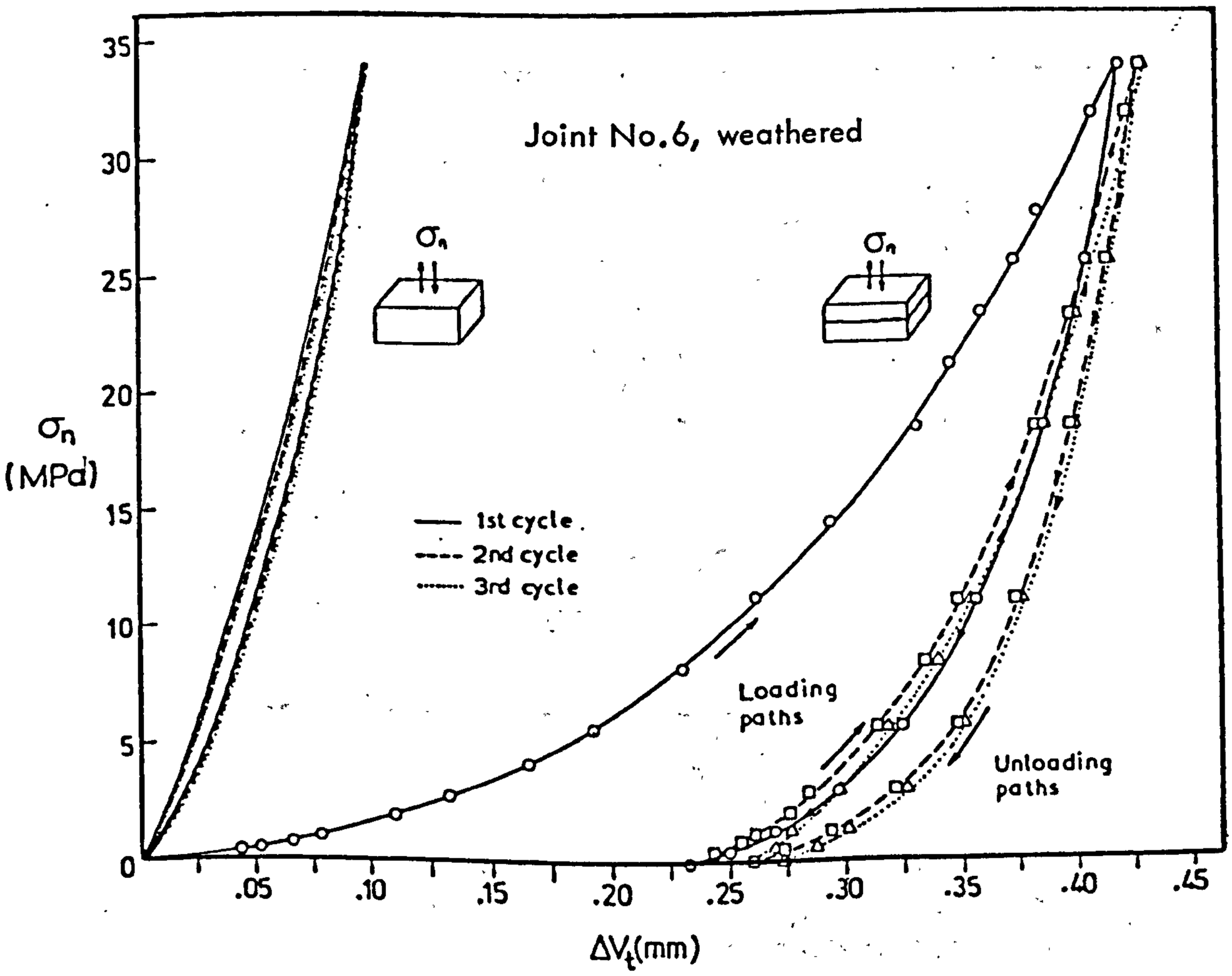

FIGURE 3.12 Normal stress (σ_n) – total deformation (ΔV_t) relationships of fresh and weathered cleavage blocks in SLATE under repeated loading cycles, and intact rock compression curves.

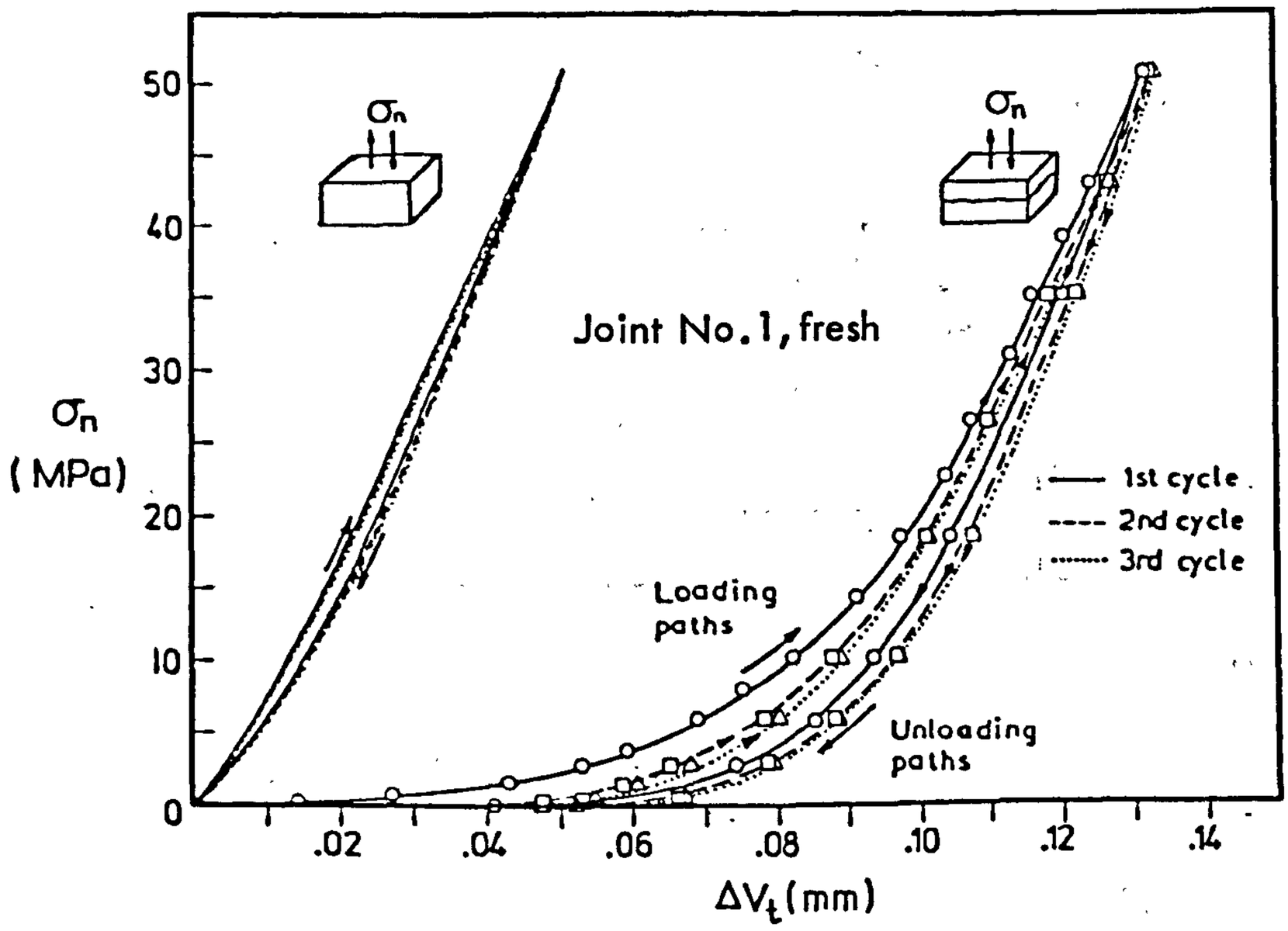

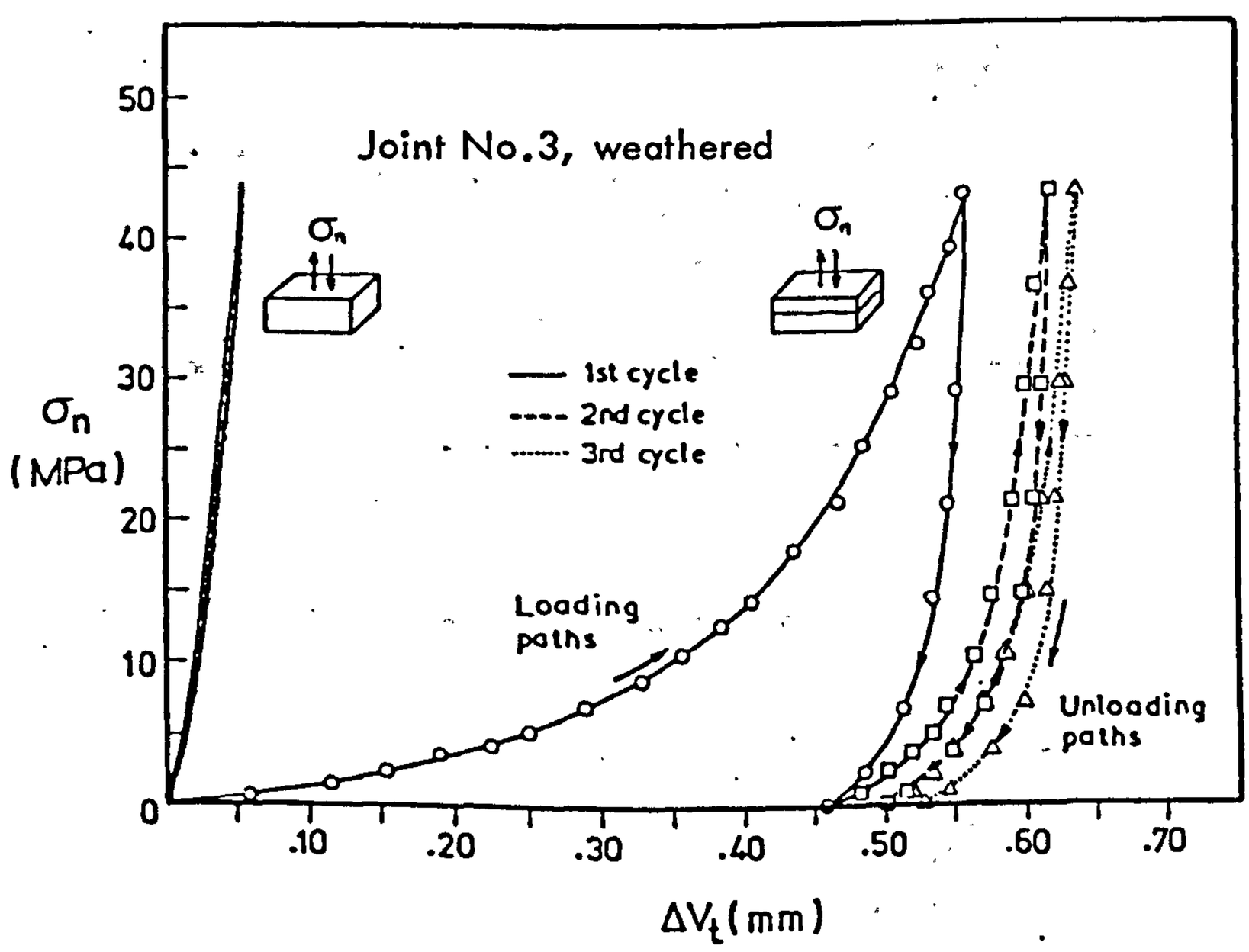

FIGURE 3.13 Normal stress (σ_n) - total deformation (ΔV_t) relationships of fresh and weathered joints in DOLERITE under repeated loading cycles, and intact rock compression curves.

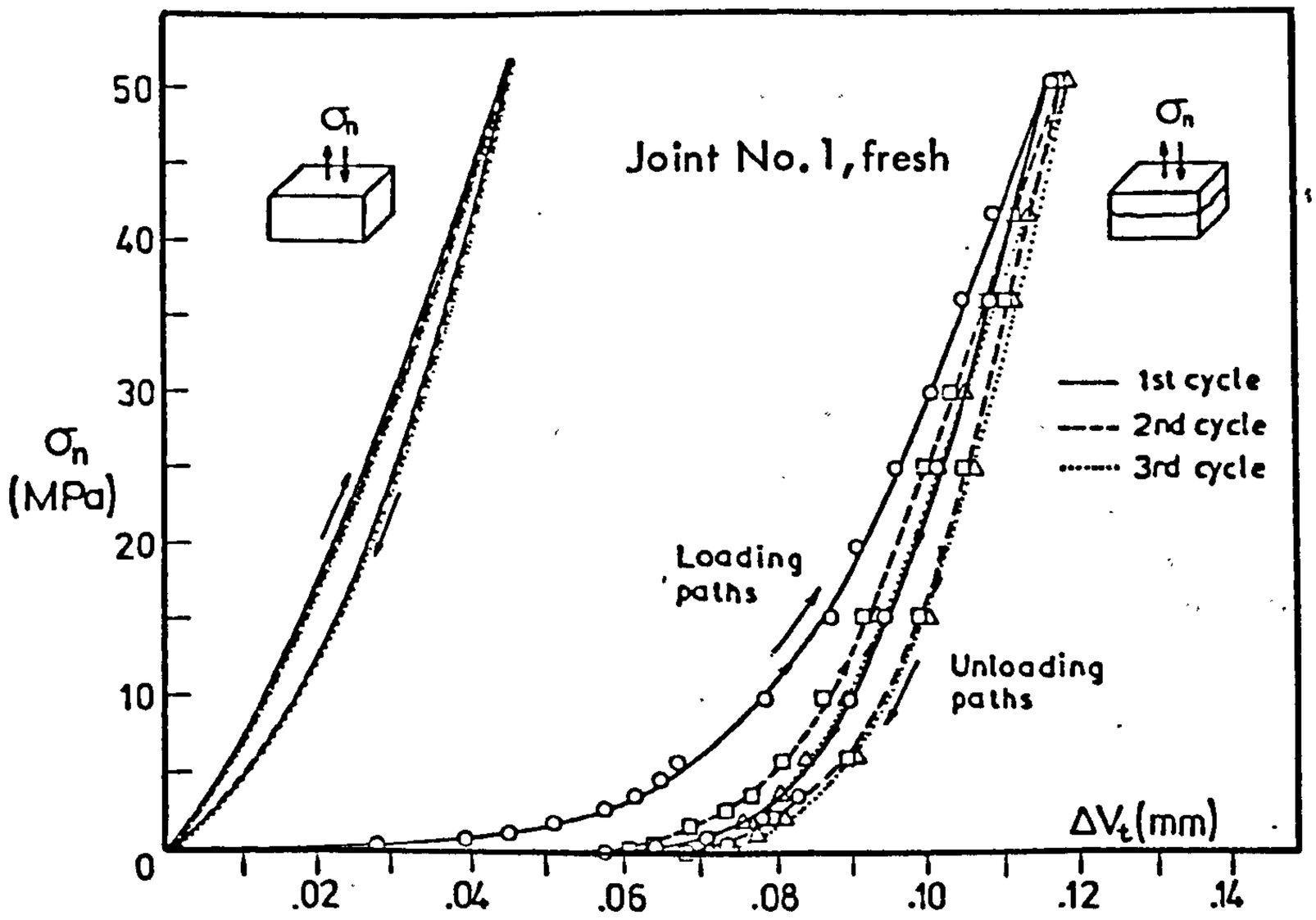

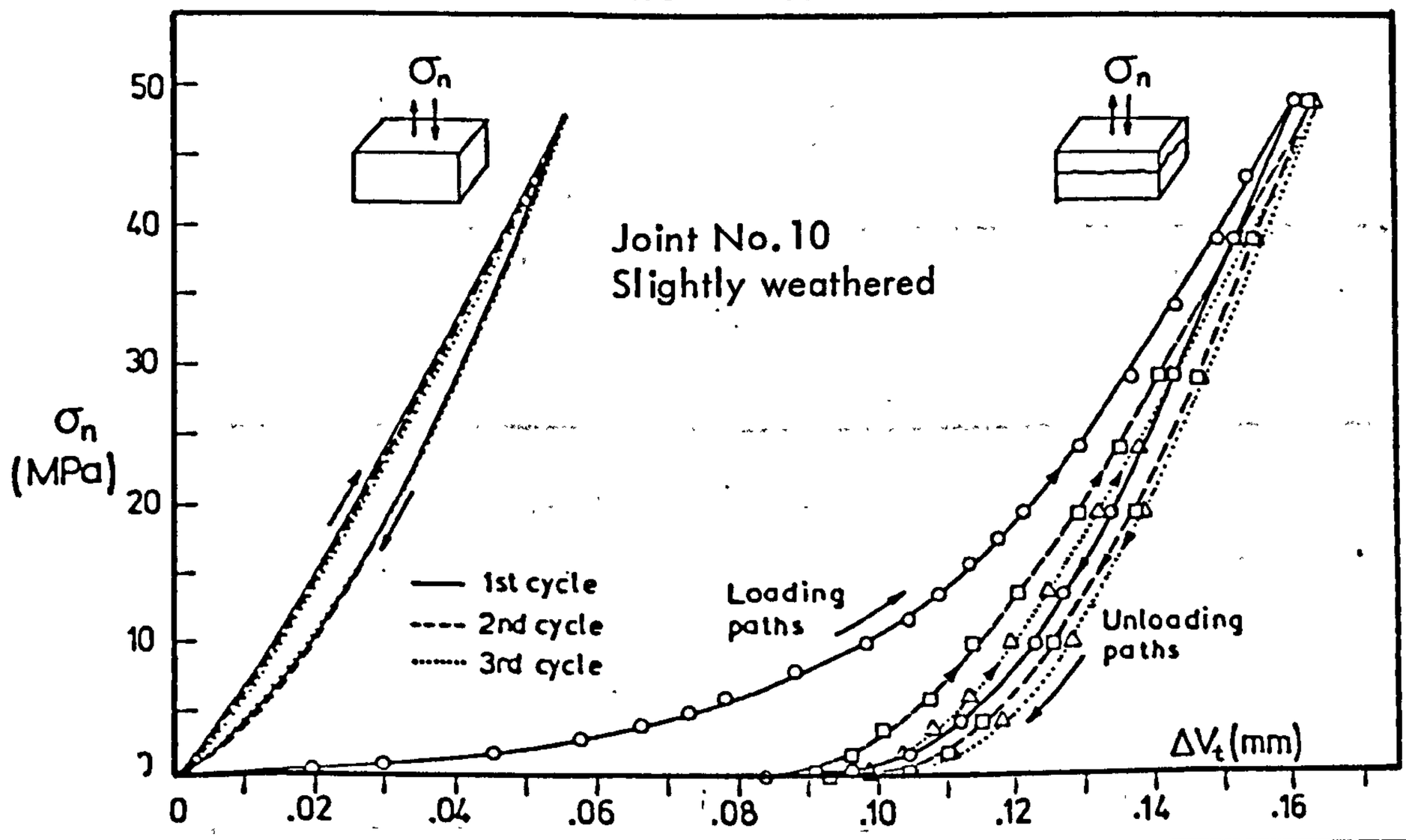

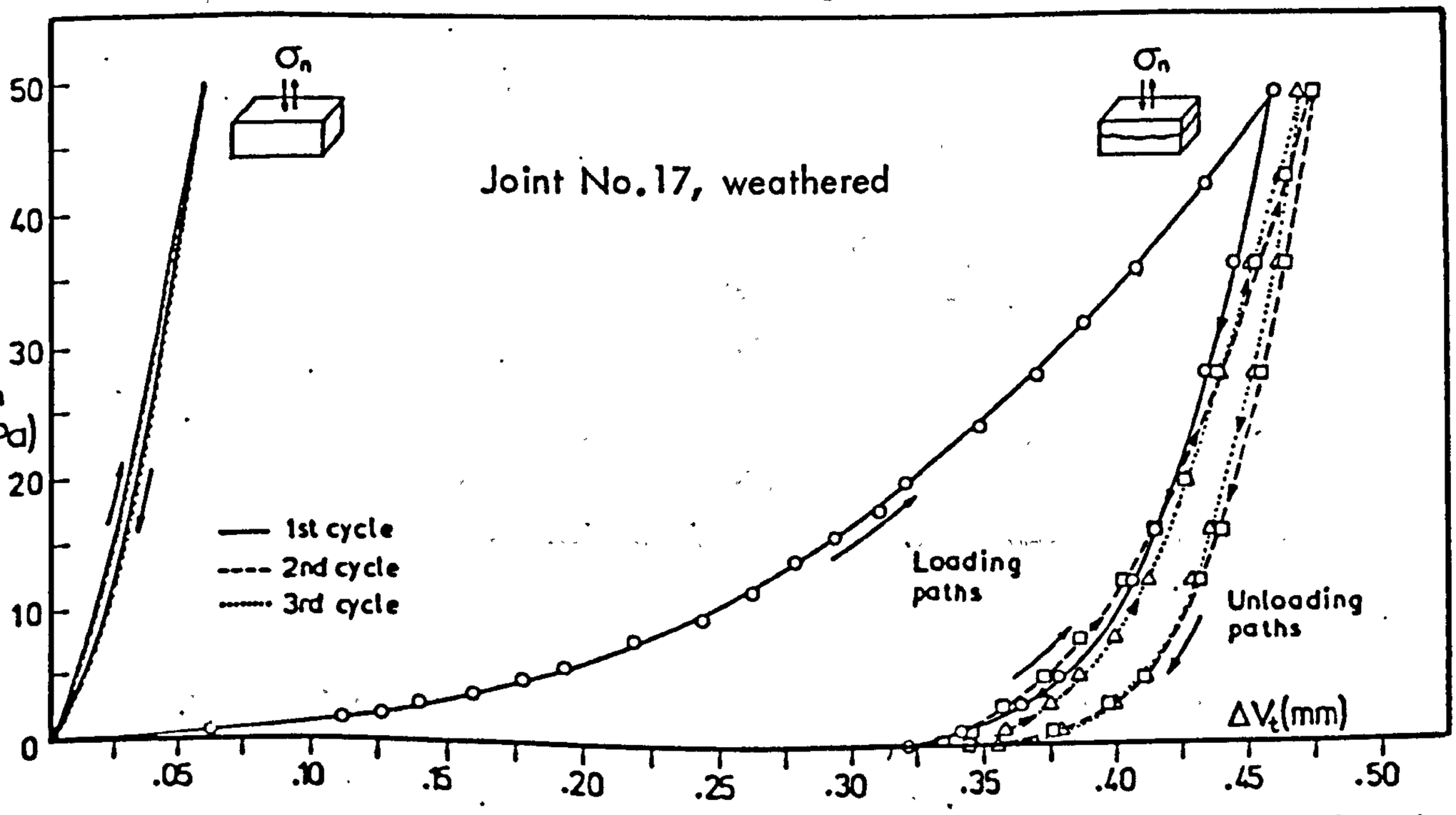

FIGURE 3.14 Normal stress (σ_n) – total deformation (ΔV_t) relationships of fresh and weathered joints in LIMESTONE under repeated loading cycles, and intact rock compression curves.

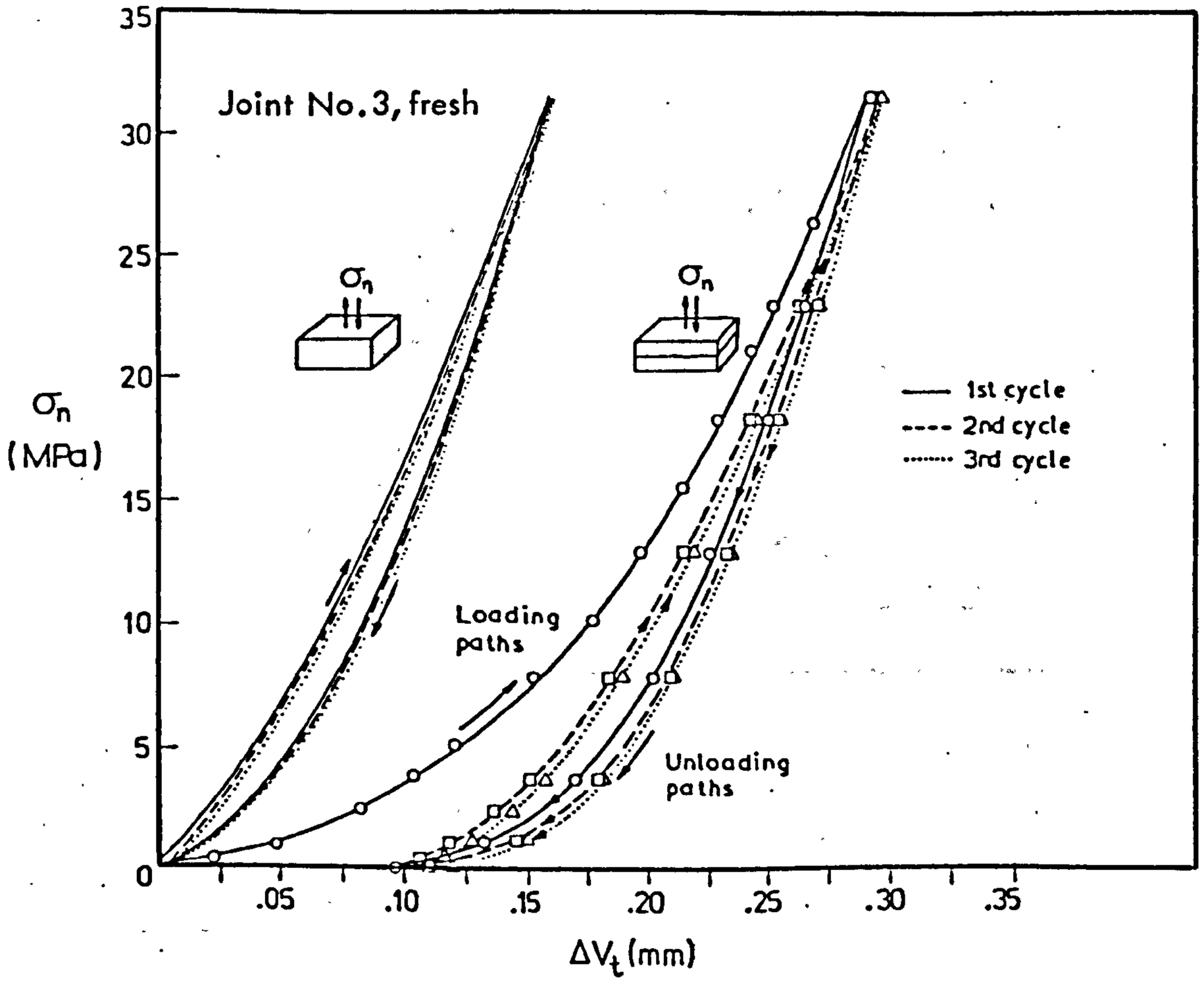

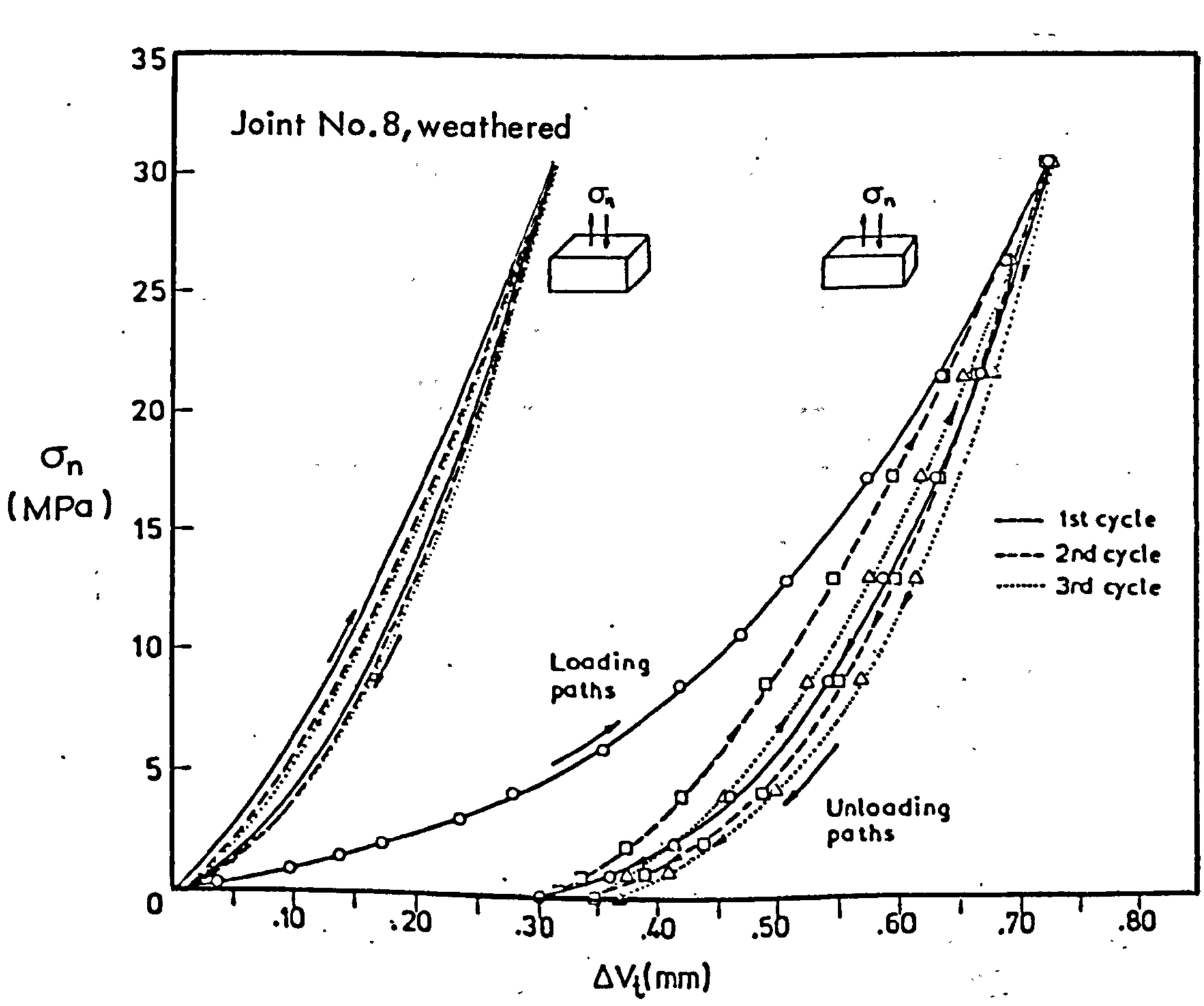

FIGURE 3.15 Normal stress (σ_n) - total deformation (ΔV_t) relationships of fresh and weathered joints in SILTSTONE under repeated loading cycles, and intact rock compression curves.

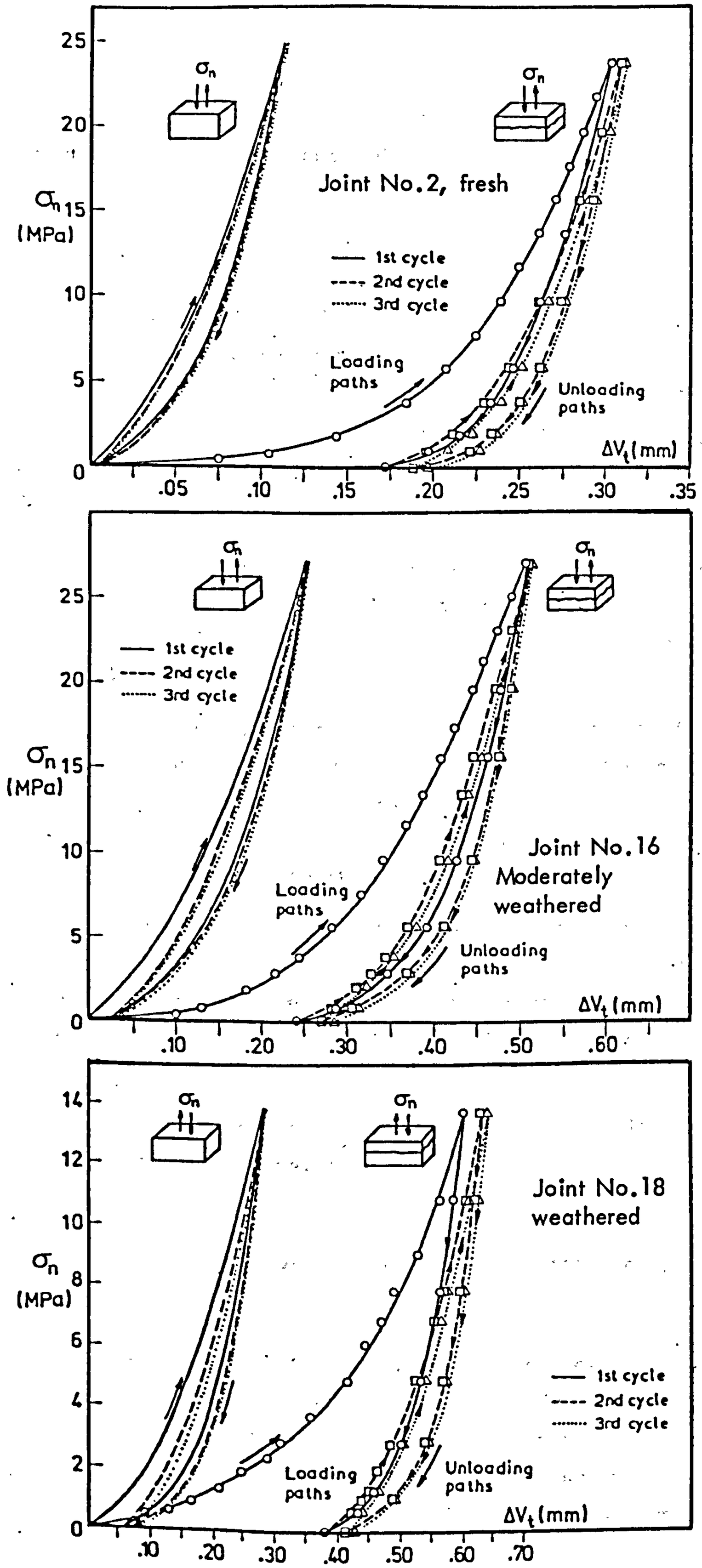

FIGURE 3.16 Normal stress (σ_n) – total deformation (ΔV_t) relationships of fresh and weathered joints in SANDSTONE under repeated loading cycles, and intact rock compression curves.

curves. Thus, at each level of normal stress the net joint closure (ΔV_j) on loading or unloading was calculated from:

$$\Delta V_j = \Delta V_t - \Delta V_r$$

where ΔV_t was the deformation of the joint block under loading or unloading and ΔV_r the corresponding deformation of its solid counterpart. The calculations were separately applied to each loading cycle. The so derived joint closure curves are presented in Figures 3.17 to 3.21. Observation of those curves reveals the following fundamental characteristics of joint normal deformation:

i) The loading paths of the normal stress-joint closure curves are highly non-linear. This type of behaviour persists throughout repeated loadings, irrespective of the rock type and the weathering state of the joint.

ii) Repeated loading after the first cycle indicates marked increase in the joint stiffness. The largest amount of closure occurs during the first loading. There is a vast difference in the closure achieved during the first and second loading. Compression for a third time shows a small further decrease in closure.

iii) Significant hysteresis persists between loading and unloading during all three cycles. At the end of the first loading a very large permanent set remains. By contrast, the increase in the amount of irrecoverable deformation at the end of the second and third cycles is small.

iv) Fresh joints are capable of some elastic recovery under the unloading path. In a relative sense, this recovery is smaller in cases of weathered joints.

v) The weathering state of walls has a profound effect on joint normal deformability.

The basic features summarized above can now be considered in further detail. Upon initial application of load all joints underwent a rapid closure probably triggered by a readjustment of the initial seating condition. The joint walls were then stabilized in an optimum interlocked position and as the normal stresses contimued to increase the rate of

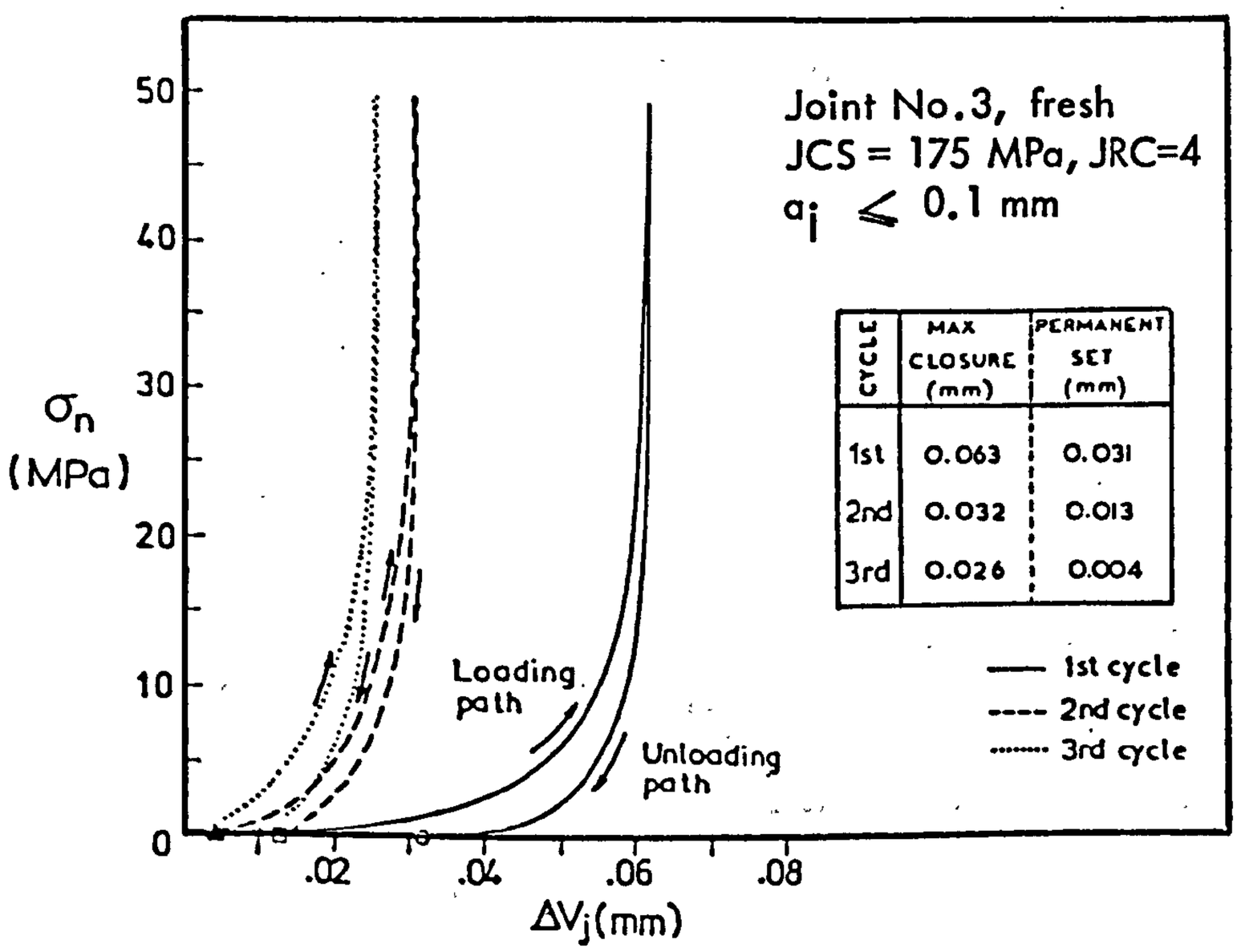

FIGURE 3.17 Normal stress (σ_n) – closure (ΔV_j) curves of fresh and weathered cleavage planes in SLATE under repeated loading cycles.

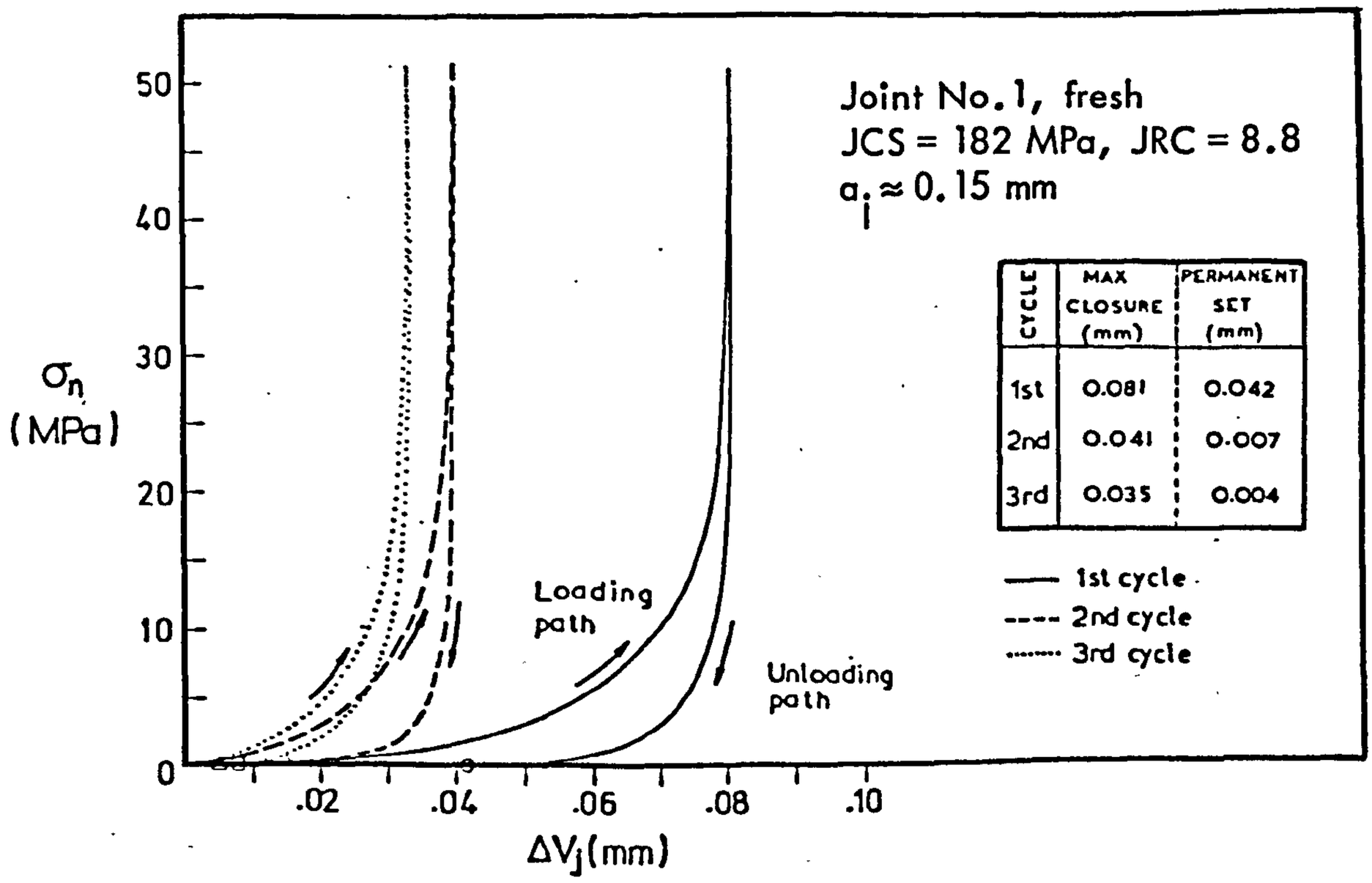

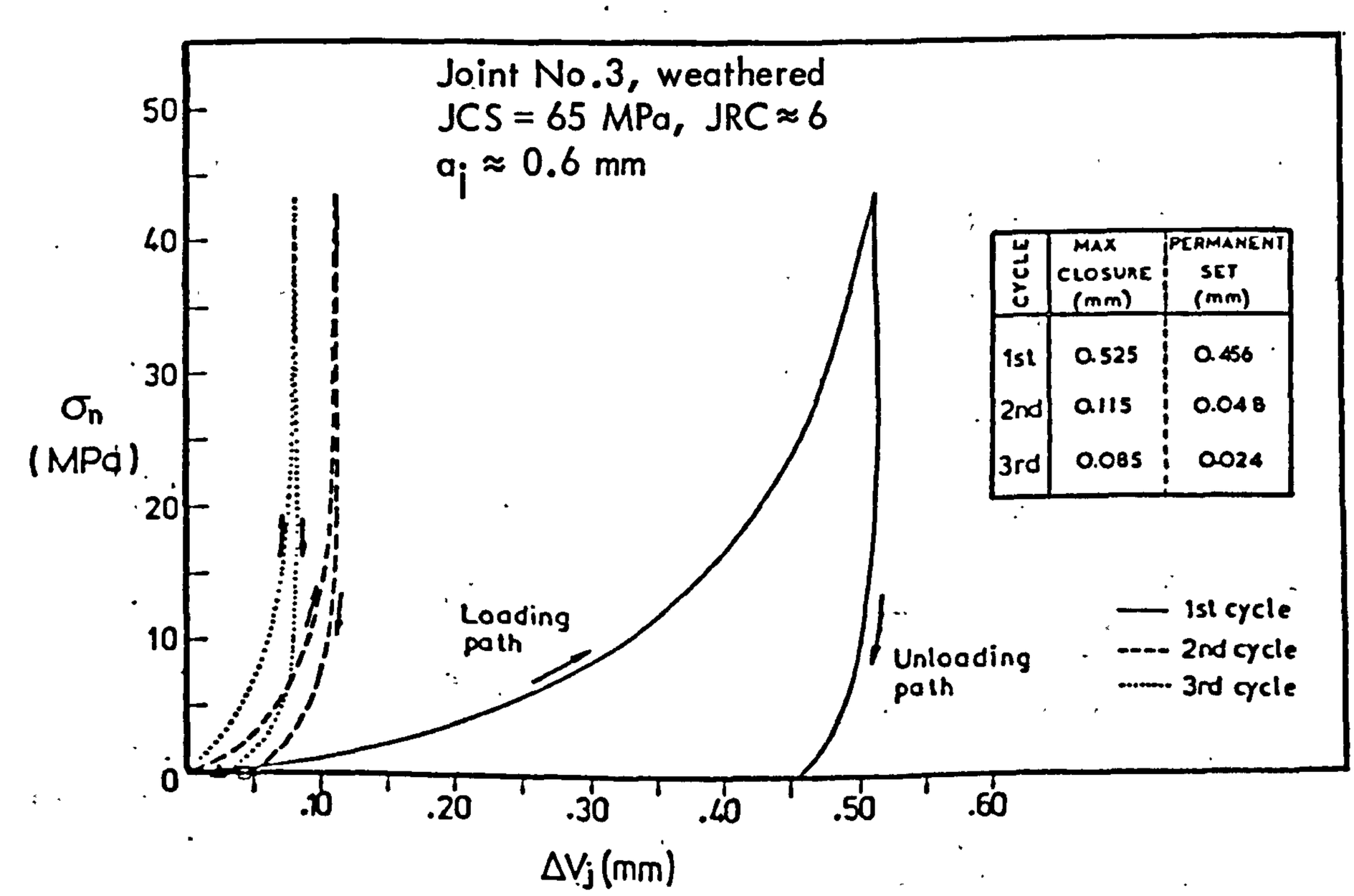

FIGURE 3.18 Normal stress (σ_n) – closure (ΔV_j) curves of fresh and weathered DOLERITE joints under repeated loading cycles.

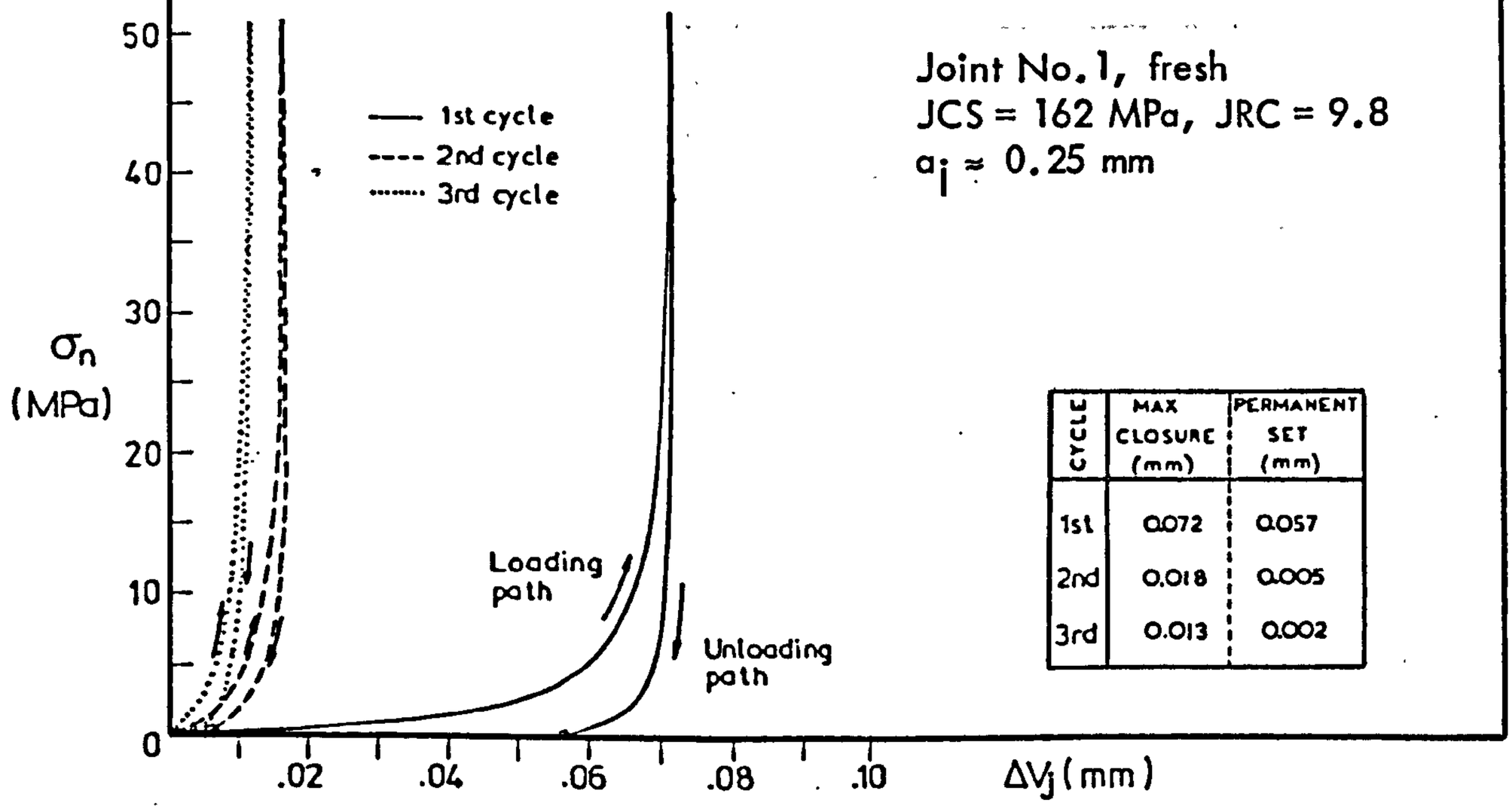

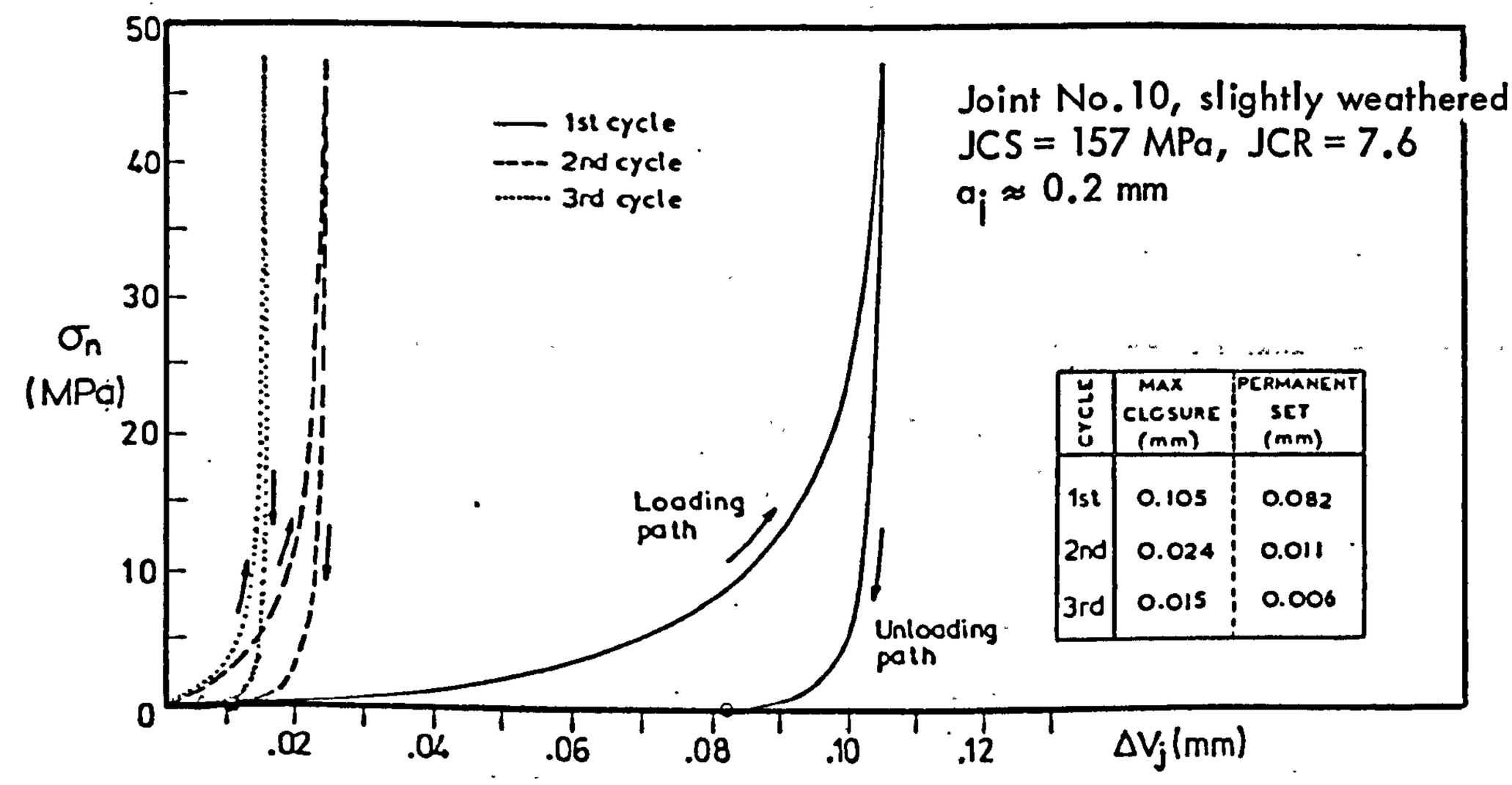

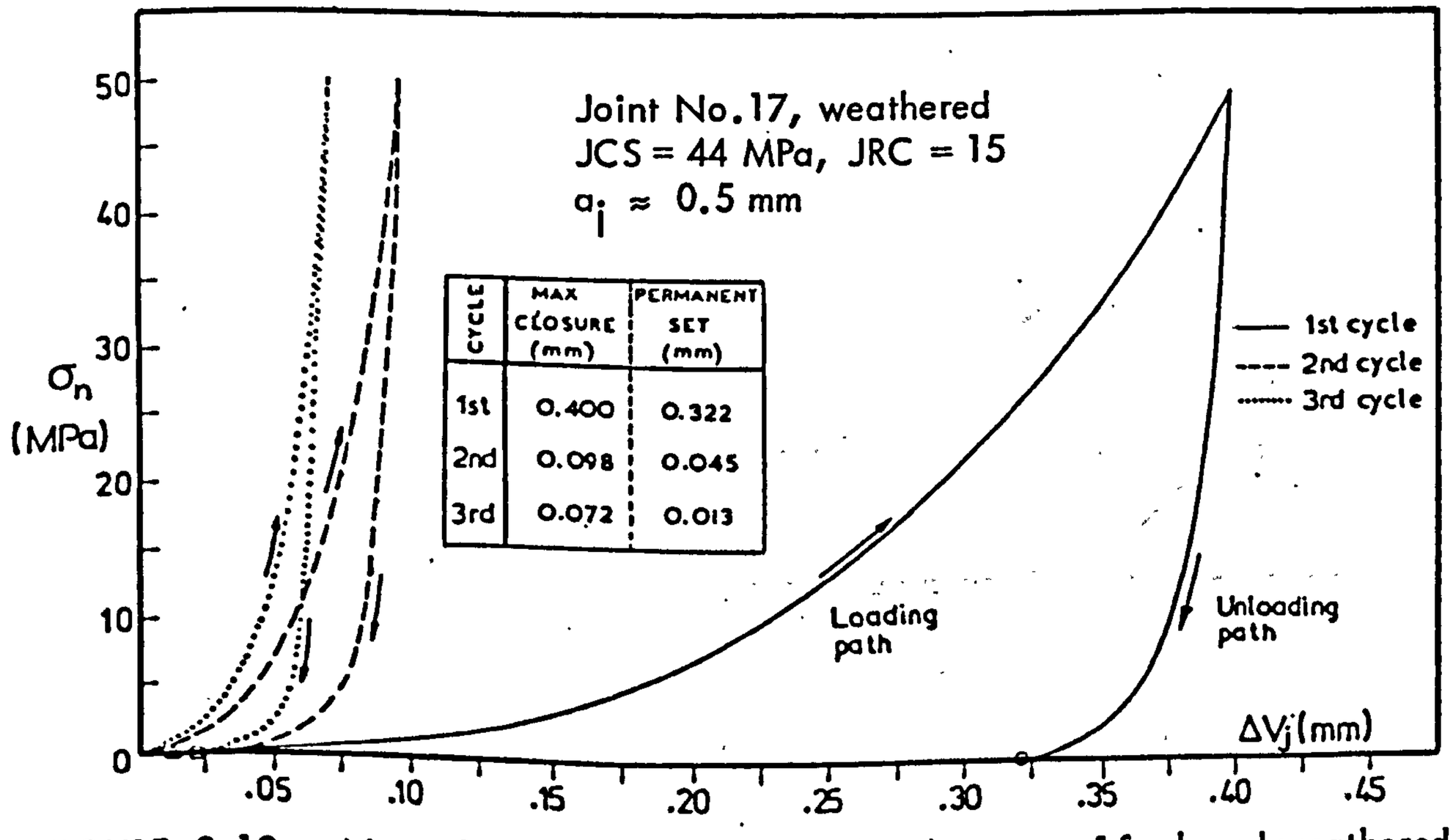

FIGURE 3.19 Normal stress (σ_n) – closure (ΔV_j) curves of fresh and weathered LIMESTONE joints under repeated loading cycles.

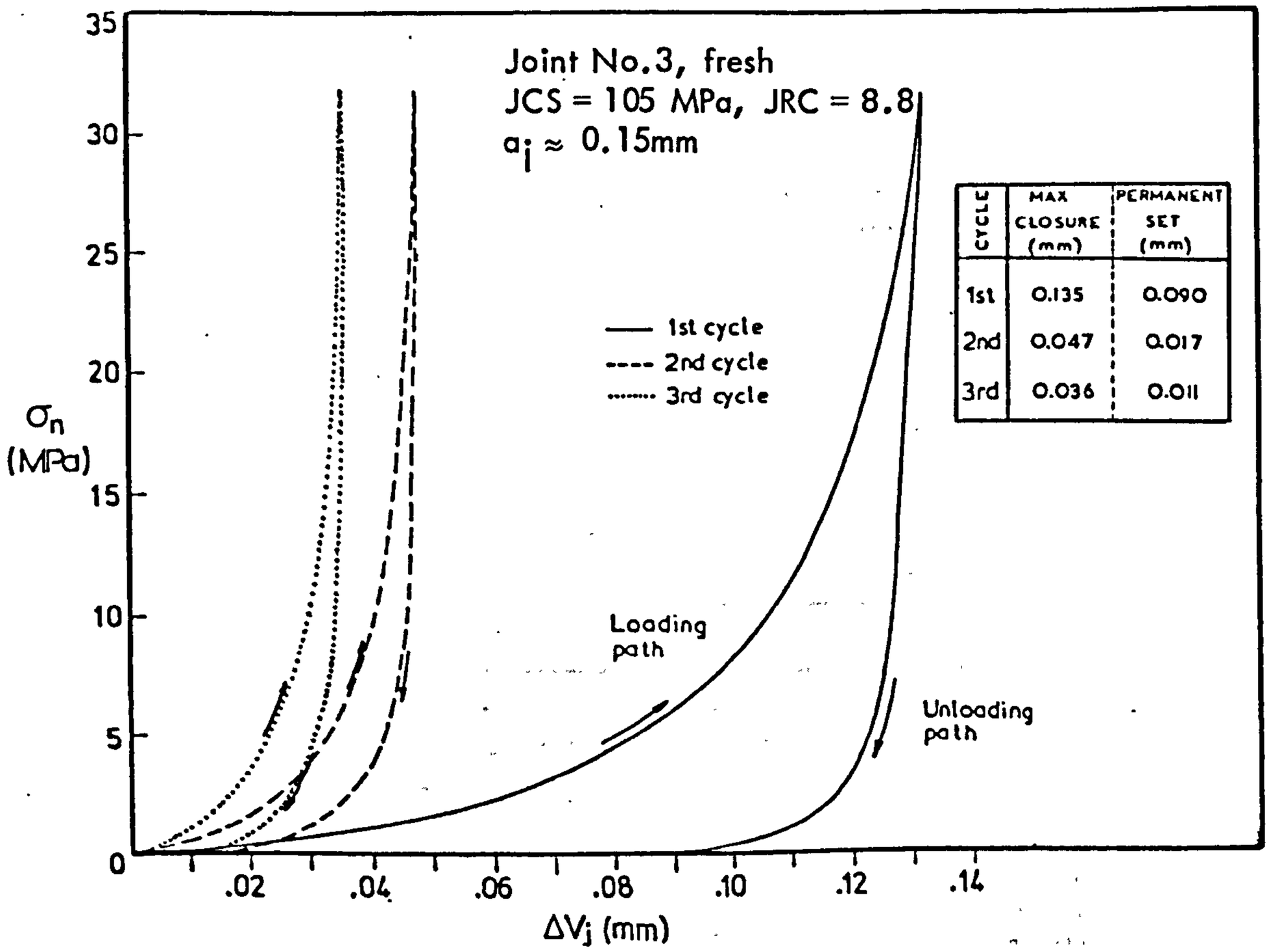

FIGURE 3.20 Normal stress (σ_n) - closure (ΔV_j) curves of fresh and weathered SILTSTONE joints under repeated loading cycles.

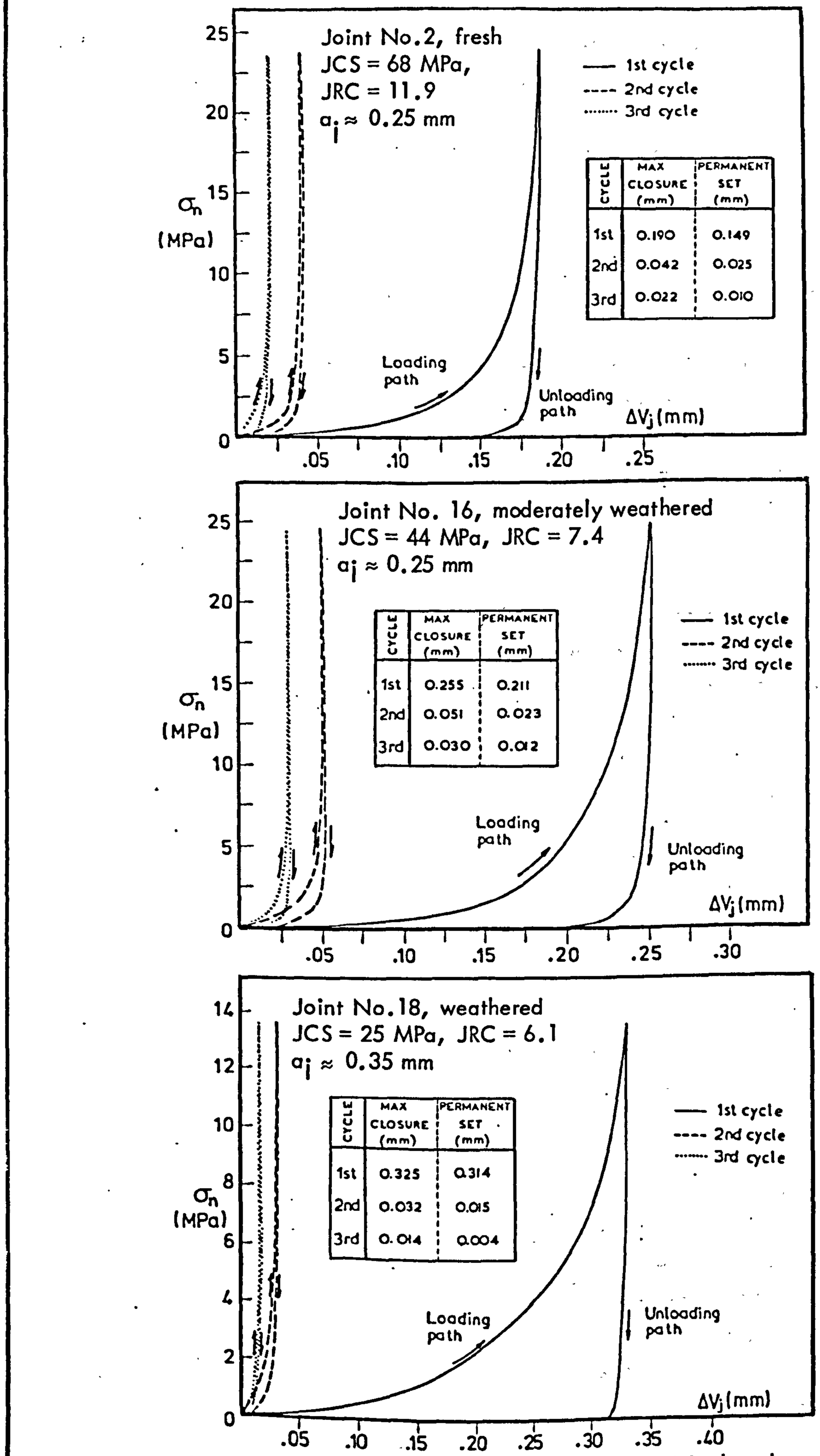

FIGURE 3.21 Normal stress (σ_n) – closure (ΔV_j) curves of fresh and weathered SANDSTONE joints under repeated loading cycles.

closure began to slow down. The stiffness of the joints started increasing drastically as the vertical displacements were controlled by asperities deforming in an effectively confined environment due to the mechanical interlock. Eventually the joints, and especially the unweathered types with very small aperture, reached a stage where very little or no displacement seemed to occur across their interface. The loading path of the closure curves appeared to become asymptotic to a vertical line representing the potential limit of closure. However it should not be implied that at this stage the joint walls will be in perfect contact over 100% of their surface outline. Iwai (1976) found that under σ_n = 30 MPa a small amount of residual flow through perfectly mating extension fractures was still possible. Typical examples of the 'impressions' of contacts obtained by inserting an extremely thin plastic sheet between the interlocked joint walls are shown in Figure 3.22 for two limestone joints (nos. 13 and 9) under the indicated levels of compression. Under the maximum stress of 35 MPa both joints were extremely near their fully closed position. The corresponding contact areas were estimated to amount to approximately 50-60% of the total sample areas. It is interesting to note the uniformity and the size of the areas of contact on the relatively planar joint no. 9, as compared to the more random pattern and variability in the size of contacts on the rough joint no. 13. From similar observations on at least two joints from each rock type it was found that at V_m the contacts represented ~ 40-70% of the total areas.

It is of interest to compare the maximum deformability of the joints in Figures 3.17 to 3.21 in relation to their approximate aperture (a_j). Fresh joints had apertures ranging from ~ 0.10 mm to ~ 0.250 mm. The maximum closures at the end of the first loading ranged between 0.063 mm and 0.190 mm. The ratio of V_m to a_j ranged from ~ 0.29 to ~ 0.90 which agrees with Goodman's comment of $V_m < a_j$; it is also quite clear that the ratio of V_m/a_j is strongly dependent on the joint wall strength (JCS). On a broad basis it can be said that joints of high JCS "closed" by relatively smaller amounts than joints of lower JCS and equal or even smaller aperture. For example, the maximum closure of limestone joint no. 1 (Figure 3.19) with JCS = 162 MPa, JRC = 9.8 and a_j = 0.250 mm was 0.072 mm, whereas the maximum closure of sandstone joint no. 2 (Figure 3.21) with JCS = 68 MPa, JRC = 11.9 and a_j = 0.250 mm was 0.190 mm. The siltstone joint no. 3 (Figure 3.20) with similar roughness (JRC = 8.8) as the limestone joint no. 1 but with lower wall strength (JCS = 105 MPa) and smaller aperture

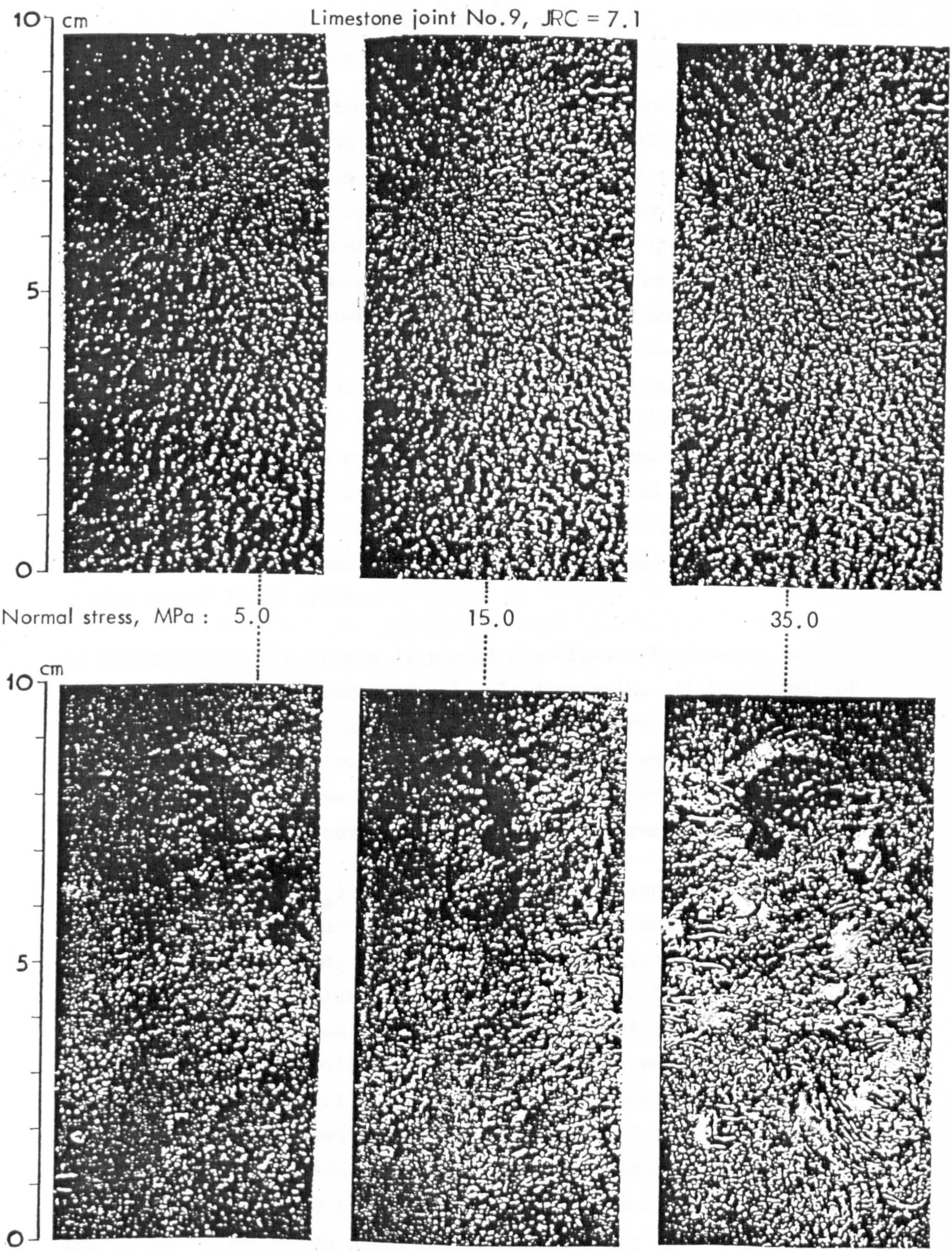

FIGURE 3.22 Illustration of the variation and distribution of the actual contact areas (white coloured features) of two interlocked limestone joints at different compression stages. Under the maximum stresses of 35 MPa both joints were very close to the state of maximum closure

(Technical note : the insert used to obtain the above "impressions" was a 'Melinex' polyester film 12 microns in thickness, manufactured by I.C.I.)

($a_j \sim 0.15$ mm) underwent larger maximum closure ($V_m = 0.135$ mm) than the limestone joint but appreciably smaller than the sandstone joint.

On second and third loading the deformability of the joints was markedly reduced. As can be seen from the V_{max} values listed in Figures 3.17 and 3.21, their difference at the end of the first and third cycles frequently approached a factor of 5 or over.. An explanation of the evident joint stiffening after the first loading may be as follows: after an initial compression under extremely high stresses the joints achieved optimum interlocking and large actual contact area through adjustment of their initial seating condition and asperity deformation. Significant seating readjustments, which would probably account for the largest part of the irrecoverable deformations at the end of the first cycle, would be almost absent in all subsequent loadings. Thus, joint deformation under second and third loading was probably due mainly to elastic deformation of wall asperities, plus some amount of plastic deformation which can explain the small permanent set at the end of those cycles.

On decompression the joints displayed significant hysteresis and initially followed a near vertical unloading path. At low levels of normal stress a certain amount of elastic recovery was observed. Since the component of solid rock deformation has been subtracted from the total deformation of the joint block, the "opening" in the unloading path must be due to recovery of elastically deformed asperities.

The maximum closure (V_m) values of the joints illustrated in Figures 3.17 to 3.21 showed large variation depending on the rock type and weathering state. Weathering effects on the present joint types caused both a decrease of the JCS value and also an increase of the aperture between the walls. The combined result was a significant increase in joint deformability. For a preliminary appraisal of the weathering effects the V_m values from the first loading listed in the respective diagrams can be compared. As shown, weathered joints in slate, dolerite and limestone showed a five- to six-fold increase in V_m as compared to the fresh ones. On the other hand, the maximum closures of the weathered sandstone joint no. 18 and of the fresh joint no. 2 differed only by a factor of approximately 2. That was because the weathered sample had relatively small aperture and the fresh joint underwent significant closure, which was over two times larger than that of the slate, dolerite and limestone joints. There exists therefore a clear interrelationship between V_m,

JCS and a_j and an attempt to combine all these variables in a quantitative form will be discussed in the next chapter.

The particular weathered sandstone joint referred to above exhibited an unusual behaviour. First unloading followed an almost vertical return to zero stress line (Fig. 3.21), the permanent set being virtually the same as the maximum closure. On recompressing the joint showed remarkably stiffer behaviour and the maximum closure at the end of the third loading was over twenty times smaller than that under first loading. The JCS was 25 MPa, the average aperture was placed between 0.3 and 0.4 mm, the total permanent deformation after all three cycles was 0.333 mm and the maximum stresses applied were approximately 14 MPa. It would appear that after the first compression the weak asperities suffered large deformations and were forced into a tight mechanical interlocking. That state was largely maintained through unloading and after the second cycle the joint block behaved virtually like a solid block, with very little contribution from the "bonded" surface to any further deformation. At the end of the tests the specimen was so tightly locked that it seemed as if it would have to be wedged apart. In any case the block was left in its interlocked position and wired safely for direct shear testing.

Mechanical interlocking of the surfaces was observed in most fresh joints from the relative weaker and deformable materials such as the sandstone and siltstone and in all the weathered types. Fresh joints in limestone, dolerite and slate could be freely plucked, although some adhesion between the joint faces was "felt". No visible signs of surface damage were found on any of the joint surfaces.

In the preceding discussions the fundamental characteristics of joint normal deformability as deduced from the compression test results have been reviewed. On a broad basis, there is agreement between the current observations and those reported by other workers (e.g. Gale, 1975; Goodman, 1976; Iwai, 1976) from tests on artificial fractures. On the other hand, the behaviour of the present joints appears to be different from that exhibited by the natural limestone and sandstone joints tested by Hungr and Coates (1978). Those authors interpreted the stress-closure relationship of those joints as close to linear due to previous compression under stresses much higher than those applied in

the tests. Although it is undoubtedly correct that joint deformability, and hence the slope of the closure curves, depends on the loading history, the normal stresses applied in those tests (up to ~ 2.5 MPa) were too low to reveal the complete joint performance. The experience from the present tests shows that much higher stresses are needed to achieve complete joint closure. Hungr and Coates also attributed joint deformability to progressive crushing of asperities, which seems to be an incorrect assumption as far as interlocked joints are concerned. Furthermore, they did not take into consideration the inevitable disturbance of the natural in-situ closure and seating condition of the joints caused by conventional sampling procedures. "Precompression" effects can only be conclusively studied if those conditions are adequately reproduced prior to the test. As far as can be deduced from the current study, the loading history of a joint does not have any effect on the mode of behaviour. Even extremely tightly locked joints, as for instance after two cycles under very high stresses, showed non-linear behaviour.

In the next chapter, the mathematical representation of the interlocked joint closure curves will be investigated, as well as the relative effects of fundamental joint system variables such as aperture, wall strength and roughness in conditioning the amounts of closure and hence joint normal stiffness.

3. Normal deformational behaviour of mismatched joints

The initial idea behind the tests on mismatched joints was to investigate the deformational characteristics and the changes in the normal stiffness when joints have been subjected to a relative shear displacement. The latter condition was approximately simulated by creating misfitted joints supported at a few discrete contact points. Preliminary tests showed that unless the two joint surfaces had a stable seating it would be practically impossible to obtain vertical displacement measurements due to excessive rotation. That was an inherent limitation in the attempted simulation of joints displaced in shear. On the other hand excessive rotations of individual joints blocks in the rock mass are also unlikely due to confinement. The best practical compromise was to create mismatched joints by a small (1 to 2 mm) lengthwise relative translational movement and a slight rotation about a vertical axis, thus achieving a stable initial seating condition.

A total of 24 joints from four different rock types were tested (7 limestone joints, 11 sandstone joints plus another two from a millstone grit formation, 3 siltstone joints and 2 slate fractures). The average vertical joint "uplift" (effectively representing the average aperture across the interface) was estimated by subtraction of the block heights when the intersecting joint was in its interlocked ($\bar{h}_i$) and mismatched ($\bar{h}_m$) positions as indicated below:

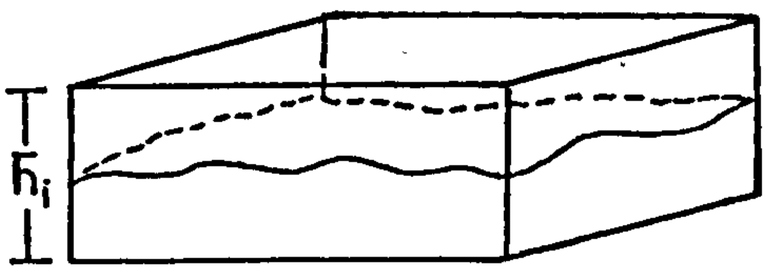

Interlocked joint

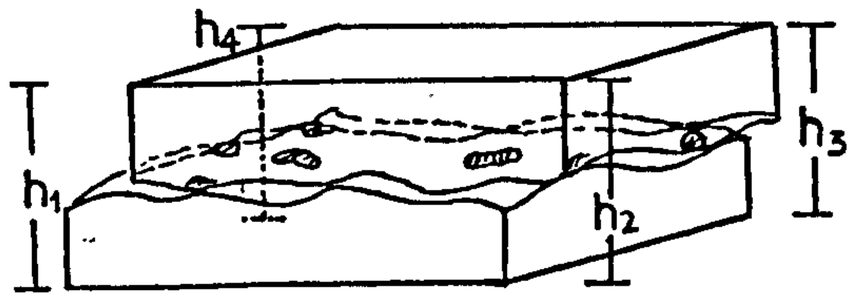

Mismatched joint

$$\bar{h}_m = \frac{h_1 + h_2 + h_3 + h_4}{4}$$

$$a_j = \bar{h}_m - \bar{h}_i$$

The measurements of h_m were taken just before initiation of the compression test. The mismatched joint block was placed in its testing position and a small normal load was applied (~ 0.15 MPa on average). Measurements were then taken by inserting telescopic gauges between the loading platens. The average apertures of the various joint types varied from 0.150 mm to 1.30 mm but the majority were between approximately 0.300 and 0.800 mm.

The load cycling procedure was the same as in the tests of the interlocked joint blocks. The normal loads were incrementally raised to a maximum level and then returned to the initial value. The two dials usually gave dissimilar displacement values and in a few cases the differences between the readings were as much as 30 to 40%. That was mainly due to readjusting movements of the upper block half, especially in cases of highly irregular surfaces, as the delicate initial balance of the mismatched walls was altered under the applied loads. Average displacement values were assumed in the derivation of the stress-deformation curves.

(a) Normal stress (σ_n)-total deformation (ΔV_t) relationships

Typical examples of the mismatched joint block compression curves obtained from the experiments are illustrated in Figure 3.23 for a variety of joints under first loading. As can be seen, the blocks displayed qualitatively similar behaviour as when tested with the joints interlocked, by following non-linear loading paths and showing typical hysteretic recovery and huge permanent sets. The factors which seemingly controlled the magnitude of the vertical displacements were the distance of separation between the joint walls, the surface roughness and the mechanical properties of the contacting asperities.

For an initial appreciation of the quantitative differences between the deformabilities of interlocked and mismatched joints a typical test case is presented in Figure 3.24, where the total deformation (ΔV_t) and closure (ΔV_j) curves of the same limestone joint (no. 10) tested in interlocked (a_j = 0.20 mm) and mismatched (a_j = 0.35 mm) positions are compared. In that particular case the stiffness of the interlocked joint was 3 to 5 times higher than that of the mismatched depending on σ_n.

(b) Normal stress (σ_n)-joint closure (ΔV_j) relationships

As shown in Figure 3.24, subtraction of the solid rock deformation (ΔV_r) from the joint block compression curves (ΔV_t) gave a highly non-linear closure (ΔV_j) curve. The unloading path showed huge hysteresis and a certain amount of elastic recovery. That pattern was typical of the behaviour exhibited by all the joints tested.

The basic mechanics of deformation of the joints can be described qualitatively. Under extremely low loads the upper block half was supported by small, point contacting asperities. As the loading increased those asperities suffered large amounts of deformation and eventually failed under the polarized stresses. The results were a rapid reduction of the original vertical distance of the joint walls, enlargement of the original contact areas, and development of new asperity contacts. The shape and size of the damaged areas indicated that in some of the rough joints, failure of the asperities originally supporting the upper block half may have triggered a small amount of translational movement, thus upsetting the initial balance. Once the walls had readjusted themselves into a new "stable" seating condition,

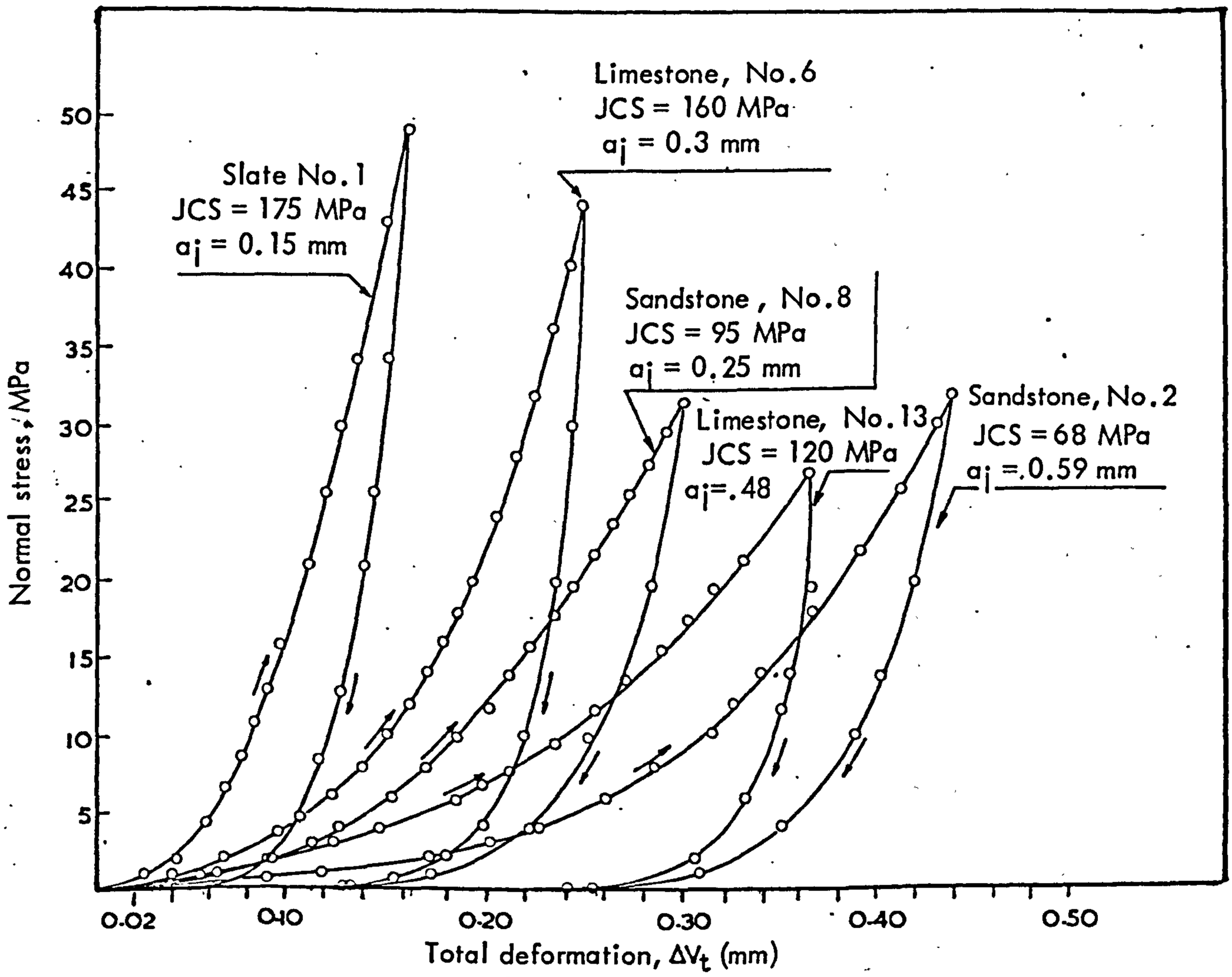

FIGURE 3.23 Normal stress - total deformation curves of mismatched joint blocks under the first loading

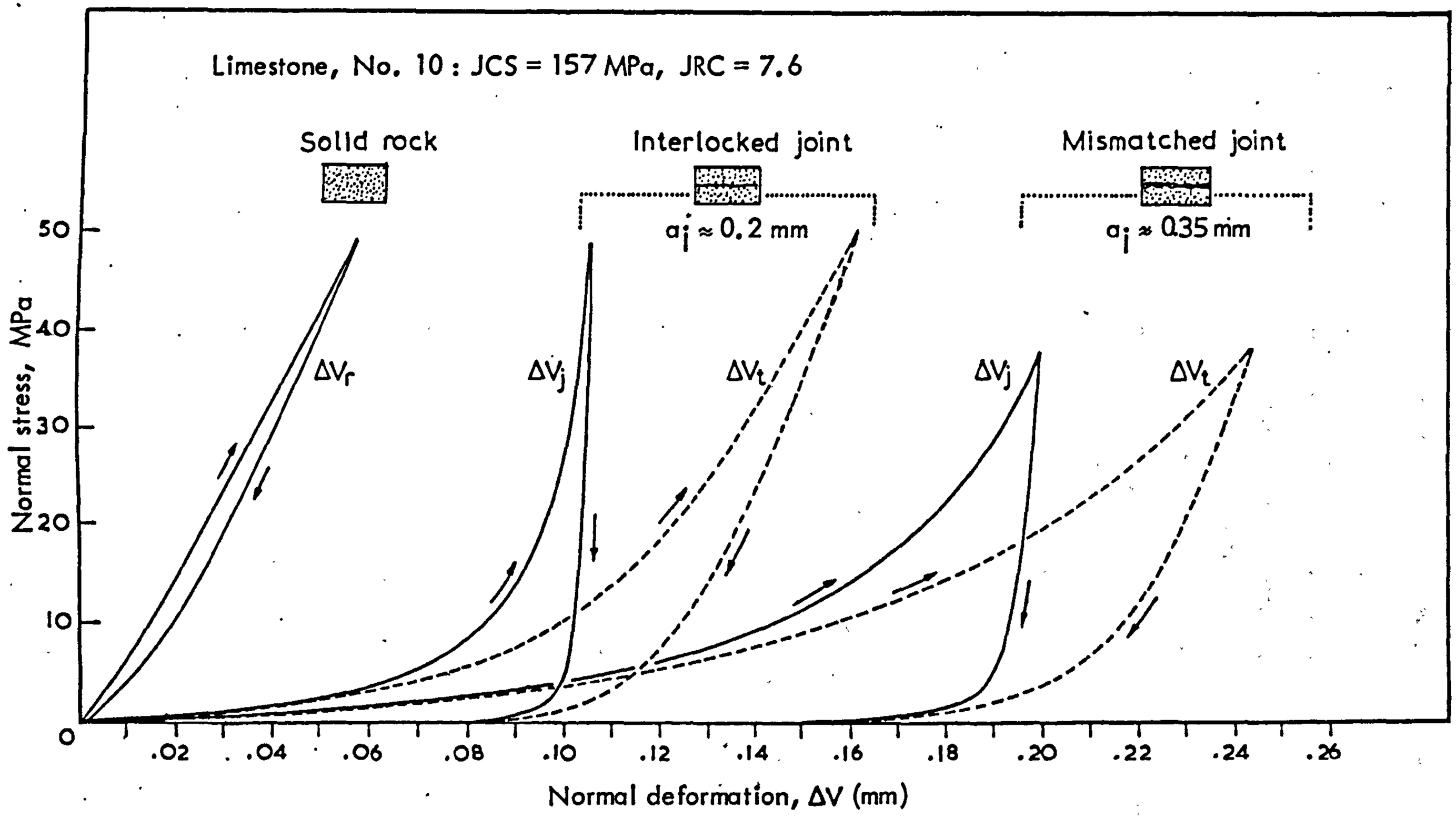

FIGURE 3.24 Comparison of total deformation (ΔV_t) and net closure curves ($\Delta V_j = \Delta V_t - \Delta V_r$) from the first loading cycle of the same joint tested in fully interlocked and mismatched positions.

further increase in the stresses caused proportional enlargement of the contact areas as the large surface protrusions deformed elastically or plastically, the rate of closure began to slow down, and the stiffness of the joint started increasing rapidly.

The distribution and extent of surface damage found on different types of joints at the end of testing is shown in the photograph of Figure 3.25. As would be expected, damaged areas on rough undulating joints were mainly concentrated on the slopes of the large irregularities (e.g. see limestone joint nos. 13 and failed joint no. 1). A relatively more uniform distribution of damaged contacts was observed on planar surfaces, e.g. as shown by the limestone joint no. 9 and sandstone joint no. 13. Planar joints lacking appreciable small scale roughness features such as the slate cleavage fractures, did not have any visible signs of damage.

As seen from the closure curves presented in Figure 3.26, the mismatched joints did not reach the closure state as when tested fully locked. Maximum stresses usually approached $\frac{1}{4}$ of JCS. Even in cases where the stresses were increased to $\sim \frac{1}{2}$ of JCS (e.g. sandstone joint no. 2 in Fig. 3.26), complete closure had not been achieved. In quite a few tests raising of the loads to such high levels resulted in block failure by tensile splitting (e.g. limestone joint no. 1 and sandstone joint no. 6 in Fig. 3.25 failed during the second loading under σ_n between $\frac{1}{3}$ and $\frac{1}{2}$ of JCS). The closure curves from repeated loadings were also non-linear but much steeper, since the vertical displacements after the first cycle were probably mostly contributed by the deformation of the asperities across their enlarged areas of contact. The curves from the third cycle applied on the particular joints are included in Fig. 3.26.

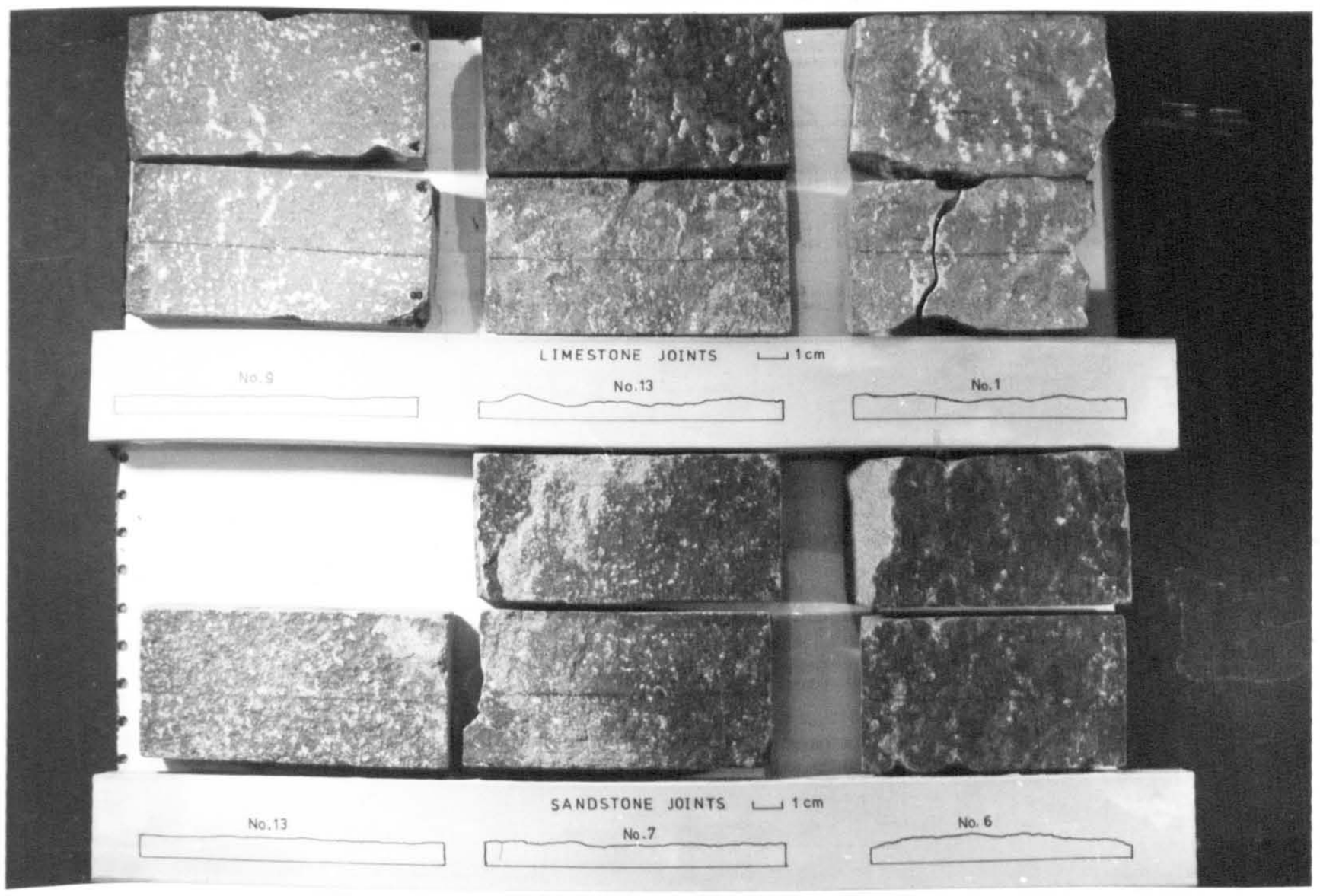

FIGURE 3.25 Photograph illustrating the distribution and extent of asperity damage (light coloured areas) found on the surfaces of mismatched joints at the end of the compression test. Maximum applied normal stresses were approximately equal to $\frac{1}{4}$ of the uniaxial compressive strength of the rock material.

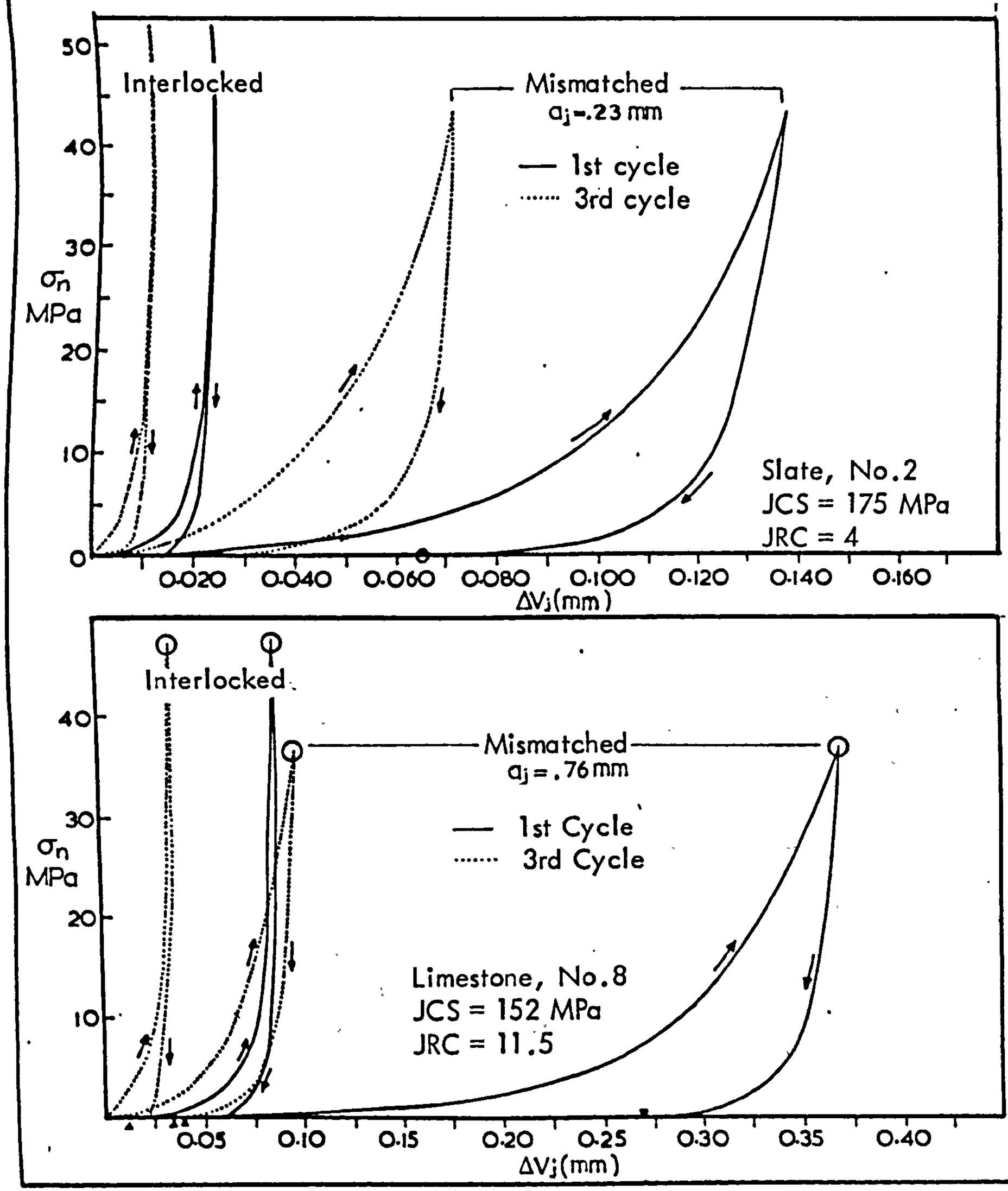

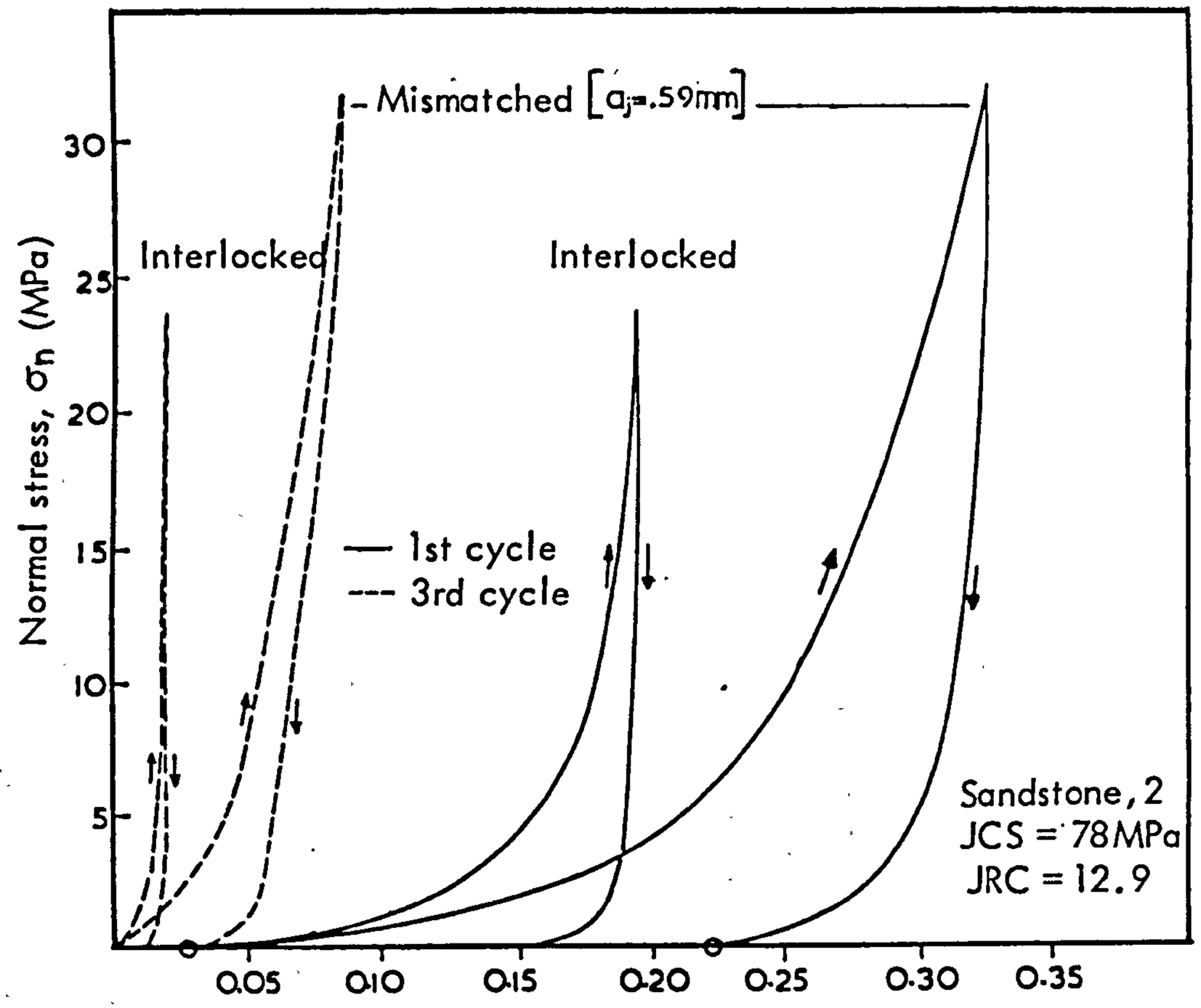

FIGURE 3.26 Normal stress – joint closure curves of mismatched specimens under the first and the third loading cycles and comparison with the corresponding curves from the interlocked tests.

3.2.4 Fundamental aspects of joint shear deformability in the pre-peak range

The shear deformation characteristics up to mobilization of peak shear strength was studied for a range of fresh and weathered joint types. The purpose of those tests was to compare the normal and shear stiffness of joints at various stress levels and to examine closely the shear stress-displacement relationship in the pre-peak region.

1. Experimental procedure

The limitations of the multistage testing procedures have already been outlined in section 3.2.2(5). The present testing sequence consisted of firstly shearing each joint under the lowest normal stress level which was usually ~ 0.25 MPa. Once the peak shear strength was reached, the shear load was released, the joint halves reassembled, and a new run performed under a higher normal stress. The chosen increments of σ_n were approximately 0.25, 0.50, 1.00 and 2.00 MPa, with small variations depending on the specimen size. A "normal" testing procedure was followed for the weathered sandstone joints and slate cleavage planes since the available specimens had very similar surface geometry.

2. Shear stress-shear displacement relationships

Typical examples of the stress-displacement relationships up to peak shear strength for a variety of joint types are illustrated in Figures 3.27 and 3.28, and the following observations can be made:

(i) The shear stress (τ)-displacement (d_n) relationships show that all joints exhibited non-linear behaviour to a greater or lesser extent. Under each level of normal stress the shear stiffness (expressed as the tangent value) varied from a maximum value at extremely low shear stress to a minimum at the peak stress region.

(ii) The amounts of displacement preceding peak shear strength were generally larger for the weathered joints, due to the poor interlocking and relatively even geometry. Depending on the level of normal stresses, the peak shear stiffness (secant values) of fresh and weathered joints of reasonably similar roughness differed by factors ranging from ~ 2.0 to ~ 3.5. An extreme case was

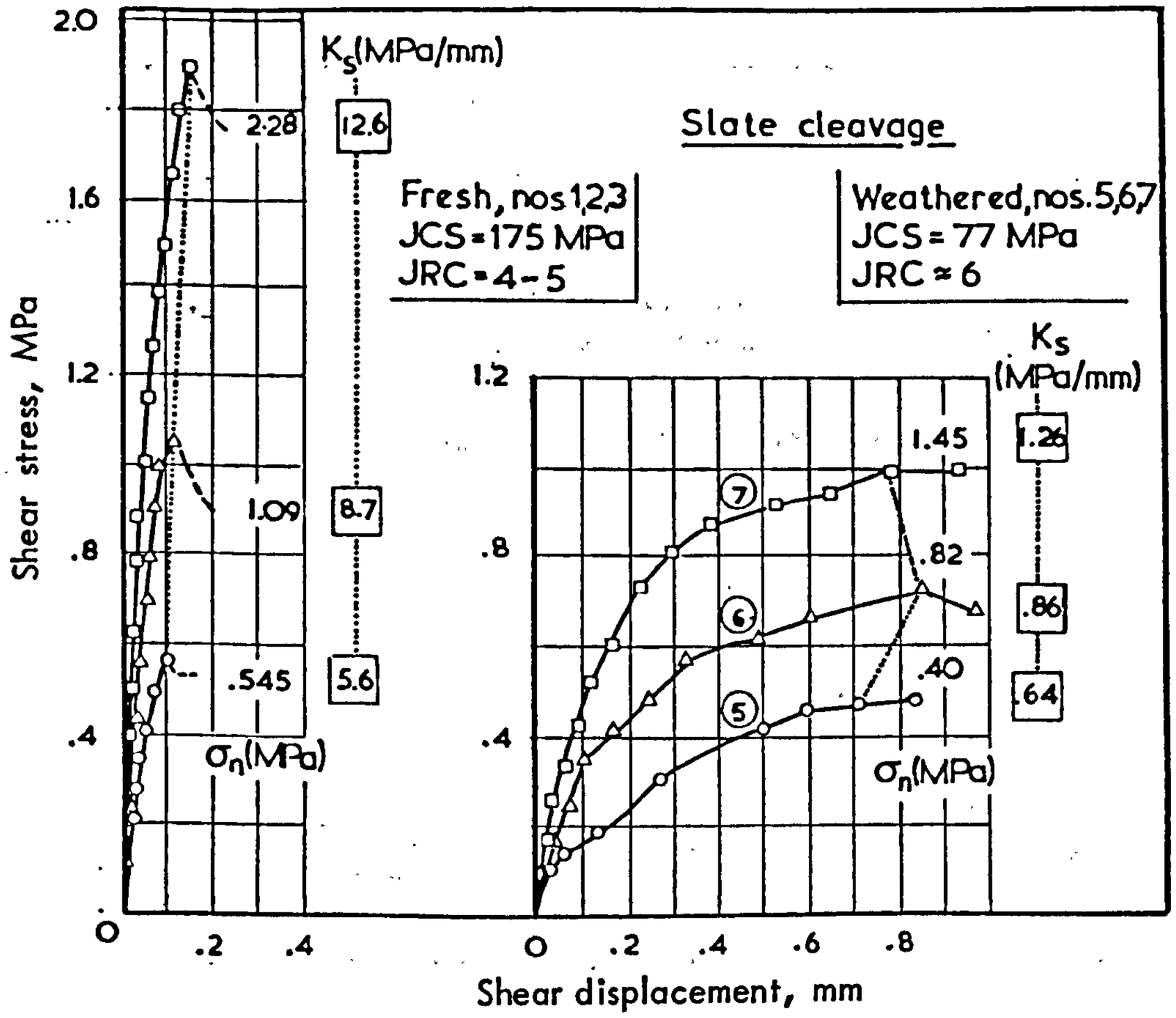

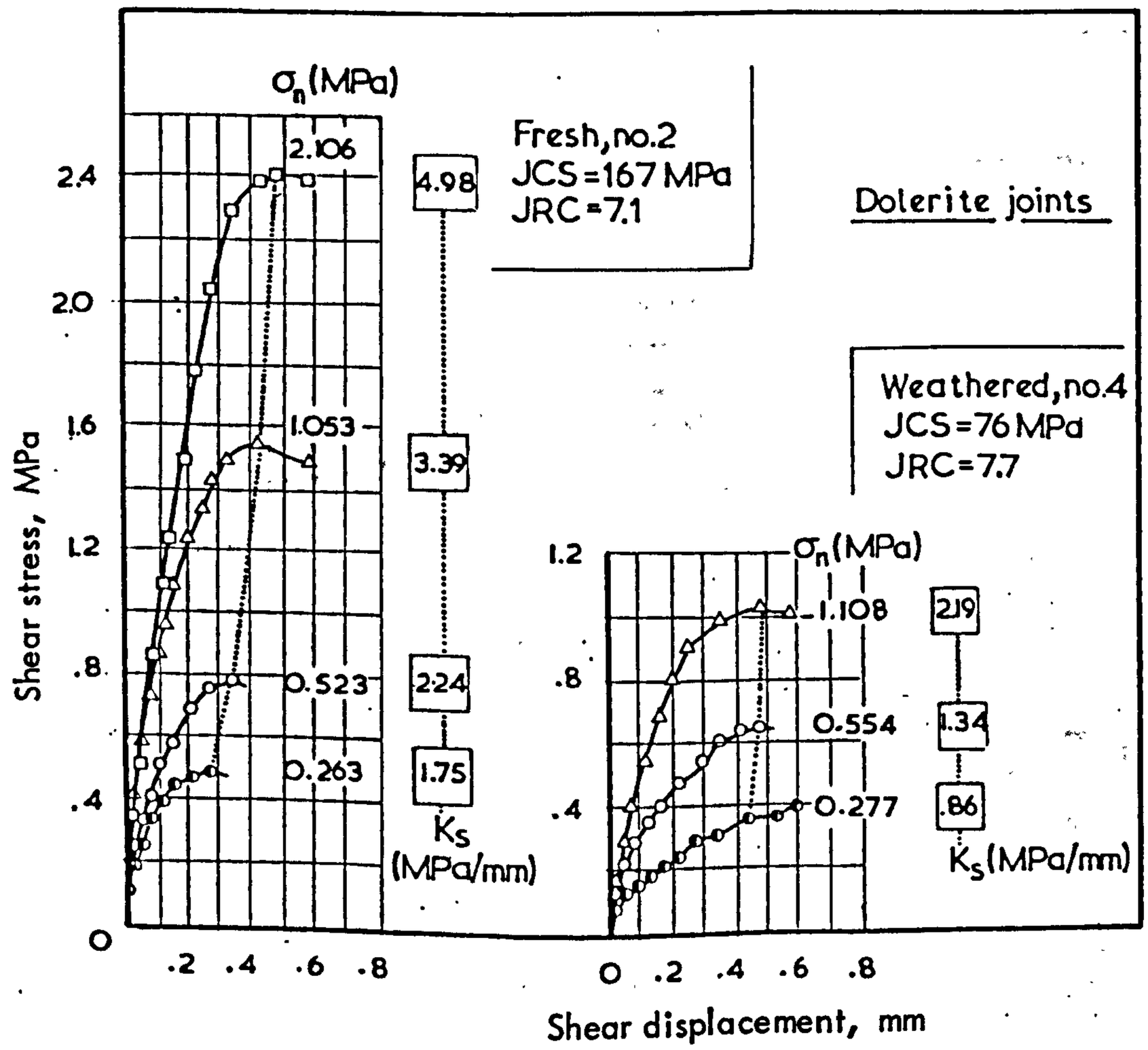

FIGURE 3.27. Shear stress – displacement relationships obtained from fresh and weathered joints in slate and dolerite at various levels of normal stress (σ_n). The included K_s data have been derived as secant peak values.

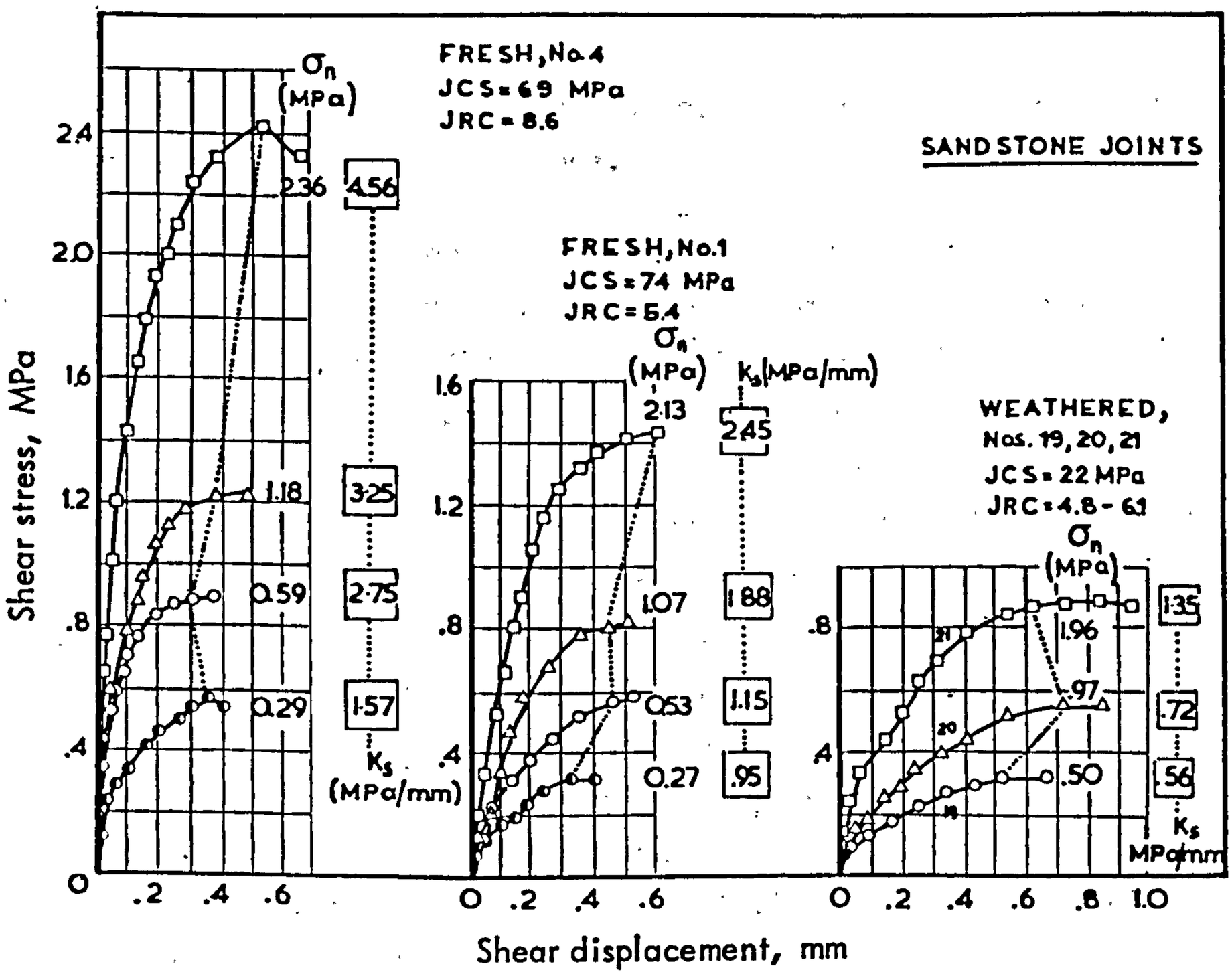

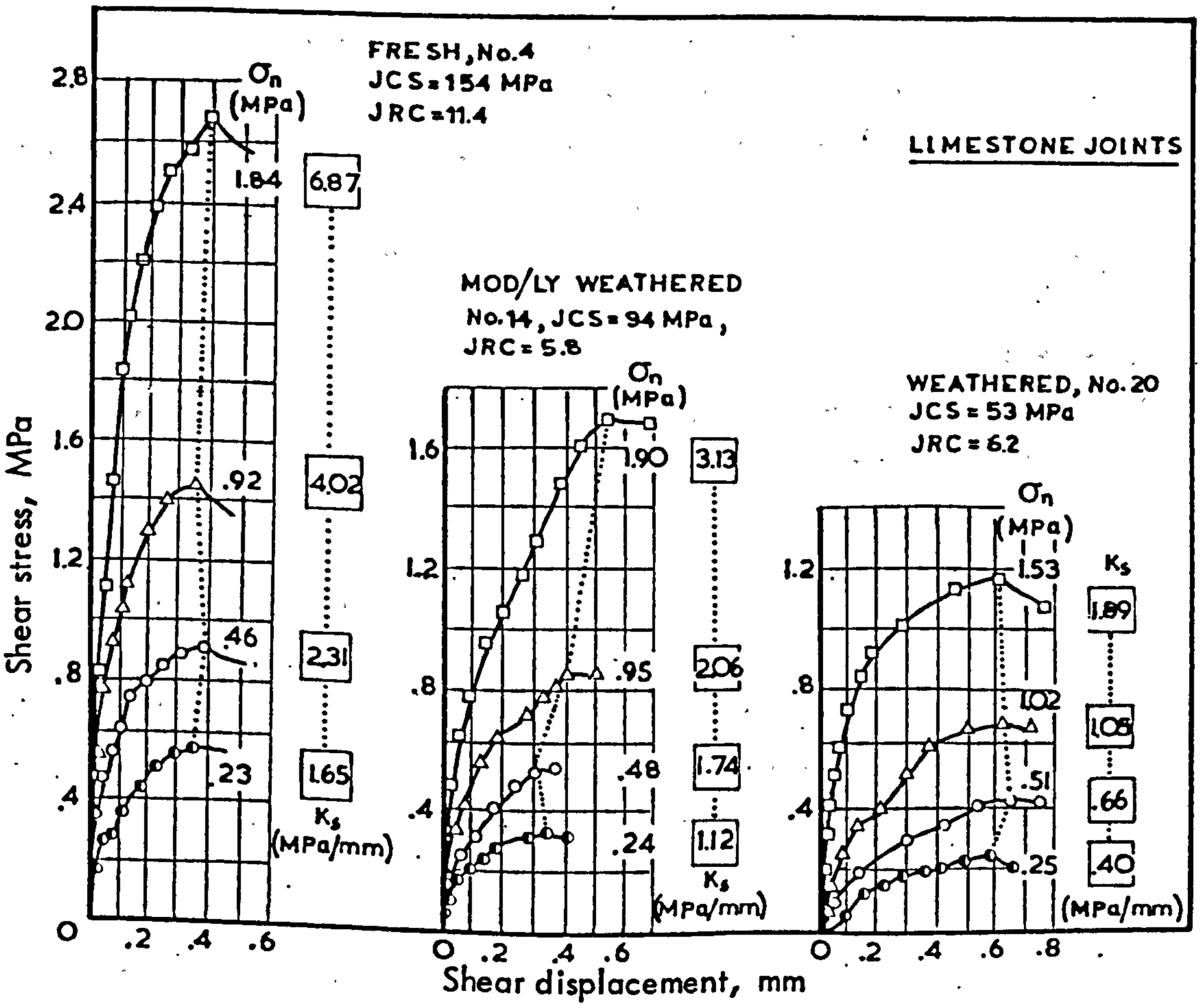

FIGURE 3.28. Shear stress – displacement relationships obtained from fresh and weathered joints in sandstone and limestone at various levels of normal stress. The included K_s data have been derived as secant peak values.

presented by the slate cleavage planes, which showed approximately one order of magnitude difference.

(iii) The peak shear stiffness (K_s) depends on the level of normal stresses applied. Generally, peak shear displacements varied by a relatively small amount compared to the increase in shear strength under increasing σ_n. Overall, the behaviour of this type and size of joints seems to agree better with the conceptual "constant displacement" model referred to in Section 1.1.4 of part one. Within the present range of σ_n the calculated secant peak K_s values increased by factors varying from ~3 to ~8 depending on the joint type and degree of weathering, although the exact variation under high σ_n cannot be known with certainty due to the multistage testing (except for the weathered slate and sandstone specimens). For a ready appraisal of the effects of weathering and normal stress on the peak shear stiffness a few typical test data have been listed in Table 3.12.

The fundamental features of joint peak shear deformability described above are commonly observed in laboratory test cases found in the literature (e.g. Guiseppe 1970, Hungr and Coates 1978). The practical relevance of shear stiffness data as extracted from small scale testing seems to depend on the size of the joints involved in a particular problem. The tests on model joints reported in part two have demonstrated that as the joint length increases the peak shear strength drops considerably whereas the peak shear displacements increase. A discussion on the scale dependency of K_s has been included in the next chapter.

Another factor which significantly affects the peak strength and indirectly so the peak shear stiffness of a joint is its past loading history. Barton (1973) demonstrated that joints pre-compressed under normal stresses considerably higher than those operating in a shear failure display higher peak resistance than if sheared under the same σ_n but without previous compression. The term joint "overclosure" was then introduced as equivalent to the term "overconsolidation" used in soil mechanics. An extreme example of the potential importance of "overclosure" effects was experienced during a shear test on a pre-compressed joint.

TABLE 3.12

Comparison of peak shear stiffness (K_s, secant values) data from fresh (F) and weathered (W) joints at different levels of normal stress (σ_n).

Joint Type	σ_n (MPa)	K_s (MPa/mm)	σ_n (MPa)	K_s (MPa/mm)
Slate: nos. 1 & 2, JRC = 4-4.5, JCS = 175 MPa (F)	0.54	5.60	1.09	8.7
Slate: nos. 5 & 6, JRC = 6-6.5, JCS = 77 MPa (W)	0.40 (no.5)	0.64	0.82 (no.6)	1.26
Dolerite: no. 2, JRC = 7.1, JCS = 167 MPa (F)	0.26	1.75	1.05	4.98
Dolerite: no. 5, JRC = 7.7, JCS = 76 MPa (W)	0.28	0.86	1.11	2.19
Sandstone: no. 4, JRC = 8.6, JCS = 69 MPa (F)	0.59	1.57	2.36	4.56
Sandstone: nos. 19 & 21, JRC = 5-6, JCS = 22 MPa (W)	0.50 (no.19)	0.56	1.96 (no.21)	1.35
Limestone: no. 4, JRC = 11.4, JCS = 154 MPa (F)	0.23	1.65	1.84	7.37
Limestone: no. 20, JRC = 8.2, JCS = 53 MPa (W)	0.25	0.40	1.53	1.89

As recalled from section 3.2.3, normal loading of a weathered sandstone joint under stresses just exceeding 50% of JCS (= 25 MPa = uniaxial compressive strength of intact rock) resulted in a very tight mechanical interlocking of the surfaces. The joint block was mounted on the portable shear box and a normal stress of ~ 2.0 MPa was applied, thus creating an overclosure ratio of approximately 1:7. As the increments of shear load were applied the deformations directly recorded by the two gauges showed very small increases. Then at approximately 1.4 MPa a sudden drop in the shear load was observed, which at first was thought to be due to the dislocation of the "bonded" walls. When the sample was removed from the apparatus it was found that shear failure had taken place through the intact material, along a subhorizontal plane located a few millimeters above the joint and near to the contact of the concrete mould with the joint block. The failed specimen is shown in the photograph in Figure 3.29, together with the stress-displacement curve up to failure. The curve of a similar but "normally"-loaded joint has also been included for comparison.

It appeared, therefore, that the shear resistance and stiffness of the "overclosed" joint had increased to the level of the intrinsic shear strength and shear modulus of the solid rock. The possibility of the influence of some external factor causing severe reduction in the mechanical strength of the material was considered. As the properties of the weathered sandstone were very much affected by the moisture content, it was firstly suspected that the material might not have completely dried after the moulding process and hence had much lower strength; however, measurements of the moisture content proved normal. Another possibility was that an unseen crack near the edges of the block opened under the applied shear loads and then propagated along the full block-half length, but that could not be checked.

The above extreme experimental case demonstrates the important role of the loading history of a joint on its peak resistance and deformational performance. Weathered joints would generally be more sensitive to "overclosure" effects as the weak and deformable asperities could achieve better mechanical interlocking than in cases of fresh joints. It would of course be unrealistic to expect that joints in weathered rock masses could be even half as tightly locked as the one tested.

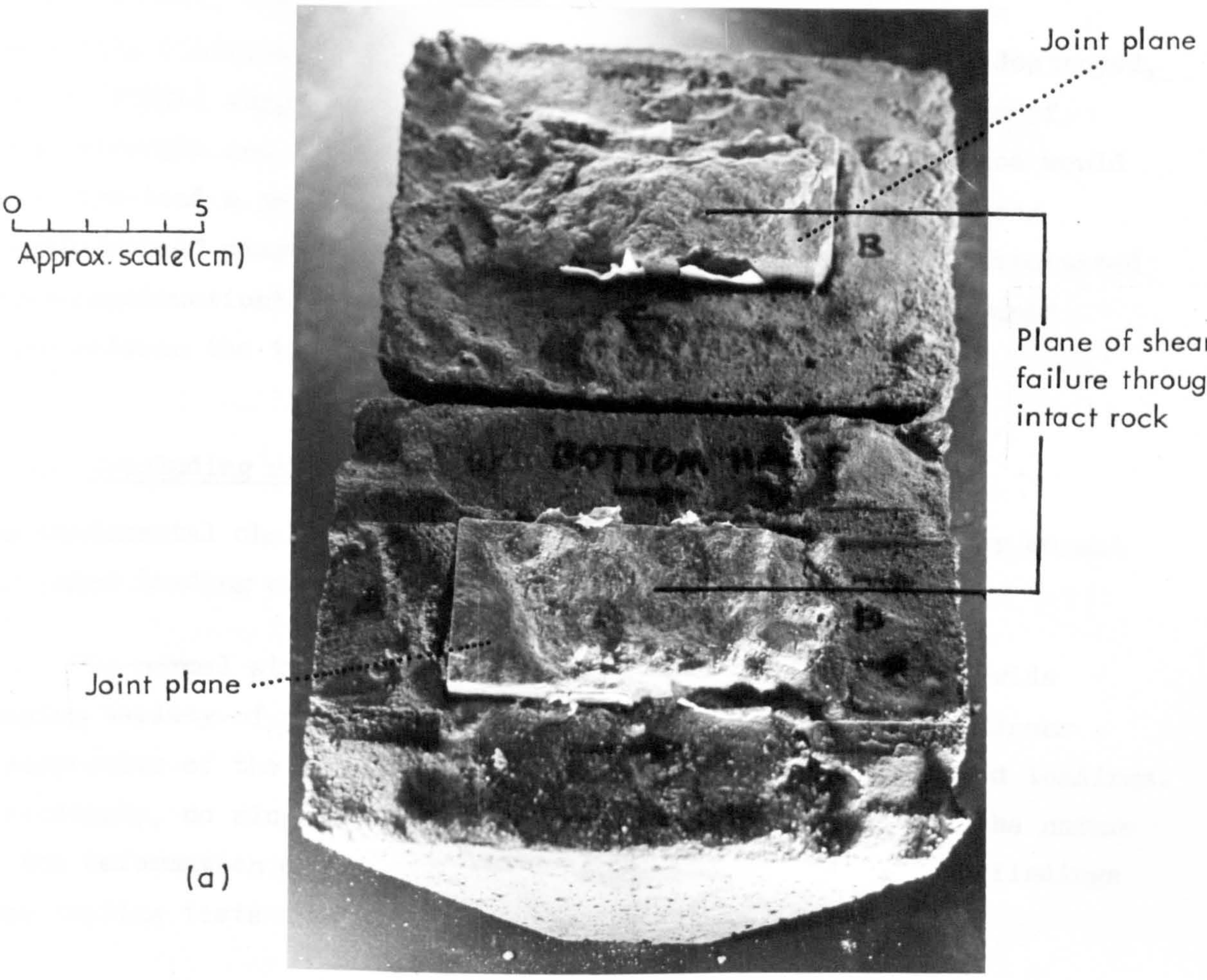

FIGURE 3.29 (a) Photograph illustrating the shear failure of the weathered sandstone joint No. 18 previously subjected to compression under maximum stresses of ~ 14 MPa.

(b) Comparison between the shear stress - displacement curves from the above pre-compressed joint and a similar one normally-loaded

Since, however, the joints sampled by conventional methods are inevitably disturbed and any natural "overclosure" effect is destroyed, Barton (1973b) suggested that in an experimental determination of shear strength and deformation properties a more valid practice would be to pre-load a joint under the current in-situ normal stresses ("undisturbed" stage) before conducting the test under the anticipated "post-construction" stress levels, provided that an "overclosure" ratio between the two stages does exist.

3.2.5 Concluding remarks

The fundamental characteristics of rock joint deformation under normal and shear loading conditions can be summarized as follows:

(i) The normal stress-normal deformation relationships of a wide ranging variety of natural interlocked joints are highly non-linear irrespective of the rock and joint type and throughout repeated loadings. Accordingly, no single value of K_n can uniquely characterize the nature of the deformation curve. This is in agreement with previous findings from loading tests on artificial rock fractures.

(ii) The derived stress-closure curves indicate that joints under compression gradually reach a state of maximum closure. The fundamental parameter of maximum joint closure is a unique joint property directly dependent upon the previous stress history. Under repeated loadings the value of Vm decreases significantly.

(iii) Preliminary quantitative considerations suggest the existence of a potential relationship between maximum closure, aperture thickness and joint wall strength. It has been verified that the amount of maximum closure is generally lower than the average thickness of joint aperture. For the present range of joint types and under maximum applied stresses approaching $\frac{1}{3}$ to $\frac{1}{2}$ of the uniaxial compressive strength of the intact rock, the closure/aperture ratio ranged between 0.3 and 0.9 depending on the joint wall strength. The actual contact areas at the state of maximum closure generally ranged between 40% and 70% of the total sample area.

(iv) Upon unloading, joints undergo strong hysteresis and display large permanent sets. A certain amount of the maximum closure may be recoverable due to the rebound of elastically deformed asperities. Hysteresis

and inelasticity are found to persist after at least three loading cycles.

(v) Artificially mismatched point-contacting joints exhibit typical non-linear stress-deformation behaviour. Under maximum applied stress ~ $\frac{1}{4}$ to $\frac{1}{3}$ of the rock compressive strength the mismatched joints had still not reached the characteristic maximum closure state of interlocked surfaces. The differences between interlocked and mismatched joint normal stiffness can be significant depending on the amount of joint opening and the joint wall strength.

(vi) The shear stress-shear deformation relationships of joints in the pre-peak range reveal variable non-linear behaviour. Non-linearity is more profound in cases of weathered joint surfaces, and least in cases of tightly interlocked fresh joints.

(vii) Non-linear behaviour implies that under a given normal stress the joint shear stiffness (K_s) will depend on the level of shear stress, in addition to a marked normal stress dependency. Joint surface variables such as roughness and weathering state have a significant influence on K_s. The relatively unimportant effects of normal stress on peak shear displacement suggest that the shear stress-deformation behaviour of natural joints may be closer to the conceptual 'constant displacement' model of John at least within the range of normal stresses of engineering interest.

(viii) Experimentally determined values of shear stiffness can be seriously affected by additional deformations due to uncontrolled movement of the external measuring point. This has been experienced on the portable shear apparatus and when testing dilatant joints. Even when the displacement measuring devices are aligned as closely as possible to the plane of shearing the measured displacement can be up to 2-3 times higher than displacements obtained directly from the joint specimen itself.

(ix) Overclosure effects will have a significant influence on joint shear strength and deformation, and hence on joint shear stiffness.

CHAPTER 3.3

ANALYSIS OF THE EXPERIMENTAL RESULTS

3.3.1 Introduction

In the review of typical experimental results reported in Chapter 3.2 the modes of joint deformation have been considered. In this chapter joint deformability will be studied from the quantitative point of view. The contents can broadly be divided into three main sections: (1) analysis of the stress-deformation curves of joints under normal and shear loading conditions; (2) processing of the experimental results and derivation of stiffness parameters; and (3) study of the variations in joint stiffness and of its relative dependence on fundamental variables defining the strength and geometry of the joint system.

3.3.2 Analytical expression of the stress-deformation relationships

The normal loading tests on joints have demonstrated that the normal stress-closure relationships for a range of natural, unfilled joint types are invariably non-linear throughout repeated loadings. Significant non-linearity was also observed in the shear stress-displacement curves of joints in direct shear. Some workers have attempted to establish an analytical representation of the stress-deformation curves. Shehata (1971, quoted in Sharp and Maini, 1972) has described the stress-closure relationship as being semi-logarithmic but Goodman (1974) has advanced a hyperbolic model. Hyperbolic functions have also been suggested for the description of the shear stress-displacement curves in the pre-peak range (Clough and Duncan, 1969, Hungr and Coates, 1978).

1. Normal stress-closure curves (joints interlocked)

At first, closure data from different joint types were plotted against logarithmically scaled normal stress. Typical examples of the relationships obtained for the loading paths from the first and third loading cycles are shown in Figure 3.30. As can be seen, the semi-log relationship fitted the data usually within an intermediate range of normal stresses showing very poor linearity in the low and high stress

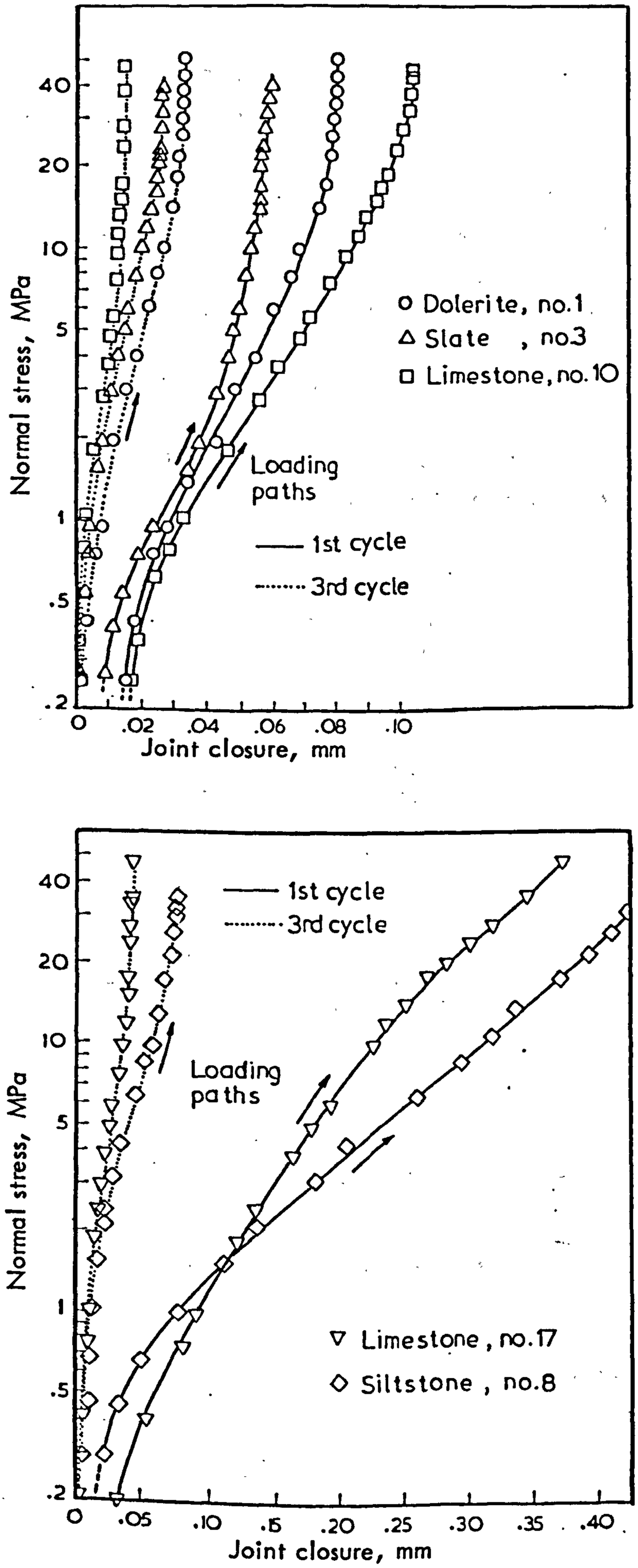

FIGURE 3.30 Semi-logarithmic plots of normal stress versus joint closure

regions. The plots for the loading paths from the third cycle were generally linear over a wider range of normal stresses. The plot for the weathered siltstone joint no. 8 showed linear relationship except only at low σ_n, whereas the plot for the weathered limestone joint no. 17 displayed extremely poor linearity virtually over the full range of stresses. Similar plots for the unloading paths were found to be non-linear over a large range of stresses. It seemed therefore that the validity of the semi-logarithmic expression depended on the joint type, the stress history and the loading mode.

Goodman (1974) proposed the empirical hyperbolic function $\sigma_n = [\Delta V_j/(V_m - \Delta V_j)] \sigma_i + \sigma_i$, which may be rearranged in the following linear form:

$$\Delta V_j = V_m - (V_m \sigma_i) \frac{1}{\sigma_n} \qquad 3.5$$

Plots of ΔV_j versus the reciprocal of normal stress for the same joint types as above, showed strong non-linearity except for in the low stress region as illustrated in Figure 3.31. An alternative version of that function was given by Goodman (1976) in the following dimensionless logarithmic form:

$$\frac{\sigma_n - \sigma_i}{\sigma_i} = C \left(\frac{\Delta V_j}{V_m - \Delta V_j}\right)^t \qquad 3.6$$

where C and t are constants.

The logarithmic relationships of dimensionless stress versus dimensionless deformation for the previous joint types and a sandstone joint are shown in Figure 3.32. The closure (ΔV_j) data represent the loading paths in the first and third cycles. The input V_m values were obtained from the intercept of the asymptotic line to the joint closure curves with the ΔV_j-axis. The seating normal stress (σ_i) value used in the calculations was arbitrarily established at 0.015 MPa. The new plots presented a completely different picture. The highly non-linear relationships of ΔV_j vs. $1/\sigma_n$ were now expressed by near perfect bilinear curves due to the logarithmic formulation. It therefore seemed that the hyperbolic function fitted well the data representing the low slope portion of the experimental joint closure curves but not

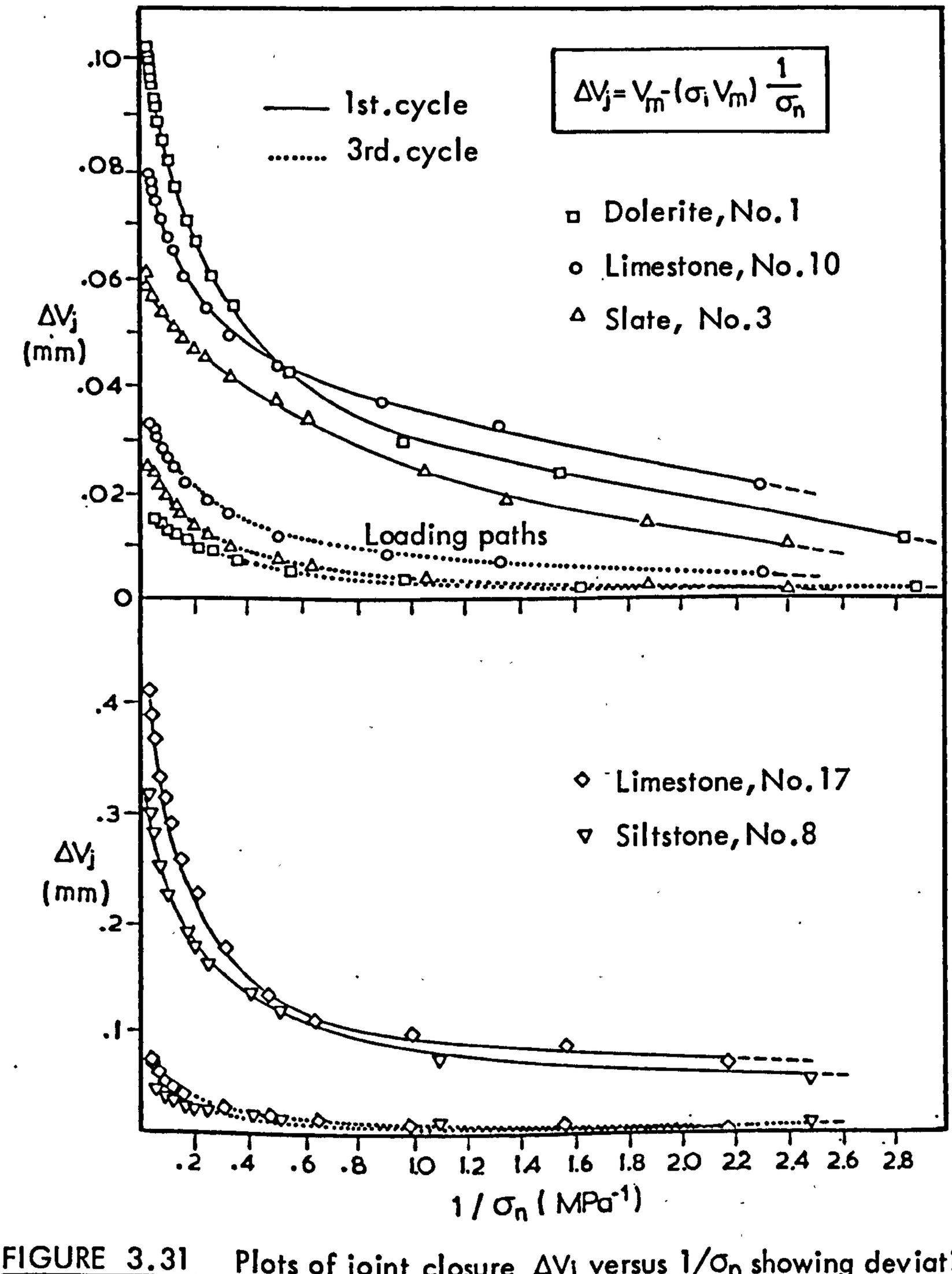

FIGURE 3.31 Plots of joint closure ΔV_j versus $1/\sigma_n$ showing deviation of the experimental data from a hyperbolic relationship as defined by Goodman's function

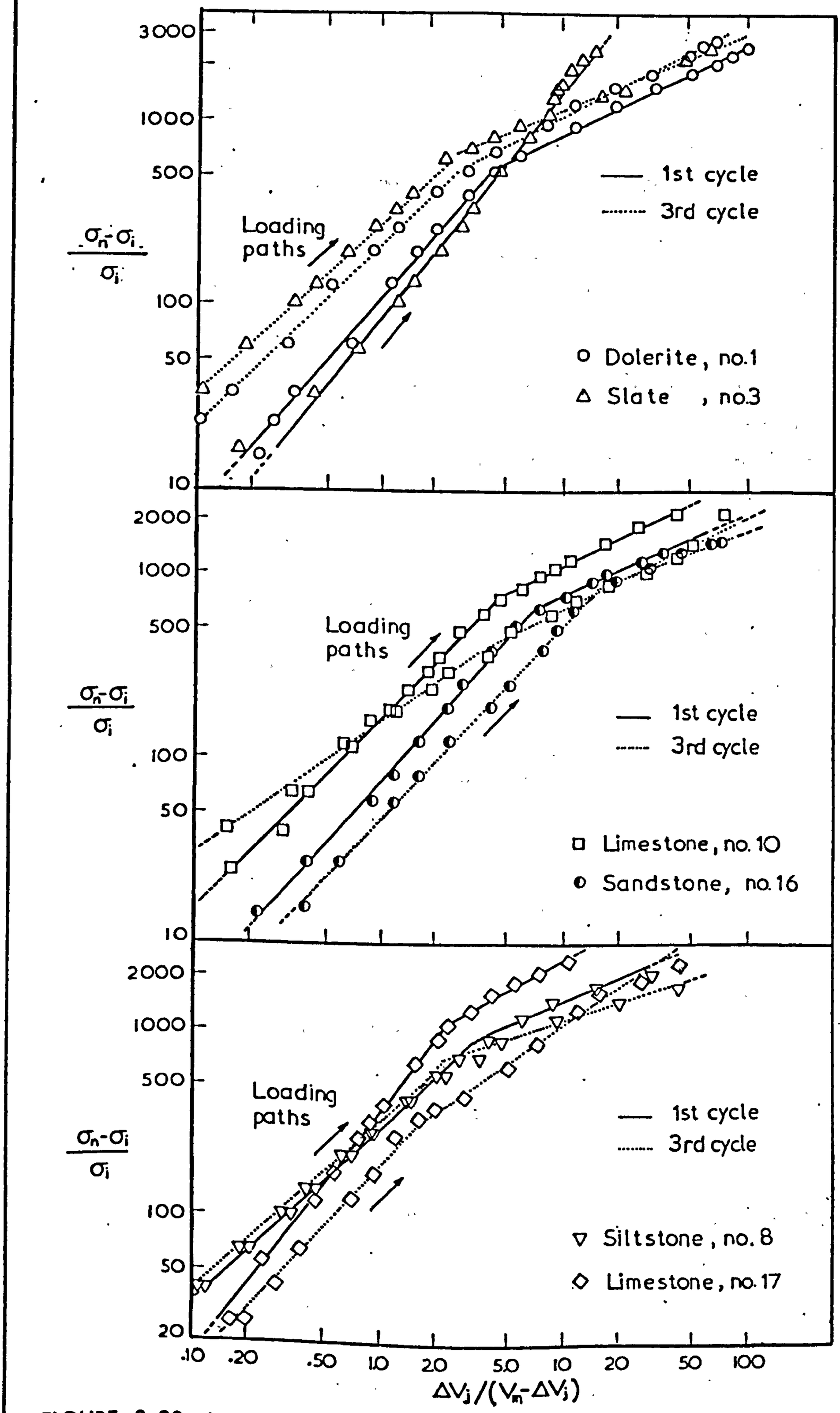

FIGURE 3.32 Logarithmic plots of dimensionless stress versus dimensionless deformation

the steeply rising part in the high stress region. Application of linear regression on both segments of the log-log relationships yielded values of t (= slope) ranging in most cases between 0.6 and 0.8. Those t values were in agreement with unpublished data by Goodman (1979, personal communication) who quoted an average value of approximately 0.7. Unfortunately, no analytical log-log plots were available to check the existence or otherwise of the type of bilinear relationship which the present data seemed to demand.

By using the C and t values from the linear regression of the relationships in Fig. 3.32, closure values (ΔV_j) for different joints were calculated and found to agree quite well with the experimental data. As it seemed that Goodman's expression gave an overall better fit than a semi-logarithmic relationship, it was decided to try another hyperbolic function. Christian and Desai (1977) reviewed an appropriate type of equation which has been used in the past to model the stress-strain relationships for soils (Kondner 1963, Duncan & Chang 1970) and rocks (Kulhaway, 1975) under triaxial compression. The basic form of that equation is:

$$\sigma = \frac{\varepsilon}{A + b\varepsilon} \qquad 3.7$$

where: σ = deviator stress

ε = axial strain

a & b = constants.

A change to the sign of the denominator was necessary for the present type of curve and hence the basic formula adopted was:

$$\sigma_n = \frac{\Delta V_j}{a - b\,\Delta V_j} \qquad 3.8$$

Rearrangement of the above expression and division by σ_n yields:

$$\frac{\Delta V_j}{\sigma_n} = a - b\,\Delta V_j \qquad 3.9$$

The latter form of equation 3.8 plots as a straight line and, conversely, a plot with axes $\Delta V_j/\sigma_n$ and ΔV_j can be used to check whether the joint

closure data fit a hyperbola. The $\Delta V_j/\sigma_n$ vs ΔV_j relationships obtained for the joint types included in the preceding analyses are illustrated in Figures 3.33 and 3.34. As seen, apart from the occasional minor discrepancies in the very low or very high stress regions, the various plots were linear throughout the normal stress range for both the first and third loading cycles, therefore indicating an overall good hyperbolic fit. Similar plots for the unloading paths, some of which have been included in the respective diagrams, also showed good linearity.

It seemed, therefore, that equation 3.8 might give a better, or at least a more consistent fit to the experimental data than Goodman's empirical formula. Since both expressions describe a hyperbolic variation of ΔV_j with σ_n, it must have been the formulation itself of Goodman's equation that exaggerated any small deviations of the experimental curves from an ideal hyperbola. The bilinear trends of the log-log relationships in Fig. 3.32 were conceivably the result of a disproportional increase of the dimensionless ratio $\Delta V_j/(V_m - \Delta V_j)$ beyond some range of $(\sigma_n - \sigma_i)/\sigma_i$ values. Trials indicated that the calculated values of the deformation ratio in the region where ΔV_j is very close to V_m were considerably different, if the V_m values were increased or decreased by no more than 2 to 4%. However, as has already been mentioned, by using the average C and t values the calculated ΔV_j values showed good agreement with the experimental ones. In order to examine the curve fitting potential of equations 3.6 and 3.8, calculated joint closure data were plotted and compared with the curves obtained experimentally. The values of ΔV_j were obtained from:

$$\Delta V_j = \frac{\sigma_n \, a}{1 + \sigma_n \, b} \qquad 3.10$$

where a and b are the intercept and slope of the $\Delta V_j/\sigma_n$ vs σ_n plots in Figs. 3.33 and 3.34 and their values were derived by linear regression. For fitting Goodman's expression, ΔV_j's were calculated from:

$$\Delta V_j = \frac{B \, V_m}{1 + B} \qquad 3.11$$

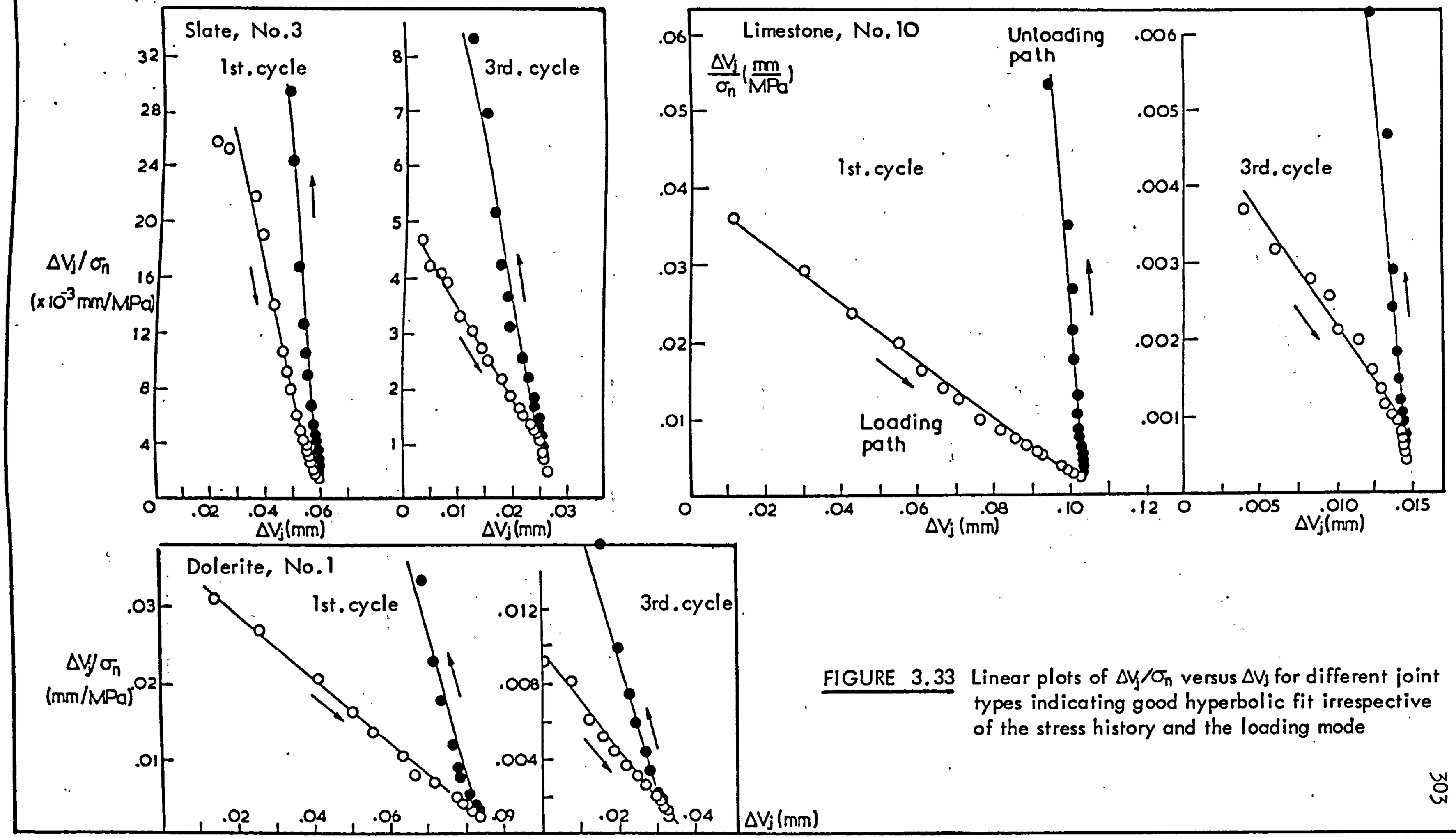

FIGURE 3.33 Linear plots of $\Delta V_j/\sigma_n$ versus ΔV_j for different joint types indicating good hyperbolic fit irrespective of the stress history and the loading mode

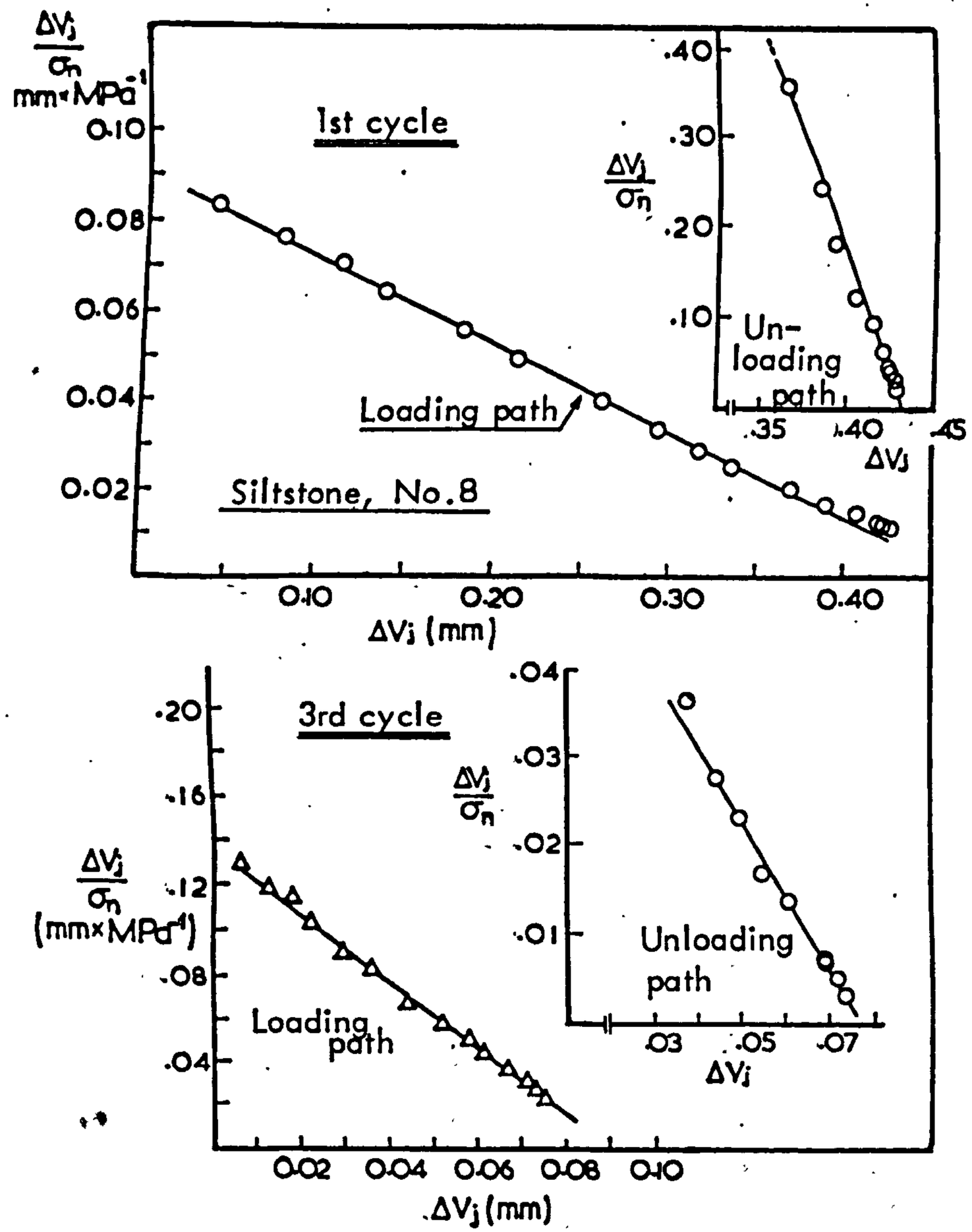

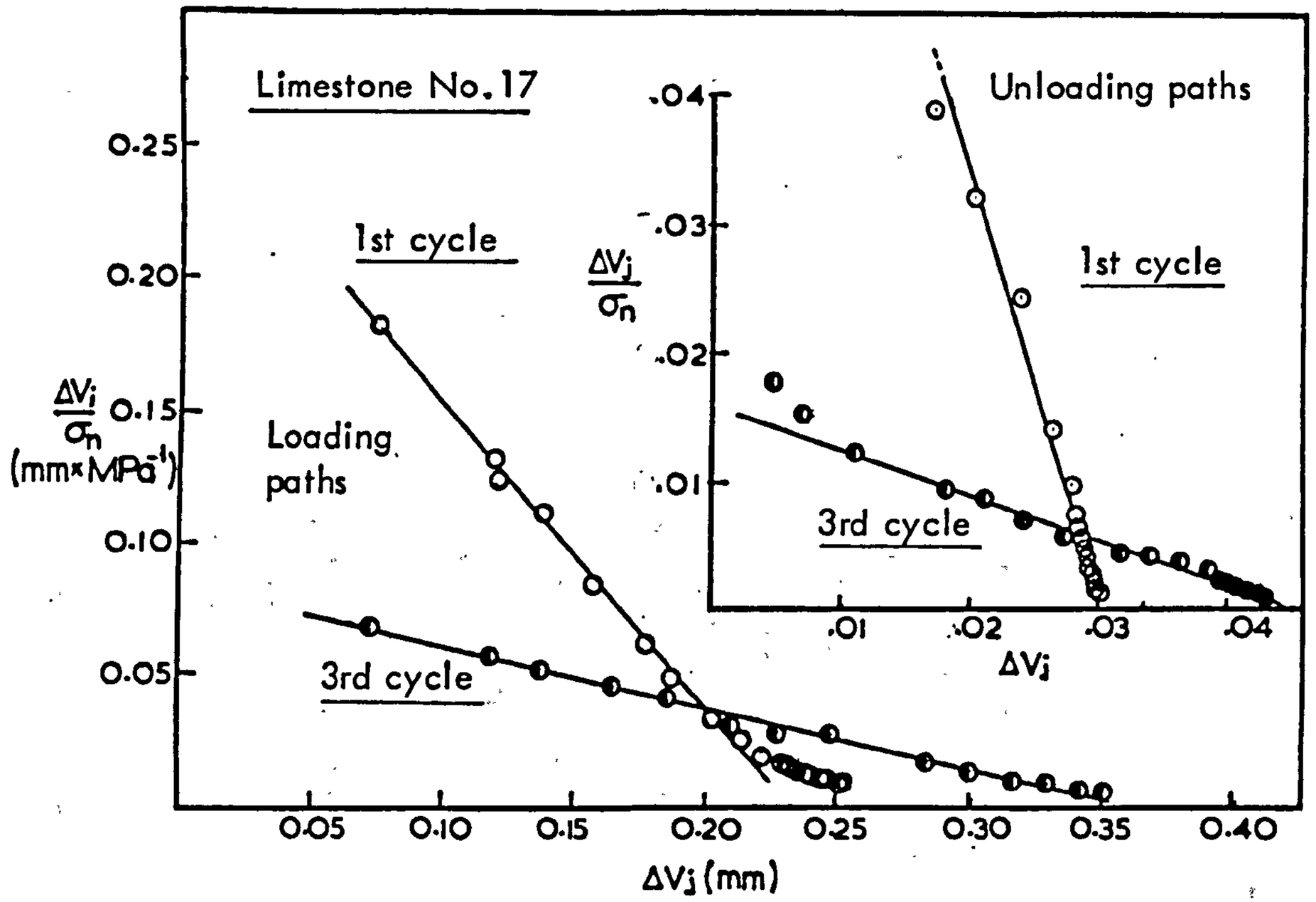

FIGURE 3.34 Linear plots of $\Delta V_j/\sigma_n$ versus ΔV_j for a range of joint types indicating a good hyperbolic fit irrespective of the stress history and the loading mode

where: $$B = \text{antilog}_{10}\left[\frac{\log_{10}\left(\frac{\sigma_n - \sigma_i}{\sigma_i}\right) - \log_{10} C}{t}\right]$$

and C and t were obtained by linear regression of the log-log relationships in Figure 3.32. Four typical examples of the degree of approximation obtained are shown in Figure 3.35 for the loading paths from the first and third cycles. Overall, equation 3.8 produced curves which followed the experimental ones closer than the curves calculated from equation 3.6, although in some cases the differences were only marginal or non-existent (for example, note the third cycle loading paths for the sandstone joint no. 16 and the limestone joint no. 10).

The analysis of the experimental joint closure curves has shown that the rate of change in closure of natural, unfilled interlocked joints can be adequately described by a hyperbolic relationship, irrespective of the joint type, stress history and loading mode. The normal stiffness (K_n) of a joint cannot, therefore, be defined by a single value; for each increment of σ_n the corresponding K_n value must be obtained from the derivative of the hyperbolic function.

In order to find the incremental stiffness by using equation 3.8, the physical meaning of the constants a and b must be considered.
Equation 3.8 may be rewritten as

$$\sigma_n = \frac{1}{\frac{a}{\Delta V_j} - b} \qquad 3.12$$

which implies that for very large values of σ_n ($\rightarrow \infty$), ΔV_j must tend to the limiting value a/b, hence

$$\frac{a}{b} = \text{asymptote to the hyperbola} = V_m \text{ (maximum joint closure)} \qquad 3.13$$

and therefore at V_m the tangent joint stiffness (K_n) will acquire an infinite value as shown below:

$$K_n = \frac{\partial \sigma_n}{\partial \Delta V_j} = \frac{a}{(a - b\,\Delta V_j)^2} \rightarrow \infty, \text{ for } \Delta V_j \rightarrow \frac{a}{b} = V_m \qquad 3.14$$

$$\text{and } \sigma_n \rightarrow \infty$$

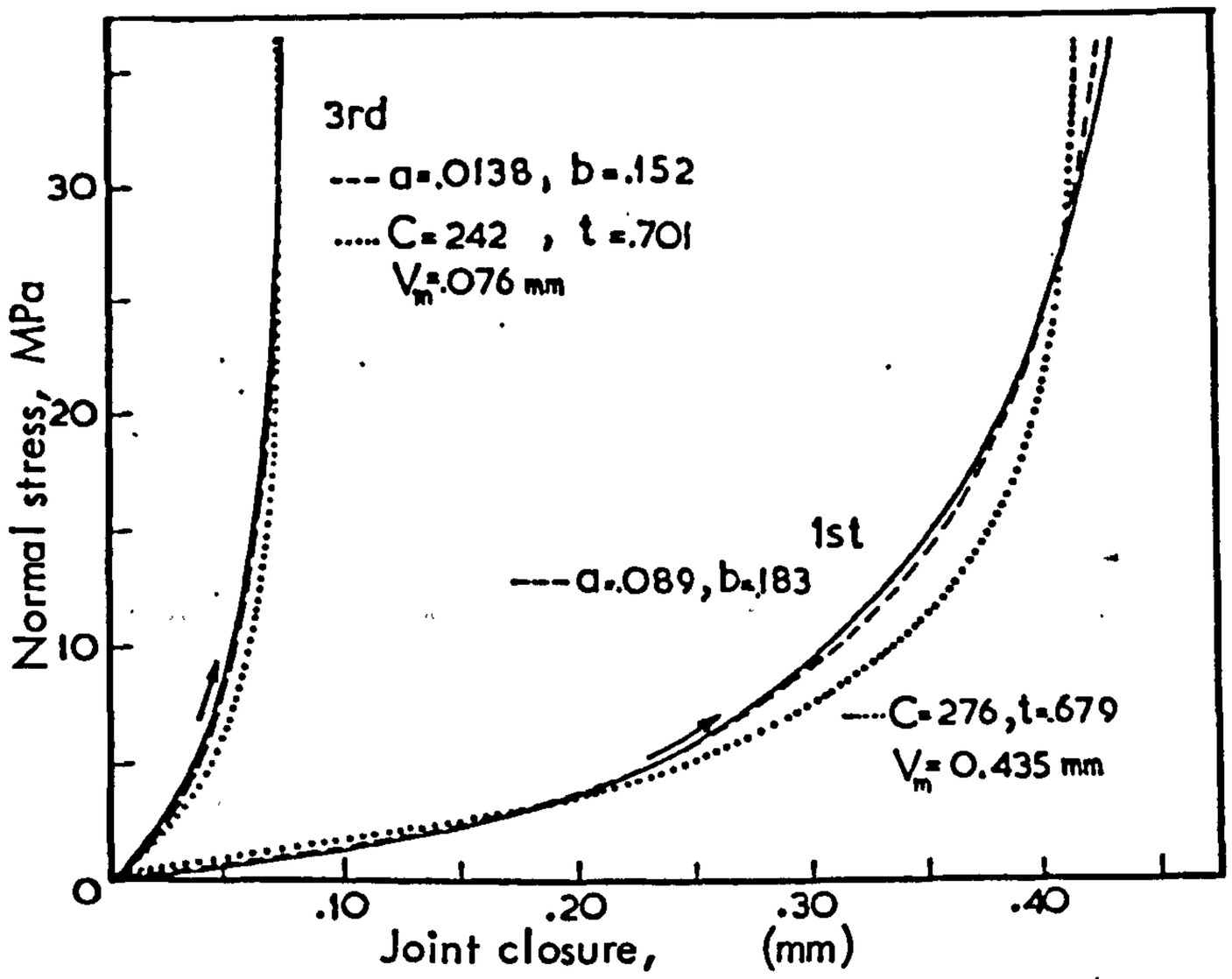

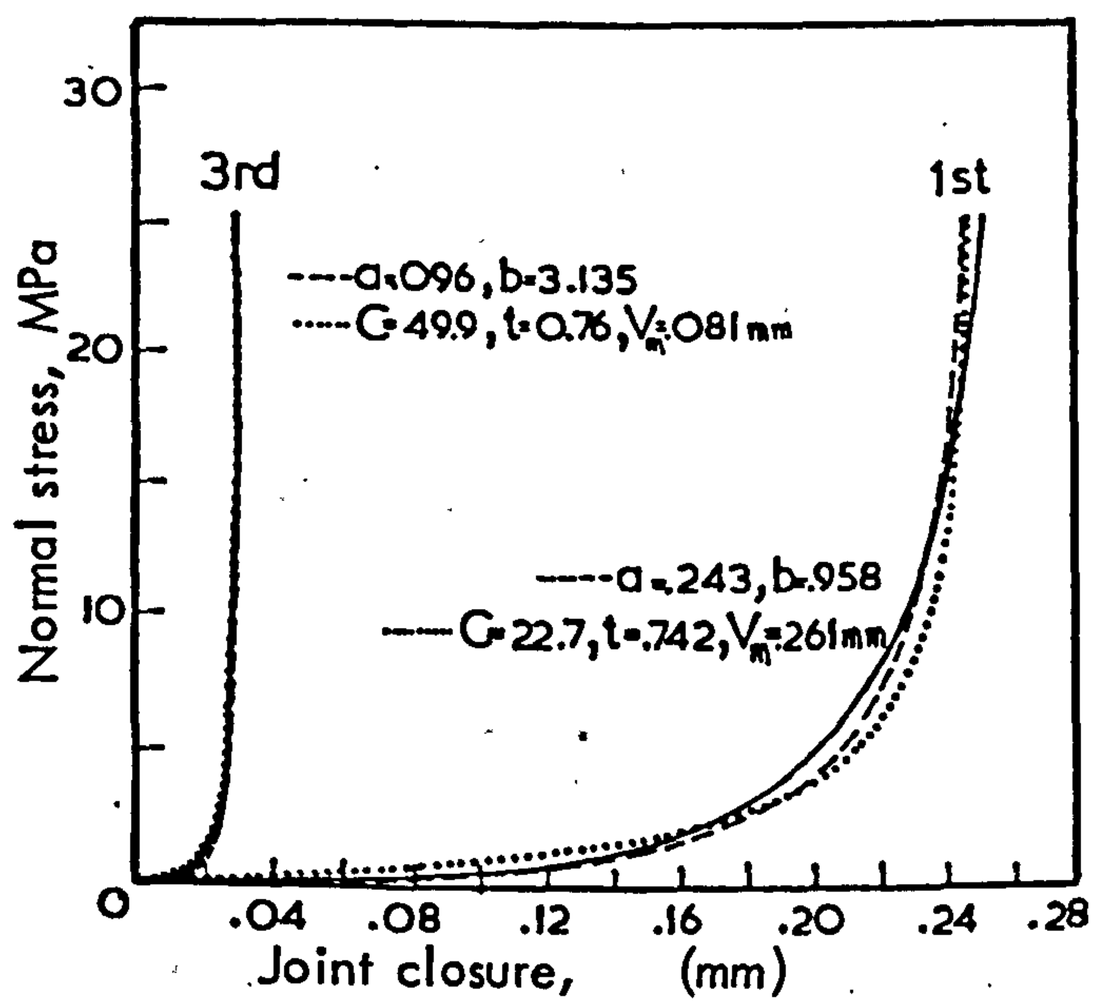

——— Experimental

----- $\sigma_n = \frac{\Delta V_j}{a - b\Delta V_j}$

..... $\frac{\sigma_n - \sigma_i}{\sigma_i} = C\left(\frac{\Delta V_j}{V_m - \Delta V_j}\right)^t$

σ_i=.015 MPa

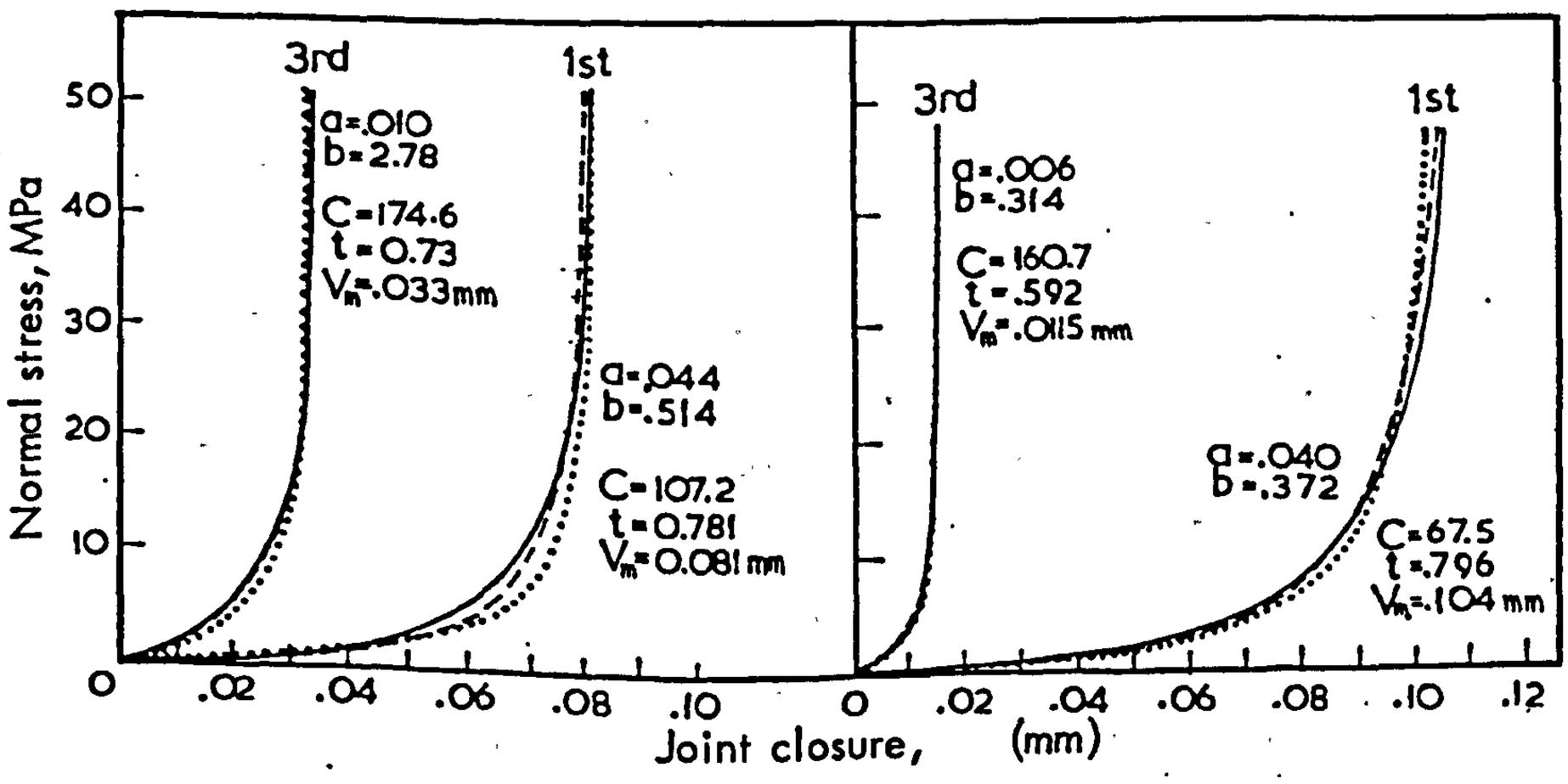

FIGURE 3.35 Comparisons between experimental closure curves under the first and third loading tests and those calculated by using functions 3·6 and 3·8

For an extremely small increment of σ_n ($\rightarrow 0$), ΔV_j will also $\longrightarrow 0$, and hence:

$$K_{ni} = \frac{1}{a} \qquad 3.15$$

therefore, constant "a" represents the reciprocal of the initial normal stiffness (K_{ni}).

The values of the initial normal stiffness (K_{ni}) and maximum joint closure (V_m) uniquely define the hyperbolic stress-closure relationship of a joint. The tangent value of normal stiffness (K_n) at any level of normal stress (σ_n) may be found from:

$$K_n = \frac{\partial \sigma_n}{\partial \Delta V_j} = \frac{a}{(a - b\,\Delta V_j)^2} = \frac{1}{a(1 - \frac{b}{a}\Delta V_j)^2} = \frac{K_{ni}}{(1 - \frac{\Delta V_j}{\Delta V_m})^2} \qquad 3.16$$

By substitution of ΔV_j for

$$V_j = \frac{\sigma_n a}{1 + \sigma_n b} = \frac{1}{\frac{1}{\sigma_n a} + \frac{b}{a}} = \frac{\sigma_n V_m}{K_{ni} V_m + \sigma_n}$$

the expression 3.16 becomes:

$$\boxed{K_n = K_{ni} \left(1 - \frac{\sigma_n}{V_m K_{ni} + \sigma_n}\right)^{-2}} \qquad 3.17$$

Both K_{ni} and V_m data of a particular joint are, of course, dependent upon the initial level of normal stress (σ_i). In an experimental determination of those parameters, the joint can be precompressed under the estimated in-situ seating stress before closure readings begin; alternatively, in cases where the experimental σ_i is zero, the compression curve may be obtained by translating the axes to a position (σ_i, ΔV_{ji}) such that σ_i and ΔV_{ji} will represent the initial stress and closure conditions respectively of the joint (Goodman and St. John, 1977). That will again lead to an appropriately reduced maximum closure (V_m) value and increased initial normal stiffness (K_{ni}).

2. Normal stress-closure curves (joints mismatched)

The closure curves of the joints with mismatched walls (Figures 3.24 and 3.26) were highly non-linear implying possible use of a hyperbolic function to express them analytically. In the only similar test known to the author, equation 3.6 had been used to approximate the closure curve of a mismatched fracture (Goodman, 1976). However, in that case the experimental curve had to be extrapolated to obtain an estimate of the maximum closure value (V_m) needed in 3.6, due to specimen failure. As stated in section 3.2.3(3), complete closure of the mismatched joints was not achieved under the applied levels of stress and hence the V_m value could only be guessed. Due to the apparent sensitivity of equation 3.6 upon the input value of V_m, that function was not tested against the present data. In any case, plots of $\Delta V_j/\sigma_n$ vs ΔV_j (according to 3.9) showed poor linearity over a wide range of stresses, as shown with a few examples in Figure 3.36.

Since the mismatched joints closure data did not fit a hyperbola to a satisfactory degree, the possibilities of fitting a power or a semi-log curve were considered. Of those two alternatives, the semi-log fit gave the best approximation. As shown in Figure 3.37, plots of closure data versus logarithmically scaled normal stress gave linear relationships except for in the very low stress region. A semi-log relationship between σ_n and ΔV_j implies that a joint will never be fully closed, which in fact is the very case for mismatched joints.

The relationships in Figure 3.37 are expressed by

$$\log_{10} \sigma_n = p + q\ \Delta V_j \qquad 3.18$$

which implies that for $\Delta V_j = 0$ (initial reference for taking closure measurements), $\log_{10} \sigma_n$ is equal to p. Hence, the intercept p represents the logarithm of the initial normal stress (σ_i). The antilog of the coefficients p in the linear regression equations included in Fig. 3.37 indicate somewhat higher σ_i values (range = .175 MPa - .268 MPa, mean = .222 MPa) than the mean experimental (~ 0.15 MPa). This is probably due to the slight deviation of the closure data from an ideal semi-log relationship over the full stress range.

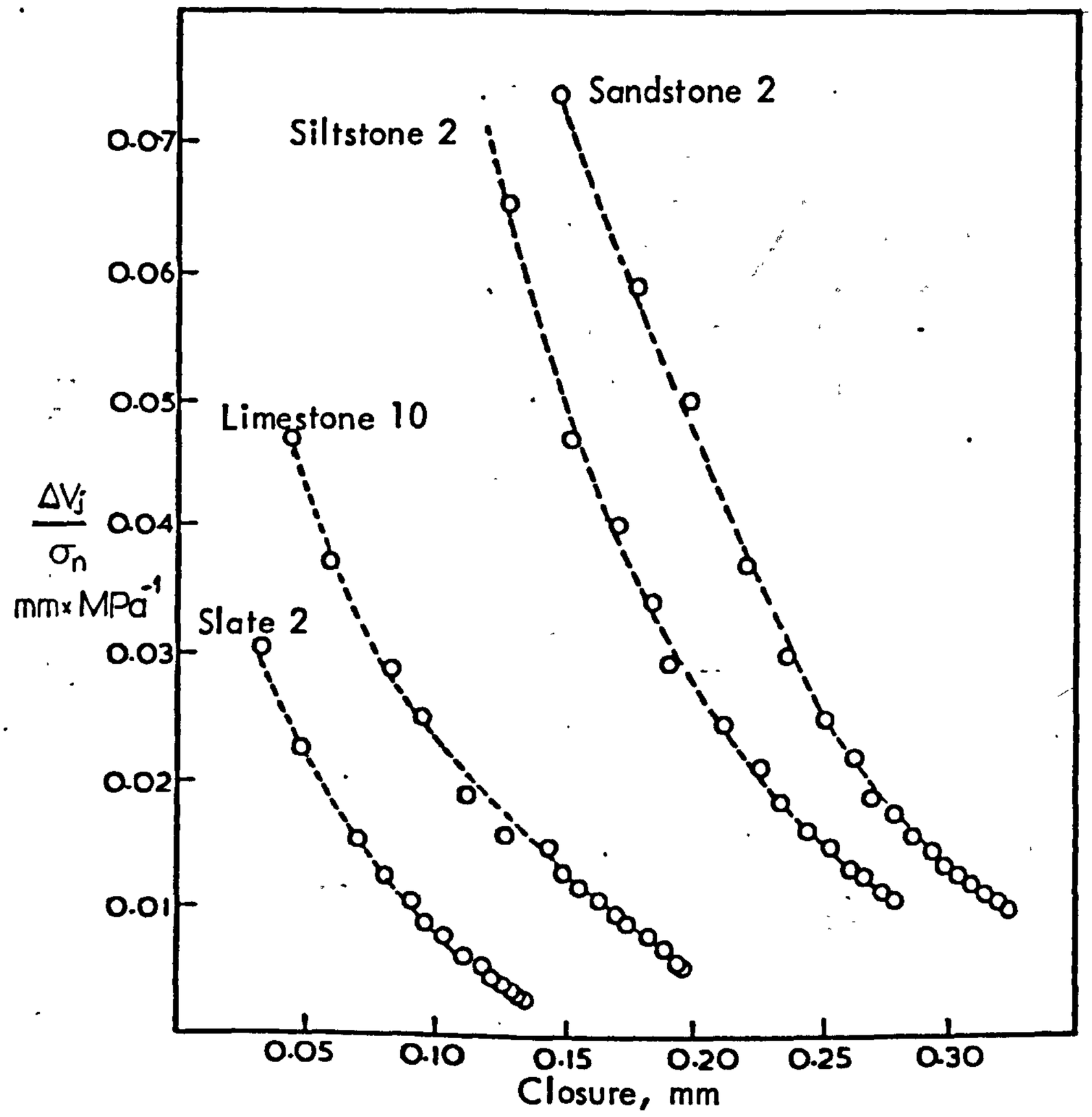

FIGURE 3.36 Non-linear plots of closure (ΔVj) / stress (σ_n) versus closure (ΔVj) indicating poor hyperbolic fit to the stress-closure relationship of mismatched joints.

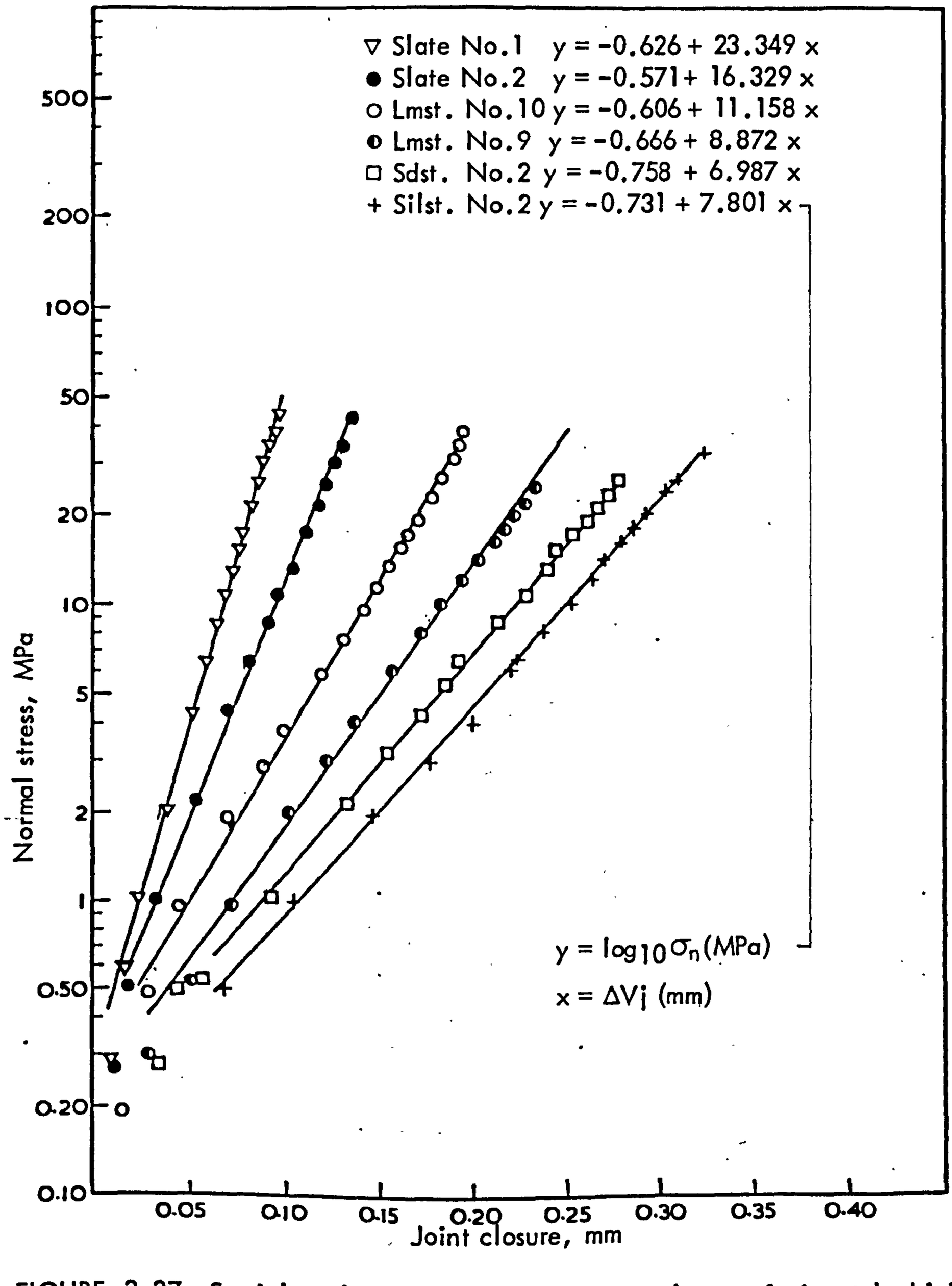

FIGURE 3.37 Semi-log plots of normal stress versus closure of mismatched joints.

The incremental normal stiffness (K_n) for mismatched joints can be calculated from the derivative of function 3.18, which may be re-written as:

$$\Delta V_j = -\frac{p}{q} + \frac{\log_{10}\sigma_n}{q} \quad \text{hence} \quad \frac{\partial \Delta V_j}{\partial \sigma_n} = \frac{1}{\sigma_n q}\log_{10} e$$

$$\text{and} \quad \frac{\partial \sigma_n}{\partial \Delta V_j} = \frac{q\sigma_n}{\log_{10} e}$$

Therefore, for each increment of σ_n, the normal stiffness can be obtained from:

$$\boxed{K_n = \frac{q\sigma_n}{0.4343}} \qquad 3.19$$

3. Shear stress-displacement curves in the pre-peak range

The typical examples of shear stress-displacement curves presented in Figures 3.27 and 3.28 have shown significant non-linearity in the range up to mobilization of the peak shear strength. The shape of the curves at constant normal stress suggests the possibility of using a hyperbolic function to depict the pre-peak shear behaviour of joints.

Clough and Duncan (1969, quoted by Kulhawy 1975) developed a hyperbolic relationship to model the shear behaviour of soil/concrete interface. The basic form of the function was the same as the one used in this study to express the stress-joint closure relationships (equation 3.8) except for the sign of the denominator:

$$\tau = \frac{d_h}{m + n\,d_h} \quad \text{or in linear form:} \quad \frac{d_h}{\tau} = m + n\,d_h \qquad 3.20$$

where τ is the shear stress, d_h is the shear displacement, and m and n are the constants of the hyperbola. The above function implies that at very small shear displacements $\tau = d_h/m$, hence the constant m represents the reciprocal of the initial shear stiffness (K_{si}), or

$$K_{si} = \frac{1}{m} \qquad 3.21$$

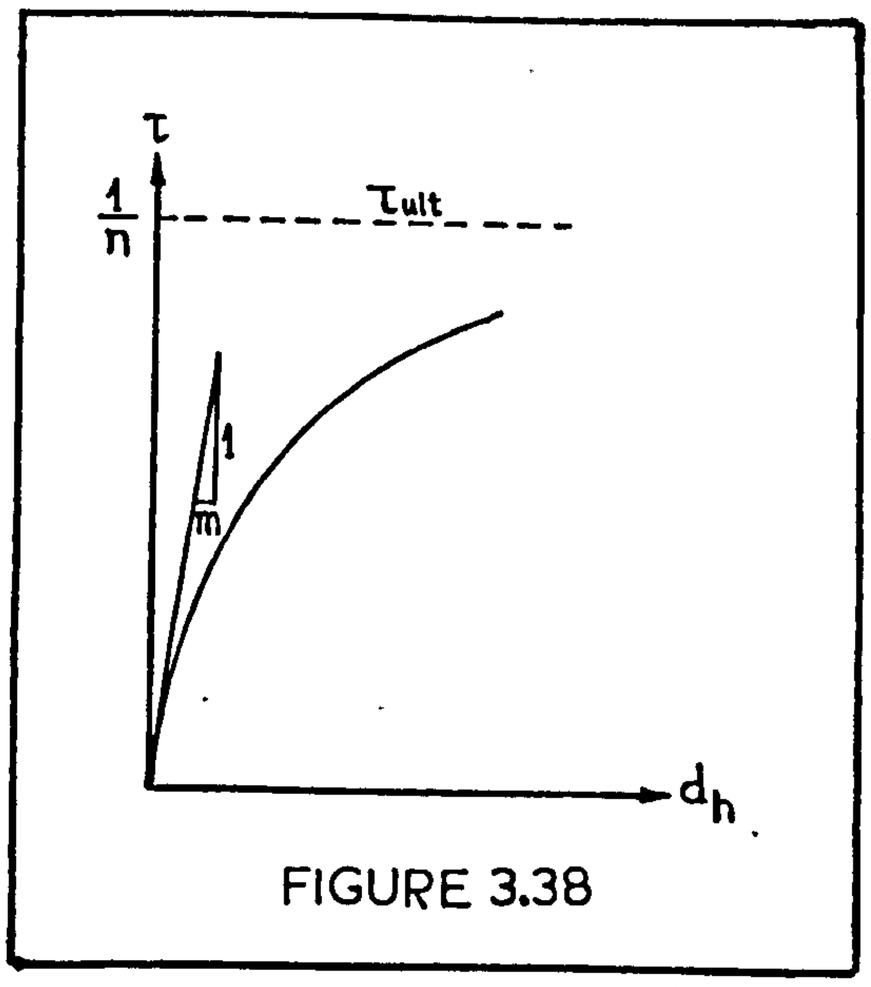

FIGURE 3.38

At large shear displacements $\tau = 1/n$, hence constant n represents the reciprocal of the horizontal asymptote (τ_{ult}), or:

$$\tau_{ult} = \frac{1}{n} \qquad 3.22$$

The above basic characteristics of the hyperbolic model for non-linear behaviour are illustrated diagrammatically in Figure 3.38.

In order to examine whether the present stress-displacement curves agreed with the hyperbolic model, plots of d_h/τ vs. d_h were prepared for various levels of normal stress, and some characteristic examples are illustrated in Figure 3.39. As seen, the data points fell essentially on straight lines, thus indicating a good hyperbolic fit in the pre-peak range. The only exception was the fresh slate cleavage fracture no. 2, which displayed minimum non-linearity (see Fig. 3.27).

For a certain level of normal stress the incremental shear stiffness (K_{st}) can be found by differentiation of the hyperbolic function (3.20):

$$K_{st} = \frac{\partial \tau}{\partial d_h} = \frac{m}{(m + nd_h)^2} \qquad 3.23$$

By solving (3.20) for $d_h = \frac{\tau m}{1-n}$ and substituting in 3.23:

$$K_{st} = \frac{1}{m}(1 - n\tau)^2 \qquad 3.24$$

Finally, by replacing 1/m by K_{si} and n by $1/\tau_{ult}$, 3.24 becomes

$$K_{st} = K_{si}\left(1 - \frac{\tau}{\tau_{ult}}\right)^2 \qquad 3.25$$

Equation 3.25 defines the tangent shear stiffness (K_{st}) as a function of the shear stress (τ) under constant normal stress. Clough and Duncan

Weathered sandstone
Nos. 19, 20, 21

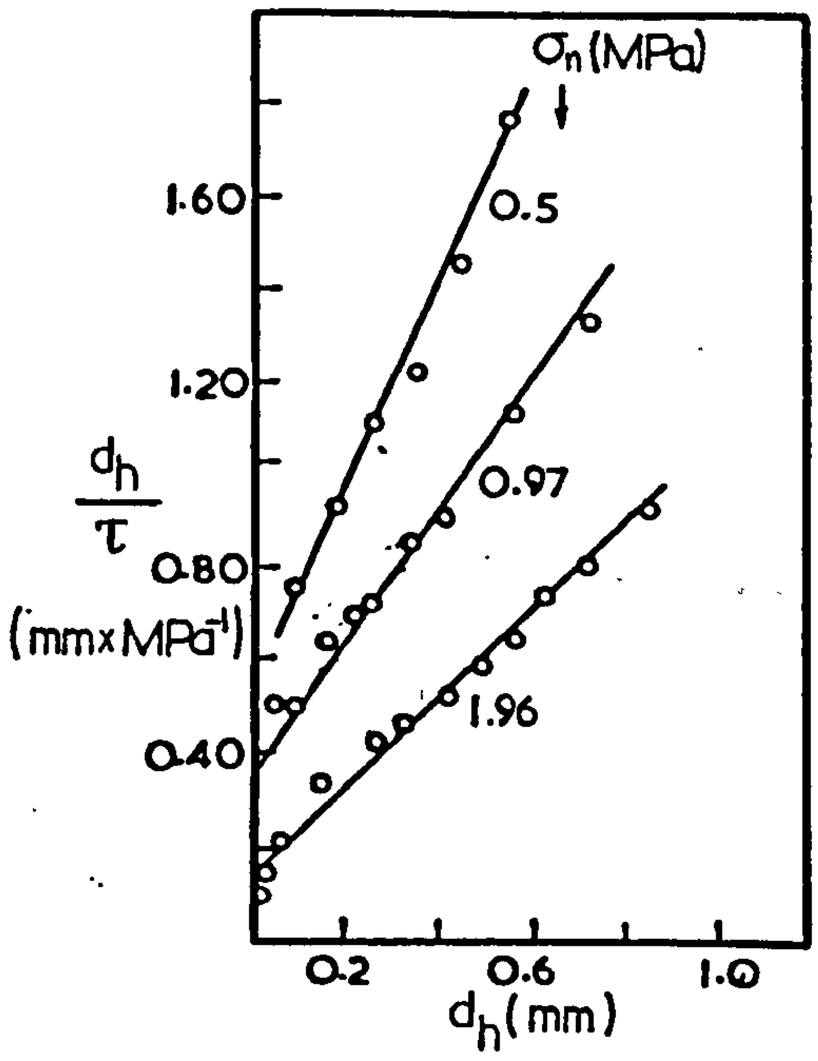

Weathered slate cleavage planes
Nos. 5, 6, 7

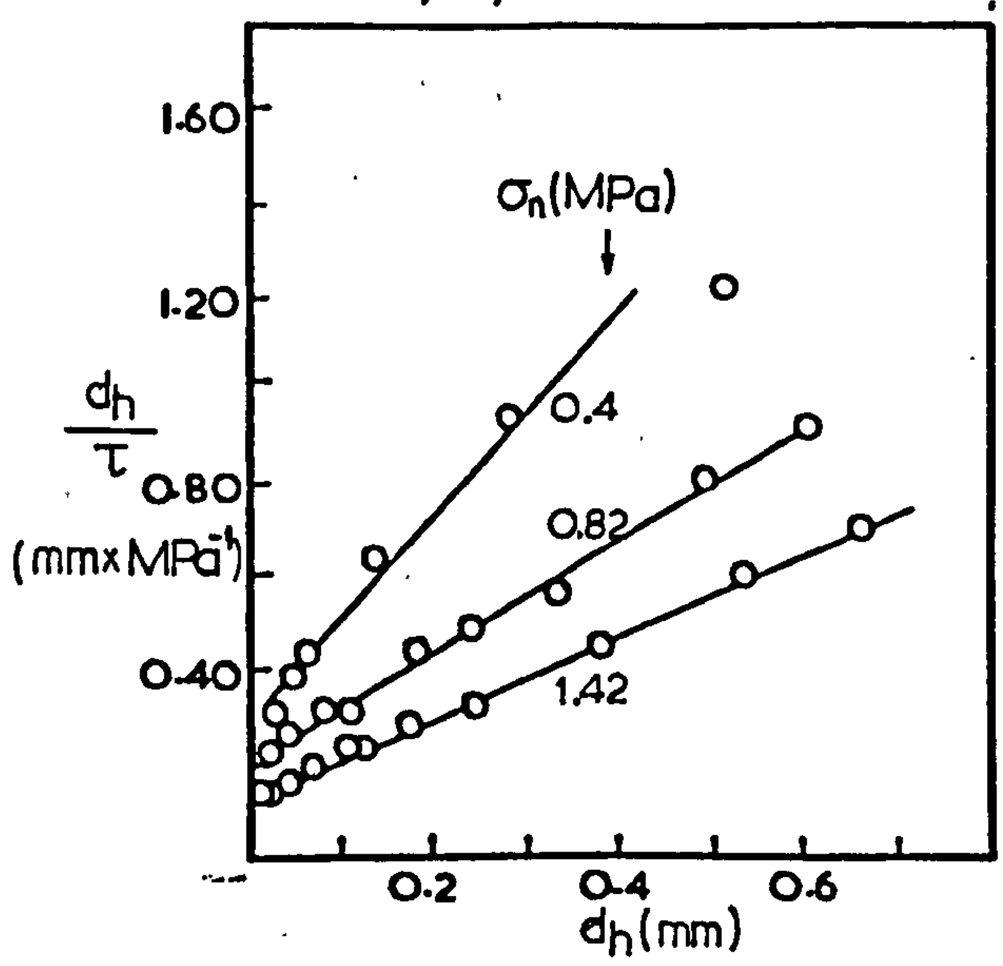

Weathered limestone
No. 20

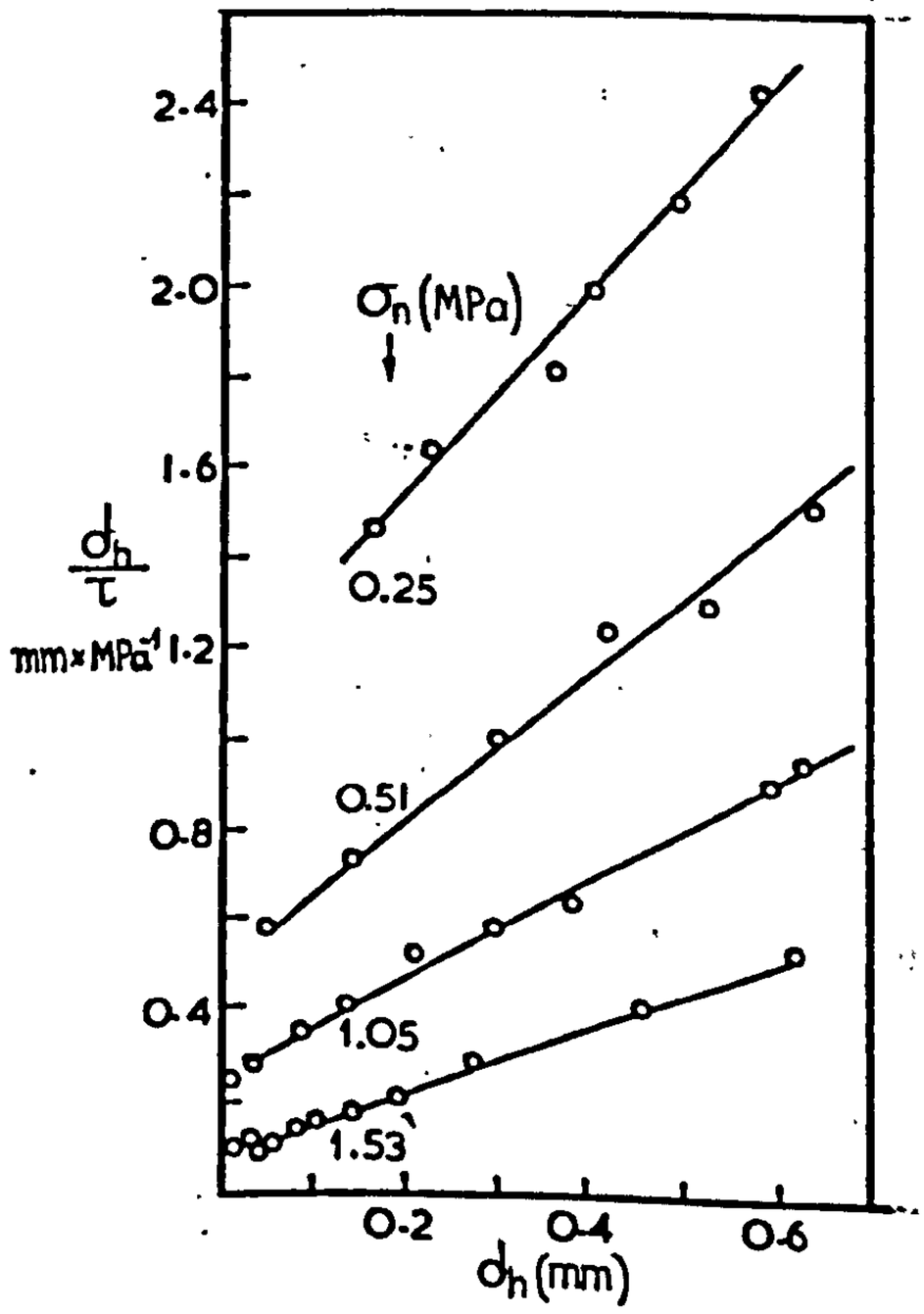

Fresh limestone, No.4

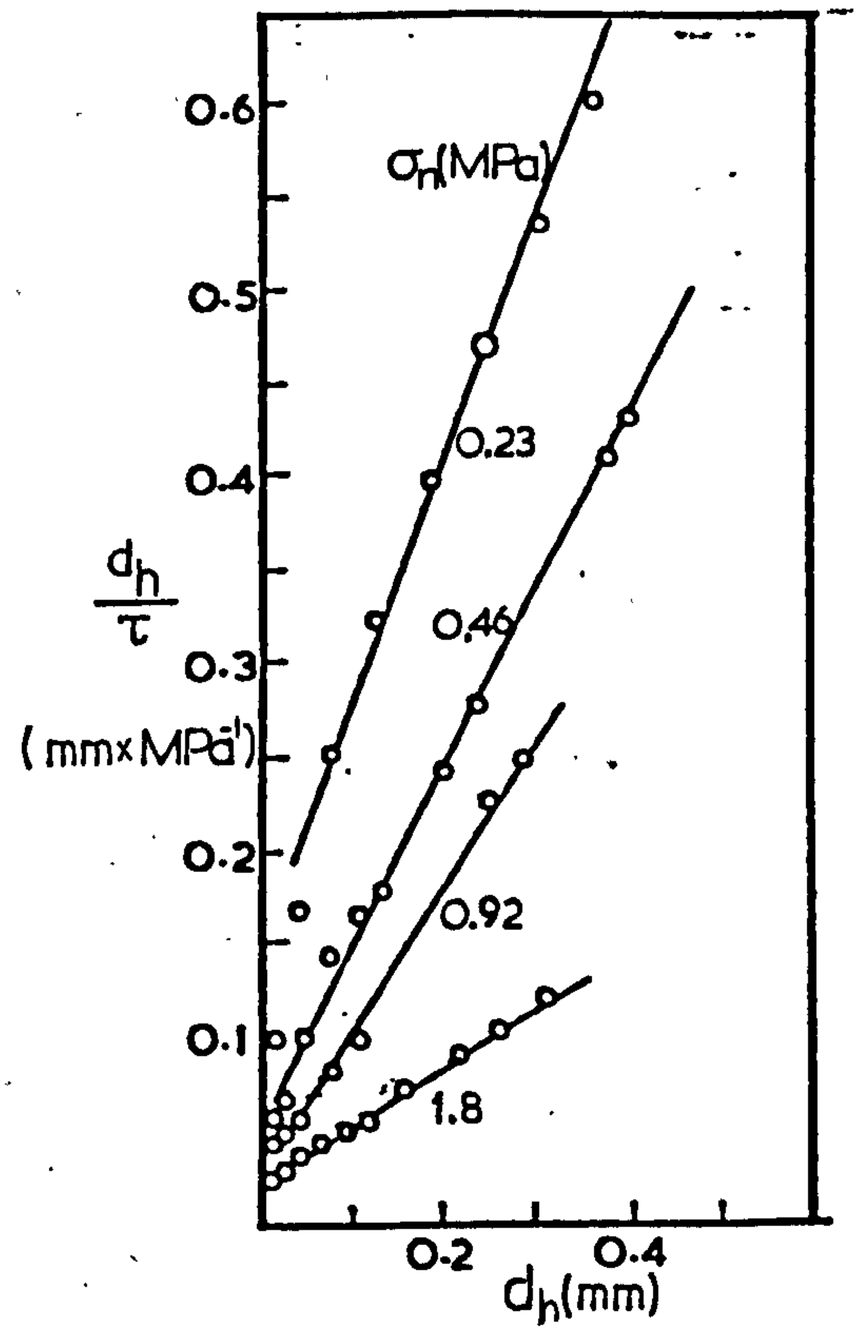

FIGURE 3.39 Linear plots of shear displacement (d_h) / stress (τ) versus d_h indicating good hyperbolic fit to the shear stress-shear displacement relationship irrespective of the normal stress level.

related the ultimate stress (τ_{ult}) value predicted by the hyperbola with the experimental peak shear stress (τ_p) by means of a coefficient which they called the failure ratio (R_f) and defined as:

$$R_f = \frac{\tau_p}{\tau_{ult}} \qquad 3.26$$

The failure ratio is always less than or equal to unity. High values of R_f indicate high degree of non-linearity. It was also stated that the initial shear stiffness (K_{si}) varied linearly with normal stress on a log-log basis:

$$K_{si} = K_j(\sigma_n)^{n_j} \qquad 3.27$$

where: K_j = stiffness number
n_j = stiffness exponent

By substitution of τ_{ult} for τ_p/R_f and K_{si} for 3.27, equation 3.25 becomes

$$\boxed{K_{st} = K_j(\sigma_n)^{n_j}\left(1 - \frac{\tau R_f}{\tau_p}\right)^2} \qquad 3.28$$

The above expression describes the shear stiffness of a joint at any level of shear and normal stresses. It is interesting to note that if the shear stress-displacement curve is linear R_f can be set equal to zero, and if the stiffness is not dependent on the normal stress n_j can be set equal to zero.

Hungr and Coates (1978) also advanced the practical validity of use of hyperbolic functions and derived a relationship uniquely defined by the "yield" point of the shear stress (τ) - displacement (d_h) curve. The basic form of their expression was:

$$\tau = \frac{ut}{t - d_h} - u \;, \quad \text{for } t < d_h \qquad 3.29$$

where u and t are constants. The two fundamental conditions considered in the definition of the hyperbola were that (a) the function must pass

through the yield point and (b) by definition the function must attain its maximum curvature at the yield point. By solving the two equations satisfying conditions (a) and (b) simultaneously for u and t and through a series of simple combinations the authors derived the following two functional relationships for the constants u and t:

$$u = -\frac{z\,a\,f\,\sigma_n^{\,2}}{a\,\sigma_n - b} \quad \text{and} \quad t = -\frac{z\,f\,b}{a(a\,\sigma_n - b)} \qquad 3.30$$

where: z = ratio of the yield (τ_y) to the peak (τ_p) stress
a = ratio of the yield secant shear stiffness (K_{sy}) to the normal stress (σ_n)
f = coefficient of friction describing the peak shear strength under σ_n.
b = scale coefficient equal to the ratio of unit length on the stress axis to the unit length on the displacement axis, allowing for cases where results of the same test were plotted to different scales.

Once the values of u and t have been derived, the incremental tangent shear stiffness (K_{st}) at any level of shear or normal stress can be calculated from:

$$K_{st} = \frac{\partial \tau}{\partial d_h} = \frac{ut}{(t - d_h)^2} \qquad 3.31$$

Hungr and Coates' hyperbolic relationship is based on a single characteristic point, that is the yield point (τ_y, d_{hy}). In order to examine its validity at various levels of shear stress, secant values of shear stiffness were calculated at points representing 25%, 50% and 75% of the peak shear stress and the peak point itself for different types of joints and levels of normal stress. The calculated values were very comparable to those obtained directly from the experimental results. Some typical examples of the observed level of agreement are presented in Table 3.13. The data listed in column 1 were calculated from Hungr and Coates' expression as

$$K_s = \frac{1}{d_h}\left(\frac{ut}{t - d_h} - u\right) \qquad 3.32$$

TABLE 3.13

Comparisons between secant shear stiffness (K_s) values calculated from hyperbolic functions and experimental data.

Shear stress level	Slate, nos. 5 and 7				Dolerite, no. 2				Limestone, no. 4			
	σ_n (MPa)	K_s (MPa/mm) CALCULATED 1	2	EXPERIMENTAL	σ_n (MPa)	K_s (MPa/mm) CALCULATED 1	2	EXPERIMENTAL	σ_n (MPa)	K_s (MPa/mm) CALCULATED 1	2	EXPERIMENTAL
at 25% τ_p	0.82	3.6	4.1	3.8	0.26	6.8	6.5	6.0	0.23	5.3	7.1	7.2
at 50% "		3.4	3.4	3.1		5.2	5.0	4.8		3.8	4.4	3.7
at 75% "		2.8	2.3	2.3		4.0	3.8	4.1		2.3	2.8	2.6
at peak		1.1	0.8	0.9		1.9	1.8	1.8		1.7	1.6	1.7
at 25% τ_p	1.45	4.5	6.0	5.7	1.05	24.4	15.7	20.5	0.92	16.4	21.3	24.1
at 50% "		3.7	4.2	4.2		13.4	10.6	9.8		12.7	16.3	18.1
at 75% "		2.8	3.0	3.1		7.4	6.6	6.2		8.0	8.6	10.4
at peak		1.4	1.2	1.3		3.9	3.8	3.8		3.3	4.1	4.1

and those in column 2 were obtained from Clough and Duncan's expression as:

$$K_s = \frac{1}{a - bd_h} \qquad 3.33$$

The three joint types referred to in Table 3.13 displayed different degrees of non-linear behaviour. The average failure ratio (R_f) values were 0.87 (slate), 0.83 (limestone) and 0.77 (dolerite). The agreement between the predicted and experimental data indicates that both hyperbolic functions may be regarded as a good representation of observed pre-peak shear behaviour irrespective of the joint type and level of normal stresses.

The analytical work presented in this section has shown that simple empirical functional relationships may offer a realistic expression of the joint deformational behaviour under normal and shear loading conditions. The obvious advantage of such relationships is that they are based on parameters which can be measured by experiment. For example the changing stiffness of a joint under compression is uniquely defined by the initial stiffness and the maximum closure. Likewise, the changing stiffness of a joint in shear can be defined by the stiffness number (K_j), exponent (n_j) and failure ratio (R_f), etc. The functional relationships can be incorporated in numerical analyses, e.g. in a finite element model modifying progressively the K_n and K_s values by the incremental or iterative procedures used in the F.E. method to simulate non-linear stress-deformation behaviour.

3.33 Data processing and presentation of joint stiffness parameters

In this section the method of analysis of the experimental stress-deformation data will be described and the derived stiffness parameters of all the types of joints tested in this study will be presented.

(1) Joint block compression test results

In discussing the general pattern of joint behaviour under normal loading, Goodman and St. John (1977) stated that the total deformation curve of a jointed block eventually becomes asymptotic to a line

representing the elastic compression of the rock material and that it is extremely close to it after the intersecting joint has reached its maximum closure state. The authors assumed that the maximum closure (V_m) can be defined as the intersection of the asymptote to the joint block compression curve with the total deformation (ΔV_t) axis, as exemplified diagrammatically in Figure 3.40. By implication the net joint closure curve could be derived by subtraction of the compression line of the intact rock (BC) from the total deformation curve (OA) as obtained from the experiment.

The above characteristics can be readily observed in the normal stress-total deformation relationships of interlocked joint blocks in the previous Figures 3.12 to 3.16. Under high normal stresses the curves - especially those obtained from fresh joints in slate, dolerite and limestone - acquired an essentially constant slope and followed paths parallel or virtually parallel to the loading paths of the independently tested solid blocks. Exceptions to that pattern were the curves of weathered joints during the first loading. Sketching of the approximate asymptotic lines showed that the agreement of the "predicted" V_m values with the experimental ones depended, as would be expected, on the degree of non-linearity in the elastic curves of the rock materials. Therefore, if the maximum closure was to be obtained in that manner, an appropriate allowance ought to be made for the over-estimate induced by the non-linearity in actual rock behaviour.

The above empirical approach presented a potential solution to the problem of evaluation of the maximum closure values of all the joints tested, since rock deformation (ΔV_r) data for each individual test case were not available, and the following steps were undertaken:

(a) formulation of an appropriate function representing the experimental normal stress-total deformation relationships

(b) fitting each set of data with that function by non-linear least squares regression to obtain statistically significant "predictions"

(c) evaluation of appropriate correction factors to allow for the non-linearity component included in the "predicted" V_m.

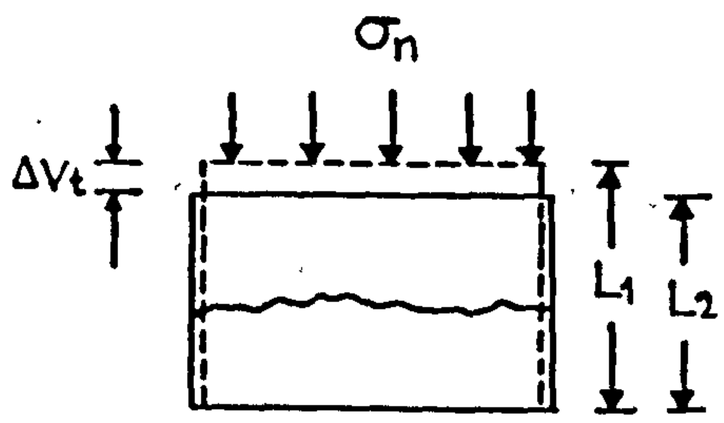

Hypothetical compression test on a jointed block

L_1 = original block height
L_2 = block height under normal stress
$L_1 - L_2$ = joint block shortening (ΔV_t total deformation)

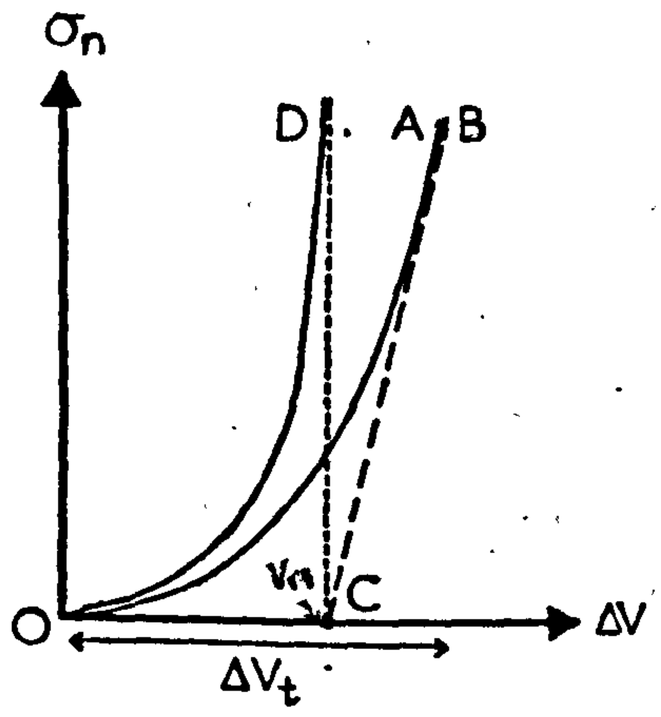

OA = joint block compression curve
BC = line representing compression of the rock material
OD = joint closure curve
V_m = maximum joint closure

FIGURE 3.40 Normal deformation of rock block containing a joint

(from Goodman and St. John, 1977)

The function which was found to fit best the experimental data was a simply modified form of the hyperbolic expression 3.10, by addition of a linear component (ΔV_r):

$$\Delta V_t = \Delta V_j + \Delta V_r = \frac{\sigma_n{}^a}{1 + \sigma_n{}^b} + \frac{\sigma_n}{c} \qquad 3.33$$

where c is a constant representing the elastic normal stiffness of the rock material. The experimental results from each joint were processed using a non-linear regression program in Algol 68 written by Powell (1979, personal communication). Each data set was fitted with

$$\Delta V_t = \frac{1}{\frac{1}{\sigma_n a} + \frac{b}{a}} + \frac{\sigma_n}{c} \qquad 3.34$$

so that for very large σ_n, 3.34 becomes

$$\Delta V_t = \frac{a}{b} + \left(\frac{1}{c}\right)\sigma_n \qquad 3.35$$

and thus, for large σ_n the slope is 1/c and the intercept is a/b, which has been defined as the maximum closure V_m.

The results from data processing showed that function 3.34 gave a very good fitting to the experimental loading paths. Of all cycles, the uncertainty in the "predicted" V_m values from the first loading curves were rarely outside the $\pm$ 1 to 4% range. Slightly wider range of uncertainty was indicated for the V_m data from the 2nd and 3rd loadings. The same applied for the "predicted" values for the initial normal stiffness coefficient K_{ni}. Detailed tables with complete experimental and analytical data have been included in Appendix IV.

In order to allow for the rock deformation component included in the "predicted" V_m, average correction quantities (Table 3.14) were evaluated from all the experimental curves available for each type of rock. The percentage variation of those values was estimated to be within the region of $\pm$ 5 to 15%.

TABLE 3.14

Average non-linearity components (ΔV_{nl}) of rock deformation

Rock type	Joint nos.	V_{nl} (mm) 1st loading	2nd loading	3rd loading	Rock weathering state
Dolerite	All	0.005	0.005	0.005	Fresh
Slate	1 to 4	0.003	0.003	0.003	Fresh (⊥)
"	5 to 7	0.020	0.020	0.020	Slightly weathered (⊥)
Limestone	All	0.006	0.006	0.006	Fresh
Siltstone	1 to 5	0.035	0.030	0.030	Fresh (//)
Siltstone	6 to 10	0.080	0.070	0.070	Slightly weathered (⊥)
Sandstone	1 to 4	0.040	0.035	0.035	Fresh (⊥)
Sandstone	5 to 8	0.030	0.025	0.025	Fresh (//)
Sandstone	9 to 12	0.050	0.050	0.045	Slightly weathered (//)
Sandstone	13 to 17	0.070	0.060	0.055	" " (⊥)
Sandstone	18 to 21	0.100	0.085	0.080	Highly weathered (⊥)

Maximum closure and initial normal stiffness data derived from the above procedure are listed in Table 3.15 and compared with the corresponding experimental values; that is, those obtained ordinarily by subtraction of the actual rock deformation curve from the joint block compression curves. As seen, the predicted and experimental parameters from both the first and third loadings were in close agreement, thus indicating that the empirical processing of the experimental data could indeed be regarded as a realistic approximation.

As stated earlier, the stress-closure relationship of a joint is uniquely defined by the initial normal stiffness and maximum closure. Those two parameters were derived for all the types of interlocked joints and are presented in Tables 3.16 to 3.20. The ± values represent the range of uncertainty implied by one standard deviation. In a few cases where no data from the 2nd or 3rd cycle have been

TABLE 3.15

Comparisons between experimental (E) and predicted (P) maximum closure and initial normal stiffness values.

	Maximum joint closure, V_m (mm)			
	1st LOADING		3rd LOADING	
Joint type	E	P	E	P
Slate, no. 3	.063	.058 ± .002	.026	.035 ± .004
Dolerite, no. 1	.081	.084 ± .001	.035	.042 ± .004
Limestone, no. 1	.072	.068 ± .002	.013	.016 ± .002
Limestone, no. 10	.105	.110 ± .002	.015	.016 ± .003
Sandstone, no. 2	.190	.173 ± .008	.022	.037 ± .007
Sandstone, no. 16	.255	.244 ± .012	.051	.058 ± .017
Siltstone, no. 3	.135	.143 ± .006	.036	.053 ± .006

	Initial normal stiffness, K_n (MPa/mm)			
	1st LOADING		3rd LOADING	
	E	P	E	P
Slate, no. 3	26.9	24.10 ± 1.77	210.20	189.10 ± 16.13
Dolerite, no. 1	22.7	26.72 ± 0.62	99.01	102.90 ± 9.03
Limestone, no. 10	25.9	27.64 ± 0.62	171.50	137.70 ± 30.78
Sandstone, no. 16	4.1	4.30 ± 0.41	26.46	32.04 ± 1.50
Siltstone, no. 3	18.0	22.42 ± 0.60	84.42	69.66 ± 3.20

TABLE 3.16

Initial normal stiffness (K_{ni}) and maximum closure (V_m) data from repeated normal loading cycles on SLATE cleavage planes.

Joint no.	1st CYCLE		2nd CYCLE		3rd CYCLE	
	K_{ni} (MPa/mm)	V_m (mm)	K_{ni} (MPa/mm)	V_m (mm)	K_{ni} (MPa/mm)	V_m (mm)
1	34.51 ± 0.92	.040 ± .0004	98.03 ± 6.24	.033 ± .001	185.20 ± 8.60	.032 ± .002
2	46.50 ± 5.59	.019 ± .0007	344.30 ± 19.71	.015 ± .001	424.40 ± 32.06	.015 ± .002
3	24.06 ± 1.76	.058 ± .002	101.10 ± 7.75	.034 ± .002	189.10 ± 16.13	.035 ± .004
4	13.10 ± .32	.106 ± .001	68.99 ± 2.08	.046 ± .001	235.50 ± 18.30	.039 ± .007
5	13.81 ± .78	.290	19.12 ± 1.90	.135 ± .01	63.58 ± 4.41	.120 ± .017
6	12.76 ± .49	.320	39.96 ± 1.64	.095	77.61 ± 2.39	.069
7	11.57 ± .48	.384	38.67 ± 0.67	.207 ± .007	49.47 ± 3.60	.165 ± .023

TABLE 3.17

Initial normal stiffness (K_{ni}) and maximum closure (V_m) data from repeated normal loading cycles on DOLERITE joints.

Joint no.	1st CYCLE		2nd CYCLE		3rd CYCLE	
	K_{ni} (MPa/mm)	V_m (mm)	K_{ni} (MPa/mm)	V_m (mm)	K_{ni} (MPa/mm)	V_m (mm)
1	26.72 ± 0.62	.084 ± .001	75.31 ± 4.47	.045 ± .002	102.90 ± 9.03	.042 ± .004
2	21.69 ± 0.96	.117 ± .003	58.98 ± 10.07	.061 ± .008	119.40 ± 2.99	.092 ± .005
3	13.29 ± 0.20	.525	33.72 ± 2.24	.135 ± .009	73.20 ± 4.03	.090 ± .001
4	10.96 ± 0.24	.454	91.53 ± 5.32	.077 ± .006	130.40 ± 5.63	.062 ± .005
5	7.06 ± 0.26	.473	24.73 ± 0.96	.238	37.48 ± 1.26	.175

TABLE 3.18

Initial normal stiffness (K_{ni}) and maximum closure (V_m) data from repeated normal loading cycles on LIMESTONE joints.

Joint no.	1st CYCLE		2nd CYCLE		3rd CYCLE	
	K_{ni} (MPa/mm)	V_m (mm)	K_{ni} (MPa/mm)	V_m (mm)	K_{ni} (MPa/mm)	V_m (mm)
1	21.63 ± 1.00	.068 ± .002	133.50 ± 24.91	.021 ± .004	159.50 ± 15.67	.016 ± .002
2	30.57 ± 1.71	.093 ± .003	56.50 ± 4.29	.053 ± .003	72.17 ± 1.58	.043 ± .001
3	10.98 ± 0.75	.104 ± .003	75.78 ± 4.85	.053 ± .003	90.23 ± 6.41	.045 ± .003
4	25.27 ± 0.75	.077 ± .001	53.92 ± 9.91	.045 ± .005	121.10 ± 17.14	.037 ± .006
5	18.68 ± .021	.097 ± .0006	74.26 ± 7.22	.037 ± .003	130.90 ± 12.72	.019 ± .002
6	9.81 ± 0.66	.094 ± .002	62.87 ± 7.81	.042 ± .004	103.00 ± 11.99	.025 ± .003
7	7.21 ± 0.87	.114 ± .002	98.38 ± 3.80	.049 ± .002	124.00 ± 15.92	.036 ± .005
8	14.51 ± 0.66	.085 ± .002	104.10 ± 6.62	.049 ± .004	126.80 ± 22.67	.032 ± .006
9	15.10 ± 0.24	.088 ± .005	108.6 ± 6.19	.041 ± .003	113.1 ± 4.19	.027 ± .001
10	27.64 ± 0.62	.110 ± .002	109.0 ± 12.81	.026 ± .002	137.7 ± 30.78	.016 ± .003
10a	24.95 ± 0.75	.069 ± .001	61.17 ± 3.78	.042 ± .002		

(Cont.)

TABLE 3.18 (Cont.)

Joint no.	1st CYCLE		2nd CYCLE		3rd CYCLE	
	K_{ni} (MPa/mm)	V_m (mm)	K_{ni} (MPa/mm)	V_m (mm)	K_{ni} (MPa/mm)	V_m (mm)
11	32.85 ± 1.15	.124 ± .005	45.83 ± 3.76	.046 ± .002	121.4 ± 10.74	.028 ± .003
12	70.22 ± 2.22	.070 ± .002	25.71 ± 6.50	.026 ± .002	53.33 ± 10.07	.019 ± .002
13	34.42 ± 0.35	.086 ± .0007	90.72 ± 2.75	.060 ± .002	168.40 ± 16.91	.039 ± .006
14	4.95 ± 0.34	.146 ± .003	47.80 ± 1.80	.087 ± .003	71.28 ± 2.35	.077 ± .003
15	8.28 ± 0.61	.156 ± .004	48.41 ± 5.37	.080 ± .006	80.12 ± 13.38	.037 ± .004
16	6.92 ± 0.20	.525				
17	12.89 ± 0.47	.400	49.44 ± 6.27	.078 ± .009	59.76 ± 5.47	.059 ± .005
18	3.84 ± 0.21	.307	43.66 ± 3.80	.070 ± .006	65.16 ± 4.83	.062 ± .006
19	6.27 ± 0.57	.319	43.99 ± 5.62	.124	42.50 ± 1.49	.114 ± .004
20	12.43 ± 1.60	.316	39.77 ± 4.89	.112	60.26 ± 8.29	.079

TABLE 3.19

Initial normal stiffness (K_{ni}) and maximum closure (V_m) data from repeated normal loading cycles on SILTSTONE joints.

Joint no.	1st CYCLE		2nd CYCLE		3rd CYCLE	
	K_{ni} (MPa/mm)	V_m (mm)	K_{ni} (MPa/mm)	V_m (mm)	K_{ni} (MPa/mm)	V_m (mm)
1	14.02 ± 2.24	.117 ± .017	21.83 ± 1.21	.099 ± .008	21.82 ± 1.13	.096 ± .007
2	25.90 ± 2.67	.123 ± .019	64.23 ± 5.94	.039 ± .010	69.06 ± 4.35	.040 ± .007
3	22.42 ± 0.60	.143 ± .006	45.75 ± 2.35	.077 ± .012	69.66 ± 3.20	.053 ± .006
4	15.82 ± 2.03	.152 ± .019				
5	16.23 ± 0.93	.140 ± .008				
6	11.22 ± 0.41	.339 ± .018	20.03 ± 2.37	.132 ± .023	25.93 ± 1.29	.130 ± .014
7	10.49 ± 0.23	.281 ± .012				
8	9.97 ± 0.19	.500 ± .018	27.01 ± 1.42	.106 ± .015	29.04 ± 1.94	.120 ± .021
9	6.95 ± 0.28	.523 ± .035	28.60 ± 0.91	.101 ± 0.14	40.93 ± 0.65	.105 ± .012
10	14.21 ± 0.13	.520 ± .017	25.07 ± 0.72	.185 ± .018	30.72 ± 1.74	.156 ± .05

TABLE 3.20

Initial normal stiffness (K_{ni}) and maximum joint closure (V_m) data from repeated normal loading cycles on SANDSTONE joints.

Joint no.	1st CYCLE		2nd CYCLE		3rd CYCLE	
	K_{ni} (MPa/mm)	V_m (mm)	K_{ni} (MPa/mm)	V_m (mm)	K_{ni} (MPa/mm)	V_m (mm)
1	3.56 ± 0.12	.246 ± .008	11.54 ± 0.67	.156 ± .013	18.30 ± 1.81	.096 ± .015
2	14.62 ± 0.28	.173 ± .008	34.94 ± 2.03	.043 ± .007	37.27 ± 2.52	.037 ± .007
3	11.88 ± 0.28	.196 ± .009	15.99 ± 1.14	.081 ± .008	24.46 ± 1.68	.066 ± .009
4	6.65 ± 0.28	.194 ± .008	31.14 ± 3.53	.068 ± .007	36.08 ± 3.47	.045 ± .006
5	16.21 ± 1.92	.128 ± .014	30.00 ± 1.31	.057 ± .003	62.08 ± 3.47	.024 ± .003
6	22.67 ± 0.62	.139 ± .005	18.68 ± 2.23	.078 ± .008	56.45 ± 2.86	.059 ± .008
7	17.21 ± 0.32	.134 ± .005	24.03 ± 1.25	.069 ± .005	23.09 ± 0.79	.054 ± .003
8	9.74 ± 0.44	.148 ± .006	20.95 ± 1.99	.049 ± .008	40.04 ± 2.39	.049 ± .005
9	7.97 ± 0.36	.200 ± .010	25.35 ± 1.66	.064 ± .010	31.94 ± 1.90	.058 ± .009
10	7.10 ± 0.20	.272 ± .008	26.62 ± 1.76	.069 ± .011	44.79 ± 5.15	.057 ± .018

(Cont.)

TABLE 3.20 (Cont.)

Joint no.	1st CYCLE		2nd CYCLE		3rd CYCLE	
	K_{ni} (MPa/mm)	V_m (mm)	K_{ni} (MPa/mm)	V_m (mm)	K_{ni} (MPa/mm)	V_m (mm)
11	25.57 ± 1.41	.197 ± .009	26.87 ± 1.61	.085 ± .011	26.99 ± 1.53	.079 ± .006
12	11.45 ± 0.49	.270 ± .018	13.12 ± 0.84	.107 ± .009	28.53 ± 1.67	.108 ± .015
13	8.51 ± 0.10	.286 ± .008	13.46 ± 0.74	.092 ± .009		
14	5.64 ± 0.42	.241 ± .017	13.97 ± 0.64	.156 ± .013	16.25 ± 1.23	.095 ± .012
15	5.16 ± 0.38	.237 ± .016	8.80 ± 0.60	.115 ± .010	18.04 ± 1.12	.120 ± .014
16	4.30 ± 0.41	.244 ± .012	19.30 ± 0.75	.096 ± .009	32.04 ± 1.50	.058 ± .017
17	8.27 ± 0.23	.216 ± .014	13.61 ± 1.43	.125 ± .013	14.80 ± 0.75	.139 ± .014
18	4.73 ± 0.25	.370 ± .038	13.67 ± 0.73	.066 ± .014	19.90 ± 0.80	.064 ± .015
19	2.60 ± 0.07	.552 ± .027	8.95 ± 0.37	.196 ± .042	11.33 ± 0.49	.095 ± .013
20	2.54 ± 0.03	.510 ± .040				
21	2.68 ± 0.04	.443 ± .018				

included, repeated loading of the particular joint was either not performed or discontinued due to specimen failure. The V_m values predicted for the weathered joints in slate, dolerite and limestone under first loading were much lower than what would be expected considering the magnitude of the total deformation (ΔV_t) and rock deformation (ΔV_r). As already pointed out, the slope of the portion of the ΔV_t-curves of weathered joints in the high stress region was artificially low due to incomplete closure, and consequently erroneous overestimates of ΔV_r were obtained. Significant increase in the steepness of the curves was observed during the second and third loadings. For example, in the case of the limestone joint no. 17 the value of c (= slope of asymptote in 3.34) increased from an initial 235.6 MPa/mm to 698.4 MPa/mm, which was within the expected range for the particular type of rock. Unless independent ΔV_r data for those joints were available, the total deformation curves were corrected by using the value of c as predicted for the third loading curve.

The empirical analysis of the stress-deformation relationships of interlocked joint blocks could not be adopted for the mismatched specimens. Even under the maximum stresses the deformation across the asperity contacts of the mismatched joint walls contributed a significant portion to the total deformation of the blocks. Consequently, the slope of the "elastic" portion of the curves was appreciably lower than that of the solid rock compression line. Ultimately, the following correction procedure was chosen: for each particular joint the V_m and K_{ni} values derived from the last loading test were used to calculate its closure curve from: $\Delta V_j = \sigma_n V_m/(K_{ni} V_m + \sigma_n)$. The closure curve was then subtracted from the experimental (total deformation, ΔV_t) curve to obtain the approximate compression line of the solid rock. In that manner it was possible to allow for the non-linearity in rock behaviour under the third loading. As it would be unlikely to encounter any significant changes in rock behaviour under its fourth loading, the calculated ΔV_r values were used to correct the ΔV_t data from the same joint when tested in mismatched position.

The experimental results for the suite of 24 mismatched joints are summarized in Table 3.21. For each specimen the following data are given: (i) the average aperture (a_j); (ii) the regression coefficient q of the semi-log plots of stress versus closure; (iii) the closure of all joints

TABLE 3.21

Summary of experimental results from normal loading tests on mismatched joints (first loading, initial normal stress ~ 0.15 MPa).

Joint no.	Average aperture a_j (mm)	Regression coefficient q	Closure (ΔV_j) at σ_n = 15 MPa (mm)
LIMESTONE			
1	0.800	3.881	0.293
6	0.300	12.199	0.151
8	0.360	6.445	0.318
9	0.450	8.872	0.208
10	0.350	11.158	0.152
13	0.480	4.866	0.270
AF	1.300	4.574	0.470
SANDSTONE			
2	0.590	6.987	0.311
3	0.380	8.082	0.210
7	0.600	5.601	0.319
8	0.250	11.390	0.175
9	0.350	5.761	0.304
10	0.490	5.073	0.314
12	0.350	9.704	0.185
13	0.480	4.042	0.352
14	0.420	6.162	0.264
16	0.250	9.408	0.184
Millstone grit			
M1	1.220	4.538	0.387
M2	0.520	6.104	0.277
SILTSTONE			
2	0.480	7.801	0.241
5	0.860	4.225	0.314
9	0.730	2.779	0.489
SLATE			
1	0.150	23.349	0.076
2	0.230	16.329	0.108

Notes: Joint nos. are as originally assigned (see Tables 3.7 to 3.11). The limestone specimen AF is an artificial extension fracture (JCS = 135 MPa, JRC = 10). M1 and M2 are two extension fractures in coarse-grained sandstone of the Millstone Grit series (JCS = 54 - 65 MPa, JRC = 9.5 for M1, and 7.8 for M2).

at the arbitrary normal stress level of 15 MPa, for ready appraisal of the differences in deformability and in place of the unobtained values of V_{max}.

(2) Direct shear test results

The ranges of the shear stiffness parameters derived from the experimental results are summarized in Table 3.22. Linear regression analyses of the d_h/τ vs d_h plots yielded the initial shear stiffness coefficient (K_{si}) at each of the normal stress levels. The log-log relationships between K_{si} and σ_n gave the values of the stiffness number (K_j) and stiffness exponent (n_j) for each of the joints. As the failure ratio (R_f) values did not display large differences under different σ_n, mean values have been included. The weathering state of joints is denoted by F, SW, MW and W as defined earlier.

TABLE 3.22

Summary of joint shear stiffness data

Joint no.	Normal stress (MPa)	Initial K_{si} (MPa/mm)	Stiffness number K_j (MPa/mm)	Stiffness exponent n_j (MPa^2/mm)	Failure ratio R_f	Secant peak K_s (MPa/mm)
SANDSTONE						
5 (SW)	.25 - 2.07	8.7 - 41.9	24.49	0.714	0.738	1.23 - 4.74
4 (F)	.29 - 2.36	10.2 - 37.6	23.64	0.624	0.724	1.57 - 4.50
3 (F)	.25 - 2.04	3.4 - 14.5	9.25	0.697	0.776	0.56 - 2.28
1 (F)	.27 - 2.13	2.2 - 10.8	6.18	0.703	0.744	0.95 - 2.46
15 (MW)	.24 - 2.04	1.2 - 4.9	3.02	0.700	0.810	0.47 - 1.59
17 (MW)	.48 - 1.45	2.7 - 6.2	4.74	0.754	0.810	0.78 - 1.73
19-21(W)	.50 - 1.96	2.1 - 6.5	3.49	0.831	0.887	0.56 - 1.35
LIMESTONE						
4 (SW)	.23 - 1.84	9.0 - 50.5	30.19	0.799	0.830	1.65 - 6.87
14 (MW)	.24 - 1.90	4.1 - 17.3	9.73	0.698	0.731	1.12 - 3.13
20 (W)	.25 - 1.53	1.0 - 10.5	5.04	1.188	0.788	0.66 - 1.89

(Cont.)

TABLE 3.22 (Cont.)

Joint no.	Normal stress (MPa)	Initial K_{si} (MPa/mm)	Stiffness number K_j (MPa/mm)	Stiffness exponent n_j (MPa^2/mm)	Failure ratio R_f	Secant peak K_s (MPa/mm)
DOLERITE						
2 (SW)	.26 - 2.11	8.2 - 19.0	17.74	0.615	0.652	1.75 - 4.98
5 (W)	.28 - 1.11	3.6 - 9.1	9.02	0.674	0.778	0.86 - 2.19
SLATE						
1-3 (F)	.54 - 2.28	K_s	-	0	0	5.6 - 12.6
5-7 (W)	.40 - 1.45	2.8 - 7.5	5.72	0.76	0.870	0.64 - 1.27

3.3.4 Discussion of results

Some introductory comments on the quantitative differences in joint stiffness were made in the last chapter. The normal and shear stiffness data listed in Tables 3.16 to 3.22 provide a complete picture of the range of variations in the deformability of the present types of joints. It is seen that considerable differences exist between the stiffness parameters of fresh joints from the five different rock types and even between joints from the same rock and of similar weathering characteristics. Weathered joints are expectedly more deformable than fresh specimens from the same rock type. An attempt has been made to express those variations in a quantitative manner based on measurable indices of joint wall strength and geometry.

1. Study of the variations in interlocked joint normal stiffness

For a ready appraisal of the variations in the normal deformability of the various types of joints, the ranges and average maximum closure (V_m) and initial normal stiffness (K_{ni}) values from all loading cycles are summarized in Table 3.23, from which the following general observations can be made:

(i) Comparison of the average maximum closure of fresh joints from all rock types shows a maximum difference by an average factor of 4.4. The highest recorded V_m value was 0.246 mm (sandstone, no. 1) and the lowest was 0.019 mm (slate, no. 2). Variations in the V_m of fresh joints also persisted under the subsequent reloadings, but the differences were less pronounced. Under the third loading the highest and lowest average closure values differed by a factor of 2.5. The maximum V_m under that cycle was 0.096 mm (sandstone, no. 1 and siltstone, no. 1) and the minimum was 0.015 mm (slate, no. 2).

(ii) Comparison of the average maximum closure of fresh and weathered joints from the same rock type shows a maximum increase by an average factor of 8.5 (slate), and a minimum increase by an average factor of 2.8 (sandstone). The average maximum closure of weathered joints in dolerite,

TABLE 3.23

Summary of K_{ni} and V_m data from all interlocked joint types.

Rock type and weathering state of joints	JCS (MPa)	No. of joints	RANGE AND AVERAGE V_m AND K_{ni} DATA											
			1st CYCLE				2nd CYCLE				3rd CYCLE			
			K_{ni} (MPa/mm)		V_m (mm)		K_{ni} (MPa/mm)		V_m (mm)		K_{ni} (MPa/mm)		V_m (mm)	
			Range	Aver.	Range	Aver.	Range	Aver.	Range	Aver.	Range	Aver.	Range	Aver.
SLATE														
Fresh	175	3	24.1-46.5	35.0	.019-.058	.039	98.0-344.3	181.1	.015-.034	.027	185.2-424.4	266.2	.015-.035	.027
Mod. weathered	142	1	-	13.1	-	.106	-	69.0	-	.046	-	235.5	-	.039
Weathered	77	3	11.6-13.8	12.7	.290-.384	.331	19.1-40.0	32.6	.095-.207	.146	49.5-77.6	63.6	.069-.165	.118
DOLERITE														
Fresh	167-182	2	21.7-26.7	24.2	.084-.117	.101	59.0-75.3	67.1	.045-.061	.053	102.9-119.4	111.2	.042-.092	.067
Weathered	60-76	3	8.1-13.4	10.8	.454-.525	.484	24.7-91.5	50.0	.077-.238	.150	37.5-130.4	80.4	.062-.175	.109
LIMESTONE														
Fresh to slightly weathered	152-170	11	7.9-30.6	18.8	.068-.114	.091	53.9-133.5	85.3	.021-.053	.042	72.2-159.5	117.9	.016-.045	.030
Mod. weathered	94-120	5	4.9-70.2	30.1	.070-.156	.116	25.7-90.7	51.7	.026-.087	.060	53.3-168.4	98.9	.019-.077	.040
Weathered	35-53	5	3.8-12.9	8.5	.307-.525	.373	39.8-49.4	44.2	.070-.124	.115	42.5-65.2	56.9	.059-.114	.079
SILTSTONE														
Fresh	105	5	14.0-25.9	18.9	.117-.152	.135	21.8-64.2	43.9	.039-.099	.072	21.8-69.7	53.5	.040-.096	.063
Mod. weathered	67	2	10.5-11.2	10.8	.281-.339	.310	20.0-21.6	20.8	.132-.277	.205	19.9-25.9	22.9	.130-.237	.184
Weathered	44	3	6.9-14.2	10.4	.500-.523	.514	27.0-28.6	27.8	.101-.106	.104	29.0-40.9	35.0	.120-.105	.113
SANDSTONE														
Fresh to slightly weathered	68-95	8	3.6-22.7	12.8	.128-.246	.170	11.5-34.9	23.4	.043-.156	.075	18.3-62.1	37.2	.024-.096	.054
Mod. weathered	64-58	9	4.3-25.6	9.3	.197-.286	.240	8.8-26.9	17.9	.064-.156	.101	14.8-44.8	26.7	.057-.139	.089
Weathered	22	4	2.3-4.7	3.1	.370-.552	.469	9.0-13.7	11.3	.066-.196	.131	11.3-19.9	15.6	.064-.095	.080

limestone, and siltstone was greater than that of the fresh specimens by average factors of 4.8, 4.0 and 3.8 respectively. The differences in the average maximum closure of fresh and weathered joints under the third loading were approximately two times smaller than above.

(iii) The initial normal stiffness (K_{ni}) coefficients are also considerably variable. The lowest average K_{ni} value of fresh joints was obtained from the sandstone group (= 12.8 MPa/mm) and the highest was obtained from the slate cleavage planes (= 35.0 MPa/mm). The minimum and maximum K_{ni} values recorded from individual specimens were 3.6 MPa/mm (sandstone, no. 1) and 70.2 MPa/mm (limestone, no. 2). The average K_{ni} coefficients of weathered joints were predictably lower by factors ranging from approximately 1.8 to 4.0.

It is generally recognized that under a certain initial stress condition the basic factors influencing the amount of joint closure, and hence the normal stiffness, are the aperture thickness, the strength and deformation properties of the asperities and the roughness of the walls. By definition the aperture represents the maximum possible amount of vertical displacement which can occur between two proximate surfaces. The maximum amount of displacement which actually occurs may be only a fraction of the aperture depending on the mechanical resistance of the surface protrusions against the applied loads and the vertical distribution of the aperture. It is also reasonable that roughness may play a part in restraining the closure of the joint surfaces.

The present results provide factual evidence of the interrelationship between the joint closure and the above variables. Study of the analytical V_m data in Tables 3.16 to 3.20 in conjunction with the strength and geometrical properties of the joints (listed in previous Tables 3.7 to 3.11) shows that: (a) the maximum closure of joints with similar average aperture thickness depends primarily on the strength of the joint walls; (b) the fluctuations in the maximum closure of joints with similar wall strength and average aperture seem to be related with the differences in the roughness of the surfaces; (c) the large increases in the closure of the present types of weathered joints are the result of the combined effect of wider apertures and much lower wall strength.

It is of practical interest to search for a functional expression of the interrelationship between the maximum closure and the joint variables. In strict terms, this would require quantification of factors such as the initial contact area ratio, the size and shape of protrusions and the perpendicular distribution of their heights, as well as the variations in aperture thickness in both the perpendicular and lateral senses. Provided that those factors could be expressed in some quantitative form, it is questionable whether a meaningful relationship could ever be arrived at, due to the complex geometry of most natural surfaces. It may therefore be preferable to divert the attention onto well understood empirical indices describing the joint wall strength and geometry such as JCS and JRC. The most problematic variable is the aperture of the walls. It is true to say that no absolute measure of the joint aperture can be obtained. The nearest approximation is usually considered to be the equivalent aperture value derived from the back-analysis of a joint permeability test. A reasonable approximation can be obtained from direct measurements with feeler gauges provided that the openings are not extremely small ($\ll$0.1 mm) and measurements are taken along representative sections of the joint, as has been discussed in section 3.2.2(4b).

It was stated earlier that the large increases in the maximum closure of weathered joints was the consequence of wider apertures (a_j) coupled with the much reduced mechanical resistance (JCS) of the weathered asperities. The relative effect of JCS and a_j on joint closure can be studied simultaneously by combining the two variables empirically in a convenient form as JCS/a_j. Large values of the ratio indicate high JCS and small a_j; small values indicate low JCS and large a_j. The ratio of JCS/a_j gives a more appropriate quantitative reference of the weathering state of the present joints than JCS alone.

A detailed picture of the weathering effects on the normal deformability of joints from each rock type is presented in Figures 3.41 to 3.44 (symbols F, SW, MW and W describe fresh, slightly weathered, moderately weathered and weathered joints respectively). The top diagram in each of the figures shows the rate of increase in the maximum closure with decreasing JCS/a_j. All V_m data correspond to the first loading cycle. The exponential relationships arise from the normalization of JCS by a_j. Plots of V_m versus JCS gave linear trends

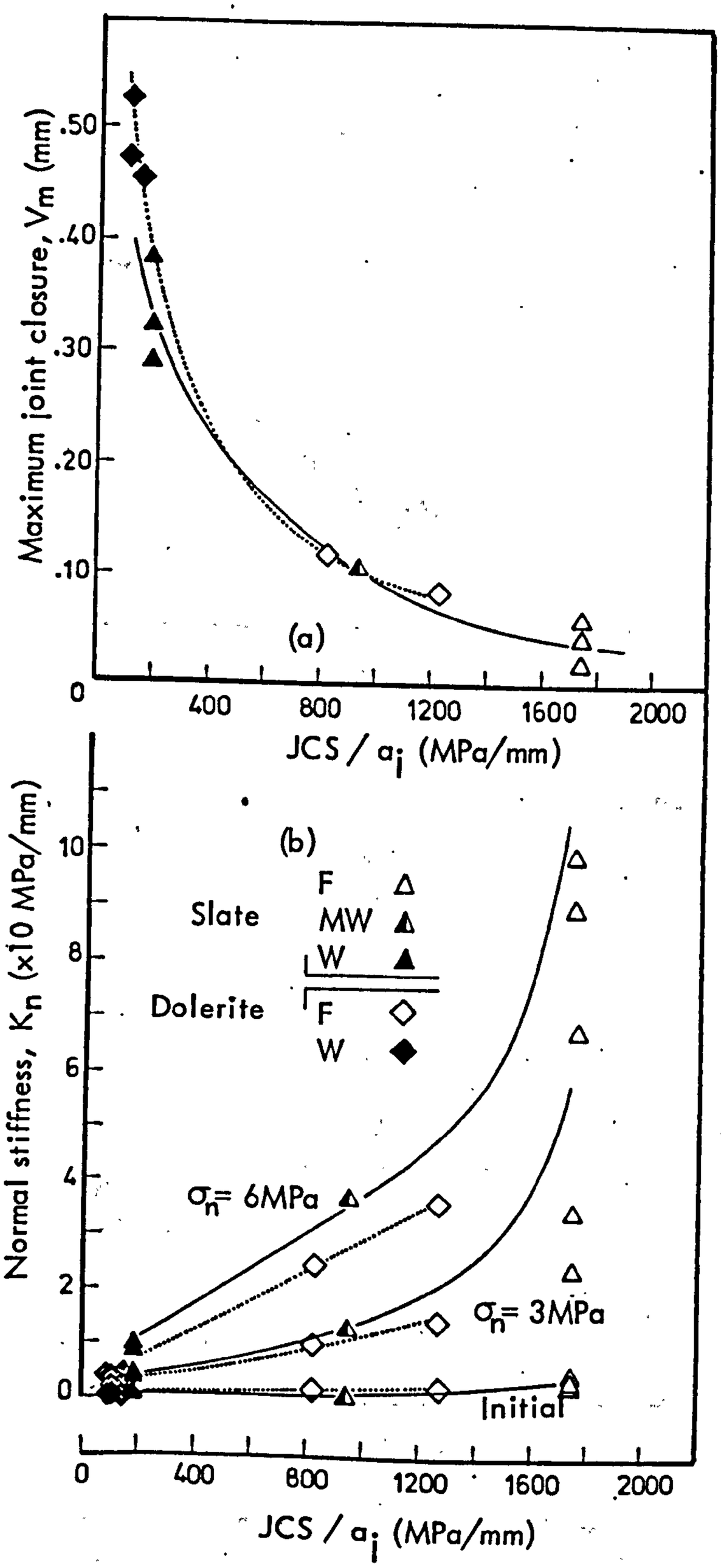

FIGURE 3.41 Weathering effects on the normal deformation of slate and dolerite joints :

(a) Variation of maximum joint closure with changing joint wall aperture (a_i) and strength (JCS)

(b) Variation of joint normal stiffness at three levels of normal stress with changing a_i and JCS

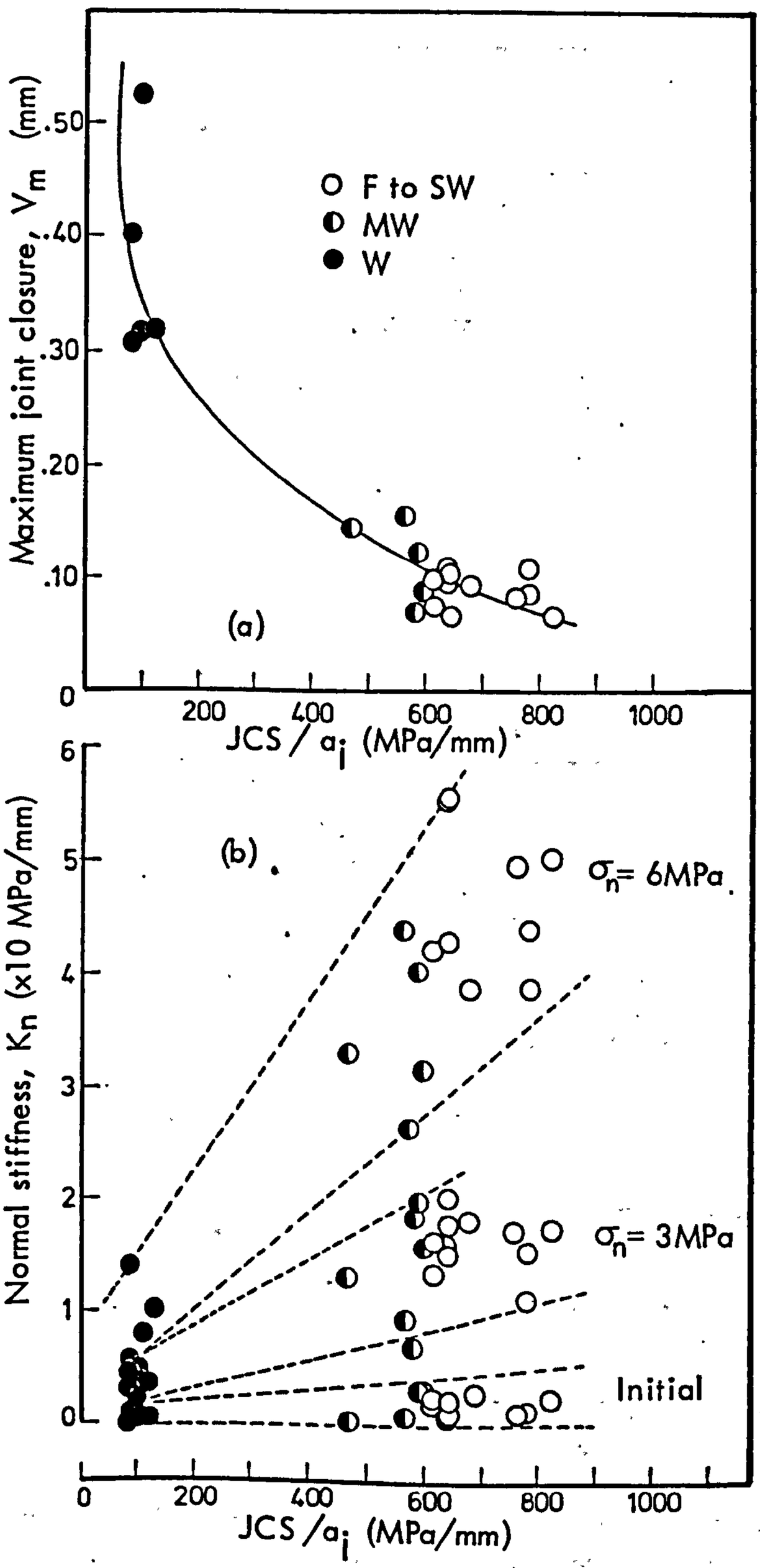

FIGURE 3.42 Weathering effects on the normal deformation of limestone joints :
(a) Variation of maximum joint closure with changing joint wall aperture (a_i) and strength (JCS)
(b) Variation of joint normal stiffness at three levels of normal stress with changing a_i and JCS

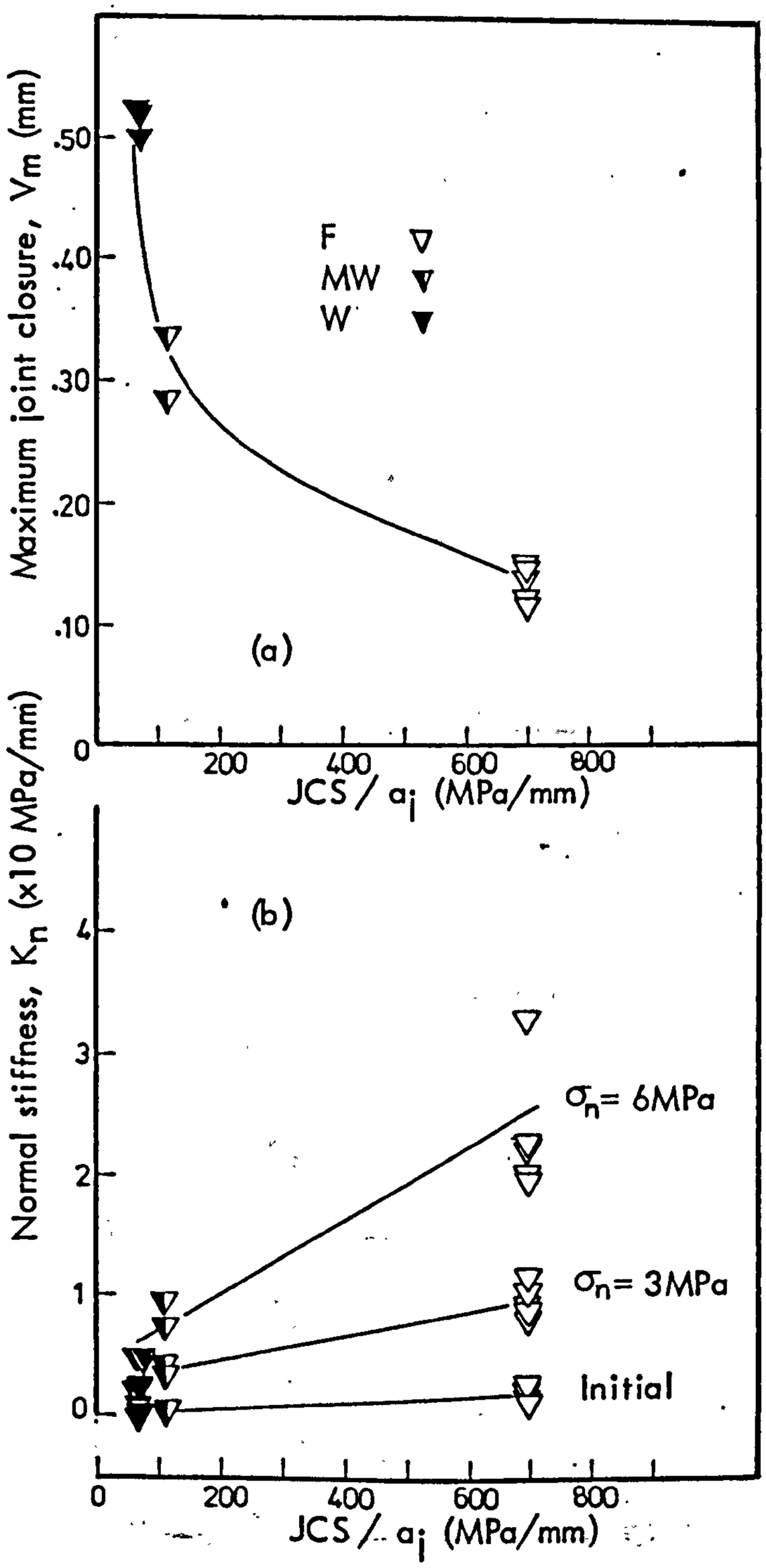

FIGURE 3.43 Weathering effects on the normal deformation of siltstone joints :
(a) Variation of maximum joint closure with changing joint wall aperture (a_i) and strength (JCS)
(b) Variation of joint normal stiffness at three levels of normal stress with changing a_i and JCS

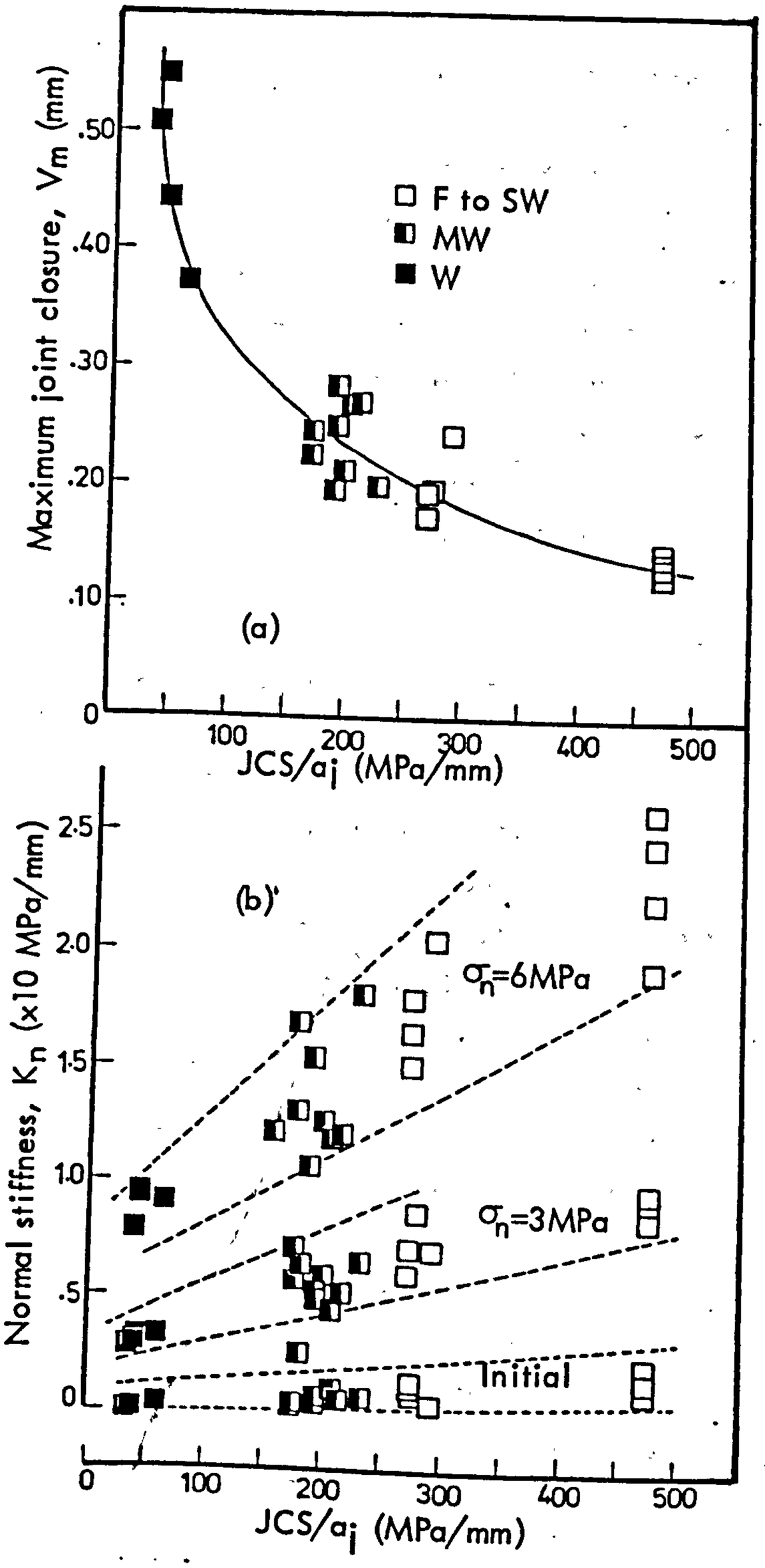

FIGURE 3.44 Weathering effects on the normal deformation of sandstone joints:
(a) Variation of maximum joint closure with changing joint wall aperture (a_j) and strength (JCS)
(b) Variation of joint normal stiffness at three levels of normal stress with changing a_j and JCS

for all joint groups except for the limestone. The bottom diagram in each of the figures illustrates the variations in the normal stiffness coefficients of the fresh and weathered joints at different levels of normal stress. The K_n coefficients are the "tangent" values calculated from equation 3.17 at σ_n equal to 3.0 and 6.0 MPa. The "initial" K_{ni} values are those listed in Tables 3.17 to 3.20. The increasing rate of change in K_n with JCS/a_j under rising normal stresses illustrates the effects of the significantly different "stiffening" paths imposed by the different a_j and JCS variables. As an extreme example, the average K_n coefficients at a very small increment of σ_n ("initial" K_{ni}) of three fresh ($a_j \sim .10$ mm, JCS = 175 MPa) and three weathered ($a_j \sim 0.40$-0.60 mm, JCS = 77 MPa) cleavage planes in slate differed by a factor of 2.2. At σ_n equal to 3.0 MPa the difference rose to an average factor of 11.7 which then increased to 17 at $\sigma_n = 6.0$ MPa.

The essential similarity between the relationships of maximum closure with JCS/a_j led to a combined plot of the V_m values of all the joints both fresh and weathered, against the respective JCS/a_j ratio values. As shown in Figure 3.45, the data combined produced a distinct non-linear relationship of high correlation. Similar plots were also prepared for the maximum closure data from the second and third cycles, and have been included in Figure 3.45. The values of average aperture a_j used for the latter two were different from those previously used. In the plot of V_m data from the second cycle the a_j value for each joint was assumed to be equal to the initial aperture minus the permanent set at the end of the first cycle. Accordingly, the a_j of the joints under the third loading was assumed to be equal to the sum of permanent sets under the previous two cycles. For purposes of comparison the regression lines of the relationships for the second and third loadings have also been drawn to the same scale of axes as the first.

Curve fitting procedures applied on the relationships in Figure 3.45 showed that the data were best fitted by a power curve:

$$V_m = C\left(\frac{JCS}{a_j}\right)^D \qquad 3.36$$

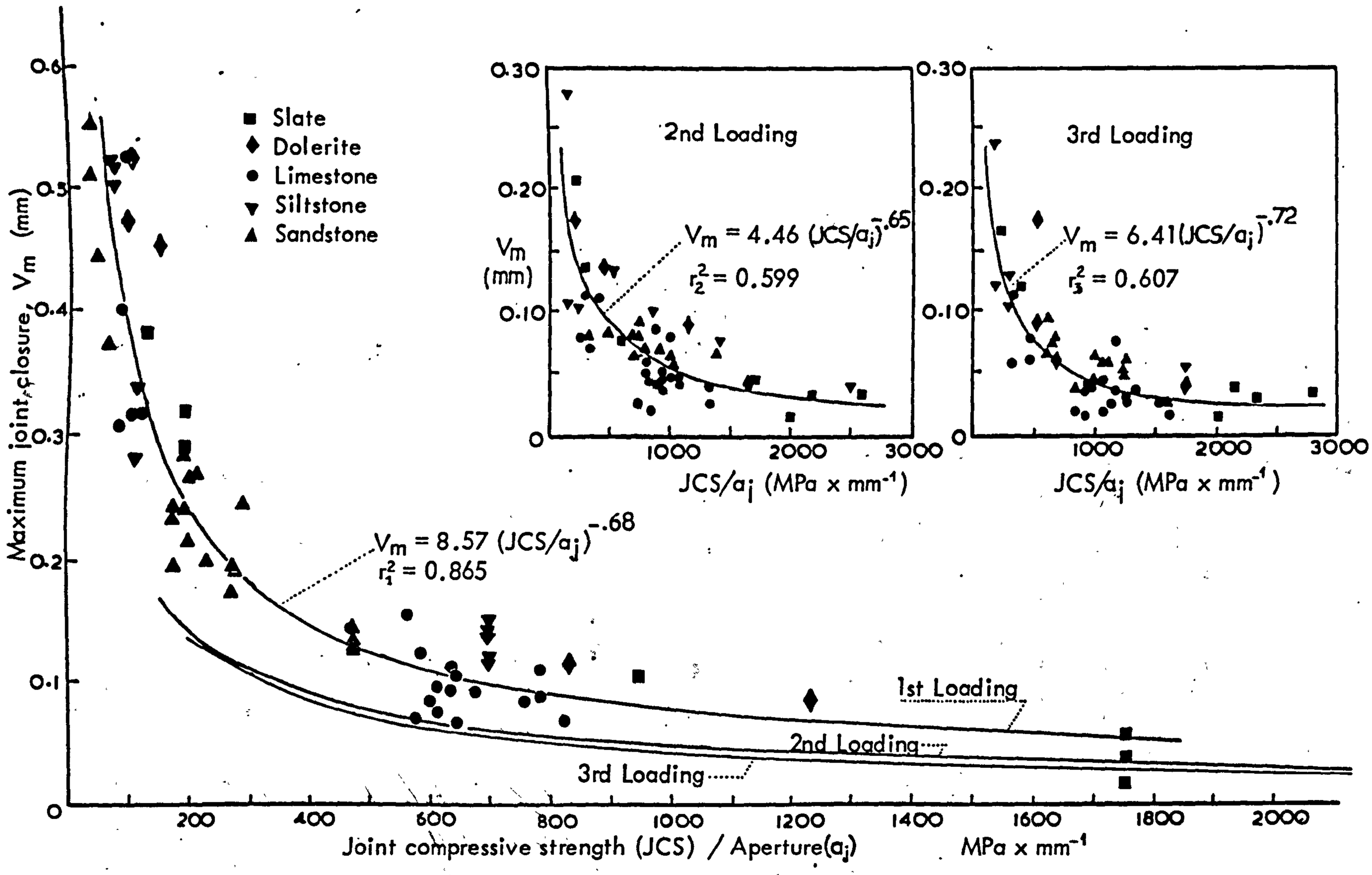

FIGURE 3.45 Relationships between maximum closure (V_m), wall strength (JCS) and aperture (a_j) of different joint types under repeated normal loading

The values of the constants C and D derived from the least square regression analysis of the data and the respective coefficients of determination (r^2) were as follows:

1st loading:	$C_1 = 8.57$	$D_1 = -0.68$	$r_1^2 = 0.865$
2nd loading:	$C_2 = 4.46$	$D_2 = -0.65$	$r_2^2 = 0.599$
3rd loading:	$C_3 = 6.41$	$D_3 = -0.72$	$r_3^2 = 0.607$

The third variable of potential influence on maximum joint closure is the surface roughness. The latter can be expressed by the empirical index of JRC. In order to examine the variations in maximum closure with JRC, a selection of V_m data from joints displaying similar aperture thicknesses was made. The selected data werefurther divided into three groups according to the JCS values, as follows: (a) JCS $>$ 140 MPa (limestone joint nos. 1 to 10a, slate cleavage no. 4, dolerite joint nos. 1 and 2); (b) JCS = 90 - 120 (limestone joint nos. 11 to 15, siltstone fracture nos. 1 to 5, sandstone joint nos. 5 to 8); (c) JCS $<$ 70 MPa (sandstone joint nos. 1 to 4 and 9 to 17).

The relationships derived by plotting the maximum closure data against the joint roughness coefficients are illustrated in Figure 3.46 for all three loading cycles. The V_m data from the first loading test presented a well defined trend of decreasing maximum closure with increasing JRC irrespective of the joint wall strength (JCS). The plots of the data from the second and third loadings showed a very high scatter but in most cases a similar trend was discernible.

An explanation for these inverse relationships between closure and surface roughness may be as follows: the mechanical interlocking between two mated surfaces becomes more effective with increasing JRC. This may have an effect upon the deformability of joints at both the very low and high levels of normal stress. Upon initiation of loading joints undergo a rapid closure through readjustment of their initial seating condition. It is logical to assume that the degrees of freedom across the interface depend on the interlocking potential between the two mated surfaces. The rate of closure at the very initial loading stages is described by the initial normal stiffness coefficient (K_{ni}). Plots of K_n versus JRC show a distinct increase in K_{ni} with increasing

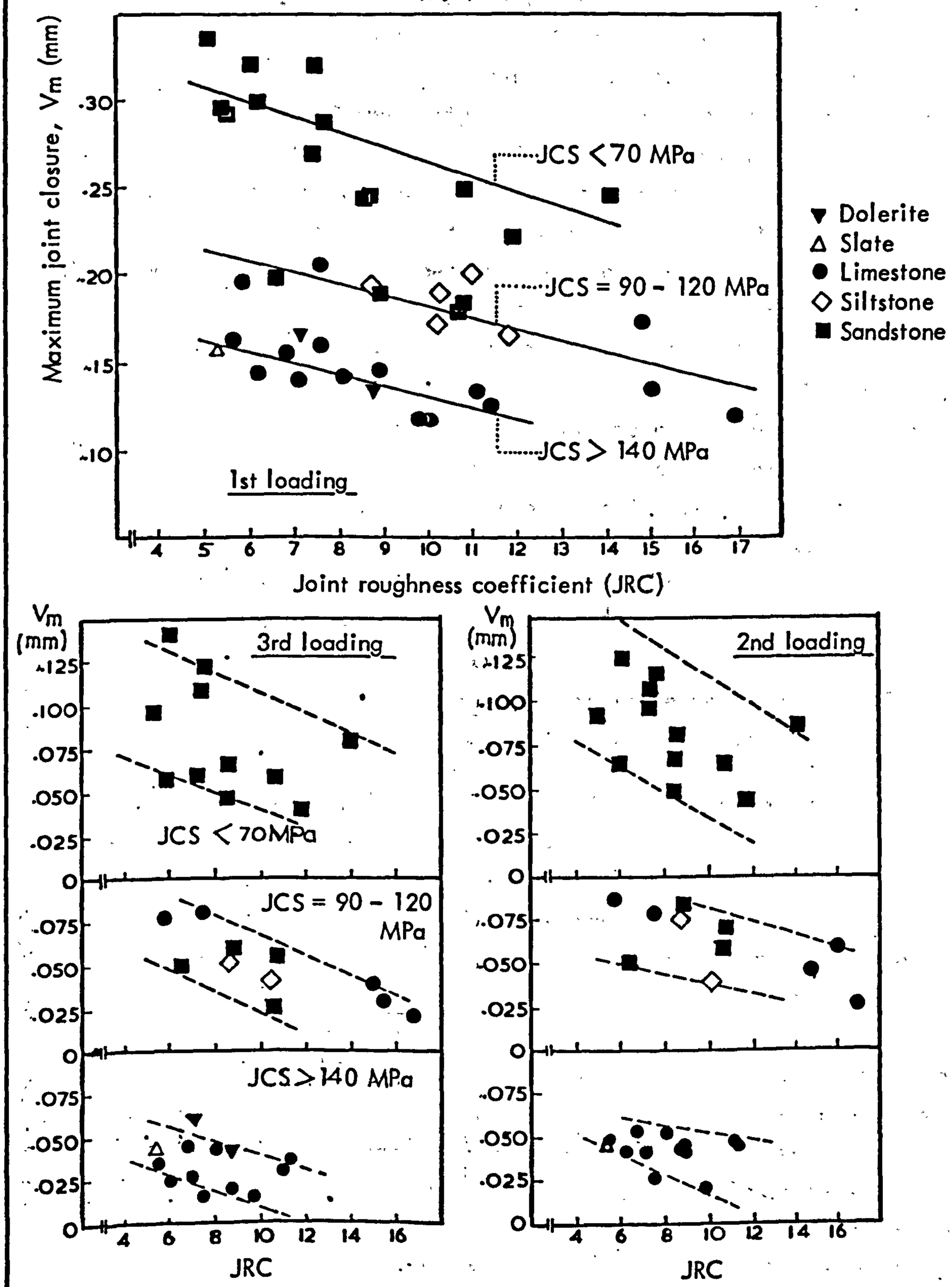

FIGURE 3.46 Relationships between maximum closure (V_m) and wall roughness (JRC) for different joint types

JRC (Figure 3.47). It is therefore plausible that the interlocking of rough surfaces reduces the amount of initial joint closure. As the normal stresses increase, the closure of the joint depends almost exclusively on the deformability of asperities. The tight mechanical interlock between the protrusions of a rough surface probably creates a very effective confined environment, thus improving the deformational response of the asperities. It is logical to expect that such an effect would be less pronounced in the cases of more regular surfaces. The impressions of the areas of actual contact presented in Figure 3.22 indicate that loads applied on very rough surfaces will be distributed over relatively larger contact areas than in cases of planar joints. The latter 2 related factors, i.e. confinement potential and relatively larger actual contact area, may also explain why roughness seemingly has some effect on joint closure under reloading, although the scatter in the data points of the high JCS joint group does not indicate roughness effects with certainty. The scatter in the JCS <70 MPa joint group is probably due to variation in the aperture thickness which depends on the permanent set(s) obtained at the end of the previous cycle(s). No relationship was found between the initial stiffness under the second and third loading tests and JRC.

The trends in Figure 3.46 indicate that within the range of JRC and JCS values considered, the variation between maximum closure and JRC can be approximated by a linear relationship. At present it is not possible to state what the relationship would be for the range of JRC below ~ 5 and over ~ 15. It would seem logical that the relationship in the two extreme ranges will experience a gradual flattening, although this can only be established experimentally. Also, it is not possible to establish with certainty what the roughness effects were, if any, in the cases of the weathered joints, due to the small number of specimens and their similar roughness. Limited experimental evidence does not indicate any deviation from the norm. Comparison between three weathered limestone joints (nos. 16, 17 and 18) shows that the closure of the relatively planar (JRC ~ 5) joint no. 16 was much larger than that of nos. 17 and 18 which were very undulating and rough (JRC = 15.0).

The established relationships between the maximum closure and the indices of wall aperture, strength and roughness were combined to yield an

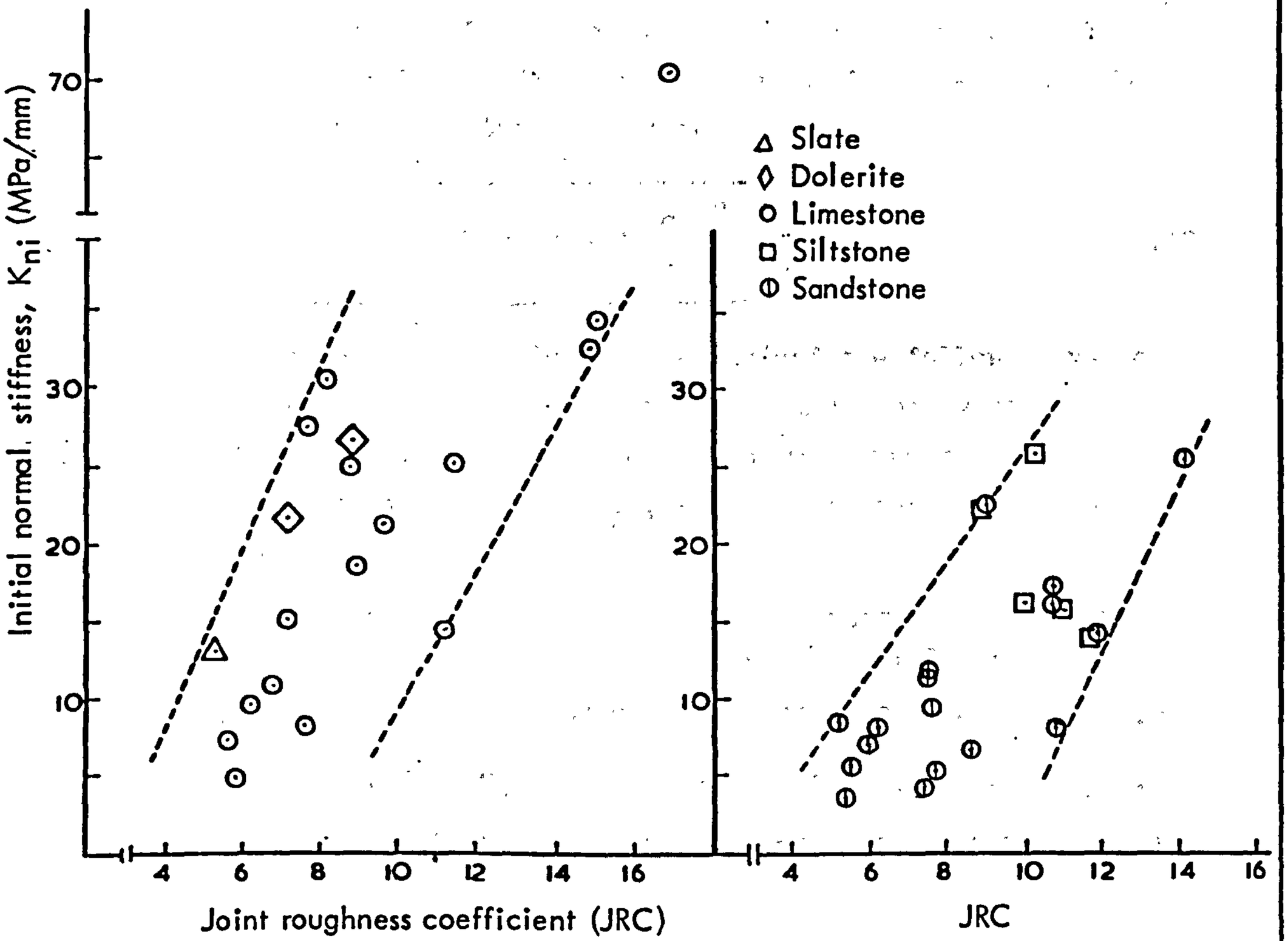

FIGURE 3.47 Relationships between the initial normal stiffness (K_{ni}) and joint wall roughness

empirical function expressing the effect of all three variables on V_m. The relationship between V_m, a_j and JCS is described by 3.36. The relationship between V_m and JRC can be given as $V_m = A - BJRC$. The two basic functions could then be combined as:

$$V_m = A + B(JRC) + C\left(\frac{JCS}{a_j}\right)^D \qquad 3.37$$

Multiple regression of all sets of data yielded the following values for constants A, B, C and D (subscripts 1, 2 and 3 below correspond to the cycle no.; $\pm$ values describe the range of uncertainty implied by one standard deviation; r_1^2, r_2^2, r_3^2 are the coefficients of determination).

$A_1 = -0.2960 \pm 0.1258$	$A_2 = -0.1005 \pm 0.0530$	$A_3 = -0.1031 \pm 0.0680$
$B_1 = -0.0056 \pm 0.0022$	$B_2 = -0.0073 \pm 0.0031$	$B_3 = -0.0074 \pm 0.0039$
$C_1 = 2.2410 \pm 0.3504$	$C_2 = 1.0082 \pm 0.2351$	$C_3 = 1.1350 \pm 0.3261$
$D_1 = -0.2450 \pm 0.1086$	$D_2 = -0.2301 \pm 0.1171$	$D_3 = -0.2510 \pm 0.1029$
$r_1^2 = 0.675$	$r_2^2 = 0.546$	$r_3^2 = 0.589$

The empirical function 3.37 does in principle represent a simple constitutive relationship describing the variations in the maximum closure of unfilled interlocked joint types displaying the following range of wall strength and geometry indices: JRC = 5-15; JCS = 22-182 MPa; $a_j \sim 0.10 - 0.60$ mm, and provided that the initial stress condition does not exceed a level of 1×10^{-3} MPa. However, the potential validity of 3.37 can only be advanced with confidence if tested against a larger number of data, which unfortunately do not exist at present. Three cases of compression tests on artificial extension fractures described by Iwai (1976) provide the only set of data whose agreement with values predicted from equation 3.36 can be examined (the JRC of those fractures which is needed in 3.37 was not given). The relevant fracture property values, the experimental maximum closure under the first loading test ($\sigma_i = 2.17 \times 10^{-3}$ MPa) and the V_m values predicted from 3.36 are shown over (numbers in brackets give the range of V_m values recorded at three measuring points around the circumference of the cylindrical specimens):

	Experimental V_m (mm) data from Iwai (1976)	Predicted V_m from 3.36
	Mean	
Granite		
JCS = 127 MPa, $a_j \sim$ 0.15 mm	0.108 (.084 - .127)	0.088 mm
Basalt		
JCS = 234 MPa, $a_j \sim$ 0.10 mm	0.050 (.019 - .072)	0.044 mm
Marble		
JCS = 98.5 MPa, $a_j \sim$ 0.05 mm	0.034 (.013 - .048)	0.049 mm

Although the JCS of the basalt sample and the a_j of the marble were slightly outside the ranges specified earlier, it can be seen that there is a reasonable agreement between the predicted and the experimental values of maximum closure of these special types of joints.

The main points arising from the above analyses can be summarized as follows:

(i) The normal stiffness coefficients of unfilled interlocked joint types show large variation. Under a certain level of normal stress the values of K_n depend on the aperture thickness, the joint wall strength, and the roughness in that order of relative importance.

(ii) Well defined trends have been observed between the maximum closure and indices describing the aforementioned joint variables. The present data indicate that within a range of aperture thicknesses between $\sim$0.10 and $\sim$0.60 and a range of JCS between 22 MPa and 182 MPa, the maximum closure decreases exponentially with decreasing a_j and increasing JCS. That relationship arises from combination of data from fresh and weathered joints from all five rock types. It should be noted that joints of large a_j usually had low JCS. No data have been included from joint types of high JCS and large a_j, or of low JCS and small a_j, although there are no indications to suggest significant deviations from the observed patterns of variation. The derived empirical function 3.36 may be used to obtain an estimate of the maximum closure of various types of joints (different JCS and a_j but similar roughness) and assuming an initial stress level in the order of 1×10^{-3} MPa.

(iii) Maximum closure data sets from joints with similar apertures indicate that within the range of JRC from ~5 to ~15, the maximum closure decreases linearly with JRC irrespective of JCS. The effects of roughness on joint closure are relatively less significant than those of JCS.

(iv) A constitute relationship describing the variations in maximum joint closure should incorporate all three fundamental joint variables of wall aperture, strength, and roughness. The simple empirical function 3.37 offers a potential solution, but its validity should be checked against a much larger number of data than the 64 data sets available from this study. The inevitable scatter in the experimental results created considerable uncertainty in the values of constants A, B, C and D. From the present data it has been found that an estimate of the maximum closure of a joint under first loading and effectively "zero" initial stress condition can be obtained from:

$$V_m = -0.269 - 0.0056\ JRC + 2.241(JCS/a_j)^{-0.245} \qquad 3.38$$

The uncertainty in the values of V_m predicted from the above relationship is 15.7% (one standard deviation about the regression lines). A similar type of relationship as 3.37 was derived for the initial normal stiffness coefficients (K_{ni}), in which the linear relationships between K_{ni} and (JCS/a_j) and K_{ni} and JRC (see previous Figures 3.41 to 3.44 and 3.47) were combined as:

$$K_{ni} = -7.154 + 1.748\ JRC + 0.0178(JCS/a_j), \quad r^2 = 0.573 \qquad 3.39$$

Intuitively, prediction of V_m and K_{ni} from 3.38 and 3.39 would enable the normal stiffness coefficient of a particular joint type at any desired level of normal stress to be obtained by using equation 3.17. The reliability of such estimates can only be tested and, hopefully, improved through experiment.

2. Comparison between interlocked and mismatched joint normal stiffness

As already noted in section 3.2.3(3) (see also Figures 3.24 and 3.25) the normal stiffness of the mismatched joints was considerably lower than the stiffness of the same specimens when loaded in fully locked position. This is an anticipated result of the stress polarisation over a relatively lower actual contact area (see Figure 3.48) and the lack of asperity confinement. A summary of the observed reductions in normal stiffness is given in Table 3.24. In order to examine the influence of the joint type the various mismatched joints have been distinguished into four groups according to their wall strength (JCS) and roughness (JRC). The average K_n (interlocked)/K_n (mismatched) ratio values have been calculated at three largely different stress levels 0.5, 5 and 15 MPa (the respective ranges of the ratios are given in brackets).

TABLE 3.24

Summary of interlocked and mismatched joint normal stiffness ratio values

		K_n(interlocked)/K_n(mismatched)		
Normal stress (MPa):		0.5	5.0	15.0
HIGH JRC	HIGH JCS: (4 spec.)	7.5 (4.5-10)	6.5 (4.5-10)	12.1 (7.7-20)
	LOW JCS: (6 spec.)	3.7 (1.4-5.6)	3.3 (2.1-7.7)	4.3 (3.0-6.6)
LOW JRC	HIGH JCS: (5 spec.)	3.1 (2.0-7.7)	3.7 (2.9-11.8)	7.1 (5.3-12.5)
	LOW JCS: (8 spec.)	1.9 (1.1-2.9)	2.0 (1.4-2.4)	3.3 (2.8-4)

Note: HIGH JCS: 120-175 MPa (mean = 156 MPa)
LOW JCS: 44-105 MPa (mean = 70 MPa)
HIGH JRC: 9.5-15 (mean = 11.0)
LOW JRC: 4.0-7.6 (mean = 6.4)

As indicated, the largest stiffness ratio values were obtained from joints of high JRC/high JCS and the smallest by the joints of low JRC/low JCS. A reason for that effect is that joints of high JRC and JCS

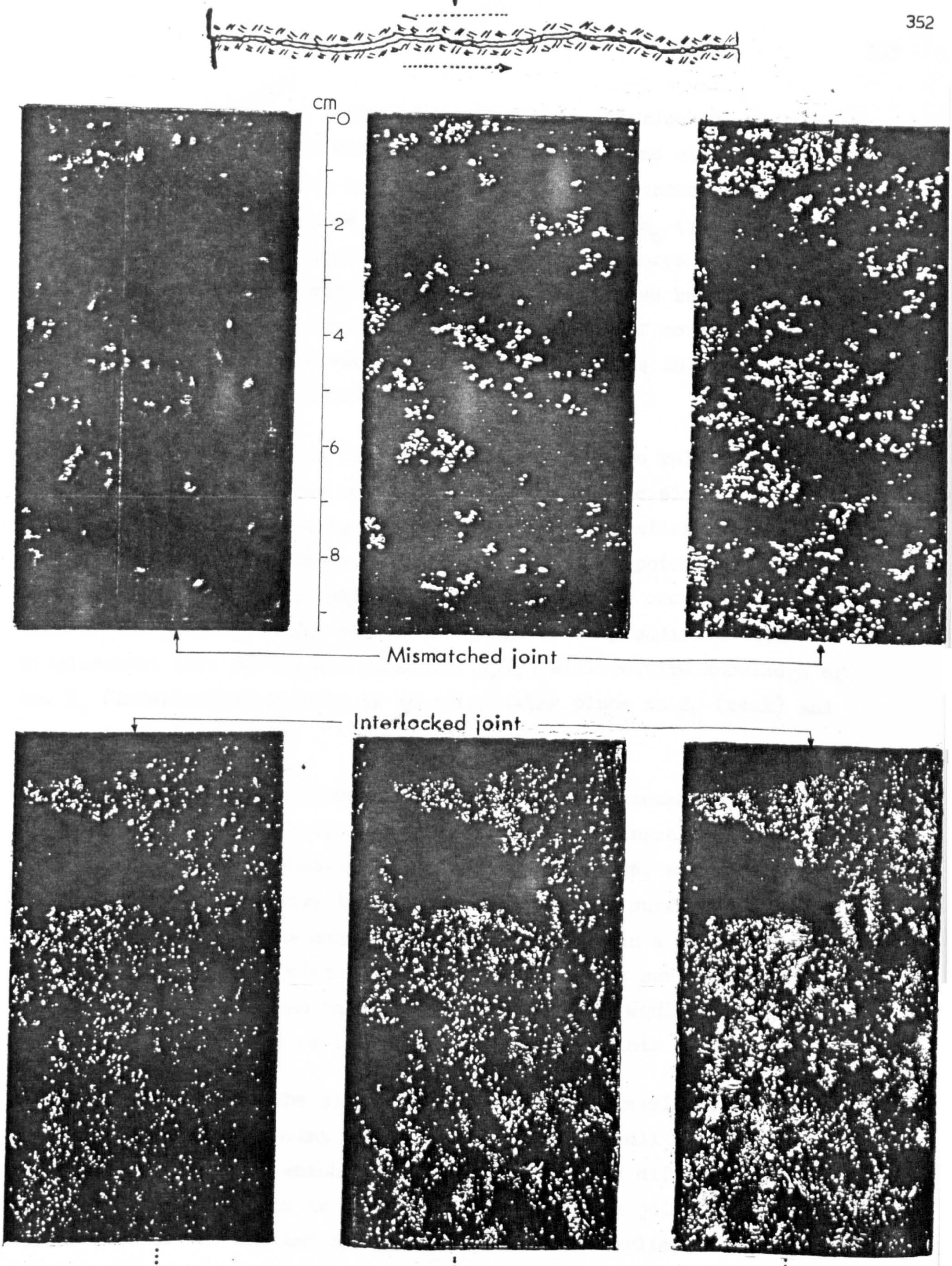

FIGURE 3.48 Comparison of the size and distribution of the actual contact area (white coloured features) of a sandstone joint loaded normally in interlocked and mismatched positions at three levels of normal stress.

generally exhibited very 'stiff' behaviour when interlocked, whereas joints of low JRC and JCS did just the opposite. Some mismatched joints of the latter group had considerable actual contact area and hence K_n (mismatched) was as expected very close to K_n (interlocked). On the other hand, the large protrusions on the surfaces of joints of high JRC prevented a similar effect. The stiffness ratio values generally show some increase with increasing level of normal stress due to the hyperbolic and semi-logarithmic variations in the closure of interlocked and mismatched joints respectively.

The purpose of mismatching the joint surfaces by some relative translation of the block halves was to enable a simplistic simulation of joints subjected to shearing displacement and examination of the related changes in stiffness. This is an aspect of potential interest because modelling of the complete joint behaviour by recent techniques whereby the joint property values are progressively modified with displacement (cf. Barton and Hansteen, 1979) will require knowledge of how K_n (interlocked) reduces as shearing takes place to d_h (peak) and thence to d_h (residual).

In the previous general comments the state of "displacement" of the mismatched joints, which obviously regulates the changes in the actual contact area and consequently in the normal stiffness, was not considered. The amount of the relative translation of the joint surfaces which was technically feasible was usually restricted to within a range of approximately $\leqslant$1 to 2 mm. Relative movement of the joint surfaces by approximately 0.5 to 1.0 mm was taken to be approximately equivalent to the peak shear displacement of the present length of joints (~ 10 cm).

A simplified model of the different stages during shearing could be envisaged in a set of joint specimens with similar wall strength and roughness, and each of which had been subjected to a different amount of shear dislocation, as in fact was the case of the joint specimens within each of the JRC and JCS groups referred to earlier. Increasing relative displacement results in progressively larger joint opening as the gradually reducing number of contact points are transferred higher onto the asperity slopes, and the stiffness of the joint drops. An illustration of the changes in stiffness with increasing joint opening due to larger shear dislocation is presented in Figure 3.49 for all the four groups of joints. The relative amount of joint opening is expressed

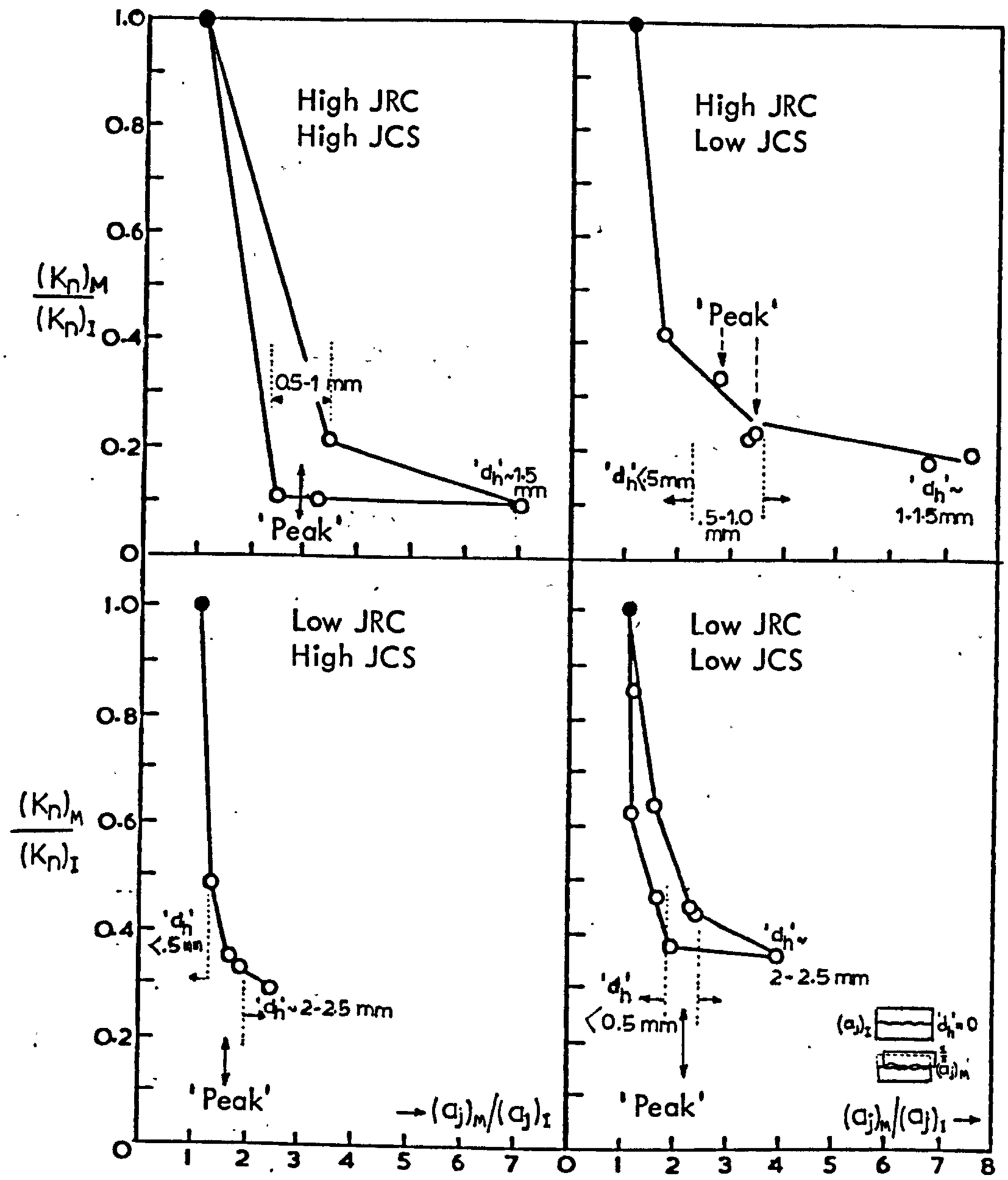

FIGURE 3.48 Illustration of the changes in joint stiffness with joint 'opening' at different stages of 'shear displacement' 'd_h'.

by the ratio of the vertical uplift $(a_j)_m$ of the upper block half (see illustration in p.280) to the aperture $(a_j)_I$ of the joint when interlocked. The value of $(a_j)_m$ and hence the $(a_j)_m/(a_j)_I$ ratio value depends on the surface roughness and the relative amount of 'shear displacement'. The stiffness ratio $(K_n)_I/(K_n)_m$ value for each joint corresponds to 'shearing' under a stress level of 0.5 MPa.

Assuming 'peak displacements' to be within the range from 0.5 to 1.0 mm, three stages of joint 'shearing' can be identified for the joint groups 2, 3 and 4: a 'pre-peak' stage ('displacement' $d_h \leq 0.5$ mm), the 'peak' stage ('d_h' > 0.5-1.0 mm) and a 'post-peak' stage ('d_h' ~ 1.5-2.5 mm). The plots in Figure 3.49 indicate that an extremely small amount of dislocation from an originally interlocked position $(K_n)_m/(K_n)_I = 1$ will cause a large reduction of the original stiffness which could amount to up to $\frac{3}{4}$ of the total reduction in stiffness from $d_h = 0$ to $d_h = d_{h(peak)}$. Small 'post-peak displacements' indicate a further reduction in stiffness but at a much lower rate. No inferences can be made at present regarding the 'post-peak' stiffness after large displacements.

It would be useful to find an empirical rule for modifying the original stiffness $K_n(I)$ at $d_h = 0$ into an effective $K_n(M)$ value at $d_h = d_{h(peak)}$. It could then be easier to modify $K_n(M)$ further for varying amounts of shear displacement (d_h). However, some basic considerations relating the changes in stiffness to the differences in the actual contact area between the 'interlocked' and 'peak' positions of a joint suggest that deduction of a rule-of-thumb would be difficult. Ladanyi and Archambault (1970) suggested equation 1.18 (p.21) to describe the ratio of the sum of contact areas at peak to the total joint area. Barton and Choubey (1977) gave a simpler version whereby A_{actual} at peak may be related to A_{total} in the ratio σ_n/JCS. If it was assumed that K_n (interlocked) represented $A_{actual} = A_{total}$ then it could be proposed that the stiffness $K_n(M)$ at the moment of peak would be reduced to $K_n(I) \times (\sigma_n/JCS)$. Since the assumption of 100% contact area for interlocked joints would be grossly unrealistic at any level of normal stress, an approximation would necessarily have the form:

$$K_n(M) = K_n(I) \times \frac{(\sigma_n/JCS)_M}{(A_{act}/A_{total})_I}$$

where $(\sigma_n/JCS)_M$ is the contact area ratio for the joint at the moment of peak under σ_n, and $(A_{act}/A_{total})_I$ is the contact area ratio for the joint in interlocked position and under the same normal stress. However the practical usefulness of the above relation is rather limited as it requires knowledge of the stress-dependent contact area ratio of the interlocked joint. It also ignores the probable influence of the surface roughness on the peak A_{actual}. There is undoubtedly much to be learned about this aspect of joint behaviour which warrants a systematic investigation. That should involve shearing of a variety of joint types and study of the behaviour under complex normal loading paths at various stages of displacement.

3. Range of joint shear stiffness parameters

The data on joint shear stiffness listed in the previous Table 3.22 show considerable variability. Under the range of normal stresses applied (0.23-2.36 MPa) the K_s (secant peak) coefficients varied between 0.47 MPa/mm and 12.6 MPa/mm. The highest K_s coefficients were obtained from the very tight slate cleavage fractures nos. 1 to 3. In fact the lowest coefficient of those specimens (5.6 MPa/mm under σ_n = 0.545 MPa) was very near to the maximum K_s obtained from all other joints under the maximum normal stresses. All three slate specimens failed in "brittle" fashion at a peak displacement between 0.1 and 0.16 mm. The peak shear displacement of the other joints ranged between 0.28 and 0.82 mm. Under rising level of normal stress $(d_h)_{peak}$ underwent only a marginal increase and consequently the K_s coefficients showed a strong dependency on normal stress.

The variation in the secant peak shear stiffness coefficients with normal stress is illustrated in Figure 3.50. The K_s data at extremely low normal stresses were derived from the results of the shear tests conducted for the determination of the JRC. The stiffness envelopes had invariably a curved shape resembling the peak shear strength envelopes of joints. The non-linear variation in K_s with σ_n is due to the non-linear variation of τ_{peak} with σ_n and the small increases in $(d_h)_{peak}$ with increasing σ_n. Distinct changes in the gentle curvature of the stiffness envelopes are due to the effects of the multistage testing procedure. The envelopes in Fig. 3.50 also demonstrate the dependency of the peak shear stiffness on joint wall strength (JCS) and roughness (JRC).

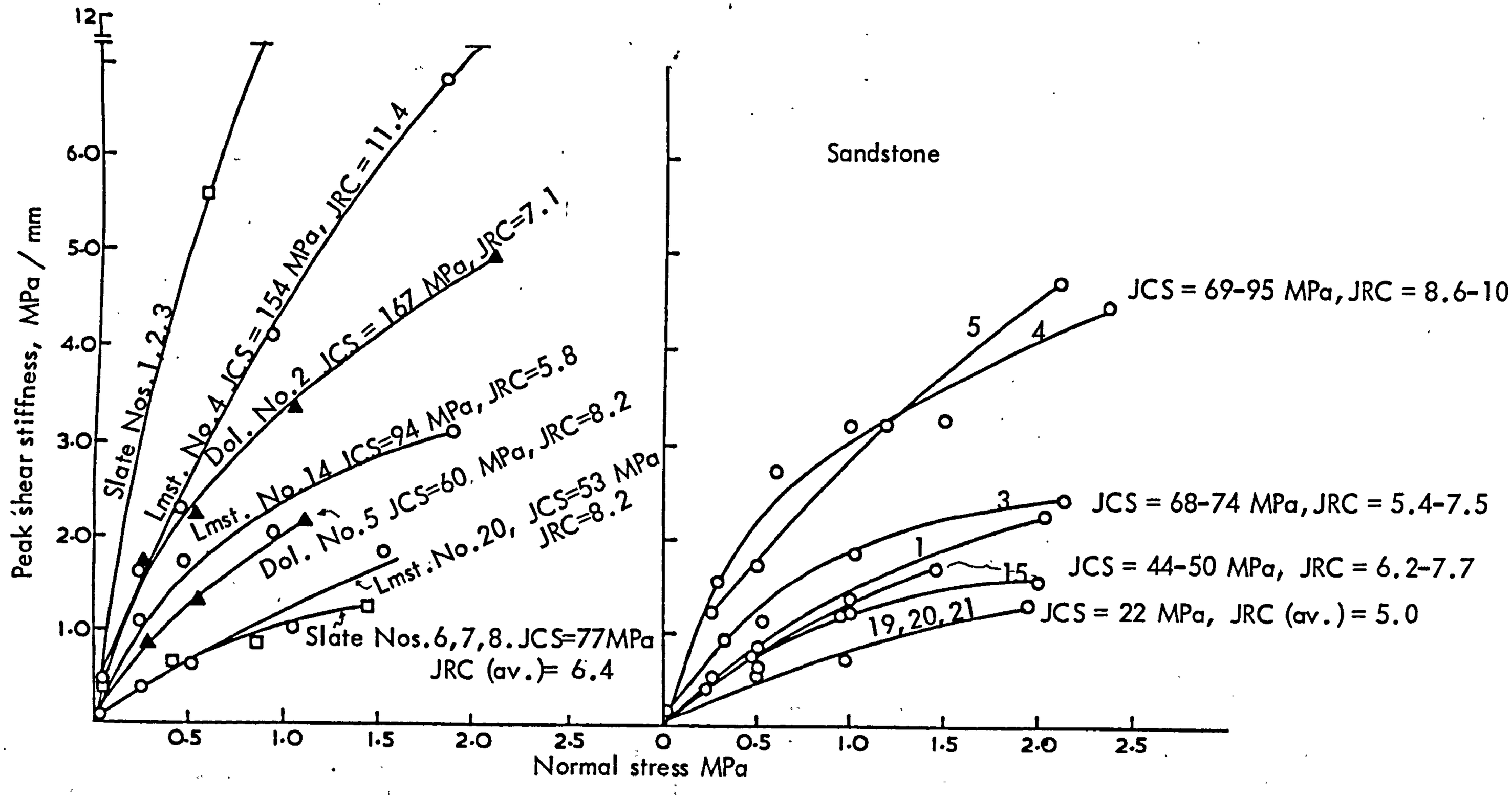

FIGURE 3.50 Variation in the peak shear stiffness (secant values) of different joint types with normal stress.

The set of parameters in Table 3.22 describing the non-linearity in joint behaviour showed the following characteristics:

(i) the failure ratio (R_f) ranged between 0.652 and 0.870. That ratio has been referred to as an index of non-linearity in joint behaviour (for linear stress-displacement relationships R_f is zero). In general, the lower R_f values were associated with well interlocked, unweathered joints of high JRC. Planar fresh and, more so, weathered joints gave the relatively higher R_f values.

(ii) The stiffness exponent n_j (= slope of the log-log relationship between initial shear stiffness K_{si} and normal stress) was very similar for all the joints; except for the n_j of a weathered limestone joint (= 1.188 MPa^2/mm) the values from all the other specimens ranged between approximately 0.6 and 0.8.

(iii) The stiffness number K_j (= intercept of the above relation) was significantly variable ranging between 3.02 and 30.19 MPa/mm. This can of course be anticipated considering the variations in K_{si} and the essential similarity in the n_j values. Correlation of the K_j values with JRC shows a proportional linear trend. This is logical since the initial stiffness of a mated joint depends on the degree of interlocking which in turn is related with the value of JRC. The best fitted line in the relationship of the 13 K_j data values and JRC is expressed by:

$$K_j = -17.19 + 3.86\ JRC \quad (r = 0.835, \text{ for } JRC > 4.5) \qquad 3.40$$

4. Anisotropy in joint deformability

A related feature of jointed rock masses that distinguishes continuum and discontinuum behaviour is the anisotropic deformability. Joint stiffness is much lower in the tangential than in the normal senses. The value of normal to peak shear stiffness ratio is not a constant but depends on the level of normal stress, the highest anisotropy being shown at low stresses.

The stiffness ratio values of the present joints are summarized in Table 3.25. The K_n/K_s values of the sandstone joints 1 to 5 and 15, 16 are the mean of the individual values at each level of σ_n, as the differences were very small. The shear stiffness of the joints under

TABLE 3.25

List of normal to peak shear stiffness ratio values at different levels of normal stress.

	Normal stress, MPa				
	.02-.05	.25	.50	1.0	2.0
SANDSTONE, F (nos. 1,3,4,5) av. K_n/K_s :	73	16	12	12	
MW (nos. 15,16) av. K_n/K_s :	124	18	16	15	
W (nos. 19,20,21) av. K_n/K_s :	130		8.4	11	14
LIMESTONE F (no. 4), K_n/K_s :	58	19.4	15.6	11.3	
MW (no. 14) " :	67	7.8	7.8	12.9	
W (no. 20) " :		35	24	21	
DOLERITE F (no. 2), K_n/K_s :	125	15.1	14.9	12.8	
W (no. 5) " :		9.6	7.2	5.7	
SLATE F (nos. 1,2,3), K_n/K_s :	88	12	27	132	
W (nos. 6,7,8) " :	122		26.2		

F: fresh; MW: moderately weathered; W: weathered

normal stresses up to 1 MPa has been considered, to avoid the possibility of using unrealistically low K_s values due to the multistage testing. For "normally" tested joints the K_s coefficients under the full σ_n range were used.

Under extremely low σ_n (.02 - .05 MPa) the K_n/K_s ratio attained maximum values ranging from 130 to 58. Within the σ_n range from .25 to 1 or 2 MPa the anisotropy was markedly reduced without showing any significant further changes. The effect of weathering on joint anisotropy is unclear. In the case of the sandstone and dolerite weathered joints the K_n/K_s values were lower than those of the fresh. For the slate cleavage planes anisotropy appeared similar in both fresh and weathered specimens,

whereas the weathered limestone joint gave higher K_n/K_s values than the fresh.

5. Scale effect on shear stiffness

The preceding discussion on the range of joint shear stiffness parameters was related to a specific joint size. However, existing evidence and the present results from the study on model joints strongly point to the significant effect of scale on peak shear stiffness, due to the dependency of both peak shear strength and displacement on the joint length.

The mean peak shear stiffness of each subdivided and full scale model was calculated from the mean gradient of the shear stress-displacement curves in Figures 2.30 to 2.40 in part two. Conversion of the model (M) K_s values to the prototype (P) scale was made according to

$$(K_s)_P = \frac{y}{\lambda} (K_s)_M \qquad 3.41$$

where y and λ are the stress (= 40) and geometric (= 30) scale factors. The variation in the K_s values with joint length (L) is illustrated in Figure 3.51. The data are plotted in three groups each comprising joints of particular morphological characteristics (nos. 1 to 5: rough, strongly undulating; nos. 6 to 8: very rough, moderately undulating; nos. 9 to 11: slightly undulating to planar). The trends show a very large reduction in the peak shear stiffness of the models with increasing joint block size. As would be anticipated, the largest reductions are associated with the highly irregular surfaces. By increasing the length of joints from 5 or 6 to 36 or 40 cm the K_s coefficients decreased by factors ranging from approximately 3 to 7 depending on the surface geometry. A near two-fold decrease in K_s is also displayed by the slightly undulating model joints nos. 9 and 10. The only case where virtually no scale effect was observed was the planar joint no. 11.

The K_s values converted to prototype scale ranged between 0.119 and 0.021 MPa/mm. The equivalent prototype joint lengths were between 1.5 and 12.0 meters and the prototype normal stress was approximately 1.0 MPa. The prototype K_s values of the model joint were plotted against the corresponding prototype lengths in the chart presented in Figure 3.3 in

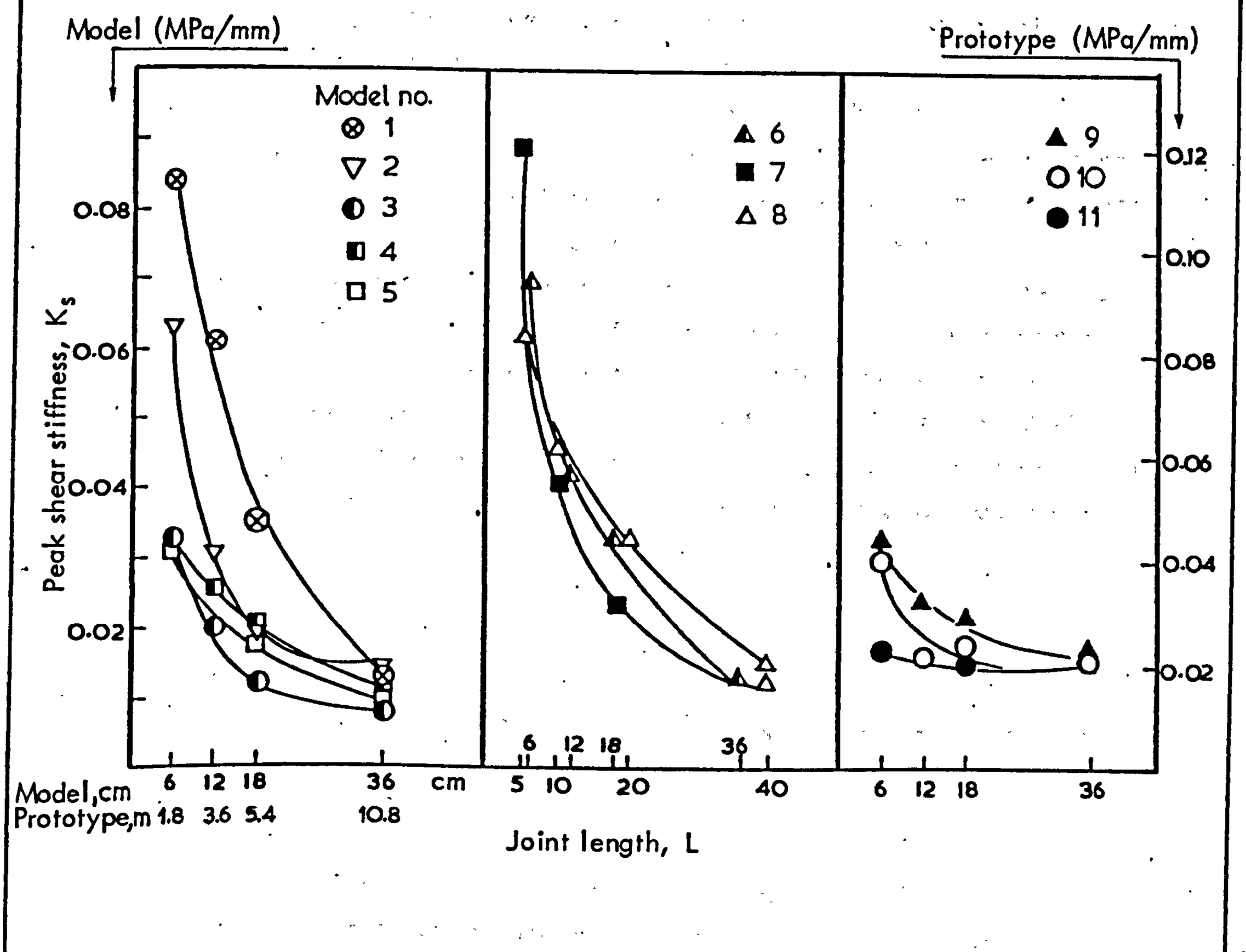

FIGURE 3.51 Effects of scale on the peak shear stiffness of model joints

Chapter 3.1, which is reproduced in Figure 3.52 containing the shear stiffness data from both the real and model joints. It is interesting to note the remarkable agreement of the data from the model joints with the general trend inferred from the current literature. All data points scatter about the $\sigma_n \sim 1$ MPa envelope. The normal stress applied on the model joints was also ~ 1 MPa.

The practical considerations made in part two with regard to the derivation of scale-free estimates of peak shear strength are obviously relevant in a prediction of values of peak shear stiffness. Due to cross-jointing and the reduced rigidity of a rock mass as scale increases, there is a limit to the length of joint that needs to be tested to be certain of avoiding the scale-effect. Correct estimates of JRC and JCS based on either index testing or appropriate correction of laboratory-size test results in relation to the average in-situ joint block size can be substituted in Barton and Choubey's empirical equation 3.1, thus allowing for the scale effect on peak shear strength. The scale-displacement effect is allowed for by the factor $100/L_c$. In the absence of measured or predicted parameters the data chart in Figure 3.52 may offer an approximation of the K_s values relevant to a particular situation.

3.3.5 Concluding remarks

The examination of possible analytical expressions for the stress-deformation relationships of rock joints leads to the following conclusions:

(i) The normal stress-normal deformation relationship of natural interlocked joints can be accurately described by a hyperbola. Equation 3.8 is found to fit the present data in a more consistent manner than Goodman's empirical function 3.6.

(ii) The normal stress-normal deformation relationship of mismatched joints is best represented by a semi-logarithmic expression (eqn. 3.18).

(iii) Non-linear shear stress-shear deformation relationships in the range up to mobilization of peak shear strength can also be approximated by hyperbolic functions (e.g. eqns. 3.20 or 3.29).

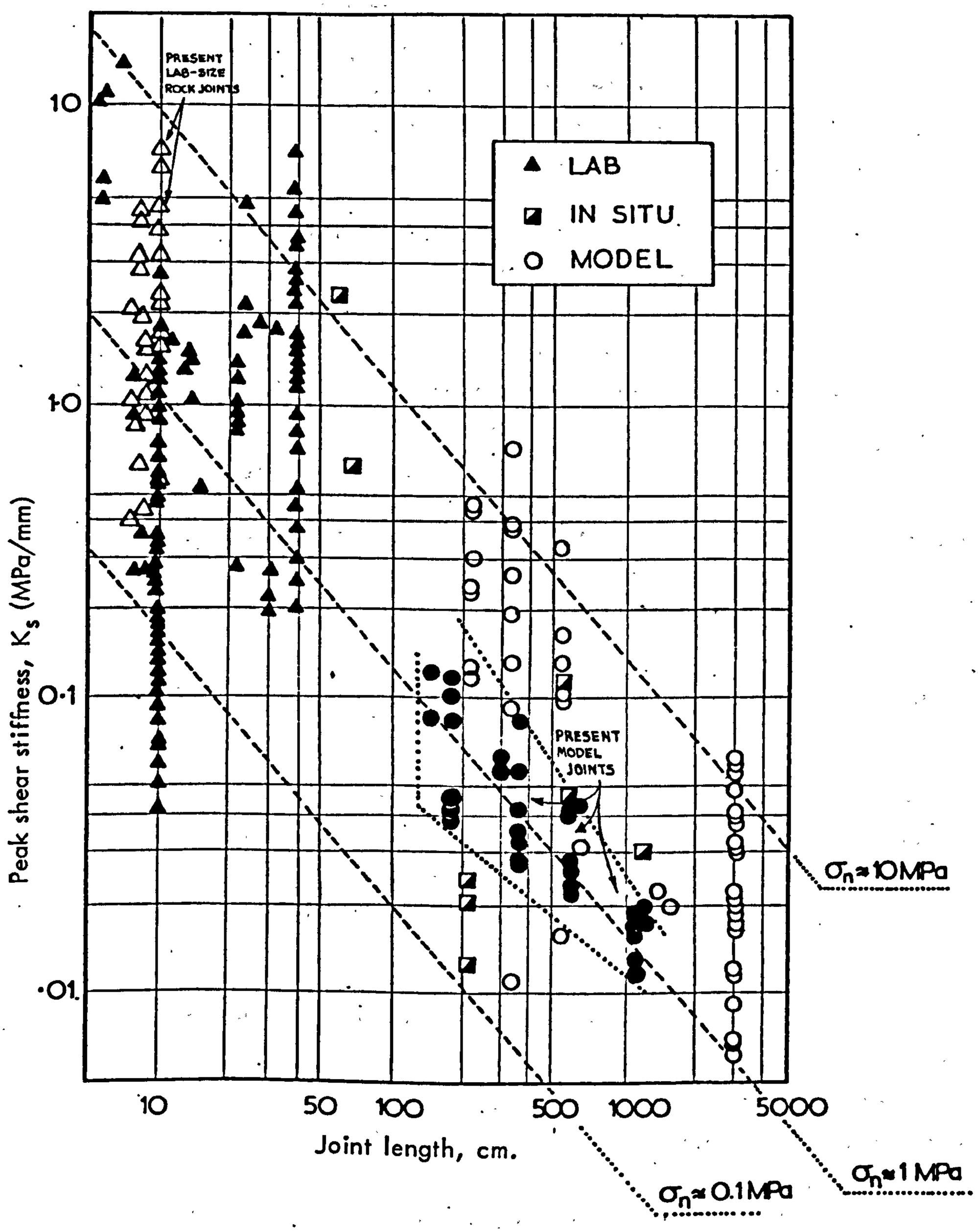

FIGURE 3.52 Comparison of peak shear stiffness (K_s) data measured from different lengths of model joints (●) with K_s data from the literature.

According to function 3.8 the hyperbolic normal stress-deformation relationship of a joint is uniquely defined by the initial normal stiffness (K_{ni}) and the maximum closure (V_m). For a particular type of joint the values of K_{ni} and V_m depend on the initial stress level (σ_i). Under the same σ_i, however, the maximum closure of different types of joints can vary substantially. From comparisons between the present experimental data the following relations have been identified:

(i) For a joint with a given aperture thickness (a_j) the amount of maximum closure depends to a large extent on the mechanical properties of asperities. For joints with similar a_j the value of V_m is inversely proportional to the asperity strength or JCS. Maximum closure data from all three tests have shown an inverse exponential relationship with the JCS/a_j ratio values. That relationship was fitted best by a power law (eqn. 3.36).

(ii) For joints with comparable JCS/a_j ratio values the maximum closure is generally lower for rougher surfaces. Specifically, an inverse linear trend exists between V_m and the surface roughness described by JRC within a range from approximately 5 to 15. The correlation between maximum closure and JRC was poor for V_m data other than those obtained from the first loading.

(iii) Combination of (i) and (ii) yields a simple constitutive relation describing the maximum joint closure as a function of aperture thickness, joint wall strength and roughness (eqn. 3.37). The latter gave a good approximation of the relationship between the maximum closure values from the first loading tests and the above joint variables.

In contrast to the very similar normal stress-normal deformation behaviour shown by all types of joints, the shear stress-shear deformation relationships indicate different degrees of non-linearity. For the present type and size of joints, and under normal stresses up to approximately 2.0 MPa, the failure ratio (R_f) values ranged between ~ 0.65 and ~ 0.89. In the case of the fresh slate cleavage planes, the R_f value was approximately zero. As a general observation, the R_f values for tightly locked joints in fresh rock were lower than 0.75. The incremental tangent shear stiffness values can be calculated from eqn. 3.28. The input parameters of stiffness number (K_j) and stiffness exponent (n_j) calculated from the present joints showed that:

(i) n_j is essentially independent of the joint type within the normal stress range up to 2.0 MPa and varies between 0.6 and 0.8. For the majority of joints n_j was between 0.7 and 0.8;

(ii) K_j depends on the type of joint and increases linearly with JRC.

In addition to the marked normal stress dependency, the effects of factors such as surface roughness and weathering on peak shear strength are clearly identified in the shear stiffness values. Comparison between the normal and peak shear stiffness of joints at different levels of normal stress showed that the K_n/K_s ratio varies with normal stress, the highest anisotropy usually occurring under low stress levels. It has not been possible to recognize any systematic difference in the anisotropic deformability of fresh and weathered joints, even in cases where the multistage testing procedure was not a complicating factor.

The results from the model tests have verified the strong scale effect on the peak shear stiffness. The amount of decrease in K_s depends on the joint type. Maximum scale effects in K_s are found for rough undulating joints and minimum to almost absent scale effects for relatively smooth and planar joints. The empirical relationship 3.1 can be used to obtain a full-scale estimate of K_s provided that allowance is made for scale effects in the JRC and JCS input values.

A comparative study of the differences in the normal stiffness of interlocked and mismatched joints led to some tentative conclusions with regard to the changes in K_n of joints subjected to shearing. These conclusions can be summarized as follows:

(i) Within the range of displacements required to mobilize the peak shear strength the original joint stiffness (K_n interlocked) will reduce at a gradually decreasing rate. The largest reductions will occur during the initial stages of displacement, and will continue at a slower rate until the joint has reached the $d_{h(peak)}$. The present results indicate that at d_h approximately equal to $\frac{1}{2}\, d_{h(peak)}$ the original K_n(interlocked) may decrease by up to three-quarters of the total reduction at the instant of peak strength. The results also suggest a further decrease in K_n at a slow rate in the immediate post-peak stages.

(ii) The amount of decrease in K_n at any stage of displacement will, in addition to its dependence on normal stress, be different for various types of joints. The results imply that the maximum decrease in K_n will be associated with joints of high JRC and JCS and the smallest with joints of low JRC and low JCS. In the present cases the relative reductions in K_n (interlocked) at an assumed $d_{h(peak)}$ for the above types of joints differed approximately by a factor of 4.

PART FOUR

SUMMARY AND CONCLUSIONS

EFFECTS OF SCALE ON THE SHEAR STRENGTH OF JOINTS

Summary of work

The experimental approach consisted of direct shear testing joint samples of various lengths prepared from eleven different 'full-size' joints 36 to 40 cm long. A rubber moulding system was used to take precise impressions of the roughness from a variety of natural joint surfaces in different rocks. A multi-component brittle material simulating a prototype rock with uniaxial compressive strength of 80 MPa was used to cast several sets of identical interlocking specimens from each pair of moulds. The 'full-size' joints were in turn subdivided into sets of equidimensional joint block samples, each of the sets representing a different average block size or joint length varying from 5-6 cm to 18-20 cm. The complete range of model joint lengths corresponded to prototype joints from 1.5 - 1.8 meters to 10.8 - 12.0 meters long. All sample sizes were tested in the same relative direction of shear and under exactly the same level of normal stress which was equivalent to approximately 1 MPa at prototype scale.

Conclusions

The results of this study show that, under the same level of normal stress, the behaviour and shear strength of different size samples of a large sized joint will change significantly as the length of sample increases:

(i) For different sized samples of the same joint, longer samples would need larger displacements than shorter samples before peak strength was attained. In effect, the peak shear displacement $(d_h)_p$ represents the distance which a joint will have to displace until it develops contacts between asperities of a size critical to the peak behaviour of that particular joint length. Small asperities regulate the peak shearing path of short joints, whereas larger irregularities become effective for correspondingly longer joints. In the present case the peak shear displacements ranged between approximately 0.5% and 1.0% of the length of joint. There may also be a proportionality

between joint length and size of 'critical' asperities. Indications are that for the present rough undulating joint types the average baselength of 'critical' asperities ranged between approximately 2% and 4% of the corresponding joint length.

(ii) The effect of the above condition on the shear behaviour with increasing scale is reflected in the shear stress-displacement relationships. Behaviour changes from 'brittle' to 'plastic', the shear stiffness reduces and the pre-peak portion of the curves usually displays higher non-linearity due to the progressive damage occurring to larger and larger asperities with increasing scale.

(iii) The involvement of small and large asperities in controlling the peak behaviour of correspondingly short and long joint samples introduces two geometrical effects on the contact areas at the instant of peak. In the first case small individual contacts develop between the small 'critical' asperities, while in the second case larger contacts are created between the slopes of the longer asperities. In addition, the larger contacts are less steeply inclined with respect to the mean joint plane than the smaller. The decreasing inclination of contacts contributes a reduced geometrical component (peak dilation angle i_p^o) to the total frictional resistance as the scale increases. The larger contact areas introduce a scale effect in the asperity failure component (S_A^o) because of the reducing joint compressive strength (JCS) with increasing size of contacts. The two effects combined result in a substantial decrease of the total friction angle (ϕ_p).

(iv) Maximum scale effects on the geometrical and asperity failure components, and hence on the peak total friction angle, are associated with rough undulating types of joints. There is a progressive decline in the scale effect as the joint roughness decreases and for almost smooth and planar joints the peak shear strength is practically independent of the length of the joint.

The conclusions from this study suggest that the peak shear strength of a closely jointed rock mass would be higher than for a wider

jointed mass because of the difference in the peak shear strength of the smaller and larger joint blocks. This in turn implies that the smaller joint blocks within the rock mass will be capable of following the individual shear paths they require in order to maintain contact with the small steep asperities and hence develop higher peak shear strength.

Experimental evidence by Barton from biaxial tests on jointed model rock masses with different cross-joint spacings (3.3, 6.4 and 12.3 meters at prototype scale) shows that the closer the spacing, or the smaller the joint block size, the higher the peak shear strength of the mass. It therefore seems probable that, unless the stress levels are high, the reduced stiffness of a closely jointed mass will offer sufficient freedom to the component blocks for individual shearing and rotation, thus 'mobilizing' the smaller scale and steeper asperities and developing higher peak shear strength.

Practical recommendations

Conventional methods of shear strength determination on samples sizes sufficiently large to allow for the scale factor are extremely costly and impractical. On the other hand empirical predictions of peak shear strength may offer not only a cheap but also a reliable alternative. Use of the indices of joint roughness coefficient (JRC) and wall compressive strength (JCS) allows incorporation of the scale effects in the estimate of shear strength in a realistic and consistent manner.

The present studies have shown that the joint roughness coefficient should only be considered as a constant for a fixed joint length. Small joint samples where peak behaviour is controlled by small steep asperities will have higher JRC values than longer joints where peak behaviour is governed by larger asperities with correspondingly flatter slopes. In addition to the scale effect on JRC, the value of joint compressive strength (JCS) will probably also be lower because of the increasing size of contact areas.

There are reasons to suggest that the naturally occurring block size may constitute a potential scale effect size limit (cf. Barton and Choubey). Accordingly, the nearest scale-free estimate of JRC could be

measured on samples of minimum length equal to the maximum cross-joint spacing. The same minimum joint length should also be the 'reference' for interpretation and correction of JRC values measured on 'laboratory' size specimens.

Analyses of the roughness on the present model joint surfaces showed a consistent similarity between the ratio of the mean inclination angles ($\overline{a^o}$) of asperities with half-baselength (= mean 'step'-size) equal to approximately 1-2% of the length of each of the two joint sizes considered, and the ratio of their respective values of JRC. If it was assumed that this type of relation was valid at larger scale, it might be possible to predict an approximate full-scale value of JRC by correcting the JRC measured on laboratory samples by an appropriate amount determined from roughness analysis of both natural joint block sizes and laboratory samples.

The difficulty of introducing independently corrected values of JRC and JCS is that prediction errors in the total friction angle can be high if there is a significant error in the input index values. The more serious error is introduced by an incorrect JRC value and when the JCS/σ_n ratio value is high. It would be useful if simple sensitivity analyses were conducted by combining the range of predicted JRC values with scale-reduced JCS values, so that the final choice of the peak friction angle(s) could be made with some knowledge of the probable range of uncertainty.

The magnitude of prediction errors would be considerably reduced if the values of JRC were actually measured on naturally occurring joint block sizes by tilt- or pull-testing as suggested by Barton & Choubey. The advantage of these methods is that when back-calculating the value of JRC the estimates of JCS and residual friction angle ϕ_r need not be very accurate due to the logarithmic formulation and the very large JCS/σ_n values. In any case, overestimates and underestimates in JCS and ϕ_r will be balanced by corresponding underestimates and overestimates of JRC. The error in the extrapolated values of total friction angle at higher stress levels would then be relatively small. An additional advantage of index testing is that the low cost involved will enable a sufficiently large number of samples to be tested, thus yielding statistically significant data.

Suggestions for future work

One of the most important limitations in simulating the shearing of joints in their natural environment by performing shear tests on individual joint samples is that the response of the surrounding rock mass is absent. It is important that subsequent studies on scale effects be directed to multiple-jointed masses. Further experimental verification is needed with regard to the inter-relationship between joint spacing, mass stiffness and shear strength. It will be of great value to test the scale model of "close joint spacing ⟶ low mass stiffness ⟶ freedom for rotation of individual blocks ⟶ higher peak shear strength" against various stress levels, since it is anticipated that the stress level will effectively control the freedom of blocks for individual rotation, and therefore influence the magnitude of the scale effect.

The experimental approach could be either via shear tests on jointed assemblies of rock blocks or by two-dimensional plane-stress jointed models tested in a biaxial loading frame. The first technique could present serious experimental difficulties, such as differential displacements at the two ends of the sheared assembly and the problem of realistic simulation of the stiffness of an assumed 'overlying rock mass'. Use of a stiff loading plate introduces variable normal stress conditions as some of the blocks become 'overstressed' whereas others are 'understressed' as a result of differential dilation along the shear plane. Alternative methods by using leaf- or coil springs to balance the stress distribution are generally impractical, the most reasonable compromise being the use of relatively stiff rubber packs between the top plate and the specimen. The problem of differential displacement could be solved by producing extension interlocked fractures to represent the cross-joints but then of course their high stiffness introduces a new variable. The second technique, using two-dimensional jointed models, will not only be technically simpler but probably more informative.

Meantime, it will be of practical value if more attention is paid to the correct interpretation of data from laboratory-size samples and to the application of realistic scale reduction factors. In Chapter 2.5 there are tentative suggestions which could be tested against larger

joints. It would be most useful if JRC values back-calculated from large scale tilt tests are compared with those predicted from laboratory samples and roughness analyses. Building up knowledge on the reliability of such predictions will not only improve the procedures but will also be of practical use where index tests are not technically feasible.

DEFORMATION OF ROCK JOINTS

Summary of work

Rock joint deformation has been studied by conducting normal compression tests and direct shear tests on a wide ranging variety of fresh and weathered natural joint samples of five different rock types, namely slate, dolerite, limestone, siltstone and sandstone. Normal loading tests involved cyclic loading of prepared single-jointed blocks and measurement of the vertical displacements. At first, all joints were compressed in fully locked position under maximum normal stresses which approached $\frac{1}{3}$ to $\frac{1}{2}$ of the uniaxial compressive strength of the intact rock (~ 20 to ~ 180 MPa). A collection of different types of joints with artificially mismatched walls was then tested. Finally, a number of joints were tested in direct shear by adopting a multistage testing procedure.

Conclusions

Normal deformation (interlocked joints)

(i) The normal stress (σ_n)-normal deformation (closure ΔV_j) relationship of natural joints is highly non-linear throughout repeated loadings and irrespective of the rock and joint type. On first unloading the joints show marked hysteresis and large permanent sets. A certain amount of recuperation also occurs because of the recovery of elastically deformed asperities. Under subsequent reloadings the amount of permanent set is considerably lower. However, it seems that several more cycles than the three applied in the present tests would be needed to obtain a reproducible stress-deformation curve with no further permanent set.

(ii) Use of hyperbolic functions enables an accurate analytical representation of the normal stress (σ_n)-closure (ΔV_j) curves of natural joints, whereby the asymptote to the hyperbola defines the fundamental property of maximum joint closure (V_m). It was found that equation 3.10

$$\Delta V_j = \frac{\sigma_n \, a}{1 + \sigma_n b} \quad , \qquad \begin{array}{l} a \text{ and } b = \text{constants of the hyperbola} \\ a/b = \text{maximum joint closure } V_m \end{array}$$

gave the most consistent fitting to the present experimental curves, irrespective of the joint type, stress history and loading mode.

(iii) The normal stress (σ_n)-total deformation (ΔV_t) relationship of joint blocks under repeated loading is accurately described by equation 3.34

$$\Delta V_t = \frac{1}{\frac{1}{\sigma_n a} + \frac{b}{a}} + \frac{\sigma_n}{c} \quad , \qquad c = \text{elastic normal stiffness of the rock material}$$

provided that the applied stresses are high enough to enter the elastic region of the solid rock. The function can be used for statistical processing of experimental ΔV_t data and prediction of the maximum joint closure (V_m) provided that the stress-deformation relationship of the rock material is linear. Otherwise, an appropriate non-linearity component should be subtracted from the predicted value.

(iv) The hyperbolic variation of joint closure (ΔV_j) with stress means that no single value of normal stiffness (K_n) can be used to characterize the stress-closure relationship. The incremental normal stiffness can be calculated from equation 3.17:

$$K_n = K_{ni}\left(1 - \frac{\sigma_n}{V_m K_{ni} + \sigma_n}\right)^{-2} \quad , \qquad K_{ni} = \text{initial normal stiffness}$$

Comparisons of the normal stiffness (K_n of different joint types under the same level of normal stress (σ_n) show that K_n is significantly variable. This is because the maximum closure (V_m), which together with the initial normal stiffness (K_{ni}) uniquely define the hyperbolic stress-closure relationship of a joint, is seriously affected by the physical characteristics of the joint surfaces.

(v) The maximum closure (V_m) is a unique joint property which depends upon the initial stress level (σ_i). Under the same σ_i the maximum closure of different joints and in particular that of fresh and weathered samples varies significantly. In fact, the value of V_m for interlocked joints depends upon the initial aperture thickness (a_j), the joint wall strength (JCS), and the wall roughness (JRC) in that order of relative importance.

(vi) From the analysis of the data the following quantitative relationships have been identified:

(a) an inverse exponential relationship between the maximum joint closure (V_m) and the ratio of wall strength (JCS) to aperture thickness, which was fitted by equation 3.36:

$$V_m = C\left(\frac{JCS}{a_j}\right)^{-D}$$

(b) an inverse linear relationship between maximum closure and wall roughness:

$$V_m = A - B\ JRC$$

From a combination of (a) and (b) a simple constitutive relationship can be advanced, describing V_m as a function of a_j, JCS and JRC:

$$V_m = A + B(JRC) + C\left(\frac{JCS}{a_j}\right)^{D}$$

Normal deformation (mismatched joints)

(vii) Mismatched joints show typically non-linear stress-deformation behaviour, hysteresis and huge permanent sets. Due to the very large aperture and the interference of surface irregularities, mismatched joints do not attain the maximum closure state observed on interlocked joints. The normal stress (σ_n)-closure (ΔV_j) curves cease to resemble a hyperbola and the relationship is best described by a semilogarithmic function:

$$\log_{10} \sigma_n = p + q\ \Delta V_j$$

(viii) Comparisons between the normal stiffness of joints tested in interlocked and mismatched positions, and assuming that a mismatched joint resembles a joint subjected to a certain shearing displacement (d_h), suggest that:

(a) the amount of reduction in the original joint stiffness K_n (interlocked) from $d_h = 0$ to $d_h = (d_h)_{peak}$ will depend upon the wall strength and roughness of the particular joint. The maximum reduction should be expected for joints of high JRC and JCS and the minimum for joints of low JRC and low JCS. The present experiments have shown that for joints of the first group, K_n (interlocked) reduced by an average factor of approximately 10 within the normal stress range up to 5 MPa. For the other group the reduction amounted to a factor of approximately 2.5.

(b) the largest part of the reduction in K_n (interlocked) occurs during the very initial stages of displacement. Subsequent changes up to $d_{h(peak)}$ and immediately after appear to occur at considerably slower rate. No information is available as to the changes in K_n after very large displacements.

Shear deformation

(ix) Joints display variable shear stress (τ)-shear deformation (d_h) behaviour within the region up to mobilization of peak shear strength, ranging from virtually linear to highly non-linear. Non-linear curves can be adequately approximated by hyperbolic functions.

(x) The peak shear stiffness (K_s)-normal stress (σ_n) relationship is non-linear irrespective of the joint type. Under the same normal stress the shear stiffness is regulated by all the factors which affect the peak shear strength (τ_p) and displacement $(d_h)_p$. The normal (K_n) to shear (K_s) stiffness ratio varies with normal stress, the highest anisotropy generally occurring under low stress levels. No systematic weathering effects have been identified in the K_n/K_s ratio values.

(xi) Two potential sources of error may affect the values of K_s measured at laboratory scale. The peak shear strength of a previously overclosed

joint will be underestimated if the overclosure ratio operating in the field is not reproduced prior to the test. The peak shear displacement may on the other hand be considerably overestimated if external deformations are not avoided or if, preferably, displacements are not measured directly on the sheared joint.

(xii) Peak shear stiffness measurements on laboratory-size samples will probably yield the absolute maximum K_s value for a particular large scale joint exposure. In fact, K_s is strongly scale dependent. This is also verified by the results from the present model joints which show a remarkable similarity with the trends of literature data. The magnitude of scale effect on K_s depends on the type of joint (e.g. rough, undulating or planar) and generally increases for rougher joint surfaces.

REFERENCES

REFERENCES

ATTEWELL, P.B. and FARMER, I.W. (1976). 'Principles of Engineering Geology', John Wiley & Sons Inc., New York, p.1045.

BARROSO (1966). "Contribution to Theme 8", Proc. 1st Cong. Int. Soc. for Rock Mechanics, Lisbon, 1966, Vol. III, pp. 588-591.

BARTON, N.R. (1970). "A low strength material for simulation of the mechanical properties of intact rock in rock mechanics models", Proc. 2nd Cong. of Int. Soc. for Rock Mech., Beograd, Vol. II, pp.99-110.

BARTON, N.R. (1971). "A model study of the behaviour of steep excavated rock slopes", Ph.D. Thesis, University of London.

BARTON, N.R. (1971). "A relationship between joint roughness and joint shear strength", Proc. Int. Symp. on Rock Mech., Nancy, Paper I-8.

BARTON, N.R. (1972). "A model study of rock joint deformation", Int. J. Rock Mech. Min. Sci., 9, pp. 579-602.

BARTON, N. (1973). "Review of a new shear-strength criterion for rock joints", Engng. Geology, 7, pp. 287-332.

BARTON, N. (1973a). "A review of the shear strength of discontinuities in rock masses with particular reference to slope stability", Norwegian Geotechnical Institute, Internal Report No. 54204-1, p.164.

BARTON, N. (1974). "A review of the shear strength of filled discontinuities in rock", Norwegian Geotechnical Institute Publication No. 105, p.38.

BARTON, N. (1976). "The shear strength of rock and rock joints", Int. J. Rock Mech. Min. Sci. & Geomech. Abstr., Vol. 13, pp. 255-279.

BARTON, N. and CHOUBEY, V. (1977). "The shear strength of rock joints in theory and practice", Rock Mechanics, 10, pp. 1-54.

BARTON, N. and BANDIS, S. (1979). Technical note: 'Some effects of scale on the shear strength of joints'. To be published. Int. J. Rock Mech. Min. Sci. and Geomech. Abstr.

BARTON, N. and HANSTEEN, H. (1979). "Large underground openings at shallow depth: Comparison of deformation magnitudes from jointed models and linear elastic finite element analyses", Norwegian Geotechnical Institute, Internal Report No. 54205-5, p.49.

BERNAIX, J. (1974). "Properties of Rock Masses", Proc. 3rd Congr. Int. Soc. for Rock Mech., Denver, Colorado, Vol. 1, Part A, pp. 9-39.

BIENIAWSKI, Z.T. and VAN HEERDEN, W.L. (1975). "The significance of in situ tests on large rock specimens", Int. J. Rock Mech. Min. Sci. & Geomech. Abstr., 12, pp. 101-113.

BOYD, J.M. (1975). "Analysis of Surface Roughness - Part 1", Imperial College, Rock Mechanics Research Report.

BROCH, E. and FRANKLIN, J.A. (1972). "The Point-Load Strength Test", Int. J. Rock Mech. Min. Sci., 9, pp. 669-697.

BROOK, N. (1977). "A method of overcoming both shape and size effects in point load testing", Proc. Conf. on Rock Engng., Newcastle, pp. 53-70.

BROWN, E.T. (1971). "Strength-size effects in rock material", Proc. Int. Symp. on Rock Mech., Nancy, Paper II-11.

BROWN, E.T., RICHARDS, L.R. and BARR, M.V. (1977). "Shear strength characteristics of the Delabole slates", Proc. Conf. on Rock Engng., Newcastle, pp. 33-51.

BYERLEE, J.D. (1967). "Frictional characteristics of granite under high confining pressure", J. Geophys. Res., 72, pp. 3639-3648.

CAWSEY, D.C. and FARRAR, N.S. (1976). "A simple sliding apparatus for the measurement of rock joint friction", Geotechnique, 26, No. 2, Technical Note, pp. 382-386.

CHAPPELL, B.A. (1975). "Friction characteristics of graphite coated bedding joints in shale", Int. J. Rock Mech. Min. Sci. & Geomech. Abstr., 12, pp. 33-39.

CHRISTIAN, J.T. and DESAI, C.S. (1977). "Constitutive laws for geologic media", in Numerical Methods in Geotechnical Engineering, Edited by Desai and Christian, pp. 65-116.

COULSON, J.H. (1970). "The effects of surface roughness on the shear strength of joints in rock", Ph.D. Thesis, University of Illinois.

COULSON, J.H. (1971). "Shear strength of flat surfaces in rock", Proc. 13th Symp. on Rock Mechanics, Urbana, Illinois. Edt. E.J. Cording ASCE, pp. 77-105.

DEERE, D.U., HENDRON, A.J., PATTON, F.D. and CORDING, E.J. (1967). "Design of surface and near-surface construction in rock", Proc. 8th Symp. of Rock Mech. on Failure and Breakage of Rock, Edt. Fairhurst, Chapter 11, pp. 237-302.

DEERE, D.U. (1974). "Geological considerations", in Rock Mechanics in Engineering Practice, Edt. Stagg and Zienkiewicz, Chapter 1, pp. 1-20.

DROZD, K. (1967). "Variations in the shear strength of a rock mass depending upon the displacements of the test blocks", Proc. Geotechn. Conf. on Shear Strength Properties of Natural Soils and Rocks, Oslo, Vol. 1, pp. 265-269.

DUNCAN, J.M. and CHANG, C.Y. (1970). "Non-linear analysis of stress and strain in soils", J. Soil Mech. Found. Div. ASCE, Vol. 96, No. SM5, pp. 1629-1653.

DUNCAN, N. and HANCOCK, K.E. (1966). "The concept of contact stress in assessment of the behaviour of rock masses as structural foundations", Proc. 1st Cong. Int. Soc. for Rock Mech., Lisbon, Vol. 2, pp. 537-542.

EINSTEIN, H.H., BAECHER, G.B. and HIRSCHFELD, R.C. (1970). "The effect of size on strength of a brittle rock", Proc. 2nd Cong. Int. Soc. for Rock Mech., Belgrade, Paper 3-2, pp. 7-12.

EVDOKIMOV, P.D. and SAPEGIN, D.D. (1970). "A large scale field shear test on rock", Proc. 2nd Cong. Int. Soc. for Rock Mech., Belgrade, 2, Paper 3-17.

FOLK, R.L. (1968). "Petrology of Sedimentary Rocks", Hemphill's Drawer M. University Station, p.170.

FRANKLIN, J., MANAILOGLOU, J. and SHERWOOD, D. (1974). "Field determination of direct shear strength", Proc. 3rd Cong. Int. Soc. for Rock Mech., Vol. IIA, Denver, Colorado, pp. 233-240.

FUMAGALLI, E. (1974). "Model simulation of rock mechanics problems", Rock Mechanics in Engng. Practice, Edt. Stagg & Zienkiewicz, Chapter 11, pp. 353-384.

GUISEPPE, B. (1970). "The shear strength of some rocks by laboratory tests", Proc. 2nd Int. Cong. Int. Soc. for Rock Mech., Belgrade, Vol. 2, Paper 3.24.

GOODMAN, R.E., TAYLOR, R.L. and BREKKE, T. (1968). "A model for the mechanics of jointed rock", J. Soil Mech. Found. Div., Proc. ASCE, Vol. 94, No. SM3, pp. 637-659.

GOODMAN, R.E. (1970). "The deformability of joints", Symposium: Determin. of the in-situ modulus of deformation of rock, A.S.T.M., S.T.P. 477, pp. 174-196.

GOODMAN, R. (1974). "The Mechanical Properties of Joints", Proc. 3rd Cong. Int. Soc. for Rock Mech., Denver, Colorado, Vol. 1, Part A, pp. 127-140.

GOODMAN, R.E. (1976). "Methods of Geological Engineering in Discontinuous Rock", West Publishing Company, p.472.

GOODMAN, R.E. and St. JOHN, C. (1977). "Finite Element Analysis for Discontinuous Rocks", in Numerical Methods in Geotechnical Engng., Edt. by Desai, C.S. and Christian, J.T., Chapter 4, pp. 148-175.

GREENSMITH, J.T. (1971). "Petrology of the Sedimentary Rocks", 5th Edition, Thomas Murby & Co., London, p.502.

GSL (1977). "The description of rock masses for engineering purposes", Report by the Geological Society Engineering Group Working Party, Q.J. Engng. Geol., Vol. 10, pp. 355-388.

GUERREIRO, M. et al. (1968). "Deformability tests and some results from three Spanish dam sites", Report II.1, Int. Symposium on Rock Mech., Madrid.

HAMROL, A. (1961). "A quantitative classification of the weathering and weatherability of rocks", Proc. 5th Int. Conf. Soil Mech. Found. Engng., Paris, Vol. 2, pp. 771-774.

HENCHER, S.R. (1976). Discussion. Geotechnique 26, no. 4, pp. 641-644.

HOBBS, D.W. (1966). "The behaviour and simulation of sedimentary rocks", National Coal Board, Mining Research Establishment, Isleworth, Middx.

HODGSON, K. and COOK, N.G. (1970). "The effects of size and stress gradient on the strength of rock", Proc. 2nd Cong. Int. Soc. for Rock Mech., Belgrade, Paper 3-5, pp. 31-34.

HOEK, E. and LONDE, P. (1974). "Surface Workings in Rock", Proc. 3rd Cong. Int. Soc. for Rock Mech., Denver, Colorado, Vol. 1, pp. 613-654.

HOEK, E. and BRAY, J. (1977). "Rock Slope Engineering", 2nd Edition, The Institution of Mining and Metallurgy, London, p.402.

HOLDRIDGE, D.A. and WALKER, E.G. (1967). "The dehydration of Gypsum and the rehydration of Plaster", Trans. Brit. Ceram. Soc. Vol. 66, pp. 485-509.

HORN, H.M. and DEERE, D.U. (1962). "Frictional Characteristics of Minerals", Geotechnique Vol. 12, pp. 319-335.

HUNGR, O. and COATES, D.F. (1978). "Deformability of joints and its relation to rock foundation settlements", Canadian Geotechnical Journal, Vol. 15, pp. 239-249.

INFANTI, N. and KANJI, M.A. (1978). "In-situ shear strength, normal and shear stiffness determinations at Agua Vermelha Project", Proc. 3rd Int. Cong. of Int. Assoc. Engng. Geol., Madrid, Session 2, Vol. 2, pp. 175-183.

ISRM (1974). Commission on Standardization of Laboratory and Field Tests of the International Society for Rock Mechanics: "Suggested methods for determining shear strength", Document No. 1, February 1974.

ISRM (1978). Commission of Standardization of Laboratory and Field Tests of the International Society for Rock Mechanics: "Suggested methods for determining hardness and abrasiveness of rocks", Int. J. Rock Mech. & Min. Sci. and Geomech. Abstr., Vol. 15, No. 3, pp. 89-99.

ISRM (1978a). Commission on Standardization of Laboratory and Field Tests of the International Society for Rock Mechanics: "Suggested methods for the quantitative description of discontinuities", Int. J. Rock Mech. and Min. Sci. & Geomech. Abstr., Vol. 15, No. 6, pp. 320-368.

IWAI, K. (1976). "Fundamental studies of fluid flow through a single fracture", Ph.D. Thesis, University of California, Berkeley, p.208.

JAGGER, J.C. (1959). "The Frictional Properties of Joints in Rock", Geofis. Pura Appl., Milano, 43, pp. 148-158.

JAEGER, J.C. (1969). "Behaviour of closely jointed rock", Proc. 11th Symp. Rock Mech., Berkeley, California, pp. 57-68.

JAEGER, J.C. (1971). "Friction of rocks and the stability of rock slopes", Geotechnique, Vol. 21, No. 2, pp. 97-134.

JOHN, K.W. (1962). "An approach to rock mechanics", Proc. American Soc. of Civil Engineers, Vol. 88, No. SM4, pp. 1-30.

JOHN, K.W. (1970). "Civil engineering approach to evaluate strength and deformability of regularly jointed rock", Proc. 11th Symposium on Rock Mechanics, pp. 69-82.

KONDRER, R.L. (1963). "Hyperbolic stress-strain response: cohesive soils", J. Soil Mech. Found. Div. ASCE, Vol. 89, No. SM1, pp. 115-143.

KRAHN, J. and N.R. MORGENSTERN (1979). "The ultimate frictional resistance of rock discontimuities", Int. J. Rock Mech. Min. Sci. & Geomech. Abstr., Vol. 16, pp. 127-133.

KRSMANOVIC, D. (1967). "Initial and residual shear strength of hard rocks", Geotechnique, Vol. 17, No. 2, pp. 145-160.

KRSMANOVIC, D. and LANGOF, Z. (1966). "Large scale laboratory tests of the shear strength of rocky material", Rock Mech. Eng. Geol., Suppl. 1, pp. 20-30.

KRSMANOVIC, D. and POPOVIC, M. (1966). "Large-scale field tests of the shear strength of limestone", Proc. 1st Cong. Int. Soc. for Rock Mech., Lisbon, Vol. 1, pp. 773-779.

KRSMANOVIC, D., TUFO, M. and LANGOF, Z. (1966). "Shear strength of rock masses and possibilities of its reproduction on models", Proc. 1st Cong. Int. Soc. for Rock Mech., Lisbon, Paper 3-52.

KULHAWY, F.H. (1975). "Stress-deformation properties of rock and rock discontimuities", Engineering Geology, Vol. 9, pp. 327-350.

KULHAWY, F.H. (1978). "Geomechanical model for rock foundation settlement", Proc. of ASCE, Geotechnical Div., Vol. 104, No. GT2, pp. 211-227.

KUTTER, H.K. (1971). "Stress distribution in direct shear test samples", Symp. Int. Soc. for Rock Mech., Nancy, Paper II-6.

LADANYI, B. and ARCHAMBAULT, G. (1970). "Simulation of shear behaviour of a jointed rock mass", Proc. 11th Symp. on Rock Mech., AIME, pp.105-125.

LAJTAI, E.Z. (1969). "Strength of discontimuous rock in direct shear", Geotechnique, Vol. 19, No. 2, pp. 218-233.

LAMA, R.D. (1978). "Influence of clay fillings on shear behaviour of joints", Proc. 3rd Int. Cong. Int. Assoc. Engng. Geol., Madrid, Vol. 2, pp. 175-183.

LAMA, R.D. and GONANO, L.P. (1976). "Size-effect considerations in the assessment of mechanical properties of rock masses", Proc. 2nd Symp. Rock Mech., Dhanbad.

LAMA, R.D. and VUTUKURI, V.S. (1978). "Handbook on mechanical properties of rock", Vol. IV, Trans. Tech. Publications.

LOCHER, H.G. and RIEDER, U.G. (1970). "Shear tests on layered Jurassic Limestone", Proc. 2nd Cong. Int. Soc. for Rock Mech., Belgrade, Vol. 2, Paper 3-1.

LONDE, P. (1973). "The role of rock mechanics in the reconnaisance of rock foundations", Q. Journal of Engng. Geology, Vol. 6, No. 1, pp.

LUNDBORG, N. "The strength-size relation of granite", Int. J. Rock Mech. and Min. Sci. Vol. 4, No. 3, pp. 269-272.

MARTIN, G.R. and MILLAR, P.J. (1974). "Joint strength characteristics of a weathered rock", Proc. 3rd Cong. Int. Soc. for Rock Mechanics, Denver, Colorado, Vol. 2A, pp. 263-270.

MILLER, R.P. (1965). "Engineering classification and index properties for intact rock", Ph.D. Thesis, Univ. Illinois, pp. 332.

MOGILEVSKAYA, S.E. (1974). "Morphology of joint surfaces in rock and its importance for engineering geological examination of dam foundations", Proc. 2nd Int. Cong. Int. Assoc. Eng. Geology, Sao Paolo, Brazil, 2, Theme VI, pp. 17.1-17.8.

MULLER, L. (1963). Discussion. Proceedings American Soc. of Civil Engineers, No. SM2, pp. 137-139.

MURRELL, S.A.F. (1965). "The effect of triaxial stress systems on the strength of rock at atmospheric temperatures", Geophysical Journal, Vol. 10, pp. 231-281.

OBERT, L. and DUVAL, W.I. (1967). "Rock mechanics and the design of structures in rock", John Wiley & Sons.

PATTON, F.D. (1966). "Multiple modes of shear failure in rock and related materials", Ph.D. Thesis, University of Illinois, p.282.

PRATT, H.R., BLACK, A.D., BROWN, W.S. and BRACE, W.F. (1972). "The effect of specimen size on the mechanical properties of unjointed Diorite", Int. J. Rock Mech. Min. Sci., Vol. 9, pp. 513-529.

PRATT, H.R., BLACK, A.D. and BRACE, W.F. (1974). "Friction and deformation of jointed Quartz Diorite", Proc. 3rd Cong. Int. Soc. for Rock Mech., Denver, Colorado, Vol. II.A, pp. 306-310.

REIK, G. and TEUTSCH, C.H.R. (1976). "The use of equivalent models in slope stability investigation", Int. J. Rock Mech. & Min. Sci. & Geomech. Abstr., Vol. 13, pp. 321-330.

RENGERS, N. (1970). "Influence of surface roughness on the friction properties of rock planes", Proc. 2nd Int. Soc. for Rock Mech., Belgrade, Vol. 1, Paper 1-31.

RICHARDS, L.R. (1975). "Shear strength of joints in weathered rock", Ph.D. Thesis, University of London.

ROCHA, M. (1974). "Present possibilities of studying foundations of concrete dams", Proc. 3rd Cong. Int. Soc. for Rock Mech., Denver, Colorado, pp. 879-897.

ROSS-BROWN, M.D. and WALTON, G. (1975). "A portable shear box for testing rock joints", Rock Mechanics, 7, pp. 129-153.

ROSSO, R.S. (1976). "A comparison of joint stiffness measurements in direct shear, triaxial compression and in situ", Int. J. Rock Mech. Min. Sci. & Geom. Abstr., Vol. 13, pp. 167-172.

RUIZ, M.D., CAMARGO, F.P., MIDEA, N.F. and NIEBLE, C.M. (1968). "Some considerations regarding the shear strength of rock masses", Int. Symp. Rock Mech., Madrid, II-5, pp. 159-169.

SALAS, J.A.J. (1968). "Mechanical Resistances", Proc. Int. Symp. on Rock Mechanics, Madrid, Theme II, pp. 115-130.

SCHNEIDER, H.J. (1976). "The friction and deformation behaviour of rock joints", Rock Mechanics, 8, pp. 169-184.

SCHNEIDER, H.J. (1978). "The laboratory direct shear test - an analysis and geotechnical evaluation", Bull. Int. Assoc. of Engng. Geology, No. 18, pp. 121-126.

SERAFIM, J.L. (1964). "Rock mechanics considerations in the design of concrete dams", in State of Stress in the Earth's Crust, Proc. Conf. on Rock Mech., Santa Monica, California, pp. 611-650.

SERAPHIM, J.L. and GUERREIRO, M. (1968). "Shear strength of rock masses at three Spanish dam sites", Int. Symp. Rock Mech., Madrid, II.4, pp. 147-158.

SHARP, J.C. and MAINI, Y.N.T. (1972). "Fundamental consideration on the hydraulic characteristics of joints in rock", Proc. Symp. on Percolation through Fissured Rock, Stuttgart, Paper No. T1-F.

SNOW, D.T. (1972). "Fundamentals and in-situ determination of permeability", Proc. Symp. on Percolation through Fissured Rock, Int. Soc. for Rock Mech., Stuttgart, Paper G1.

STEPHENSON, D.E. and TRIANDAFILIDIS, G.E. (1974). "Influence of specimen size and geometry on uniaxial compressive strength of rock", Bull. Assoc. of Engng. Geologists, Vol. XI, No. 1, pp. 29-47.

STIMPSON, B. (1970). "Modelling materials for engineering rock mechanics", Int. J. Rock Mech. Min. Sci., Vol. 7, pp. 77-121.

TALOBRE, J.A. La mechanique des roches, Dunod, Paris. (1957).

TSE, R. and CRUDEN, D.M. (1979). "Estimating joint roughness co-efficients", Int. J. Rock Mech. & Min. Sci. & Geomech. Abstr., Vol. 16, No. 5, pp. 303-307.

VUTUKURI, V.S., LAMA, R.D. and SALUJA, S.S. (1974). "Handbook on mechanical properties of rocks", Vol. 1, Trans. Tech. Publications.

WAREHAM, B.F. and SHERWOOD, D.E. (1974). "The relevance of size of sample and type of test in determining shear properties for use in stability analysis", Proc. 3rd Cong. Int. Soc. for Rock Mech., Denver, Colorado, Vol. II.A, pp. 316-321.

WITHERSPOON, P.A. and GALE, J.E. (1977). "Mechanical and hydraulic properties of rocks related to induced seismicity", Engng. Geology, Vol. 11, pp. 23-55.

APPENDICES

APPENDIX I

1. PHYSICAL PROPERTIES OF THE COMPOSITE MODELLING MATERIALS

A list of the materials that were combined into a variety of mixes has been given in section 2.2.4 , and some information about their physical characteristics is presented here.

(a) Cementing materials

Plaster is the most commonly used binder in multi-component mixes. The material is easily obtainable, it is easy to cast, sets relatively fast, shows very little shrinkage, its properties can be changed by addition of various fillers and is relatively cheap.

The main disadvantages are the sensitivity of its properties to external factors such as the source of raw material, production conditions and atmospheric moisture. It is generally advisable to test each new supply of plaster and store it in air-tight containers.

The mechanical properties of dry plaster, i.e. dried plaster-water mixes, have been summarized by Stimpson (1970), and some very brief notes are included here.

Uniaxial compressive strength (σ_c) may range from 2.5 to 7.6 MPa, Young's Modulus (E_T) can vary between 2.5 and 18 GPa and Poisson's ratio (ν) is of the order of 0.06 and 0.304.

The σ_c/σ_t ratio varies between 2 and 8 depending upon the type of plaster. With increasing amount of water, σ_c, σ_t and E decrease and ν rises or stays constant.

Depending upon the type of plaster and testing conditions (e.g. rate of strain) the stress-strain curves can be either linear or non-linear. Most non-linear curves possess a linear region at low stresses.

The dependence of the properties of the plaster upon its hydration state makes curing conditions very critical. Hobbs (1966) tested the effect of curing temperature on sand-plaster mixes and found that curing at 25°-30°C gave slightly lower σ_c, σ_t and E_T values. By drying at 90°C, σ_c and E_T decreased by up to 85% due to the breakdown of the dihydrate.

Three types of plaster were tried, namely, plaster of Paris, dental and pink plaster, and the first one was finally adopted.

Plaster of Paris (P.P.) is the hemihydrate of calcium sulphate and has the composition $CaSO_4.\frac{1}{2}H_2O$. It is commercially produced by calcination of gypsum ($CaSO_4.2H_2O$) at 190°-200°C. Addition of water results in reversal of the above process and needle-like crystals of dihydrate ($CaSO_4.2H_2O$) are formed:

$$CaSO_4.\tfrac{1}{2}H_2O + {}^{3}/2\ H_2O \longrightarrow CaSO_4.2H_2O$$

The hydration process requires 18.6 grams of water for every 100 grams of plaster.

Dental plaster (D.P.) is the hemihydrate of β-calcium sulphate. It resembles P.P. in that neither contain impurities. Dental plaster is produced by calcination at higher temperatures than P.P. Dental plaster was found to be slightly weaker than plaster of Paris.

Finally, pink plaster contains various additives which retard its setting time to over 1 hour compared to the 5-10 mins of the other two types.

Control tests on plaster of Paris consisted of compression and diametrical point loading of cylindrical specimens 2.5 cm D/5.0 cm L, prepared from a mix of equal quantities of water and plaster (W:P.P. = 1:1) and cured at 90° ± 5°C for 2 days.

The three different batches of P.P. supplied during the course of work showed very similar properties (σ_c = 552 ± 50 kPa and σ_t = 125.5 ± 15 kPa).

Care was taken to store the plaster in a moisture-free environment and was always kept in air-tight containers.

The suppliers were: C.F. Thackray Ltd., Leeds.

(b) Frictional fillers

Sand was used as the basic frictional filler and five different types were tried before the choice of the optimum one. The varieties of sands differed both in grain-size and sorting, including:

- Very fine sand (VF)
- Fine (silver) sand (F)

- Medium-coarse sand (MC)
- Coarse sand (C)
- Very coarse sand (VC).

Letters in brackets are the assigned symbols for brief description of each sand type.

The grain size distribution of the five sands obtained by sieve analysis is presented in Figure 1. From the cumulative graphs two statistical parameters, namely graphic mean and graphic standard deviation, were derived by methods given in Folk (1968). The various derived parameters together with the dry densities of the sands are presented in Table 1.

The type of sand finally chosen was the silver sand (F-type). The reasons of the choice will be explained in the relevant context.

Suppliers: Cawoods Building Materials Ltd., Leeds.

(c) Other additives

Three different additives were combined with the basic sand/plaster/water mixtures in the attempt to improve the properties of the latter, namely:

Barytes ($BaSO_4$) : Finely-ground powder. Specific gravity = 4.35. Used as a dense filler to increase the density and reduce the deformation of mixes.
Other types of similar additives that have been used in the past are red lead (Pb_3O_3) (Barton, 1970), iron ore and magnetite powder.

Calcined Alumina (Burntisland grade, Al_2O_3) : Silt-size powder of specific gravity 3.8. Used mainly to increase the σ_c/σ_t ratio and improve the brittleness of the material.
Use of alumina has not been reported in the literature.

Kaolinite powder (pure) : Clay size fraction, specific gravity 2.6.
Use of clay has been reported to increase the brittleness of materials (Stimpson, 1970). Its present use proved unsuccessful.

Suppliers of barytes: Donated by St. John's Colliery, NCB, Nr. Normanton, Yorks.

Suppliers of alumina : B.A. Chemicals Ltd., Chalfont Park, Bucks.

TABLE 1

Description of type and dry densities of sands

Type of sand	GRAPHIC MEAN $= \frac{\phi_{16\%} + \phi_{50\%} + \phi_{87\%}}{3}$ values in mm	SAND UNIFORMITY Graphic std.dev. $= \frac{\phi_{84\%} - \phi_{16\%}}{4} + \frac{\phi_{95\%} - \phi_{5\%}}{6.6}$		DENSITY gr/cm^3
			Description	
VF	0.21	0.31	Very well sorted	1.51
F	0.27	0.50	Moderately well sorted	1.62
MC	0.47	0.56	" "	1.74
C	0.79	0.29	Very well sorted	1.53
VC	1.39	0.25	" "	1.50

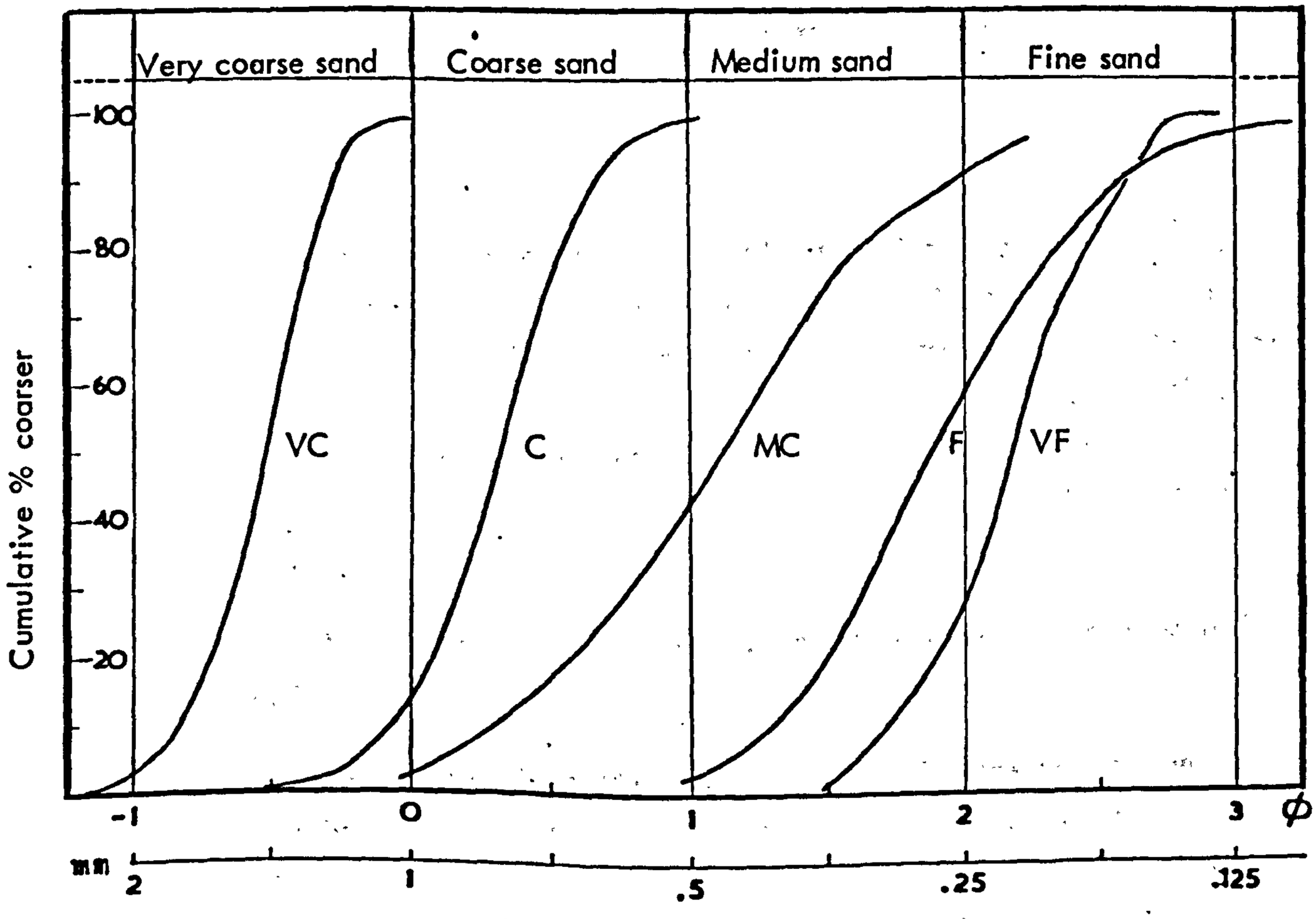

FIGURE 1 Grain-size analyses of modelling sands

2. DETAILS OF TEST SPECIMEN PREPARATION

(a) Mixing

The mixing of the various components was carried out in a Kenwood A901 mixer of double orbital type. Blending duration was standardized for similar mixes and the same speed was used throughout (setting 4).

The mixing of the materials was performed at three consecutive stages: dry mixing of fillers (5 minutes) ⟶ addition of water and 5 minutes of wet blending ⟶ addition of plaster quantity. The duration of mixing of all components depended upon the quantity of plaster and water and for the various combinations tried, it ranged between 20 seconds and 3 minutes. In general, blending was continued until the mixture reached a "creamy-but-pourable" state.

The latter condition was essential for two reasons: firstly, it almost eliminated the amount of "bleeding" of the specimens during setting and secondly, enabled preparation of compositionally homogeneous specimens. With regard to the latter, it should be pointed out that careless mixing resulted in a layer of "watery substance" on the top of the mixture which was inevitably poured in the first two or three moulds.

(b) Casting

The blended mixtures were poured into cylindrical moulds made of acrylic plastic. The average inside diameter of the cylinders was 25.67 mm (std. dev. = 0.240, n = 20). The moulds were of two different lengths; the longer ones (with average length of 51.22 mm, std. dev. = 0.2) were used to cast specimens for compression tests; the shorter ones (average length 21.26 mm, std. dev. = 0.22) provided specimens for axial point load testing.

After the plaster had set, the excess material was gently scraped off the mould ends.

Removal of the specimens from the moulds originally presented a small problem. A lubricant oil was firstly used to cover the walls of the moulds and ease specimen removal. However, that method proved disadvantageous for the following reasons. Firstly, it caused considerable delays as one had to wait until the specimens were hard enough to withstand without disturbance (mainly end compaction) the pressure necessary

for their extraction. Secondly, in quite a few instances miniature surficial pores were observed on the walls of the specimens. Closer observation of the "lubricated" cylinders revealed the existence of many air-bubbles trapped under the thin oil film, which were thought to be responsible for the defective specimen surface finish. Use of less oil proved to be ineffective.

Another set of moulds was then prepared with longitudinal slits along them. Once the mix had apparently set the moulds were placed for a few minutes in the oven at 60°-70°C. That resulted in a very small radial expansion of the plastic and by gently pulling the slit sides apart the specimen could very easily be pushed out. The possibility of mould deformation due to the repeated heating cycles was considered and measurements of dimensions were taken regularly by a micrometer. No measurable change was recorded throughout the course of the investigation.

(c) Curing

The basic characteristic of multi-component mixtures cemented with plaster is that a much larger amount of water is needed to make the mix pourable than that required for the hydration process.

Removal of the excess or free water can be achieved through evaporation by exposing the specimens either at room or oven temperature. The effect of curing temperature upon the properties of plaster has been briefly discussed in section 2.2.4.

During the course of this work a range of temperatures was tried, varying from room temperature (~20°C) to oven (80°-85°C). As expected, that variation was found to be critical for the strength of the mixes tested. The curing temperature used for the final model material was 50°-55°C which allowed the desired strength properties to be obtained.

The curing procedures will be discussed further in connection with the various mixes.

3. NOTES ON THE TESTING PROCEDURES

(a) Uniaxial Compression Tests

Compression tests were performed on standard size (25 mm D/50 mm L) cylindrical specimens using an Instron Compression Machine. Uniaxial strength was calculated from:

$$\sigma_c = \frac{L \times 9.807}{c.s.a.} \times 10^{-3} \quad kPa$$

where L = load in kgms

c.s.a. = cross sectional area in m^2 (= $517.5 \times 10^{-6} m^2$).

(b) Indirect tensile strength tests

(i) Point load tests

- Axial testing, T_{500}

The tests were performed on 25 mm D/20 mm L cylindrical specimens having the optimum cross sectional area of 500 mm^2 as has been recommended by Brook (1977).

The T_{500} index was obtained from:

$$T_{500} = \frac{L \times 9.807}{c.s.a.} \times 10^{-3} \quad kPa$$

where L = load in kgms

c.s.a. = cross sectional area in m^2 (= $500 \times 10^{-6} m^2$).

- Diametrical testing, T_o (Broch and Franklin, 1972)

The standard compression cylinders were point load tested diametrically and T_o was derived from:

$$T_o = \frac{L \times 9.807}{d^2} \times 10^{-3} \quad kPa$$

where L = load in kgms

d = specimen diameter in m (= 25.667×10^{-3}m).

(ii) Brazilian test (σ_{tb})

The test was performed on 25 mm diameter/8 mm thick discs and σ_{tb} was calculated from:

$$\sigma_{tb} = \frac{2L \times 9.807}{\pi Dt} \times 10^{-3} \quad kPa$$

where L = load in kgms

D = diameter of disc in meters (= 25.667×10^{-3}m)

t = thickness of disc in meters (= 8×10^{-3}m).

(c) Measurements of axial deformation

Use of strain gauges for measurements of axial and lateral strains of model specimens poses a number of practical problems. For instance, a thin coating of high modulus plaster on the specimen surface may result in underestimation of deformability if the gauge is directly attached on it. The inverse error can be induced by concealed pores near the specimen's surface. Furthermore, the time-consuming preparation and the cost when a large number of tests are involved, are not justified in view of the uncertainties involved.

Consequently, it was decided to measure the axial deformation of the loaded specimens by means of a dial gauge mounted on the Instron compression machine. The gauge is calibrated to measure the downwards movement of the loading ram of the apparatus to an accuracy of 0.001 mm.

During compression of a specimen the total movement of the loading ram is the sum of the axial "shortening" of the specimen and the vertical suppression of the base plate. Therefore, under any load F the displacement (D) of the loading end is:

$$D = (L - L') + d$$

where: L = original length of specimen

L' = reduced length of specimen due to axial deformation under F

d = base plate suppression under F.

If D can be corrected for d then the axial deformation (L - L') will be equal to (D - d), and hence axial strain (ε) will be:

$$\varepsilon = \frac{L - L'}{L}$$

The average movement (d) of the base plate under various loads was measured from a series of compression tests on a steel cylinder. Mechanical dial gauges (0.001 mm) were also used to cross-check the readings of the machine gauge. The displacements recorded by all gauges were almost identical.

The normal load-base plate deflection relationship was perfectly linear for both load cells used in the experiments. Linear regression analysis of the data gave the following two calibration equations:

CCM-cell: 0-50 kgms: $Y(\text{kgms}) = 2.367\ (\text{kgms}) + 0.445\ X\ (\mu\text{m})$, $r = +0.998$

CFM-cell: 0-5000 kgms: $Y(\text{kgms}) = 7.782\ (\text{kgms}) + 6.085\ X\ (\mu\text{m})$, $r = +0.989$

Use of the above equations enabled corrections of the total displacement of the loading ram recorded during each experiment.

Care was exercised during the test specimen preparation to ensure flatness of the ends. A very good finish of the latter was achieved by lapping them with a glass plate after extraction from the moulds.

The axial deformation at failure was recorded for every specimen of a given mix, and an average value was assigned. The deformation of 3-4 specimens from each mix was measured at regular load increments and the average values were used to draw the stress-strain curve for that material. From that curve the secant and tangent (at 50% σ_c) values of Young's Modulus were calculated.

(d) Density and Porosity Evaluation

The density (ρ) of the mixes was calculated according to

$$\rho = \frac{\text{Mass}}{\text{Volume}}$$

A batch of cylindrical specimens was weighed after completion of curing and the average mass was divided by the average volume of the specimen to derive mass per unit volume or density in gms/cm^3.

Porosity was evaluated indirectly on the assumption that the volume occupied by free water in the "wet" mix is equal to the volume of pores in the cured mix. Then porosity can be evaluated by dividing the weight of the evaporated water by the mass of the cured specimen.

4. PROPERTIES OF THE VARIOUS TRIAL MIXES

(a) Behaviour of the Sand (S)-Plaster (PP)- Water (W) system

(a.1) Different sand types

The physical characteristics of the five different sand types tested have been given in Table 1, section 1 of this appendix. According to their grain size the various sands have been described as: very fine (VF); fine (F); medium-coarse (MC); coarse (C); very coarse (VC).

The above varieties were used to prepare five mixes with the same amount of plaster and water. Each mixture consisted of the following quantities:

Sand = 600 grms/Plaster = 100 grms/Water = 200 grms

During the preparation of the mixes it was observed that grain size influenced their viscosity. For the same amount of water the mixtures of the coarse sands were rather "watery", while the ones with finer sands were much "thicker". That indicated the generally higher water requirements for saturation of finer grained materials due to their relatively larger surface area.

After preparation, the specimens were at first left to dry at room temperature for 24 hours to avoid development of vapour pore pressures, and then put in a ventilated oven at 80°C.

During the curing period regular recordings of the water loss were made. The specimens were considered as cured when no measurable changes of mass weight could be recorded. The latter meant that all the free water that was originally retained in the pores had evaporated.

Figure 2 shows the rate of moisture loss of the cylindrical specimens under room and oven temperatures. As shown, an apparent total loss of free water was achieved after ~ 35 hours of combined curing. The specimens were removed from the oven after $1\frac{1}{2}$ days.

The experimental results from uniaxial compression and point load (T_{500}) tests on the various mixtures are given in Table 2. Two additional mixes with combined sands were also tested (denoted 1 and 2 in Table 2).

The results showed that both σ_c and T_{500} varied with sand type.

The three "uniform" sands VF, C and VC gave weaker mixes than the graded sands F and MC, as shown in Figure 3. Such behaviour can be attributed to the better interlocking between the different sized grains in F and MC. Uniform grain size will result in looser packing of the grains, particularly in cases of coarse sands. It is interesting to note that the very fine sand (VF) of the uniform varieties exhibited much higher strength than the other two types (C and VC) because of the better mechanical bonding of the small grains. The closer packing of the sand structure that resulted from combinations of C and VC with VF resulted in mixes with strength higher than that of the original C and VC mixtures (Table 2 and Figure 3).

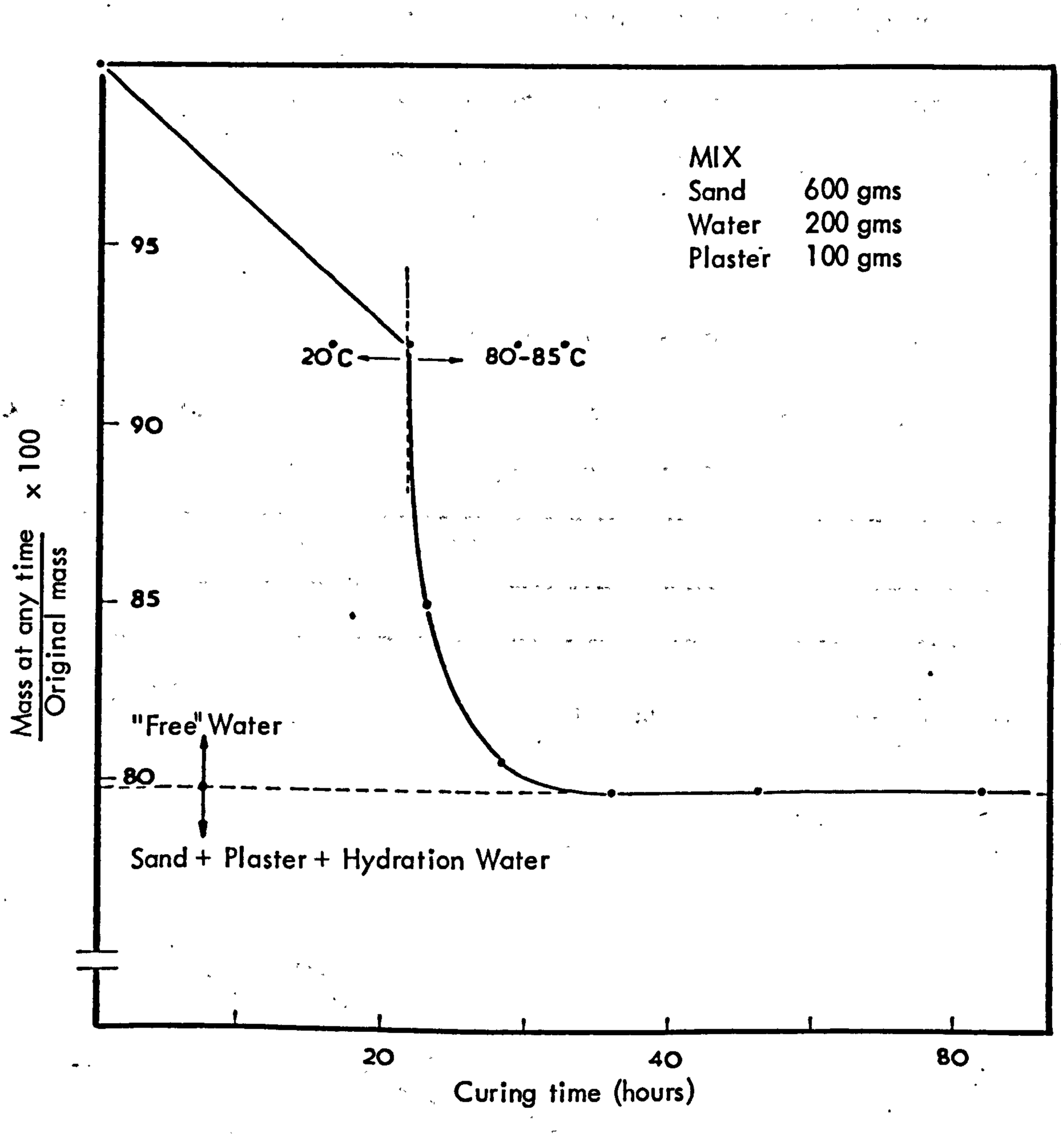

FIGURE 2 Curing of 25mm diameter / 50mm length cylindrical specimens of sand-plaster-water mixes.

TABLE 2

Different sand types

Sand type	Components (grms) S	PP	W	Proportions PP:S	W:S	Strength properties (kPa) No. of spec.	σ_c	No. of spec.	T_{500}	$\frac{\sigma_c}{T_{500}}$	Density ρ (g/cm^3)	Failure strain % ε_f
VF	600	100	200	1:6	1:3	8	91.87	5	17.73	5.2	1.52	1.35
F	"	"	"	"	"	9	115.34	7	22.53	5.1	1.53	1.11
MC	"	"	"	"	"	7	118.12	8	25.60	5.0	1.57	1.45
C	"	"	"	"	"	6	77.03	7	13.13	5.9	1.53	1.72
VC	"	"	"	"	"	6	52.72	5	12.02	4.4	1.56	2.10
(1)	600	100	200	1:6	1:3	8	67.84	3	12.23	5.55	1.59	-
(2)	"	"	"	"	"	9	86.19	9	16.07	5.4	1.56	-

(1) : 300VF + 300VC; (2) : 300VF + 300C

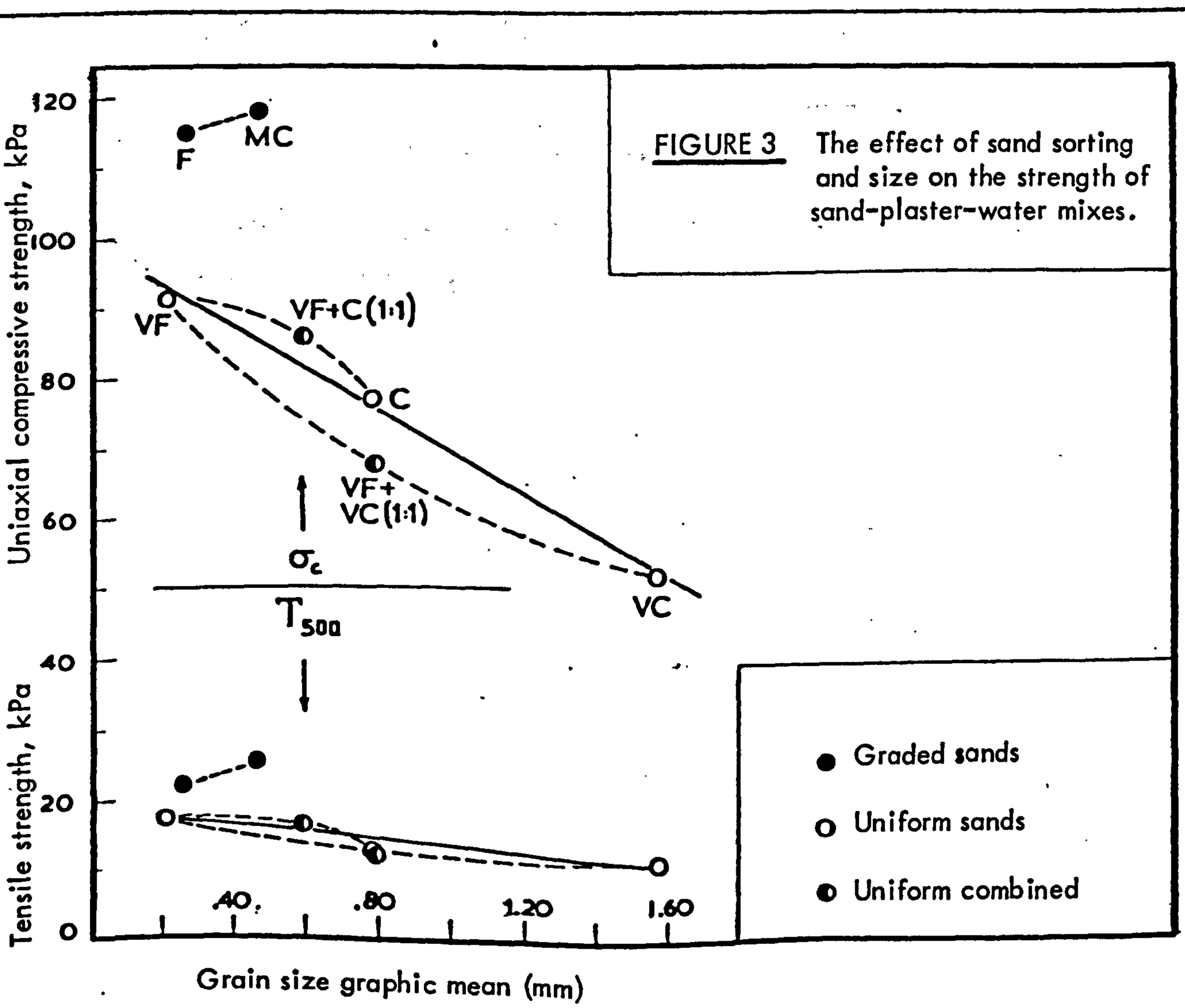

FIGURE 3 The effect of sand sorting and size on the strength of sand-plaster-water mixes.

It would appear therefore that the load carrying capacity of the sand structure decreases with increasing grain size especially in cases of uniform sands. The small amount of contact between the grains would reduce the internal frictional resistance of the material and increase its deformability. (2.1% strain at failure was recorded for the VC sand type.) In view of the above the very coarse (VC) and coarse (C) sand types were eliminated from any further testing.

(a.2) Properties of the VF, F and MC sand types mixed with various plaster quantities

The VF, F and MC types of sand were mixed with various amounts of plaster to gain some information about the range of strengths that could be achieved. The quantity of sand and water was kept constant for all mixes at 600 grms and 200 cm^3 respectively. Curing of the specimens followed the procedure described in the last section (24 hrs at 20°C and 36 hrs at 85°C).

For each type of mix the amount of plaster was increased to the maximum quantity that would still allow a workable mix to be obtained. The VF sand could only be mixed with up to 150 grms of plaster before it reached its workability limit. For the MC and F sands the maximum plaster quantities were 200 and 250 grms respectively.

The experimental results are given in Table 3, and the variations in σ_c and T_{500} are shown in Fig. 4.

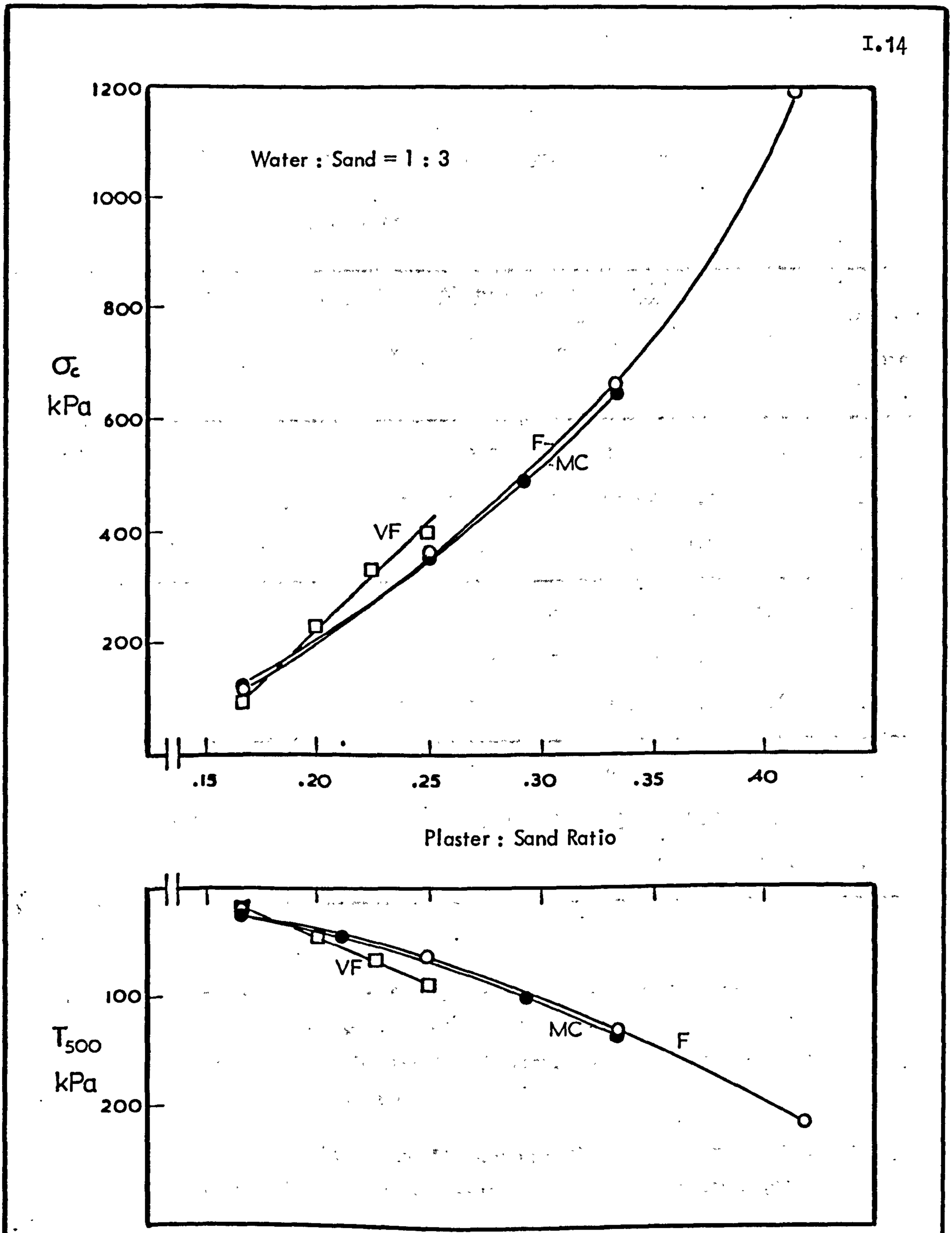

FIGURE 4 The effect of different plaster quantities on the uniaxial compressive (σ_c) and indirect tensile (T500) strength of sand-plaster-water mixes.

TABLE 3

Properties of Sand-Plaster-Water materials with constant S and W and varying PP

Curing: 24 hrs at 20°C + 36 hrs at 85°C.

Sand type	Components (gr)			Proportions		Strength properties (kPa)				$\frac{\sigma_c}{T_{500}}$	Density ρ (g/cm^3)	% strain at failure ε_f
	S	W	PP	PP:S	W:S	No. of spec.	σ_c	No. of spec.	T_{500}			
VF	600	200	120	1:5	1:3	6	229.8	7	44.76	5.1	1.51	1.14
			135	1:4.4		7	332.7	5	64.94	5.1	1.54	1.15
			150	1:4		6	399.0	6	87.26	4.6	1.53	1.42
F	600	200	150	1:4	1:3	9	363.05	8	64.28	5.7	1.59	1.13
			200	1:3		10	664.10	7	128.75	5.2	1.62	1.13
			250	1:24		8	1187.9	6	213.37	5.6	1.62	1.06
MC	600	200	150	1:4	1:3	8	353.5	6	83.36	4.2	1.58	1.50
			175	1:3.4		8	493.43	8	95.80	5.2	1.63	1.55
			200	1:3		7	642.40	7	135.14	4.7	1.64	1.52

Measurements of the axial strain at failure showed the high deformability of the mixes. The F-sand material was comparatively the least deformable while the highest strain was exhibited by the MC-mixture. A similar pattern was also observed for the σ_c/T_{500} ratio values.

On the basis of the above results, the MC-sand was discarded from any further testing. The VF-sand was also rejected because of its high water requirements and hence low mixture strength.

(a.3) Properties of silver sand/plaster mixes with different water contents

The critical factor that controls the deformational behaviour of a model material is the volume of the pore space left after evaporation of the free water. As has already been discussed, the water requirement of a mix is related to the grain size of the filler and the amount of plaster used.

Since the silver sand/plaster system formed the basis of all subsequent combinations, the effects of different water quantities upon the properties of the above components was studied in order to draw some guidelines for future optimization of proportions.

Eight sets of specimens were prepared by using a constant S:P ratio of 6:1 and varying the amount of water. The relative quantities and the test results are presented in Table 4.

TABLE 4

For all mixes S:P = 6:1

Mix type	Components (gr) S	PP	W	W:S	Density ρ (g/cm^3)	Porosity P %	Strength properties (kPa) No. of spec.	σ_c	No. of spec.	T_{500}	% strain at failure ε_f
1	600	100	250	1:2.4	1.39	44.8	6	50.2	7	8.32	2.0
2			200	1:3.0	1.53	42	9	116.3	7	22.5	1.4
3			190	1:3.16	1.57	41.5	9	132.2	9	25.4	1.5
4			185	1:3.24	1.57	42	8	172.2	9	34.0	1.2
5			180	1:3.33	1.61	40	10	184.2	11	40.0	1.4
6			175	1:3.45	1.59	36	8	179.2	6	31.1	1.1
7			170	1:3.53	1.62	38	6	185.5	7	37.1	0.9
8			165	1:3.64	1.64	38	5	189.2	7	38.5	1.1

As expected, increasing water content results in decreasing density, increasing porosity and hence decreasing strength. The variation of those properties with volume of water is illustrated in Figure 5.

The minimum amount of water required for saturation of the 700 grms of the sand/plaster mix was 165 grms, i.e. a proportion of W:(S+P) of 1:4.24. Depending upon the water content the deformation of the specimens at failure was $\varepsilon_f = 2\%$ at W = 250 cm^3 and $\varepsilon_f \approx 1\%$ at W = 165 cm^3. A small decrease in the value of the σ_c/T_{500} ratios was observed-from 6 to 4.9 - with decreasing water.

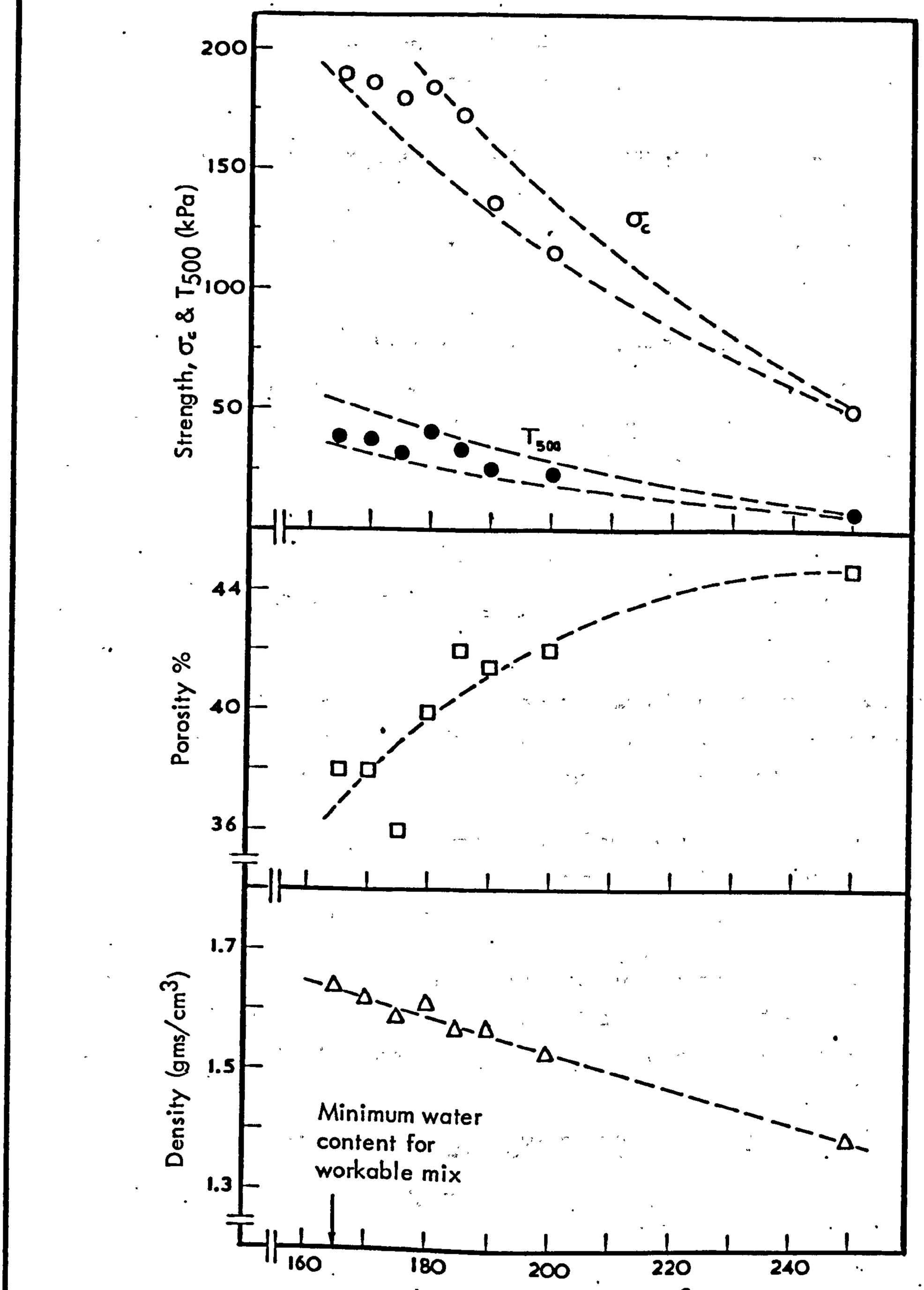

FIGURE 5 The effect of different water contents on the strength, porosity and density of silver sand-plaster mixes.

For all materials : sand = 600 gms, plaster = 100 gms

As will soon be discussed, use of fillers enabled considerable improvement of the minimum water requirements of the silver sand-plaster system.

(a.4) Summary of properties of the SAND:PLASTER:WATER system

The test results from the various trial mixes of the three basic material components gave sufficient information on the general behaviour of the system and pointed out the disadvantages of those combinations.

Compressive strengths up to 1.2 MPa were obtained (F-sand mix) under high temperature curing conditions, and obviously the target value of ~ 2.0 MPa could easily be reached if different curing temperatures were employed. However the mixes hardly approximated any of the requirements of the model material.

Densities were generally low being approximately 1.5 - 1.6 grms/cm^3. The porosity of the mixtures was of the order of 38 to 42% and the materials were very deformable.

The average axial strain at failure was estimated to be over 1% which was unacceptable in view of the range specified (.15 - .4%). Furthermore, the σ_c/T_{500} ratio was generally low being approximately 5 on average.

The selected sand type (silver sand) was also combined with two other varieties of plaster, namely dental and pink. The latter was immediately rejected because of its extremely long setting period.

Dental plaster mixtures exhibited behaviour and properties similar to those of the mixes of plaster of Paris. Comparatively, the former type was found to be slightly weaker than PP. A summary of the properties is given below.

Mix : 600 grms SAND/200 grms WATER/250 grms PLASTER

	PP-Mix	DP-mix
σ_c (kPa)	1188	1052
T_{500} (kPa)	213.4	184.0
σ_c/T_{500}	5.6	5.7
% ε_f	1.06	1.31

At this stage the investigation was directed towards improvement of the basic sand/plaster/water mixture with the aid of various additives.

(b) Properties of the Sand-Plaster-Water system combined with other fillers

(b.1) Use of Barytes (B), Kaolinite (K) and Alumina (A) as fillers

A set of five mixes with different barytes to sand ratios (1:1, 1:2, 1:3, 1:4, 1:5) was prepared to investigate the effects of the dense filler upon the properties of the silver sand/plaster/water system. The quantities of plaster and water were kept constant in all the materials to proportions of PP:(B+S) = 1:6 and W:(B+S) = 1:3 (average water requirement for similar quantities of sand and plaster). The test specimens were cured by oven drying at 80°C for 1½ days, after exposing them at room temperature for 24 hours.

The test results are presented in Table 5.

Inclusion of the high specific gravity barytes caused an increase of the strength and density of the basic sand/plaster/water mixture. Comparatively, the materials with high barytes content - B:S = 1:2 and 1:1 - showed the best behaviour with σ_c/T_{500} values of 7.5 and 6.0 and axial deformation at failure 0.30 and 0.87 respectively. However, the latter was still at unacceptable levels.

Another interesting observation was that barytes appeared to reduce the water requirements of the mixes. As mentioned in sub-section a.3, a quantity of 600 grms sand and 100 grms plaster required 165 cm^3 of water for the mix to reach its workability limit. A similar quantity of combined sand and barytes (400 gr S + 200 gr B) with 100 grms of plaster needed 125 cm^3 to reach similar viscosity. A series of mixes was prepared with different B:S proportions and constant plaster content (P:Filler = 1:6). The quantity of water added to each combination was sufficient to provide a workable mixture. The decreasing water requirements with increasing barytes content can clearly be seen in Figure 6.

A new set of specimens was prepared with the same B:S ratios as those presented in Table 5, but with smaller water content (W:Filler = 1:4). Those test results are included in Table 6 (Mix types: F6, F7, F8, F9). In Figure 7 a comparison of the compressive strength values of the same mixes with different water contents is shown.

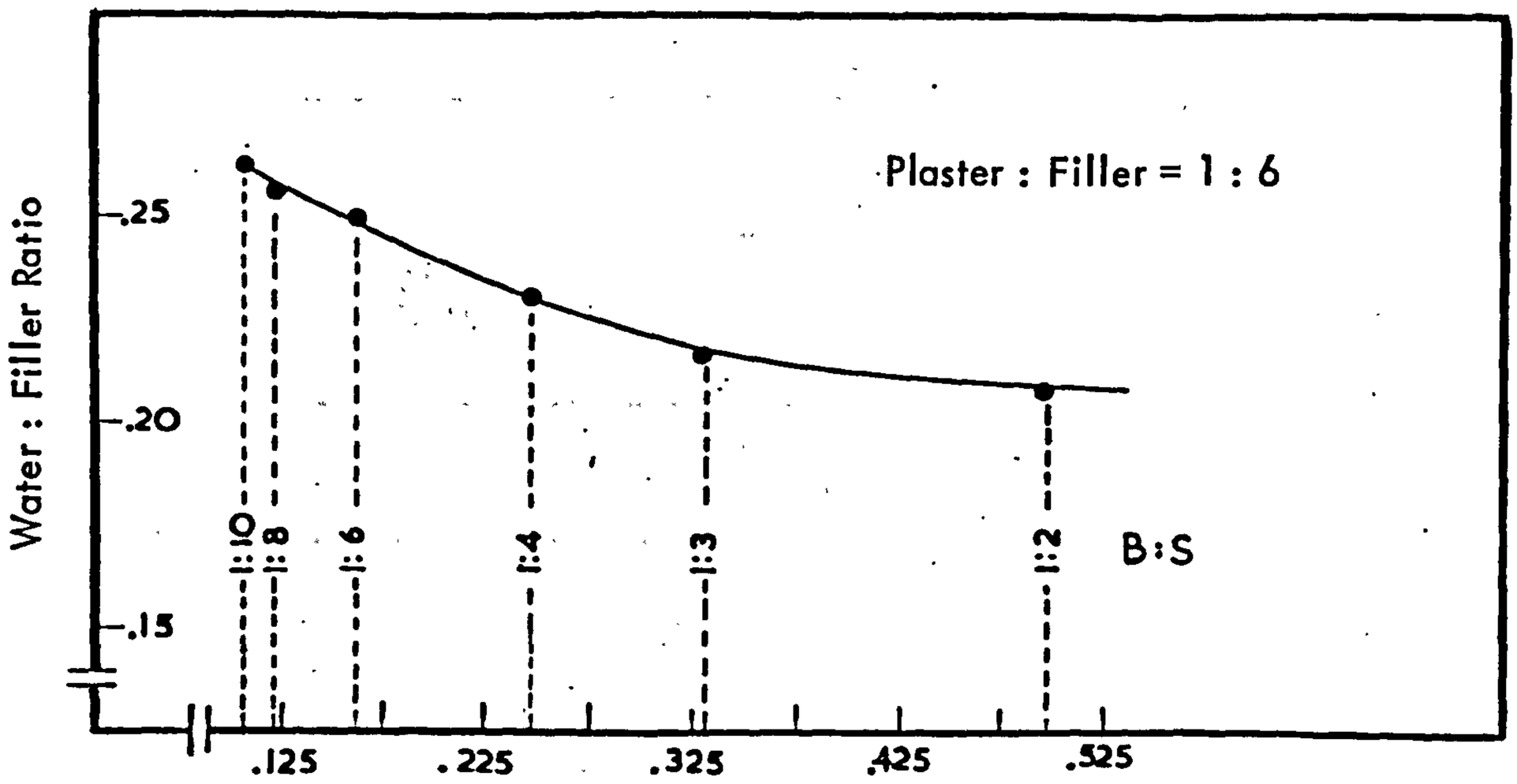

FIGURE 6 The water requirements of silver sand mixes with increasing barytes content.

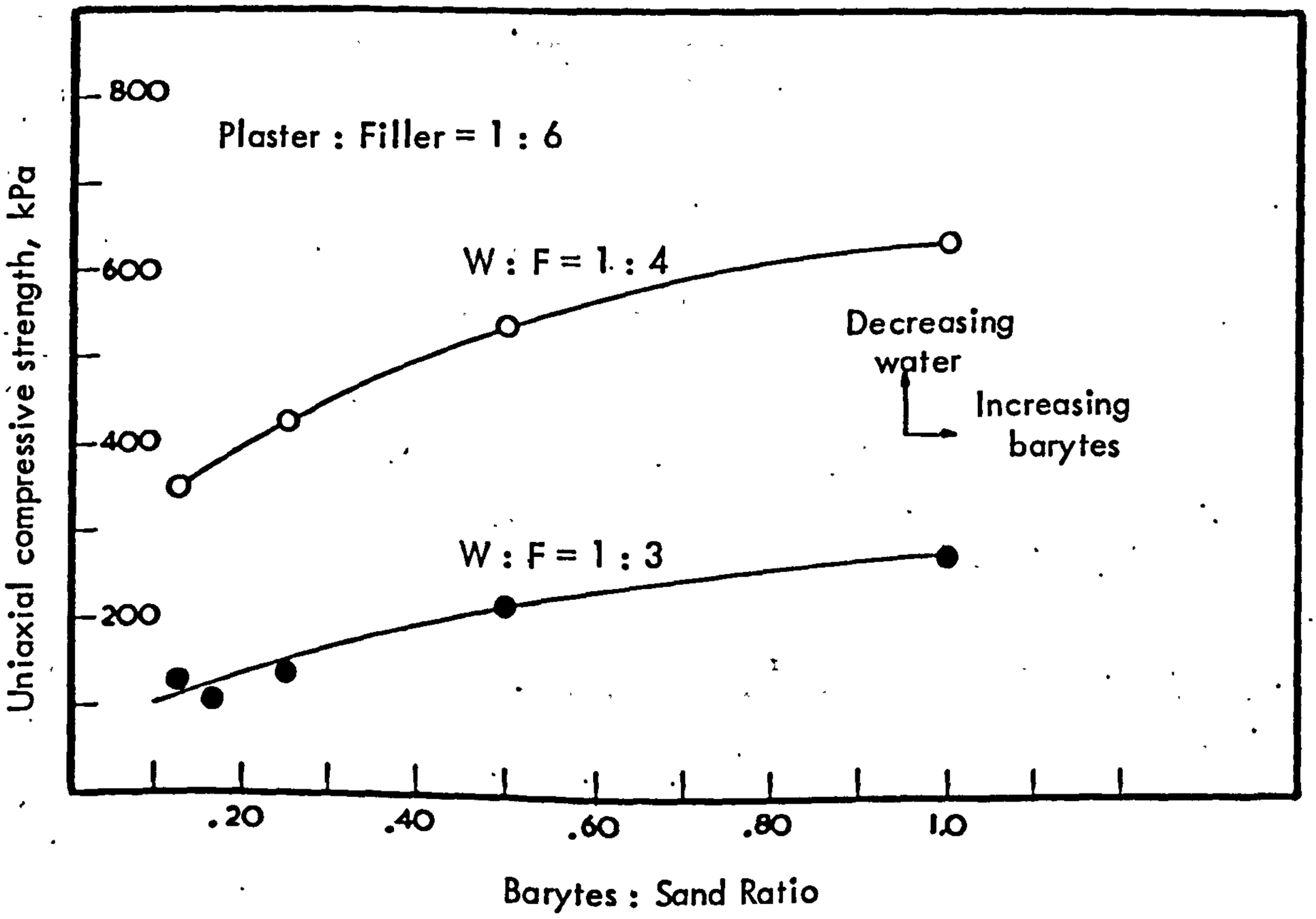

FIGURE 7 The effect of different barytes and water contents on the uniaxial compressive strength of sand-plaster-water mixes.

TABLE 5

Different B:S proportions combined with constant amounts of plaster and water

Mix	Components (grms)				Proportions			ρ grm/cm^3	Strength properties				$\frac{\sigma_c}{T_{500}}$	Axial deformation at failure % ϵ_f
	S	B	PP	W	B:S	P:F	W:F		No. of spec.	σ_c kPa	No.	T_{500} kPa		
F1	560	70	105	210	1:8	1:6	1:3	1.59	8	128.33	10	22.61	5.7	1.12
F2	540	90	105	210	1:6			1.59	9	120.39	8	23.83	5.05	1.10
F3	480	120	100	200	1:4	"	"	1.63	7	130.16	9	25.48	5.0	1.03
F4	400	200	100	200	1:2			1.65	6	217.04	8	28.93	7.5	0.90
F5	300	300	100	200	1:1			1.70	8	239.85	6	39.75	6.0	0.87

F = (B+S)

The densities, strain at failure and σ_c/T_{500} ratios of the two materials are given below.

Mix proportions → PLASTER : FILLER = 1:6	W:F = 1:3			W:F = 1:4		
↓	ρ(g/cm^3)	% ε_f	σ_c/T_{500}	(g/cm^3)	% ε_f	σ_c/T_{500}
B:S = 1:8	1.59	1.12	5.7	1.76	0.95	4.2
= 1:4	1.63	1.33	5.0	1.79	0.95	4.85
= 1:2	1.65	1.10	7.5	1.84	0.90	5.30
= 1:1	1.70	1.02	6.0	1.91	0.87	4.55

The last results showed that a smaller amount of water resulted in higher densities and lower deformation at failure. However the σ_c/T_{500} ratio appeared to decrease with decreasing water content. A similar trend was observed in the case of the sand/plaster mixes described in section a.3.

The water-to-filler proportion of 1:4 was used for a new set of mixes with different B:S and P:(B+S) ratios, which were tested to enable choice of the most promising combination for further development.

A total of sixteen mixtures were prepared by using four B:S ratios each combined with four different plaster quantities. The test results are given in Table 6.

The material with B:S proportion of 1:2 seemed to be of relatively better quality than the other three, especially with regard to deformability. The σ_c/T_{500} ratio continued to remain low (around 5) for all mixes.

Evidently the inclusion of barytes resulted in an overall improvement of the performance of the sand/plaster/water mixes. However further investigation was required to increase the brittleness of the materials to levels approaching the set specifications.

Parallel to the development of mixtures with barytes, the potential use of two other fillers was studied, namely Kaolinite and Alumina.

As reported in section 1 of this appendix, use of clay has been found to increase the brittleness of model materials.

TABLE 6

Properties of materials with different barytes and plaster contents

Mix	Components (grms)				Proportions			ρ	Strength properties, kPa				$\frac{\sigma_c}{T_{500}}$	Deformation properties			
	S	B	W	PP	B:S	P:F	W:F	gr/cm³	No. of spec.	σ_c	No.	T_{500}		$\%\varepsilon_f$	σ_c kPa	$E_{T50\%}$ MPa	$\frac{E_T}{\sigma_c}$
F10	560	70	157.5	157.5	1:8	1:4	1:4	1.75	6	828.40	5	144.24	4.74	0.88	828	189	228
F11				126	1:8	1:5	1:4	1.74	6	460.92	4	85.17	5.41	0.98	474	91	192
F6				105	1:8	1:6	1:4	1.76	6	334.33	7	78.84	4.24	0.95	302	50	166
F12				90	1:8	1:7	1:4	1.73	7	223.52	7	46.28	4.83	0.99	238	38	160
F13	480	120	150	150	1:4	1:4	1:4	1.81	6	935.10	7	169.74	5.51	1.08	988	109	110
F14				120	1:4	1:5	1:4	1.81	6	537.16	4	129.1	4.16	0.98	525	68	130
F7				100	1:4	1:6	1:4	1.79	8	425.72	4	86.98	4.85	0.95	417	86	207
F15				85.7	1:4	1:7	1:4	1.78	8	284.60	2	55.7	5.11	0.95	282	54	191
F16	400	200	150	150	1:2	1:4	1:4	1.86	6	1112.53	3	194.3	5.73	0.79	1148	294	256
F17				120	1:2	1:5	1:4	1.87	7	663.51	6	124.42	5.33	0.85	610	159	261
F8				100	1:2	1:6	1:4	1.84	7	537.95	5	101.91	5.28	0.90	614	174	283
F18				85.7	1:2	1:7	1:4	1.84	6	346.48	4	66.44	5.21	0.87	303	86	285

(Cont.)

TABLE 6 (Cont.)

Mix	Component (grms)				Proportions			ρ	Strength properties, kPa				$\frac{\sigma_c}{T_{500}}$	Deformation properties			
	S	B	W	PP	B:S	P:F	W:F	gr/cm^3	No. of spec.	σ_c	No.	T_{500}		% ϵ_f	σ_c kPa	$E_{T50\%}$ MPa	$\frac{E_T}{\sigma_c}$
F19	300	300	150	150	1:1	1:4	1:4	1.92	5	1141.07	5	238.31	4.79	1.28	1052	153	145
F20				120	1:1	1:5	1:4	1.91	6	862.97	6	159.97	5.39	0.92	850	164	193
F9				100	1:1	1:6	1:4	1.91	7	638.35	6	140.17	4.55	0.87	651	217	334
F21				85.7	1:1	1:7	1:4	1.91	7	437.70	4	80.8	5.42	0.92	418	58	139

However, attempts to use Kaolinite as a filler proved unsuccessful. The main problem was the very high water requirements of the mixtures. A combination of Kaolinite:Sand of 1:8 and plaster:filler of 1:5.25 required a water:filler proportion of 1:3 for the mix to be workable. That material showed considerable compressive strength (777 kPa) which was higher than that of proportionally similar mixes of sand/barytes. The hydrogen bonding in the clay substance was presumably the reason for that strength.
High axial strain (0.98%) was recorded at the moment of failure, and the $\sigma c/T_{500}$ ratio was 5.2.

Combinations of different quantities of alumina with sand gave more promising results. Four mixes were prepared with A:S ratios of 1:1, 1:2, 1:4 and 1:8. The same plaster quantity was used in all cases in a proportion P:(A+S) = 1:5. Although the mixtures needed a considerable amount of water they showed an interesting behaviour.
The test results are presented in Table 7. The amount of water added to each combination was sufficient for saturation of the components in a workable mix.

The high water content of the mixes resulted in low densities (ρ). The materials with high alumina content were very deformable (ε_f = .9%) but the other two (FA3 and FA4) which required less water showed strains at failure of 0.6 and 0.74%. The other interesting feature was the relatively higher $\sigma c/T_{500}$ ratios (6.6 and 7.1). Repeat tests on the latter two materials confirmed the results.

At that stage it was decided to investigate the combined effect of alumina and barytes upon the sand:plaster:water system.

TABLE 7

Properties of materials with different alumina contents

Mix	Components (gr)			Proportions			ρ gr/cm^3	Strength properties (kPa)				$\frac{\sigma_c}{T_{500}}$	Deformation properties		
	S	A	W	A:S	W:F	PP:F		No. of spec.	σ_c	No. of spec.	T_{500}		ε_f %	$E_{T_{50}}$	E_T/σ_c
FA1	300	300	290	1:1	1:2.1	1:5	1.4	7	450.44	6	94.74	4.75	0.90	144	324
FA2	400	200	250	1:2	1:2.4	1:5	1.49	8	391.39	5	73.4	5.3	0.88	94	225
FA3	480	120	200	1:4	1:3	1:5	1.57	8	378.36	4	57.42	6.6	0.60	88	232
FA4	560	120	200	1:8	1:3	1:5	1.59	8	325.57	4	45.65	7.1	0.74	66	212

(b.2) Properties of mixes with combined fillers

A number of combinations between the various components was tried in order to achieve an optimum proportion of S:(B+A) with the minimum water requirements. The one that was finally chosen consisted of sand combined with the filler (75% B, 25% A) in a proportion of 2 to 1. The optimum amount of water was in a proportion of 1W to 4(S+B+A).

The test results on specimens prepared from the last material with various plaster quantities are presented in Table 8. All specimens were cured for 24 hours at room temperature and for 36 hours at 85°C.

The behaviour of that material was found to fulfil the various specifications to an acceptable degree. Its strength was of course lower than that required, but much higher σ_c values could be obtained by adopting a different curing temperature. Earlier tests on Sand/Barytes mixes revealed a ten-fold difference in strength between the materials cured at room temperature and at 85°C (2.86 MPa and 0.292 MPa respectively). The curing temperature chosen for the final material was 50°-55°C.

An extensive experimental programme was undertaken to establish the design curve of the material and to test its reproducibility. The details on the properties of the final model material are discussed in Chapter 2.2

The following Tables 9 and 10 summarise the experimental results from the final material and will be referred to in the relevant context in Chapter 2.2

TABLE 8

Properties of material with Barytes and Alumina combined

Proportions: S:(B+A) = 2:1

B:A = 3:1

W:(S+B+A) = 1:4

PP:(S+B+A) = 1:7.5 (1), 1:8.6 (2), 1:10 (3), 1:12 (4), 1:15 (5), 1:20 (6)

Numbers in brackets are the mix type in Table .

Mix type	Components (grms) S	B	A	W	PP	Density ρ gr/cm^3	Compressive strength No.	σ_c (kPa)	Point load strength (kPa) Axial No.	T_{500}	Diametral No.	T_o	$\frac{\sigma_c}{T_{500}}$	$\frac{\sigma_c}{T_o}$	Strain at failure % ε_f
1	400	150	50	150	80	1.80	6	486.8	5	58.5	5	60.9	6.2	8.0	0.42
2					70	1.79	6	363.7	4	60.8	4	53.6	6.0	6.8	0.39
3					60	1.82	6	269.0	5	45.0	6	40.0	6.0	6.7	0.43
4					50	1.78	5	196.8	6	29.5	5	28.5	7.3	6.9	0.45
5					40	1.77	5	136.0	3	20.6	4	19.1	6.6	7.3	0.40
6					20	1.79	5	103.8	4	15.40	4	14.8	6.7	7.0	0.50

TABLE 9

Experimental results from uniaxial compression tests on final model material

Plaster of Paris : 85gr		80 gr		75 gr		70 gr		65 gr		62.2 gr		55 gr		50 gr		40 gr	
spec.no	σ_c (MPa)																
1	3.523	1	3.220	1	2.812	1	2.509	1	2.216	1	2.093	1	1.221	1	1.221	1	.678
2	2.750	2	2.860	2	2.788	2	2.651	2	1.894	2	2.122	2	1.307	2	1.240	2	.716
3	3.220	3	3.305	3	2.708	3	2.803	3	2.216	3	1.960	3	1.174	3	1.115	3	.847
4	3.372	4	2.973	4	2.651	4	2.571	4	2.112	4	1.951	4	1.222	4	1.383	4	.758
5	3.258	5	3.371	5	2.754	5	2.494			5	2.084	5	1.278	5	1.322	5	.811
										6	2.093	6	1.392	6	1.221	6	.744
										7	2.059			7	1.306	7	.695
										8	2.084			8	1.200	8	.720
										9	1.951					9	.758
										10	1.895						
$\bar{\sigma}_c$ = 3.425 MPa		$\bar{\sigma}_c$ = 3.146 MPa		$\bar{\sigma}_c$ = 2.743 MPa		$\bar{\sigma}_c$ = 2.606 MPa		$\bar{\sigma}_c$ = 2.110 MPa		$\bar{\sigma}_c$ = 2.030 MPa		$\bar{\sigma}_c$ = 1.266MPa		$\bar{\sigma}_c$ = 1.251		$\bar{\sigma}_c$ = .747	
S = .2168		S = .2197		S = .0643		S = .1262		S = .1518		S = .0807		S = .0774		S = .0832		S = .0542	
V = 6.33%		V = 6.985%		V = 2.345%		V = 4.843%		V = 7.194%		V = 3.976%		V = 6.117%		V = 6.65%		V = 7.256%	
6	3.428	6	2.973	6	2.547	6	2.387	5	1.898			7	1.397				
7	3.248	7	3.125	7	2.860	7	2.235	6	2.178			8	1.300				
8	3.427	8	2.992	8	2.879	8	2.216	7	1.960			9	1.458				
9	3.182	9	2.964	9	2.784	9	2.329	8	1.989			10	1.411				
10	3.300	10	2.955	10	2.784	10	2.356	9	1.894			11	1.312				
$\bar{\sigma}_c$ = 3.317 MPa		$\bar{\sigma}_c$ = 3.002 MPa		$\bar{\sigma}_c$ = 2.771 MPa		$\bar{\sigma}_c$ = 2.305 MPa		$\bar{\sigma}_c$ = 1.987 MPa				$\bar{\sigma}_c$ = 1.376 MPa					
S = .1093		S = .0702		S = .1322		S = .0755		S = .1159				S = .0678					
V = 3.295%		V = 2.339%		V = 4.770%		V = 3.277%		V = 5.841%				V = 4.93%					

(Cont.)

TABLE 9 (Cont.)

85 gr	80 gr	75 gr	70 gr	65 gr	62.2 gr	55 gr	50 gr	40 gr
11 3.5649	11 3.1347							
12 3.4948	12 3.1063							
13 3.5459	13 3.004							
14 3.6747	14 3.1821							
15 3.5990	15 3.3715							
16 3.6937	16 3.2579							
$\bar{\sigma}_c$=3.595 MPa	17 3.3904							
S = .0767	$\bar{\sigma}_c$=3.207 MPa							
V = 2.135%	S = .1417							
	V = 4.419%							

Quantities of components

Sand = 400 grms

Barytes = 150 grms

Alumina = 50 grms

Water = 150 cm^3

$\bar{\sigma}_c$ = average compressive strength

S = standard deviation

V = coeff. of variation

Average of all tests

$\bar{\sigma}_c$=3.455 MPa	$\bar{\sigma}_c$=3.129 MPa	$\bar{\sigma}_c$=2.757 MPa	$\bar{\sigma}_c$ = 2.456 MPa	$\bar{\sigma}_c$ = 2.05 MPa	$\bar{\sigma}_c$ = 2.030 MPa	$\bar{\sigma}_c$=1.316 MPa	$\bar{\sigma}_c$=1.251MPa	$\bar{\sigma}_c$= .747MPa
S= .1794	S= .1691	S= .0991	S = .1866	S = .1405	S = .0807	S = .0901	S = .0832	S = .0542
V=5.192%	V=5.403%	V=3.595%	V = 7.598%	V = 6.887%	V = 3.976%	V = 6.849%	V = 6.65%	V = 7.256%

TABLE 10

Experimental results on indirect tensile strength of final model material

Plaster quantity ⟶ 85 (grms)	80	75	70	65	55
AXIAL POINT LOADING (T_{500})					
1 .606	1 .584	1 .498	1 .459	1 .328	1 .286
2 .582	2 .549	2 .518	2 .481	2 .343	2 .308
3 .639	3 .574	3 .503	3 .447	3 .362	3 .270
4 .600	4 .508	4 .489	4 .456	4 .312	4 .260
5 .635	5 .553	5 .480	5 .421	5 .366	5 .279
6 .613	6 .455	6 .455	6 .431	6 .384	6 .304
	7 .575	7 .474	7 .459		
T_{500} = 0.612MPa	T_{500} = .573MPa	T_{500} = .488 MPa	T_{500} = .450 MPa	T_{500} = .349 MPa	T_{500} = .284 MPa
S = 0.0216	S = 0.0197	S = 0.0207	S = 0.0199	S = 0.0266	S = 0.0188
%V = 3.5	%V = 3.4	%V = 4.2	%V = 4.4	%V = 7.6	%V = 6.6

(Cont.)

TABLE 10 (Cont.)

85	80	75	70	65	50	40
DOUBLE POINT. Tdp (DIAMETRAL)						
1 .569	1 .521	1 .472	1 .454	1 .344	1 .176	1 .089
2 .551	2 .499	2 .503	2 .405	2 .339	2 .191	2 .107
3 .567	3 .517	3 .436	3 .402	3 .341	3 .194	3 .113
4 .567	4 .506	4 .557	4 .409	4 .377	4 .173	4 .110
5 .578	5 .499	5 .476	5 .435	5 .409	5 .189	5 .098
6 .562	6 .424	6 .470	6 .391	6 .417	6 .183	6 .104
	7 .447		7 .424		7 .186	
			8 .432		8 .179	
			9 .421			
T_{dp} = .566MPa S = .0089 σ_c/T_{dp} = 6.1	T_{dp} = .488MPa S = .0371 σ_c/T_{dp} = 6.4	T_{dp} = .469MPa S = .0221 σ_c/T_{dp} = 5.9	T_{dp} = .419MPa S = .0195 σ_c/T_{dp} = 5.9	T_{dp} = .371MPa S = .0353 σ_c/T_{dp} = 5.5	T_{dp} = .184MPa S = .00745 σ_c/T_{dp} = 6.8	T_{dp} = .103MPa S = .0088 σ_c/T_{dp} = 7.2
BRAZILIAN (DISC) TEST, σ_{tb}						
1 .461	1 .420	1 .429	1 .332	1 .239		1 .131
2 .515	2 .446	2 .390	2 .367	2 .285		2 .137
3 .458	3 .374	3 .470	3 .362	3 .287		3 .119
4 .659	4 .422	4 .339	4 .354	4 .287		4 .116
5 .517	5 .419	5 .389	5 .306	5 .347		5 .133

(Cont.)

TABLE 10 (Cont.)

85	80	75	70	65	50	40
6 .419	6 .370		6 .379	6 .299		
7 .527	7 .470		7 .375	7 .257		
8 .427	8 .427			8 .334		
9 .504				9 .257		
10 .401						
11 .439						
12 .519						
σ_{tb} = .473MPa	σ_{tb} = .421MPa	σ_{tb} = .403MPa	σ_{tb} = .353MPa	σ_{tb} = .288MPa		σ_{tb} = .127MPa
S = .0418	S = .0298	S = .04905	S = .0261	S = .0354		S = .0092
σ_c/σ_{tb} = 7.3	σ_c/σ_{tb} = 7.4	σ_c/σ_{tb} = 6.8	σ_c/σ_{tb} = 7	σ_c/σ_{tb} = 7.1		σ_c/σ_{tb} = 5.9

APPENDIX II

Tables 11 to 21 containing the cumulative mean direct shear test results from model joints (see p.141).

Symbols:

L = length of individual joint blocks

d_h = shear displacement

τ = cumulative mean shear stress at corresponding d_h

d_v = cumulative mean vertical displacement at d_h.

TABLE 11

MODEL No. 1

L = 6 cm			L = 12 cm			L = 18 cm			L = 36 cm		
d_h (mm)	τ (kPa)	d_v (mm x 10^{-2})	d_h (mm)	τ (kPa)	d_v (mm x 10^{-2})	d_h (mm)	τ (kPa)	d_v (mm x 10^{-2})	d_h (mm)	τ (kPa)	d_v (mm x 10^{-2})
.24	40.7	0.0	.22	31.3	-0.2	.25	24.0	-2.0	0.20	13.0	-2.0
.40	50.1	2.0	.44	46.3	1.8	.45	31.0	-3.0	0.35	16.8	-2.0
.58	55.3	4.4	.60	50.3	4.0	.60	35.5	-1.0	0.50	18.4	-2.0
.67*	56.4	8.0	.80	52.1	8.8	.70	38.8	+0.5	0.60	18.5	-2.0
.77	56.2	12.0	.86*	52.6	10.5	.90	40.1	5.0	0.75	19.9	-1.5
.98	56.0	19.0	.97	52.4	14.6	1.10	41.5	9.0	1.00	23.8	-0.5
1.20	54.9	23.5	1.20	52.1	21.0	1.20*	41.8	11.0	1.20	26.0	0.0
1.60	49.1	33.0	1.60	50.3	31.0	1.50	39.7	18.4	1.50	28.1	2.0
2.20	44.8	44.0	2.20	47.4	50.2	2.10	38.8	32.0	1.80	32.2	4.0
2.60	43.2	50.0	2.60	46.1	56.0	2.50	38.7	41.1	2.30	35.1	9.5
3.20	42.6	58.0	3.20	44.2	67.5	3.20	38.1	55.0	2.70*	36.2	17.5
3.80	42.2	63.0	3.80	42.0	76.0	3.70	36.2	61.0	3.00	35.9	26.0
4.80	40.0	72.0	4.5	43.0	91.0	4.70	35.4	78.0	3.60	35.8	38.0
			5.0	41.7	101.0	5.70	34.6	94.0	4.60	35.6	58.0
			5.5	41.1	106.0	6.50	34.7	101.0	5.50	34.6	74.0
									6.50	34.0	88.0

TABLE 12

MODEL No. 2

L = 6 cm			L = 12 cm			L = 18 cm			L = 36 cm		
d_h (mm)	τ (kPa)	d_v (mm x 10^{-2})	d_h (mm)	τ (kPa)	d_v (mm x 10^{-2})	d_h (mm)	τ (kPa)	d_v (mm x 10^{-2})	d_h (mm)	τ (kPa)	d_v (mm x 10^{-2})
0.24	40.8	0.0	0.23	16.8	-0.5	0.20	15.9	-1.0	0.12	8.8	0.0
0.42	46.2	4.4	0.40	24.5	-0.5	0.37	20.0	+0.5	0.28	16.7	-1.5
0.51	47.8	6.2	0.50	26.8	-0.2	0.50	25.6	1.0	0.50	20.0	-1.5
0.71	50.2	12.0	0.72	32.5	0.0	0.70	27.0	4.0	0.70	23.0	-0.5
0.80*	50.5	14.2	0.86	35.9	2.2	0.90	29.3	8.0	0.85	24.0	0.0
1.00	50.3	19.0	1.10	38.2	7.0	1.15	32.6	12.0	1.00	26.0	+0.5
1.30	49.3	27.0	1.25*	39.1	10.5	1.30	33.2	14.2	1.35	29.0	2.0
1.80	47.4	37.0	1.65	38.1	19.0	1.80	34.2	20.5	1.80	30.5	5.5
2.20	45.1	45.0	2.00	37.3	26.5	1.82*	34.4	24.5	2.00	31.3	6.0
2.80	43.9	57.0	2.80	35.3	40.0	2.20	34.1	31.0	2.20*	31.3	8.5
3.30	41.9	65.0	3.30	33.6	49.0	2.60	33.7	38.0	2.55	31.0	15.0
4.00	39.5	78.0	4.00	32.1	67.0	3.50	33.6	50.0	3.40	30.2	31.0
4.90	38.5	95.0	4.80	31.3	83.0	4.0	33.5	59.0	4.0	29.8	41.0
			5.80	30.1	99.5	4.5	31.9	66.0	4.8	29.1	55.0
						5.5	32.0	78.0	5.8	29.0	64.0
						6.0	31.0	82.5			

TABLE 13

MODEL No. 3

L = 6 cm			L = 12 cm			L = 18 cm			L = 36 cm		
d_h (mm)	τ (kPa)	d_v (mm x 10^{-2})	d_h (mm)	τ (kPa)	d_v (mm x 10^{-2})	d_h (mm)	τ (kPa)	d_v (mm x 10^{-2})	d_h (mm)	τ (kPa)	d_v (mm x 10^{-2})
0.20	28.7	-0.2	0.22	17.2	-1.4	0.20	16.5	-0.4	0.25	12.7	-0.5
0.38	35.8	+1.0	0.41	18.9	-1.0	0.40	21.0	+0.2	0.40	15.1	-0.5
0.47	39.1	2.0	0.73	26.4	+3.0	0.65	25.5	0.5	0.54	16.6	-0.5
0.70	44.1	5.5	0.90	29.2	4.5	1.00	26.6	3.0	0.74	16.9	-0.5
1.00	48.9	11.0	1.30	33.2	10.0	1.40	30.3	10.9	1.10	19.0	0.0
1.23	49.8	13.0	1.50	34.8	13.0	1.80	32.4	18.0	1.40	21.2	+0.5
1.45	51.1	17.5	1.70	36.6	16.0	2.20	33.1	23.9	1.60	22.0	1.0
1.55*	51.5	20.0	1.90*	37.8	18.8	2.60	33.9	29.5	2.00	22.7	2.0
1.70	50.6	24.5	2.30	36.8	27.0	2.80*	34.3	35.7	2.30	24.0	3.0
2.00	49.5	31.0	2.80	36.0	30.8	3.20	34.0	42.5	2.9	25.5	8.0
2.4	47.9	40.0	3.30	35.1	38.3	4.00	32.9	49.0	3.3	26.5	12.0
2.8	46.4	47.5	3.80	33.6	45.4	5.00	32.3	64.0	3.5*	27.0	16.0
3.4	45.2	55.5	4.80	35.0	60.0	6.00	32.5	76.0	4.0	27.3	24.0
3.8	44.6	62.5	5.80	32.3	72.5	7.00	32.0	85.5	4.8	28.2	38.0
4.8	43.5	71.0	6.80	32.3	77.0				5.2	28.5	43.5
									6.2	29.4	56.0
									8.2	29.9	82.0

TABLE 14

MODEL No. 4

L = 6 cm			L = 12 cm			L = 18 cm			L = 36cm		
d_h (mm)	τ (kPa)	d_v (mm x 10^{-2})	d_h (mm)	τ (kPa)	d_v (mm x 10^{-2})	d_h (mm)	τ (kPa)	d_v (mm x 10^{-2})	d_h (mm)	τ (kPa)	d_v (mm x 10^{-2})
0.13	21.2	-0.2	0.10	13.5	0.0	0.16	15.0	0.0	0.10	10.0	0.0
0.30	15.8	-0.4	0.20	20.6	-0.7	0.40	22.7	-0.6	0.15	12.6	0.0
0.49	33.5	12.4	0.52	29.2	+0.6	0.65	27.0	+1.0	0.25	14.0	-0.5
0.87	39.2	9.6	0.87	34.0	3.5	0.80	30.4	3.8	0.40	17.5	-0.5
1.10	41.0	12.1	1.25	36.2	8.0	1.20	32.9	11.2	0.65	20.4	-1.0
1.26*	42.0	15.5	1.45*	37.5	11.0	1.60*	33.5	17.8	0.90	21.5	-1.0
1.66	41.5	22.9	1.68	36.6	15.0	1.80	33.3	20.0	1.40	23.9	0.0
1.86	41.6	26.5	2.00	37.3	19.0	2.00	33.5	25.4	1.80	24.7	2.5
2.10	41.7	30.2	2.45	36.6	25.5	2.40	33.5	30.0	2.20*	25.7	4.5
2.70	40.0	38.0	3.15	37.4	33.5	2.80	33.2	36.5	2.45	25.2	7.5
2.90	39.5	40.0	3.6	36.0	42.5	3.50	32.7	46.0	3.00	26.0	14.0
3.40	38.6	44.5	4.2	34.3	49.8	4.00	32.2	54.0	3.80	26.3	21.0
3.90	37.6	46.5	5.2	34.1	63.0	5.00	31.7	66.5	4.50	26.6	24.5
4.40	37.2	52.0	6.00	33.2	71.5	6.00	31.2	77.5	5.00	27.5	29.0
4.80	36.3	54.0				7.00	31.0	85.0	6.00	28.2	39.0
						7.90	31.3		7.00	29.0	43.5
									8.00	29.0	51.0
									9.00	29.2	58.0

TABLE 15

MODEL No. 5

L = 6 cm		
d_h (mm)	τ (kPa)	d_v (mm x 10^{-2})
0.13	21.0	0.0
0.31	24.4	+0.2
0.60	32.4	2.1
0.90	37.2	4.6
1.10	38.9	5.6
1.30*	39.9	7.0
1.50	39.7	8.2
1.90	40.2	12.4
2.30	39.7	16.5
2.70	40.4	19.9
3.50	38.8	27.9
4.00	38.1	31.0
4.50	36.0	32.0
5.00	35.1	36.0

L = 12 cm		
d_h (mm)	τ (kPa)	d_v (mm x 10^{-2})
0.10	18.1	0.5
0.25	29.0	1.3
0.60	31.1	4.3
0.80	34.6	6.9
1.20	39.3	14.3
1.35	39.6	15.9
1.65	40.4	21.5
2.00*	41.0	27.2
2.20	40.9	30.0
2.60	40.5	38.7
3.60	39.2	48.0
4.30	38.6	54.0
4.80	38.4	58.3
5.80	37.0	67.0
6.80	37.0	76.5

L = 18 cm		
d_h (mm)	τ (kPa)	d_v (mm x 10^{-2})
0.18	18.0	0.0
0.28	20.0	0.0
0.40	22.6	1.0
0.80	26.4	5.1
0.98	28.5	7.2
1.40	30.4	12.8
1.80*	32.3	19.0
2.00	31.1	25.1
2.40	30.8	28.0
3.00	30.4	36.6
3.40	30.2	42.0
4.00	30.0	49.5
4.80	30.0	57.7
5.80	30.0	60.4
6.80	30.2	63.5
7.80	30.0	66.0

L = 36 cm		
d_h (mm)	τ (kPa)	d_v (mm x 10^{-2})
0.22	10.0	0.0
0.35	13.5	0.0
0.46	15.0	1.0
0.87	19.7	3.8
1.20	22.6	7.5
1.70	25.0	13.0
2.10	27.2	18.0
2.30	27.6	20.5
2.90*	29.0	24.0
3.00	29.2	29.0
3.70	29.1	36.0
4.70	28.9	44.0
5.70	28.5	48.5
6.7	28.5	52.0

TABLE 16

MODEL No. 6

L = 6 cm			L = 12 cm			L = 18 cm			L = 36 cm		
d_h (mm)	τ (kPa)	d_v (mm x 10^{-2})	d_h (mm)	τ (kPa)	d_v (mm x 10^{-2})	d_h (mm)	τ (kPa)	d_v (mm x 10^{-2})	d_h (mm)	τ (kPa)	d_v (mm x 10^{-2})
0.18	27.4	0.4	0.15	14.8	0.0	0.12	9.4	0	0.10	8.1	0.0
0.34	37.4	2.0	0.30	24.3	1.2	0.40	21.4	-1.0	0.25	12.5	-0.5
0.52	43.0	6.5	0.51	30.6	3.3	0.58	26.6	0.0	0.50	15.3	0.0
0.62*	43.7	8.8	0.72	33.5	6.7	0.75	28.3	2.0	0.65	17.7	0.2
1.00	41.6	16.5	0.82*	34.5	9.0	0.90*	29.5	3.1	0.90	20.3	0.5
1.40	38.0	23.8	1.00	34.2	12.2	1.30	26.7	8.9	1.30	21.5	1.0
2.00	34.6	31.0	1.60	31.4	19.4	1.70	25.7	12.0	1.80*	23.3	3.0
2.40	33.1	35.0	2.20	29.9	26.1	2.20	26.3	17.0	2.30	23.4	7.5
2.80	32.0	38.5	3.00	27.9	32.2	3.00	25.6	23.0	3.00	23.0	15.0
3.40	31.1	42.0	3.80	27.1	36.8	3.40	25.4	25.5	3.80	22.8	24.2
3.80	30.5	44.0	4.80	26.3	42.0	3.80	25.5	29.0	4.20	23.0	27.0
4.20	30.0	45.8	5.80	26.1	46.5	4.50	26.0	35.0	5.00	22.5	32.0
4.80	29.0	48.0	6.40	26.0	48.0	5.50	24.5	38.2	6.00	22.3	37.5
						6.50	23.8	40.0	7.00	22.4	41.0

TABLE 17

MODEL No. 7

L = 5 cm			L = 10 cm			L = 20 cm			L = 40 cm		
d_h (mm)	τ (kPa)	d_v (mm x 10^{-2})	d_h (mm)	τ (kPa)	d_v (mm x 10^{-2})	d_h (mm)	τ (kPa)	d_v (mm x 10^{-2})	d_h (mm)	τ (kPa)	d_v (mm x 10^{-2})
0.13	28.7	0.0	0.10	19.6	-0.2	0.10	14.5	-0.9	0.08	10.2	0.0
0.30	44.5	0.10	0.25	31.1	+0.3	0.25	20.9	-1.0	0.15	12.7	-0.80
0.48	54.7	2.00	0.60	42.8	5.7	0.40	24.8	+0.2	0.40	14.4	-1.00
0.66*	58.7	5.00	0.80	43.9	9.7	0.80	29.0	5.3	0.60	17.0	+0.50
1.00	56.8	18.20	0.90	44.5	13.8	1.10	31.4	9.9	0.75	19.8	1.50
1.40	54.4	26.8	1.10*	44.7	16.7	1.35*	32.1	15.5	1.00	21.2	4.40
1.80	50.8	33.5	1.30	43.5	20.5	1.60	31.3	21.2	1.25	24.0	7.00
2.30	47.8	40.0	1.60	42.5	26.7	1.95	30.6	27.1	1.75	25.3	13.20
2.70	45.8	45.5	2.30	40.2	40.6	2.20	30.4	30.6	2.00*	25.7	17.00
3.10	44.2	51.0	3.20	37.7	52.5	2.60	30.3	37.2	2.50	26.0	23.80
3.70	42.2	59.5	4.30	36.4	65.5	3.00	30.1	43.2	3.00	25.7	30.40
4.40	41.8	67.0	5.30	34.9	76.2	3.80	29.7	53.8	3.80	25.6	40.50
4.90	40.9	73.0	5.80	34.8	82.8	4.80	29.5	61.5	4.80	25.3	50.00
						5.80	29.4	75.0	5.80	25.4	54.80
						6.80	29.4	71.0	6.80	25.3	59.30
									7.80	25.3	62.50
									8.80	25.3	65.00

TABLE 18

MODEL No. 8

L = 5 cm			L = 10 cm			L = 20 cm			L = 40 cm		
d_h (mm)	τ (kPa)	d_v (mm x 10^{-2})	d_h (mm)	τ (kPa)	d_v (mm x 10^{-2})	d_h (mm)	τ (kPa)	d_v (mm x 10^{-2})	d_h (mm)	τ (kPa)	d_v (mm x 10^{-2})
0.12	31.0	0.0	0.10	21.3	-0.2	0.10.	15.5	-0.5	0.20	12.0	-0.5
0.30	41.7	0.5	0.30	33.0	+1.3	0.30	24.8	-0.5	0.30	14.0	-0.5
0.40	43.4	1.2	0.50	39.5	2.8	0.50	27.8	+0.5	0.50	17.9	-0.5
0.60	47.4	4.0	0.80	45.0	6.3	0.80	31.1	3.8	0.70	20.7	0.0
0.80*	50.0	8.0	1.00*	46.0	8.4	1.00*	32.7	6.5	1.00	24.3	+3.0
1.00	48.8	12.5	1.30	45.4	13.0	1.20	31.9	9.5	1.30	24.7	6.0
1.20	47.9	17.0	1.60	44.4	17.5	1.60	31.4	16.0	1.70*	25.7	11.0
1.60	45.8	23.5	2.00	42.9	25.0	2.00	31.5	22.0	1.90	25.5	13.8
2.30	43.4	31.0	2.60	41.3	32.5	2.40	31.5	28.0	2.60	26.0	22.5
2.90	40.7	36.5	3.20	40.0	40.0	3.20	31.8	37.0	3.30	26.0	33.5
3.30	39.3	39.5	3.60	48.4	44.0	3.60	31.5	40.0	4.3	26.5	47.0
3.90	37.3	44.0	4.10	38.0	38.2	4.20	31.5	43.5	4.8	26.6	52.0
4.40	36.2	47.5	4.60	37.5	51.5	4.60	31.5	46.5	5.30	26.7	56.5
4.90	35.4	51.0	5.20	37.0	56.0	5.60	31.5	52.0	5.80	26.2	61.0
			5.80	35.5	58.1	6.60	31.0	57.5	6.30	26.7	63.0
									6.80	27.0	66.0

TABLE 19

MODEL No. 9

L = 6 cm			L = 12 cm			L = 20 cm			L = 40 cm		
d_h (mm)	τ (kPa)	d_v (mm x 10^{-2})	d_h (mm)	τ (kPa)	d_v (mm x 10^{-2})	d_h (mm)	τ (kPa)	d_v (mm x 10^{-2})	d_h (mm)	τ (kPa)	d_v (mm x 10^{-2})
0.12	24.9	0.0	0.22	18.9	-0.5	0.20	19.0	-0.5	0.20	10.2	-0.2
0.30	29.5	-0.5	0.40	20.5	-0.5	0.40	22.4	-1.0	0.50	16.6	-0.5
0.50	32.6	+0.5	0.55	25.7	0.0	0.60	24.3	+0.2	0.70	18.5	-0.2
0.90	35.4	4.1	0.90	29.8	2.5	1.00	26.1	2.5	0.90	22.1	-0.2
1.10*	35.8	6.5	1.10	30.3	3.50	1.20*	26.5	4.3	1.10	23.2	0.0
1.40	37.4	10.5	1.30*	31.1	5.0	1.40	26.5	6.1	1.40*	24.0	+0.5
1.90	37.8	14.4	1.70	30.9	9.7	1.80	26.4	8.5	1.80	23.8	+2.0
2.30	38.1	17.8	2.10	30.7	14.9	2.20	26.3	12.5	2.00	23.7	3.4
2.70	37.8	21.0	2.70	30.1	21.0	2.60	26.2	17.4	2.40	23.8	7.0
3.40	37.6	25.0	3.20	28.9	26.0	3.00	26.0	20.3	2.80	23.3	11.0
3.90	37.1	28.1	3.70	28.7	32.7	3.50	26.1	24.5	3.40	22.4	16.4
4.40	36.9	32.0	4.90	28.5	36.0	4.80	25.8	28.9	4.00	22.0	21.4
4.90	36.7	34.5	4.70	28.6	41.7	4.50	26.0	34.0	4.80	21.7	27.8
			5.70	28.6	47.5	5.50	25.5	41.5	5.60	21.4	35.9
						6.50	25.4	45.0	6.60	21.7	40.0
						7.50	25.0	46.5	7.60	21.7	45.0

TABLE 20

MODEL No. 10

L = 6 cm			L = 12 cm			L = 18 cm			L = 36 cm		
d_h (mm)	τ (kPa)	d_v (mm x 10^{-2})	d_h (mm)	τ (kPa)	d_v (mm x 10^{-2})	d_h (mm)	τ (kPa)	d_v (mm x 10^{-2})	d_h (mm)	τ (kPa)	d_v (mm x 10^{-2})
0.10	20.6	0.0	0.10	14.2	0.0	0.30	19.7	0.0	0.20	12.2	0.0
0.30	24.3	0.0	0.40	20.2	-0.05	0.50	21.0	-0.06	0.40	17.5	-0.05
0.70	26.8	+0.2	0.80	22.7	-0.05	0.90	22.6	0.00	0.70	19.8	-0.07
0.91*	27.2	+0.4	1.00	23.8	0.0	1.10	23.3	0.15	0.90	20.7	-0.05
1.10	27.3	1.2	1.40	25.4	0.8	1.30*	23.6	1.0	1.30*	21.0	0.00
1.30	27.9	2.1	1.60*	26.2	0.15	1.70	24.1	2.7	1.70	21.0	+0.06
1.50	28.1	3.0	1.90	27.2	3.10	2.10	24.4	4.8	2.40	21.0	2.2
1.90	28.1	4.7	2.30	27.7	5.5	2.50	24.7	6.8	3.00	21.3	4.5
2.30	28.0	7.2	2.75	28.0	8.8	2.90	24.5	8.5	3.40	21.4	6.4
2.70	27.8	10.0	3.20	28.6	10.5	3.40	24.1	10.5	4.00	21.5	9.0
3.40	27.5	13.4	3.70	28.9	13.5	4.40	24.1	14.2	4.60	21.2	12.0
4.40	27.5	16.8	4.70	28.6	18.0	5.40	24.0	17.5	5.60	20.6	16.5
4.90	27.0	18.0	5.70	28.0	22.0	6.40	24.0	19.5	6.60	20.6	21.8
									7.60	20.8	23.5

TABLE 21

MODEL No. 11

L = 6 cm			L = 12 cm			L = 18 cm			L = 36 cm		
d_h (mm)	τ (kPa)	d_v (mm x 10^{-2})	d_h (mm)	τ (kPa)	d_v (mm x 10^{-2})	d_h (mm)	τ (kPa)	d_v (mm x 10^{-2})	d_h (mm)	τ (kPa)	d_v (mm x 10^{-2})
0.20	12.5	0.2	0.20	11.7	0.2	0.15	9.0	0.0	0.10	7.0	0.0
0.35	14.9	0.5	0.45	16.5	0.6	0.30	11.2	0.0	0.25	11.6	-0.2
0.60	16.7	0.8	0.60	17.7	0.8	0.70	15.5	0.3	0.50	15.0	-0.4
0.90	21.0	1.5	1.00	17.8	2.0	1.10	18.0	0.5	0.90	18.2	0.0
1.10	21.9	2.3	1.20	20.2	2.4	1.30	19.5	0.8	1.30*	20.2	0.5
1.30	22.6	3.4	1.40	20.9	3.2	1.70	19.5	1.5	1.60	20.2	1.2
1.50	22.1	4.0	1.90	20.7	4.5	2.30	19.5	3.4	2.00	20.2	2.0
1.90	22.3	5.0	2.40	20.5	6.9	2.90	19.3	5.0	2.50	19.6	4.0
2.50	21.8	7.5	2.90	20.5	8.5	3.30	19.3	6.2	3.00	19.0	5.5
2.90	21.5	9.0	3.80	20.4	10.5	4.30	19.3	8.5	4.00	19.2	7.7
3.90	21.3	11.0	4.80	20.3	12.5	5.30	19.0	10.0	5.00	19.3	9.5
4.90	21.2	13.0	5.80	20.0	14.0	6.30	19.0	11.5	6.00	18.4	11.0

APPENDIX III

This appendix has been included as a supplement to Chapter 3.2 in part three. It contains additional information on the Schmidt hammer index testing method of rock surface hardness, on the preparation and compression testing of joint blocks and detailed notes on specimen preparation and shear testing of joints in a portable shear box.

1. Notes on Schmidt hammer testing of rock surfaces

The Schmidt hammer was originally designed by E. Schmidt for testing concrete. The hammer is a simple device recording the rebound of a spring loaded plunger after its impact with a surface. A longitudinal section of the instrument is shown in Figure III.1.

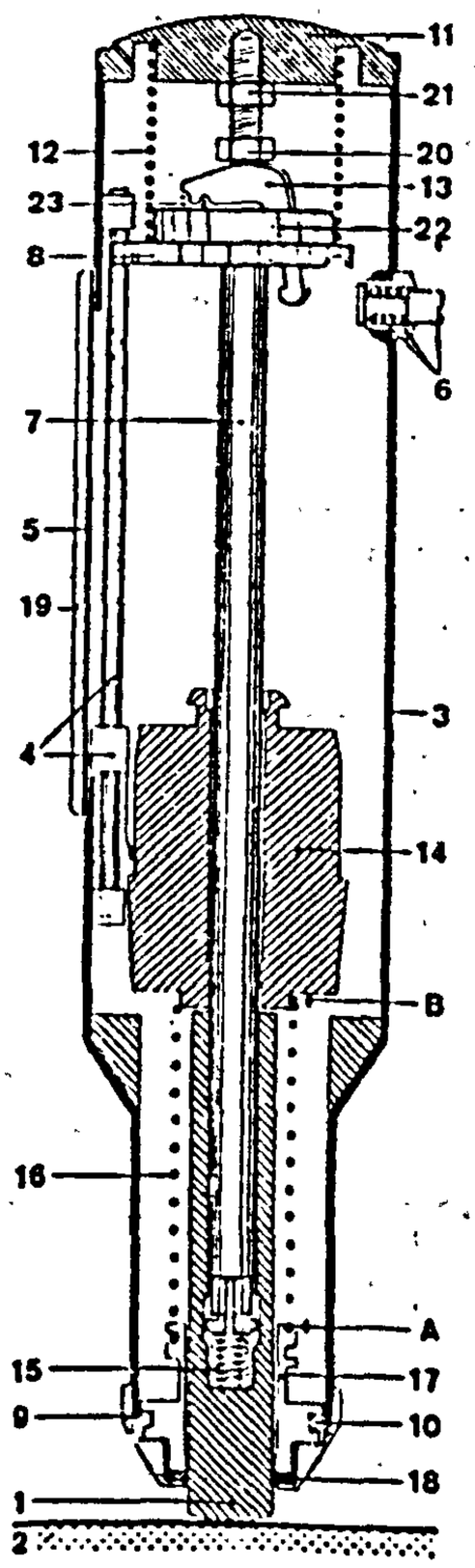

1 Impact plunger
2 Tested surface
3 Housing compl.
4 Rider with guide rod
5
6 Pushbutton compl.
7 Hammer guide bar
8 Disk
9 Cap
10 Two part ring
11 Rear cover
12 Compression
13 Pawl
14 Hammer mass
15 Retaining spring
16 Impact spring
17 Guide sleeve
18 Felt washer
19 Scale
20 Trip screw
21 Lock nut
22 Pin
23 Pawl spring

FIGURE III.1. Longitudinal section and description of components of a Schmidt hammer (from manufacturer's manual).

Briefly, under pressure the compression spring (12) at the top of the device contracts, while the impact spring (16) extends. Just before the plunger (1) disappears in the housing (3) the impact mass (14) of the hammer is released and due to the tension developed in the impact spring (16) it strikes the end of the plunger. After the impact the hammer mass rebounds to a certain height which is indicated by a pointer (4) on a scale (5). The reading on the scale represents the rebound height as a percentage of the forward travel of the impact mass and is termed the rebound number (R).

There are a number of Schmidt hammer types differing in the amount of impact energy (in fact, spring stiffness), which are tabulated below with the manufacturer's specifications and recommendations for use.

Hammer type	Impact energy (mkg)	Recommended use
"N"	.225	For testing concrete in ordinary building and bridge construction
"L"	:075	For testing small and impact sensitive parts of concrete or artificial stone
"M"	3.0	For massive concrete, concrete road pavements, airfield runways
"P" (pendulum type)	.09	For low hardness and strength materials (4.8 to 24 MPa)
"PT"	.09	For extremely low strength materials (.5 to 8 MPa)

The L-type hammer is the one most commonly used for testing of rock surfaces, as it is non-destructive even when applied on hand-specimens and is capable of measuring strength values from 20 up to 300 MPa.

Miller (1965) investigated the potential application of the Schmidt hammer for the purpose of indexing of rock substances. By testing a suite of rock types he found a reasonable correlation between the rebound number, R (in the range from approximately 25 to 60) and unconfined

compressive strength (σ_c) measured on conventional cylindrical specimens. Best linearity in the original arithmetic plot of σ_c vs R was observed in the range of rebound numbers from approximately 40 to 55. An improved correlation was subsequently obtained when he multiplied the rebound number by the dry unit weight (γ in kN/m^3) and he was able to derive the following semi-logarithmic relationship:

$$\log \sigma_c = 0.00088\ \gamma R + 1.01, \quad r = 0.943$$

The above relationship and an approximate measure of the anticipated scatter is shown in Figure III.2.

Appreciation of the significance of the hardness of the joint surfaces as opposed to that of the underlying rock substance has led to the use of the Schmidt hammer for direct testing of joint surfaces and derivation of an index representing the joint compressive strength (JCS). Despite its simplicity the test is sensitive to a number of external factors and for optimum results the following operational instructions should be noted (summarized mainly from ISRM, 1978b):

(a) the hammer should be applied in a direction perpendicular to the test surface

(b) for a given surface the rebound number is minimum when the hammer is used vertically downwards (rebound against gravity) and maximum when used vertically upwards. Miller's equation and Figure III.2 apply to vertical downwards tests on horizontal surfaces. For any other testing direction the rebound numbers should be appropriately corrected, as shown in Table III.1.

(c) if the impulse is sufficient to move the surface being tested, the resulting rebound will be artificially low. This problem may arise in field testing of a closely spaced and loose joint structure. Specimens tested in the laboratory should be sufficiently large (for example blocks at least 20 cm in each direction, Barton and Choubey 1977) or otherwise they should be rigidly clamped on a heavy base.

(d) the test surface should be smooth and flat over the area covered by the plunger. Crushing of loose grains also produces artificially low readings.

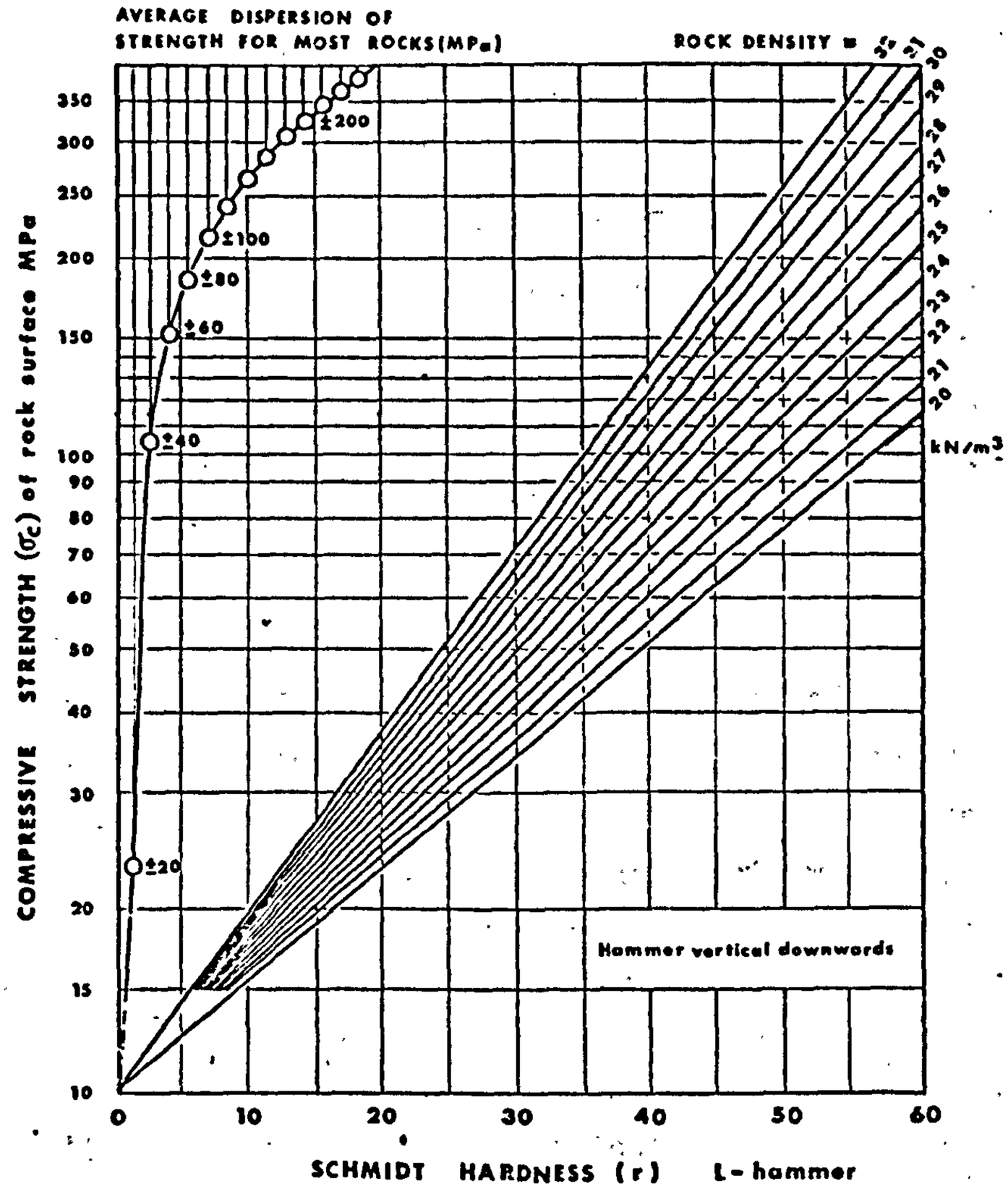

FIGURE III.2. Correlation chart for Schmidt (L.) hammer, relating rock density, compressive strength and rebound number.
(After Miller, 1965).

TABLE III.1

Corrections for reducing measured Schmidt hammer rebound (r) when the hammer is not used vertically downwards

Rebound r	Downwards α = −90°	Downwards α = −45°	Upwards α = +90°	Upwards α = +45°	Horizontal α = 0°
10	0	−0.8	—	—	−3.2
20	0	−0.9	−8.8	−6.9	−3.4
30	0	−0.8	−7.8	−6.2	−3.1
40	0	−0.7	−6.6	−5.3	−2.7
50	0	−0.6	−5.3	−4.3	−2.2
60	0	−0.4	−4.0	−3.3	−1.7

It is important to consider the factor (d) in some detail. Rebound numbers are affected by the roughness (both microscopic and megascopic) of the surface being tested. Dixon (1969) gave a broad classification of various surface textures as an aid to the appraisal of the rebound test (Figure III.3). The rebound numbers from rough surfaces (e.g. see "hackly" type in Fig. III.3) show larger scatter and the mean value is usually lower than that of a planar surface of the same rock type. Since the correlations between the uniaxial compressive strength and the rebound number are based on tests on flat surfaces, some more standardized procedure is necessary for the assessment of the JCS index from direct testing of natural joint surfaces. The ISRM (1978b) recommends that tests are performed in groups of 10 (i.e. 10 tests per joint, or 10 tests per unit area of a large critical discontinuity), applying the hammer to a new part of the surface before each impact. The five lowest readings of each group of 10 are discounted and the mean value of the five highest readings is quoted. The overall mean R value for a set of joints can then be obtained from a number of individual sets of 10 tests conducted on different joint exposures.

For a better appreciation of the effects of surface roughness on the rebound numbers, a few experiments were conducted on smooth, saw-cut surfaces and rough tension fractures of three rock types, namely a coarse-grained granite, a medium-grained sandstone and a fine-grained dolerite (Whin Sill). A group of twenty readings were firstly taken by applying the hammer on the sides of the blocks, which were then split in tension and the same number of tests was repeated on the rough fractures. The results of those tests are summarized in Table III.2.

The mean R values of all the readings taken from the rough fractures were in all cases lower than the means for the planar surfaces, by an amount ranging from approximately 4 to 8. It should be noted that extremely low R values which were occasionally obtained have been excluded from those presented in Table III.2. Assuming a unit weight value of 25 kN/m^3 for all three rock types, the σ_c estimates would differ by 15 to 33%. For example in the case of the granite the relevant values would be 175 ($\pm$ 70) and 117 ($\pm$ 45). By eliminating the ten lowest readings obtained from the fractures, the remaining readings gave means very close to those obtained from the flat surfaces, especially in the case of the medium- and fine-grained rocks. A

smooth, planar

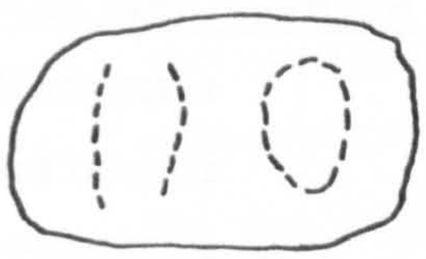

smooth, non-planar

D = 0-6 mm
w = 8-15 mm

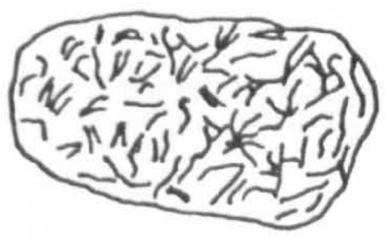

hackly

D = 0-6 mm
w = 3-8 mm

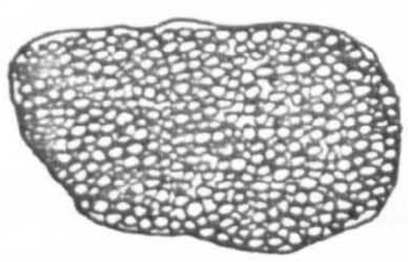

granular

D = 1-3 mm
w = 1-4 mm

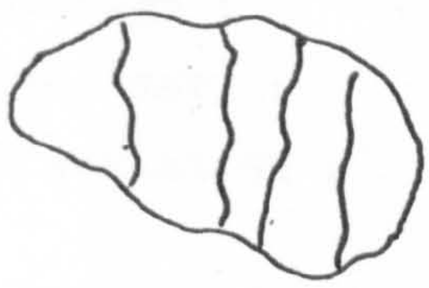

scaly

D = .5-1.5 mm
w = 1-10 mm

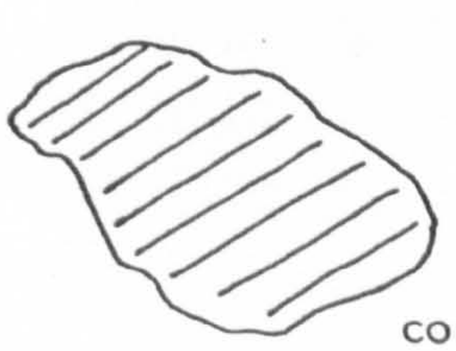

corrugated

D = 2-4 mm
w = 2-10 mm

FIGURE III.3 Classification of surface textures on joint surfaces as used by the Department of Mines, South Australia. (from Dixon, 1969)

TABLE III.2

Comparison of rebound numbers from Schmidt hammer testing of artificial smooth and rough rock surfaces.

	TESTS ON SMOOTH SAW-CUT SURFACES	TESTS ON ROUGH TENSION FRACTURES	
			Excluding
	All	All	10 lowest
1. COARSE-GRAINED GRANITE			
Minimum :	53	42	49
Maximum :	59	56	56
Average :	56	48.1	51.8
Std. dev. :	1.6	4.5	3.7
% variation :	2.9	9.1	7.0
2. MEDIUM-GRAINED SANDSTONE			
Minimum :	43	37	42
Maximum :	48	51	51
Average :	45.1	41.7	44.2
Std. dev. :	1.5	3.3	2.7
% variation :	3.1	8.0	6.0
3. FINE-GRAINED WINDSTONE			
Minimum :	48	44	49
Maximum :	59	56	56
Average :	52.7	49	51.6
Std. dev. :	2.7	3.2	2.3
% variation :	5.1	6.5	4.5

relatively larger deviation was still present in the case of the granite, presumably due to the coarse grain size. However, for practical purposes such differences are insignificant considering the anticipated scatter in the predicted σ_c values. The above testing procedure was adopted for the fresh and weathered joint surfaces as discussed in the relevant section 3.2.2(4) of Chapter 3.2.

2. Joint block preparation and compression testing

The experimental set-up described in section 3.2.2(5) of Chapter 3.2 meant that the accuracy of the vertical displacement measurements could be affected by poor quality contact between the bottom side of the block and the basal plate. Consequently, proper surface preparation was of primary significance in order to eliminate such influences to the maximum practical level.

Both the leading ends of the joint blocks were ground by using a horizontal grinder with a clamping device to accommodate the prismatic specimens. The first stage of treatment aimed at producing flat surfaces and improving the parallelism between the loading ends and the joint plane. As a second stage the block sides which would be in contact with the basal platen during the compression tests were subjected to several stages of progressively finer grinding, and then polished on a lapping wheel using a 600 grade silicon carbide.

Some difficulties were experienced during the grinding of the joint blocks from the highly weathered sandstone. Because of the weakness of the cementing material, many quartz grains were actually removed rather than ground, thus ending with an inferior quality finish. In order to strengthen the intergranular bonding those surfaces were treated with a thin epoxy resin mixture consisting of equal parts of araldite CY 219 and versamid 140 thinned with acetone. The mixture was allowed to impregnate 2 to 3 mm of the rock surfaces and on drying it provided a remarkably effective bonding, enabling the surfaces to be ground and lapped safely.

In order to compare the deformation values recorded by the dial gauges in the present experimental set-up with those obtained by using some other conventional technique, and so to test the effectiveness of the preparatory procedures and the relative sensitivity of the displacement

measuring devices, a series of compression tests was conducted on intact specimens of five different rock types. During each test direct measurements of strain were taken by two electrical resistance strain gauges, and the average of these values were then compared with the values of strain calculated from the average deformations recorded by the dial gauges. The tested rock specimens are described below:

(1) sandstone (coarse-grained) : cylinder, 73.41 mm diameter/65.52 mm length
(2) sandstone (medium-grained) : prism, 83.00 mm x 50.24 mm x 67.98 mm
(3) limestone (medium- to fine-grained) : cylinder, 73.41 mm diameter/ 132.52 mm length
(4) limestone (medium- to fine-grained) : cylinder 73.41 mm diameter/ 70.55 mm length
(5) sandstone metamorphosed (fine-grained) : prism, 76.45 mm x 69.90 mm x 76.32 mm.

Two 10 mm strain gauges were attached on each specimen on diametrically opposite positions on the circumference of the cylinders and on opposing sides of the blocks. The average stress-strain curves obtained from the direct and indirect measurements of strain are shown in Figure III.4. As seen, the curves derived for the two sandstone samples showed a very good agreement during both loading and unloading. Reasonably comparable also were the curves for the limestone specimen no. 3. Significant deviation was found in the case of limestone specimen no. 4, while for specimen no. 5 an unusual discrepancy was observed.

A ready explanation for the larger strains calculated for specimen no. 4 from the dial gauges could be that an additional amount of deformation had been recorded due to imperfect rock-platen contact. However, it should be noted that both specimens no. 3 and 4 were drilled from adjacent positions of the same block of perfectly fresh, compact limestone material. Comparison between the curves of specimen nos. 3 and 4 shows that those derived from the dial gauge measurements are virtually parallel which could be expected considering the type of rock being tested. On the other hand, the two strain gauge curves show a substantial difference in slope, with curve no. 4 being steeper than no. 3. It is not unlikely therefore that some external factor affected the strain gauge measurements for specimen no. 4.

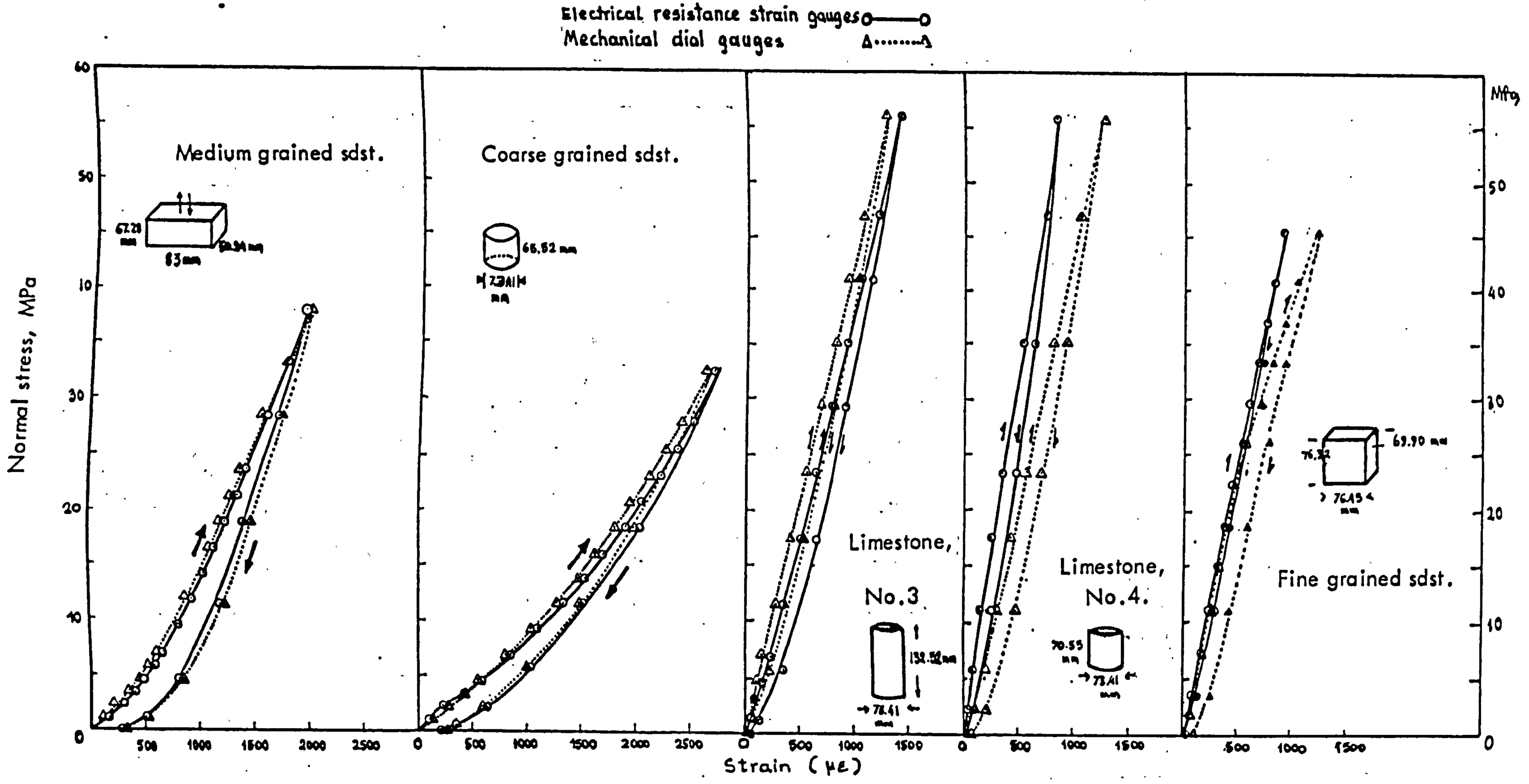

FIGURE III.4 Comparison of average stress-strain of intact specimens of five rock types obtained from direct and indirect measurements of strain by using electrical resistance gauges and mechanical dial gauges.

In the case of specimen no. 5 it can be seen that although the two curves are extremely close for normal stresses up to approximately 20 MPa, from then onwards the dial gauge curve began to deviate. The calculated strain at 45 MPa was approximately 20% higher than that directly measured by the strain gauges. There is a possible explanation for that anomaly. The block contained an extremely fine crack running across it diagonally at approximately 75° to the direction of loading. It is conceivable that a small elastic movement occurred along that crack and added to the overall block deformation measured by the dial gauges. Because of their relative position the strain gauges could not record that additional strain.

The above comparative study showed that careful sample preparation could enable acceptably accurate measurements of joint block deformation. Although it is unlikely that the platen-contact effects were completely eliminated, the amount of extra deformation would be insignificant compared to the magnitude of joint block displacements and certainly within the tolerance of the experimental error.

3. Direct shear testing of joints on a portable shear apparatus

The apparatus consists of two halves, the lower half being fitted with two hydraulic rams for forward and reverse shear movement and the upper with a ram for normal loads. The box is designed to accept rock samples of no more than 115 mm x 125 mm in face area or cores of up to 102 mm diameter. The general lay-out of the apparatus and casting moulds is shown in the manufacturer's design reproduced in Figure III.5.

The two halves of the joint sample to be tested are usually wired or taped together, then fitted into special clamps for horizontal alignment, appropriately positioned in the shear plane of the apparatus, and the moulding material is poured. Once the bottom section has set sufficiently hard, the sample is inverted and the top is cast in the other half of the mould. Once the mounted joint has been encased in the apparatus and a small normal load has been applied to prevent any movement of the joint, the wire or tape holding the two halves is cut and the test normal load can be applied. The most convenient shearing procedure is to apply suitable increments of shear load and monitor the shear displacements. During the shearing process the normal load is

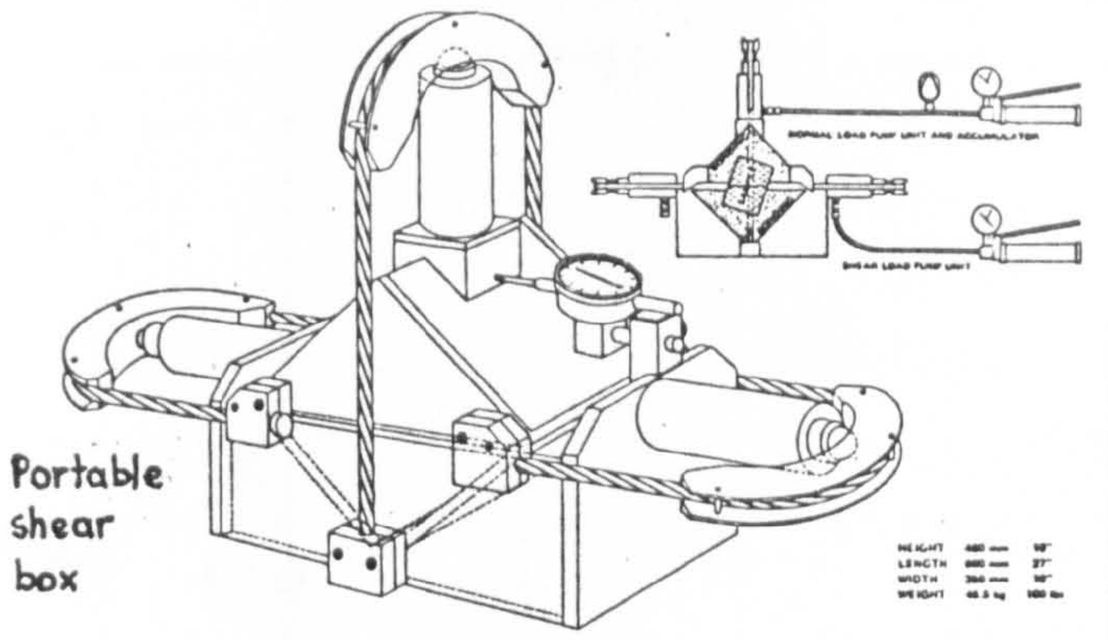

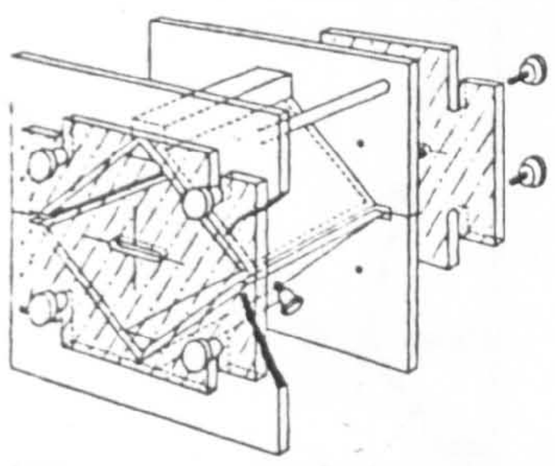

Sample mould former

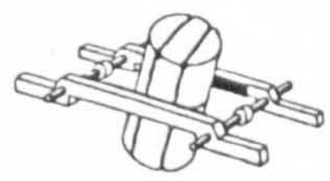

Sample locating clamp

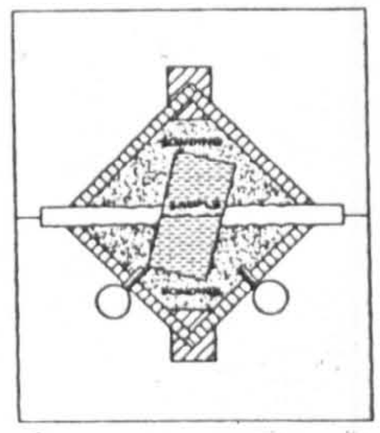

Sectional view of sample in mould

FIGURE III.5

maintained constant by a hydraulic intensifier, the low pressure side being a pneumatic reservoir. The hydraulic and pneumatic pressures are balanced by means of the hydraulic hand pump and an air pump respectively, such that the maintainer float lower edge rises approximately half way up the viewing parts in the outer body at the required load.

Testing trials showed that the standard configuration for measuring the shear displacement (Figure III.5(a))is inappropriate when testing dilatant surfaces, as has been outlined in section 3.2.2(5c) of Chapter 3.2. Some striking examples of the type of difficulties experienced are illustrated in the shear load-displacement curves in Figure III.6.

In order to ensure accurate measurements of shear displacements a different system was adopted. The unused hydraulic ram was removed

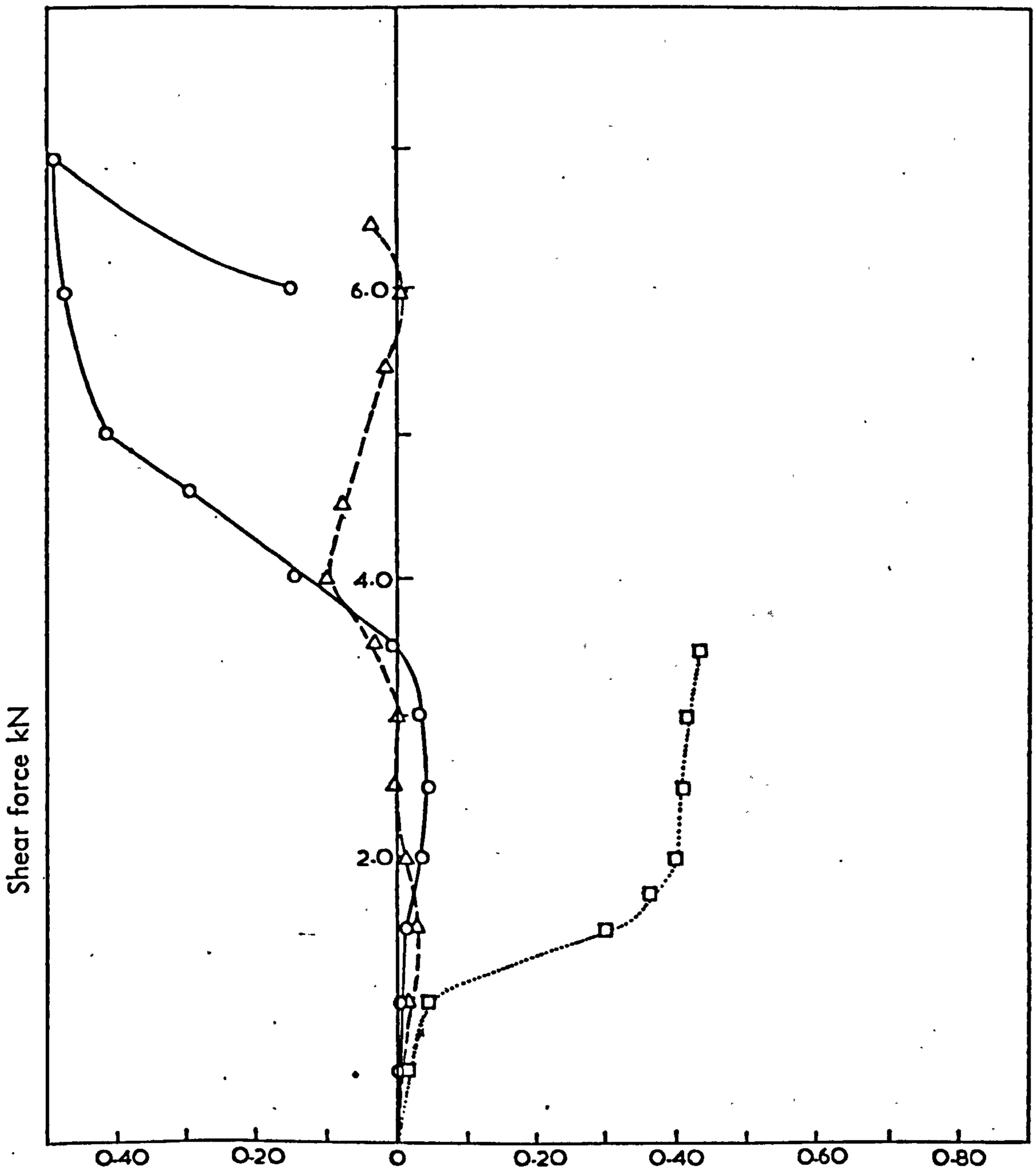

FIGURE III.6 Effects of rotation of the upper box during shearing of dilatant surfaces in the portable shear box.

from the lower box-half and two dial gauges were fitted at an appropriate height so that their spindles could go through the existing holes for the ram screws. By attaching an extension to the standard spindle length, the ends were brought to rest on the projecting side of the upper joint half at a distance of one or two millimeters above the shear plane, as shown diagrammatically in Figure III.7.

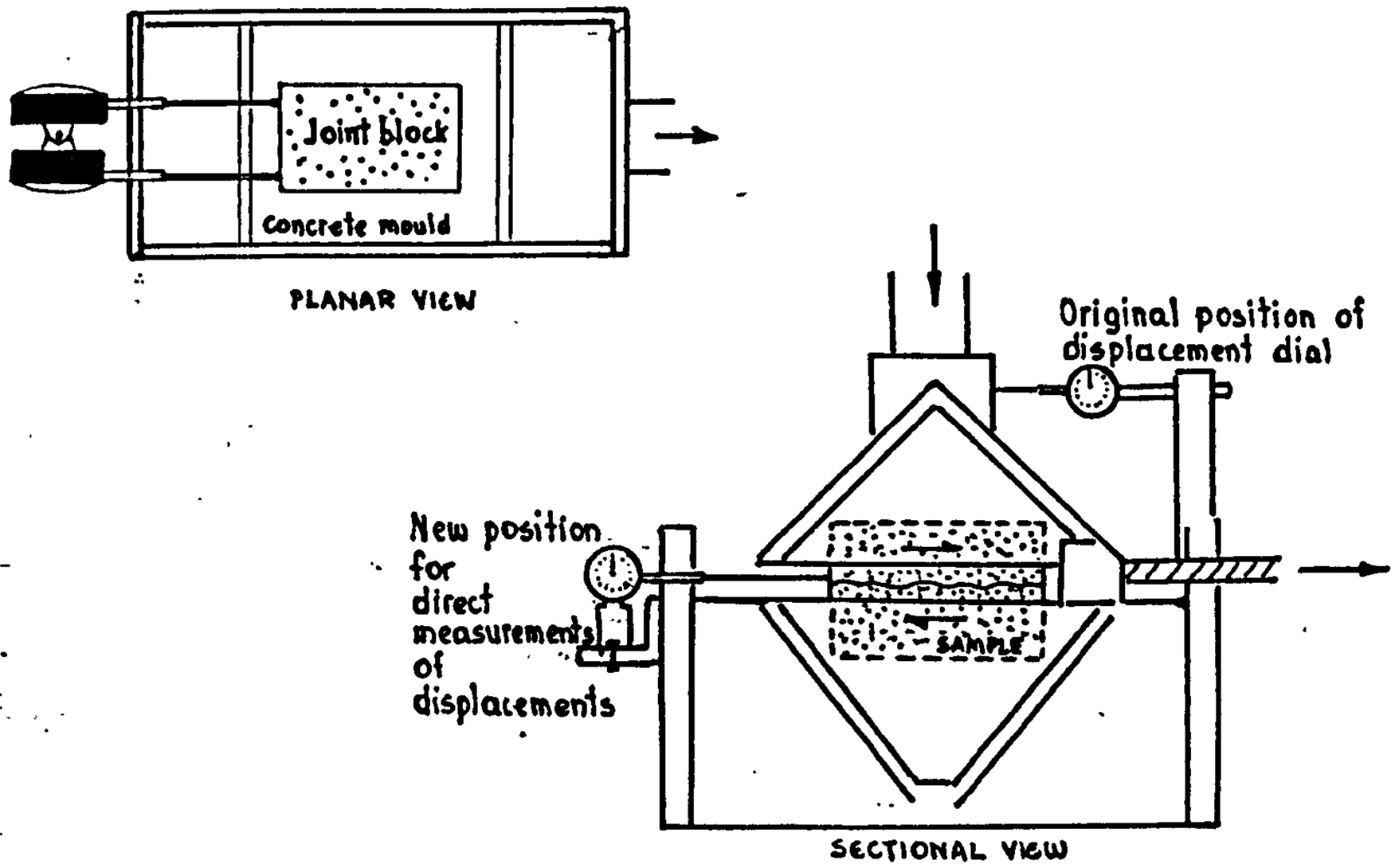

Figure III.7 Diagrammatic illustration of the standard and a modified positioning of dial gauges for measuring the shear displacements.

The positioning of the dial spindles near the corners of the joint also enables a check to be made on any excessive horizontal rotation of the upper half. However, in all the tests carried out the differences in the readings of the two dials were never in excess of $\pm$ 0.05 mm. Average displacement values were used in the plotting of the shear stress-shear displacement diagrams.

A number of tests were carried out with simultaneous recording of the displacements by both the standard and modified dial arrangement. A typical example of the differences obtained is illustrated by the family of curves in Figure III.8, as derived from multistage testing of a tightly locked dilatent joint in sandstone. As shown, the direct measurements

were two to three times smaller than the indirect ones which had, of course, an analogous effect on the calculated values of peak shear stiffness.

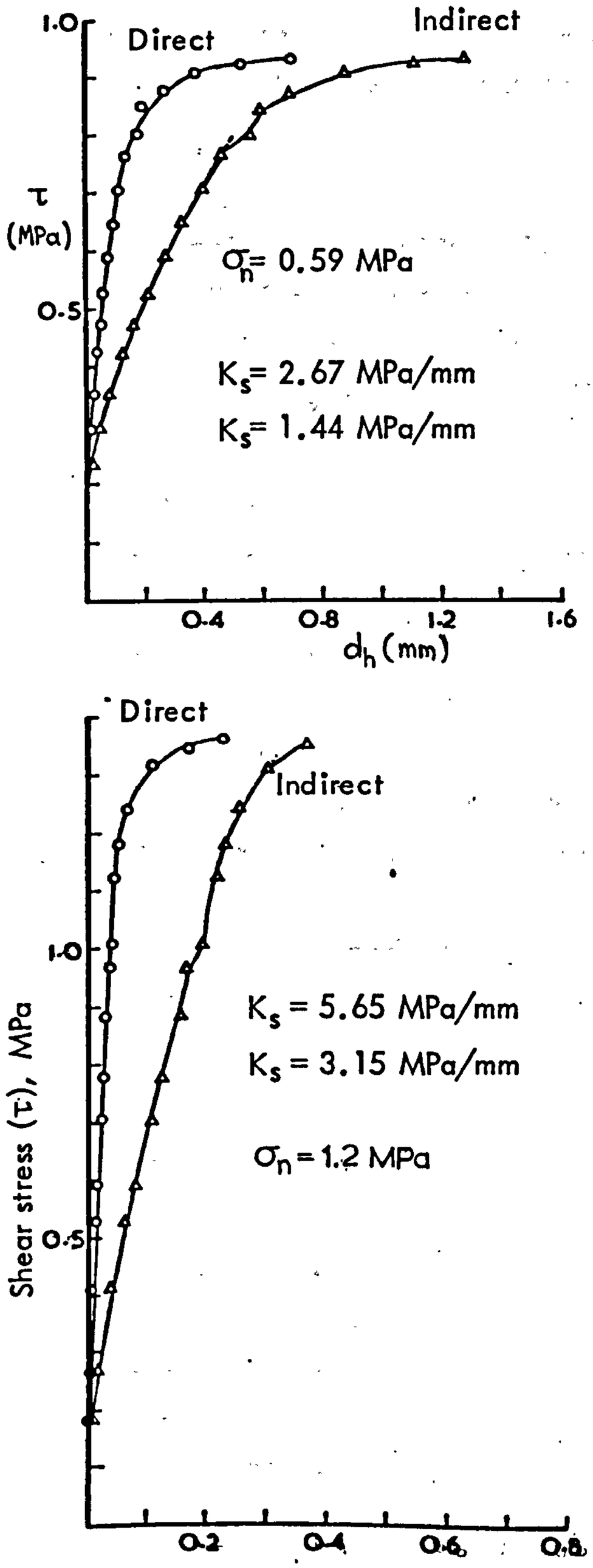

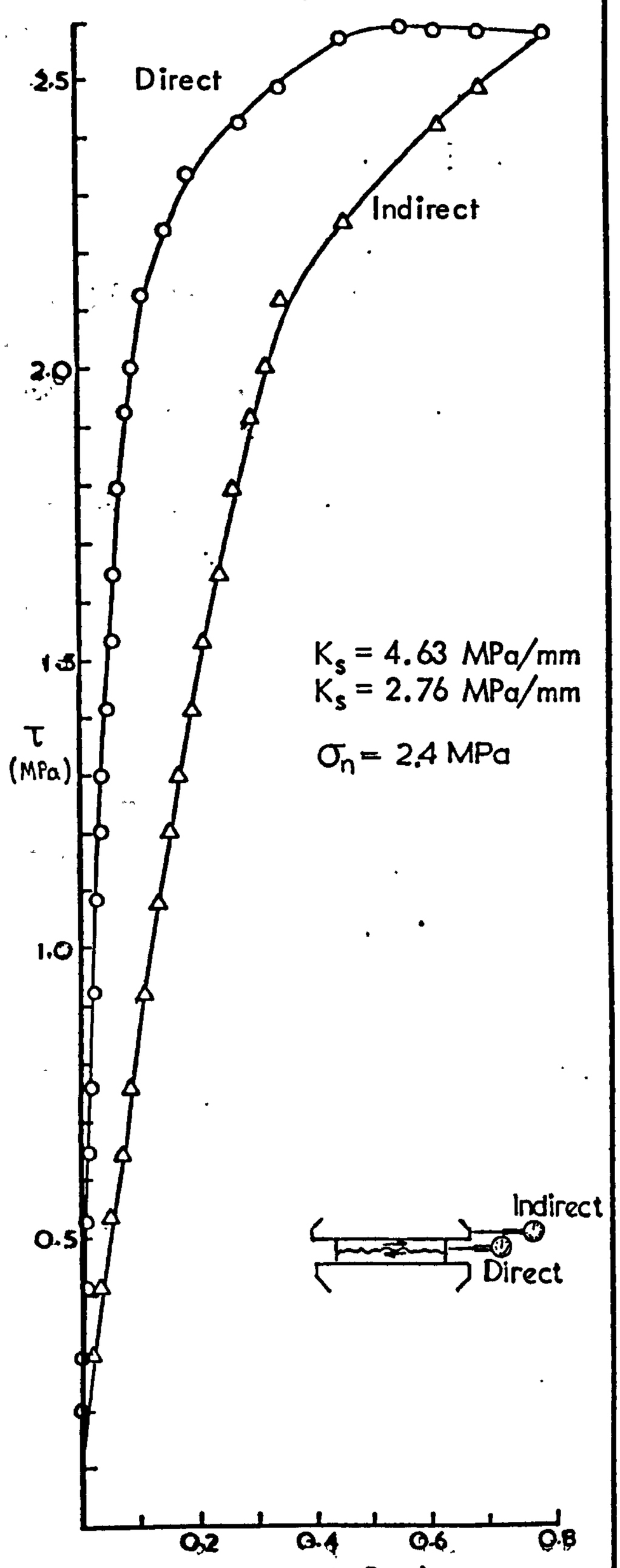

FIGURE III. 8 Comparisons of shear stress (τ) – shear displacement (d_h) diagrams obtained from direct and indirect measurements of shear displacement

APPENDIX IV

This appendix contains analytical records of the experimental data and the results from the non-linear regression analysis.

Symbols

SIGMA = normal stress in MPa units

DELTA (V) MEASURED = experimental total deformation of joint blocks

DELTA (V) CALCULATED = regression value

% DIFF = $\lceil (\text{DELTA (V)}_M - \text{DELTA (V)}_C)/\text{DELTA (V)}_M \rceil \times 100$

A = initial normal stiffness (K_{ni}) in MPa/mm

B = maximum joint closure (V_m) in mm

C = elastic stiffness of intact rock in MPa/mm

SD = one standard deviation

% = $\lceil SD/(A \text{ or } B \text{ or } C) \rceil \times 100$

The data plotted in the diagrams are the experimental total deformation values. The three loading cycles are drawn as:

△—△ 1st cycle

▽—▽ 2nd cycle

□—□ 3rd cycle

The results from the various joint types are presented in the following order:

Slate : SL 1 to 7

Dolerite : DOL 1 to 5

Limestone : LMST 1 to 20

Siltstone : SLST 1 to 10

Sandstone : SDST 1 to 21.

SL : 1

1st loading

SOLUTION

A=	34.51	SD =	0.9175	% =	2.659
B=	0.04258	SD =	4.1638 -4	% =	0.9778
C=	602.7	SD =	4.822	% =	0.6961

COMPUTED RESIDUALS

SIGMA	DELTA(V) MEASURED	DELTA(V) CALCULATED	DIFF	% DIFF
0.9891	0.01900	0.01856	0.00044	2.33
2.065	0.02800	0.02786	0.00014	0.50
3.140	0.03300	0.03354	-0.00054	1.63
4.215	0.03700	0.03766	-0.00066	1.78
6.366	0.04400	0.04378	0.00022	0.49
8.517	0.04900	0.04861	0.00039	0.80
12.82	0.05700	0.05670	0.00030	0.52
17.12	0.06400	0.06393	0.00007	0.11
21.42	0.07100	0.07077	0.00023	0.33
25.72	0.07700	0.07741	-0.00041	0.53
30.02	0.08400	0.08393	0.00007	0.08
34.32	0.09000	0.09038	-0.00038	0.42
38.63	0.09700	0.09678	0.00022	0.23
42.93	0.1030	0.1031	-0.0001	0.14
48.30	0.1110	0.1111	-0.0001	0.05
54.53	0.1160	0.1158	0.0002	0.18

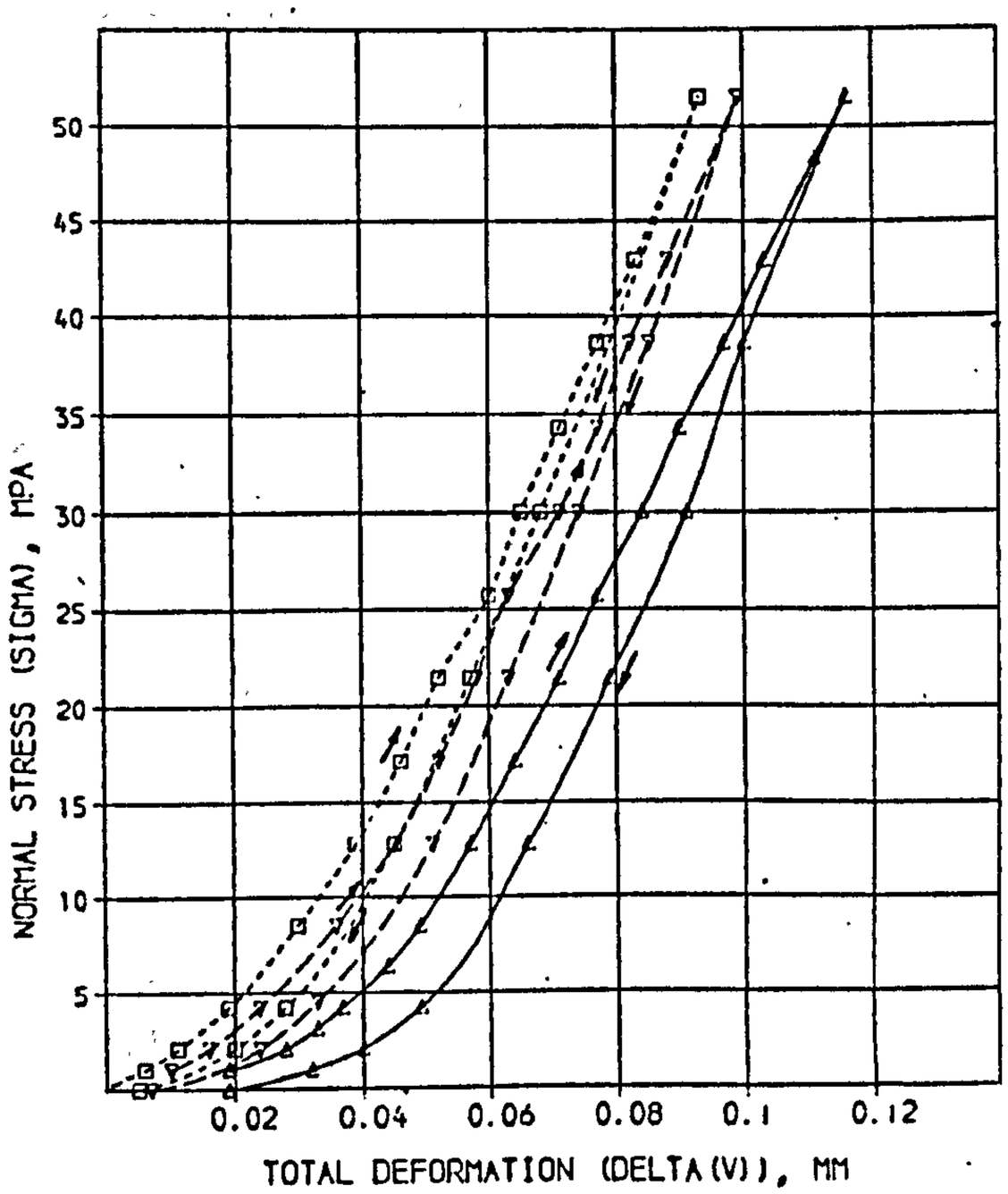

2nd loading

SOLUTION

A=	98.33	SD =	0.241	% =	0.367
B=	0.03577	SD =	0.001407	% =	3.932
C=	783.0	SD =	17.94	% =	2.291

COMPUTED RESIDUALS

SIGMA	DELTA(V) MEASURED	DELTA(V) CALCULATED	DIFF	% DIFF
0.9890	0.01000	0.00913	0.00087	8.67
2.065	0.01600	0.01590	0.00010	0.65
4.215	0.02400	0.02491	-0.00091	3.79
8.517	0.03600	0.03622	-0.00022	0.60
12.82	0.04500	0.04446	0.00054	1.19
17.12	0.05200	0.05156	0.00044	0.85
21.42	0.05800	0.05810	-0.00010	0.17
25.72	0.06300	0.06435	-0.00135	2.11
30.02	0.07100	0.07037	0.00063	0.88
34.32	0.07700	0.07629	0.00071	0.92
38.63	0.08200	0.08215	-0.00015	0.18
42.93	0.08800	0.08790	0.00010	0.11
51.53	0.09900	0.09931	-0.00031	0.31

3rd loading

SOLUTION

A=	185.2	SD =	8.601	% =	4.643
B=	0.03509	SD =	0.001622	% =	4.621
C=	826.1	SD =	18.81	% =	2.277

COMPUTED RESIDUALS

SIGMA	DELTA(V) MEASURED	DELTA(V) CALCULATED	DIFF	% DIFF
0.9890	0.006300	0.005851	0.000169	2.81
2.065	0.01100	0.01096	0.00004	0.36
4.215	0.01900	0.01891	0.00009	0.49
8.517	0.03000	0.03021	-0.00021	0.70
12.82	0.03900	0.03860	0.00040	0.51
17.12	0.04600	0.04616	-0.00016	0.34
21.42	0.05200	0.05285	-0.00085	1.63
25.72	0.06000	0.05914	0.00086	1.43
30.02	0.06500	0.06518	-0.00018	0.28
34.32	0.07100	0.07104	-0.00004	0.06
38.63	0.07700	0.07660	0.00040	0.27
42.93	0.08300	0.08244	0.00056	0.67
51.53	0.09300	0.09353	-0.00053	0.57

SL: No. 2

1st loading

SOLUTION

A=	46.50	SD =	5.594	% =	12.03
B=	0.02237	SD =	0.000669	% =	2.988
C=	821.3	SD =	11.98	% =	1.459

COMPUTED RESIDUALS

SIGMA	DELTA(V) MEASURED	DELTA(V) CALCULATED	DIFF	% DIFF
1.002	0.01200	0.01220	-0.00020	1.64
2.092	0.01600	0.01749	0.00151	7.95
4.271	0.02200	0.02319	-0.00119	5.42
6.451	0.02600	0.02712	-0.00112	4.31
8.630	0.03000	0.03047	-0.00047	1.58
10.81	0.03300	0.03357	-0.00057	1.73
12.99	0.03700	0.03653	0.00047	1.27
15.17	0.04000	0.03941	0.00059	1.49
17.35	0.04300	0.04223	0.00077	1.79
19.53	0.04500	0.04502	-0.00002	0.04
21.71	0.04800	0.04778	0.00022	0.46
26.06	0.05300	0.05325	-0.00025	0.47
30.42	0.05800	0.05868	0.00032	0.55
34.78	0.06500	0.06407	0.00093	1.43
39.14	0.07000	0.06945	0.00055	0.78
43.50	0.07400	0.07481	-0.00081	1.10
47.86	0.08000	0.08017	-0.00017	0.21
52.22	0.08500	0.08551	-0.00051	0.61

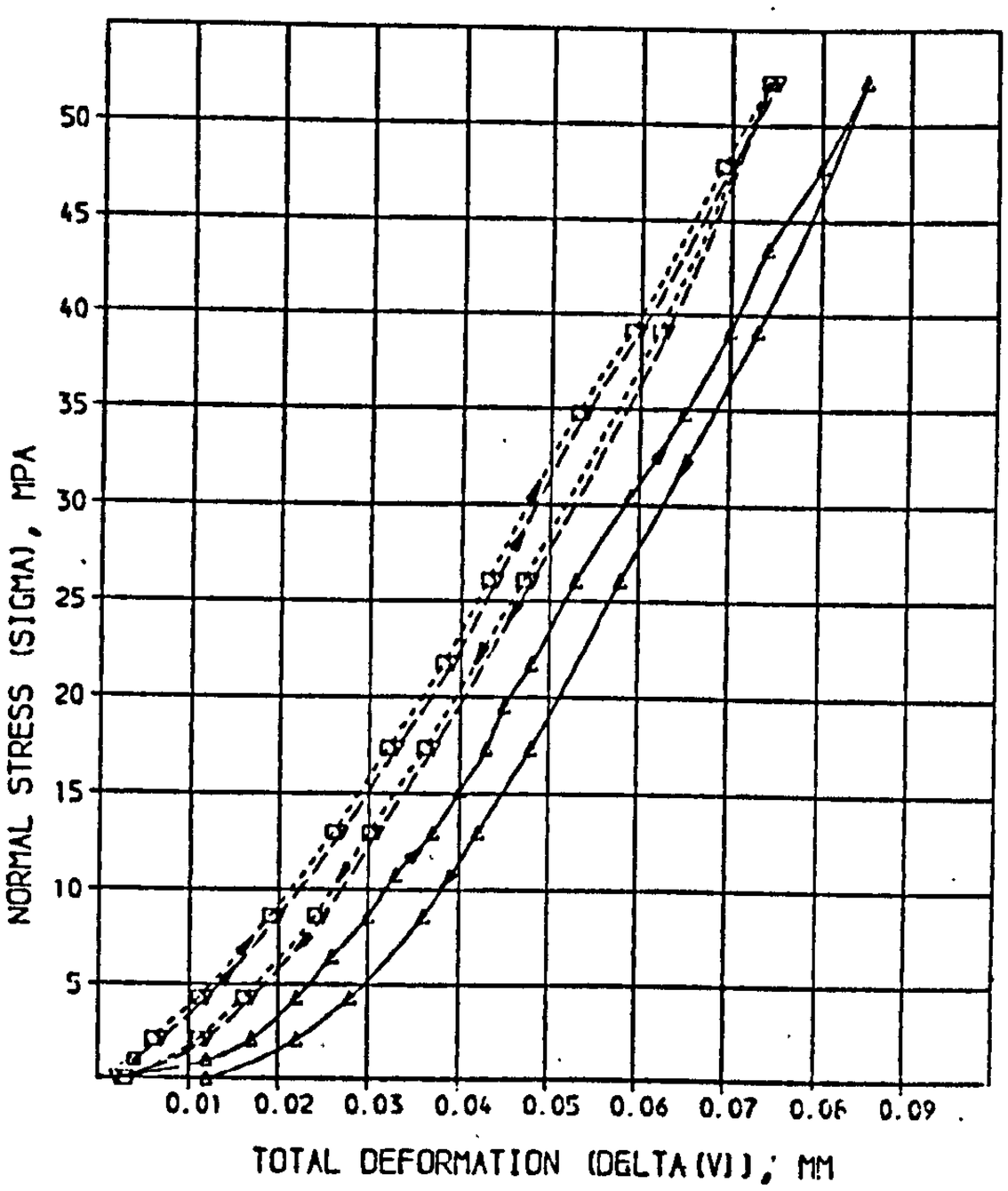

2nd loading

SOLUTION

A=	344.3	SD =	19.71	% =	5.725
B=	0.01835	SD =	0.001000	% =	5.448
C=	890.6	SD =	13.07	% =	1.468

COMPUTED RESIDUALS

SIGMA	DELTA(V) MEASURED	DELTA(V) CALCULATED	DIFF	% DIFF
1.002	0.004000	0.003697	0.000303	9.08
2.092	0.007000	0.006913	0.000087	1.24
4.271	0.01200	0.01220	-0.00020	1.64
8.630	0.02000	0.02028	-0.00028	1.42
12.99	0.02700	0.02693	0.00007	0.26
17.35	0.03300	0.03293	0.00007	0.21
21.71	0.03900	0.03859	0.00041	1.06
26.06	0.04400	0.04403	-0.00003	0.06
34.78	0.05400	0.05458	-0.00058	1.07
39.14	0.06000	0.05974	0.00026	0.43
47.86	0.07000	0.06995	0.00005	0.08
52.22	0.07500	0.07500	-0.00000	0.00

3rd loading

SOLUTION

A=	424.4	SD =	32.06	% =	7.554
B=	0.01828	SD =	0.001593	% =	8.714
C=	899.5	SD =	19.70	% =	2.190

COMPUTED RESIDUALS

SIGMA	DELTA(V) MEASURED	DELTA(V) CALCULATED	DIFF	% DIFF
1.002	0.004000	0.003205	0.000795	19.88
2.092	0.006000	0.006208	-0.000208	3.47
4.271	0.01100	0.01124	-0.00024	2.17
8.630	0.01900	0.01922	-0.00022	1.16
12.99	0.02600	0.02586	0.00014	0.44
17.35	0.03200	0.03192	0.00008	0.25
21.71	0.03800	0.03760	0.00040	1.05
26.06	0.04300	0.04306	-0.00006	0.13
34.78	0.05300	0.05361	-0.00061	1.15
39.14	0.05900	0.05877	0.00023	0.39
47.86	0.06900	0.06894	0.00006	0.09
52.22	0.07400	0.07397	0.00003	0.04

SL : No. 3

1st loading

SOLUTION

A=	24.06	SD =	1.765	% =	7.337
B=	0.06071	SD =	0.002124	% =	3.499
C=	754.6	SD =	39.75	% =	5.268

COMPUTED RESIDUALS

SIGMA	DELTA(V) MEASURED	DELTA(V) CALCULATED	DIFF	% DIFF
0.3680	0.008000	0.012705	-0.004705	58.82
0.5310	0.01400	0.01689	-0.00289	20.64
0.7360	0.02000	0.02132	-0.00132	6.58
0.9400	0.02500	0.02502	-0.00002	0.07
1.553	0.03600	0.03334	0.00266	7.38
1.961	0.04000	0.03739	0.00261	6.52
2.983	0.04600	0.04471	0.00129	2.81
4.005	0.05100	0.04979	0.00121	2.37
5.026	0.05400	0.05370	0.00030	0.56
6.048	0.05700	0.05691	0.00009	0.15
8.091	0.06200	0.06215	-0.00015	0.23
10.13	0.06600	0.06649	-0.00049	0.74
12.18	0.07000	0.07034	-0.00034	0.49
14.22	0.07400	0.07390	0.00010	0.14
16.26	0.07700	0.07725	-0.00025	0.33
18.31	0.08000	0.08048	-0.00048	0.60
20.35	0.08300	0.08361	-0.00061	0.73
22.39	0.08600	0.08666	-0.00066	0.77
24.44	0.08900	0.08966	-0.00066	0.75
28.52	0.09500	0.09555	-0.00055	0.57
32.61	0.1000	0.1013	-0.0013	1.31
36.69	0.1040	0.1070	-0.0030	2.89
49.78	0.1180	0.1126	0.0054	4.54

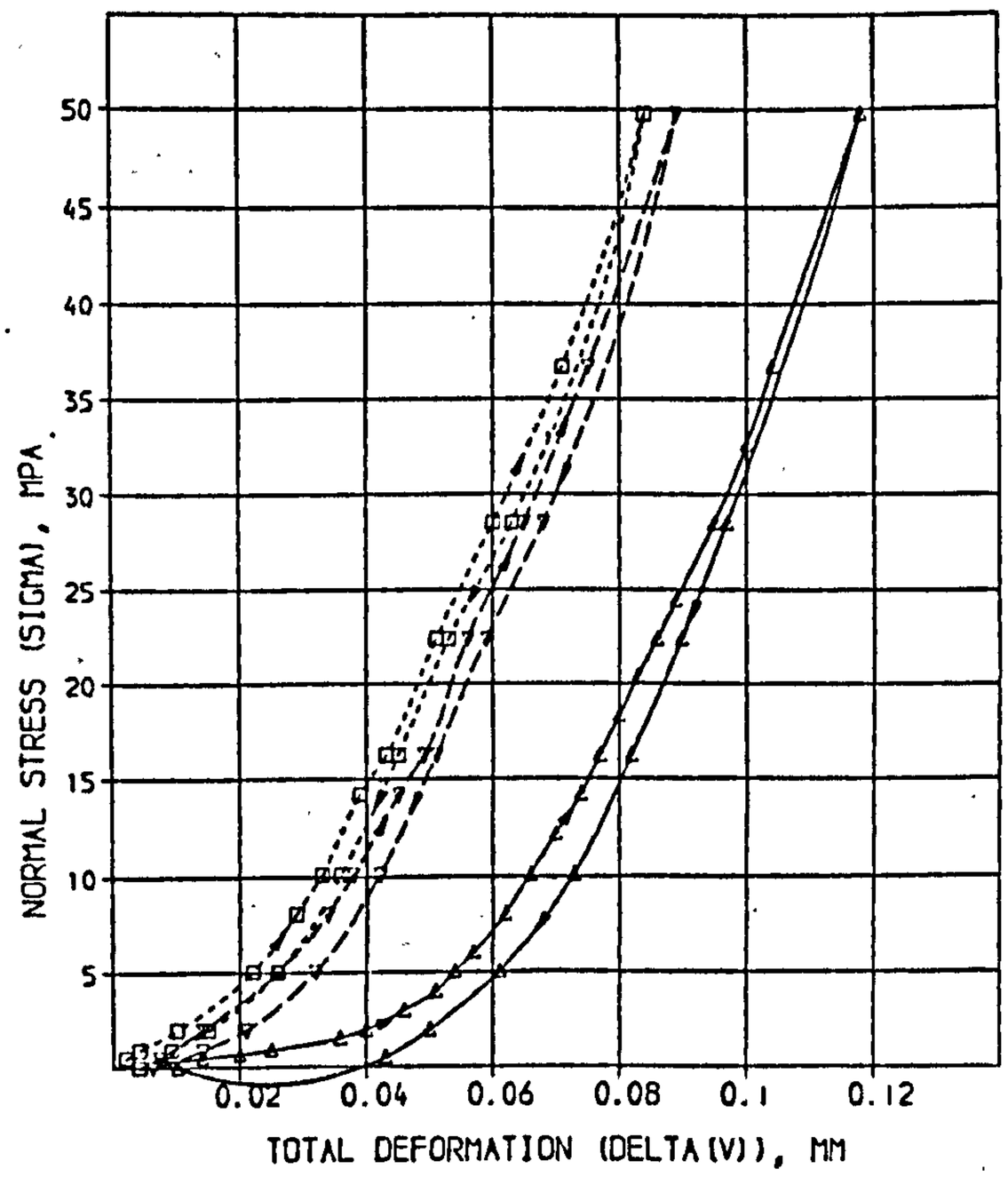

2nd loading

SOLUTION

A=	101.1	SD =	7.731	% =	7.664
B=	0.03703	SD =	0.001906	% =	5.147
C=	901.1	SD =	33.05	% =	3.668

COMPUTED RESIDUALS

SIGMA	DELTA(V) MEASURED	DELTA(V) CALCULATED	DIFF	% DIFF
0.5310	0.007000	0.005588	0.001412	25.89
0.9400	0.009000	0.008473	0.000527	5.86
1.961	0.01450	0.01490	-0.00040	2.77
5.026	0.02600	0.02680	-0.00080	3.06
8.091	0.03400	0.03427	-0.00027	0.80
11.13	0.03800	0.03828	-0.00028	0.73
14.22	0.04500	0.04509	-0.00009	0.20
16.26	0.04900	0.04814	0.00086	1.75
22.39	0.05600	0.05657	-0.00057	1.02
28.52	0.06500	0.06454	0.00046	0.95
36.69	0.07500	0.07432	0.00068	0.91
49.78	0.08900	0.08964	-0.00068	0.77

3rd loading

SOLUTION

A=	189.1	SD =	10.13	% =	8.528
B=	0.03816	SD =	0.003904	% =	10.23
C=	971.4	SD =	61.57	% =	6.356

COMPUTED RESIDUALS

SIGMA	DELTA(V) MEASURED	DELTA(V) CALCULATED	DIFF	% DIFF
0.5310	0.002500	0.003102	-0.000602	24.46
0.9400	0.004000	0.005505	-0.001505	34.12
1.961	0.01000	0.01017	-0.00017	1.72
5.026	0.02200	0.02084	0.00116	5.28
8.091	0.02900	0.02850	0.00050	1.73
10.13	0.03300	0.03271	0.00029	0.87
14.22	0.03900	0.03995	-0.00095	2.44
16.26	0.04300	0.04317	-0.00017	0.39
22.39	0.05100	0.05191	-0.00091	1.78
28.52	0.06000	0.05981	0.00019	0.31
36.69	0.07100	0.06946	0.00154	1.89
49.78	0.08400	0.08458	-0.00058	0.69

SL : No. 4

1st loading

SOLUTION

A=	13.10	SD =	0.3185	% =	2.431
B=	0.1095	SD =	0.001136	% =	1.037
C=	983.4	SD =	33.38	% =	3.394

COMPUTED RESIDUALS

SIGMA	DELTA(V) MEASURED	DELTA(V) CALCULATED	DIFF	% DIFF
0.2800	0.01700	0.01817	-0.00117	6.86
0.6300	0.03700	0.03406	0.00294	7.95
1.156	0.05000	0.05005	-0.00005	0.09
1.681	0.06100	0.06080	0.00020	0.33
2.557	0.07200	0.07276	-0.00076	1.06
3.432	0.08000	0.08073	-0.00073	0.92
4.308	0.08600	0.08655	-0.00055	0.64
5.184	0.09100	0.09106	-0.00006	0.07
6.935	0.09600	0.09781	-0.00181	1.89
8.686	0.1030	0.1028	0.0002	0.15
10.44	0.1060	0.1069	-0.0009	0.86
12.19	0.1110	0.1104	0.0006	0.54
14.82	0.1160	0.1149	0.0011	0.92
17.44	0.1200	0.1190	0.0010	0.87
20.94	0.1250	0.1238	0.0012	0.95
24.45	0.1290	0.1283	0.0007	0.52
27.95	0.1330	0.1326	0.0004	0.29
31.45	0.1360	0.1367	-0.0007	0.55
34.95	0.1410	0.1408	0.0002	0.16
38.46	0.1440	0.1447	-0.0007	0.49
41.96	0.1480	0.1486	-0.0006	0.40

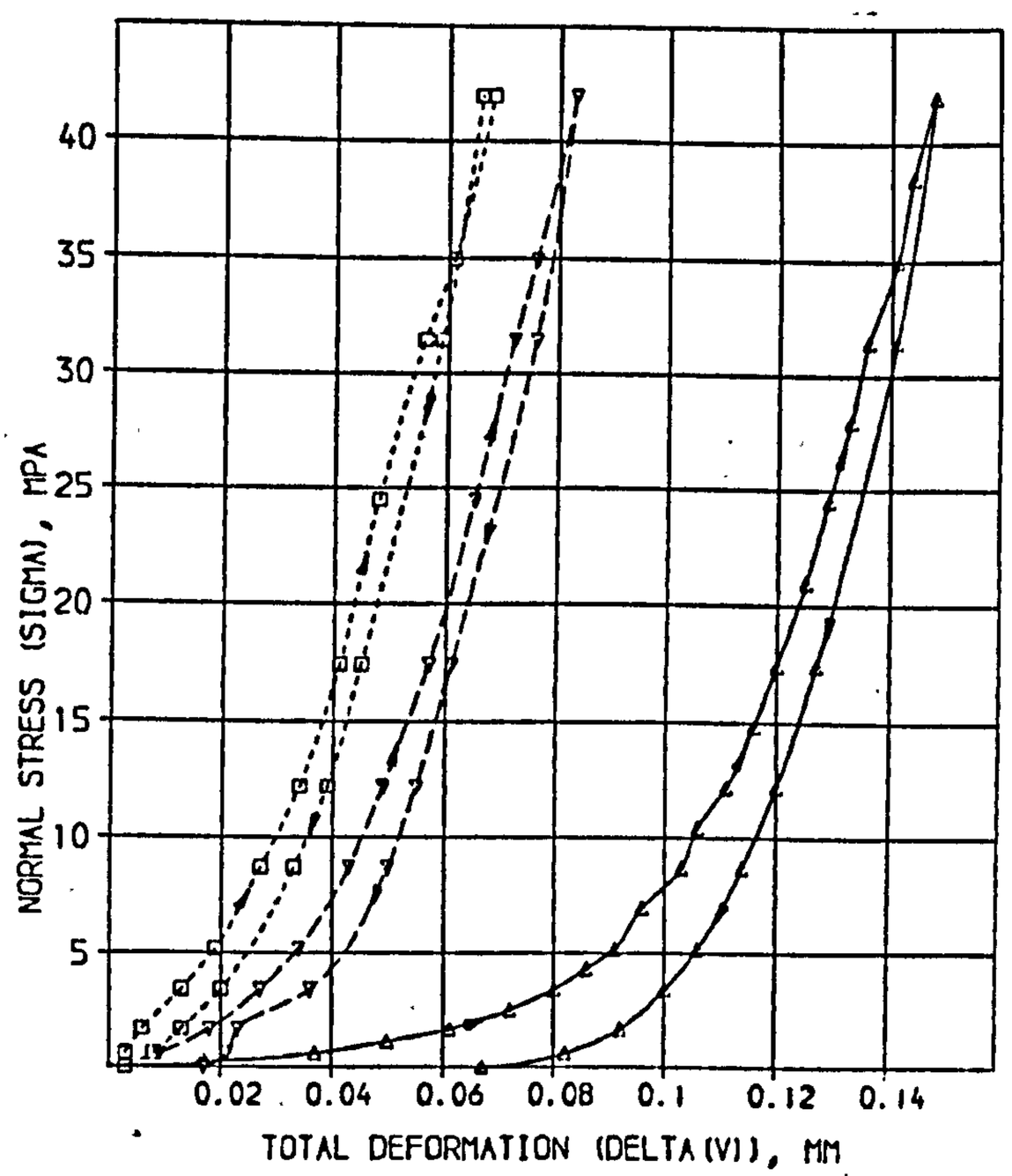

2nd loading

SOLUTION

A=	68.94	SD =	2.041	% =	3.017
B=	0.04351	SD =	0.001100	% =	2.268
C=	1103.	SD =	31.52	% =	2.859

COMPUTED RESIDUALS

SIGMA	DELTA(V) MEASURED	DELTA(V) CALCULATED	DIFF	% DIFF
0.6300	0.009000	0.008257	0.000743	8.26
1.081	0.01300	0.01274	0.00026	1.42
3.432	0.02700	0.02767	-0.00067	2.49
5.184	0.03400	0.03418	-0.00018	0.53
8.686	0.04300	0.04290	0.00010	0.24
12.19	0.04900	0.04914	-0.00014	0.24
17.44	0.05700	0.05652	0.00048	0.85
24.45	0.06500	0.06464	0.00010	0.24
31.45	0.07200	0.07257	-0.00057	0.51
34.95	0.07600	0.07547	0.00053	0.05
41.96	0.08300	0.08294	0.00002	0.03

3rd loading

SOLUTION

A=	235.5	SD =	18.31	% =	7.772
B=	0.04199	SD =	0.007506	% =	17.40
C=	1257.	SD =	186.7	% =	14.86

COMPUTED RESIDUALS

SIGMA	DELTA(V) MEASURED	DELTA(V) CALCULATED	DIFF	% DIFF
0.6300	0.003000	0.003010	-0.000010	0.53
1.681	0.006000	0.007454	-0.001454	25.97
3.432	0.01300	0.01355	-0.00055	4.22
5.184	0.01910	0.01867	0.00043	2.28
8.686	0.02700	0.02655	0.00045	1.68
12.19	0.03400	0.03288	0.00112	3.29
17.44	0.04100	0.04067	0.00033	0.80
24.45	0.04300	0.04435	-0.00135	2.82
31.45	0.05600	0.05697	-0.00097	1.73
34.95	0.06100	0.06054	0.00046	0.75
41.96	0.06300	0.06237	0.00063	0.92

SL : No. 5

1st loading

SOLUTION

A=	13.81	SD =	0.7774	% =	5.629
B=	0.2562	SD =	0.01110	% =	4.334
C=	246.8	SD =	15.08	% =	0.354

COMPUTED RESIDUALS

SIGMA	DELTA(V) MEASURED	DELTA(V) CALCULATED	DIFF	% DIFF
0.2920	0.02300	0.02071	0.00229	9.94
0.6560	0.04100	0.04273	0.00027	12.80
1.021	0.06700	0.06151	0.00549	8.19
1.385	0.08100	0.07769	0.00331	4.09
1.750	0.09300	0.09188	0.00112	1.21
3.573	0.1360	0.1432	-0.0072	5.30
5.396	0.1670	0.1766	-0.0096	5.76
7.219	0.1920	0.2012	-0.0092	4.79
9.041	0.2290	0.2228	0.0062	3.59
10.86	0.2480	0.2373	0.0107	4.32
15.42	0.2680	0.2709	-0.0029	1.08
18.16	0.2860	0.2880	-0.0020	0.70
21.80	0.3100	0.3088	0.0012	0.39
25.45	0.3290	0.3281	0.0009	0.29
29.09	0.3490	0.3463	0.0027	0.77
32.74	0.3640	0.3639	0.0001	0.03
36.38	0.3820	0.3809	0.0011	0.28
40.03	0.3960	0.3976	-0.0016	0.41
43.68	0.4120	0.4140	-0.0020	0.49

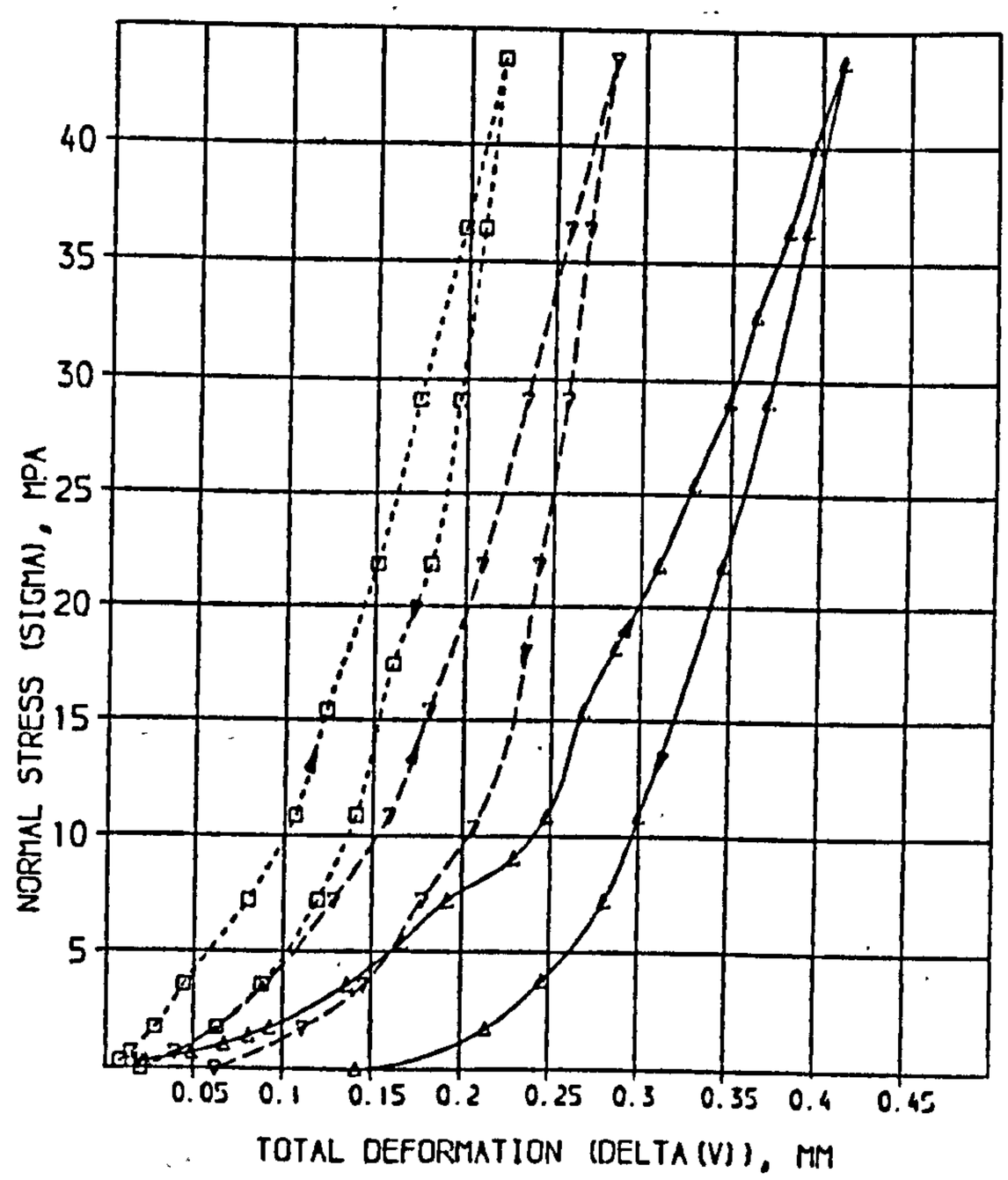

2nd loading

SOLUTION

A=	19.12	SD =	1.899	% =	9.931
B=	0.1543	SD =	0.01004	% =	6.512
C=	313.7	SD =	23.85	% =	7.603

COMPUTED RESIDUALS

SIGMA	DELTA(V) MEASURED	DELTA(V) CALCULATED	DIFF	% DIFF
0.2920	0.01300	0.01485	0.00317	17.61
0.6560	0.03900	0.03017	0.00883	22.63
1.750	0.06300	0.06310	-0.00010	0.16
3.573	0.09000	0.09606	-0.00606	6.74
7.219	0.1290	0.1328	-0.0048	3.77
11.86	0.1590	0.1523	0.0067	1.70
15.42	0.1810	0.1791	0.0019	1.07
21.80	0.2090	0.2058	0.0032	1.51
29.09	0.2340	0.2333	0.0007	0.30
36.38	0.2590	0.2576	-0.0014	0.46
43.68	0.2830	0.2843	-0.0013	0.45

3rd loading

SOLUTION

A=	63.58	SD =	4.404	% =	6.953
B=	0.1400	SD =	0.01706	% =	12.19
C=	426.7	SD =	50.79	% =	11.90

COMPUTED RESIDUALS

SIGMA	DELTA(V) MEASURED	DELTA(V) CALCULATED	DIFF	% DIFF
0.2920	0.008000	0.005131	0.002869	35.86
0.6560	0.01400	0.01115	0.00285	20.38
1.750	0.02300	0.02210	0.00090	3.91
3.573	0.04400	0.04447	-0.00447	10.16
7.219	0.08000	0.07961	0.00039	0.49
11.86	0.1060	0.1024	0.0036	3.42
15.42	0.1230	0.1249	-0.0019	1.53
21.80	0.1510	0.1505	0.0005	0.35
29.09	0.1740	0.1753	-0.0013	0.77
36.38	0.1980	0.1977	0.0003	0.15
43.68	0.2190	0.2186	0.0004	0.17

SL : No. 6

1st loading_

SOLUTION

A=	12.76	SD =	0.4543	% =	3.874
B=	0.2680	SD =	0.009461	% =	3.531
C=	188.9	SD =	9.443	% =	5.000

COMPUTED RESIDUALS

SIGMA	DELTA(V) MEASURED	DELTA(V) CALCULATED	DIFF	% DIFF
0.2560	0.02500	0.02002	0.00498	19.92
0.5120	0.04400	0.03761	0.00639	14.52
0.7540	0.05100	0.04649	0.00451	8.85
0.9380	0.06000	0.06265	0.00335	5.07
1.364	0.08800	0.08363	0.00437	4.96
2.075	0.1100	0.1122	-0.0022	1.99
2.786	0.1330	0.1351	-0.0021	1.55
4.207	0.1650	0.1701	-0.0051	3.09
5.657	0.1930	0.1970	-0.0040	2.06
8.471	0.2290	0.2358	-0.0068	2.95
11.31	0.2620	0.2657	-0.0037	1.41
14.16	0.2630	0.2608	0.0022	0.75
15.58	0.3040	0.3022	0.0018	0.59
17.00	0.3160	0.3131	0.0029	0.91
18.42	0.3320	0.3235	0.0085	2.55
21.26	0.3460	0.3434	0.0026	0.74
23.45	0.3600	0.3580	0.0020	0.55
25.53	0.3750	0.3715	0.0035	0.94
27.66	0.3840	0.3849	-0.0009	0.25
29.79	0.3960	0.3981	-0.0021	0.54
31.92	0.4080	0.4111	-0.0031	0.75
34.05	0.4200	0.4238	-0.0038	0.91

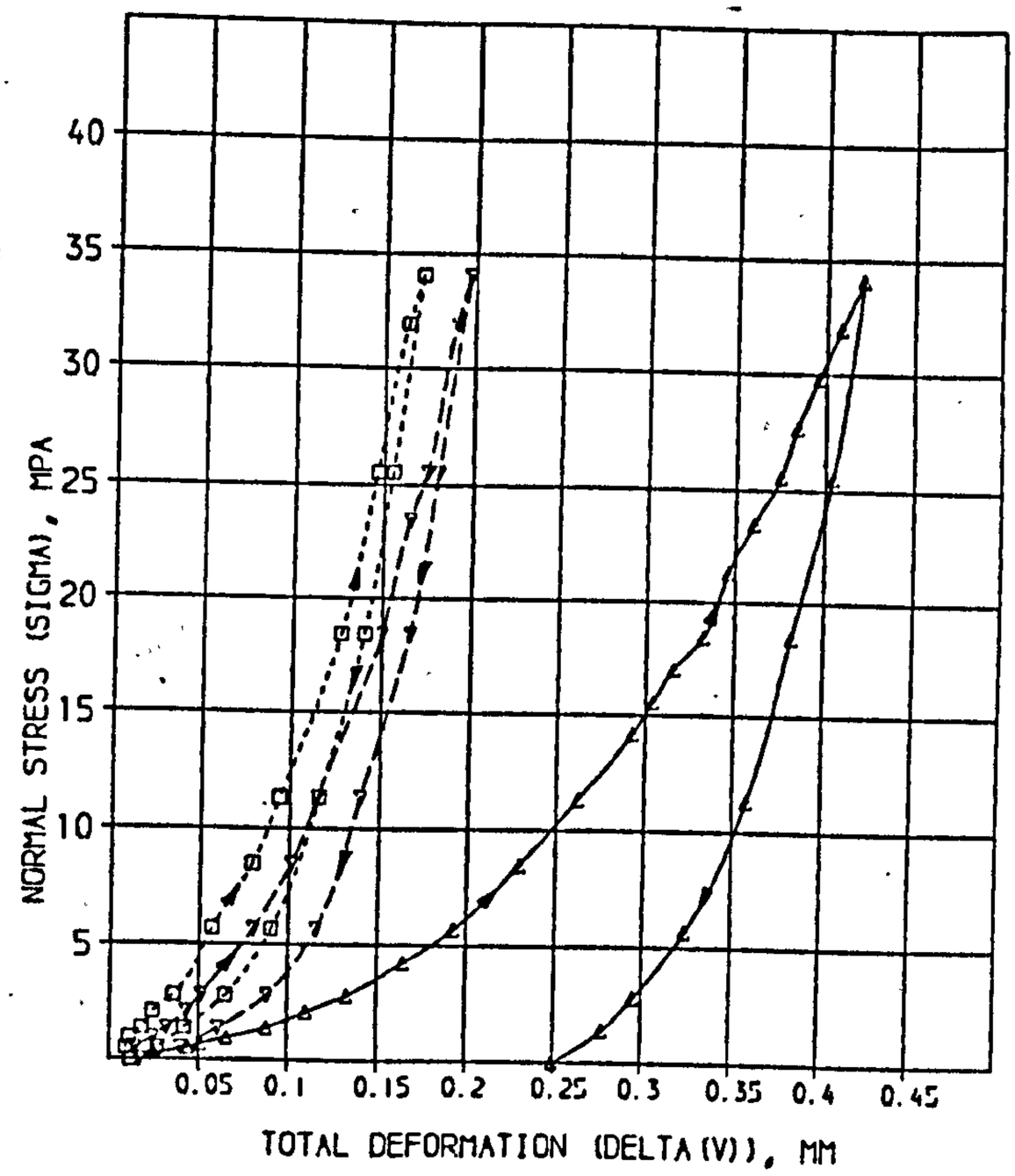

2nd loading_

SOLUTION

A=	39.90	SD =	1.633	% =	4.093
B=	0.1237	SD =	0.007391	% =	5.743
C=	395.5	SD =	27.41	% =	6.931

COMPUTED RESIDUALS

SIGMA	DELTA(V) MEASURED	DELTA(V) CALCULATED	DIFF	% DIFF
0.5120	0.01400	0.01295	0.00105	7.52
0.9380	0.02400	0.02224	0.00176	7.40
1.364	0.03200	0.03043	0.00157	4.92
2.075	0.04300	0.04224	0.00076	1.76
2.786	0.05100	0.05220	-0.00120	2.48
5.657	0.08000	0.08171	-0.00171	2.14
8.471	0.1010	0.1015	-0.0005	0.49
11.31	0.1150	0.1171	-0.0021	1.79
14.42	0.1500	0.1472	0.0028	1.88
23.45	0.1650	0.1644	0.0002	0.10
25.53	0.1740	0.1717	0.0023	1.34
31.92	0.1900	0.1915	-0.0015	0.82
34.05	0.1970	0.1979	-0.0009	0.46

3rd loading_

SOLUTION

A=	77.61	SD =	4.194	% =	5.404
B=	0.1815	SD =	0.03032	% =	16.81
C=	831.1	SD =	320.4	% =	38.55

COMPUTED RESIDUALS

SIGMA	DELTA(V) MEASURED	DELTA(V) CALCULATED	DIFF	% DIFF
0.5120	0.009000	0.006982	0.002018	22.43
0.9380	0.01100	0.01240	-0.00140	15.27
1.364	0.01800	0.01760	0.00034	1.86
2.075	0.02400	0.02580	-0.00180	7.50
2.786	0.03600	0.03352	0.00268	7.44
5.657	0.05700	0.05881	-0.00181	3.18
8.471	0.07900	0.07855	0.00065	0.82
11.31	0.09400	0.09444	-0.00044	0.47
13.42	0.1270	0.1250	0.0020	1.56
25.53	0.1460	0.1477	-0.0017	1.16
31.92	0.1630	0.1643	-0.0013	0.83
34.05	0.1710	0.1694	0.0016	0.95

SL : No. 7

1st loading _

SOLUTION

A=	11.57	SD =	0.4674	% =	4.040
B=	0.2661	SD =	0.007628	% =	2.867
C=	192.9	SD =	6.811	% =	3.531

COMPUTED RESIDUALS

SIGMA	DELTA(V) MEASURED	DELTA(V) CALCULATED	DIFF	% DIFF
0.2930	0.02500	0.02464	0.00036	1.44
0.8430	0.06600	0.06157	0.00643	9.46
1.210	0.08500	0.08134	0.00366	4.30
1.760	0.1100	0.1059	0.0041	3.72
2.676	0.1370	0.1376	-0.0006	0.44
3.593	0.1570	0.1618	-0.0049	3.14
5.426	0.1460	0.1479	-0.0019	0.96
7.305	0.2190	0.2251	-0.0061	2.77
9.092	0.2440	0.2459	-0.0019	0.78
10.92	0.2600	0.2642	-0.0042	1.63
14.59	0.2640	0.2654	-0.0014	0.47
18.26	0.3270	0.3224	0.0046	1.42
21.92	0.3520	0.3470	0.0050	1.42
25.59	0.3750	0.3702	0.0048	1.28
29.26	0.3960	0.3924	0.0036	0.90
32.92	0.4160	0.4140	0.0020	0.48
36.59	0.4350	0.4351	-0.0001	0.03
40.25	0.4560	0.4559	0.0001	0.02
44.01	0.4690	0.4769	-0.0079	1.68

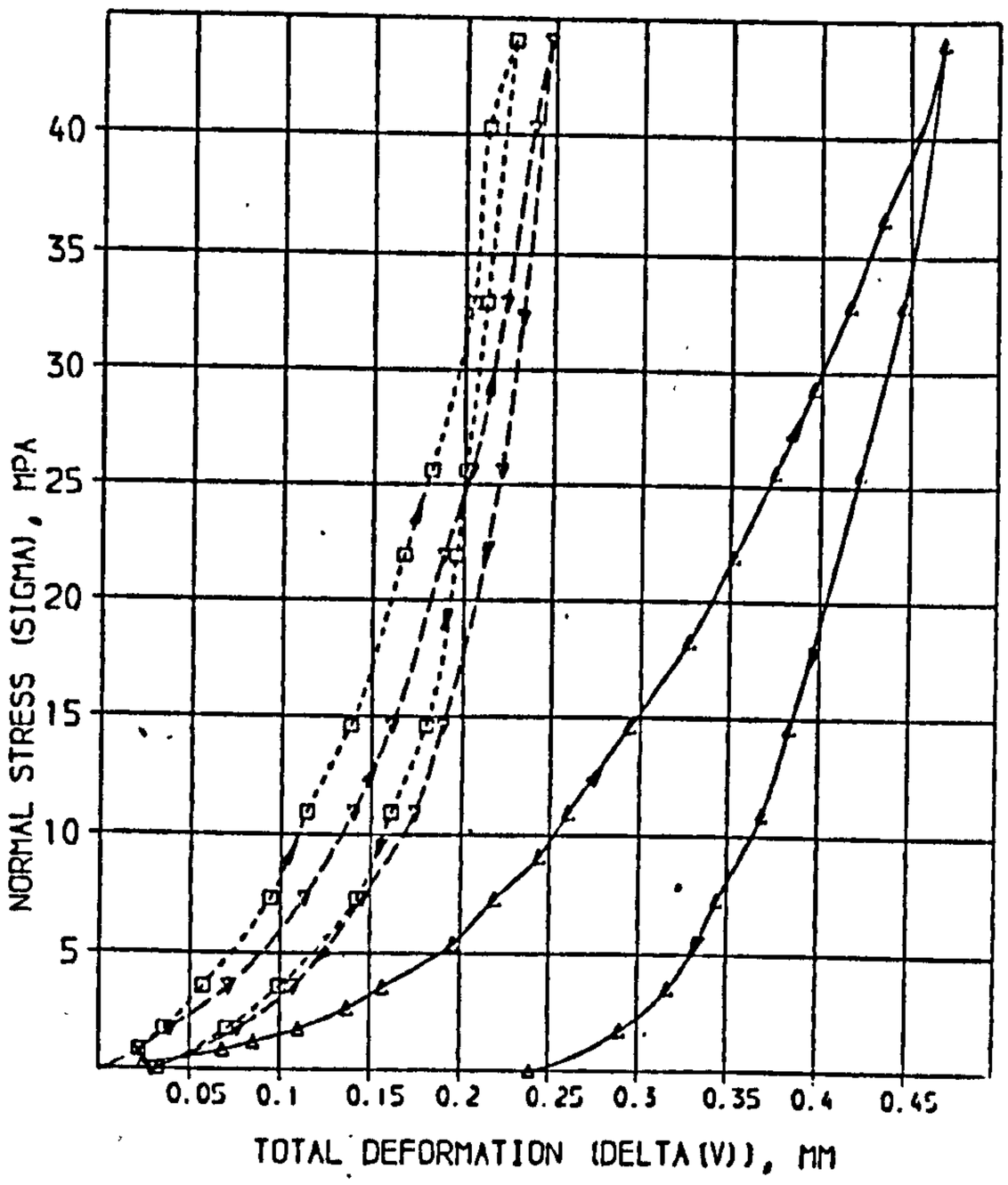

2nd loading _

SOLUTION

A=	38.67	SD =	0.6742	% =	1.743
B=	0.2275	SD =	0.006503	% =	2.884
C=	720.9	SD =	62.99	% =	8.170

COMPUTED RESIDUALS

SIGMA	DELTA(V) MEASURED	DELTA(V) CALCULATED	DIFF	% DIFF
0.8430	0.02200	0.02099	0.00101	4.60
1.760	0.03900	0.04041	-0.00141	3.10
3.590	0.07100	0.07059	0.00041	0.57
7.305	0.1130	0.1127	0.0003	0.27
10.92	0.1400	0.1406	-0.0006	0.12
14.59	0.1610	0.1609	0.0001	0.08
21.92	0.1900	0.1918	-0.0018	0.95
25.59	0.2040	0.2025	0.0015	0.73
32.92	0.2230	0.2223	0.0007	0.33
40.25	0.2330	0.2339	-0.0009	0.39
44.01	0.2470	0.2467	0.0003	0.11

3rd loading _

SOLUTION

A=	49.47	SD =	3.602	% =	7.282
B=	0.1849	SD =	0.02334	% =	12.62
C=	599.5	SD =	135.4	% =	22.25

COMPUTED RESIDUALS

SIGMA	DELTA(V) MEASURED	DELTA(V) CALCULATED	DIFF	% DIFF
0.8430	0.02200	0.01701	0.00499	22.69
1.760	0.03600	0.03277	0.00323	8.96
3.590	0.05700	0.05811	-0.00111	1.94
7.305	0.09400	0.09447	-0.00047	0.51
10.92	0.1140	0.1188	-0.0048	4.25
14.59	0.1330	0.1330	0.0000	0.00
21.92	0.1670	0.1670	-0.0000	0.02
25.59	0.1820	0.1789	0.0031	1.69
32.92	0.2040	0.1996	0.0044	2.14
40.25	0.2130	0.2178	-0.0048	2.26
44.01	0.2270	0.2265	0.0005	0.21

DOL: No. 1

1st loading -

SOLUTION

A=	26.72	SD =	0.6203	% =	2.321
B=	0.08913	SD =	0.001100	% =	1.233
C=	1080.	SD =	30.01	% =	2.778

COMPUTED RESIDUALS

SIGMA	DELTA(V) MEASURED	DELTA(V) CALCULATED	DIFF	% DIFF
0.4340	0.01400	0.01414	-0.00014	1.00
0.7500	0.02700	0.02630	0.00070	2.60
1.982	0.04300	0.04233	0.00067	1.56
3.014	0.05300	0.05259	0.00041	0.77
4.047	0.05900	0.05988	-0.00088	1.48
6.111	0.06100	0.06982	-0.00082	1.19
8.176	0.07500	0.07662	-0.00162	2.17
10.24	0.08200	0.08183	0.00017	0.21
14.37	0.09100	0.08980	0.00120	1.32
18.50	0.09700	0.09613	0.00087	0.90
22.63	0.1020	0.1016	0.0004	0.39
26.76	0.1070	0.1067	0.0003	0.32
30.89	0.1110	0.1114	-0.0004	0.35
35.02	0.1160	0.1159	0.0001	0.07
39.14	0.1200	0.1203	-0.0003	0.25
43.27	0.1240	0.1246	-0.0006	0.48
51.33	0.1330	0.1327	0.0003	0.19

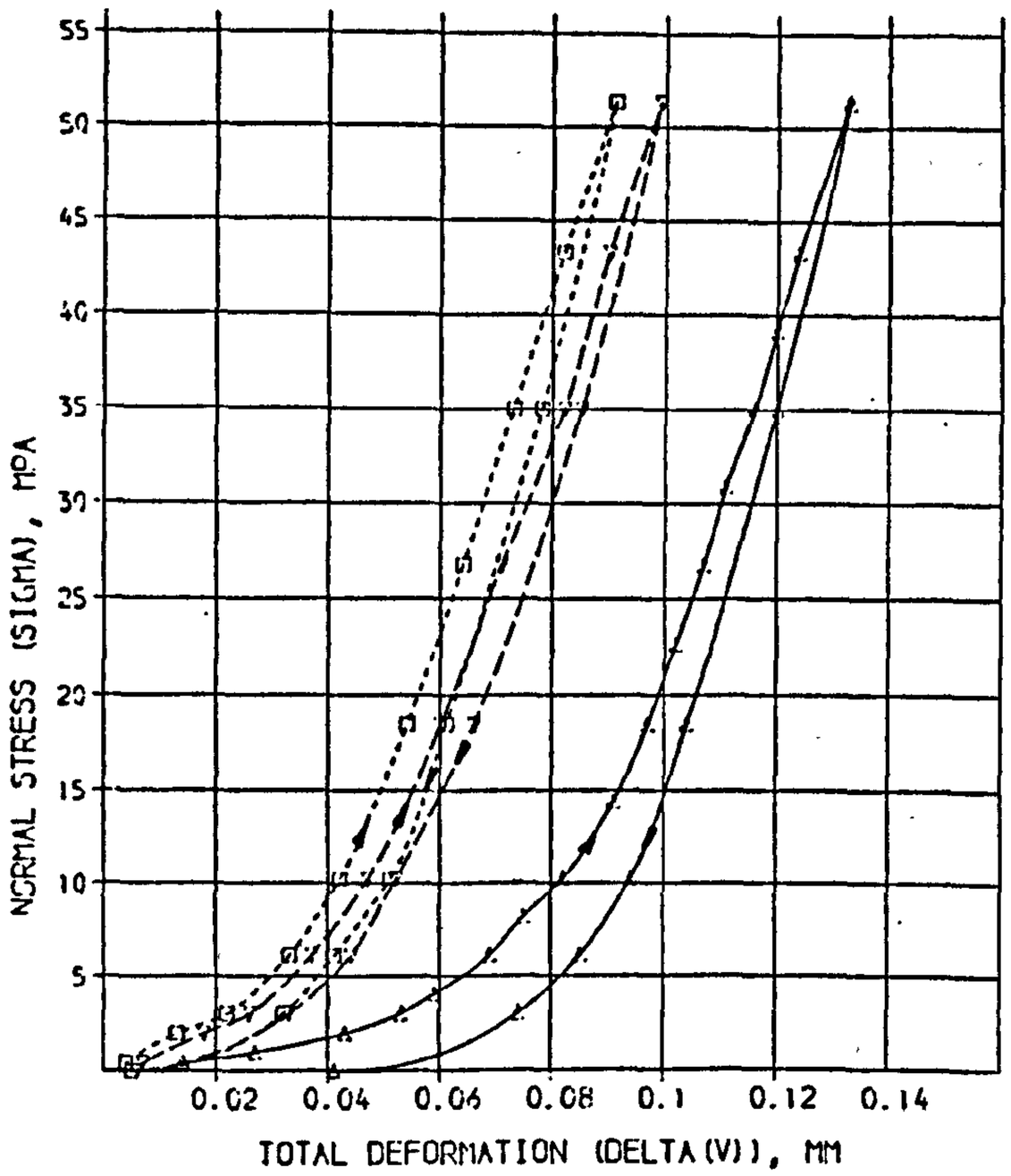

2nd loading -

SOLUTION

A=	75.31	SD =	4.474	% =	5.941
B=	0.04965	SD =	0.002186	% =	4.403
C=	969.6	SD =	40.53	% =	4.185

COMPUTED RESIDUALS

SIGMA	DELTA(V) MEASURED	DELTA(V) CALCULATED	DIFF	% DIFF
0.4340	0.007000	0.005611	0.001389	19.84
1.982	0.01300	0.01424	-0.00124	6.91
3.014	0.02600	0.02527	0.00073	2.82
6.111	0.03700	0.03710	-0.00010	0.28
10.24	0.04700	0.04693	0.00007	0.15
13.50	0.06000	0.06058	-0.00058	0.63
26.76	0.07100	0.07116	-0.00016	0.22
35.02	0.08200	0.08094	0.00106	1.25
43.27	0.09000	0.09054	-0.00054	0.36
51.33	0.09900	0.09921	-0.00021	0.22

3rd loading -

SOLUTION

A=	102.9	SD =	9.055	% =	8.781
B=	0.04711	SD =	0.003746	% =	7.950
C=	1087.	SD =	80.85	% =	7.440

COMPUTED RESIDUALS

SIGMA	DELTA(V) MEASURED	DELTA(V) CALCULATED	DIFF	% DIFF
0.4340	0.004000	0.004271	-0.000271	6.77
1.982	0.01300	0.01550	-0.00250	19.20
3.014	0.02200	0.02083	0.00117	5.30
6.111	0.03300	0.03189	0.00111	3.35
10.24	0.04200	0.04139	0.00061	1.44
13.50	0.05400	0.05435	-0.00035	0.65
26.76	0.06400	0.06451	-0.00051	0.79
35.02	0.07300	0.07360	-0.00060	0.83
43.27	0.08200	0.08218	-0.00018	0.21
51.33	0.09100	0.09027	0.00073	0.80

DOL.: No. 2

1st loading

SOLUTION

A=	21.69	SD =	0.9589	% =	4.411
B=	0.1216	SD =	0.003081	% =	2.534
C=	553.3	SD =	21.65	% =	3.913

COMPUTED RESIDUALS

SIGMA	DELTA(V) MEASURED	DELTA(V) CALCULATED	DIFF	% DIFF
0.4610	0.02300	0.01892	0.00408	17.72
0.9640	0.03700	0.03429	0.00271	7.33
1.488	0.04400	0.04654	0.00246	5.01
2.012	0.05700	0.05625	0.00075	1.31
3.059	0.07000	0.07082	-0.00082	1.17
4.107	0.07500	0.08146	-0.00246	3.12
5.155	0.08700	0.08975	-0.00275	3.10
6.203	0.09300	0.09652	-0.00352	3.79
8.298	0.1040	0.1073	-0.0033	3.13
10.39	0.1150	0.1153	-0.0008	0.66
12.49	0.1250	0.1230	0.0020	1.63
14.58	0.1310	0.1293	0.0017	1.28
16.68	0.1370	0.1351	0.0019	1.36
20.87	0.1480	0.1457	0.0023	1.58
25.06	0.1570	0.1553	0.0017	1.08
29.25	0.1660	0.1644	0.0016	0.96
33.44	0.1740	0.1731	0.0009	0.49
37.63	0.1800	0.1816	-0.0016	0.91
41.83	0.1890	0.1900	-0.0010	0.51
46.02	0.1980	0.1982	-0.0002	0.08
50.21	0.2050	0.2063	-0.0013	0.62

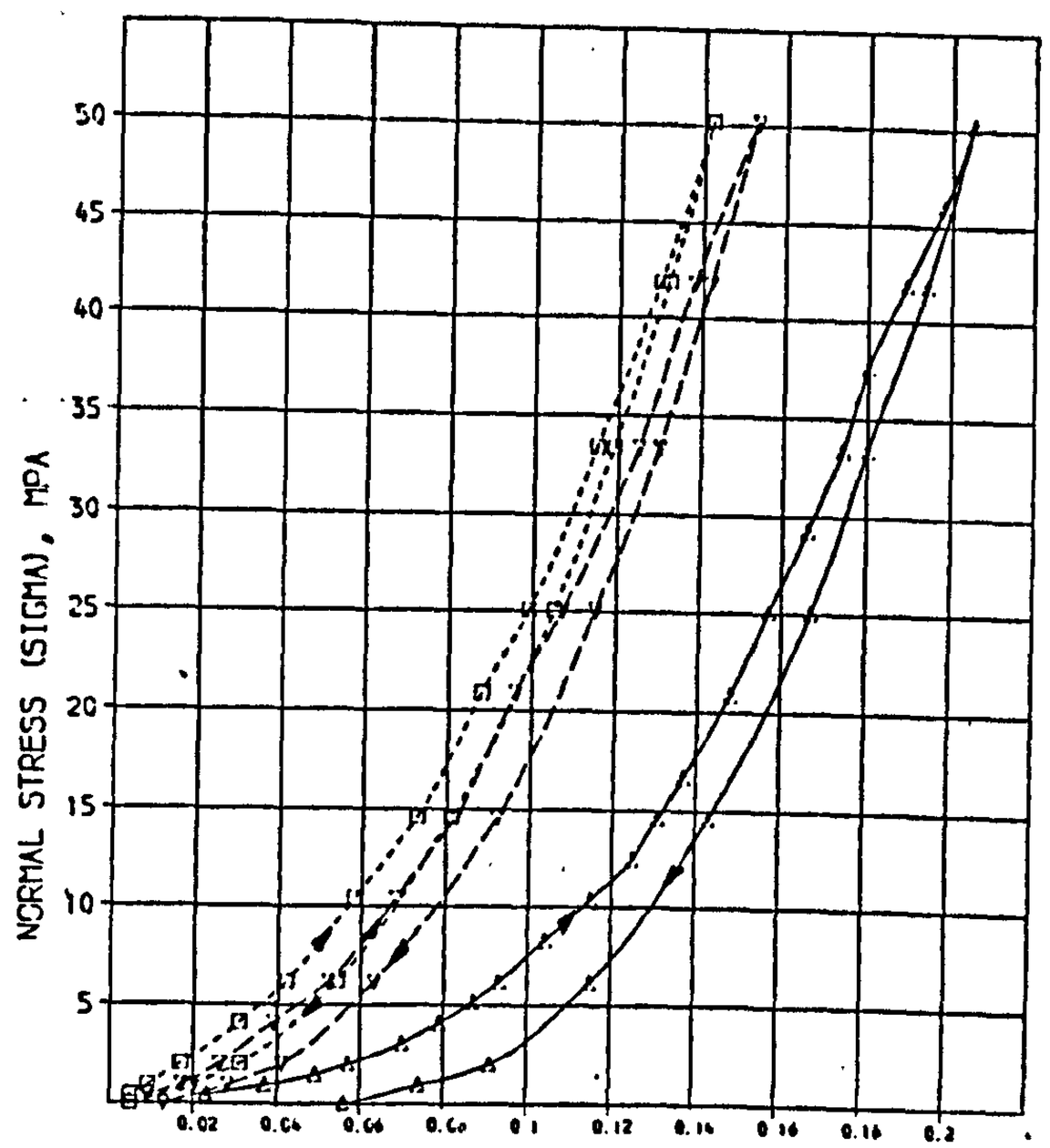

2nd loading

SOLUTION

A=	58.98	SD =	10.07	% =	17.07
B=	0.06558	SD =	0.008202	% =	12.60
C=	535.8	SD =	48.63	% =	9.077

COMPUTED RESIDUALS

SIGMA	DELTA(V) MEASURED	DELTA(V) CALCULATED	DIFF	% DIFF
0.4610	0.009000	0.007844	0.001156	12.84
0.9640	0.01700	0.01488	0.00212	12.45
2.012	0.02600	0.02620	-0.00020	0.75
4.107	0.03900	0.04144	-0.00244	6.25
6.203	0.05200	0.05197	0.00003	0.06
10.39	0.06300	0.06714	0.00086	1.21
14.58	0.08200	0.07904	0.00296	3.61
20.87	0.08600	0.09428	-0.00828	9.62
25.06	0.1070	0.1056	0.0054	5.20
33.44	0.1250	0.1212	0.0038	3.05
41.83	0.1380	0.1381	-0.0001	0.07
50.21	0.1530	0.1546	-0.0016	1.05

3rd loading

SOLUTION

A=	119.4	SD =	2.995	% =	2.509
B=	0.09727	SD =	0.005153	% =	5.277
C=	787.6	SD =	43.59	% =	5.534

COMPUTED RESIDUALS

SIGMA	DELTA(V) MEASURED	DELTA(V) CALCULATED	DIFF	% DIFF
0.4610	0.005000	0.004299	0.000701	14.01
0.9640	0.009000	0.008680	0.000320	3.56
2.012	0.01700	0.01692	0.00008	0.48
4.107	0.03100	0.03063	0.00037	1.20
6.203	0.04200	0.04174	0.00026	0.61
10.39	0.05800	0.05912	-0.00112	1.94
14.58	0.07300	0.07266	0.00034	0.47
20.87	0.08800	0.08899	-0.00099	1.13
25.06	0.09900	0.09829	0.00071	0.72
33.44	0.1150	0.1147	0.0003	0.30
41.83	0.1300	0.1292	0.0008	0.58
50.21	0.1420	0.1427	-0.0007	0.53

DOL : No. 3

1st loading

SOLUTION

A=	13,29	SD =	0,1991	% =	1,499
B=	0,5760	SD =	0,01392	% =	2,417
C=	562,1	SD =	78,02	% =	13,99

COMPUTED RESIDUALS

SIGMA	DELTA(V) MEASURED	DELTA(V) CALCULATED	DIFF	% DIFF
0,3630	0,02500	0,02673	-0,00173	6,91
0,9800	0,06300	0,06712	0,00088	1,29
1,814	0,1150	0,1137	0,0013	1,14
2,542	0,1520	0,1481	0,0039	2,54
3,632	0,1900	0,1918	-0,0018	0,97
4,540	0,2240	0,2225	0,0015	0,65
5,448	0,2500	0,2492	0,0008	0,31
7,264	0,2890	0,2934	-0,0044	1,53
9,081	0,3270	0,3287	-0,0017	0,53
10,90	0,3550	0,3578	-0,0028	0,78
12,71	0,3340	0,3322	0,0018	0,48
14,40	0,4040	0,4027	0,0013	0,32
16,16	0,4350	0,4376	-0,0026	0,59
20,30	0,4670	0,4580	0,0090	1,92
25,43	0,4840	0,4880	-0,0040	0,82
29,16	0,5050	0,5076	-0,0026	0,52
32,60	0,5250	0,5249	0,0001	0,02
36,32	0,5420	0,5404	0,0016	0,29
39,05	0,5550	0,5511	0,0039	0,70
43,59	0,5640	0,5675	-0,0035	0,63

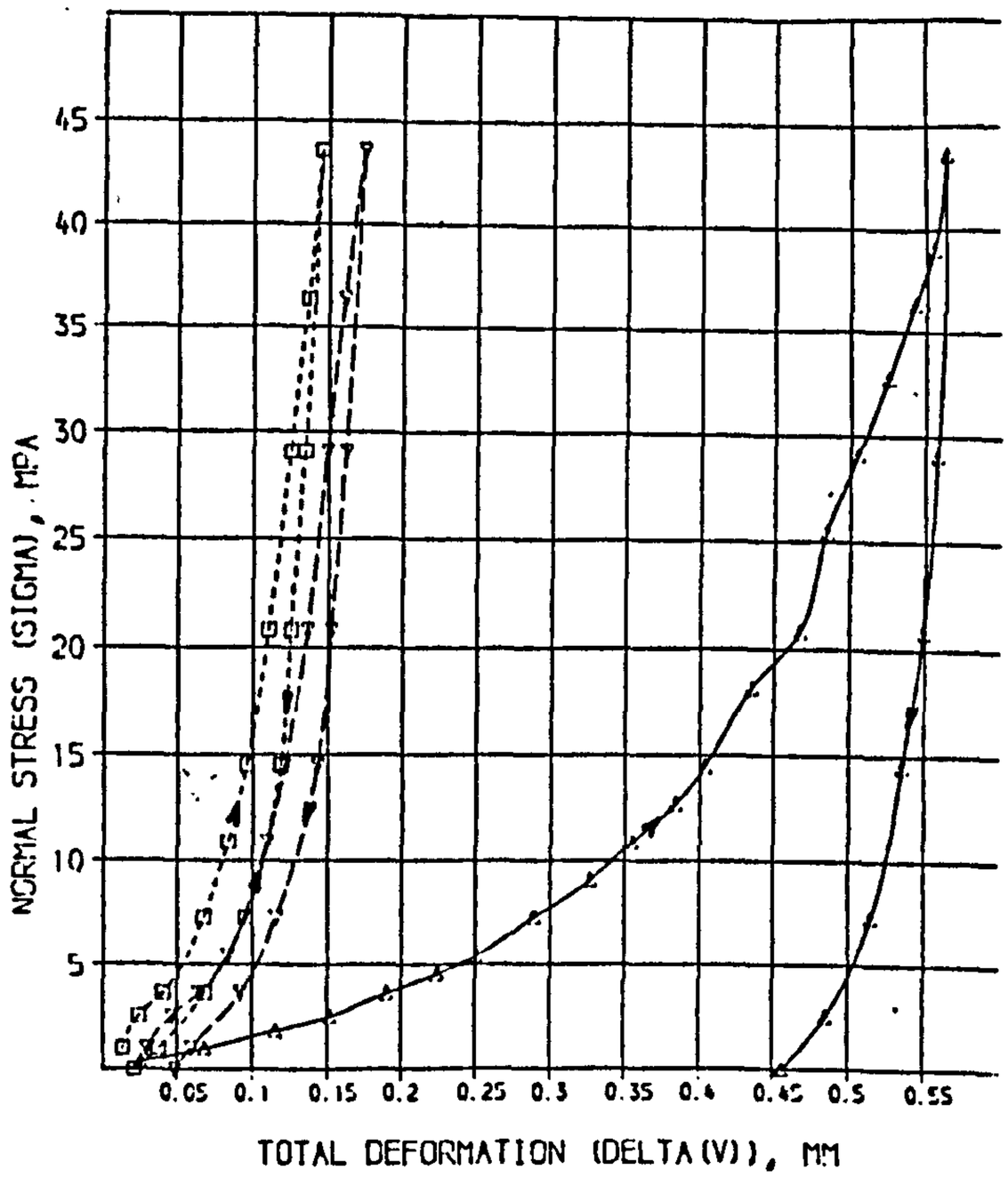

2nd loading

SOLUTION

A=	33,72	SD =	2,244	% =	6,653
B=	0,1307	SD =	0,009535	% =	6,684
C=	651,4	SD =	175,7	% =	18,47

COMPUTED RESIDUALS

SIGMA	DELTA(V) MEASURED	DELTA(V) CALCULATED	DIFF	% DIFF
0,0800	0,02900	0,02508	0,00392	13,50
2,542	0,04000	0,05103	-0,00563	12,23
3,632	0,06400	0,06466	-0,00066	0,98
5,448	0,08300	0,08043	0,00257	2,85
7,264	0,09400	0,09236	0,00164	1,74
10,90	0,1090	0,1090	0,0000	0,03
14,53	0,1210	0,1207	0,0003	0,21
20,79	0,1360	0,1357	0,0003	0,20
29,06	0,1490	0,1507	-0,0017	1,16
36,32	0,1610	0,1614	-0,0018	1,13
43,59	0,1740	0,1719	0,0021	1,23

3rd loading

SOLUTION

A=	73,20	SD =	4,029	% =	5,504
B=	0,0947	SD =	0,00146	% =	15,42
C=	810	SD =	62,99	% =	7,78

COMPUTED RESIDUALS

SIGMA	DELTA(V) MEASURED	DELTA(V) CALCULATED	DIFF	% DIFF
0,0800	0,01300	0,01272	0,00028	2,12
2,542	0,02400	0,02955	-0,00555	23,13
3,632	0,04000	0,03950	0,00064	1,59
7,264	0,06700	0,06455	0,00265	3,95
10,90	0,08300	0,08182	0,00118	1,42
14,53	0,09600	0,09485	0,00115	1,20
21,79	0,1100	0,1114	-0,0014	1,10
29,06	0,1240	0,1262	-0,0022	1,77
36,32	0,1360	0,1360	0,0000	0,03
43,58	0,1450	0,1434	0,0016	0,80

DOL : No. 4

1st loading

SOLUTION

A=	10.96	SD =	0.2391	% =	2.181
B=	0.3281	SD =	0.004582	% =	1.397
C=	509.1	SD =	28.57	% =	4.768

COMPUTED RESIDUALS

SIGMA	DELTA(V) MEASURED	DELTA(V) CALCULATED	DIFF	% DIFF
0.6040	0.02200	0.02773	-0.00573	26.03
1.207	0.05300	0.05136	0.00161	3.03
1.811	0.07200	0.07192	0.00008	0.11
2.414	0.09100	0.08987	0.00113	1.24
3.017	0.1050	0.1057	-0.0007	0.70
4.526	0.1410	0.1385	0.0025	1.76
6.035	0.1640	0.1642	-0.0002	0.12
7.544	0.1840	0.1850	-0.0010	0.54
9.053	0.2030	0.2023	0.0007	0.33
10.56	0.2170	0.2171	-0.0001	0.03
12.07	0.2290	0.2299	-0.0009	0.38
13.58	0.2400	0.2411	-0.0011	0.48
15.08	0.2500	0.2512	-0.0012	0.49
18.10	0.2700	0.2686	0.0014	0.51
21.12	0.2830	0.2833	-0.0003	0.12
24.14	0.2970	0.2962	0.0008	0.28
27.16	0.3080	0.3076	0.0004	0.12
30.17	0.3180	0.3180	-0.0000	0.01
33.19	0.3280	0.3276	0.0004	0.11
36.21	0.3370	0.3366	0.0004	0.12
39.23	0.3450	0.3450	-0.0000	0.01
42.24	0.3520	0.3530	-0.0010	0.30
45.26	0.3610	0.3607	0.0003	0.08
48.28	0.3680	0.3681	-0.0001	0.03

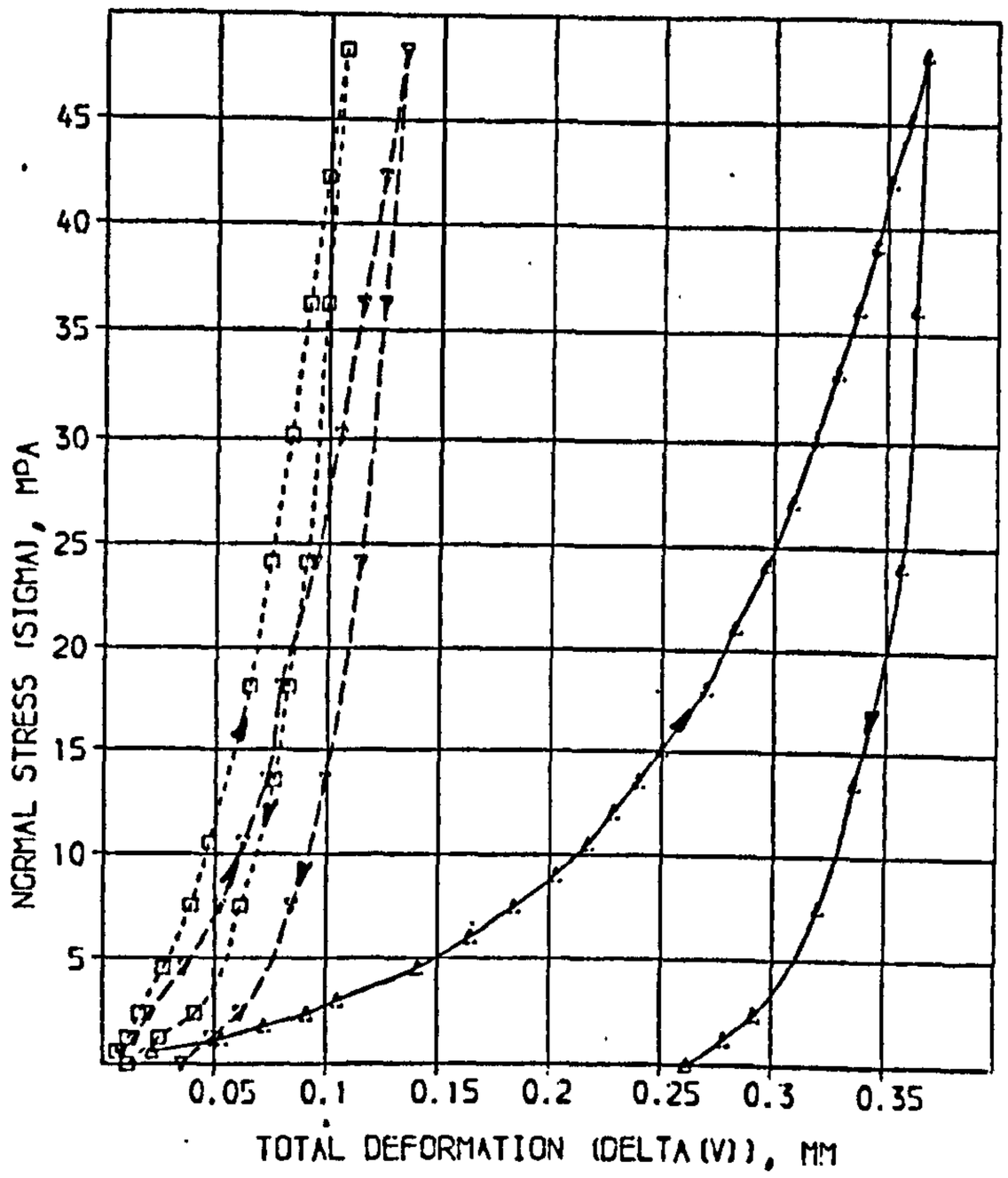

2nd loading

SOLUTION

A=	91.53	SD =	5.310	% =	5.807
B=	0.08213	SD =	0.006303	% =	7.670
C=	768.7	SD =	61.53	% =	8.005

COMPUTED RESIDUALS

SIGMA	DELTA(V) MEASURED	DELTA(V) CALCULATED	DIFF	% DIFF
0.6040	0.008300	0.006894	0.001106	15.83
1.207	0.01400	0.01293	0.00107	7.62
2.414	0.02100	0.02311	-0.00211	10.03
4.526	0.03600	0.03678	-0.00078	2.11
7.544	0.05200	0.05096	0.00104	2.00
11.56	0.06200	0.06173	0.00027	0.44
15.58	0.07300	0.07055	0.00245	3.36
18.10	0.07900	0.08100	-0.00200	3.29
24.14	0.09400	0.09406	-0.00006	0.06
30.17	0.1050	0.1050	-0.0000	0.02
36.21	0.1150	0.1151	-0.0001	0.13
42.24	0.1250	0.1247	0.0003	0.24
48.28	0.1340	0.1339	0.0001	0.07

3rd loading

SOLUTION

A=	130.4	SD =	5.643	% =	4.317
B=	0.06683	SD =	0.004619	% =	6.902
C=	964.2	SD =	67.30	% =	6.980

COMPUTED RESIDUALS

SIGMA	DELTA(V) MEASURED	DELTA(V) CALCULATED	DIFF	% DIFF
0.6040	0.006000	0.004959	0.001041	17.35
1.207	0.01100	0.00950	0.00162	14.69
2.414	0.01600	0.01700	-0.00100	6.27
4.526	0.02700	0.02754	-0.00054	2.00
7.544	0.03900	0.03883	0.00017	0.43
11.56	0.04700	0.04756	-0.00056	1.20
17.10	0.06500	0.06387	0.00113	1.73
24.14	0.07400	0.07413	-0.00013	0.17
31.17	0.08300	0.08313	-0.00013	0.15
38.21	0.09100	0.09140	-0.00040	0.44
42.24	0.09900	0.09919	-0.00019	0.19
48.28	0.1070	0.1067	0.0003	0.31

DOL : No 5

1st loading

SOLUTION

A=	7,056	SD =	0,2504	% =	3,660
B=	0,3073	SD =	0,007295	% =	2,370
C=	133,3	SD =	4,295	% =	3,223

COMPUTED RESIDUALS

SIGMA	DELTA(V) MEASURED	DELTA(V) CALCULATED	DIFF	% DIFF
0,5300	0,06600	0,06494	0,00106	2,52
0,7950	0,09500	0,08842	0,00658	6,93
1,325	0,1310	0,1263	0,0045	3,40
1,855	0,1590	0,1557	0,0023	1,47
2,651	0,1850	0,1890	-0,0040	2,19
3,976	0,2230	0,2269	-0,0039	2,63
5,301	0,2540	0,2581	-0,0041	1,61
6,626	0,2750	0,2815	-0,0065	2,37
7,952	0,2990	0,3014	-0,0024	0,81
9,277	0,3180	0,3190	-0,0010	0,31
10,60	0,3370	0,3330	0,0040	0,59
11,25	0,3690	0,3639	0,0051	1,38
15,90	0,3940	0,3901	0,0039	0,98
18,55	0,4190	0,4146	0,0044	1,01
21,20	0,4430	0,4383	0,0047	1,06
23,85	0,4040	0,4011	0,0029	0,62
26,50	0,4321	0,4334	-0,0014	0,28
29,16	0,5040	0,5052	-0,0012	0,25
33,13	0,5310	0,5373	-0,0063	1,22

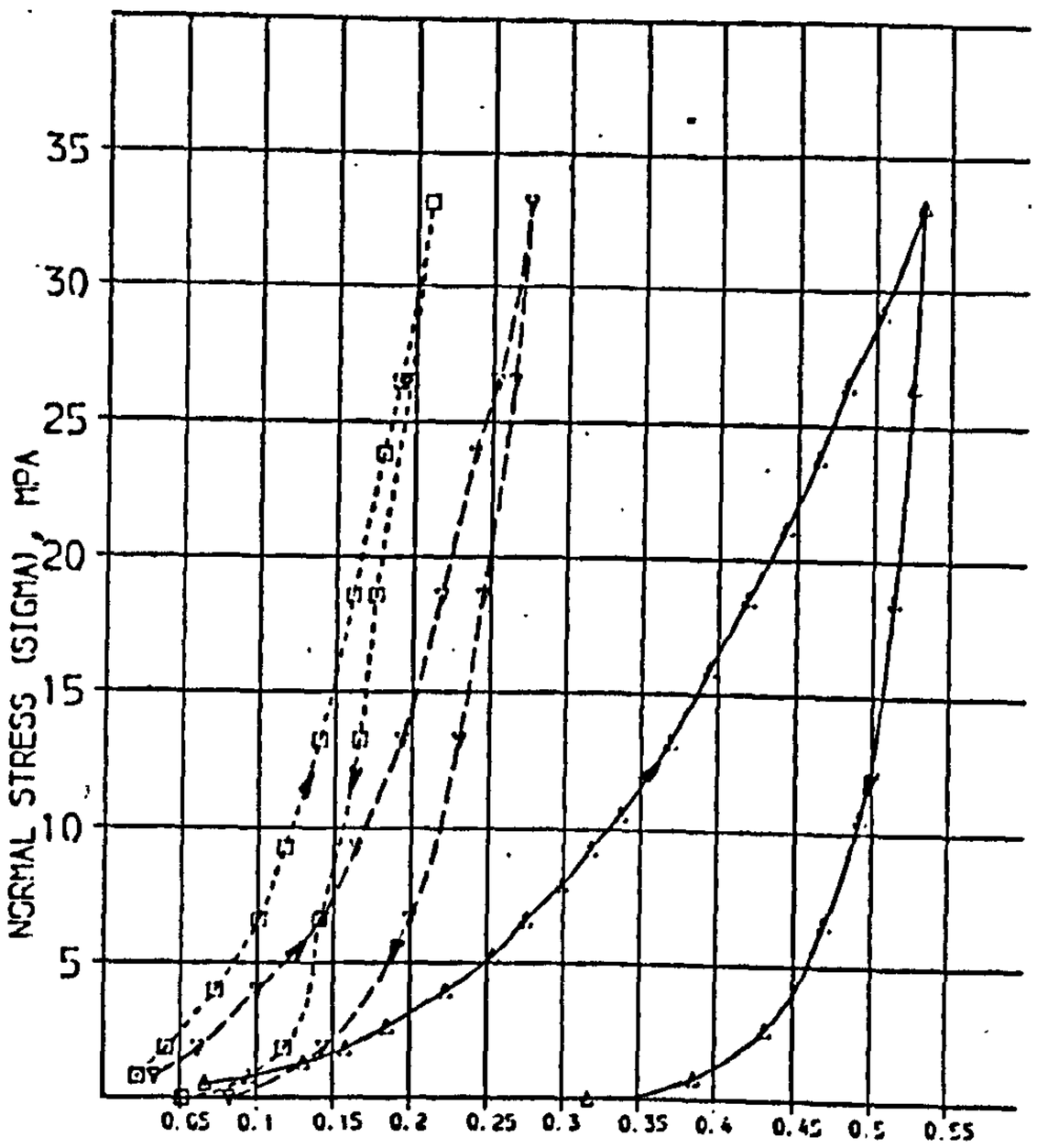

2nd loading

SOLUTION

A=	24,73	SD =	0,9651	% =	3,895
B=	0,2300	SD =	0,01298	% =	5,643
C=	430,8	SD =	55,79	% =	12,95

COMPUTED RESIDUALS

SIGMA	DELTA(V) MEASURED	DELTA(V) CALCULATED	DIFF	% DIFF
0,7950	0,03300	0,03005	0,00295	8,93
1,855	0,06100	0,06087	0,00013	0,21
3,976	0,1000	0,1059	-0,0059	5,86
6,626	0,1420	0,1397	0,0023	1,63
9,277	0,1640	0,1641	-0,0001	0,07
13,25	0,1930	0,1917	0,0013	0,68
19,55	0,2180	0,2191	-0,0011	0,50
23,85	0,2300	0,2411	-0,0041	0,87
26,50	0,2570	0,2509	0,0021	0,84
33,13	0,2730	0,2732	-0,0002	0,07

3rd loading

SOLUTION

A=	37,48	SD =	1,257	% =	3,355
B=	0,1601	SD =	0,008241	% =	5,172
C=	452,1	SD =	38,41	% =	8,497

COMPUTED RESIDUALS

SIGMA	DELTA(V) MEASURED	DELTA(V) CALCULATED	DIFF	% DIFF
0,7950	0,02200	0,02049	0,00151	6,86
1,855	0,04000	0,04191	-0,00191	4,78
3,976	0,07200	0,07261	-0,00061	0,85
6,626	0,1010	0,0987	0,0023	2,29
9,277	0,1170	0,1176	-0,0006	0,64
13,25	0,1400	0,1395	0,0005	0,33
19,55	0,1610	0,1620	-0,0010	0,64
23,85	0,1800	0,1807	-0,0007	0,39
26,50	0,1900	0,1892	0,0008	0,43
33,13	0,2070	0,2069	0,0001	0,07

LMST : No. 1

1st loading_

SOLUTION

A=	21.63	SD =	1.005	% =	8.636
B=	0.07409	SD =	0.002122	% =	2.864
C=	1099.	SD =	73.91	% =	6.727

COMPUTED RESIDUALS

SIGMA	DELTA(V) MEASURED	DELTA(V) CALCULATED	DIFF	% DIFF
0.4090	0.02870	0.02422	0.00448	15.63
0.9200	0.04010	0.03906	0.00101	2.52
1.431	0.04640	0.04754	-0.00114	2.46
1.941	0.05190	0.05307	-0.00117	2.26
2.962	0.05840	0.06009	-0.00169	2.89
3.984	0.06270	0.06454	-0.00184	2.93
5.005	0.06560	0.06776	-0.00216	3.29
6.027	0.06750	0.07031	-0.00281	4.16
10.09	0.07640	0.07744	0.00196	2.47
15.56	0.08610	0.08437	0.00373	4.24
20.30	0.09170	0.08955	0.00215	2.34
25.41	0.09640	0.09479	0.00161	1.67
30.52	0.1007	0.0998	0.0009	0.86
36.65	0.1058	0.1057	0.0001	0.05
42.78	0.1097	0.1116	-0.0019	1.70
50.76	0.1177	0.1191	-0.0014	1.18

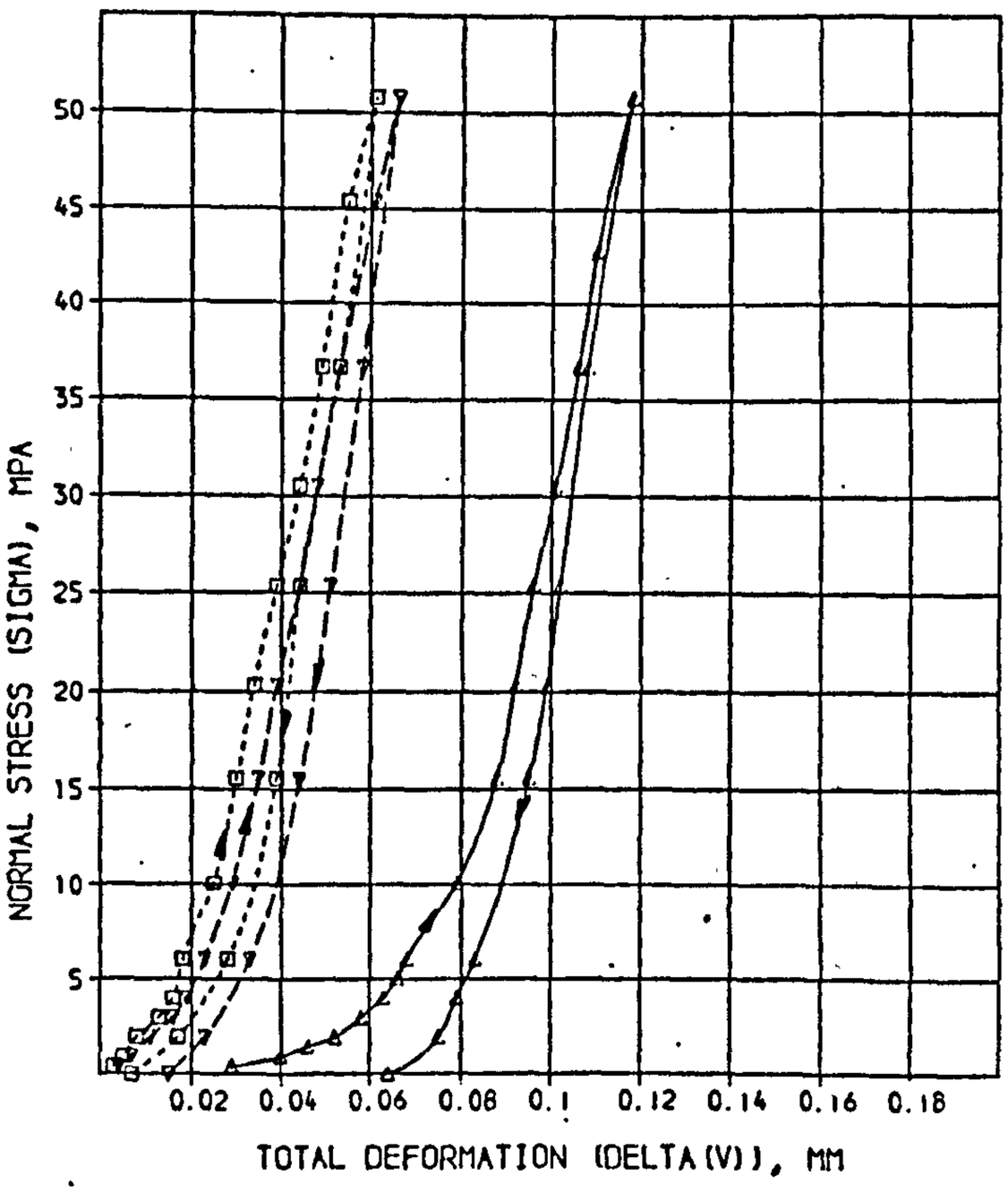

2nd loading_

SOLUTION

A=	133.5	SD =	44.91	% =	18.67
B=	0.02719	SD =	0.003799	% =	13.97
C=	1265.	SD =	120.4	% =	9.989

COMPUTED RESIDUALS

SIGMA	DELTA(V) MEASURED	DELTA(V) CALCULATED	DIFF	% DIFF
0.4090	0.004100	0.003077	0.001023	24.95
0.9200	0.007000	0.006226	0.000774	11.06
1.941	0.01150	0.01101	0.00049	4.28
2.960	0.01650	0.01455	0.00195	11.80
3.984	0.01200	0.01758	-0.00558	44.80
6.027	0.02300	0.02173	0.00127	5.51
10.09	0.02900	0.02797	0.00103	3.55
15.56	0.03500	0.03454	0.00066	1.88
20.30	0.03900	0.03911	-0.00011	0.27
25.41	0.04400	0.04387	0.00013	0.30
30.52	0.04900	0.04942	-0.00042	0.87
36.65	0.05300	0.05370	-0.00070	1.32
45.40	0.06100	0.06105	-0.00005	0.09
51.79	0.06600	0.06551	0.00049	0.74

3rd loading_

SOLUTION

A=	159.5	SD =	15.07	% =	9.821
B=	0.02230	SD =	0.001618	% =	7.254
C=	1289.	SD =	56.14	% =	4.356

COMPUTED RESIDUALS

SIGMA	DELTA(V) MEASURED	DELTA(V) CALCULATED	DIFF	% DIFF
0.4090	0.003200	0.004617	0.000565	18.23
0.9200	0.004500	0.005296	-0.000796	17.68
1.941	0.008000	0.009378	-0.001378	17.22
2.960	0.01300	0.01244	0.00056	4.43
3.984	0.01600	0.01487	0.00113	7.05
6.027	0.01850	0.01870	-0.00020	1.08
10.09	0.02500	0.02432	0.00068	2.74
15.56	0.03000	0.03022	-0.00022	0.74
20.30	0.03400	0.03475	-0.00075	2.13
25.41	0.03900	0.03928	-0.00028	0.71
30.52	0.04400	0.04365	0.00035	0.79
36.65	0.04900	0.04876	0.00024	0.48
45.40	0.05500	0.05590	-0.00090	1.64
51.79	0.06100	0.06025	0.00075	1.23

LMST : No. 2

1st loading

SOLUTION

A=	30.57	SD =	1.708	% =	5.586
B=	0.09870	SD =	0.003446	% =	3.492
C=	502.5	SD =	20.21	% =	4.021

COMPUTED RESIDUALS

SIGMA	DELTA(V) MEASURED	DELTA(V) CALCULATED	DIFF	% DIFF
0.3730	0.01270	0.01160	0.00110	8.64
0.6400	0.02580	0.02317	0.00263	10.20
1.775	0.04220	0.04005	0.00211	4.99
2.708	0.05290	0.05208	0.00082	1.56
3.643	0.06070	0.06124	-0.00054	0.89
5.510	0.07150	0.07474	-0.00324	4.54
7.375	0.08020	0.08474	-0.00454	5.66
9.247	0.09140	0.09282	-0.00142	1.56
11.11	0.1005	0.0997	0.0008	0.75
12.98	0.1068	0.1059	0.0009	0.82
14.85	0.1124	0.1116	0.0008	0.72
16.59	0.1234	0.1219	0.0015	1.21
23.20	0.1357	0.1336	0.0021	1.51
27.93	0.1469	0.1446	0.0023	1.53
32.60	0.1557	0.1552	0.0005	0.32
37.27	0.1654	0.1655	-0.0001	0.04
41.94	0.1739	0.1755	-0.0016	0.93
46.51	0.1840	0.1852	-0.0012	0.68

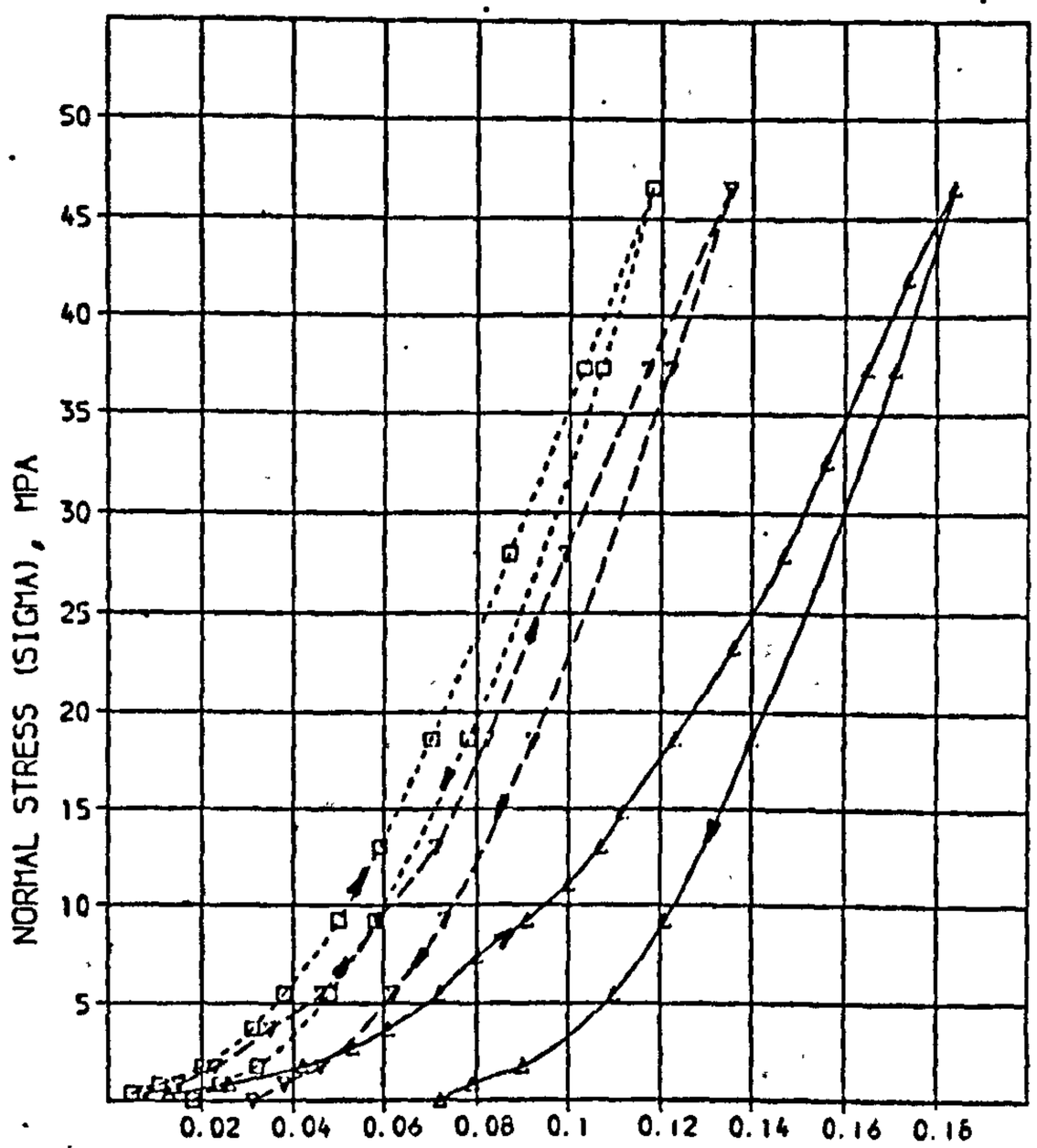

2nd loading

SOLUTION

A=	56.53	SD =	4.286	% =	7.586
B=	0.05365	SD =	0.003209	% =	5.870
C=	584.5	SD =	24.57	% =	4.204

COMPUTED RESIDUALS

SIGMA	DELTA(V) MEASURED	DELTA(V) CALCULATED	DIFF	% DIFF
0.3730	0.008200	0.006684	0.001516	18.49
0.7400	0.01510	0.01330	0.00180	11.34
1.775	0.02320	0.02350	-0.00030	1.27
3.643	0.03500	0.03695	-0.00195	5.56
5.510	0.04550	0.04605	-0.00055	1.22
9.247	0.05900	0.05900	0.00000	0.00
12.98	0.07100	0.06893	0.00207	2.91
13.59	0.08200	0.08156	0.00044	0.51
27.93	0.09900	0.10022	-0.00122	1.23
37.27	0.1170	0.1176	-0.0006	0.54
46.51	0.1350	0.1343	0.0007	0.50

3rd loading

SOLUTION

A=	72.17	SD =	1.578	% =	2.186
B=	0.04361	SD =	0.000714	% =	1.643
C=	638.8	SD =	7.142	% =	1.124

COMPUTED RESIDUALS

SIGMA	DELTA(V) MEASURED	DELTA(V) CALCULATED	DIFF	% DIFF
0.3800	0.004800	0.005340	-0.000540	11.37
0.7400	0.01060	0.01071	-0.00011	1.00
1.775	0.01950	0.01911	0.00039	1.99
3.646	0.03050	0.03044	0.00006	0.06
5.510	0.03820	0.03833	-0.00013	0.33
9.247	0.04950	0.04972	-0.00022	0.44
12.98	0.05900	0.05859	0.00041	0.70
13.59	0.07000	0.07000	0.00000	0.01
27.93	0.08650	0.08691	-0.00041	0.47
37.27	0.1030	0.1026	0.0002	0.22
46.51	0.1190	0.1180	-0.0000	0.01

LMST: No.3

1st loading

SOLUTION

A=	10.98	SD =	0.7491	% =	6.821
B=	0.1098	SD =	0.002983	% =	2.716
C=	438.6	SD =	17.38	% =	3.963

COMPUTED RESIDUALS

SIGMA	DELTA(V) MEASURED	DELTA(V) CALCULATED	DIFF	% DIFF
0.3930	0.03400	0.02786	0.00611	17.98
0.8420	0.04100	0.04707	0.00193	3.94
1.305	0.06000	0.06014	-0.00014	0.24
1.777	0.06800	0.06947	-0.00147	2.17
2.712	0.07800	0.08220	-0.00320	4.05
3.648	0.08600	0.08885	-0.00285	3.24
5.516	0.1010	0.1027	-0.0017	1.69
7.388	0.1090	0.1113	-0.0023	2.07
9.256	0.1190	0.1183	0.0007	0.61
11.12	0.1270	0.1244	0.0026	2.02
14.87	0.1330	0.1355	-0.0025	1.87
18.61	0.1500	0.1456	0.0044	2.95
23.29	0.1610	0.1575	0.0035	2.16
27.96	0.1710	0.1690	0.0020	1.14
33.57	0.1830	0.1826	0.0004	0.23
39.19	0.1950	0.1959	-0.0009	0.46
46.57	0.2100	0.2133	-0.0033	1.55

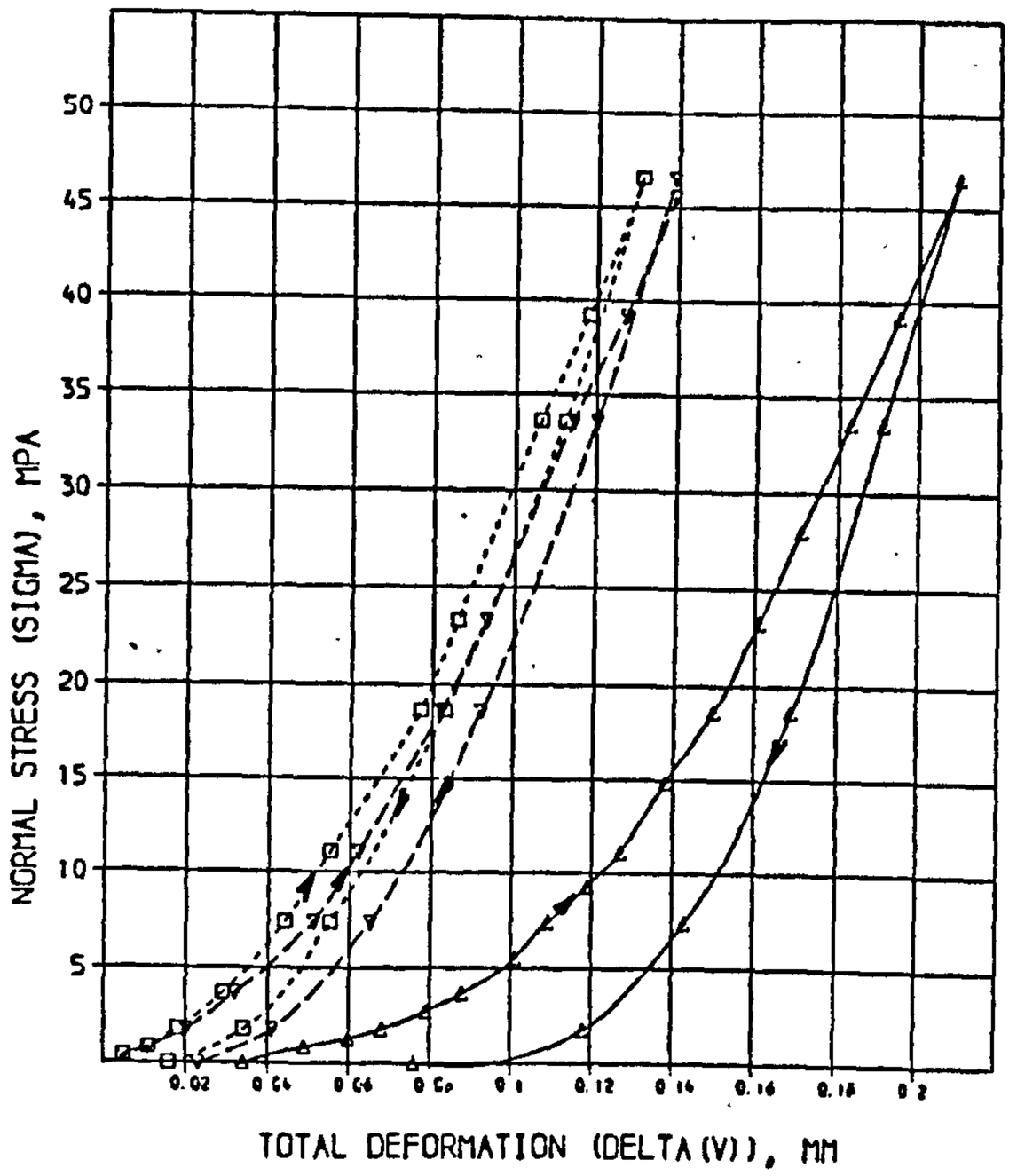

2nd loading

SOLUTION

A=	75.73	SD =	4.854	% =	6.405
B=	0.05837	SD =	0.003342	% =	5.727
C=	533.9	SD =	19.42	% =	3.653

COMPUTED RESIDUALS

SIGMA	DELTA(V) MEASURED	DELTA(V) CALCULATED	DIFF	% DIFF
0.3930	0.005000	0.005502	-0.000502	10.05
0.8420	0.01130	0.01092	0.00038	3.33
1.777	0.02000	0.02010	-0.00010	0.49
3.648	0.03200	0.03356	-0.00156	4.11
7.388	0.05300	0.05054	0.00246	4.64
11.12	0.06200	0.06284	-0.00084	1.36
18.61	0.08200	0.08234	-0.00034	0.42
23.29	0.09300	0.09303	-0.00003	0.03
33.57	0.1140	0.1148	-0.0008	0.74
39.19	0.1270	0.1265	0.0007	0.59
45.56	0.1390	0.1390	0.0000	0.03

3rd loading

SOLUTION

A=	90.23	SD =	6.406	% =	7.100
B=	0.05103	SD =	0.003251	% =	6.364
C=	545.6	SD =	19.36	% =	3.549

COMPUTED RESIDUALS

SIGMA	DELTA(V) MEASURED	DELTA(V) CALCULATED	DIFF	% DIFF
0.3930	0.004700	0.004754	-0.000054	0.71
0.8420	0.01100	0.00943	0.00157	14.24
1.777	0.01300	0.01247	0.00053	2.94
3.648	0.02900	0.02945	-0.00045	0.88
7.388	0.04400	0.04500	-0.00100	2.27
11.12	0.05500	0.05650	-0.00150	2.72
18.61	0.07650	0.07505	0.00145	1.89
23.29	0.08600	0.08533	0.00067	0.77
33.57	0.1065	0.1064	0.0001	0.05
39.19	0.1180	0.1175	0.0005	0.39
46.57	0.1310	0.1310	-0.0008	0.64

LMST : No. 4

1st loading

SOLUTION

A=	25.27	SD =	0.7408	% =	2.967
B=	0.08275	SD =	0.001147	% =	1.386
C=	403.1	SD =	6.539	% =	1.326

COMPUTED RESIDUALS

SIGMA	DELTA(V) MEASURED	DELTA(V) CALCULATED	DIFF	% DIF
0.4766	0.01580	0.01631	-0.00051	3.22
1.567	0.03970	0.03863	0.00107	2.71
2.578	0.05210	0.05092	0.00118	2.27
3.608	0.06020	0.05970	0.00050	0.82
4.639	0.06550	0.06645	-0.00095	1.44
5.669	0.07090	0.07195	-0.00105	1.48
6.700	0.07560	0.07665	-0.00105	1.39
7.851	0.08040	0.08127	-0.00087	1.08
10.16	0.08900	0.08923	-0.00023	0.26
13.91	0.09890	0.10015	-0.00025	0.25
18.05	0.1116	0.1108	0.0008	0.76
22.18	0.1212	0.1206	0.0006	0.49
25.26	0.1292	0.1276	0.0016	1.20
30.46	0.1393	0.1392	0.0001	0.08
35.55	0.1507	0.1502	0.0005	0.30
40.74	0.1610	0.1613	-0.0003	0.21
45.84	0.1718	0.1721	-0.0003	0.18
51.04	0.1823	0.1830	-0.0007	0.38

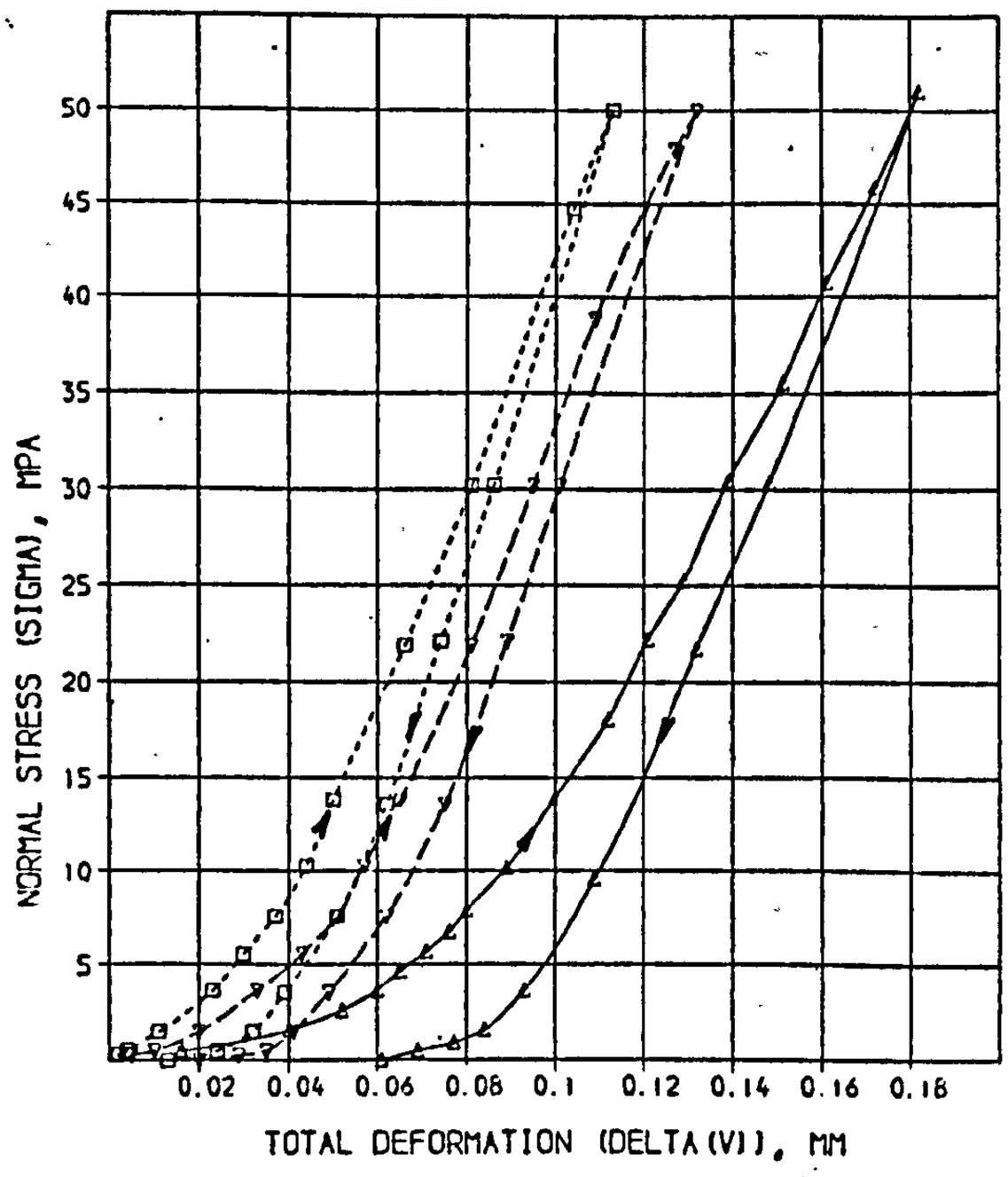

2nd loading

SOLUTION

A=	53.02	SD =	9.913	% =	18.58
B=	0.05122	SD =	0.005219	% =	10.17
C=	633.7	SD =	42.62	% =	6.726

COMPUTED RESIDUALS

SIGMA	DELTA(V) MEASURED	DELTA(V) CALCULATED	DIFF	% DIFF
0.2740	0.005100	0.005055	0.000045	0.88
0.4760	0.01000	0.008820	0.001172	11.19
1.487	0.01960	0.02027	-0.00067	3.43
3.608	0.03300	0.03471	-0.00171	5.17
5.553	0.04250	0.04297	-0.00047	1.11
7.552	0.05100	0.04942	0.00158	3.09
11.22	0.05750	0.05660	0.00090	1.57
13.82	0.06500	0.06450	0.00050	0.77
21.90	0.08100	0.08005	0.00095	1.18
31.19	0.09500	0.09457	0.00043	0.45
39.85	0.1050	0.1091	-0.0041	3.94
44.75	0.1130	0.1169	-0.0039	3.19
47.90	0.1270	0.1240	0.0030	2.34
51.00	0.1320	0.1274	0.0046	3.45

3rd loading

SOLUTION

A=	121.1	SD =	17.14	% =	14.15
B=	0.04327	SD =	0.005847	% =	13.51
C=	705.7	SD =	51.94	% =	7.360

COMPUTED RESIDUALS

SIGMA	DELTA(V) MEASURED	DELTA(V) CALCULATED	DIFF	% DIFF
0.2740	0.002310	0.002558	-0.000258	10.34
0.4760	0.004000	0.004277	-0.000277	6.92
1.487	0.01100	0.01107	-0.00007	0.09
3.605	0.02310	0.02274	0.00036	1.55
5.530	0.02990	0.03005	-0.00015	0.51
7.552	0.03700	0.03624	0.00076	2.04
11.28	0.04350	0.04325	0.00025	0.63
13.82	0.05000	0.05096	-0.00096	1.91
21.90	0.06000	0.06095	0.00005	0.08
31.19	0.08100	0.07965	0.00135	1.67
44.75	0.09800	0.10215	-0.00415	4.23
51.00	0.1130	0.1100	0.0030	2.64

LMST: No.5

1st loading

SOLUTION:

A=	12.68	SD =	0.2007	% =	1.120
B=	0.1028	SD =	0.000660	% =	0.6427
C=	708.6	SD =	0.494	% =	1.340

COMPUTED RESIDUALS

SIGMA	DELTA(V) MEASURED	DELTA(V) CALCULATED	DIFF	% DIF
0.3960	0.02580	0.02452	0.00128	4.97
0.8130	0.04210	0.04064	0.00146	3.47
0.9910	0.04550	0.04580	-0.00030	0.66
1.784	0.06120	0.06192	-0.00072	1.17
2.181	0.06650	0.06742	-0.00092	1.38
2.855	0.07380	0.07460	-0.00080	1.08
3.767	0.08200	0.08168	0.00032	0.39
4.758	0.08790	0.08740	0.00050	0.57
5.749	0.09150	0.09190	-0.00040	0.44
7.732	0.09840	0.09886	-0.00046	0.47
9.714	0.1038	0.1043	-0.0005	0.51
11.70	0.1088	0.1090	-0.0002	0.16
13.68	0.1128	0.1131	-0.0003	0.30
15.66	0.1174	0.1170	0.0004	0.36
17.64	0.1205	0.1206	-0.0001	0.09
19.63	0.1249	0.1241	0.0008	0.66
24.58	0.1332	0.1323	0.0009	0.68
29.54	0.1412	0.1401	0.0011	0.77
34.49	0.1478	0.1477	0.0001	0.06
39.45	0.1549	0.1552	-0.0003	0.17
44.40	0.1626	0.1625	0.0001	0.06
49.36	0.1687	0.1698	-0.0011	0.65

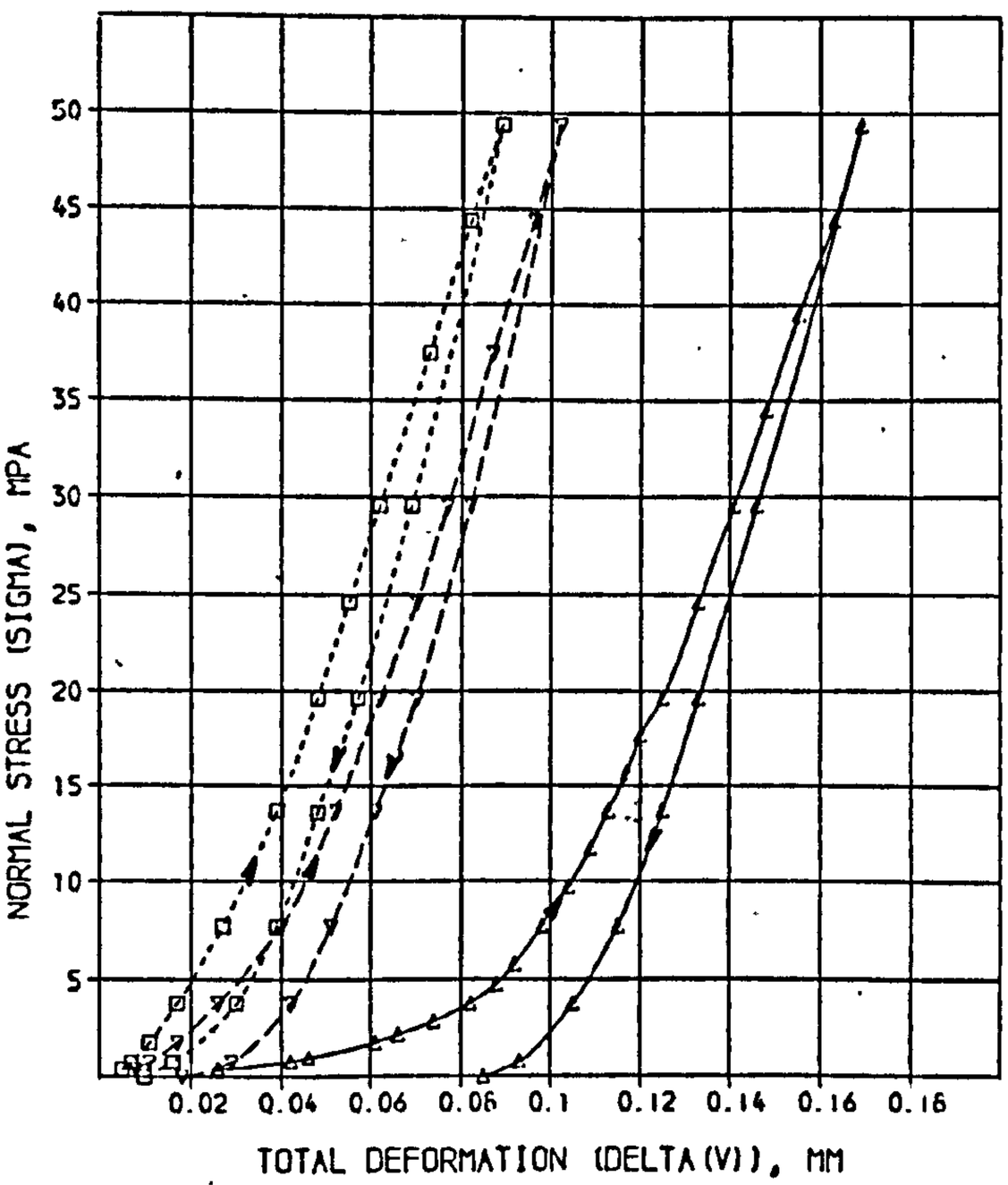

2nd loading

SOLUTION:

A=	74.26	SD =	7.215	% =	9.715
B=	0.04318	SD =	0.002678	% =	6.201
C=	794.4	SD =	36.20	% =	4.557

COMPUTED RESIDUALS

SIGMA	DELTA(V) MEASURED	DELTA(V) CALCULATED	DIFF	% DIFF
0.3960	0.008000	0.005245	0.002755	34.44
0.7921	0.01100	0.00955	0.00145	13.18
1.784	0.01750	0.01768	-0.00018	1.04
3.766	0.02600	0.02800	-0.00200	7.94
7.732	0.04000	0.04020	-0.00020	0.64
13.68	0.05200	0.05220	-0.00020	0.39
19.62	0.06200	0.06182	0.00018	0.29
24.58	0.07000	0.06914	0.00086	1.23
29.54	0.07700	0.07614	0.00086	1.12
37.47	0.08700	0.08695	0.00005	0.06
44.41	0.09600	0.09618	-0.00018	0.18
49.36	0.1020	0.1027	-0.0007	0.67

3id loading

SOLUTION

A=	130.9	SD =	14.72	% =	9.714
B=	0.02513	SD =	0.001582	% =	6.295
C=	753.1	SD =	19.08	% =	2.534

COMPUTED RESIDUALS

SIGMA	DELTA(V) MEASURED	DELTA(V) CALCULATED	DIFF	% DIFF
0.3960	0.004500	0.003226	0.001274	28.32
0.7920	0.007100	0.005927	0.001173	16.52
1.784	0.01100	0.01120	-0.00020	1.86
3.766	0.01750	0.01841	-0.00091	5.22
7.732	0.02700	0.02790	-0.00090	3.32
13.68	0.03900	0.03843	0.00057	1.47
19.62	0.04300	0.04256	0.00044	0.87
24.58	0.05500	0.05480	0.00020	0.36
29.54	0.06200	0.06184	0.00016	0.26
37.47	0.07300	0.07286	0.00014	0.19
44.41	0.08200	0.08257	-0.00057	0.45
49.36	0.08900	0.08910	-0.00010	0.12

1st loading_

SOLUTION

A=	5.812	SD =	0.0646	% =	0.773
B=	0.09961	SD =	0.002346	% =	2.356
C=	581.6	SD =	24.09	% =	4.142

COMPUTED RESIDUALS

SIGMA	DELTA(V) MEASURED	DELTA(V) CALCULATED	DIFF	% DIFF
0.3530	0.03400	0.02704	0.00696	20.48
0.8580	0.04500	0.04804	-0.00304	6.76
1.364	0.06000	0.06037	-0.00037	0.62
1.870	0.06100	0.06863	0.00037	0.53
2.881	0.07800	0.07933	-0.00133	1.71
3.892	0.08500	0.08631	-0.00131	1.54
5.915	0.09300	0.09565	-0.00265	2.85
7.936	0.1010	0.1023	-0.0013	1.32
9.958	0.1080	0.1078	0.0002	0.16
14.00	0.1190	0.1172	0.0018	1.53
18.05	0.1280	0.1255	0.0025	1.94
22.09	0.1350	0.1334	0.0016	1.21
26.13	0.1420	0.1410	0.0010	0.74
32.20	0.1530	0.1520	0.0010	0.63
40.29	0.1660	0.1665	-0.0005	0.31
50.39	0.1820	0.1842	-0.0022	1.20

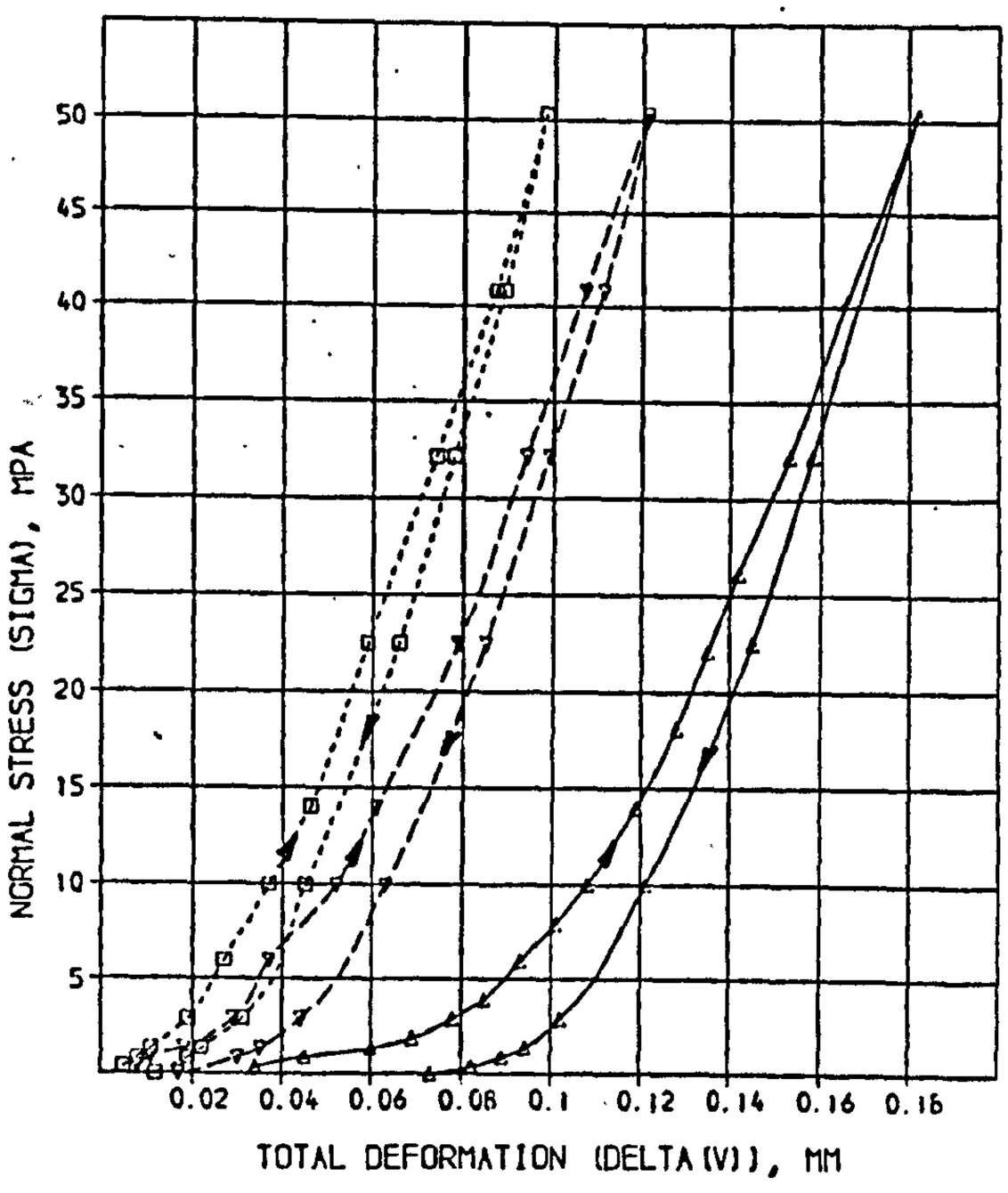

2rd loading_

SOLUTION

A=	62.87	SD =	7.810	% =	12.42
B=	0.04815	SD =	0.003925	% =	8.150
C=	655.6	SD =	36.70	% =	5.593

COMPUTED RESIDUALS

SIGMA	DELTA(V) MEASURED	DELTA(V) CALCULATED	DIFF	% DIFF
0.3500	0.008000	0.005524	0.002476	30.95
0.8510	0.01150	0.01180	-0.00030	2.17
1.360	0.01300	0.01200	0.00100	7.55
2.880	0.02000	0.02787	-0.00113	5.90
5.940	0.03700	0.04096	-0.00396	10.69
9.970	0.05200	0.05214	-0.00014	0.28
14.00	0.06100	0.06094	0.00006	0.09
22.50	0.07900	0.07676	0.00244	2.84
32.20	0.09400	0.09313	0.00087	0.93
40.80	0.1070	0.1071	-0.0001	0.05
50.30	0.1210	0.1221	-0.0011	0.94

3rd loading_

SOLUTION

A=	103.0	SD =	11.99	% =	11.65
B=	0.03144	SD =	0.002504	% =	7.964
C=	719.7	SD =	27.67	% =	3.845

COMPUTED RESIDUALS

SIGMA	DELTA(V) MEASURED	DELTA(V) CALCULATED	DIFF	% DIFF
0.3500	0.005100	0.003554	0.001546	30.32
0.8510	0.008200	0.007727	0.000473	5.77
1.360	0.01150	0.01119	0.00031	2.69
2.880	0.01900	0.01880	0.00020	1.04
5.940	0.02700	0.02860	-0.00160	5.93
9.970	0.03650	0.03759	-0.00109	2.97
14.00	0.04600	0.04499	0.00101	2.20
22.50	0.05900	0.05875	0.00025	0.43
32.20	0.07400	0.07331	0.00069	0.93
40.80	0.08700	0.08582	0.00118	1.36
50.30	0.09800	0.09943	-0.00143	1.46

LMST: No. 7

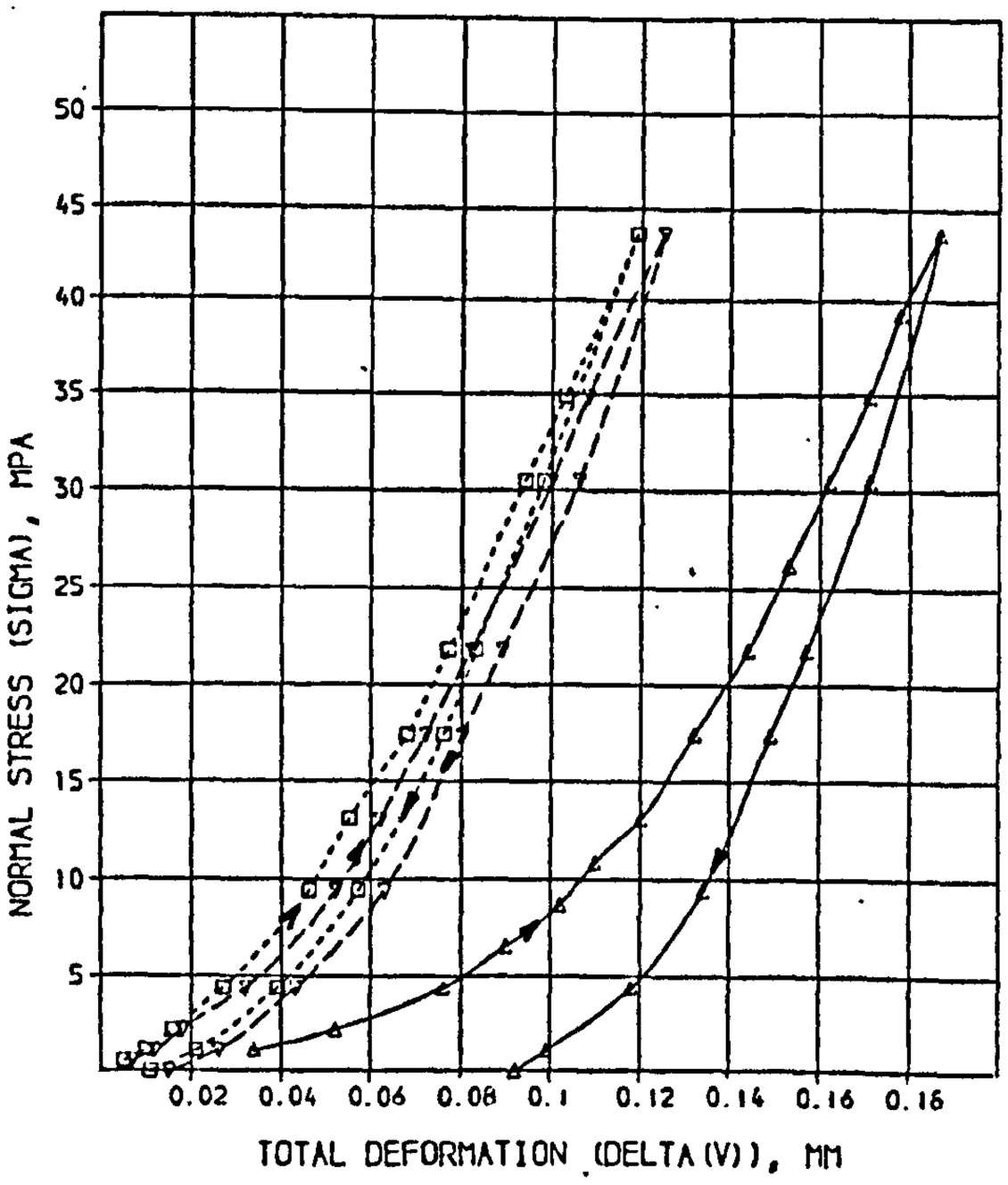

1st loading

SOLUTION

A=	7.21	SD =	0.8716	% =	3.203
B=	0.1205	SD =	0.002502	% =	2.077
C=	577.7	SD =	19.15	% =	3.314

COMPUTED RESIDUALS

SIGMA	DELTA(V) MEASURED	DELTA(V) CALCULATED	DIFF	% DIFF
1.090	0.03400	0.03195	0.00205	6.03
2.179	0.05200	0.05188	0.00012	0.23
4.359	0.07600	0.07632	-0.00032	0.42
6.538	0.09000	0.09157	-0.00157	1.75
8.717	0.1020	0.1027	-0.0007	0.64
10.90	0.1100	0.1115	-0.0015	1.36
13.08	0.1200	0.1190	0.0010	0.85
17.43	0.1320	0.1316	0.0004	0.30
21.79	0.1440	0.1425	0.0015	1.06
26.15	0.1530	0.1523	0.0007	0.43
30.51	0.1620	0.1616	0.0004	0.23
34.90	0.1710	0.1706	0.0004	0.25
38.23	0.1780	0.1791	-0.0011	0.62
43.59	0.1870	0.1875	-0.0005	0.28

2nd loading

SOLUTION

A=	98.38	SD =	3.793	% =	3.861
B=	0.05484	SD =	0.002106	% =	3.951
C=	573.2	SD =	14.35	% =	2.504

COMPUTED RESIDUALS

SIGMA	DELTA(V) MEASURED	DELTA(V) CALCULATED	DIFF	% DIFF
0.5120	0.006500	0.005640	0.000854	13.13
1.090	0.01200	0.01112	0.00088	7.34
2.179	0.01350	0.01458	-0.00108	7.83
4.359	0.03200	0.03211	-0.00011	0.35
9.450	0.05150	0.05139	0.00011	0.20
13.08	0.06200	0.06164	0.00036	0.58
17.40	0.07200	0.07221	-0.00021	0.30
21.79	0.08200	0.08197	0.00003	0.04
30.51	0.1000	0.0998	0.0002	0.18
34.90	0.1090	0.1084	-0.0004	0.35
43.59	0.1250	0.1248	0.0002	0.12

3rd loading

SOLUTION

A=	124.0	SD =	15.92	% =	12.85
B=	0.04206	SD =	0.005371	% =	12.77
C=	530.5	SD =	30.46	% =	5.813

COMPUTED RESIDUALS

SIGMA	DELTA(V) MEASURED	DELTA(V) CALCULATED	DIFF	% DIFF
0.5120	0.004900	0.004726	0.000174	3.55
1.090	0.009500	0.009324	0.000172	1.82
2.179	0.01600	0.01650	-0.00050	3.15
4.359	0.02750	0.02737	0.00013	0.48
9.450	0.04600	0.04492	0.00108	2.35
13.08	0.05500	0.05473	0.00027	0.49
17.40	0.06150	0.06450	-0.00300	5.95
21.79	0.07700	0.07501	0.00199	2.58
30.51	0.09400	0.09343	0.00057	0.60
34.90	0.1030	0.1024	0.0006	0.60
43.59	0.1100	0.1107	-0.0007	0.62

LMST: No. 8

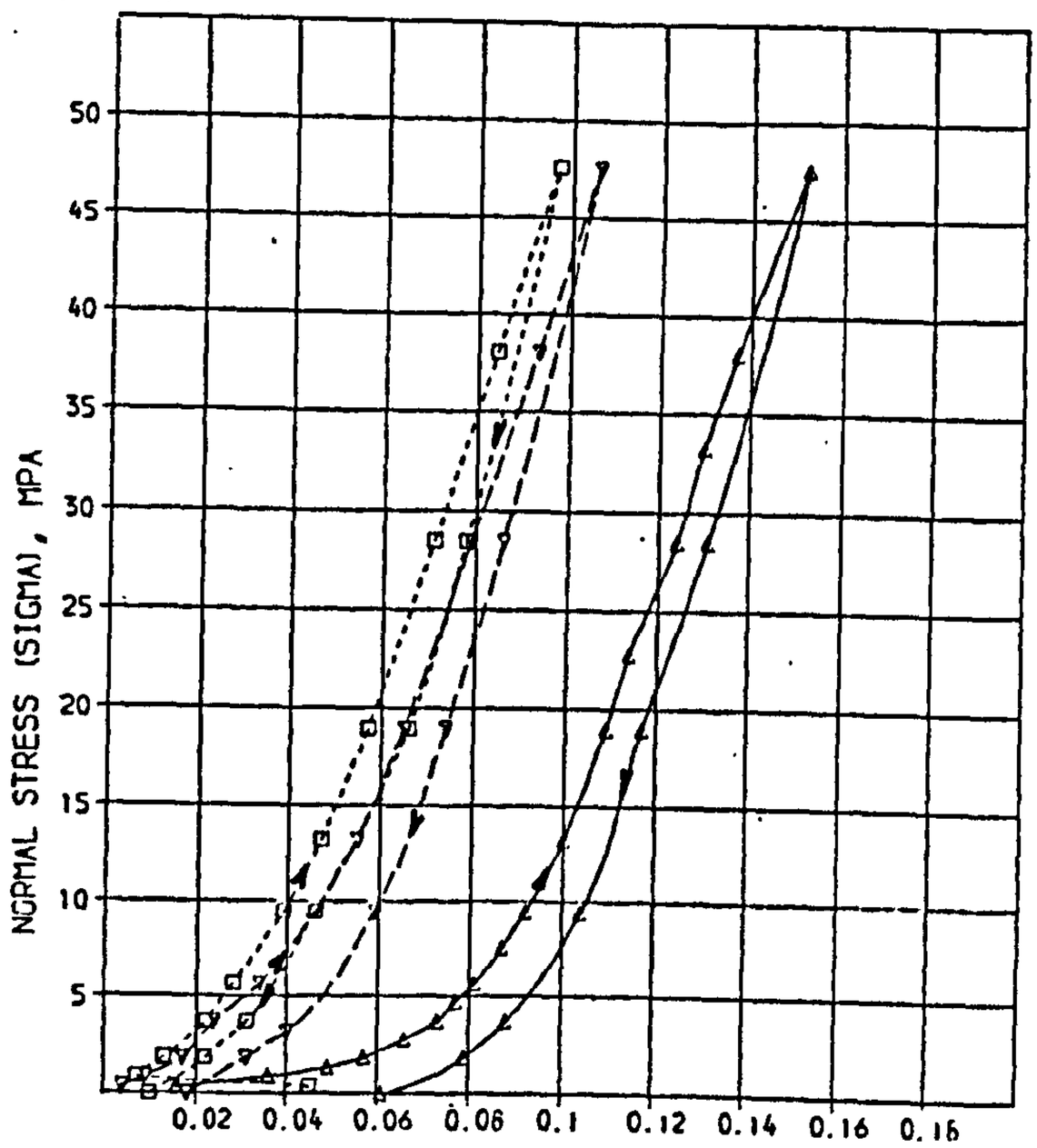

1st loading_

SOLUTION

A=	14.51	SD =	0.6610	% =	4.556
B=	0.0°071	SD =	0.001753	% =	1.933
C=	762.7	SD =	29.73	% =	3.897

COMPUTED RESIDUALS

SIGMA	DELTA(V) MEASURED	DELTA(V) CALCULATED	DIFF	% DIFF
0.3810	0 01590	0.02086	-0.00496	31.23
0.857C	0 03610	0.03690	-0.00080	2.21
1.334	C.04670	0.04741	0.00129	2.65
1.810	C.05690	0.05488	0.00201	3.53
2.763	C 06040	0.06506	0.00134	2.01
3.715	0 07250	0.07185	0.00065	0.90
4.667	0.07680	0.07687	-0.00007	0.10
5.620	0.08080	0.08086	-0.00006	0.08
7.525	0.08700	0.08707	-0.00007	0.08
9.430	0.09160	0.09196	-0.00036	0.40
13.24	0.09180	0.09186	-0.00006	0.06
18.95	0.1090	0.1097	-0.0007	0.61
22.76	0.1140	0.1156	-0.0016	1.40
28.48	0.1245	0.1240	0.0005	0.37
33.24	0.1305	0.1308	-0.0003	0.26
38.00	0.1370	0.1375	-0.0005	0.36
47.53	0.1519	0.1506	0.0013	0.87

2nd loading_

SOLUTION

A=	104.1	SD =	0.617	% =	6.357
B=	0.05502	SD =	0.003855	% =	7.008
C=	839.2	SD =	50.45	% =	5.987

COMPUTED RESIDUALS

SIGMA	DELTA(V) MEASURED	DELTA(V) CALCULATED	DIFF	% DIFF
0.3810	0.003900	0.003886	0.000014	0.36
0.8570	0.008600	0.008183	0.000617	7.01
1.810	0.01700	0.01537	0.00163	9.59
3.715	0.02400	0.02607	-0.00207	8.64
5.620	0.03350	0.03395	-0.00045	1.33
9.430	0.04600	0.04547	0.00053	1.16
13.24	0.05500	0.05418	0.00082	1.49
18.95	0.06500	0.06483	0.00017	0.26
28.48	0.07900	0.07974	-0.00074	0.94
38.00	0.09300	0.09309	-0.00009	0.10
47.53	0.1060	0.1057	0.0003	0.25

3rd loading_

SOLUTION

A=	126.8	SD =	22.07	% =	17.87
B=	0.03765	SD =	0.006352	% =	16.82
C=	749.6	SD =	70.04	% =	9.344

COMPUTED RESIDUALS

SIGMA	DELTA(V) MEASURED	DELTA(V) CALCULATED	DIFF	% DIFF
0.3810	0.004500	0.003290	0.001210	26.88
0.8570	0.007500	0.006872	0.000628	8.37
1.810	0.01300	0.01276	0.00024	1.82
3.715	0.02200	0.02143	0.00057	2.59
5.620	0.02850	0.02785	0.00065	2.28
9.430	0.03250	0.03757	-0.00507	15.61
13.24	0.04700	0.04535	0.00165	3.55
18.95	0.05700	0.05535	0.00165	2.89
28.48	0.07100	0.07023	0.00077	1.08
38.00	0.08400	0.08414	-0.00014	0.16
47.53	0.09700	0.09706	-0.00002	0.64

LMST: No.9

1st loading

SOLUTION

A=	15.10	SD =	0.2445	% =	1.619
B=	0.09449	SD =	0.000599	% =	0.6338
C=	679.5	SD =	7.372	% =	1.085

COMPUTED RESIDUALS

SIGMA	DELTA(V) MEASURED	DELTA(V) CALCULATED	DIFF	% DIFF
0.4000	0.02100	0.02128	-0.00028	1.34
0.9000	0.03900	0.03788	0.00112	2.88
1.902	0.05700	0.05679	0.00021	0.37
2.902	0.06700	0.06766	-0.00066	0.92
3.903	0.07400	0.07494	-0.00094	1.27
4.903	0.08000	0.08041	-0.00041	0.51
5.904	0.08500	0.08479	0.00021	0.25
7.905	0.09200	0.09165	0.00035	0.35
9.907	0.09700	0.09717	-0.00017	0.18
11.91	0.1020	0.1019	0.0001	0.09
15.91	0.1110	0.1101	0.0009	0.79
24.92	0.1260	0.1260	-0.0000	0.03
29.92	0.1340	0.1342	-0.0002	0.16
35.93	0.1440	0.1438	0.0002	0.17
41.93	0.1530	0.1531	-0.0001	0.05
49.83	0.1650	0.1652	-0.0002	0.11

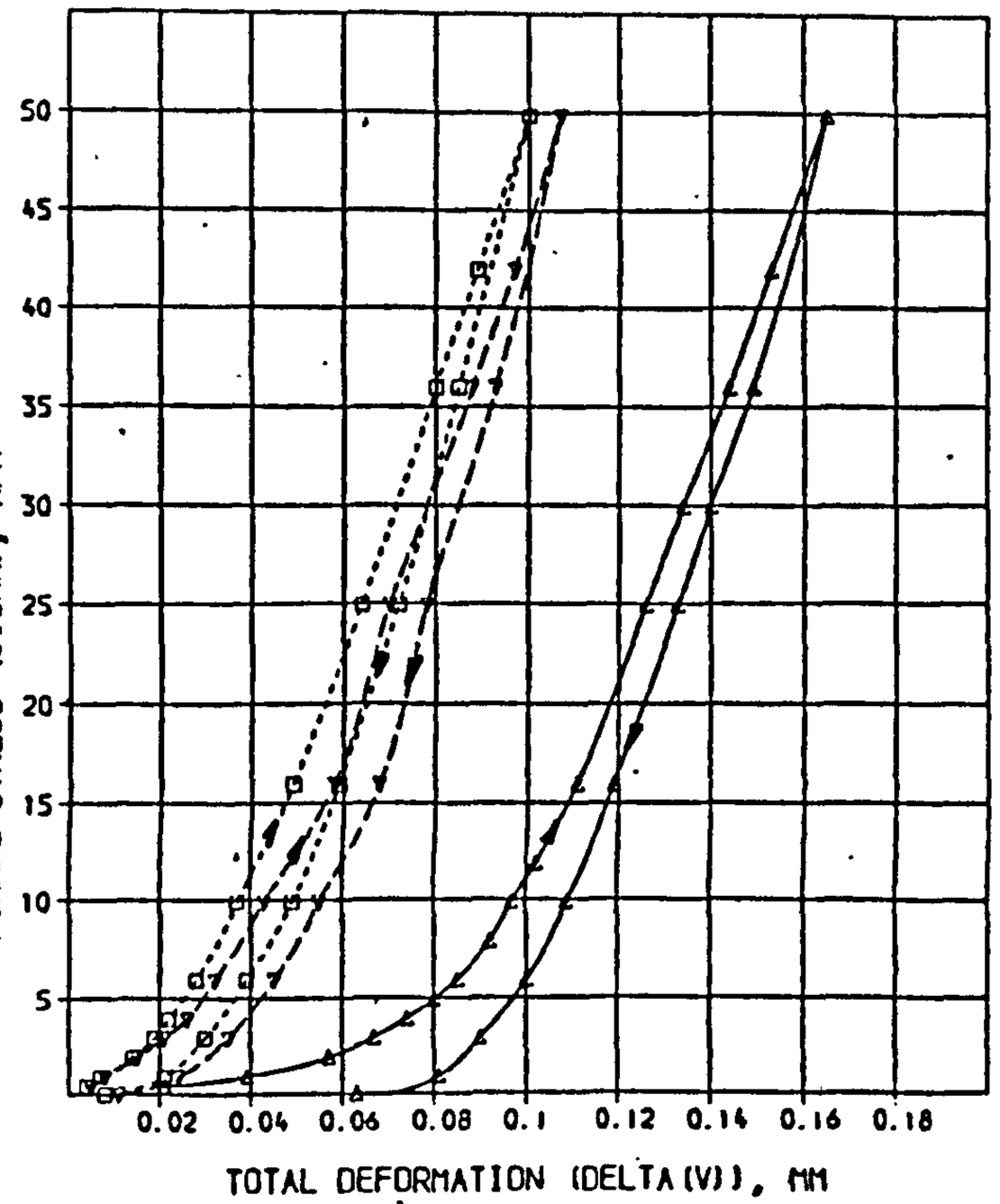

2nd loading

SOLUTION

A=	108.6	SD =	6.194	% =	5.701
B=	0.04674	SD =	0.002867	% =	6.135
C=	766.9	SD =	31.46	% =	4.102

COMPUTED RESIDUALS

SIGMA	DELTA(V) MEASURED	DELTA(V) CALCULATED	DIFF	% DIFF
0.4000	0.004500	0.003935	0.000565	12.56
0.9000	0.008200	0.008211	-0.000011	0.13
1.902	0.01500	0.01522	-0.00022	1.45
2.902	0.02100	0.02078	0.00022	1.04
3.903	0.02600	0.02540	0.00060	2.30
5.904	0.03200	0.03285	-0.00085	2.58
9.907	0.04300	0.04382	-0.00082	1.91
15.91	0.05300	0.05018	0.00282	5.14
24.92	0.07000	0.07132	-0.00132	1.89
35.93	0.08800	0.08780	0.00020	0.22
41.93	0.09700	0.09630	0.00064	0.65
49.83	0.1070	0.1074	-0.0004	0.37

3rd loading

SOLUTION

A=	113.1	SD =	4.193	% =	3.707
B=	0.03259	SD =	0.001015	% =	3.113
C=	712.0	SD =	10.50	% =	1.475

COMPUTED RESIDUALS

SIGMA	DELTA(V) MEASURED	DELTA(V) CALCULATED	DIFF	% DIFF
0.4000	0.004000	0.003752	0.000248	6.19
0.9000	0.007500	0.007660	-0.000160	4.13
1.902	0.01400	0.01376	0.00024	1.68
2.902	0.01900	0.01843	0.00057	2.99
3.903	0.02200	0.02224	-0.00024	1.10
5.904	0.02800	0.02836	-0.00036	1.27
9.907	0.03700	0.03767	-0.00067	1.80
15.91	0.04900	0.04880	0.00020	0.40
24.92	0.06400	0.06359	0.00041	0.65
35.93	0.08000	0.08002	-0.00002	0.03
41.93	0.08900	0.08883	0.00017	0.17
49.83	0.1000	0.1003	-0.0003	0.33

LMST; No. 10

1st loading

SOLUTION

A=	27.66	SD =	0.6145	% =	2.241
B=	0.1162	SD =	0.001602	% =	1.430
C=	896.7	SD =	30.86	% =	3.441

COMPUTED RESIDUALS

SIGMA	DELTA(V) MEASURED	DELTA(V) CALCULATED	DIFF	% DIFF
0.6350	0.01900	0.01984	0.00001	0.07
1.020	0.02190	0.02914	0.00076	2.54
1.789	0.04540	0.04356	0.00184	4.06
2.753	0.05760	0.05669	0.00091	1.58
3.715	0.06600	0.06645	-0.00045	0.69
4.677	0.07330	0.07410	-0.00080	1.09
5.639	0.07800	0.08031	-0.00231	2.96
7.563	0.08770	0.08998	-0.00228	2.60
9.483	0.09610	0.09738	0.00072	0.73
11.41	0.1045	0.1034	0.0011	1.06
13.34	0.1091	0.1085	0.0006	0.55
15.26	0.1132	0.1130	0.0002	0.18
17.18	0.1171	0.1171	0.0000	0.04
17.18	0.1171	0.1171	0.0000	0.04
19.11	0.1207	0.1208	-0.0001	0.06
23.92	0.1294	0.1291	0.0003	0.23
28.73	0.1367	0.1365	0.0002	0.12
33.55	0.1444	0.1435	0.0009	0.66
38.35	0.1507	0.1500	0.0007	0.48
43.16	0.1557	0.1563	-0.0006	0.37
47.98	0.1614	0.1624	-0.0010	0.62

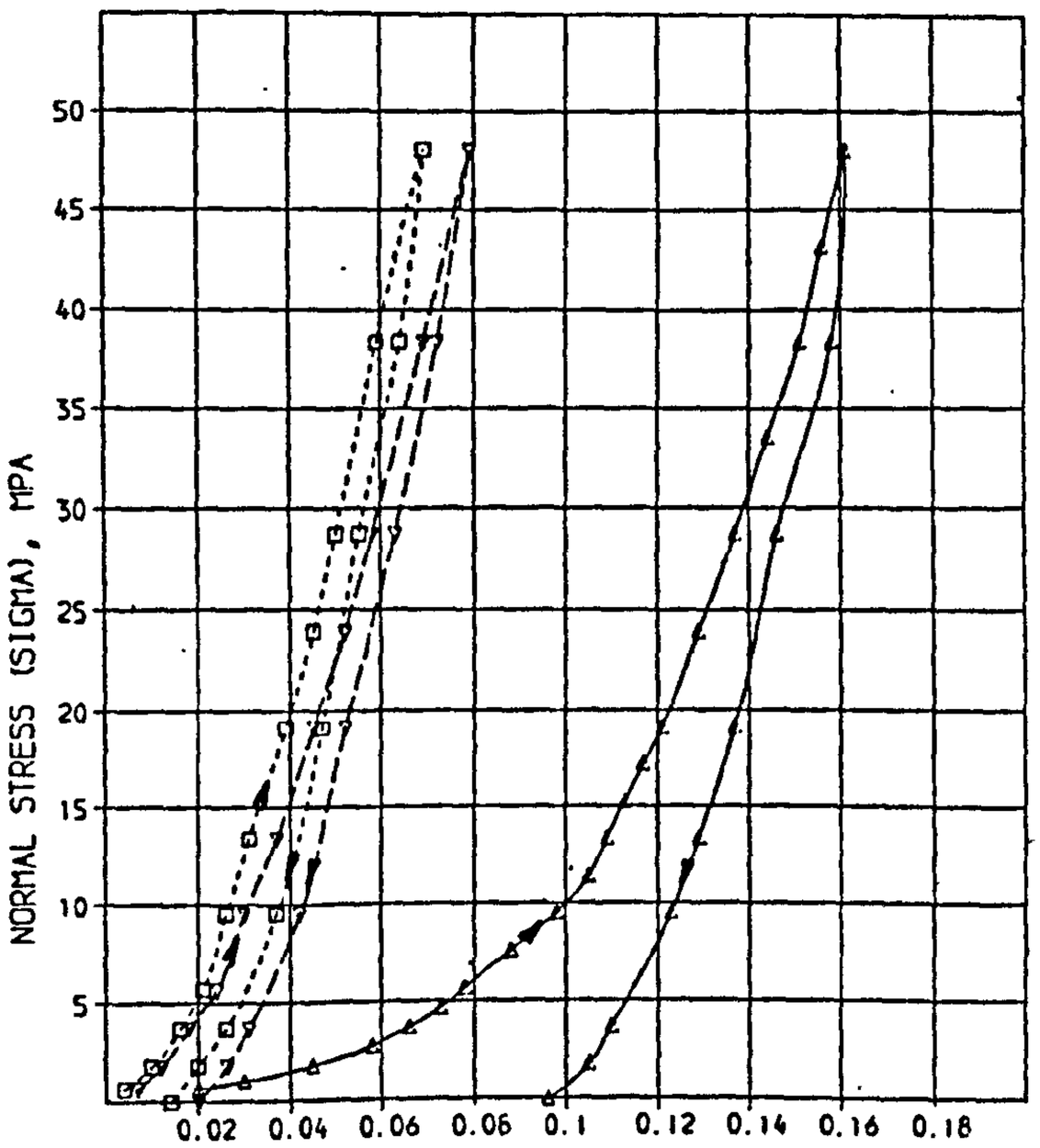

SOLUTION

A=	100.0	SD =	12.41	% =	11.70
B=	0.02503	SD =	0.001815	% =	6.961
C=	865.3	SD =	31.95	% =	3.655

COMPUTED RESIDUALS

SIGMA	DELTA(V) MEASURED	DELTA(V) CALCULATED	DIFF	% DIFF
0.6350	0.007100	0.005496	0.001604	22.60
1.730	0.01200	0.01214	-0.00014	1.17
3.715	0.01850	0.01907	-0.00057	3.05
5.640	0.02400	0.02385	0.00015	0.61
9.490	0.03000	0.03105	-0.00105	3.43
13.34	0.03650	0.03690	-0.00040	1.11
19.11	0.04500	0.04477	0.00023	0.50
23.92	0.05150	0.05094	0.00056	1.10
28.73	0.05300	0.05691	0.00109	1.87
33.35	0.06900	0.06857	0.00043	0.62
47.98	0.07900	0.08004	-0.00104	1.31

SOLUTION

A=	137.7	SD =	30.78	% =	22.35
B=	0.02102	SD =	0.003027	% =	13.81
C=	978.9	SD =	66.31	% =	6.774

COMPUTED RESIDUALS

SIGMA	DELTA(V) MEASURED	DELTA(V) CALCULATED	DIFF	% DIFF
0.6350	0.003500	0.004458	-0.000958	27.37
1.789	0.01050	0.00998	0.00052	4.91
3.715	0.01600	0.01589	0.00011	0.70
5.640	0.02100	0.02004	0.00096	4.57
9.490	0.02650	0.02633	0.00017	0.66
13.34	0.02800	0.03150	-0.00350	12.51
19.11	0.03950	0.03845	0.00105	2.65
23.92	0.04500	0.04390	0.00110	2.44
28.73	0.05000	0.04919	0.00081	1.63
33.35	0.05950	0.05950	0.00000	0.00
47.98	0.06900	0.06964	-0.00064	0.93

LMST : No. 10a

1st loading

SOLUTION

A=	24.05	SD =	0.7541	% =	3.023
B=	0.07544	SD =	0.001128	% =	1.495
C=	941.3	SD =	27.66	% =	2.939

COMPUTED RESIDUALS

SIGMA	DELTA(V) MEASURED	DELTA(V) CALCULATED	DIFF	% DIFF
0.4040	0.01350	0.01376	-0.00026	1.94
0.8650	0.02510	0.02468	0.00042	1.69
1.346	0.03390	0.03284	0.00101	2.99
1.827	0.04040	0.03910	0.00130	3.21
2.788	0.04700	0.04800	-0.00010	0.21
3.750	0.05350	0.05422	-0.00072	1.34
4.711	0.05730	0.05891	-0.00161	2.81
5.672	0.06050	0.06267	-0.00217	3.59
7.259	0.06740	0.06762	-0.00022	0.33
9.519	0.07440	0.07310	0.00130	1.74
11.44	0.07750	0.07694	0.00056	0.72
13.36	0.08030	0.08033	-0.00003	0.04
15.29	0.08340	0.08342	-0.00002	0.02
19.13	0.08040	0.08001	0.00039	0.43
23.94	0.09040	0.09538	0.00102	1.06
28.75	0.1019	0.1014	0.0005	0.54
33.56	0.1068	0.1071	-0.0003	0.27
38.36	0.1127	0.1127	0.0000	0.02
47.88	0.1227	0.1235	-0.0008	0.62

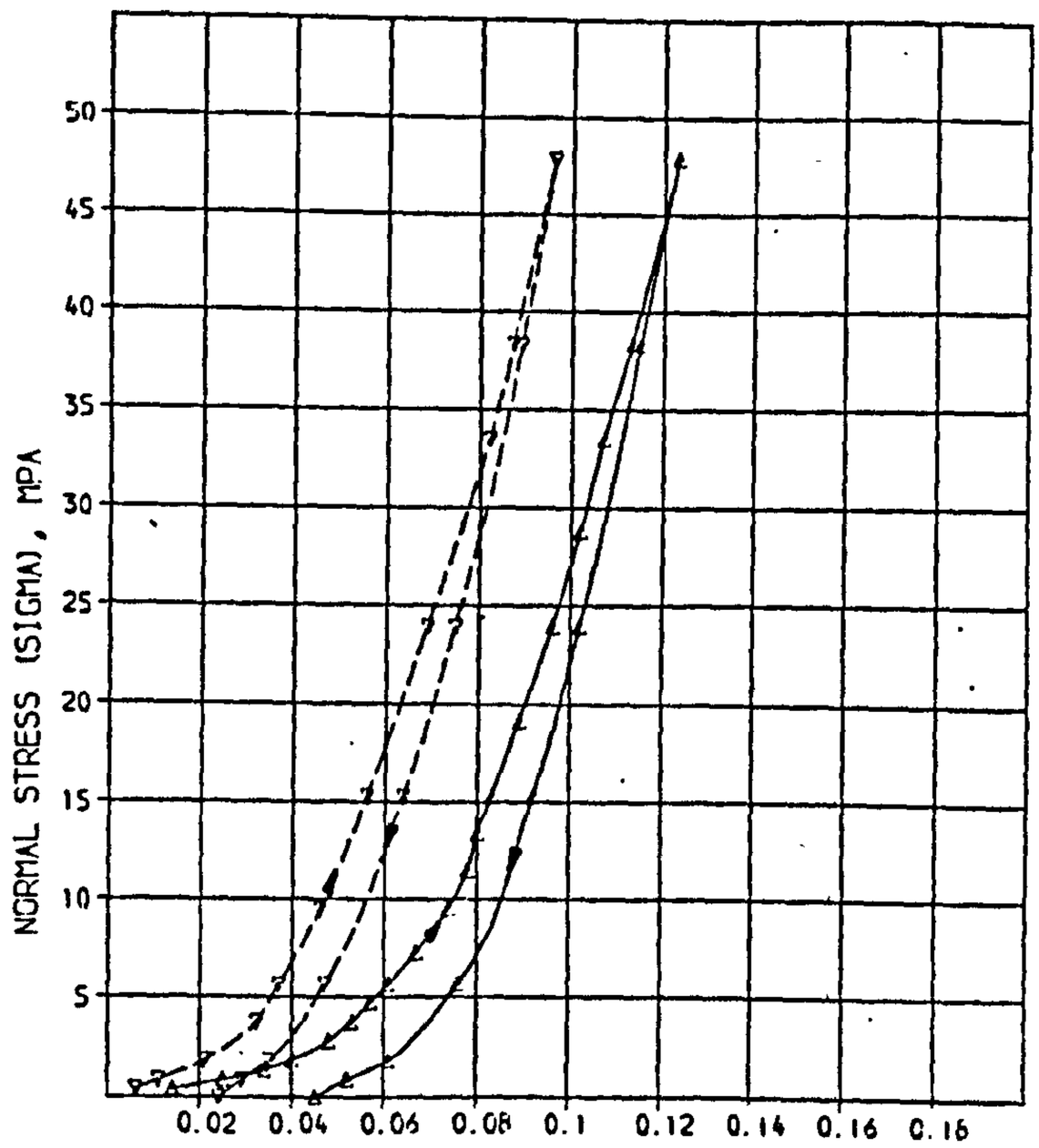

2nd loading

SOLUTION

A=	61.17	SD =	3.787	% =	6.185
B=	0.04817	SD =	0.002028	% =	4.210
C=	924.7	SD =	38.91	% =	4.208

COMPUTED RESIDUALS

SIGMA	DELTA(V) MEASURED	DELTA(V) CALCULATED	DIFF	% DIFF
0.4040	0.006000	0.000245	-0.000245	4.08
0.8650	0.01150	0.01187	-0.00037	3.19
1.827	0.02100	0.02041	0.00059	2.80
3.750	0.03200	0.03103	0.00097	3.03
5.672	0.03700	0.03784	-0.00084	2.26
9.519	0.04650	0.04704	-0.00058	1.25
15.29	0.05600	0.05692	-0.00092	1.65
23.94	0.06950	0.06878	0.00072	1.03
33.56	0.08200	0.08058	0.00142	1.73
38.36	0.08650	0.08622	0.00028	0.32
47.88	0.09630	0.09710	-0.00110	1.21

LMST: No. 11

1st loading

SOLUTION

A=	32.85	SD =	1.151	% =	3.503
B=	0.12E6	SD =	0.004777	% =	3.686
C=	703.	SD =	143.6	% =	20.02

COMPUTED RESIDUALS

SIGMA	DELTA(V) MEASURED	DELTA(V) CALCULATED	DIFF	% DIFF
0.8320	0.02010	0.02194	-0.00184	9.17
1.295	0.03340	0.03140	0.00200	5.98
1.758	0.04170	0.03947	0.00223	5.34
2.683	0.05340	0.05254	0.00086	1.62
3.609	0.06200	0.06273	-0.00073	1.18
4.533	0.07030	0.07094	-0.00064	0.92
5.458	0.07750	0.07776	-0.00026	0.33
7.309	0.08700	0.08852	-0.00152	1.75
9.159	0.09580	0.09678	-0.00088	0.92
11.01	0.1012	0.1034	-0.0022	2.22
12.86	0.1071	0.1090	-0.0019	1.80
14.71	0.1172	0.1138	0.0034	2.86
18.41	0.1247	0.1220	0.0027	2.20
22.11	0.1300	0.1287	0.0013	0.98
25.81	0.1351	0.1347	0.0004	0.33
29.51	0.1427	0.1400	-0.0013	0.95
33.21	0.1483	0.1450	-0.0007	0.47
36.91	0.1544	0.1497	-0.0003	0.18

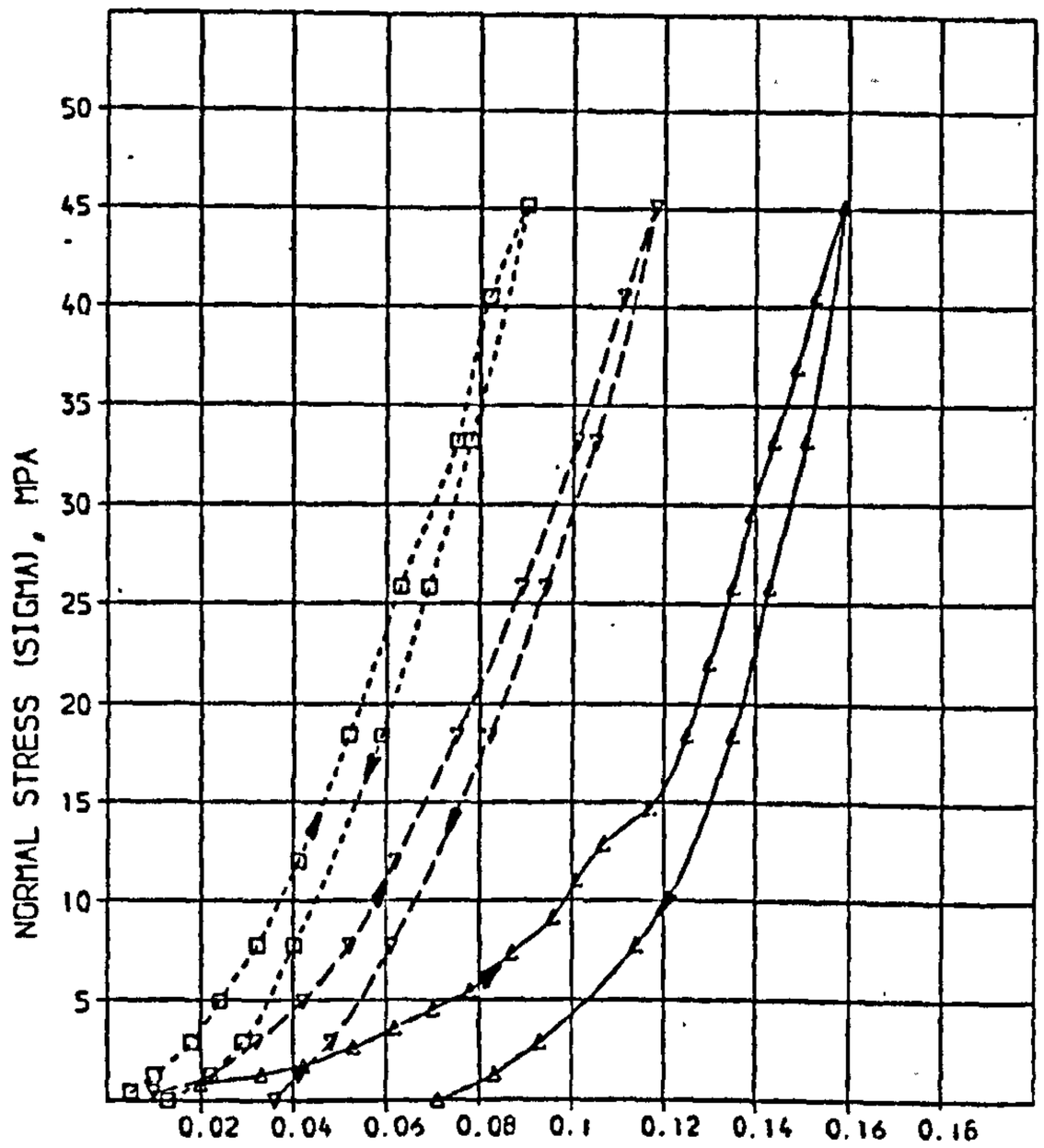

2nd loading

SOLUTION

A=	45.83	SD =	3.705	% =	8.215
B=	0.05242	SD =	0.002443	% =	4.659
C=	650.1	SD =	24.71	% =	3.801

COMPUTED RESIDUALS

SIGMA	DELTA(V) MEASURED	DELTA(V) CALCULATED	DIFF	% DIFF
0.4500	0.01050	0.00896	0.00154	14.64
1.295	0.02290	0.02185	0.00105	7.49
2.930	0.03150	0.03331	-0.00181	5.75
4.940	0.04290	0.04287	0.00087	2.07
7.690	0.05150	0.05177	-0.00027	0.53
12.00	0.06290	0.06214	-0.00014	0.22
17.41	0.07500	0.07464	0.00031	0.41
25.81	0.08900	0.08756	0.00144	1.50
33.21	0.1010	0.1000	0.0010	1.02
40.50	0.1115	0.1114	-0.0003	0.26
45.10	0.1180	0.1192	-0.0012	0.98

3rd loading

SOLUTION

A=	121.4	SD =	10.74	% =	8.849
B=	0.03414	SD =	0.002568	% =	7.523
C=	770.3	SD =	31.55	% =	4.095

COMPUTED RESIDUALS

SIGMA	DELTA(V) MEASURED	DELTA(V) CALCULATED	DIFF	% DIFF
0.4500	0.005000	0.003947	0.001053	21.46
1.295	0.01000	0.00981	0.00019	1.93
2.930	0.01800	0.01794	0.00006	0.34
4.940	0.02450	0.02497	-0.00047	1.93
7.690	0.03200	0.03216	-0.00016	0.50
12.00	0.04050	0.04094	-0.00044	1.09
17.41	0.05200	0.05175	0.00025	0.48
25.81	0.06300	0.06290	0.00010	0.16
33.21	0.07500	0.07344	0.00156	2.09
40.50	0.08200	0.08351	-0.00151	1.84
45.10	0.09000	0.08978	0.00022	0.25

LMST: No. 12

1st loading

SOLUTION

A=	70.22	SD =	2.221	% =	3.163
B=	0.07635	SD =	0.002315	% =	3.123
C=	579.0	SD =	15.13	% =	2.613

COMPUTED RESIDUALS

SIGMA	DELTA(V) MEASURED	DELTA(V) CALCULATED	DIFF	% DIFF
0.2000	0.003000	0.003091	-0.000091	3.04
0.3400	0.005300	0.005140	0.000160	3.02
0.7000	0.008600	0.010026	-0.001426	16.58
1.301	0.02050	0.01716	0.00334	16.31
2.202	0.02590	0.02603	-0.00013	0.51
2.702	0.02690	0.03025	-0.00035	1.17
3.706	0.03720	0.03761	-0.00041	1.09
4.703	0.04360	0.04380	-0.00020	0.46
5.704	0.04480	0.04421	0.00059	1.19
7.705	0.05800	0.05833	-0.00033	0.57
9.707	0.06560	0.06595	-0.00035	0.53
11.71	0.07170	0.07259	-0.00089	1.25
13.71	0.07810	0.07857	-0.00047	0.60
15.71	0.08340	0.08406	-0.00066	0.79
17.71	0.08860	0.08920	-0.00060	0.68
19.71	0.09480	0.09407	0.00073	0.77
24.72	0.1066	0.1054	0.0012	1.09
29.72	0.1169	0.1160	0.0009	0.76
34.72	0.1268	0.1261	0.0007	0.54
39.73	0.1362	0.1359	0.0003	0.23
44.73	0.1468	0.1473	-0.0005	0.36
49.73	0.1540	0.1548	-0.0008	0.53

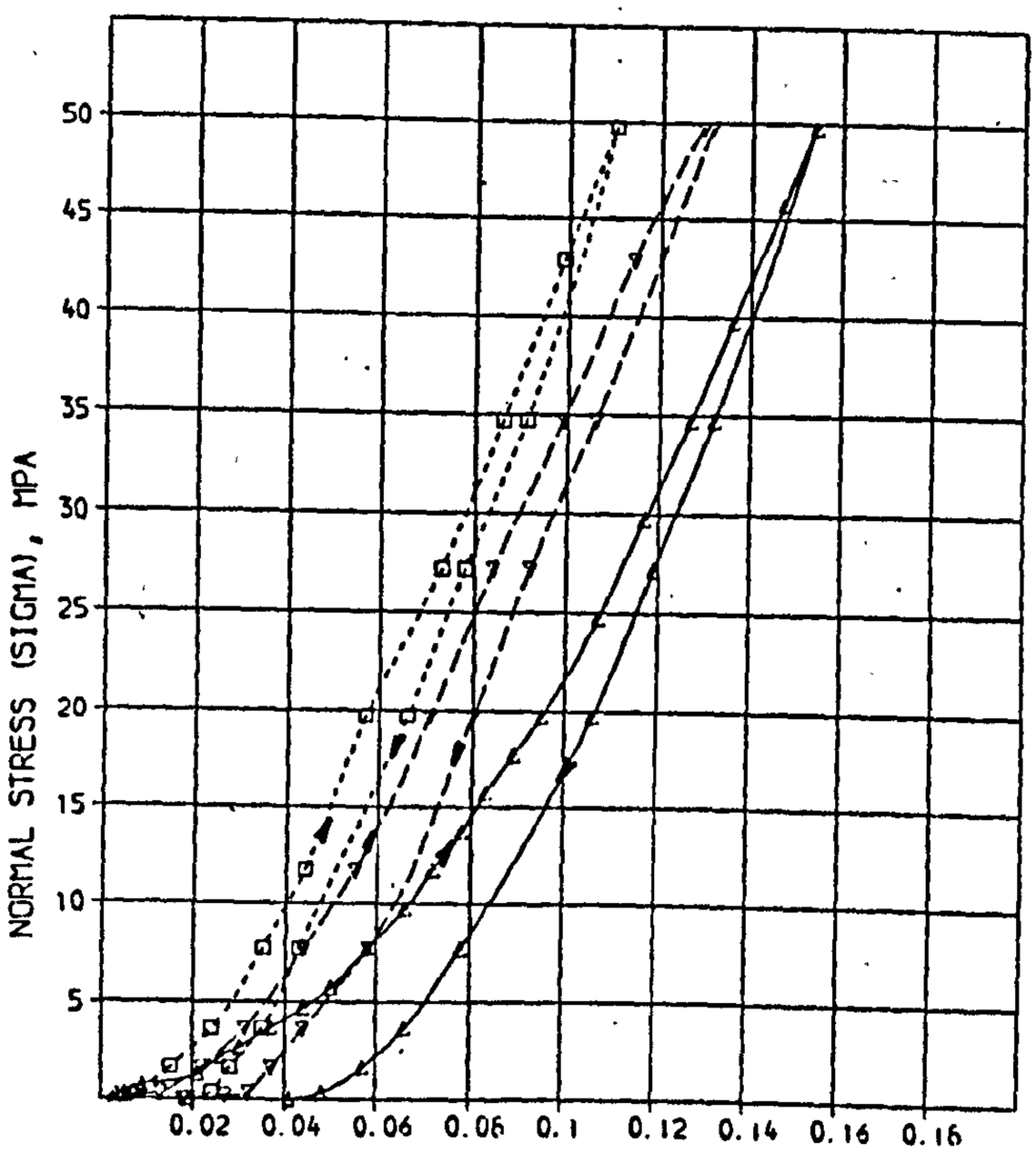

2nd loading

SOLUTION

A=	25.71	SD =	6.501	% =	25.28
B=	0.03152	SD =	0.002456	% =	7.790
C=	509.2	SD =	17.83	% =	3.509

COMPUTED RESIDUALS

SIGMA	DELTA(V) MEASURED	DELTA(V) CALCULATED	DIFF	% DIFF
0.2000	0.007100	0.006632	0.000468	6.59
0.3400	0.01300	0.00998	0.00302	23.20
1.670	0.02250	0.02491	-0.00231	11.40
3.630	0.03350	0.03591	-0.00241	7.90
7.705	0.04400	0.04360	0.00032	0.72
11.71	0.05500	0.05252	0.00248	4.50
17.71	0.07100	0.06906	0.00194	2.73
27.17	0.08400	0.08407	-0.00007	0.08
34.72	0.09350	0.09414	-0.00064	0.63
42.86	0.1120	0.1153	-0.0033	2.92
49.73	0.1310	0.1289	0.0021	1.63

3rd loading

SOLUTION

A=	53.33	SD =	10.07	% =	18.89
B=	0.02512	SD =	0.001769	% =	7.043
C=	571.6	SD =	14.93	% =	2.612

COMPUTED RESIDUALS

SIGMA	DELTA(V) MEASURED	DELTA(V) CALCULATED	DIFF	% DIFF
0.2000	0.004500	0.003613	0.000887	19.71
0.3400	0.008000	0.005680	0.002320	29.00
1.670	0.01520	0.01686	-0.00166	10.92
3.632	0.02400	0.02470	-0.00070	2.93
7.705	0.03500	0.03488	0.00012	0.36
11.71	0.04350	0.04302	0.00048	1.10
19.71	0.05700	0.05800	-0.00100	1.75
27.17	0.07300	0.07147	0.00153	2.10
34.72	0.08600	0.08492	0.00108	1.25
42.86	0.09900	0.09955	-0.00055	0.34
49.73	0.1105	0.1115	-0.0010	0.86

LMST : No. 13

1st loading

SOLUTION

A=	-4.42	SD =	0.3462	% =	1.011
B=	0.60210	SD =	0.000675	% =	0.7328
C=	852.7	SD =	12.05	% =	1.413

COMPUTED RESIDUALS

SIGMA	DELTA(V) MEASURED	DELTA(V) CALCULATED	DIFF	% DIFF
0.4770	0.01690	0.01667	0.00023	1.33
0.9540	0.02880	0.02855	0.00025	0.87
1.526	0.03400	0.03402	-0.00002	0.05
1.908	0.04490	0.04451	0.00039	0.87
2.862	0.05460	0.05493	-0.00033	0.60
3.816	0.06170	0.06242	-0.00072	1.17
4.770	0.06860	0.06818	0.00042	0.61
5.724	0.07380	0.07283	0.00097	1.31
7.632	0.07870	0.08006	-0.00039	0.48
9.540	0.08510	0.08572	-0.00062	0.72
11.45	0.08470	0.08540	-0.00070	0.78
13.36	0.09380	0.09449	-0.00069	0.73
15.26	0.09770	0.09817	-0.00047	0.48
17.17	0.1014	0.1016	-0.0002	0.17
19.08	0.1054	0.1048	0.0006	0.61
22.89	0.1116	0.1107	0.0011	0.98
26.71	0.1169	0.1163	0.0006	0.54
30.53	0.1222	0.1216	0.0006	0.51
34.34	0.1268	0.1267	0.0001	0.07
38.16	0.1317	0.1317	-0.0000	0.02
41.98	0.1368	0.1366	0.0002	0.12
45.79	0.1409	0.1415	-0.0006	0.42
47.70	0.1434	0.1439	-0.0005	0.34

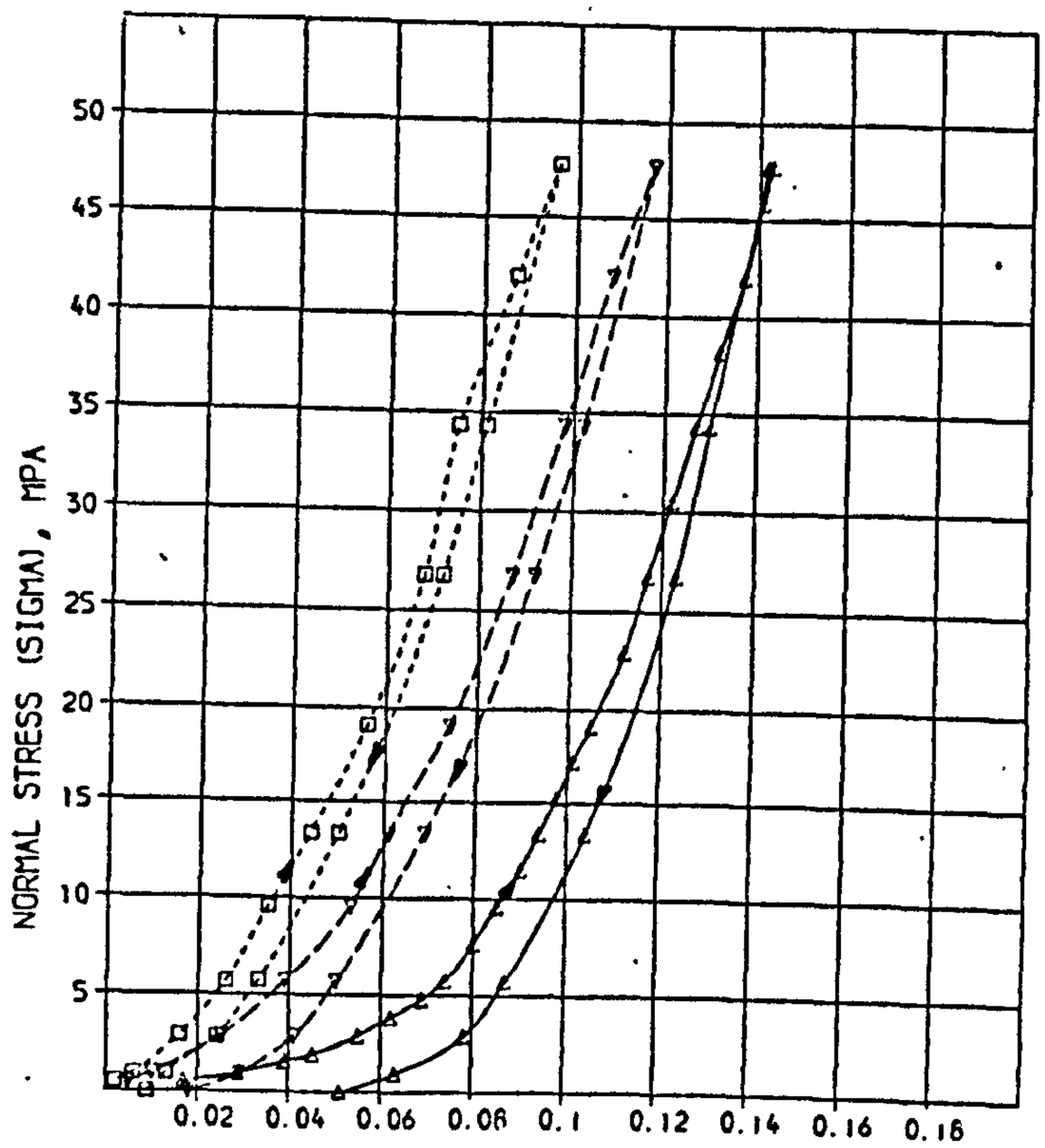

2nd loading

SOLUTION

A=	90.72	SD =	2.745	% =	3.026
B=	0.06603	SD =	0.002082	% =	3.152
C=	824.4	SD =	25.02	% =	3.035

COMPUTED RESIDUALS

SIGMA	DELTA(V) MEASURED	DELTA(V) CALCULATED	DIFF	% DIFF
0.4770	0.005100	0.005449	-0.000349	6.84
0.9540	0.01000	0.01023	-0.00023	2.29
2.862	0.02500	0.02482	0.00018	0.72
5.724	0.03900	0.03921	-0.00021	0.53
9.540	0.05300	0.05213	0.00087	1.63
13.36	0.06100	0.06180	-0.00080	1.30
19.08	0.07350	0.07340	0.00010	0.14
26.71	0.08450	0.08433	0.00017	0.19
34.34	0.09800	0.09788	0.00012	0.12
41.98	0.1080	0.1087	-0.0007	0.66
47.70	0.1170	0.1165	0.0005	0.41

3rd loading

SOLUTION

A=	168.4	SD =	16.91	% =	10.04
B=	0.04510	SD =	0.005943	% =	13.27
C=	854.5	SD =	71.00	% =	8.310

COMPUTED RESIDUALS

SIGMA	DELTA(V) MEASURED	DELTA(V) CALCULATED	DIFF	% DIFF
0.4770	0.002500	0.003224	-0.000724	28.95
0.9540	0.005800	0.006150	-0.000350	6.03
2.862	0.01650	0.01569	0.00081	4.89
5.724	0.02600	0.02608	-0.00008	0.31
9.540	0.03550	0.03627	-0.00077	2.18
13.36	0.04400	0.04439	-0.00039	0.88
19.08	0.05600	0.05459	0.00141	2.53
26.71	0.06750	0.06637	0.00113	1.67
34.34	0.07500	0.07711	-0.00211	2.82
41.98	0.08650	0.08731	-0.00081	0.94
47.70	0.09600	0.09472	0.00128	1.33

LMST : No. 14

1st loading

SOLUTION

A=	4.950	SD =	0.3409	% =	6.887
B=	0.1517	SD =	0.002718	% =	1.791
C=	458.6	SD =	16.69	% =	3.640

COMPUTED RESIDUALS

SIGMA	DELTA(V) MEASURED	DELTA(V) CALCULATED	DIFF	% DIFF
0.7570	0.07240	0.07781	-0.00541	7.48
1.472	0.1049	0.1037	0.0012	1.16
1.997	0.1174	0.1146	0.0028	2.37
3.049	0.1311	0.1284	0.0027	2.07
4.100	0.1392	0.1372	0.0020	1.45
5.151	0.1448	0.1437	0.0011	0.79
8.305	0.1557	0.1573	-0.0016	1.00
10.41	0.1636	0.1642	-0.0006	0.38
12.51	0.1702	0.1704	-0.0002	0.13
16.72	0.1799	0.1817	-0.0018	0.98
20.92	0.1899	0.1921	-0.0022	1.16
26.18	0.2098	0.2046	0.0052	2.48
31.43	0.2122	0.2167	-0.0045	2.14
36.69	0.2254	0.2287	-0.0033	1.46
44.05	0.2445	0.2453	-0.0008	0.31
52.36	0.2682	0.2638	0.0044	1.66

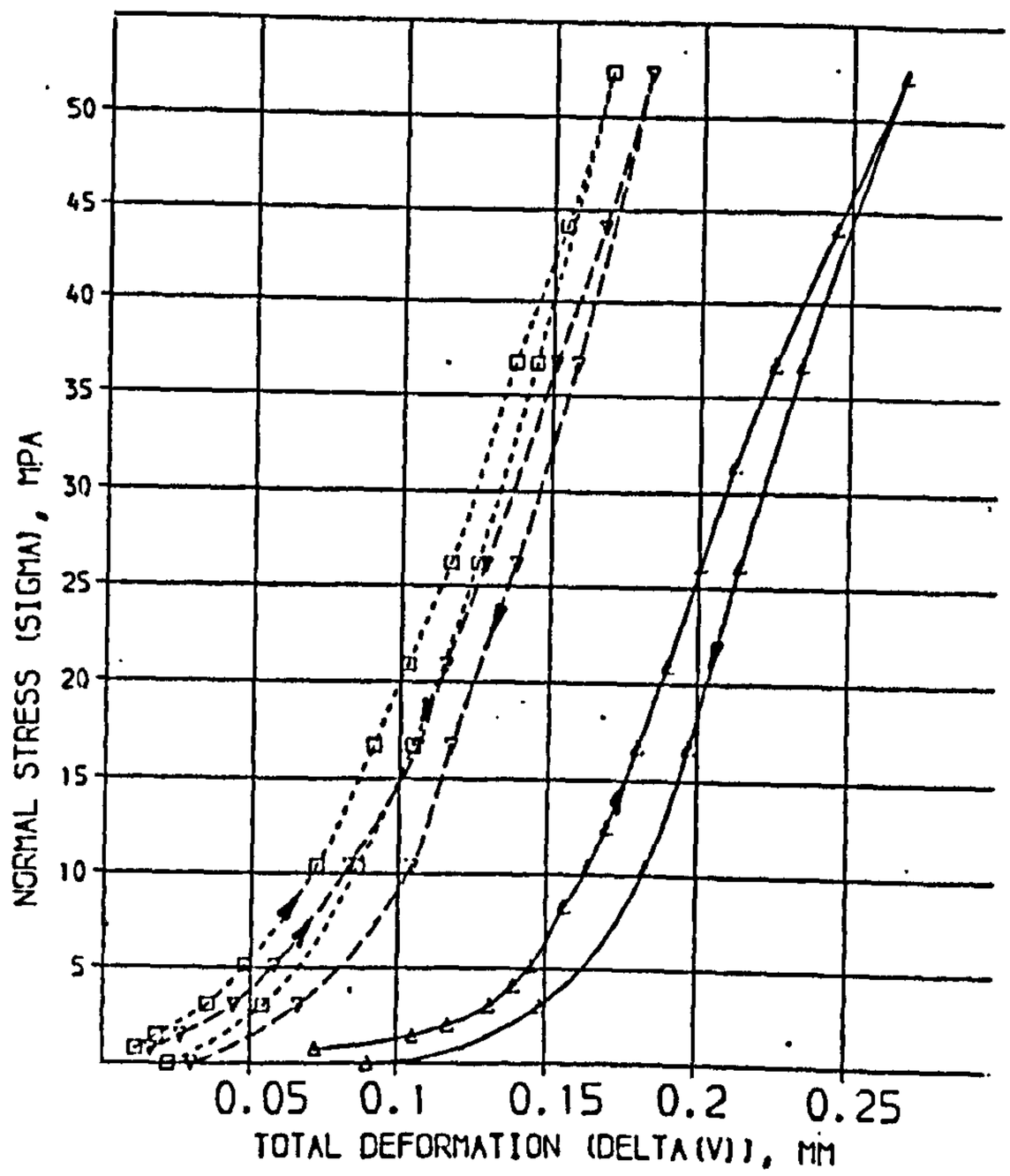

2nd loading

SOLUTION

A=	47.80	SD =	1.796	% =	3.758
B=	0.09283	SD =	0.002734	% =	2.949
C=	538.3	SD =	15.09	% =	2.803

COMPUTED RESIDUALS

SIGMA	DELTA(V) MEASURED	DELTA(V) CALCULATED	DIFF	% DIFF
0.7570	0.01600	0.01494	0.00106	6.65
1.470	0.02650	0.02585	0.00067	2.52
3.049	0.04400	0.04347	0.00053	1.20
5.151	0.05800	0.05944	-0.00144	2.49
10.41	0.08300	0.08445	-0.00145	1.72
16.72	0.1060	0.1044	0.0016	1.48
20.92	0.1155	0.1155	0.0000	0.04
26.18	0.1280	0.1280	-0.0000	0.01
36.69	0.1510	0.1510	0.0000	0.01
44.05	0.1670	0.1662	0.0008	0.49
52.36	0.1820	0.1829	-0.0009	0.47

3rd loading

SOLUTION

A=	71.28	SD =	2.346	% =	3.292
B=	0.08275	SD =	0.002646	% =	3.197
C=	550.9	SD =	13.89	% =	2.521

COMPUTED RESIDUALS

SIGMA	DELTA(V) MEASURED	DELTA(V) CALCULATED	DIFF	% DIFF
0.7570	0.01100	0.01059	0.00041	1.94
1.470	0.01800	0.01918	-0.00118	6.54
3.049	0.03450	0.03373	0.00077	2.22
5.151	0.04800	0.04793	0.00007	0.15
10.41	0.07200	0.07172	0.00028	0.39
16.72	0.09100	0.09155	-0.00055	0.58
20.92	0.1020	0.1025	-0.0005	0.52
26.18	0.1160	0.1151	0.0009	0.81
36.69	0.1370	0.1379	-0.0009	0.65
44.05	0.1540	0.1529	0.0011	0.68
52.36	0.1690	0.1694	-0.0004	0.25

LMST : No. 15

1st loading

SOLUTION

A=	8.276	SD =	0.6100	% =	7.370
B=	0.1621	SD =	0.003927	% =	2.423
C=	702.5	SD =	47.12	% =	6.708

COMPUTED RESIDUALS

SIGMA	DELTA(V) MEASURED	DELTA(V) CALCULATED	DIFF	% DIFF
0.5120	0.05650	0.04550	0.01300	22.22
1.051	0.07660	0.07260	0.00391	5.10
2.076	0.09580	0.10140	-0.00560	5.85
3.074	0.1132	0.1172	-0.0040	3.54
3.748	0.1194	0.1247	-0.0053	4.42
5.098	0.1307	0.1356	-0.0049	3.72
7.795	0.1473	0.1494	-0.0021	1.40
10.49	0.1582	0.1586	-0.0004	0.27
13.18	0.1661	0.1659	0.0002	0.14
15.89	0.1732	0.1721	0.0011	0.66
18.58	0.1791	0.1776	0.0015	0.84
21.28	0.1849	0.1827	0.0022	1.17
23.98	0.1904	0.1876	0.0028	1.47
26.67	0.1958	0.1923	0.0035	1.80
29.37	0.2007	0.1968	0.0039	1.95
33.42	0.2067	0.2034	0.0033	1.61
40.16	0.2149	0.2140	0.0009	0.42
46.90	0.2228	0.2243	-0.0015	0.68
53.65	0.2314	0.2345	-0.0031	1.33
60.39	0.2411	0.2445	-0.0034	1.41

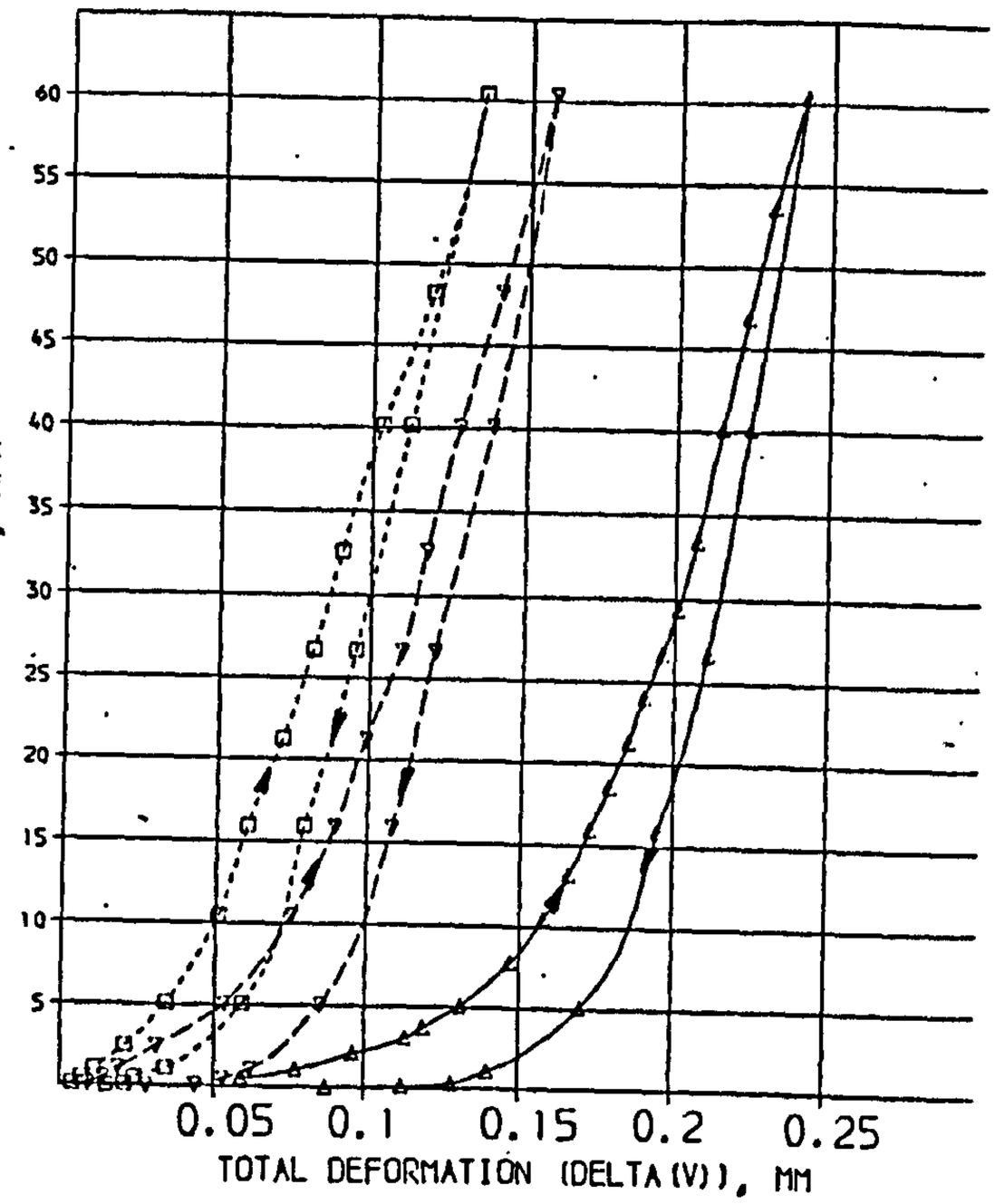

2nd loading

SOLUTION

A=	48.41	SD =	5.369	% =	11.09
B=	0.08564	SD =	0.006118	% =	7.144
C=	781.8	SD =	67.51	% =	8.610

COMPUTED RESIDUALS

SIGMA	DELTA(V) MEASURED	DELTA(V) CALCULATED	DIFF	% DIFF
0.1070	0.009000	0.002292	0.006708	74.54
0.5120	0.01420	0.01007	0.00413	29.09
1.051	0.01990	0.01866	0.00124	6.21
2.400	0.03100	0.03447	-0.00347	11.19
5.097	0.05300	0.05374	-0.00074	1.41
10.49	0.07500	0.07480	0.00020	0.27
15.89	0.08900	0.08824	0.00076	0.85
21.28	0.09900	0.09889	0.00011	0.11
26.67	0.1100	0.1082	0.0018	1.61
32.67	0.1180	0.1174	0.0006	0.18
40.16	0.1260	0.1290	-0.0030	2.38
43.25	0.1410	0.1406	0.0004	0.30
61.39	0.1530	0.1574	0.0006	0.39

3rd loading

SOLUTION

A=	80.12	SD =	13.34	% =	16.70
B=	0.04292	SD =	0.004128	% =	9.619
C=	629.5	SD =	31.15	% =	4.948

COMPUTED RESIDUALS

SIGMA	DELTA(V) MEASURED	DELTA(V) CALCULATED	DIFF	% DIFF
0.1070	0.003500	0.001465	0.002035	58.14
0.5120	0.006300	0.005875	0.000425	6.24
1.051	0.01100	0.01192	-0.00092	8.51
2.400	0.02050	0.02145	-0.00095	4.65
5.097	0.03400	0.03372	0.00028	0.81
10.49	0.05100	0.04899	0.00201	3.95
15.89	0.06000	0.06054	-0.00054	0.87
21.28	0.07100	0.07055	0.00045	0.35
26.67	0.08050	0.08038	0.00012	0.15
32.67	0.08800	0.09073	-0.00273	3.10
40.16	0.1010	0.1033	-0.0023	2.30
43.25	0.1220	0.1167	0.0053	4.34
61.39	0.1350	0.1365	-0.0015	1.14

LMST : No. 16

1st loading

SOLUTION

A=	0.922	SD =	0.1984	% =	2.867
B=	0.4396	SD =	0.01300	% =	2.957
C=	122.2	SD =	6.733	% =	5.508

COMPUTED RESIDUALS

SIGMA	DELTA(V) MEASURED	DELTA(V) CALCULATED	DIFF	% DIFF
0.4580	0.05500	0.06590	-0.01090	19.82
1.056	0.1150	0.1222	-0.0072	6.23
1.682	0.1740	0.1703	0.0037	2.15
2.305	0.2120	0.2083	0.0037	1.73
2.927	0.2450	0.2395	0.0055	2.25
3.550	0.2709	0.2658	0.0051	1.90
4.795	0.3085	0.3082	0.0003	0.10
6.040	0.3396	0.3418	-0.0022	0.64
7.286	0.3648	0.3697	-0.0049	1.35
8.656	0.3947	0.3961	-0.0014	0.35
10.777	0.4140	0.4153	-0.0013	0.31
12.52	0.4531	0.4560	-0.0029	0.65
14.76	0.4677	0.4652	0.0025	0.51
17.25	0.5158	0.5148	0.0010	0.19
19.74	0.5439	0.5424	0.0015	0.28
22.86	0.5771	0.5750	0.0021	0.36
26.78	0.6917	0.6139	-0.0022	0.36

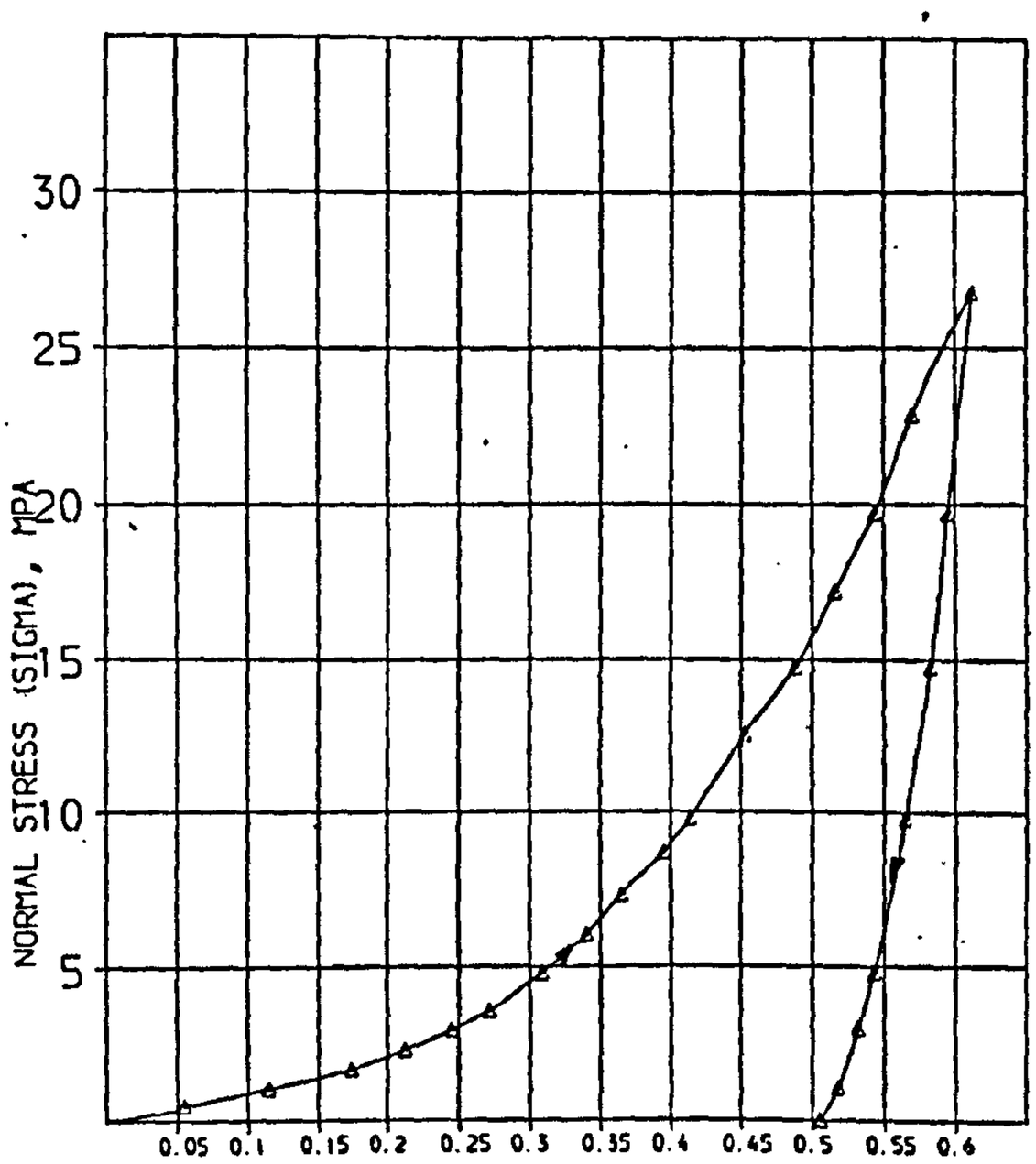

LMST : No. 17

1st loading

SOLUTION

A=	12.89	SD =	0.4660	% =	3.615
B=	0.2760	SD =	0.007257	% =	2.629
C=	235.6	SD =	6.082	% =	3.854

COMPUTED RESIDUALS

SIGMA	DELTA(V) MEASURED	DELTA(V) CALCULATED	DIFF	% DIF
0.4030	0.03370	0.02979	0.00391	11.61
0.9080	0.06260	0.05996	0.00264	4.21
1.916	0.1107	0.1047	0.0060	5.39
2.421	0.1259	0.1220	0.0039	3.08
2.926	0.1386	0.1370	0.0016	1.18
3.535	0.1597	0.1616	-0.0019	1.21
4.943	0.1781	0.1815	-0.0034	1.89
5.952	0.1923	0.1980	-0.0057	2.96
7.965	0.2175	0.2246	-0.0071	3.28
8.987	0.2445	0.2459	-0.0014	0.57
12.00	0.2620	0.2639	-0.0019	0.71
14.02	0.2783	0.2797	-0.0014	0.49
16.04	0.2932	0.2940	-0.0008	0.26
18.26	0.3101	0.3085	0.0016	0.52
20.07	0.3207	0.3197	0.0010	0.33
24.11	0.3493	0.3428	0.0065	1.85
28.14	0.3701	0.3645	0.0056	1.52
32.28	0.3890	0.3856	0.0034	0.87
36.21	0.4073	0.4050	0.0023	0.56
42.27	0.4335	0.4340	-0.0005	0.11
49.33	0.4590	0.4668	-0.0078	1.70

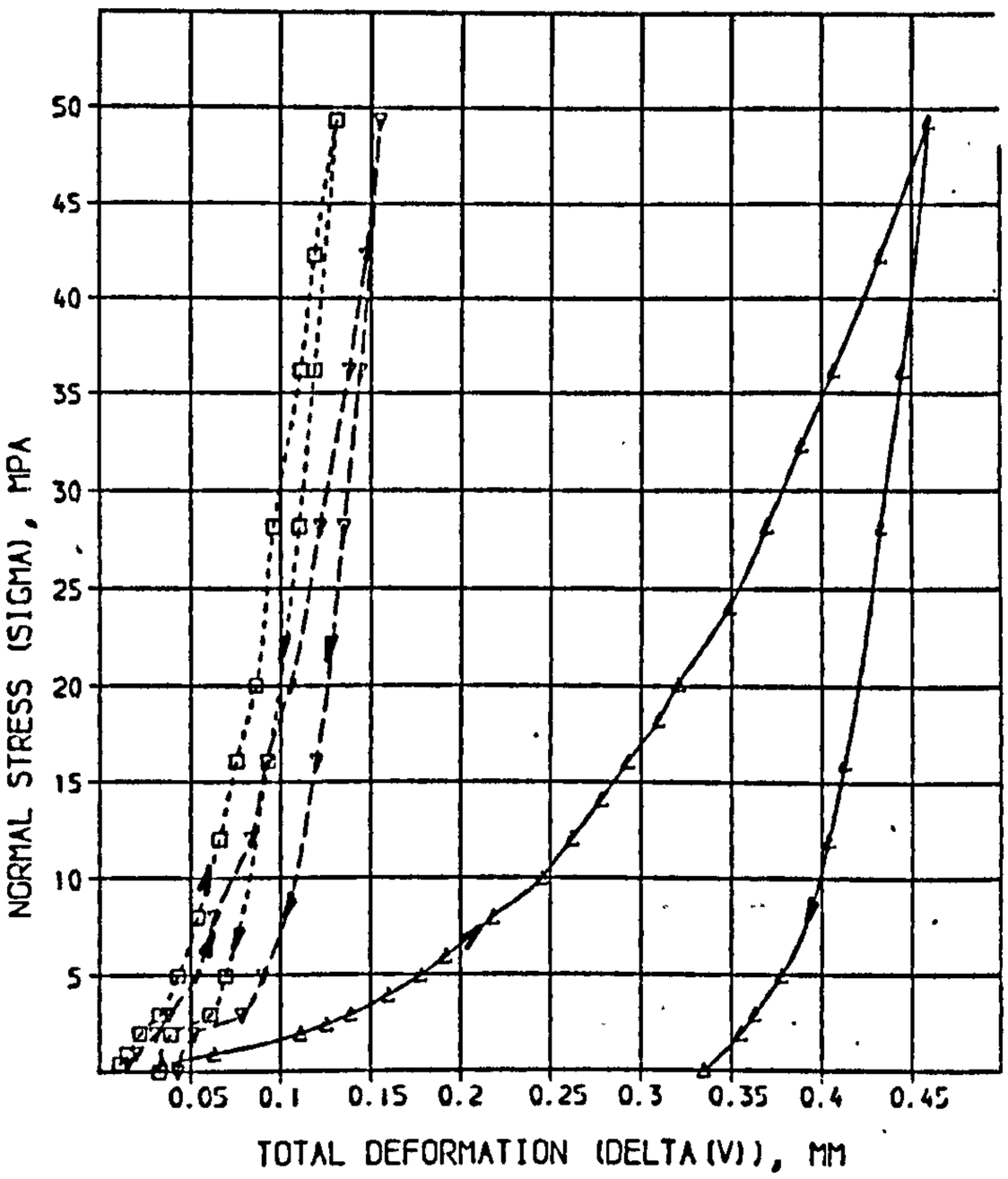

2nd loading

SOLUTION

A=	49.44	SD =	9.275	% =	12.69
B=	0.08387	SD =	0.008576	% =	10.22
C=	605.7	SD =	63.50	% =	10.48

COMPUTED RESIDUALS

SIGMA	DELTA(V) MEASURED	DELTA(V) CALCULATED	DIFF	% DIFF
0.4030	0.01500	0.00809	0.00691	46.03
0.9080	0.02000	0.01657	0.00343	17.17
1.916	0.03050	0.02967	0.00083	2.72
2.926	0.03800	0.03953	-0.00153	4.03
4.943	0.05300	0.05377	-0.00077	1.46
7.969	0.06250	0.06832	-0.00582	9.32
12.00	0.08300	0.08215	0.00085	1.03
16.04	0.09200	0.09315	-0.00115	1.22
20.00	0.1050	0.1025	0.0025	2.39
28.14	0.1220	0.1196	0.0024	2.00
36.21	0.1375	0.1350	0.0025	1.79
42.27	0.1470	0.1462	0.0008	0.57
49.33	0.1550	0.1588	-0.0038	2.46

3rd loading

SOLUTION

A=	59.76	SD =	5.406	% =	9.147
B=	0.06485	SD =	0.004549	% =	7.015
C=	698.4	SD =	45.71	% =	6.546

COMPUTED RESIDUALS

SIGMA	DELTA(V) MEASURED	DELTA(V) CALCULATED	DIFF	% DIFF
0.4030	0.01100	0.00649	0.00451	39.22
0.9080	0.01500	0.01361	0.00139	9.26
1.946	0.02200	0.02447	-0.00247	11.21
2.926	0.03300	0.03209	0.00091	2.76
4.943	0.04250	0.04343	-0.00093	2.19
7.969	0.05400	0.05504	-0.00104	1.93
12.00	0.06600	0.06620	-0.00020	0.31
16.04	0.07500	0.07520	-0.00020	0.26
20.00	0.08600	0.08296	0.00304	3.53
28.14	0.09600	0.09729	-0.00129	1.35
36.21	0.1110	0.1104	0.0006	0.51
42.27	0.1190	0.1199	-0.0009	0.78
49.33	0.1310	0.1306	0.0004	0.18

LMST : No. 18

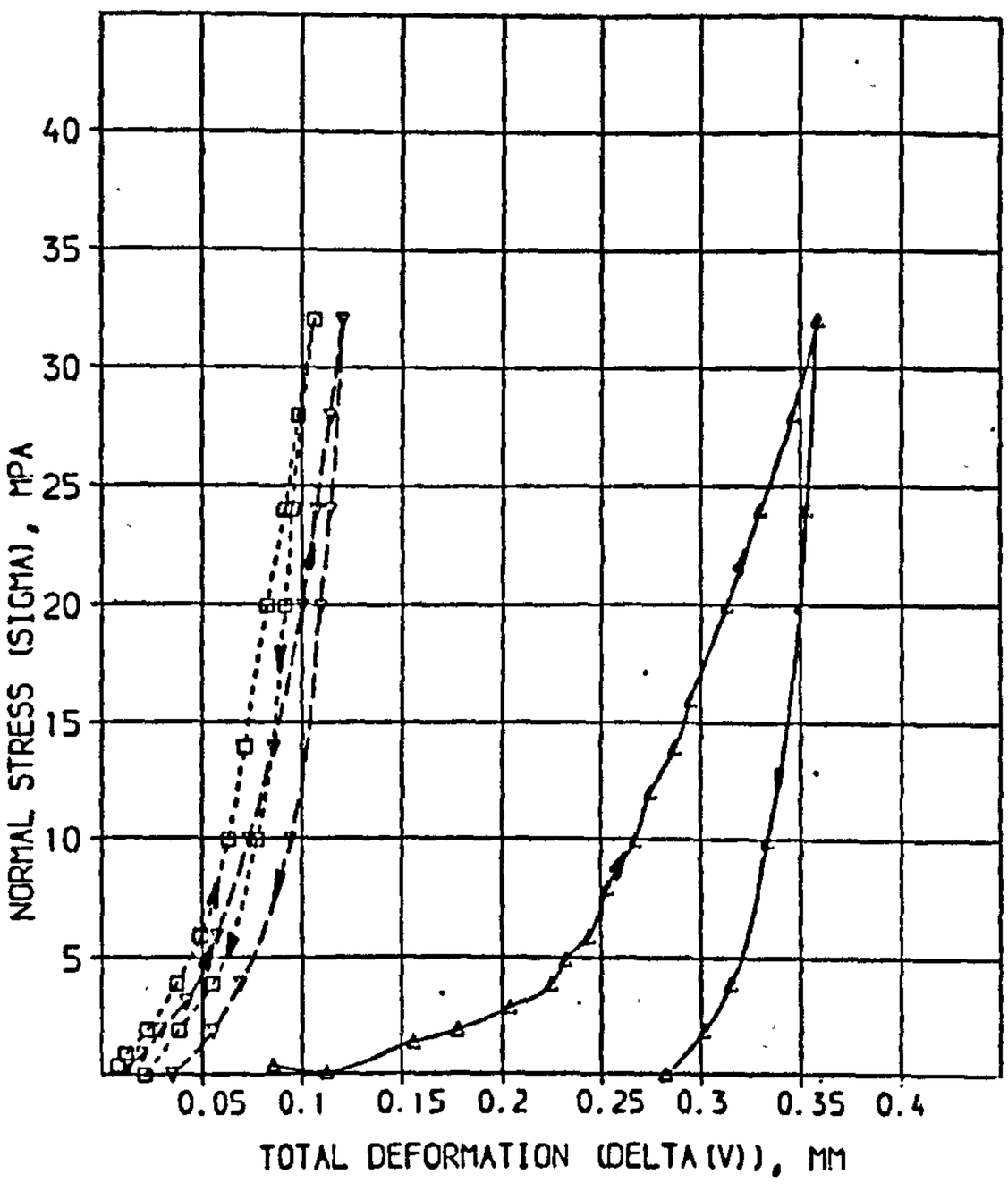

1st loading

SOLUTION

A=	3.836	SD =	0.2082	% =	5.424
B=	0.2576	SD =	0.005512	% =	2.140
C=	294.5	SD =	19.13	% =	6.771

COMPUTED RESIDUALS

SIGMA	DELTA(V) MEASURED	DELTA(V) CALCULATED	DIFF	% DIFF
0.4010	0.08500	0.07569	0.00931	10.95
0.9030	0.1120	0.1260	-0.0140	12.52
1.404	0.1560	0.1559	0.0001	0.05
1.906	0.1780	0.1761	0.0019	1.08
2.909	0.2040	0.2021	0.0019	0.92
3.913	0.2250	0.2189	0.0061	2.70
4.916	0.2320	0.2312	0.0008	0.36
5.918	0.2440	0.2408	0.0032	1.30
7.925	0.2530	0.2559	-0.0029	1.16
9.931	0.2670	0.2680	-0.0010	0.38
12.02	0.2750	0.2788	-0.0038	1.39
13.94	0.2870	0.2879	-0.0009	0.31
16.00	0.2950	0.2970	-0.0020	0.67
19.96	0.3134	0.3133	0.0001	0.04
23.98	0.3298	0.3289	0.0009	0.29
27.99	0.3456	0.3439	0.0017	0.49
32.00	0.3587	0.3586	0.0001	0.03

2nd loading

SOLUTION

A=	43.66	SD =	3.798	% =	8.700
B=	0.07647	SD =	0.006378	% =	8.341
C=	612.5	SD =	68.15	% =	11.13

COMPUTED RESIDUALS

SIGMA	DELTA(V) MEASURED	DELTA(V) CALCULATED	DIFF	% DIFF
0.4010	0.01300	0.00885	0.00415	31.89
0.9030	0.01950	0.01775	0.00175	8.95
1.906	0.02900	0.03090	-0.00190	6.56
3.155	0.04200	0.04230	-0.00030	0.73
5.918	0.05700	0.05855	-0.00155	2.72
9.931	0.07300	0.07344	-0.00044	0.61
13.94	0.08500	0.08445	0.00055	0.64
19.96	0.1000	0.0981	0.0019	1.90
23.98	0.1070	0.1063	0.0007	0.68
27.99	0.1140	0.1140	-0.0000	0.01
32.00	0.1200	0.1215	-0.0015	1.24

3rd loading

SOLUTION

A=	65.19	SD =	4.868	% =	7.466
B=	0.06845	SD =	0.006133	% =	8.959
C=	716.4	SD =	80.88	% =	11.29

COMPUTED RESIDUALS

SIGMA	DELTA(V) MEASURED	DELTA(V) CALCULATED	DIFF	% DIFF
0.4010	0.008000	0.006204	0.001796	22.46
0.9030	0.01200	0.01278	-0.00078	6.50
1.906	0.02150	0.02315	-0.00165	7.66
3.913	0.03700	0.03744	-0.00044	1.19
5.918	0.04900	0.04728	0.00172	3.50
9.931	0.06250	0.06109	0.00141	2.26
13.94	0.07100	0.07131	-0.00031	0.44
19.96	0.08200	0.08380	-0.00180	2.20
23.98	0.09050	0.09118	-0.00068	0.75
27.99	0.09800	0.09811	-0.00011	0.11
32.00	0.1060	0.1047	0.0013	1.19

LMST : No. 19

1st loading_

SOLUTION

A=	6.266	SD =	0.5673	% =	9.053
B=	0.2322	SD =	0.01062	% =	4.573
C=	272.3	SD =	22.77	% =	8.347

COMPUTED RESIDUALS

SIGMA	DELTA(V) MEASURED	DELTA(V) CALCULATED	DIFF	% DIFF
0.2940	0.04900	0.04011	0.00889	18.15
0.4900	0.06700	0.06029	0.00671	10.01
0.6860	0.08900	0.07691	0.01209	13.58
0.9810	0.1040	0.0971	0.0069	6.64
1.471	0.1210	0.1221	-0.0011	0.92
1.964	0.1370	0.1400	-0.0030	2.61
2.942	0.1540	0.1661	-0.0121	7.88
3.923	0.1710	0.1857	-0.0147	7.45
5.884	0.1960	0.2077	-0.0117	5.98
7.846	0.2180	0.2246	-0.0066	3.04
11.77	0.2530	0.2494	0.0036	1.28
15.96	0.2820	0.2713	0.0107	3.80
19.62	0.3010	0.2881	0.0129	4.30
24.52	0.3160	0.3091	0.0069	2.20
29.42	0.3370	0.3291	0.0079	2.34
34.32	0.3510	0.3486	0.0024	0.69
39.23	0.3650	0.3677	-0.0027	0.74
47.07	0.3840	0.3974	-0.0134	3.59

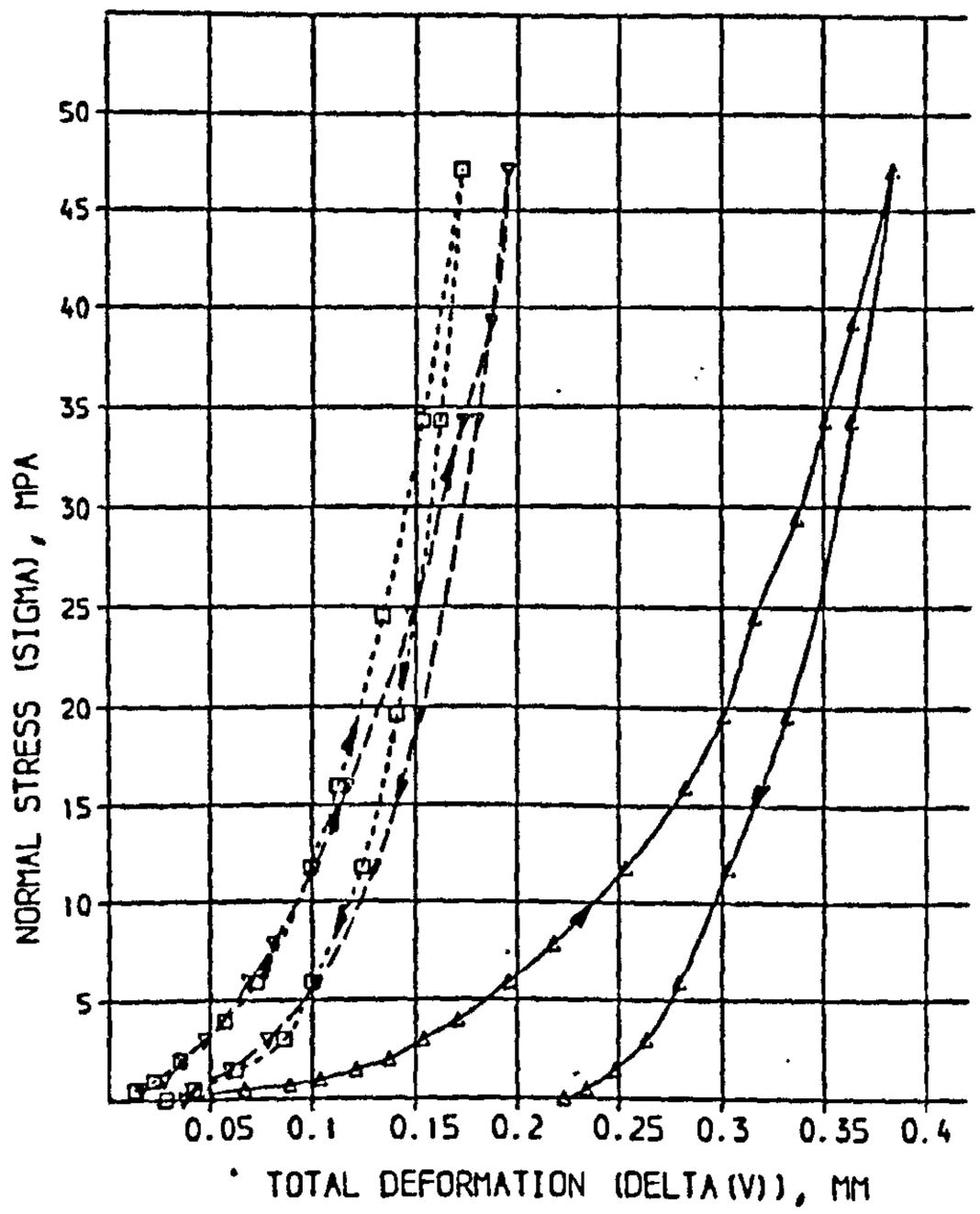

2nd loading_

SOLUTION

A=	42.50	SD =	1.494	% =	3.514
B=	0.1198	SD =	0.004291	% =	3.581
C=	725.3	SD =	44.49	% =	6.133

COMPUTED RESIDUALS

SIGMA	DELTA(V) MEASURED	DELTA(V) CALCULATED	DIFF	% DIFF
0.4900	0.01300	0.01119	0.00181	13.90
0.9810	0.02200	0.02071	0.00129	5.88
1.964	0.03500	0.03600	-0.00100	3.02
3.923	0.05700	0.05755	-0.00055	0.96
5.884	0.07300	0.07234	0.00066	0.90
11.77	0.09900	0.09980	-0.00080	0.87
15.96	0.1120	0.1128	-0.0008	0.76
24.52	0.1340	0.1330	0.0010	0.73
34.32	0.1530	0.1517	0.0013	0.87
47.07	0.1720	0.1730	-0.0010	0.59

3rd loading_

SOLUTION

A=	43.99	SD =	5.662	% =	12.76
B=	0.1063	SD =	0.01293	% =	12.16
C=	448.5	SD =	51.60	% =	11.51

COMPUTED RESIDUALS

SIGMA	DELTA(V) MEASURED	DELTA(V) CALCULATED	DIFF	% DIFF
0.4900	0.01600	0.01118	0.00482	30.16
0.9810	0.02700	0.02062	0.00638	25.63
1.964	0.03600	0.03582	0.00018	0.50
2.942	0.04700	0.04761	-0.00061	1.30
5.884	0.06900	0.07235	-0.00335	4.86
7.846	0.08100	0.08410	-0.00310	3.83
11.77	0.1010	0.1023	-0.0013	1.30
15.96	0.1170	0.1178	-0.0008	0.69
24.52	0.1480	0.1439	0.0041	2.74
34.32	0.1730	0.1701	0.0029	1.68
39.23	0.1870	0.1824	0.0046	2.44
47.07	0.1950	0.2010	-0.0060	3.41

LMST : No. 20

1st loading

SOLUTION

A=	12,43	SD =	1,549	% =	12,86
B=	0.2168	SD =	0,02503	% =	10,62
C=	182.1	SD =	23,03	% =	12,65

COMPUTED RESIDUALS

SIGMA	DELTA(V) MEASURED	DELTA(V) CALCULATED	DIFF	% DIFF
0.3460	0.03900	0.02656	0,01244	31,89
0.8090	0.06800	0.05444	0,01356	19,95
1.154	0.07600	0.07153	0,00467	6,15
1.731	0.09200	0.09428	-0,00228	2,48
2.308	0.1050	0.1127	-0.0077	7,31
4.615	0.1570	0.1662	-0.0092	5,30
6.923	0.1760	0.1940	-0.0180	10,25
9.231	0.2220	0.2165	0.0055	1,59
13.84	0.2630	0.2575	0.0055	2,10
18.46	0.3010	0.2905	0.0105	3,48
23.07	0.3290	0.3208	0.0082	2,49
27.84	0.3570	0.3566	0.0004	0,11
34.62	0.3810	0.3912	-0.0102	2,68

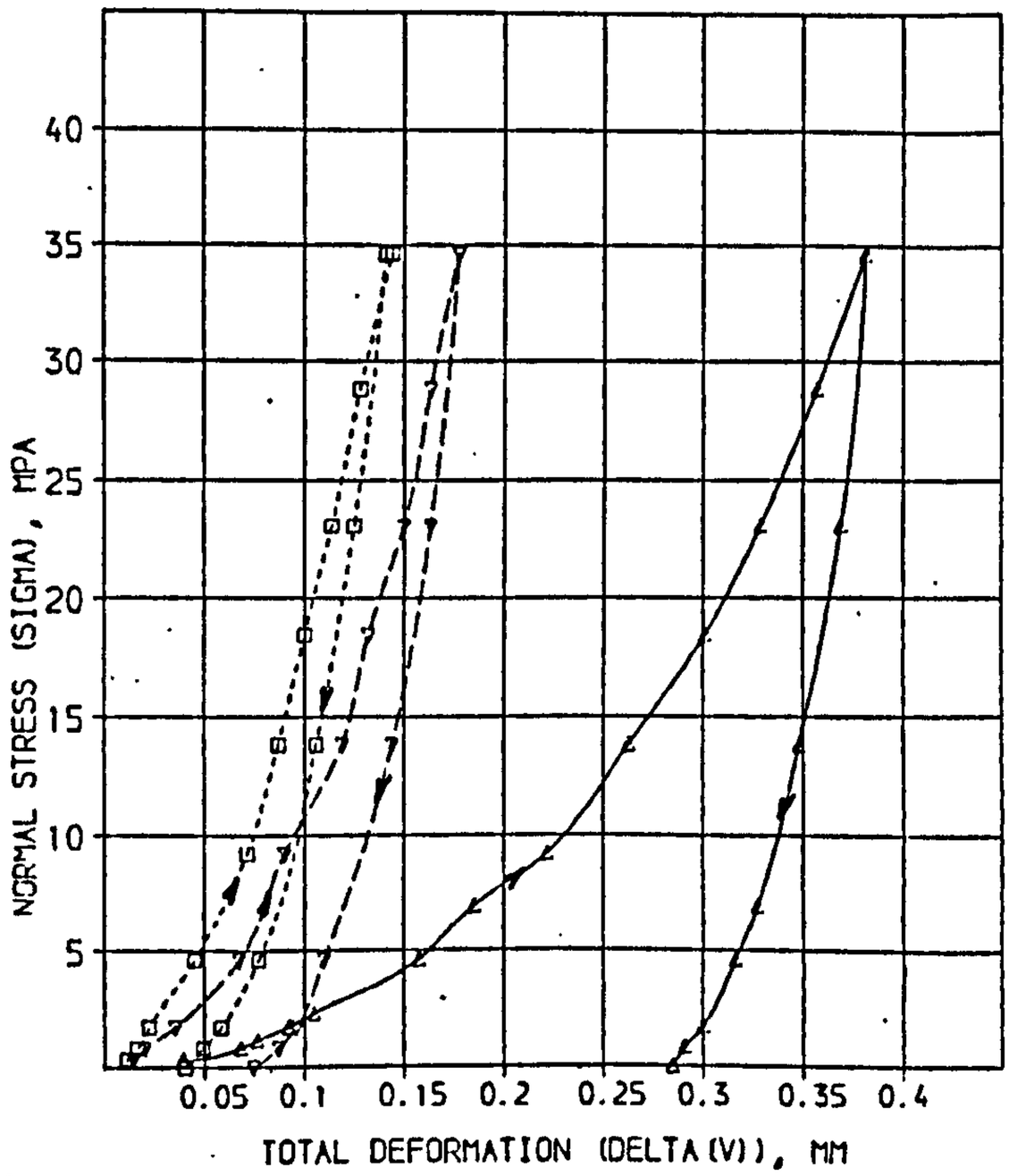

2nd loading

SOLUTION

A=	20.26	SD =	0,291	% =	13,76
B=	0.06980	SD =	0,009506	% =	13,62
C=	424.4	SD =	43,19	% =	10,18

COMPUTED RESIDUALS

SIGMA	DELTA(V) MEASURED	DELTA(V) CALCULATED	DIFF	% DIFF
0.3461	0.01100	0.00612	0,00488	44,36
0.8090	0.01600	0.01315	0,00285	17,80
1.731	0.02200	0.02445	-0,00245	11,04
4.615	0.04500	0.04739	-0,00239	5,32
9.231	0.07100	0.06970	0,00130	1,83
13.84	0.08700	0.08616	0,00084	0,96
18.46	0.1000	0.1005	-0.0005	0,35
23.07	0.1140	0.1134	0.0006	0,51
27.84	0.1280	0.1289	-0.0009	0,69
34.62	0.1440	0.1438	0.0002	0,12

3rd loading

SOLUTION

A=	39,77	SD =	4,895	% =	12,50
B=	0.1084	SD =	0,01346	% =	12,42
C=	418.6	SD =	58,98	% =	14,09

COMPUTED RESIDUALS

SIGMA	DELTA(V) MEASURED	DELTA(V) CALCULATED	DIFF	% DIFF
0.3460	0.01400	0.00888	0,00512	36,57
0.8080	0.02000	0.01904	0,00096	4,80
1.731	0.03500	0.03519	-0,00019	0,54
4.615	0.06700	0.06706	-0,00006	0,09
9.231	0.09000	0.09592	-0,00592	6,58
13.84	0.1190	0.1157	0.0033	2,78
18.46	0.1320	0.1319	0.0001	0,04
23.07	0.1500	0.1464	0.0036	2,38
27.84	0.1630	0.1632	-0.0002	0,11
34.62	0.1770	0.1791	-0.0021	1,17

SLST : No. 1

1st loading_

SOLUTION

A=	14.02	SD =	2.245	% =	16.01
B=	0.1518	SD =	0.01646	% =	10.84
C=	147.0	SD =	12.98	% =	8.827

COMPUTED RESIDUALS

SIGMA	DELTA(V) MEASURED	DELTA(V) CALCULATED	DIFF	% DIFF
0.4290	0.02800	0.02838	-0.00038	1.35
0.9400	0.05700	0.05289	0.00411	7.21
1.961	0.08500	0.08613	-0.00113	1.33
2.983	0.1060	0.1089	-0.0029	2.72
4.005	0.1240	0.1264	-0.0024	1.91
8.048	0.1530	0.1534	-0.0004	0.28
8.091	0.1770	0.1752	0.0018	1.00
10.13	0.1980	0.1944	0.0036	1.82
12.18	0.2160	0.2121	0.0039	1.83
14.22	0.2340	0.2288	0.0052	2.23
16.26	0.2490	0.2449	0.0041	1.66
18.31	0.2340	0.2605	-0.0265	11.33
20.35	0.2800	0.2759	0.0041	1.48
22.39	0.2650	0.2901	0.0041	1.37
24.40	0.3090	0.3062	0.0028	0.90
28.52	0.3360	0.3353	0.0007	0.22

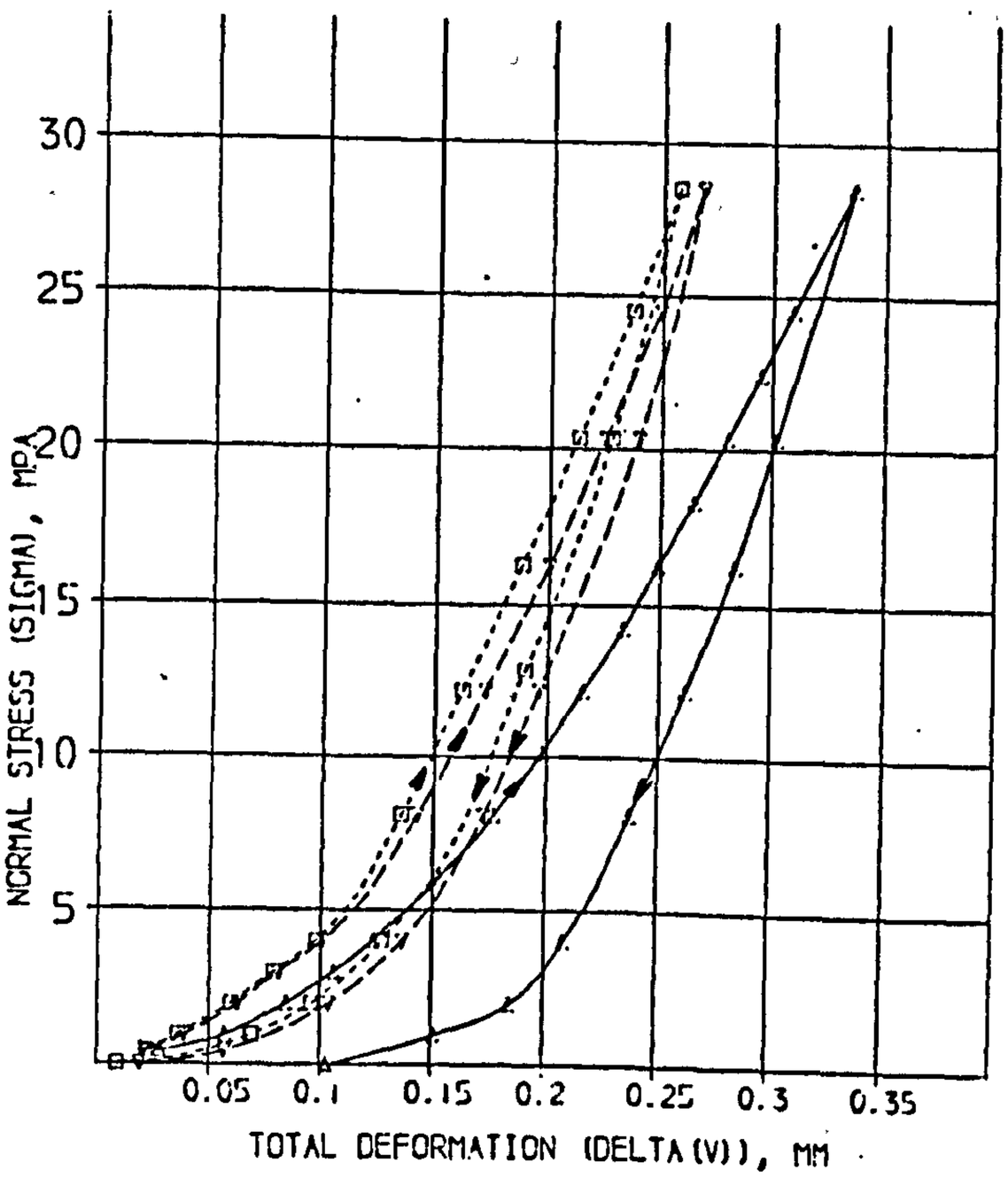

2nd loading_

SOLUTION

A=	21,83	SD =	1,207	% =	5,529
B=	0.1337	SD =	0,007338	% =	5,489
C=	191.1	SD =	8,709	% =	4,558

COMPUTED RESIDUALS

SIGMA	DELTA(V) MEASURED	DELTA(V) CALCULATED	DIFF	% DIFF
0.4290	0.02100	0.01938	0.00162	7.73
0.9400	0.03900	0.03748	0.00152	3.88
1.961	0.06300	0.06399	-0.00099	1.56
2.983	0.08100	0.08314	-0.00214	2.69
4.005	0.1010	0.0983	0.0027	2.68
8.091	0.1370	0.1406	-0.0036	2.62
12.18	0.1720	0.1716	0.0004	0.24
16.26	0.2000	0.1984	0.0016	0.78
20.35	0.2250	0.2234	0.0010	0.70
24.40	0.2490	0.2476	0.0014	0.56
28.52	0.2690	0.2705	-0.0025	0.94

3rd loading_

SOLUTION

A=	21,82	SD =	1,134	% =	5,196
B=	0.1262	SD =	0,006211	% =	4,921
C=	200.3	SD =	8,243	% =	4,115

COMPUTED RESIDUALS

SIGMA	DELTA(V) MEASURED	DELTA(V) CALCULATED	DIFF	% DIFF
0.4290	0.02200	0.01913	0.00285	12.94
0.9400	0.03600	0.03681	-0.00081	2.25
1.961	0.06000	0.06228	-0.00228	3.81
2.983	0.07900	0.08052	-0.00152	1.92
4.005	0.09300	0.09478	0.00322	3.28
8.091	0.1360	0.1346	0.0014	1.06
12.18	0.1620	0.1637	-0.0017	1.08
16.26	0.1380	0.1891	-0.0011	0.59
20.35	0.2130	0.2124	0.0002	0.11
24.40	0.2370	0.2357	0.0013	0.54
28.52	0.2570	0.2575	-0.0005	0.18

SLST : No 2

1st loading_

SOLUTION

A=	25.90	SD =	2.604	% =	10.28
B=	0.1582	SD =	0.01813	% =	11.46
C=	252.2	SD =	32.87	% =	13.03

COMPUTED RESIDUALS

SIGMA	DELTA(V) MEASURED	DELTA(V) CALCULATED	DIFF	% DIFF
0.9970	0.04300	0.03491	0.00809	18.81
2.081	0.06500	0.06153	0.00347	5.34
3.165	0.08000	0.08149	-0.00149	1.86
4.249	0.09500	0.09738	-0.00238	2.50
6.417	0.1180	0.1220	-0.0040	3.38
8.584	0.1360	0.1411	-0.0051	3.76
10.75	0.1530	0.1572	-0.0042	2.72
12.92	0.1690	0.1713	-0.0023	1.38
15.09	0.1800	0.1842	0.0058	3.04
17.25	0.2010	0.1962	0.0048	2.36
19.42	0.2120	0.2076	0.0044	2.06
21.59	0.2240	0.2186	0.0054	2.43
25.93	0.2380	0.2394	-0.0014	0.59
30.26	0.2530	0.2593	-0.0063	2.50

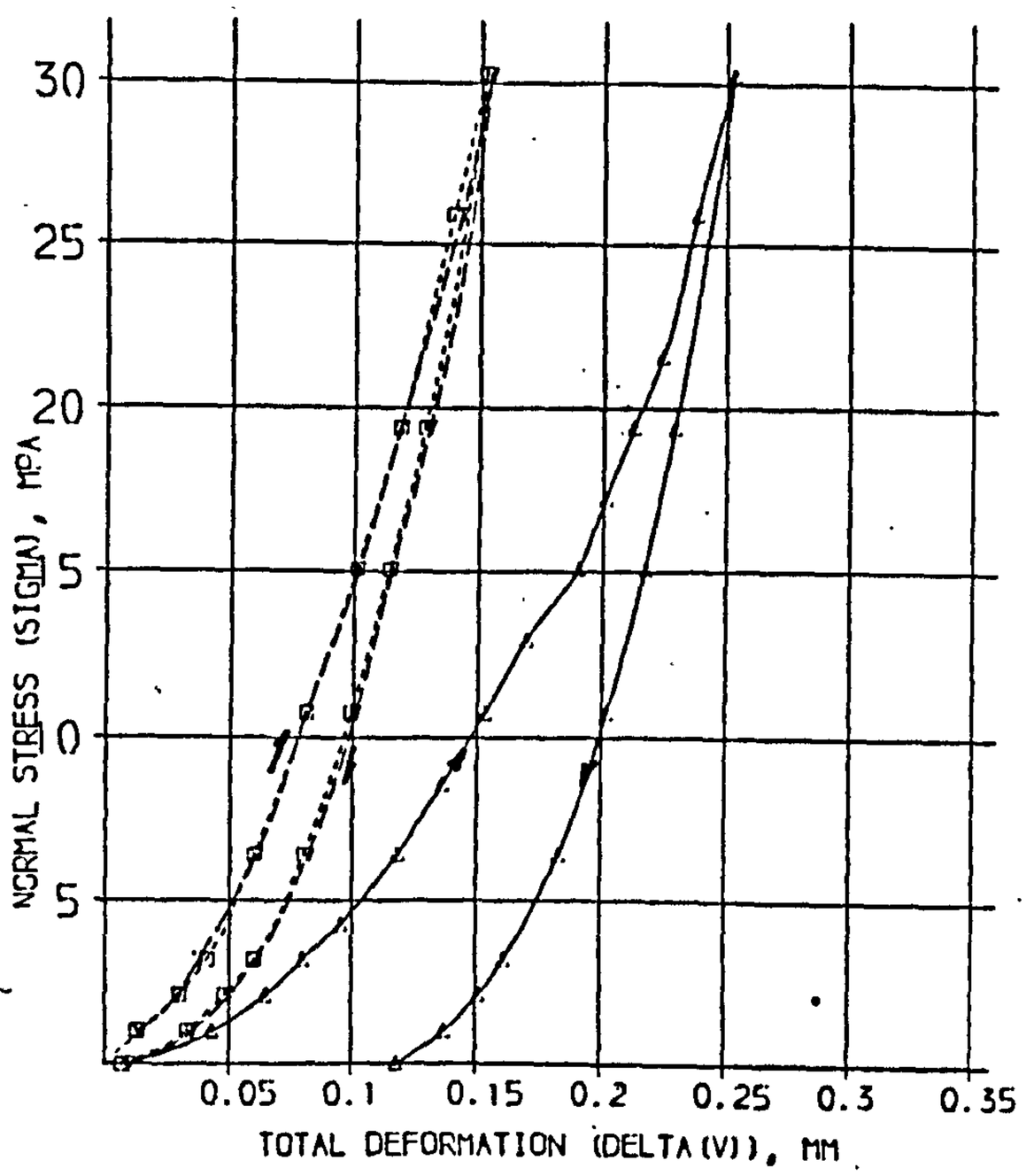

2nd loading_

SOLUTION

A=	69.06	SD =	4.351	% =	6.301
B=	0.07453	SD =	0.006877	% =	9.227
C=	330.6	SD =	19.14	% =	5.789

COMPUTED RESIDUALS

SIGMA	DELTA(V) MEASURED	DELTA(V) CALCULATED	DIFF	% DIFF
0.9970	0.01400	0.01511	-0.00111	7.93
2.081	0.02900	0.02775	0.00125	4.30
3.165	0.03800	0.03795	0.00005	0.13
6.417	0.06100	0.06077	0.00023	0.38
10.75	0.08100	0.08291	-0.00191	2.36
15.09	0.1020	0.1012	0.0008	0.77
19.42	0.1180	0.1177	0.0003	0.29
25.93	0.1420	0.1406	0.0014	0.97
30.26	0.1540	0.1552	-0.0012	0.79

3rd loading_

SOLUTION

A=	64.23	SD =	5.944	% =	9.254
B=	0.07351	SD =	0.009147	% =	12.44
C=	339.0	SD =	27.65	% =	8.155

COMPUTED RESIDUALS

SIGMA	DELTA(V) MEASURED	DELTA(V) CALCULATED	DIFF	% DIFF
0.9970	0.01300	0.01570	-0.00270	21.21
2.082	0.03000	0.02864	0.00136	4.54
3.165	0.04100	0.03884	0.00216	5.28
6.417	0.06000	0.06120	-0.00120	2.13
10.75	0.08130	0.08279	-0.00179	2.21
15.09	0.1010	0.1005	0.0005	0.49
19.42	0.1180	0.1164	0.0016	1.34
25.93	0.1390	0.1387	0.0003	0.23
30.26	0.1520	0.1529	-0.0009	0.56

SLST : No. 3

1st loading

SOLUTION

A=	22.42	SD =	0.5957	% =	2.658
B=	0.1782	SD =	0.005047	% =	2.832
C=	228.7	SD =	7.359	% =	3.218

COMPUTED RESIDUALS

SIGMA	DELTA(V) MEASURED	DELTA(V) CALCULATED	DIFF	% DIFF
0.5580	0.02400	0.02428	-0.00028	1.18
1.222	0.04800	0.04709	0.00091	1.90
2.551	0.08300	0.08061	0.00239	2.88
3.880	0.1040	0.1048	-0.0008	0.75
5.209	0.1210	0.1236	-0.0026	2.19
7.867	0.1520	0.1526	-0.0006	0.40
10.52	0.1760	0.1752	0.0008	0.45
13.18	0.1940	0.1944	-0.0004	0.22
15.84	0.2120	0.2116	0.0004	0.19
18.50	0.2270	0.2275	-0.0005	0.20
21.15	0.2430	0.2424	0.0006	0.24
23.18	0.2560	0.2534	0.0026	1.01
26.47	0.2700	0.2706	-0.0006	0.23
31.79	0.2460	0.2473	-0.0013	0.45

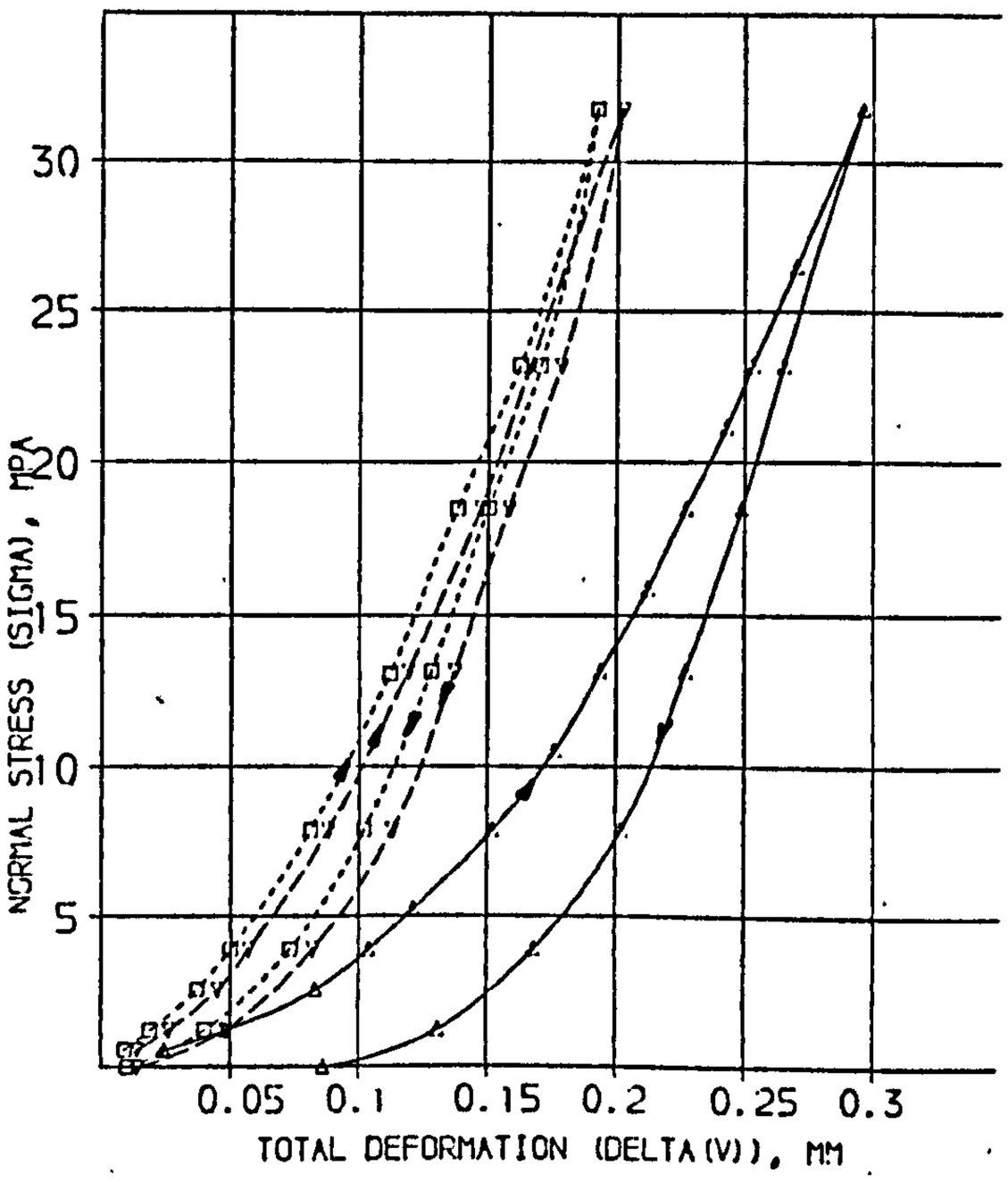

2nd loading

SOLUTION

A=	45.75	SD =	2.348	% =	5.132
B=	0.08835	SD =	0.005550	% =	6.053
C=	255.5	SD =	9.014	% =	3.703

COMPUTED RESIDUALS

SIGMA	DELTA(V) MEASURED	DELTA(V) CALCULATED	DIFF	% DIFF
0.5580	0.01400	0.01290	0.00110	7.84
1.222	0.02600	0.02529	0.00071	2.72
2.555	0.04500	0.04422	0.00078	1.74
3.880	0.05700	0.05840	-0.00140	2.56
7.867	0.08800	0.08910	-0.00110	1.31
13.18	0.1100	0.1104	-0.0004	0.17
18.50	0.1470	0.1449	0.0021	1.42
23.18	0.1660	0.1660	0.0000	0.03
31.79	0.2020	0.2028	-0.0008	0.40

3rd loading

SOLUTION

A=	69.66	SD =	3.209	% =	4.607
B=	0.1122	SD =	0.011.9	% =	10.69
C=	308.3	SD =	24.01	% =	7.786

COMPUTED RESIDUALS

SIGMA	DELTA(V) MEASURED	DELTA(V) CALCULATED	DIFF	% DIFF
0.5580	0.009000	0.009287	-0.000287	3.19
1.222	0.01900	0.01914	-0.00014	0.71
2.555	0.03700	0.03593	0.00107	2.89
3.880	0.05000	0.04981	0.00019	0.33
7.867	0.08100	0.08180	-0.00080	0.99
13.10	0.1120	0.1124	-0.0008	0.69
18.50	0.1380	0.1389	-0.0009	0.64
23.18	0.1620	0.1591	0.0029	1.79
31.79	0.1920	0.1932	-0.0012	0.61

SLST : No. 4

1st loading

SOLUTION

A=	15.82	SD =	2.034	% =	12.85
B=	0.1874	SD =	0.01827	% =	9.749
C=	132.5	SD =	9.402	% =	7.095

COMPUTED RESIDUALS

SIGMA	DELTA(V) MEASURED	DELTA(V) CALCULATED	DIFF	% DIFF
0.5200	0.03400	0.03189	0.00211	6.21
1.136	0.06600	0.06061	0.00539	8.17
2.377	0.1030	0.1013	0.0017	1.62
3.616	0.1280	0.1303	-0.0023	1.77
4.854	0.1530	0.1530	0.0000	0.01
7.330	0.1890	0.1888	0.0002	0.13
9.807	0.1950	0.2179	-0.0229	11.76
12.28	0.2470	0.2437	0.0033	1.34
14.76	0.2740	0.2675	0.0065	2.39
17.24	0.2950	0.2900	0.0050	1.70
19.71	0.3170	0.3117	0.0053	1.68
22.19	0.3400	0.3326	0.0072	2.12
24.67	0.3550	0.3535	0.0015	0.43
29.62	0.3400	0.3939	-0.0039	1.00
34.57	0.4280	0.4335	-0.0055	1.29

SLST : No. 5

SOLUTION

A=	16.23	SD =	0.9317	% =	5.741
B=	0.1748	SD =	0.007338	% =	4.197
C=	167.1	SD =	6.043	% =	3.616

COMPUTED RESIDUALS

SIGMA	DELTA(V) MEASURED	DELTA(V) CALCULATED	DIFF	% DIFF
0.5210	0.03700	0.03024	0.00676	18.27
1.142	0.06000	0.05701	0.00299	4.99
2.383	0.09300	0.09407	-0.00107	1.15
3.625	0.1160	0.1198	-0.0038	3.24
4.866	0.1370	0.1396	-0.0026	1.87
7.349	0.1670	0.1701	-0.0031	1.86
9.832	0.1960	0.1945	0.0015	0.76
12.31	0.2180	0.2158	0.0022	1.02
14.80	0.2340	0.2352	-0.0012	0.53
17.28	0.2560	0.2536	0.0024	0.95
19.76	0.2750	0.2711	0.0039	1.40
24.75	0.3050	0.3048	0.0002	0.06
29.69	0.3350	0.3373	-0.0023	0.68
34.66	0.3680	0.3690	-0.0010	0.27

SLST : No. 6

1st loading

SOLUTION

A=	11.22	SD =	0.4128	% =	3.678
B=	0.4191	SD =	0.01636	% =	3.904
C=	115.6	SD =	5.010	% =	4.342

COMPUTED RESIDUALS

SIGMA	DELTA(V) MEASURED	DELTA(V) CALCULATED	DIFF	% DIFF
0.5070	0.05200	0.04517	0.00683	13.13
0.9580	0.07500	0.07922	-0.00422	5.62
1.522	0.1150	0.1156	-0.0006	0.56
2.085	0.1470	0.1468	0.0002	0.15
3.213	0.1620	0.1679	-0.0059	3.09
4.340	0.2450	0.2387	0.0063	2.56
6.594	0.3120	0.3017	0.0103	3.29
8.849	0.3450	0.3503	-0.0053	1.54
11.10	0.3810	0.3906	-0.0096	2.52
13.36	0.4240	0.4257	-0.0017	0.40
15.61	0.4560	0.4573	-0.0013	0.30
17.87	0.4680	0.4666	0.0014	0.29
22.38	0.5480	0.5402	0.0078	1.42
26.88	0.5880	0.5897	-0.0017	0.28
31.39	0.6420	0.6365	0.0055	0.85
35.90	0.6800	0.6817	-0.0017	0.25
38.16	0.7000	0.7038	-0.0038	0.54

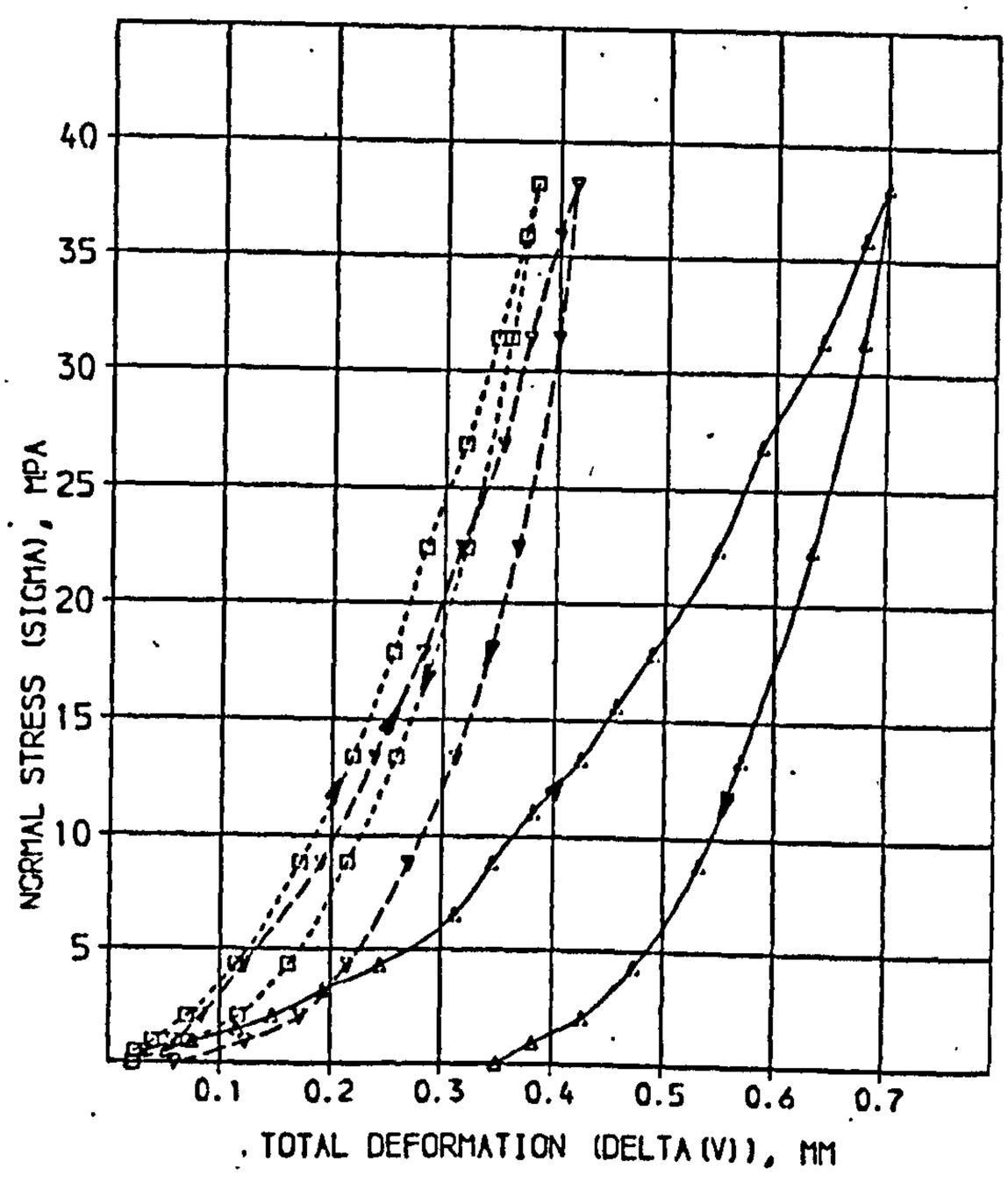

2nd loading

SOLUTION

A=	20.03	SD =	2.375	% =	11.85
B=	0.2071	SD =	0.02203	% =	10.63
C=	164.4	SD =	13.81	% =	8.399

COMPUTED RESIDUALS

SIGMA	DELTA(V) MEASURED	DELTA(V) CALCULATED	DIFF	% DIFF
0.5070	0.03200	0.02563	0.00637	19.89
0.9580	0.05700	0.04468	0.01232	21.62
2.085	0.08300	0.08195	0.00105	1.27
4.340	0.1210	0.1323	-0.0113	9.32
8.849	0.1900	0.1948	-0.0048	2.54
13.39	0.2380	0.2396	-0.0016	0.66
17.87	0.2810	0.2768	0.0042	1.50
22.38	0.3150	0.3109	0.0041	1.32
26.88	0.3510	0.3429	0.0081	2.30
31.39	0.3740	0.3739	0.0001	0.03
35.90	0.4000	0.4040	-0.0040	1.01
38.16	0.4150	0.4189	-0.0039	0.94

3rd loading

SOLUTION

A=	25.93	SD =	1.292	% =	4.982
B=	0.2054	SD =	0.01127	% =	5.488
C=	188.5	SD =	8.519	% =	4.520

COMPUTED RESIDUALS

SIGMA	DELTA(V) MEASURED	DELTA(V) CALCULATED	DIFF	% DIFF
0.5070	0.02300	0.02055	0.00245	10.67
0.9580	0.03900	0.03640	0.00260	6.66
2.085	0.07000	0.06886	0.00114	1.63
4.340	0.1140	0.1153	-0.0013	1.11
8.849	0.1710	0.1752	-0.0042	2.45
13.39	0.2180	0.2180	-0.0000	0.00
17.87	0.2550	0.2531	0.0019	0.76
22.38	0.2830	0.2847	-0.0017	0.59
26.88	0.3180	0.3141	0.0039	1.24
31.39	0.3450	0.3422	0.0028	0.82
35.90	0.3690	0.3694	-0.0004	0.10
38.16	0.3790	0.3827	-0.0037	0.98

SLST : No. 7

1st loading

SOLUTION

A=	10.49	SD =	0.2346	% =	2.237
B=	0.3613	SD =	0.008608	% =	2.382
C=	88.71	SD =	2.014	% =	2.270

COMPUTED RESIDUALS

SIGMA	DELTA(V) MEASURED	DELTA(V) CALCULATED	DIFF	% DIFF
1.066	0.08300	0.09121	-0.00821	9.89
2.127	0.1550	0.1539	0.0011	0.72
3.191	0.2040	0.2012	0.0028	1.40
4.261	0.2410	0.2393	0.0017	0.71
5.316	0.2730	0.2709	0.0021	0.75
6.382	0.3000	0.2987	0.0013	0.45
7.446	0.3230	0.3234	-0.0004	0.13
8.509	0.3460	0.3459	0.0001	0.02
9.573	0.3670	0.3668	0.0002	0.06
10.64	0.3850	0.3863	-0.0013	0.35
12.76	0.4210	0.4225	-0.0015	0.36
14.89	0.4540	0.4559	-0.0019	0.42
17.02	0.4860	0.4874	-0.0014	0.29
19.15	0.5170	0.5175	-0.0005	0.09
21.27	0.5470	0.5465	0.0005	0.09
23.40	0.5760	0.5748	0.0012	0.21
25.53	0.6040	0.6024	0.0016	0.26
27.65	0.6290	0.6295	-0.0005	0.09

SLET : No. B

1st loading

SOLUTION

A=	9.973	SD =	0.1909	% =	1.914
B=	0.5796	SD =	0.01595	% =	2.752
C=	127.8	SD =	5.714	% =	4.470

COMPUTED RESIDUALS

SIGMA	DELTA(V) MEASURED	DELTA(V) CALCULATED	DIFF	% DIFF
0.4620	0.03700	0.04651	-0.00951	25.71
1.011	0.09000	0.09419	0.00481	4.86
1.561	0.1360	0.1355	0.0005	0.40
2.111	0.1730	0.1716	0.0014	0.83
3.210	0.2350	0.2321	0.0029	1.25
4.310	0.2780	0.2813	-0.0033	1.18
6.509	0.3530	0.357[illegible]	-0.0049	1.39
8.774	0.4180	0.4180	-0.0000	0.01
10.91	0.4690	0.4641	0.0049	1.04
13.10	0.5070	0.5047	0.0023	0.45
17.61	0.5730	0.5742	-0.0012	0.20
21.90	0.6270	0.6299	-0.0029	0.46
26.30	0.6830	0.6809	0.0021	0.31
	0.7250	0.7279	-0.0029	0.40

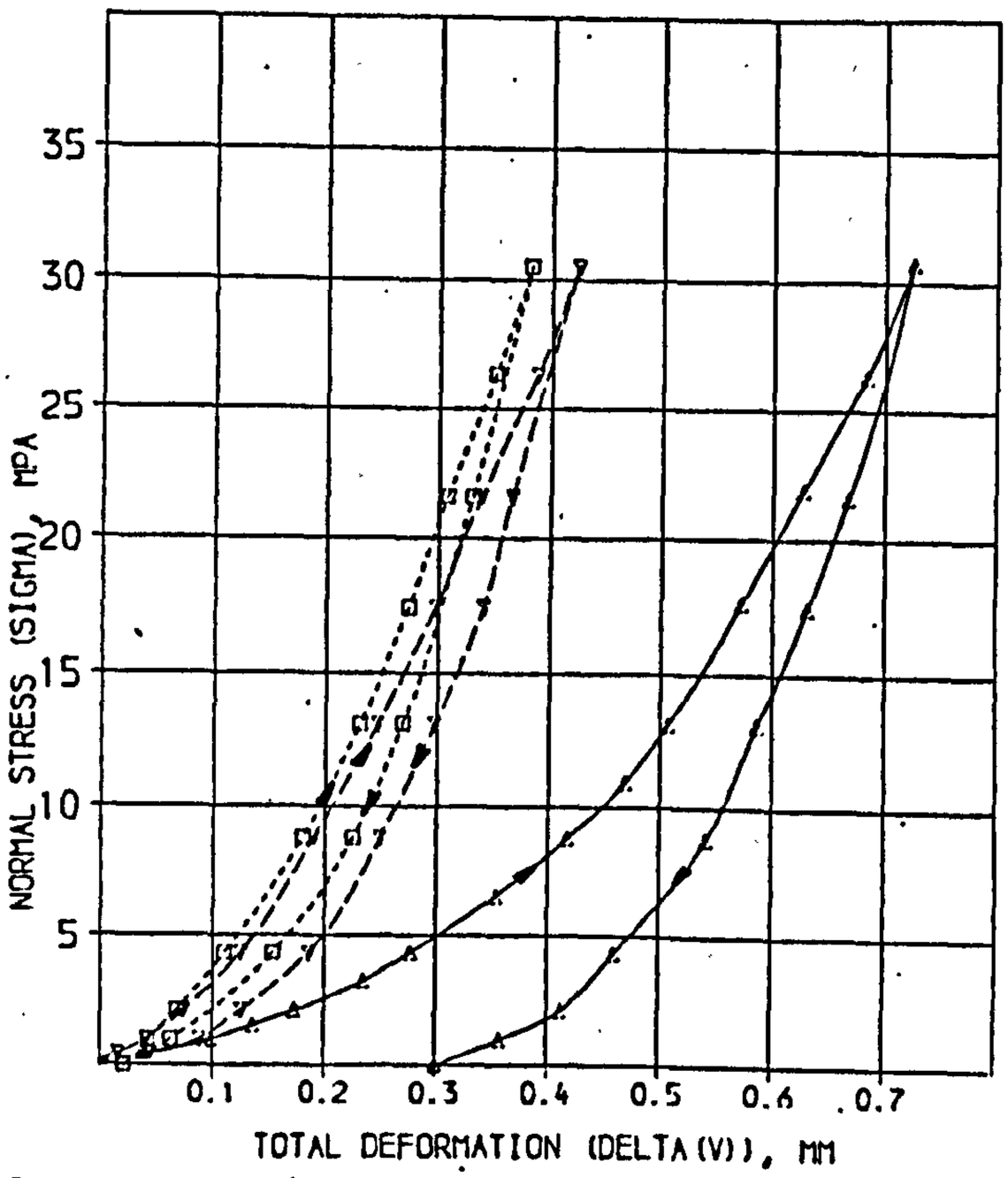

2nd loading

SOLUTION

A=	27,01	SD =	1,425	% =	5,277
B=	0.1805	SD =	0,01263	% =	7,001
C=	112,9	SD =	4,109	% =	3,693

COMPUTED RESIDUALS

SIGMA	DELTA(V) MEASURED	DELTA(V) CALCULATED	DIFF	% DIFF
0.4620	0,01600	0,01972	-0,00372	23,22
1.011	0.04100	0,03996	0,00104	2,55
2.111	0.07400	0,07324	0,00076	1,03
4.310	0.1250	0.1229	0,0021	1,71
8.774	0.1900	0,1937	-0,0037	1,96
13.10	0.2470	0,2470	-0,0000	0,23
17.41	0.2980	0,2952	0,0028	0,94
21.60	0.3380	0,3386	-0,0006	0,17
26.30	0.3870	0,3852	0,0018	0,46
30.50	0.4240	0,4258	-0,0018	0,41

3rd loading

SOLUTION

A=	29,04	SD =	1,937	% =	6,668
B=	0.1949	SD =	0,01971	% =	10,11
C=	139,7	SD =	9,343	% =	6,686

COMPUTED RESIDUALS

SIGMA	DELTA(V) MEASURED	DELTA(V) CALCULATED	DIFF	% DIFF
1.011	0.04300	0,03677	0,00623	14,49
2.111	0.06800	0,06805	-0,00005	0,07
4.310	0.1110	0.1151	-0.0041	3,68
8.774	0.1800	0,1813	-0,0013	0,69
13.10	0.2310	0,2298	0,0012	0,51
17.41	0.2740	0,2717	0,0023	0,86
21.60	0.3080	0,3090	-0,0010	0,32
26.30	0.3500	0,3486	0,0014	0,41
30.50	0.3810	0,3820	-0,0010	0,43

SLST : No. 9

1st loading

SOLUTION

A=	6.949	SD =	0.2793	% =	4.019
B=	0.6026	SD =	0.03406	% =	5.652
C=	113.5	SD =	13.77	% =	12.13

COMPUTED RESIDUALS

SIGMA	DELTA(V) MEASURED	DELTA(V) CALCULATED	DIFF	% DIFF
0.4300	0.06500	0.05990	0.00510	7.85
0.9430	0.1240	0.1191	0.0049	3.98
1.968	0.1880	0.2100	-0.0220	11.69
2.922	0.2620	0.2734	0.0086	3.05
4.017	0.3400	0.3304	0.0096	2.82
6.067	0.4110	0.4100	0.0010	0.25
8.116	0.4650	0.4690	-0.0040	0.86
10.17	0.5160	0.5163	-0.0003	0.06
12.21	0.5550	0.5563	-0.0013	0.24
14.26	0.5910	0.5915	-0.0005	0.08
16.31	0.6240	0.6232	0.0008	0.13
18.36	0.6520	0.6524	-0.0004	0.07
20.41	0.6800	0.6798	0.0002	0.03
22.46	0.7060	0.7058	0.0002	0.04
24.51	0.7310	0.7306	0.0004	0.06

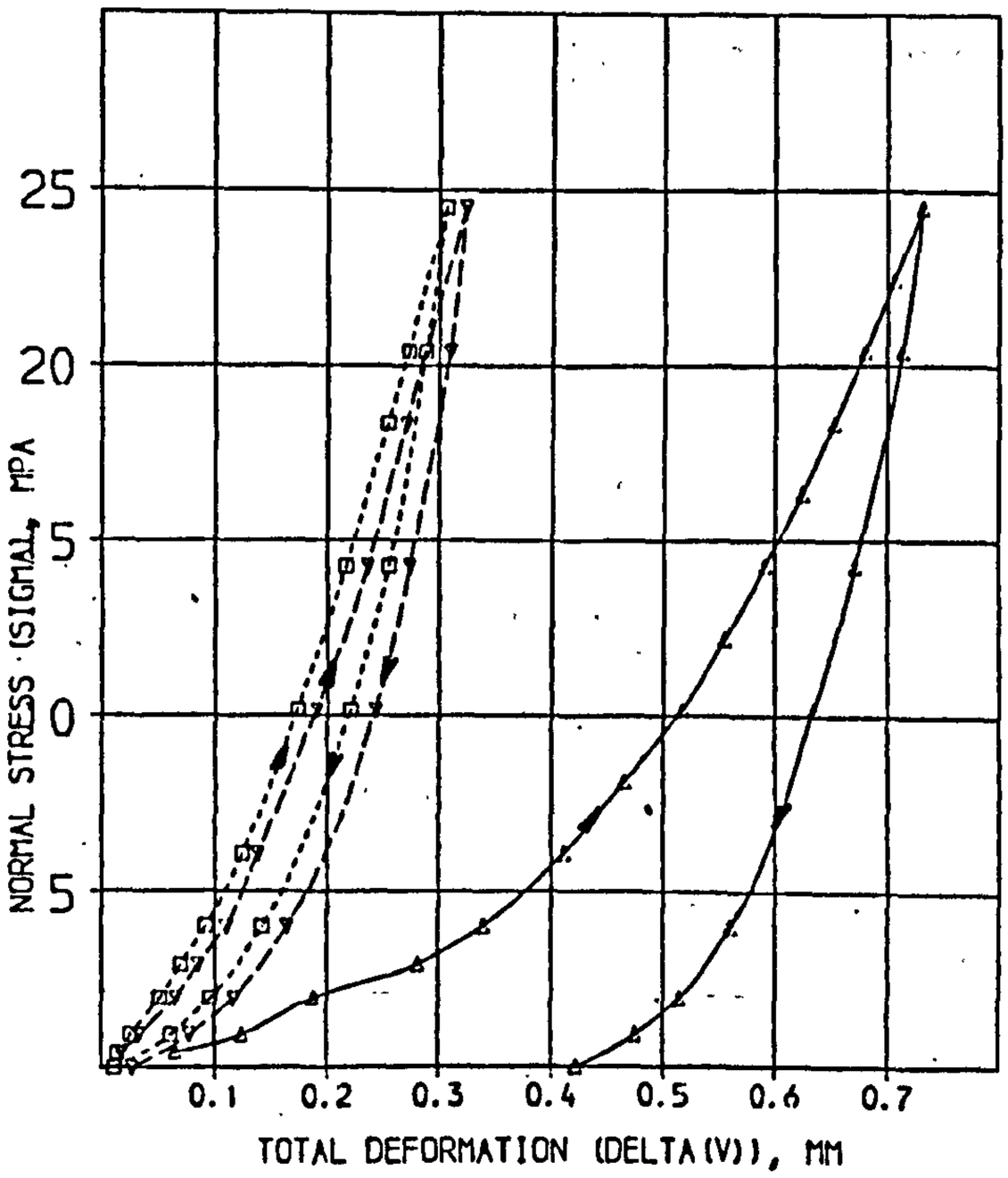

2nd loading

SOLUTION

A=	28,60	SD =	0,9044	% =	3,176
B=	0.1764	SD =	0,01134	% =	6,428
C=	138,7	SD =	0,457	% =	4,640

COMPUTED RESIDUALS

SIGMA	DELTA(V) MEASURED	DELTA(V) CALCULATED	DIFF	% DIFF
0,4300	0.01800	0,01695	0,00105	5,82
0,9430	0.03300	0,03457	-0,00157	4,77
1,968	0.06500	0,06368	0,00132	2,03
2,922	0.08500	0,08575	-0,00075	0,89
4,017	0.1090	0,1071	0,0019	1,70
6,067	0.1380	0,1400	-0,0020	1,48
10,17	0.1900	0,1912	-0,0012	0,64
14,26	0.2360	0,2331	0,0029	1,23
18,36	0.2700	0,2707	-0,0007	0,27
20,41	0.2880	0,2886	-0,0006	0,19
24,51	0.3230	0,3230	0,0000	0,01

3rd loading

SOLUTION

A=	40,93	SD =	0,6462	% =	1,584
B=	0.1800	SD =	0,009590	% =	5,329
C=	146,2	SD =	2,102	% =	3,550

COMPUTED RESIDUALS

SIGMA	DELTA(V) MEASURED	DELTA(V) CALCULATED	DIFF	% DIFF
0,4300	0.01400	0,01287	0,00113	8,09
0,9430	0.02600	0,02687	-0,00087	3,36
1,968	0.05100	0,05140	-0,00040	0,79
2,922	0.07000	0,07110	-0,00110	1,56
4,017	0.09200	0,09098	0,00102	1,11
6,067	0.1240	0,1228	0,0012	0,99
10,17	0.1730	0,1739	-0,0009	0,53
14,26	0.2160	0,2162	-0,0002	0,08
18,36	0.2540	0,2540	0,0000	0,01
20,41	0.2720	0,2718	0,0002	0,07
24,51	0.3060	0,3060	0,0000	0,01

SLST : No.10

1st loading

SOLUTION

A=	14.21	SD =	0.1321	% =	0.9297
B=	0.5998	SD =	0.01477	% =	2.463
C=	182.6	SD =	9.959	% =	5.455

COMPUTED RESIDUALS

SIGMA	DELTA(V) MEASURED	DELTA(V) CALCULATED	DIFF	% DIFF
0.6010	0.04250	0.04281	-0.00031	0.72
1.002	0.06450	0.06859	0.00091	1.31
1.603	0.10000	0.10374	-0.00374	3.74
2.003	0.1260	0.1251	0.0009	0.70
3.005	0.1705	0.1728	-0.0023	1.36
4.007	0.2146	0.2138	0.0008	0.38
5.009	0.2500	0.2495	0.0005	0.21
6.010	0.2810	0.2810	0.0000	0.00
8.014	0.3400	0.3346	0.0054	1.59
10.02	0.3780	0.3790	-0.0010	0.26
12.02	0.4150	0.4168	-0.0018	0.44
14.02	0.4478	0.4499	-0.0021	0.47
16.03	0.4820	0.4794	0.0026	0.54
20.03	0.5285	0.5306	-0.0021	0.39
22.04	0.5550	0.5533	0.0017	0.31
24.04	0.5733	0.5746	-0.0013	0.22
26.04	0.5950	0.5946	0.0004	0.06

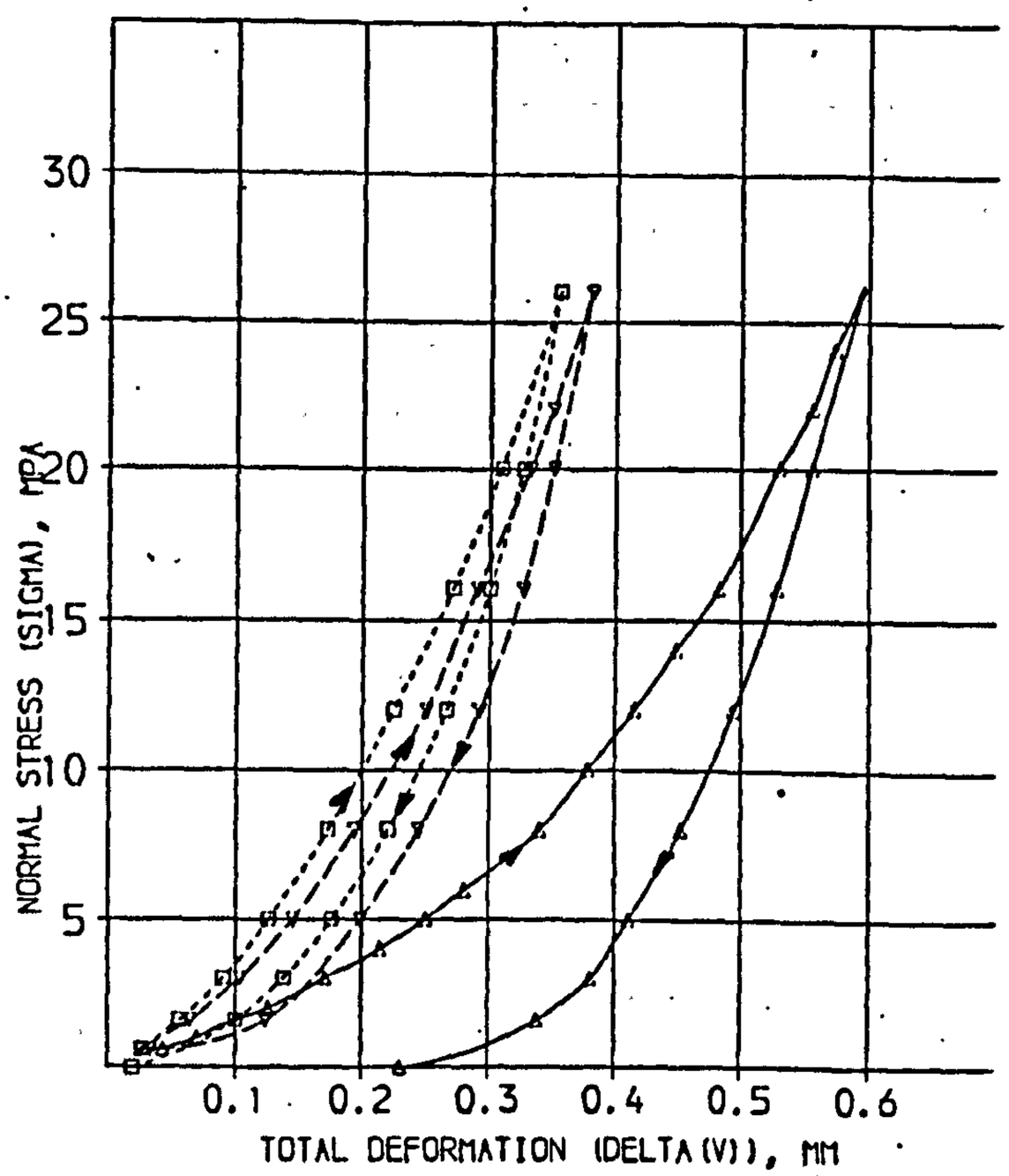

2nd loading

SOLUTION

A=	25.07	SD =	0.7228	% =	2.884
B=	0.2549	SD =	0.01608	% =	6.545
C=	146.8	SD =	9.158	% =	6.237

COMPUTED RESIDUALS

SIGMA	DELTA(V) MEASURED	DELTA(V) CALCULATED	DIFF	% DIFF
0.6010	0.02500	0.02601	-0.00101	4.04
1.603	0.06400	0.06204	0.00196	3.06
3.005	0.1030	0.1020	0.0010	0.97
5.009	0.1450	0.1461	-0.0011	0.78
8.014	0.1940	0.1964	-0.0024	1.24
12.02	0.2500	0.2483	0.0017	0.68
16.03	0.2900	0.2914	-0.0014	0.49
20.03	0.3320	0.3297	0.0023	0.70
22.04	0.3490	0.3477	0.0013	0.37
26.04	0.3800	0.3820	-0.0020	0.53

3rd loading

SOLUTION

A=	30.72	SD =	1.744	% =	5.677
B=	0.2267	SD =	0.03277	% =	14.46
C=	146.0	SD =	17.28	% =	11.83

COMPUTED RESIDUALS

SIGMA	DELTA(V) MEASURED	DELTA(V) CALCULATED	DIFF	% DIFF
0.6010	0.02600	0.02213	0.00387	14.89
1.603	0.05600	0.05340	0.00260	4.64
3.005	0.09000	0.08892	0.00108	1.20
5.009	0.1260	0.1291	-0.0031	2.50
8.014	0.1730	0.1762	-0.0032	1.83
12.02	0.2250	0.2258	-0.0008	0.38
16.03	0.2710	0.2678	0.0032	1.18
20.03	0.3090	0.3054	0.0036	1.18
26.04	0.3540	0.3572	-0.0032	0.89

SDST : No. 1

1st loading

SOLUTION

A=	3.566	SD =	0.1202	% =	3.374
B=	0.2862	SD =	0.005515	% =	1.927
C=	110.4	SD =	4.107	% =	3.721

COMPUTED RESIDUALS

SIGMA	DELTA(V) MEASURED	DELTA(V) CALCULATED	DIFF	% DIFF
0.1250	0.03300	0.03238	0.00062	1.89
0.3340	0.08100	0.07362	0.00738	9.11
0.7510	0.1310	0.1282	0.0028	2.17
1.168	0.1620	0.1634	-0.0014	0.83
1.586	0.1850	0.1885	-0.0035	1.91
2.003	0.2050	0.2078	-0.0028	1.35
3.046	0.2380	0.2420	-0.0040	1.67
4.090	0.2620	0.2661	-0.0041	1.57
5.133	0.2850	0.2852	-0.0002	0.08
6.176	0.3050	0.3016	0.0034	1.13
8.263	0.3330	0.3296	0.0034	1.02
9.306	0.3450	0.3422	0.0028	0.81
10.35	0.3570	0.3543	0.0027	0.76
12.44	0.3800	0.3772	0.0028	0.75
14.52	0.3480	0.3990	-0.0010	0.25
16.61	0.4180	0.4201	-0.0021	0.50
18.70	0.4380	0.4408	-0.0028	0.63

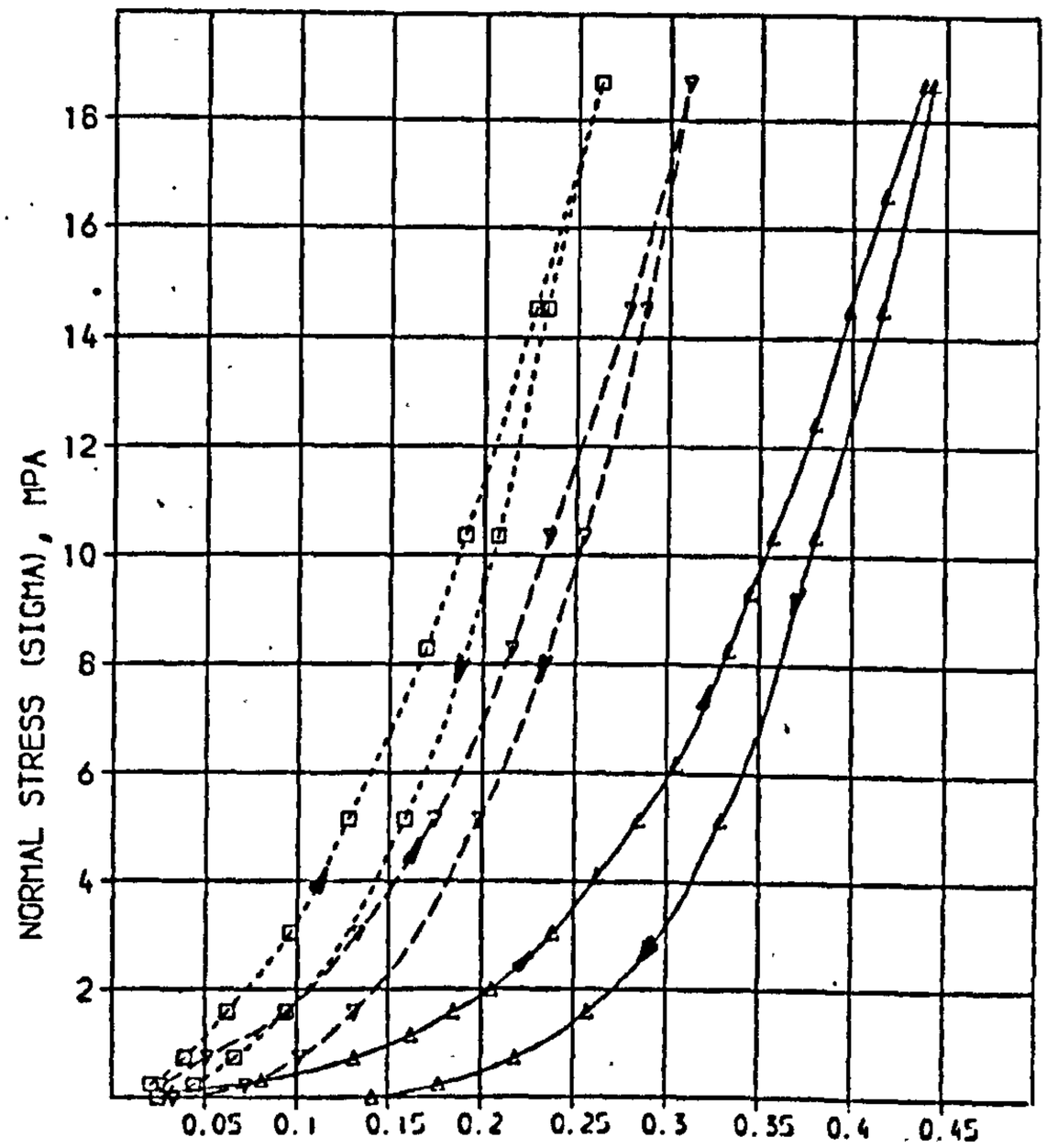

2nd loading

SOLUTION

A=	11.54	SD =	0.6719	% =	5.823
B=	0.1967	SD =	0.01192	% =	6.062
C=	137.2	SD =	10.53	% =	7.673

COMPUTED RESIDUALS

SIGMA	DELTA(V) MEASURED	DELTA(V) CALCULATED	DIFF	% DIFF
0.2500	0.02700	0.02135	0.00567	20.98
0.7510	0.05100	0.04793	-0.00307	6.57
1.586	0.09400	0.09239	0.00161	1.71
3.046	0.1330	0.1346	-0.0016	1.32
5.133	0.1740	0.1730	0.0004	0.24
8.263	0.2150	0.2142	0.0008	0.35
10.35	0.2350	0.2364	-0.0014	0.61
14.52	0.2780	0.2756	0.0024	0.87
18.70	0.3100	0.3113	-0.0013	0.43

3rd loading

SOLUTION

A=	18.30	SD =	1.814	% =	9.909
B=	0.1309	SD =	0.01422	% =	10.86
C=	126.9	SD =	10.53	% =	8.301

COMPUTED RESIDUALS

SIGMA	DELTA(V) MEASURED	DELTA(V) CALCULATED	DIFF	% DIFF
0.2500	0.02100	0.01434	0.00666	31.72
0.7510	0.03900	0.03716	0.00184	4.72
1.586	0.06200	0.06464	-0.00264	4.26
3.046	0.09000	0.09720	-0.00120	1.33
5.133	0.1270	0.1297	-0.0027	2.13
8.263	0.1690	0.1666	0.0024	1.42
10.35	0.1900	0.1879	0.0021	1.13
14.52	0.2270	0.2262	0.0008	0.09
18.70	0.2620	0.2634	-0.0014	0.53

SDST : No. 2

1st loading

SOLUTION

A=	14.622	SD =	0.2791	% =	1.908
B=	0.2127	SD =	0.005624	% =	2.644
C=	234.7	SD =	15.09	% =	6.430

COMPUTED RESIDUALS

SIGMA	DELTA(V) MEASURED	DELTA(V) CALCULATED	DIFF	% DIFF
0.4200	0.07500	0.06545	0.00955	12.73
0.9210	0.1040	0.1068	-0.0028	2.69
1.921	0.1430	0.1489	-0.0059	4.10
3.923	0.1840	0.1868	-0.0028	1.51
5.924	0.2070	0.2076	-0.0006	0.31
7.926	0.2240	0.2230	0.0010	0.45
9.927	0.2380	0.2358	0.0022	0.92
11.93	0.2490	0.2473	0.0017	0.68
13.93	0.2610	0.2580	0.0030	1.15
15.93	0.2700	0.2682	0.0018	0.67
17.93	0.2790	0.2780	0.0010	0.35
19.93	0.2870	0.2876	-0.0006	0.21
21.94	0.2960	0.2970	-0.0010	0.34
23.94	0.3030	0.3063	-0.0033	1.08

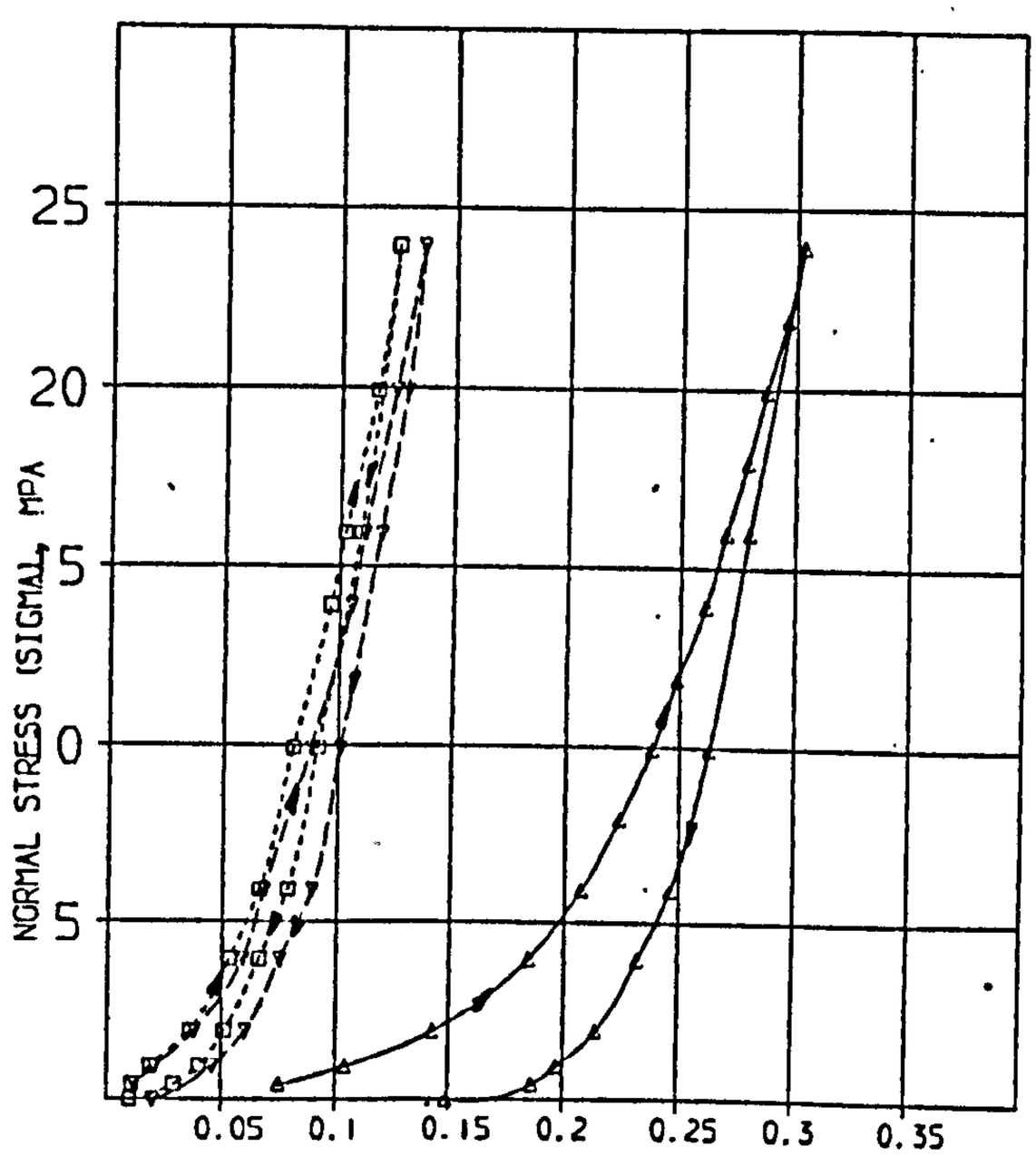

2nd loading

SOLUTION

A=	34.94	SD =	2.026	% =	5.799
B=	0.07830	SD =	0.004503	% =	5.824
C=	362.1	SD =	22.54	% =	6.170

COMPUTED RESIDUALS

SIGMA	DELTA(V) MEASURED	DELTA(V) CALCULATED	DIFF	% DIFF
0.4200	0.01200	0.01158	0.00042	3.49
0.9210	0.02100	0.02220	-0.00120	6.02
1.921	0.03800	0.03760	0.00040	1.04
3.923	0.05900	0.05696	0.00204	3.45
5.924	0.06800	0.06992	-0.00192	2.83
7.927	0.08800	0.08879	-0.00079	0.90
13.93	0.1050	0.1039	0.0011	1.04
15.93	0.1110	0.1106	0.0002	0.17
19.93	0.1240	0.1239	0.0001	0.09
23.94	0.1360	0.1364	-0.0004	0.28

3rd loading

SOLUTION

A=	37.27	SD =	2.342	% =	6.287
B=	0.07222	SD =	0.004845	% =	6.709
C=	393.3	SD =	28.14	% =	7.155

COMPUTED RESIDUALS

SIGMA	DELTA(V) MEASURED	DELTA(V) CALCULATED	DIFF	% DIFF
0.4200	0.01100	0.01082	0.00018	1.68
0.9210	0.01900	0.02075	-0.00175	9.23
1.921	0.03600	0.03496	0.00104	2.89
3.923	0.05300	0.05281	0.00019	0.37
5.924	0.06600	0.06472	0.00128	1.94
9.927	0.08060	0.08263	-0.00203	2.57
13.93	0.09600	0.09594	0.00006	0.06
15.93	0.1020	0.1023	-0.0003	0.27
19.93	0.1160	0.1143	0.0017	1.47
23.94	0.1250	0.1256	-0.0006	0.63

SDST : No. 3

1st loading

SOLUTION

A=	11.88	SD =	0.2754	% =	2.318
B=	0.2360	SD =	0.006700	% =	2.839
C=	170.5	SD =	8.459	% =	4.961

COMPUTED RESIDUALS

SIGMA	DELTA(V) MEASURED	DELTA(V) CALCULATED	DIFF	% DIFF
0.2500	0.01100	0.02270	-0.00179	8.41
0.4560	0.03700	0.03564	0.00131	3.54
0.6420	0.05100	0.04774	0.00326	6.40
1.034	0.07300	0.06965	0.00335	4.59
1.426	0.09000	0.08793	0.00207	2.30
1.819	0.1030	0.1035	-0.0005	0.52
2.211	0.1160	0.1170	-0.0010	0.88
2.990	0.1370	0.1395	-0.0025	1.81
3.780	0.1550	0.1577	-0.0027	1.72
4.761	0.1740	0.1764	-0.0024	1.41
5.741	0.1910	0.1922	-0.0012	0.64
6.722	0.2050	0.2060	-0.0010	0.48
7.703	0.2180	0.2182	-0.0002	0.09
8.684	0.2300	0.2293	0.0007	0.30
9.664	0.2410	0.2396	0.0014	0.58
10.64	0.2500	0.2492	0.0008	0.31
11.63	0.2610	0.2583	0.0027	1.03
13.59	0.2800	0.2753	0.0047	1.68
16.50	0.2980	0.2985	-0.0005	0.16
18.00	0.3080	0.3097	-0.0017	0.57
20.00	0.3220	0.3243	-0.0023	0.70

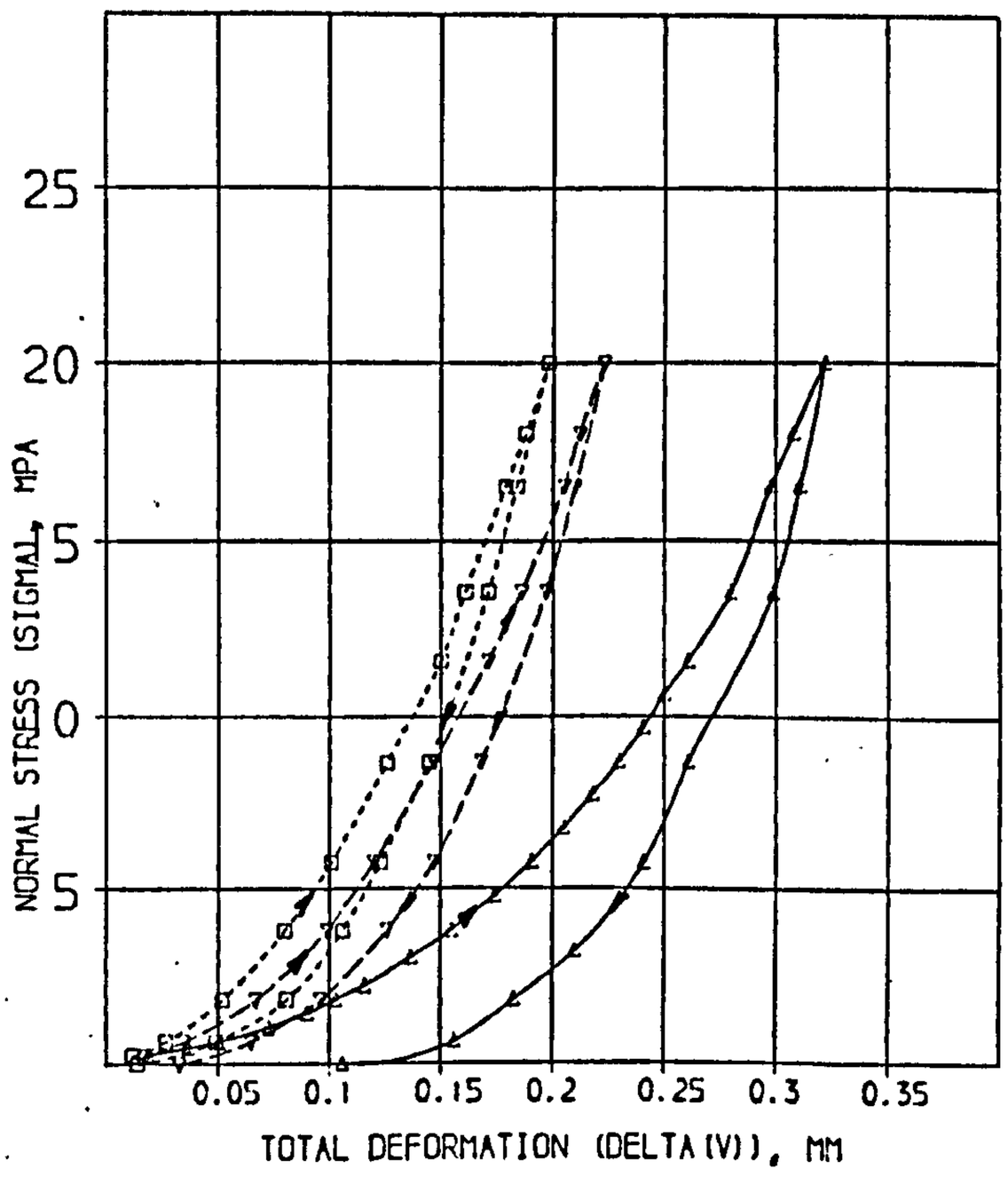

2nd loading

SOLUTION

A=	15.99	SD =	1.138	% =	7.117
B=	0.1151	SD =	0.006270	% =	5.445
C=	166.1	SD =	7.905	% =	4.796

COMPUTED RESIDUALS

SIGMA	DELTA(V) MEASURED	DELTA(V) CALCULATED	DIFF	% DIFF
0.2500	0.01300	0.01527	0.00273	15.16
0.6420	0.03500	0.03364	0.00136	3.90
1.819	0.06700	0.06818	-0.00118	1.76
3.780	0.09900	0.10019	-0.00119	1.20
5.741	0.1200	0.1218	-0.0018	1.46
8.684	0.1470	0.1475	-0.0005	0.20
11.63	0.1710	0.1694	0.0016	0.92
13.59	0.1860	0.1832	0.0028	1.49
16.50	0.2050	0.2024	0.0021	1.01
18.00	0.2120	0.2124	-0.0004	0.40
20.00	0.2230	0.2259	-0.0029	1.28

3rd loading

SOLUTION

A=	24.46	SD =	1.689	% =	6.905
B=	0.1010	SD =	0.006812	% =	6.745
C=	181.8	SD =	9.440	% =	5.192

COMPUTED RESIDUALS

SIGMA	DELTA(V) MEASURED	DELTA(V) CALCULATED	DIFF	% DIFF
0.2500	0.01200	0.01066	0.00134	11.20
0.6420	0.02700	0.02496	0.00204	9.77
1.819	0.05200	0.05285	-0.00085	1.60
3.780	0.08000	0.08187	-0.00187	2.33
5.741	0.1010	0.1022	-0.0012	1.18
8.648	0.1260	0.1261	-0.0001	0.10
11.63	0.1500	0.1473	0.0027	1.82
13.59	0.1610	0.1602	0.0008	0.49
16.50	0.1790	0.1786	0.0004	0.22
18.00	0.1880	0.1878	0.0002	0.10
20.00	0.1980	0.1999	-0.0019	0.96

SDST : No. 4

1st loading

SOLUTION

A=	6.653	SD =	0.2774	% =	4.171
B=	0.2343	SD =	0.004516	% =	1.927
C=	384.3	SD =	23.47	% =	6.100

COMPUTED RESIDUALS

SIGMA	DELTA(V) MEASURED	DELTA(V) CALCULATED	DIFF	% DIFF
0.2360	0.04200	0.05145	0.01057	25.16
0.6140	0.06500	0.06782	-0.00282	4.34
1.182	0.1040	0.1041	-0.0001	0.13
2.363	0.1460	0.1475	-0.0015	0.91
4.726	0.1360	0.1385	-0.0025	1.33
7.080	0.2100	0.2105	-0.0005	0.23
9.511	0.2260	0.2260	-0.0000	0.01
11.82	0.2370	0.2377	-0.0007	0.29
14.18	0.2400	0.2411	0.0011	0.43
16.54	0.2580	0.2571	0.0009	0.35
18.95	0.2670	0.2657	0.0013	0.48
21.27	0.2750	0.2736	0.0014	0.53
23.63	0.2820	0.2812	0.0008	0.29
28.36	0.2960	0.2953	0.0002	0.08
37.81	0.3210	0.3233	-0.0023	0.70

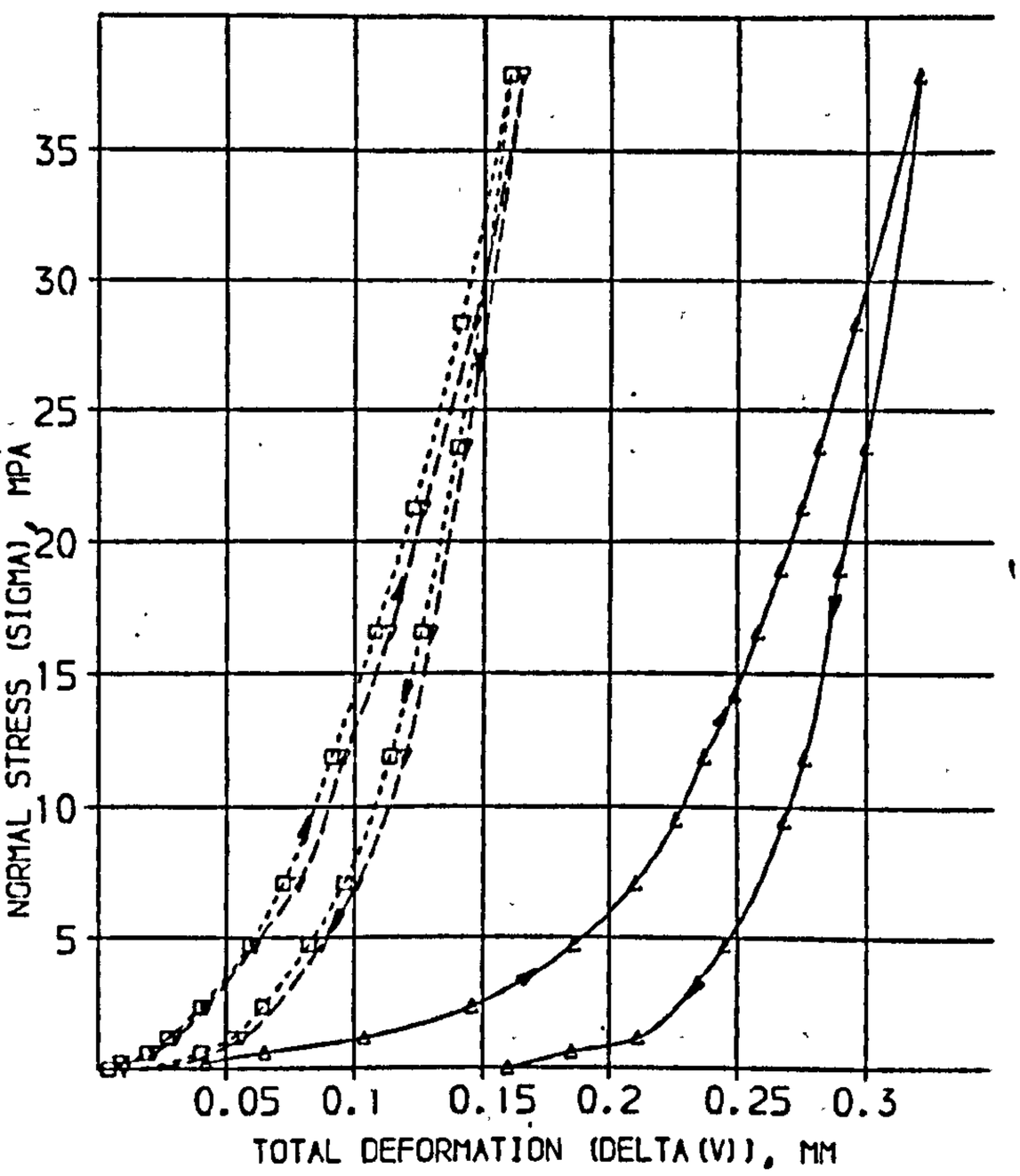

2nd loading

SOLUTION

A=	31.14	SD =	3.589	% =	11.53
B=	0.08032	SD =	0.006247	% =	7.778
C=	408.1	SD =	30.16	% =	7.390

COMPUTED RESIDUALS

SIGMA	DELTA(V) MEASURED	DELTA(V) CALCULATED	DIFF	% DIFF
0.2360	0.008000	0.007503	0.000497	6.21
0.6140	0.02200	0.01754	0.00466	21.20
1.182	0.03000	0.02867	0.00133	4.42
2.363	0.04200	0.04481	-0.00281	6.69
4.726	0.06100	0.06411	-0.00311	5.09
7.089	0.07800	0.07675	0.00125	1.61
11.82	0.09400	0.09525	-0.00125	1.32
16.54	0.1100	0.1105	-0.0005	0.28
21.27	0.1270	0.1240	0.0030	2.37
23.36	0.1460	0.1433	0.0027	1.85
37.81	0.1650	0.1680	-0.0030	1.81

3rd loading

SOLUTION

A=	36.03	SD =	3.467	% =	9.609
B=	0.08033	SD =	0.005845	% =	7.276
C=	429.1	SD =	29.42	% =	6.948

COMPUTED RESIDUALS

SIGMA	DELTA(V) MEASURED	DELTA(V) CALCULATED	DIFF	% DIFF
0.2360	0.009000	0.006594	0.002406	26.69
0.6140	0.01900	0.01547	0.00353	18.57
1.182	0.02700	0.02604	0.00096	3.62
2.363	0.04000	0.04158	-0.00158	3.96
4.726	0.05900	0.06080	-0.00180	3.06
7.089	0.07200	0.07354	-0.00154	2.13
11.82	0.09100	0.09204	-0.00104	1.14
16.54	0.1080	0.1069	0.0011	1.02
21.27	0.1230	0.1203	0.0027	2.23
23.36	0.1410	0.1390	0.0020	1.45
37.81	0.1600	0.1627	-0.0027	1.70

SDST : No. 5

1st loading

SOLUTION

A=	16.21	SD =	1.920	% =	11.84
B=	0.1585	SD =	0.01329	% =	8.386
C=	229.8	SD =	20.28	% =	8.826

COMPUTED RESIDUALS

SIGMA	DELTA(V) MEASURED	DELTA(V) CALCULATED	DIFF	% DIFF
0.4510	0.03400	0.02563	0.01337	34.29
1.077	0.05700	0.05150	0.00550	9.65
1.704	0.07000	0.07061	-0.00061	0.88
2.331	0.08400	0.08554	-0.00154	1.83
3.584	0.1040	0.1079	-0.0039	3.76
4.838	0.1200	0.1246	-0.0046	3.82
6.091	0.1340	0.1380	-0.0040	2.98
7.345	0.1440	0.1494	-0.0054	3.75
9.852	0.1660	0.1686	-0.0026	1.56
12.36	0.1820	0.1850	-0.0030	1.65
14.86	0.2200	0.1998	0.0202	9.16
19.88	0.2290	0.2269	0.0021	0.93
22.39	0.2410	0.2396	0.0014	0.58
24.89	0.2520	0.2520	-0.0000	0.01
27.40	0.2630	0.2642	-0.0012	0.44
29.91	0.2750	0.2761	-0.0011	0.41
32.41	0.2850	0.2879	-0.0029	1.03
34.92	0.2980	0.2996	-0.0016	0.54

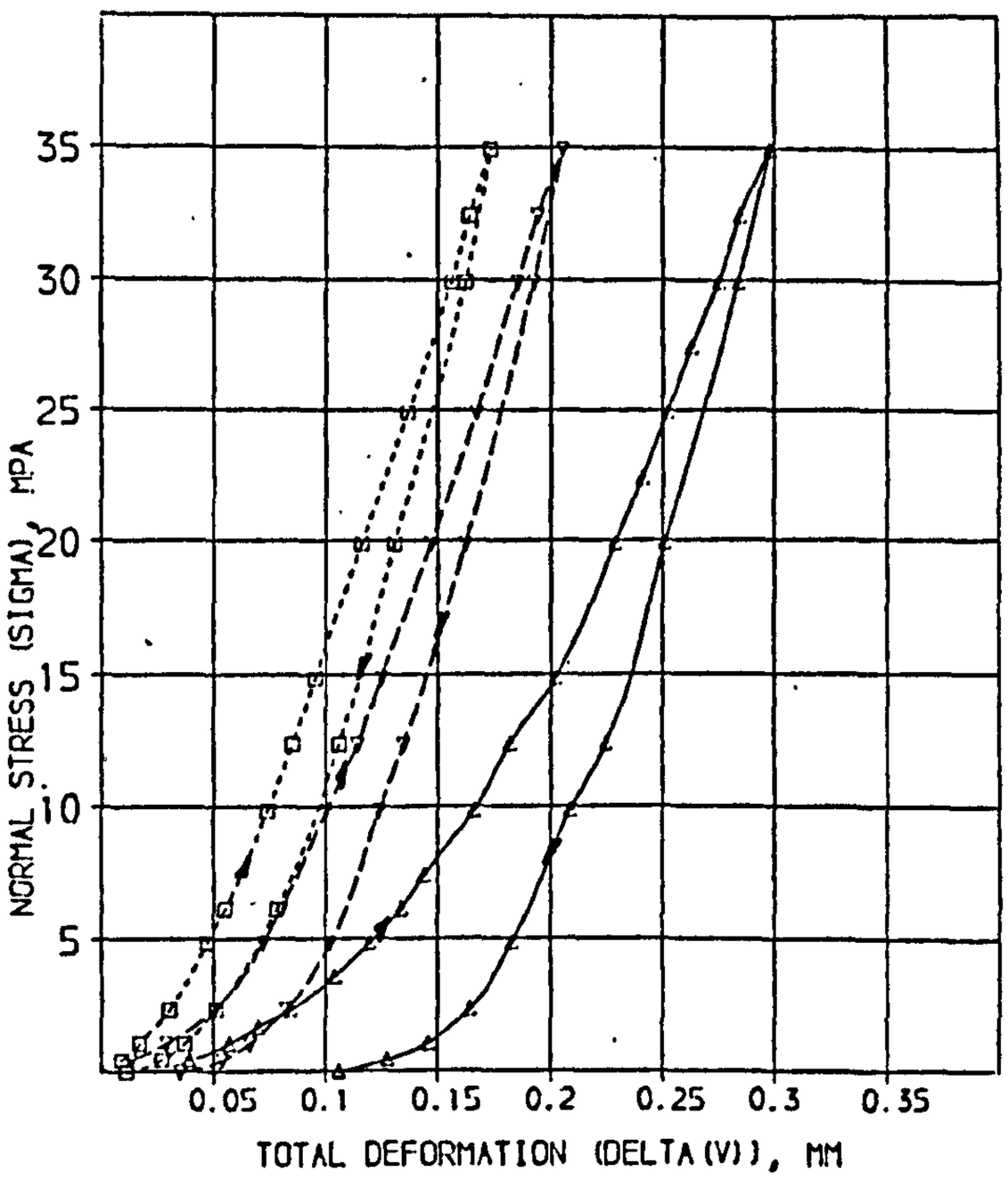

2nd loading

SOLUTION

A=	30.03	SD =	1.305	% =	4.351
B=	0.08184	SD =	0.002213	% =	2.704
C=	272.3	SD =	4.638	% =	1.722

COMPUTED RESIDUALS

SIGMA	DELTA(V) MEASURED	DELTA(V) CALCULATED	DIFF	% DIFF
0.4510	0.01300	0.01450	-0.00150	10.42
1.077	0.02900	0.02891	0.00009	0.32
2.331	0.05000	0.04842	0.00158	3.17
4.838	0.07200	0.07205	-0.00005	0.07
6.091	0.08000	0.08069	-0.00069	0.87
9.852	0.1000	0.1017	-0.0017	1.69
12.36	0.1140	0.1137	0.0003	0.29
14.86	0.1250	0.1244	0.0006	0.46
19.88	0.1470	0.1453	0.0016	0.78
24.89	0.1670	0.1659	0.0011	0.66
29.91	0.1850	0.1855	-0.0005	0.26
32.41	0.1940	0.1951	-0.0011	0.57
34.92	0.2050	0.2047	0.0003	0.14

3rd loading

SOLUTION

A=	62.03	SD =	3.406	% =	5.504
B=	0.04891	SD =	0.001993	% =	4.074
C=	270.5	SD =	3.912	% =	1.446

COMPUTED RESIDUALS

SIGMA	DELTA(V) MEASURED	DELTA(V) CALCULATED	DIFF	% DIFF
0.4510	0.009000	0.007993	0.001007	11.19
1.077	0.01700	0.01679	0.00021	1.25
2.331	0.03000	0.02986	0.00014	0.47
4.838	0.04700	0.04794	-0.00094	1.99
6.091	0.05500	0.05510	-0.00010	0.19
9.852	0.07400	0.07381	0.00019	0.26
12.36	0.08300	0.08296	0.00004	0.05
14.86	0.09500	0.09555	-0.00055	0.58
19.88	0.1160	0.1159	0.0001	0.06
24.89	0.1370	0.1356	0.0014	1.01
29.91	0.1560	0.1550	0.0010	0.65
32.41	0.1640	0.1645	-0.0005	0.33
34.92	0.1730	0.1741	-0.0011	0.64

SDST : No.6

Id loading

SOLUTION

A=	22.67	SD =	0.6143	% =	2.733
B=	0.1688	SD =	0.004220	% =	2.499
C=	243.5	SD =	6.513	% =	2.675

COMPUTED RESIDUALS

SIGMA	DELTA(V) MEASURED	DELTA(V) CALCULATED	DIFF	% DIFF
0.5150	0.02300	0.02214	0.00086	3.73
1.128	0.04700	0.04307	0.00393	8.36
2.354	0.07400	0.07397	0.00003	0.04
3.580	0.09500	0.09631	-0.00131	1.38
4.805	0.1120	0.1137	-0.0017	1.54
7.257	0.1390	0.1403	-0.0013	0.97
9.709	0.1600	0.1610	-0.0010	0.61
12.16	0.1780	0.1784	-0.0004	0.21
14.61	0.1950	0.1938	0.0012	0.61
17.06	0.2090	0.2080	0.0010	0.48
19.52	0.2220	0.2213	0.0007	0.31
21.97	0.2360	0.2340	0.0020	0.84
24.42	0.2470	0.2462	0.0008	0.30
26.87	0.2580	0.2581	-0.0001	0.06
29.32	0.2690	0.2698	-0.0008	0.29
31.77	0.2800	0.2812	-0.0012	0.42
34.23	0.2920	0.2924	-0.0004	0.14

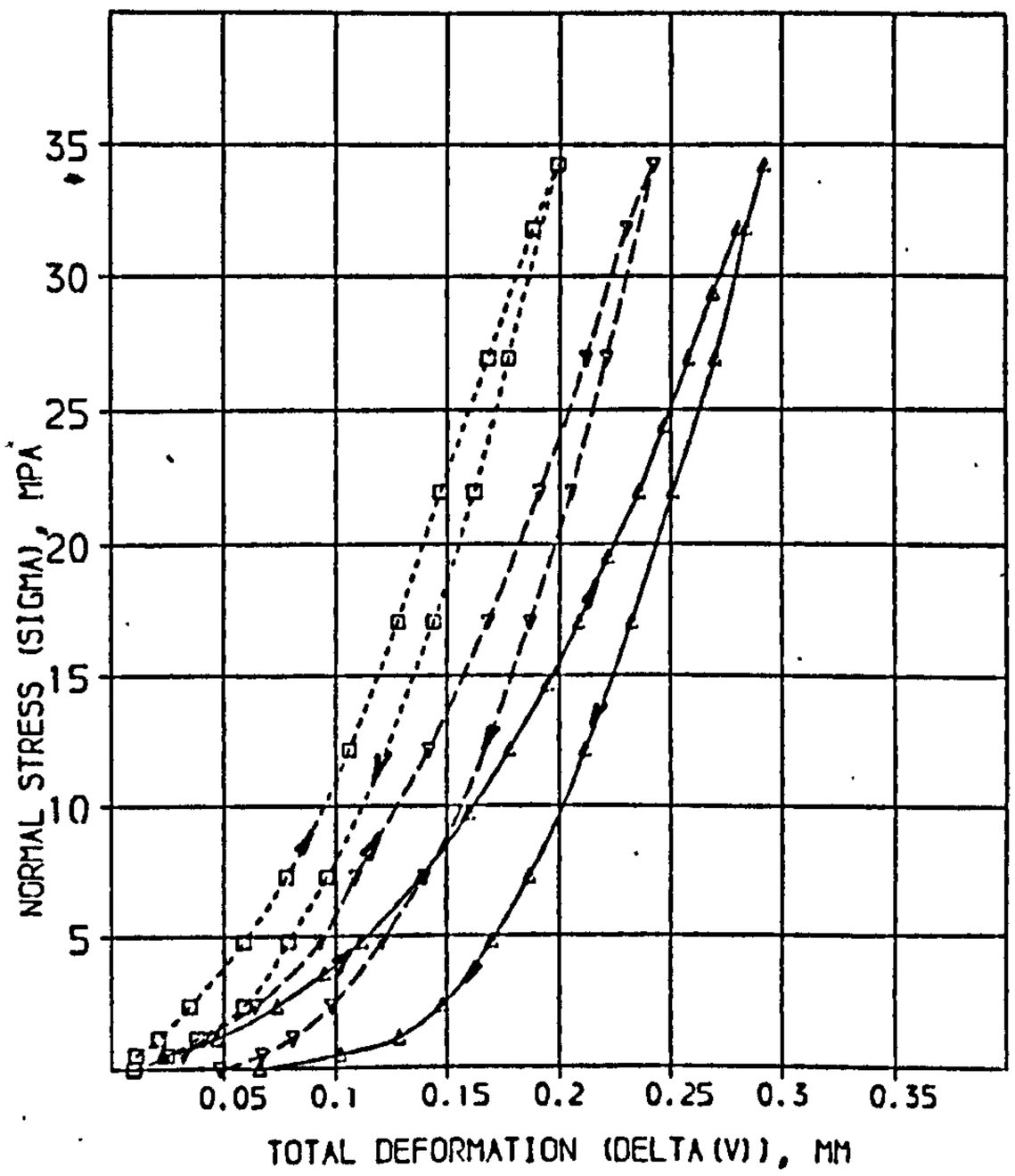

SOLUTION

A=	18.68	SD =	2.230	% =	11.94
B=	0.1023	SD =	0.007162	% =	6.984
C=	234.4	SD =	12.22	% =	5.213

COMPUTED RESIDUALS

SIGMA	DELTA(V) MEASURED	DELTA(V) CALCULATED	DIFF	% DIFF
0.5150	0.03200	0.02394	0.00806	25.19
1.128	0.04100	0.04280	-0.00180	4.54
2.354	0.06400	0.06667	-0.00267	4.17
4.805	0.09300	0.09397	-0.00097	1.04
7.257	0.1090	0.1123	-0.0033	3.00
12.16	0.1420	0.1407	0.0013	0.93
17.06	0.1680	0.1652	0.0028	1.66
21.97	0.1910	0.1883	0.0027	1.42
26.87	0.2120	0.2106	0.0014	0.66
31.77	0.2300	0.2323	-0.0023	1.09
34.23	0.2420	0.2434	-0.0014	0.58

SOLUTION

A=	56.45	SD =	2.857	% =	5.061
B=	0.08440	SD =	0.005000	% =	5.924
C=	276.7	SD =	9.078	% =	3.281

COMPUTED RESIDUALS

SIGMA	DELTA(V) MEASURED	DELTA(V) CALCULATED	DIFF	% DIFF
0.5150	0.01100	0.01009	0.00091	8.23
1.128	0.02100	0.02023	0.00077	3.65
2.354	0.03500	0.03642	-0.00142	4.05
4.805	0.05900	0.05974	-0.00074	1.26
7.257	0.07800	0.07717	0.00083	1.06
12.16	0.1060	0.1046	0.0014	1.34
17.06	0.1280	0.1276	0.0004	0.29
21.97	0.1470	0.1487	-0.0017	1.19
26.87	0.1680	0.1688	-0.0008	0.47
31.77	0.1880	0.1882	-0.0002	0.11
34.23	0.1990	0.1978	0.0012	0.61

SDST : No.7

1st loading _

SOLUTION

A=	17.207	SD =	0.3234	% =	1.879
B=	0.1642	SD =	0.004259	% =	2.594
C=	215.4	SD =	10.48	% =	4.866

COMPUTED RESIDUALS

SIGMA	DELTA(V) MEASURED	DELTA(V) CALCULATED	DIFF	% DIFF
0.1410	0.01600	0.01814	-0.00014	0.76
0.3430	0.04300	0.03846	0.00451	10.49
0.5450	0.05600	0.05431	0.00369	6.37
0.7480	0.07400	0.07743	0.00157	1.98
1.150	0.08500	0.08626	-0.00126	1.49
1.957	0.1100	0.1114	-0.0014	1.28
2.361	0.1180	0.1203	-0.0023	1.98
2.765	0.1260	0.1278	-0.0018	1.44
3.168	0.1320	0.1342	-0.0022	1.70
3.975	0.1430	0.1450	-0.0020	1.39
4.984	0.1540	0.1558	-0.0018	1.19
5.993	0.1640	0.1649	-0.0009	0.57
7.002	0.1720	0.1730	-0.0010	0.56
8.011	0.1810	0.1803	0.0007	0.41
10.03	0.1860	0.1934	0.0026	1.32
12.05	0.2120	0.2054	0.0066	3.10
14.06	0.2190	0.2167	0.0023	1.03
15.50	0.2280	0.2245	0.0035	1.53
17.00	0.2330	0.2324	0.0006	0.25
18.35	0.2430	0.2445	-0.0015	0.63
22.00	0.2520	0.2579	-0.0059	2.36

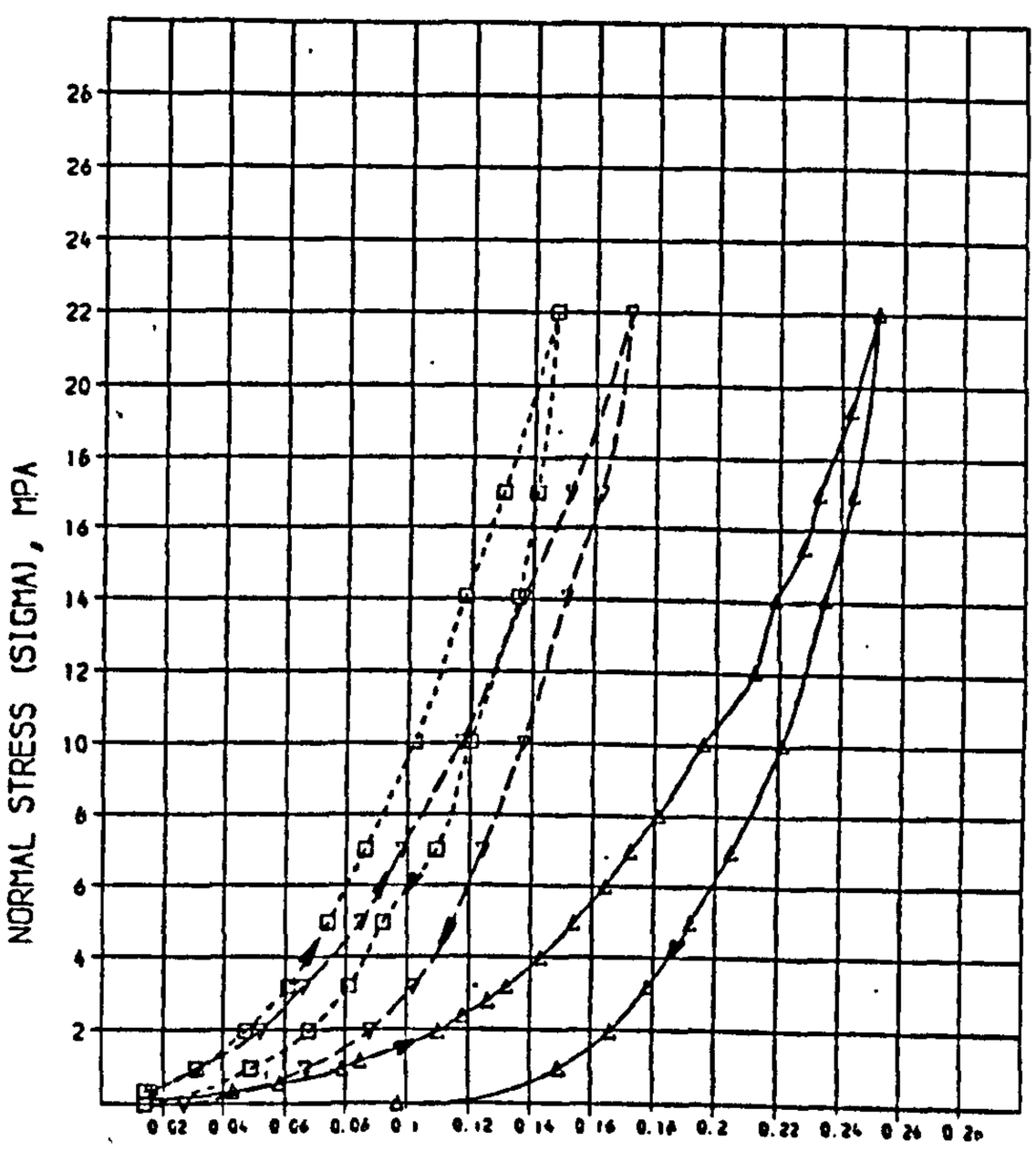

2nd loading _

SOLUTION

A=	24.03	SD =	1.250	% =	5.203
B=	0.09445	SD =	0.004508	% =	4.773
C=	253.7	SD =	12.25	% =	4.822

COMPUTED RESIDUALS

SIGMA	DELTA(V) MEASURED	DELTA(V) CALCULATED	DIFF	% DIFF
0.3430	0.01600	0.01375	0.00225	14.06
0.7480	0.03100	0.03150	-0.00050	1.62
1.957	0.05200	0.05144	0.00056	1.07
3.168	0.06600	0.06751	-0.00151	2.29
4.984	0.08500	0.08454	0.00046	0.54
7.002	0.09300	0.09392	-0.00092	0.94
10.03	0.1170	0.1160	0.0004	0.38
14.06	0.1370	0.1367	0.0003	0.19
17.00	0.1520	0.1503	0.0017	1.10
22.00	0.1710	0.1723	-0.0013	0.77

3rd loading _

SOLUTION

A=	23.09	SD =	0.7949	% =	3.454
B=	0.07907	SD =	0.002078	% =	2.628
C=	294.1	SD =	8.115	% =	2.759

COMPUTED RESIDUALS

SIGMA	DELTA(V) MEASURED	DELTA(V) CALCULATED	DIFF	% DIFF
0.3430	0.01410	0.01367	0.00053	2.35
0.7480	0.03100	0.03023	0.00075	2.43
1.957	0.04700	0.04750	-0.00050	1.19
3.168	0.06100	0.06094	0.00006	0.11
4.984	0.07400	0.07482	-0.00082	1.11
7.002	0.08600	0.08655	-0.00055	0.62
10.03	0.1020	0.1010	0.0010	0.98
14.06	0.1180	0.1176	0.0002	0.17
17.00	0.1300	0.1292	0.0008	0.60
22.00	0.1470	0.1478	-0.0008	0.56

SDST : No. 8

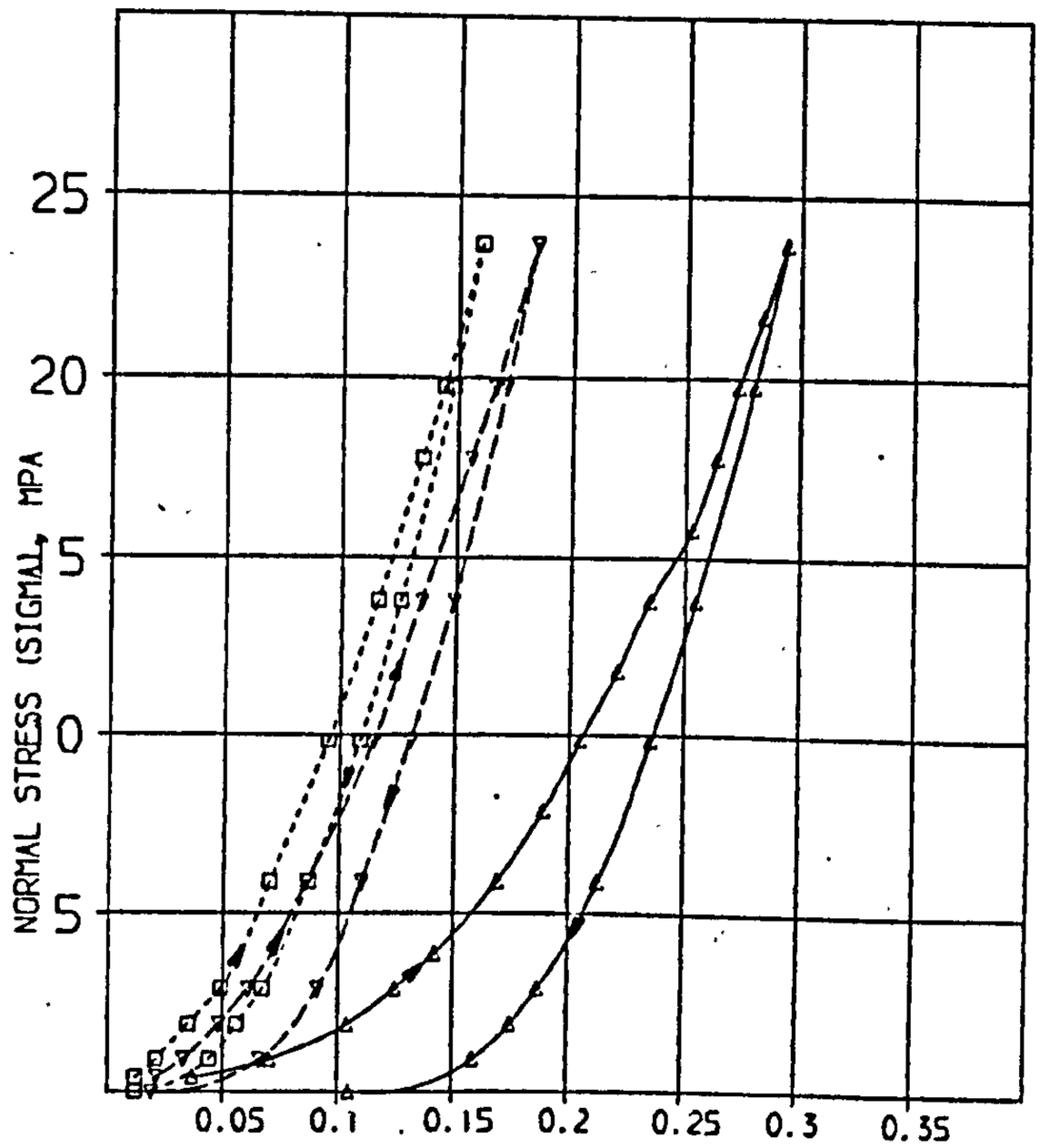

1st loading

SOLUTION:

A=	6.745	SD =	0.4354	% =	4.468
B=	0.1778	SD =	0.005200	% =	2.925
C=	179.8	SD =	7.157	% =	3.981

COMPUTED RESIDUALS

SIGMA	DELTA(V) MEASURED	DELTA(V) CALCULATED	DIFF	% DIFF
0.4190	0.03700	0.03695	0.00005	0.13
0.9110	0.07000	0.06634	0.00366	5.24
1.902	0.1040	0.1036	0.0004	0.37
2.893	0.1250	0.1273	-0.0023	1.83
3.883	0.1420	0.1445	-0.0025	1.79
5.864	0.1690	0.1699	-0.0009	0.51
7.846	0.1890	0.1893	-0.0003	0.15
9.827	0.2050	0.2058	-0.0008	0.40
11.81	0.2210	0.2207	0.0003	0.12
13.79	0.2350	0.2347	0.0003	0.15
15.77	0.2530	0.2479	0.0051	2.01
17.75	0.2640	0.2607	0.0033	1.24
19.73	0.2730	0.2732	-0.0002	0.08
21.71	0.2840	0.2854	-0.0014	0.51
23.69	0.2940	0.2975	-0.0035	1.19

2nd loading

SOLUTION:

A=	20.05	SD =	1.994	% =	9.518
B=	0.07444	SD =	0.005002	% =	6.720
C=	204.4	SD =	9.153	% =	4.479

COMPUTED RESIDUALS

SIGMA	DELTA(V) MEASURED	DELTA(V) CALCULATED	DIFF	% DIFF
0.4190	0.02100	0.01782	0.00318	15.17
0.9110	0.03300	0.03191	0.00109	3.31
1.902	0.04300	0.05021	-0.00721	4.60
2.893	0.06100	0.06252	-0.00152	2.50
5.864	0.08600	0.08750	-0.00150	1.74
9.827	0.1150	0.1123	0.0027	2.32
13.79	0.1350	0.1344	0.0006	0.48
17.75	0.1560	0.1553	0.0007	0.46
19.73	0.1660	0.1655	0.0005	0.28
23.69	0.1840	0.1858	-0.0018	0.96

3rd loading

SOLUTION

A=	39.94	SD =	4.556	% =	5.900
B=	0.06915	SD =	0.004445	% =	6.428
C=	238.7	SD =	9.458	% =	3.962

COMPUTED RESIDUALS

SIGMA	DELTA(V) MEASURED	DELTA(V) CALCULATED	DIFF	% DIFF
0.4190	0.01200	0.01086	0.00114	9.46
0.9110	0.02100	0.02097	0.00003	0.15
1.902	0.03500	0.03617	-0.00117	3.34
2.893	0.04900	0.04750	0.00150	3.06
5.864	0.07000	0.07138	-0.00138	2.25
9.827	0.09500	0.09513	-0.00013	0.16
13.79	0.1160	0.1154	0.0006	0.53
17.75	0.1350	0.1344	0.0006	0.59
19.73	0.1440	0.1433	0.0007	0.47
23.69	0.1600	0.1612	-0.0012	0.74

SDST : No.9

1st loading

SOLUTION

A=	7.973	SD =	0.3508	% =	4.475
B=	0.2498	SD =	0.008896	% =	3.562
C=	169.0	SD =	11.28	% =	0.674

COMPUTED RESIDUALS

SIGMA	DELTA(V) MEASURED	DELTA(V) CALCULATED	DIFF	% DIFF
0.3030	0.03000	0.03478	0.00122	3.40
0.5060	0.05400	0.05360	0.00540	9.10
1.011	0.09500	0.09000	0.00491	5.17
1.517	0.1150	0.1170	0.0020	1.70
2.022	0.1380	0.1378	0.0002	0.14
2.528	0.1520	0.1547	-0.0027	1.76
3.033	0.1640	0.1687	-0.0047	2.88
4.044	0.1880	0.1913	-0.0033	1.75
5.055	0.2050	0.2091	-0.0041	2.00
6.066	0.2210	0.2239	-0.0029	1.33
7.077	0.2350	0.2368	-0.0018	0.76
8.088	0.2470	0.2483	-0.0013	0.52
9.099	0.2600	0.2588	0.0012	0.48
10.11	0.2710	0.2685	0.0025	0.93
12.15	0.2910	0.2863	0.0047	1.60
14.15	0.3080	0.3027	0.0053	1.72
16.18	0.3240	0.3181	0.0059	1.82
18.20	0.3370	0.3328	0.0042	1.24
20.22	0.3450	0.3470	-0.0020	0.59
22.63	0.3540	0.3635	-0.0095	2.68

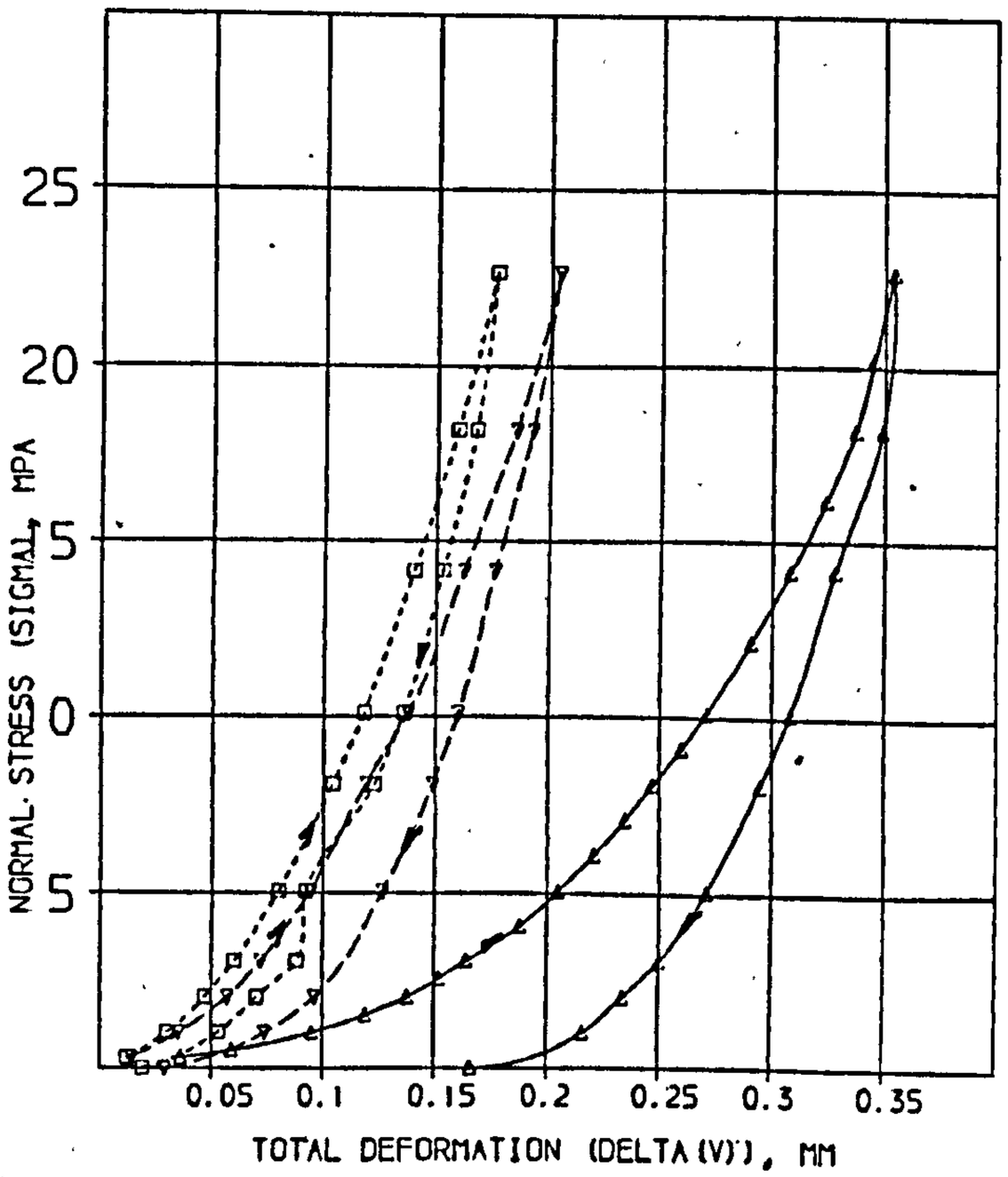

2nd loading

SOLUTION

A=	25.35	SD =	1.664	% =	6.567
B=	0.1130	SD =	0.008299	% =	7.283
C=	215.3	SD =	14.01	% =	6.795

COMPUTED RESIDUALS

SIGMA	DELTA(V) MEASURED	DELTA(V) CALCULATED	DIFF	% DIFF
0.3030	0.01400	0.01223	0.00177	12.65
1.011	0.03500	0.03425	0.00075	2.15
2.022	0.05700	0.05633	0.00067	1.18
3.033	0.07200	0.07247	-0.00047	0.66
5.055	0.09400	0.09605	-0.00205	2.16
8.088	0.1190	0.1210	-0.0020	2.17
10.11	0.1380	0.1357	0.0023	1.70
14.15	0.1620	0.1604	0.0016	0.96
18.20	0.1850	0.1830	0.0020	1.08
22.63	0.2040	0.2063	-0.0023	1.13

3rd loading

SOLUTION

A=	31.94	SD =	1.896	% =	5.937
B=	0.1030	SD =	0.007606	% =	7.402
C=	257.8	SD =	18.58	% =	7.207

COMPUTED RESIDUALS

SIGMA	DELTA(V) MEASURED	DELTA(V) CALCULATED	DIFF	% DIFF
0.3030	0.01200	0.00986	0.00214	17.82
1.011	0.03000	0.02813	0.00187	6.22
2.022	0.04700	0.04705	-0.00005	0.11
3.033	0.06000	0.06117	-0.00117	1.95
5.055	0.08000	0.08200	-0.00200	2.50
8.088	0.1040	0.1046	-0.0006	0.56
10.11	0.1180	0.1169	0.0011	0.91
14.15	0.1400	0.1384	0.0016	1.11
18.20	0.1590	0.1576	0.0014	0.74
22.63	0.1760	0.1777	-0.0017	0.96

SDST : No. 10

1st loading

SOLUTION

A=	7.098	SD =	0.1977	% =	2.786
B=	0.3217	SD =	0.006521	% =	2.027
C=	145.1	SD =	4.681	% =	3.227

COMPUTED RESIDUALS

SIGMA	DELTA(V) MEASURED	DELTA(V) CALCULATED	DIFF	% DIFF
0.4780	0.05500	0.05868	-0.00398	7.24
0.9810	0.1000	0.1034	-0.0034	3.44
1.514	0.1450	0.1387	0.0063	4.34
2.047	0.1710	0.1662	0.0048	2.81
3.113	0.2070	0.2070	-0.0000	0.02
4.179	0.2340	0.2369	-0.0029	1.22
6.311	0.2750	0.2798	-0.0048	1.73
8.443	0.3090	0.3114	-0.0024	0.79
10.57	0.3360	0.3375	-0.0015	0.44
12.71	0.3610	0.3603	0.0007	0.19
14.84	0.3830	0.3811	0.0019	0.50
16.97	0.4030	0.4005	0.0025	0.61
19.10	0.4230	0.4190	0.0040	0.93
21.23	0.4390	0.4369	0.0021	0.49
23.37	0.4550	0.4542	0.0008	0.19
25.50	0.4700	0.4710	-0.0010	0.22
27.63	0.4840	0.4876	-0.0036	0.75
29.76	0.5030	0.5040	-0.0010	0.19

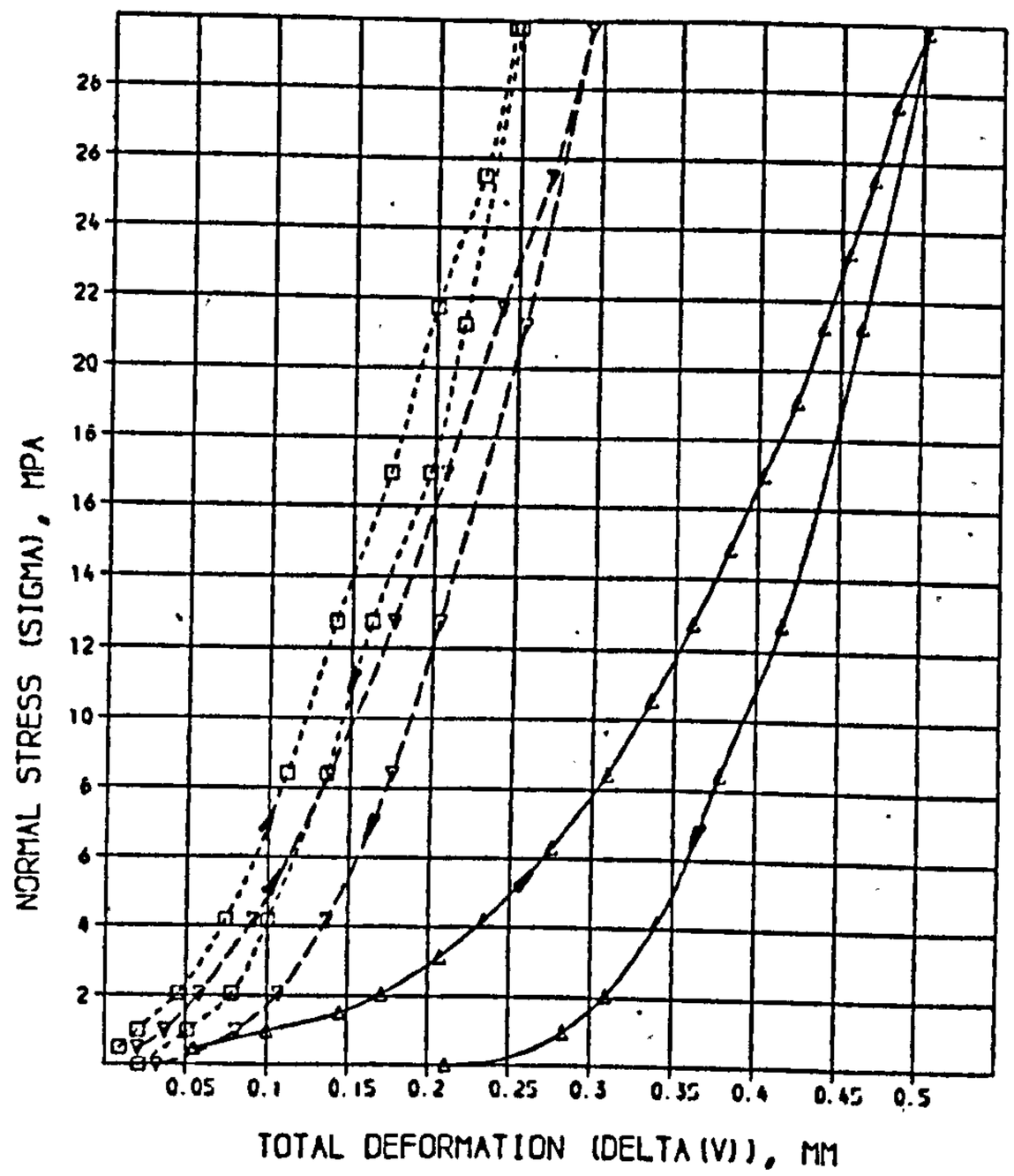

2nd loading

SOLUTION

A=	26,62	SD =	1,757	% =	6,597
B=	0.1143	SD =	0,006943	% =	6,073
C=	155,2	SD =	5,190	% =	3,338

COMPUTED RESIDUALS

SIGMA	DELTA(V) MEASURED	DELTA(V) CALCULATED	DIFF	% DIFF
0.4780	0.02000	0.01860	0.00140	7,02
0.9810	0.03710	0.03419	0.00291	7,80
2.047	0.05300	0.05910	-0.00110	2,00
4.179	0.09100	0.09307	-0.00207	2,28
8.443	0.1370	0.1384	-0.0014	1,05
12.71	0.1760	0.1741	0.0019	1,06
16.97	0.2070	0.2063	0.0007	0,34
21.23	0.2400	0.2405	-0.0005	0,13
25.50	0.2660	0.2665	0.0045	0,95
29.76	0.2930	0.2955	-0.0045	0,85

3rd loading

SOLUTION

A=	44,79	SD =	5,152	% =	11,50
B=	0.1021	SD =	0,01516	% =	14,85
C=	186,1	SD =	14,12	% =	7,592

COMPUTED RESIDUALS

SIGMA	DELTA(V) MEASURED	DELTA(V) CALCULATED	DIFF	% DIFF
0.4780	0.009000	0.012230	-0.003250	35,89
0.9810	0.02000	0.02331	-0.00331	16,53
2.047	0.04500	0.04257	0.00243	5,40
4.179	0.07400	0.07121	0.00279	3,77
8.443	0.1110	0.1116	-0.0006	0,55
12.71	0.1400	0.1434	-0.0034	2,43
16.97	0.1730	0.1716	0.0014	0,79
21.23	0.2000	0.2011	-0.0011	0,57
25.50	0.2280	0.2236	0.0044	1,92
29.76	0.2460	0.2485	-0.0025	1,00

SDST : No. 11

1st loading

SOLUTION

A=	25.567	SD =	1.4141	% =	5.534
B=	0.2471	SD =	0.007905	% =	3.199
C=	155.4	SD =	0.591	% =	0.174

COMPUTED RESIDUALS

SIGMA	DELTA(V) MEASURED	DELTA(V) CALCULATED	DIFF	% DIFF
0.3020	0.05600	0.04643	0.00957	17.09
0.6790	0.09400	0.08604	0.00796	8.47
1.433	0.1360	0.1353	0.0007	0.51
1.811	0.1490	0.1521	-0.0031	2.08
2.565	0.1730	0.1774	-0.0044	2.53
2.942	0.1830	0.1873	-0.0043	2.37
3.319	0.1910	0.1961	-0.0051	2.66
3.696	0.2000	0.2039	-0.0039	1.95
4.630	0.2180	0.2205	-0.0025	1.13
5.582	0.2340	0.2342	-0.0002	0.09
6.525	0.2470	0.2461	0.0009	0.36
7.468	0.2580	0.2568	0.0012	0.48
8.411	0.2680	0.2665	0.0015	0.54
9.354	0.2790	0.2757	0.0033	1.20
11.24	0.2970	0.2925	0.0045	1.50
13.13	0.3120	0.3082	0.0038	1.22
15.01	0.3270	0.3230	0.0040	1.22
16.90	0.3410	0.3373	0.0037	1.08
18.78	0.3510	0.3512	-0.0002	0.05
22.60	0.3690	0.3784	-0.0094	2.56

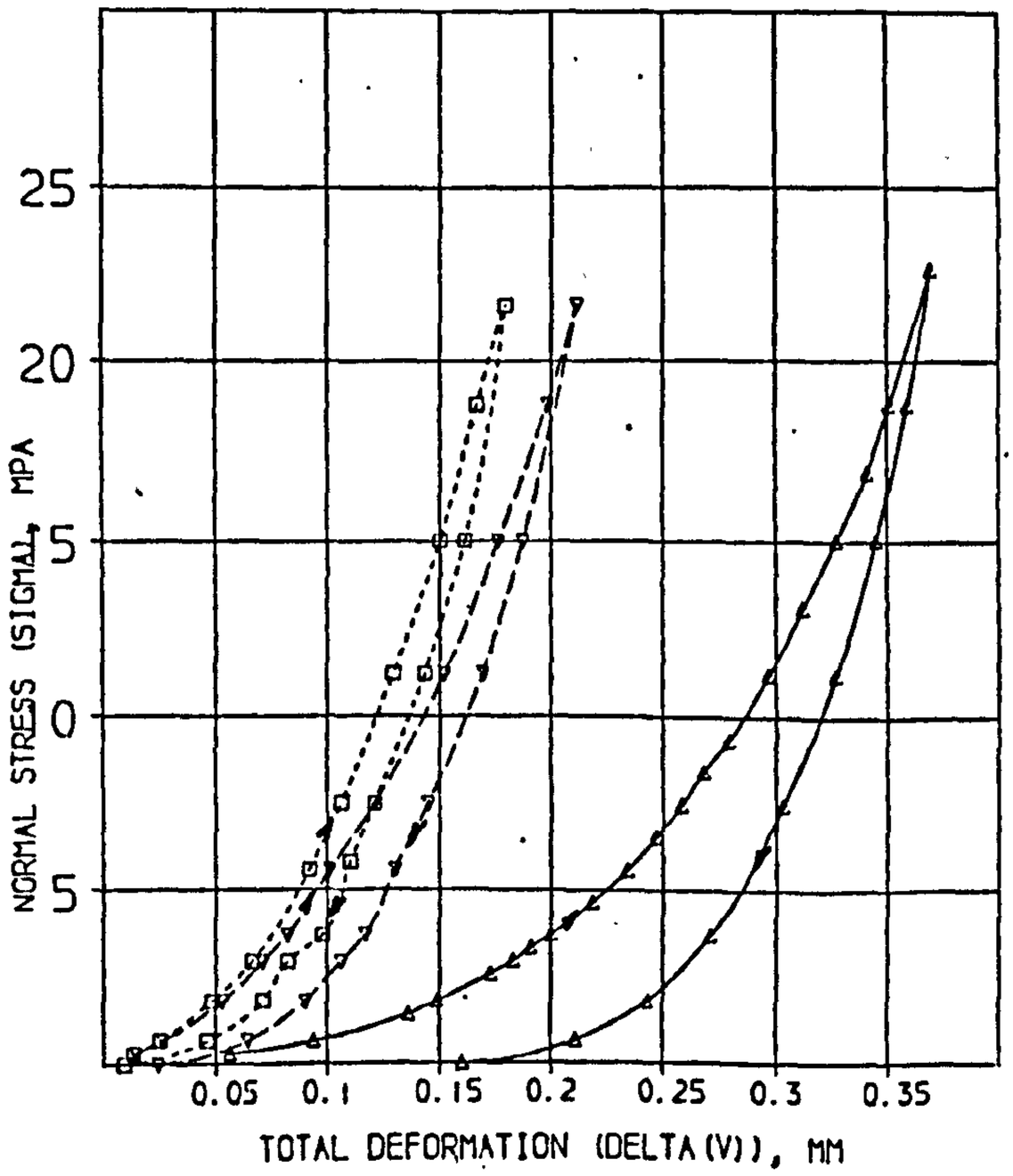

2nd loading

SOLUTION

A=	26,87	SD =	1,612	% =	6,001
B=	0,1139	SD =	0,009241	% =	7,774
C=	196,3	SD =	13,24	% =	6,729

COMPUTED RESIDUALS

SIGMA	DELTA(V) MEASURED	DELTA(V) CALCULATED	DIFF	% DIFF
0.3020	0.01400	0.01180	0.00220	15,69
0.6790	0.02600	0.02429	0.00171	6,57
1.811	0.05300	0.05222	0.00078	1,48
2.942	0.07100	0.07195	-0.00095	1,33
3.696	0.08200	0.08255	-0.00055	0,67
5.582	0.1010	0.1040	-0.0030	2,95
7.468	0.1210	0.1214	-0.0004	0,18
11.24	0.1520	0.1497	0.0023	1,52
15.01	0.1750	0.1743	0.0017	0,97
18.78	0.1980	0.1970	0.0010	0,49
21.60	0.2110	0.2133	-0.0023	1,10

3rd loading

SOLUTION

A=	25,65	SD =	0,9501	% =	3,649
B=	0,1022	SD =	0,003854	% =	3,770
C=	244,5	SD =	9,143	% =	3,739

COMPUTED RESIDUALS

SIGMA	DELTA(V) MEASURED	DELTA(V) CALCULATED	DIFF	% DIFF
0.3020	0.01300	0,01159	0,00141	9,29
0.6790	0.02500	0,02380	0,00120	4,79
1.811	0.04800	0,04917	-0,00117	2,43
2.942	0.06600	0,06608	-0,00008	0,13
5.582	0.09200	0,09238	-0,00038	0,42
7.468	0.1060	0,1062	-0,0002	0,19
11.24	0.1200	0,1289	0,0001	0,11
15.01	0.1510	0,1484	0,0016	1,06
18.78	0.1660	0,1665	-0,0005	0,31
21.60	0.1790	0,1795	-0,0005	0,28

SDST : 12

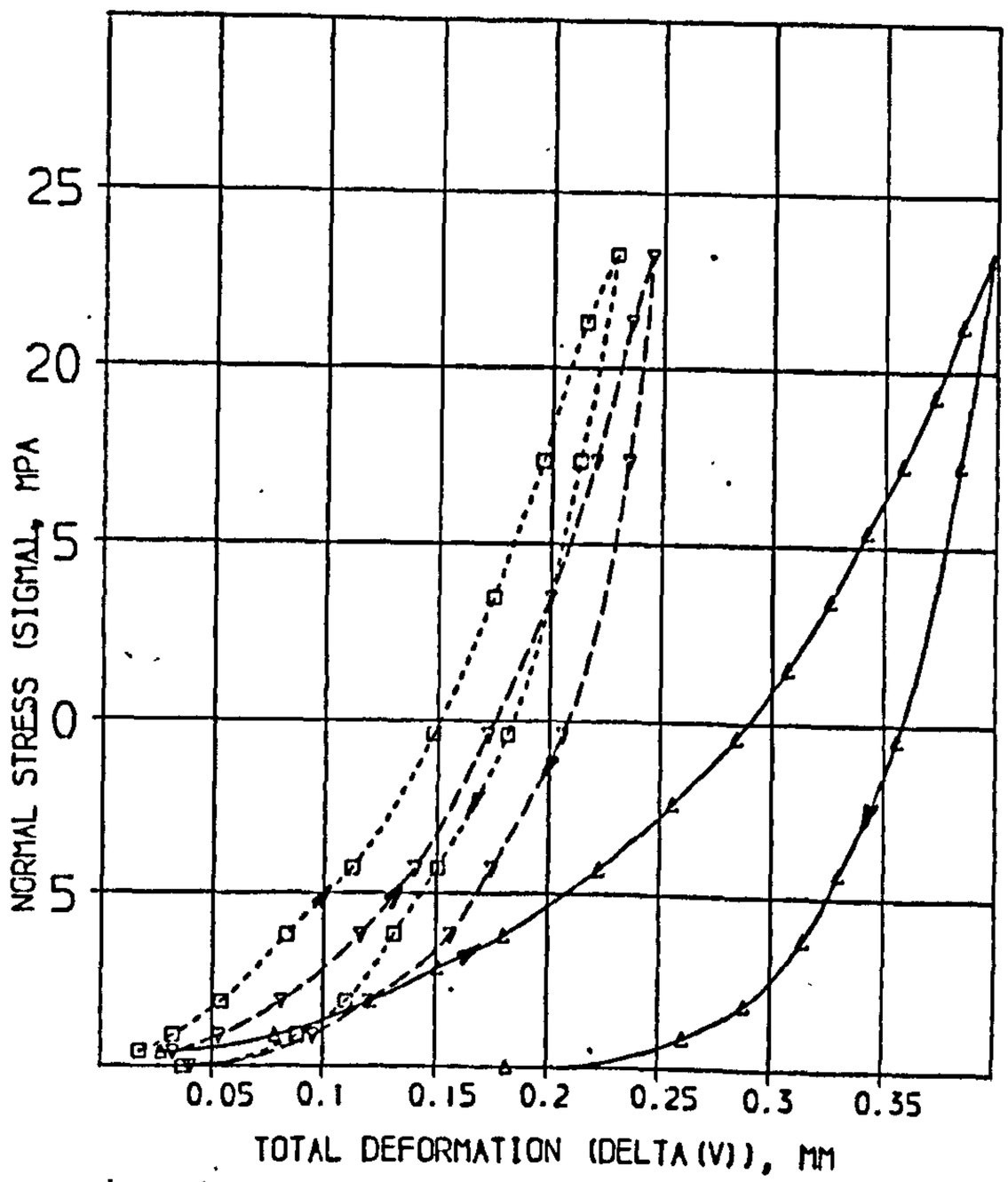

1st loading_

SOLUTION

A=	11.45	SD =	0.4866	% =	4.268
B=	0.3205	SD =	0.01772	% =	5.529
C=	188.2	SD =	21.40	% =	11.37

COMPUTED RESIDUALS

SIGMA	DELTA(V) MEASURED	DELTA(V) CALCULATED	DIFF	% DIFF
0.4070	0.02700	0.03417	-0.00717	26.54
0.8920	0.07800	0.06742	0.01058	13.56
1.861	0.1210	0.1177	0.0033	2.69
3.830	0.1510	0.1546	-0.0036	2.38
3.799	0.1800	0.1832	-0.0032	1.79
5.737	0.2230	0.2260	-0.0030	1.33
7.675	0.2560	0.2576	-0.0016	0.63
9.613	0.2840	0.2830	0.0010	0.34
11.55	0.3070	0.3046	0.0024	0.78
13.44	0.3260	0.3236	0.0024	0.72
15.43	0.3420	0.3409	0.0011	0.32
17.37	0.3580	0.3569	0.0011	0.32
19.30	0.3720	0.3719	0.0001	0.03
21.24	0.3850	0.3862	-0.0012	0.30
23.18	0.3980	0.3999	-0.0019	0.47

2nd loading_

SOLUTION

A=	13.12	SD =	0.8423	% =	6.421
B=	0.1574	SD =	0.008227	% =	5.226
C=	220.2	SD =	16.44	% =	7.471

COMPUTED RESIDUALS

SIGMA	DELTA(V) MEASURED	DELTA(V) CALCULATED	DIFF	% DIFF
0.4070	0.03200	0.02772	0.00428	13.38
0.7920	0.05300	0.05143	0.00157	2.96
1.861	0.08100	0.08265	-0.00165	2.29
3.799	0.1160	0.1184	-0.0024	2.40
5.737	0.1400	0.1411	-0.0011	0.81
9.613	0.1720	0.1721	-0.0001	0.05
13.49	0.2000	0.1962	0.0038	1.91
17.37	0.2220	0.2195	0.0025	1.14
21.24	0.2360	0.2374	-0.0014	0.59
23.18	0.2450	0.2470	-0.0020	0.83

3rd loading_

SOLUTION

A=	28.53	SD =	1.667	% =	5.841
B=	0.1533	SD =	0.01451	% =	9.469
C=	235.2	SD =	25.11	% =	10.67

COMPUTED RESIDUALS

SIGMA	DELTA(V) MEASURED	DELTA(V) CALCULATED	DIFF	% DIFF
0.4070	0.01700	0.01476	0.00224	13.06
0.3920	0.03200	0.02976	0.00224	7.01
1.861	0.05400	0.05300	0.00054	0.62
3.799	0.08300	0.08740	-0.00440	5.30
5.737	0.1120	0.1114	0.0006	0.58
9.613	0.1480	0.1462	0.0018	1.21
13.49	0.1740	0.1731	0.0009	0.53
17.37	0.1960	0.1965	-0.0005	0.14
21.24	0.2150	0.2174	-0.0024	1.11
23.18	0.2260	0.2273	0.0013	0.67

SDST : No 13

1st loading

SOLUTION

A=	6.514	SD =	0.1031	% =	1.210
B=	0.3557	SD =	0.004651	% =	1.308
C=	130.4	SD =	2.657	% =	2.037

COMPUTED RESIDUALS

SIGMA	DELTA(V) MEASURED	DELTA(V) CALCULATED	DIFF	% DIFF
0.2130	0.02500	0.02501	-0.00001	0.03
0.4250	0.04600	0.04703	-0.00103	2.25
0.6380	0.06600	0.06678	0.00121	1.78
0.8510	0.08700	0.08455	0.00245	2.81
1.276	0.1190	0.1152	0.0038	3.17
1.915	0.1540	0.1525	0.0015	0.99
2.446	0.1780	0.1777	0.0003	0.18
2.978	0.1680	0.1692	-0.0012	0.60
3.510	0.2160	0.2179	-0.0019	0.86
4.042	0.2320	0.2343	-0.0023	1.00
4.574	0.2450	0.2491	-0.0041	1.66
5.106	0.2620	0.2624	-0.0004	0.16
6.169	0.2850	0.2859	-0.0009	0.30
8.297	0.3250	0.3242	0.0008	0.25
10.42	0.3570	0.3555	0.0015	0.41
12.55	0.3840	0.3828	0.0012	0.32
14.68	0.4080	0.4074	0.0006	0.15
16.81	0.4320	0.4302	0.0018	0.41
18.93	0.4540	0.4518	0.0022	0.49
21.06	0.4730	0.4724	0.0006	0.12
23.19	0.4810	0.4824	-0.0014	0.28
25.31	0.5100	0.5118	-0.0018	0.34
27.44	0.5300	0.5307	-0.0007	0.13

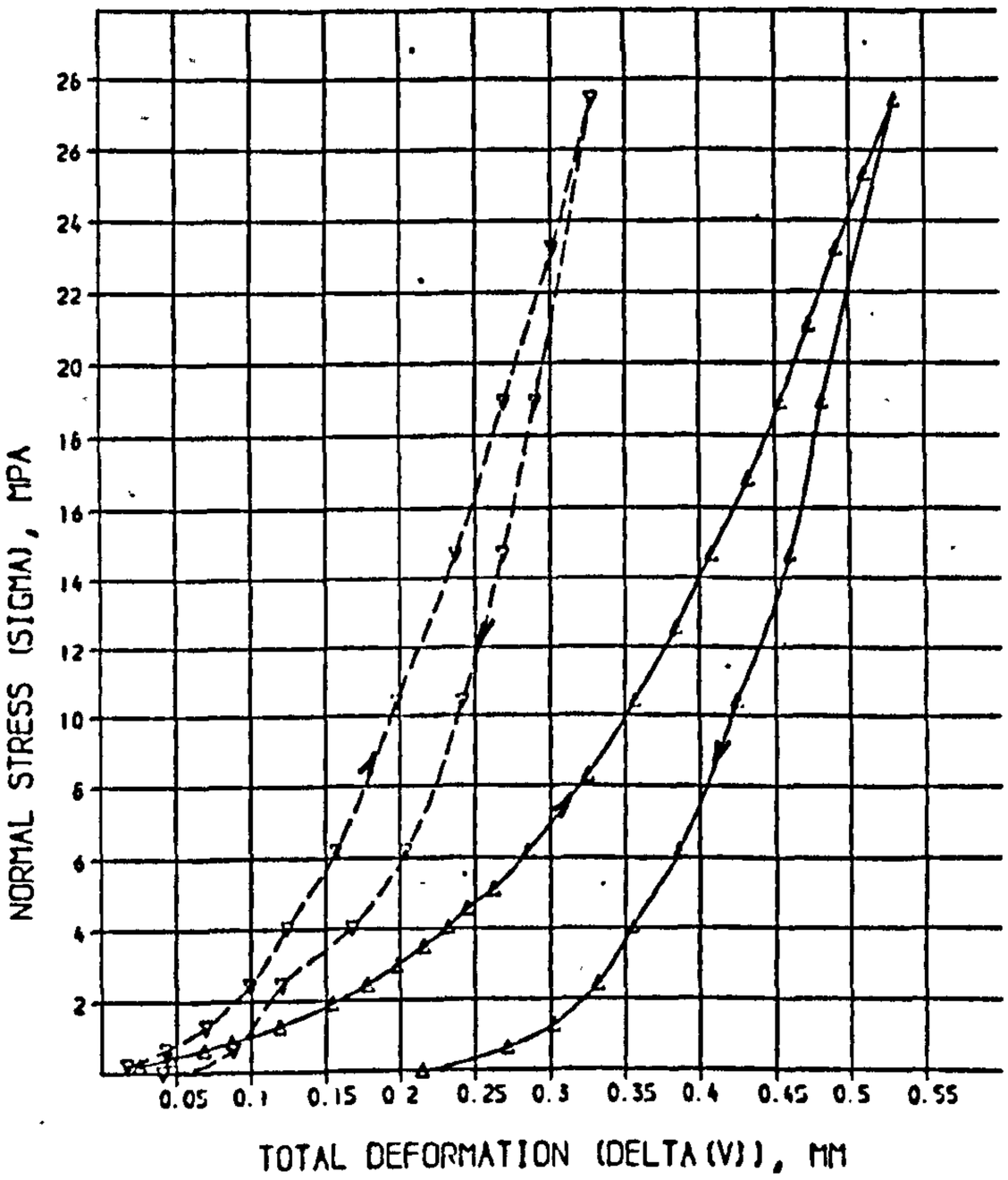

2nd loading

SOLUTION

A=	13.40	SD =	0.7301	% =	5.469
B=	0.1517	SD =	0.006229	% =	4.106
C=	145.1	SD =	4.848	% =	3.341

COMPUTED RESIDUALS

SIGMA	DELTA(V) MEASURED	DELTA(V) CALCULATED	DIFF	% DIFF
0.2130	0.01700	0.01580	0.00120	7.07
0.6380	0.04200	0.04051	0.00149	3.54
1.276	0.06900	0.06713	0.00187	2.70
2.446	0.09900	0.09955	-0.00055	0.54
4.042	0.1240	0.1280	-0.0040	3.74
6.169	0.1570	0.1565	0.0005	0.33
10.42	0.1930	0.1987	-0.0007	0.33
14.68	0.2370	0.2343	0.0027	1.12
18.93	0.2690	0.2674	0.0016	0.60
23.19	0.3010	0.2992	0.0018	0.59
27.44	0.3270	0.3305	-0.0035	1.01

SDST : No. 14

1st loading

SOLUTION

A=	5.635	SD =	0.4109	% =	7.292
B=	0.3110	SD =	0.01543	% =	4.962
C=	93.32	SD =	5.872	% =	6.292

COMPUTED RESIDUALS

SIGMA	DELTA(V) MEASURED	DELTA(V) CALCULATED	DIFF	% DIFF
0.4000	0.07000	0.06208	0.00792	11.32
0.8760	0.1200	0.1130	0.0070	5.81
1.828	0.1830	0.1784	0.0046	2.53
3.780	0.2100	0.2205	-0.0105	5.02
3.732	0.2420	0.2516	-0.0096	3.97
5.637	0.2920	0.2977	-0.0057	1.94
7.541	0.3300	0.3332	-0.0032	0.96
9.445	0.3680	0.3635	0.0045	1.21
11.35	0.3980	0.3910	0.0070	1.75
13.25	0.4240	0.4167	0.0073	1.72
15.16	0.4470	0.4412	0.0058	1.30
17.06	0.4690	0.4648	0.0041	0.88
18.97	0.4880	0.4879	0.0001	0.01
20.87	0.5060	0.5106	-0.0046	0.90
22.77	0.5250	0.5328	-0.0078	1.49

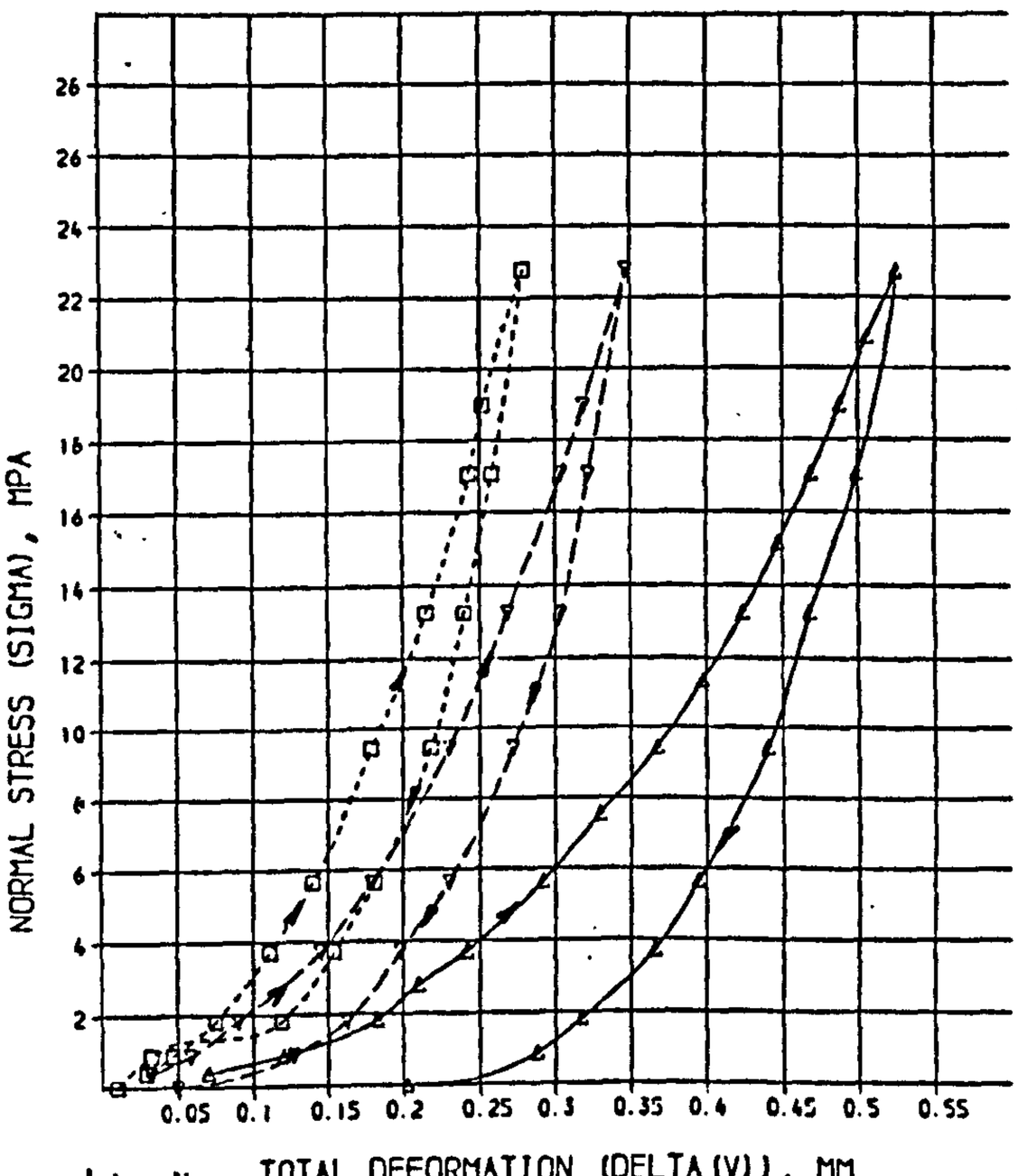

2nd loading

SOLUTION

A=	13.97	SD =	0.6401	% =	4.580
B=	0.2159	SD =	0.01146	% =	5.309
C=	143.3	SD =	8.745	% =	6.065

COMPUTED RESIDUALS

SIGMA	DELTA(V) MEASURED	DELTA(V) CALCULATED	DIFF	% DIFF
0.4000	0.03210	0.02805	0.00395	12.33
0.8760	0.05800	0.05467	0.00333	5.74
1.823	0.09000	0.09417	-0.00417	4.63
3.732	0.1450	0.1455	-0.0005	0.23
5.637	0.1790	0.1798	-0.0008	0.46
9.445	0.2300	0.2293	0.0007	0.30
13.25	0.2630	0.2680	0.0000	0.00
17.06	0.3040	0.3021	0.0019	0.63
18.97	0.3190	0.3182	0.0008	0.25
22.77	0.3470	0.3490	-0.0020	0.57

3rd loading

SOLUTION

A=	16.25	SD =	1.227	% =	7.551
B=	0.1496	SD =	0.01033	% =	7.242
C=	156.2	SD =	10.48	% =	6.710

COMPUTED RESIDUALS

SIGMA	DELTA(V) MEASURED	DELTA(V) CALCULATED	DIFF	% DIFF
0.4000	0.02900	0.02370	0.00530	18.28
0.8760	0.04600	0.04524	0.00076	1.66
1.828	0.07500	0.07591	-0.00091	1.21
3.732	0.1110	0.1145	-0.0035	3.12
5.637	0.1400	0.1406	-0.0006	0.42
9.445	0.1790	0.1794	-0.0004	0.23
13.25	0.2150	0.2112	0.0038	1.77
17.06	0.2430	0.2401	0.0029	1.19
18.97	0.2520	0.2540	-0.0020	0.79
22.77	0.2790	0.2809	-0.0019	0.67

SDST : No. 15

1st loading_

SOLUTION

A=	5.150	SD =	0.3979	% =	7.714
B=	0.3060	SD =	0.01452	% =	4.736
C=	78.40	SD =	3.913	% =	4.990

COMPUTED RESIDUALS

SIGMA	DELTA(V) MEASURED	DELTA(V) CALCULATED	DIFF	% DIFF
0.4140	0.08300	0.06888	0.01411	17.00
0.9060	0.1270	0.1232	0.0038	2.97
1.891	0.1850	0.1911	-0.0061	3.29
3.875	0.2340	0.2345	-0.0005	0.20
3.860	0.2560	0.2667	-0.0107	4.19
5.829	0.3100	0.3155	-0.0055	1.78
7.798	0.3530	0.3544	-0.0014	0.39
9.768	0.3910	0.3885	0.0025	0.65
11.74	0.4250	0.4199	0.0051	1.20
13.71	0.4610	0.4497	0.0113	2.45
15.67	0.4820	0.4784	0.0036	0.74
17.64	0.5090	0.5065	0.0025	0.50
19.61	0.5370	0.5339	0.0031	0.58
21.58	0.5560	0.5610	-0.0050	0.89
23.55	0.5790	0.5877	-0.0087	1.51

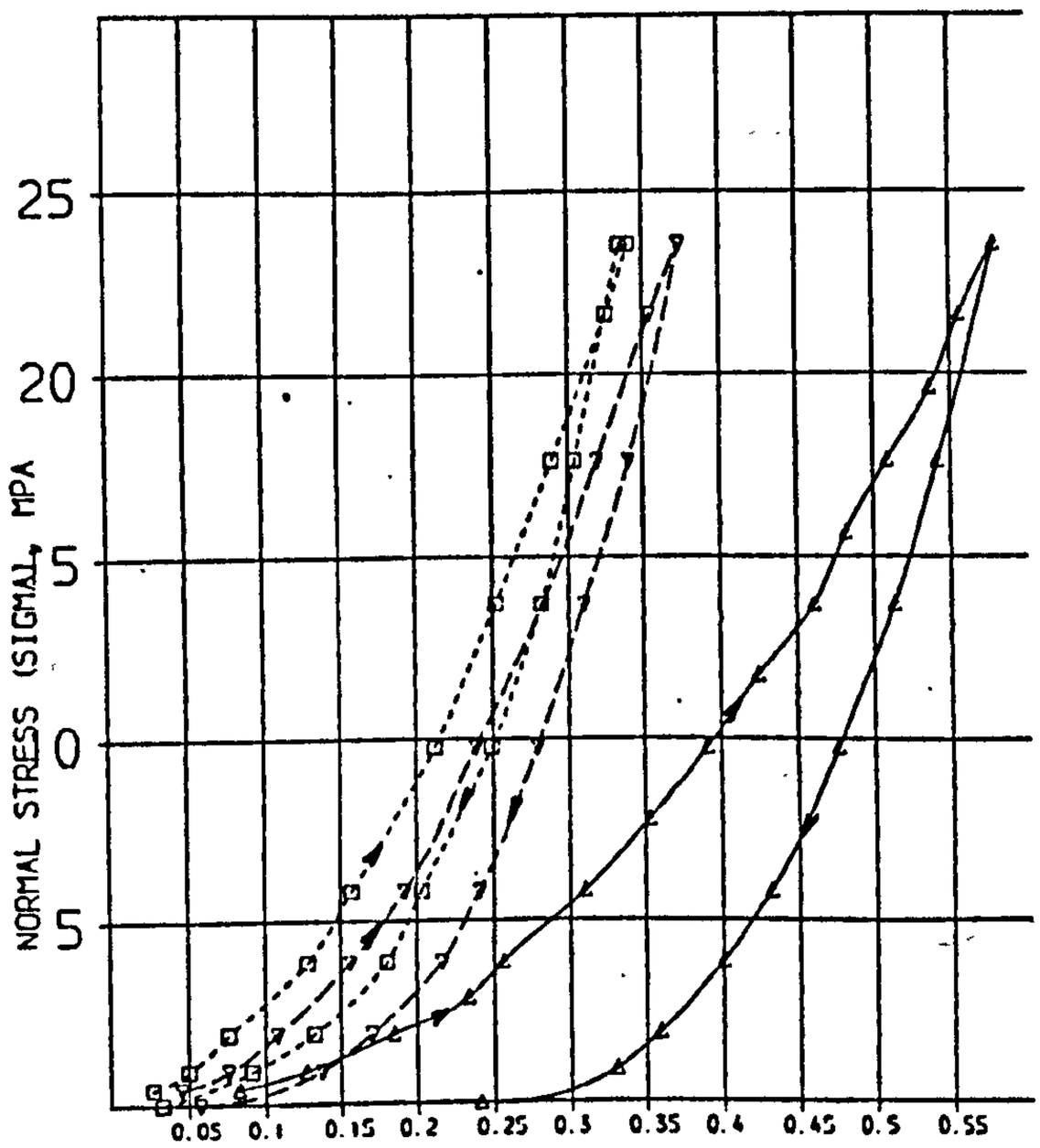

2nd loading_

SOLUTION

A=	8.304	SD =	0.6013	% =	6.829
B=	0.1750	SD =	0.007604	% =	4.459
C=	112.2	SD =	4.242	% =	3.780

COMPUTED RESIDUALS

SIGMA	DELTA(V) MEASURED	DELTA(V) CALCULATED	DIFF	% DIFF
0.4140	0.04500	0.04075	0.00425	9.44
0.9060	0.07600	0.07288	0.00312	4.11
1.891	0.1098	0.1155	-0.0055	4.89
3.860	0.1560	0.1593	-0.0033	2.23
5.829	0.1920	0.1904	0.0016	0.85
9.768	0.2390	0.2382	0.0008	0.33
13.71	0.2830	0.2793	0.0037	1.24
17.64	0.3190	0.3181	0.0009	0.27
21.58	0.3540	0.3550	-0.0010	0.46
23.55	0.3730	0.3741	-0.0011	0.50

3rd loading_

SOLUTION

A=	18.04	SD =	1.117	% =	6.190
B=	0.1750	SD =	0.01242	% =	7.094
C=	125.8	SD =	6.841	% =	5.436

COMPUTED RESIDUALS

SIGMA	DELTA(V) MEASURED	DELTA(V) CALCULATED	DIFF	% DIFF
0.4140	0.02700	0.03358	0.00342	12.68
0.9060	0.05000	0.04622	0.00378	7.55
1.891	0.07600	0.08059	-0.00459	6.04
3.860	0.1280	0.1270	0.0010	0.82
5.829	0.1570	0.1599	-0.0029	1.82
9.768	0.2120	0.2079	0.0041	0.98
13.71	0.2520	0.2512	0.0008	0.30
17.64	0.2890	0.2887	0.0003	0.11
21.58	0.3250	0.3242	0.0008	0.24
23.55	0.3400	0.3415	-0.0015	0.45

SDST: No 16

1st loading

SOLUTION

A=	4.297	SD =	0.4107	% =	9.556
B=	0.2865	SD =	0.01270	% =	4.432
C=	114.4	SD =	6.977	% =	6.097

COMPUTED RESIDUALS

SIGMA	DELTA(V) MEASURED	DELTA(V) CALCULATED	DIFF	% DIFF
0.4080	0.1000	0.0749	0.0251	25.13
0.8930	0.1270	0.1282	-0.0012	0.98
1.864	0.1800	0.1888	-0.0088	4.90
2.835	0.2150	0.2245	-0.0095	4.42
3.806	0.2420	0.2497	-0.0077	3.19
5.748	0.2820	0.2862	-0.0042	1.48
7.690	0.3150	0.3141	0.0009	0.27
9.632	0.3390	0.3382	0.0008	0.24
11.57	0.3690	0.3601	0.0089	2.42
13.52	0.3870	0.3807	0.0063	1.63
15.50	0.4070	0.4008	0.0062	1.52
17.40	0.4250	0.4196	0.0054	1.27
19.34	0.4420	0.4383	0.0037	0.83
21.28	0.4550	0.4568	-0.0018	0.40
23.23	0.4740	0.4750	-0.0010	0.21
25.17	0.4880	0.4930	-0.0050	1.03
27.11	0.5040	0.5104	-0.0069	1.37

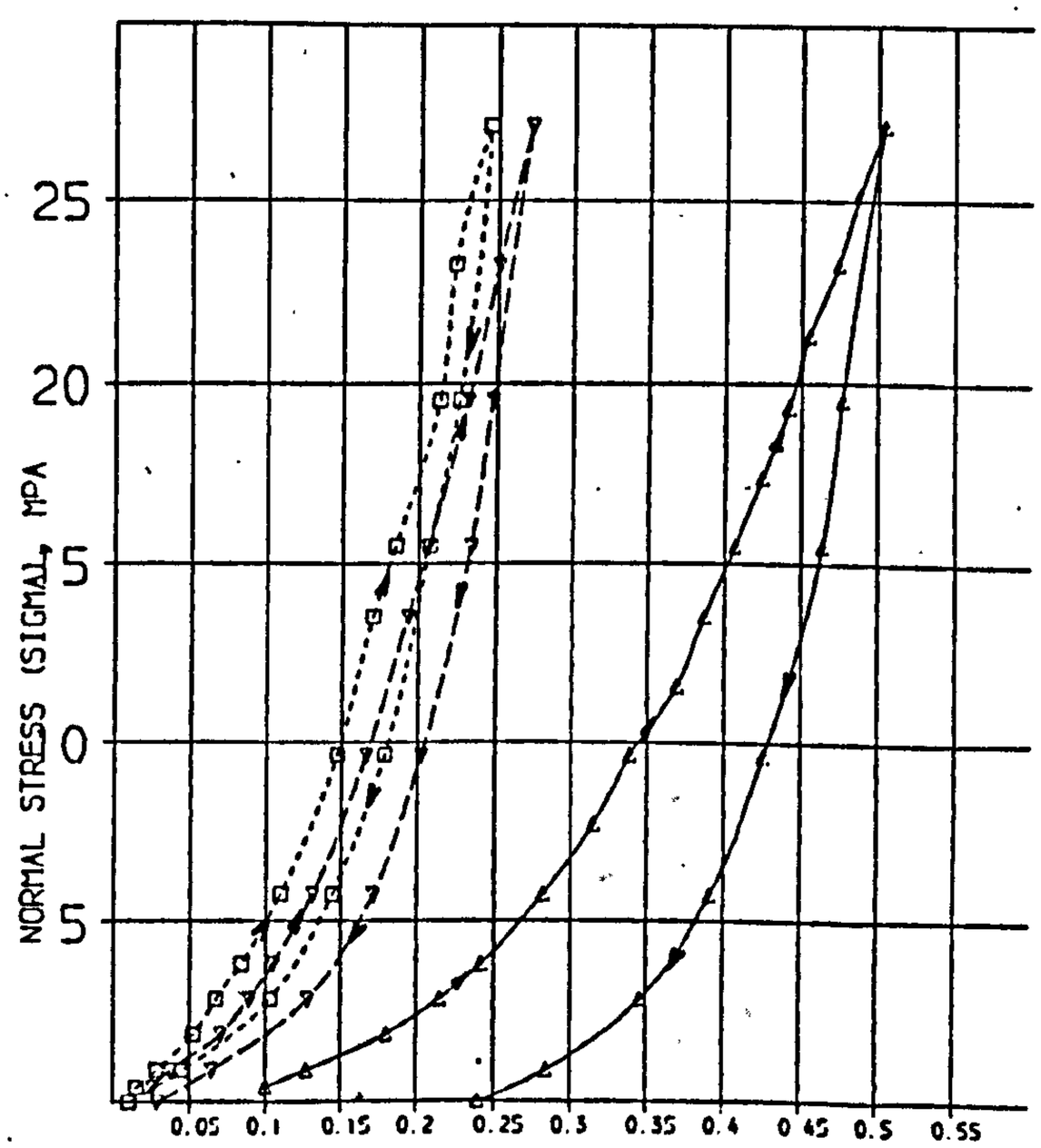

2nd loading

SOLUTION

A=	19.30	SD =	0.7515	% =	3.895
B=	0.1563	SD =	0.006334	% =	4.053
C=	205.6	SD =	8.941	% =	4.348

COMPUTED RESIDUALS

SIGMA	DELTA(V) MEASURED	DELTA(V) CALCULATED	DIFF	% DIFF
0.4080	0.02500	0.02061	0.00439	17.56
0.8930	0.03700	0.04005	-0.00305	8.24
1.864	0.07000	0.06877	0.00123	1.76
2.835	0.08900	0.08956	-0.00056	0.58
3.820	0.1050	0.1059	-0.0009	0.87
5.748	0.1310	0.1305	0.0005	0.41
9.632	0.1660	0.1659	0.0001	0.08
13.52	0.1930	0.1935	-0.0005	0.28
15.50	0.2060	0.2062	-0.0002	0.11
19.54	0.2320	0.2304	0.0016	0.68
23.23	0.2510	0.2513	-0.0003	0.12
27.11	0.2720	0.2725	-0.0005	0.18

3rd loading

SOLUTION

A=	32.04	SD =	1.500	% =	4.683
B=	0.1127	SD =	0.01005	% =	8.918
C=	210.4	SD =	29.74	% =	14.12

COMPUTED RESIDUALS

SIGMA	DELTA(V) MEASURED	DELTA(V) CALCULATED	DIFF	% DIFF
0.4080	0.01500	0.01339	0.00161	10.76
0.8930	0.02800	0.02734	0.00066	2.36
1.864	0.05200	0.05049	0.00151	2.91
2.835	0.06700	0.06911	-0.00211	3.14
3.820	0.08400	0.08481	-0.00081	0.97
5.748	0.1100	0.1095	0.0005	0.47
9.632	0.1470	0.1457	0.0013	0.89
13.52	0.1720	0.1751	-0.0031	1.81
15.50	0.1850	0.1852	-0.0002	0.11
19.54	0.2130	0.2076	0.0054	2.52
23.23	0.2230	0.2263	-0.0033	1.49
27.11	0.2450	0.2444	0.0006	0.09

SDST : No. 17

1st loading_

SOLUTION

A=	6.271	SD =	0.2277	% =	2.752
B=	0.3143	SD =	0.009939	% =	3.162
C=	86.13	SD =	3.305	% =	3.838

COMPUTED RESIDUALS

SIGMA	DELTA(V) MEASURED	DELTA(V) CALCULATED	DIFF	% DIFF
0.2150	0.02400	0.02650	0.00250	8.61
0.4880	0.06400	0.05534	0.00866	13.53
0.9770	0.1000	0.0972	0.0028	2.80
1.465	0.1310	0.1303	0.0007	0.54
1.953	0.1560	0.1575	-0.0015	0.97
2.442	0.1790	0.1806	-0.0016	0.89
2.930	0.1960	0.2006	-0.0046	2.33
3.419	0.2160	0.2183	-0.0023	1.04
3.907	0.2330	0.2341	-0.0011	0.47
4.884	0.2620	0.2618	0.0002	0.06
5.861	0.2840	0.2858	-0.0018	0.63
6.838	0.3080	0.3071	0.0009	0.28
7.814	0.3270	0.3266	0.0004	0.13
8.791	0.3420	0.3447	-0.0027	0.78
9.768	0.3630	0.3617	0.0013	0.37
10.74	0.3810	0.3779	0.0031	0.83
11.72	0.3950	0.3934	0.0016	0.41
13.67	0.4290	0.4229	0.0061	1.42
15.63	0.4520	0.4510	0.0010	0.23
17.58	0.4760	0.4780	-0.0020	0.42
19.54	0.5000	0.5042	-0.0042	0.85

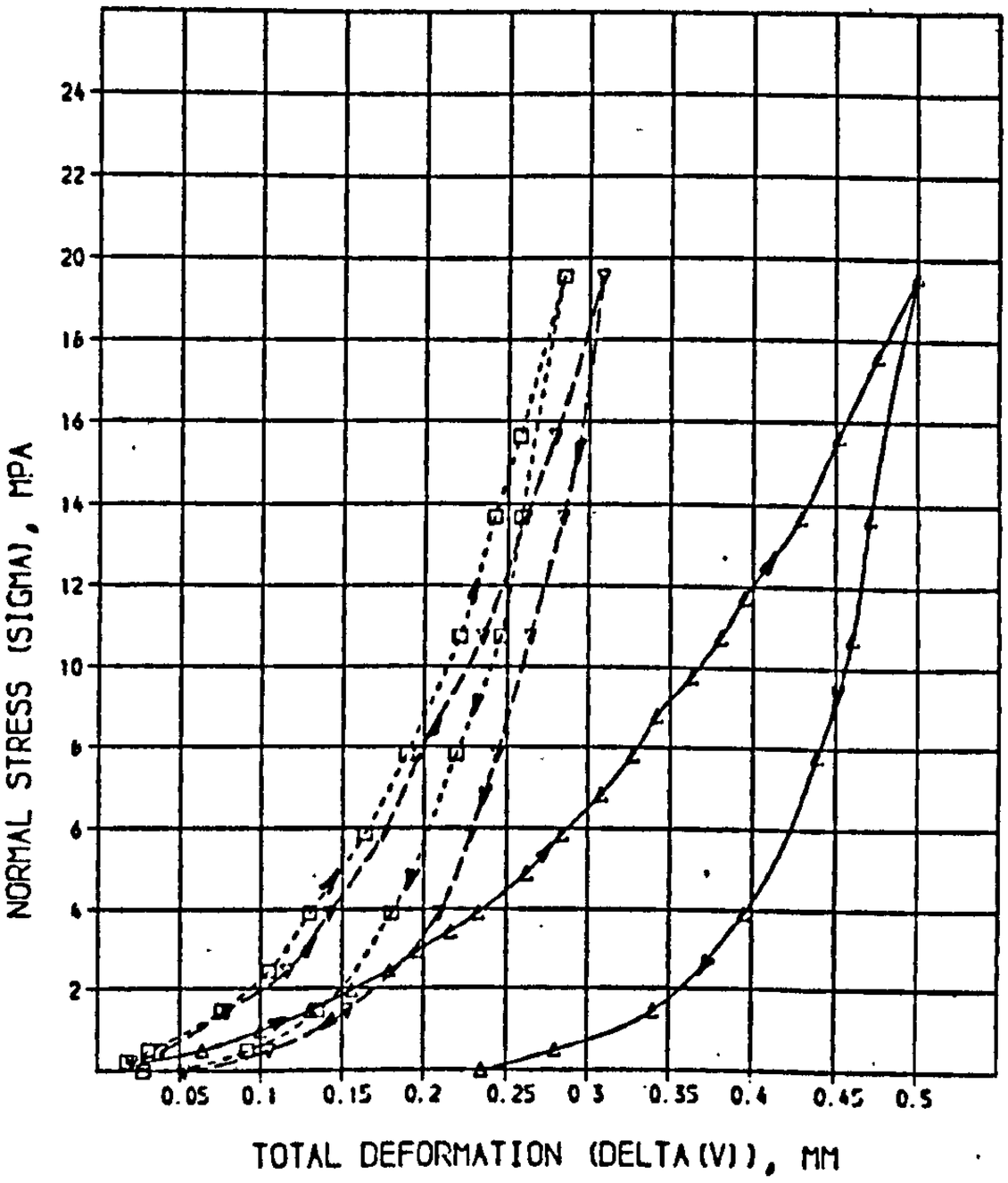

2nd loading_

SOLUTION

A=	12.34	SD =	0.8107	% =	6.569
B=	0.1802	SD =	0.01147	% =	6.369
C=	130.9	SD =	9.003	% =	6.877

COMPUTED RESIDUALS

SIGMA	DELTA(V) MEASURED	DELTA(V) CALCULATED	DIFF	% DIFF
0.2150	0.02100	0.01753	0.00347	16.53
0.4880	0.03900	0.03615	0.00285	7.30
1.465	0.07900	0.08275	-0.00375	4.75
2.442	0.1160	0.1130	0.0030	2.62
3.907	0.1420	0.1447	-0.0027	1.88
5.861	0.1750	0.1754	-0.0004	0.22
7.814	0.1970	0.1999	-0.0029	1.50
9.74	0.2350	0.2313	0.0037	1.57
13.67	0.2610	0.2594	0.0016	0.62
15.63	0.2790	0.2771	0.0019	0.67
19.54	0.3080	0.3110	-0.0030	0.98

3rd loading_

SOLUTION

A=	14.80	SD =	0.7511	% =	5.074
B=	0.1944	SD =	0.01245	% =	6.400
C=	168.4	SD =	14.54	% =	8.631

COMPUTED RESIDUALS

SIGMA	DELTA(V) MEASURED	DELTA(V) CALCULATED	DIFF	% DIFF
0.2150	0.01800	0.01479	0.00321	17.82
0.4880	0.03100	0.03104	-0.00004	0.27
1.465	0.07610	0.07428	0.00182	2.26
2.442	0.1050	0.1037	0.0013	1.20
3.907	0.1300	0.1351	-0.0051	3.96
5.861	0.1640	0.1652	-0.0012	0.72
7.814	0.1890	0.1885	0.0005	0.28
9.74	0.2210	0.2171	0.0039	1.77
13.67	0.2420	0.2414	0.0002	0.10
15.63	0.2570	0.2570	0.0000	0.01
19.54	0.2340	0.2855	-0.0015	0.52

SDST : no. 18

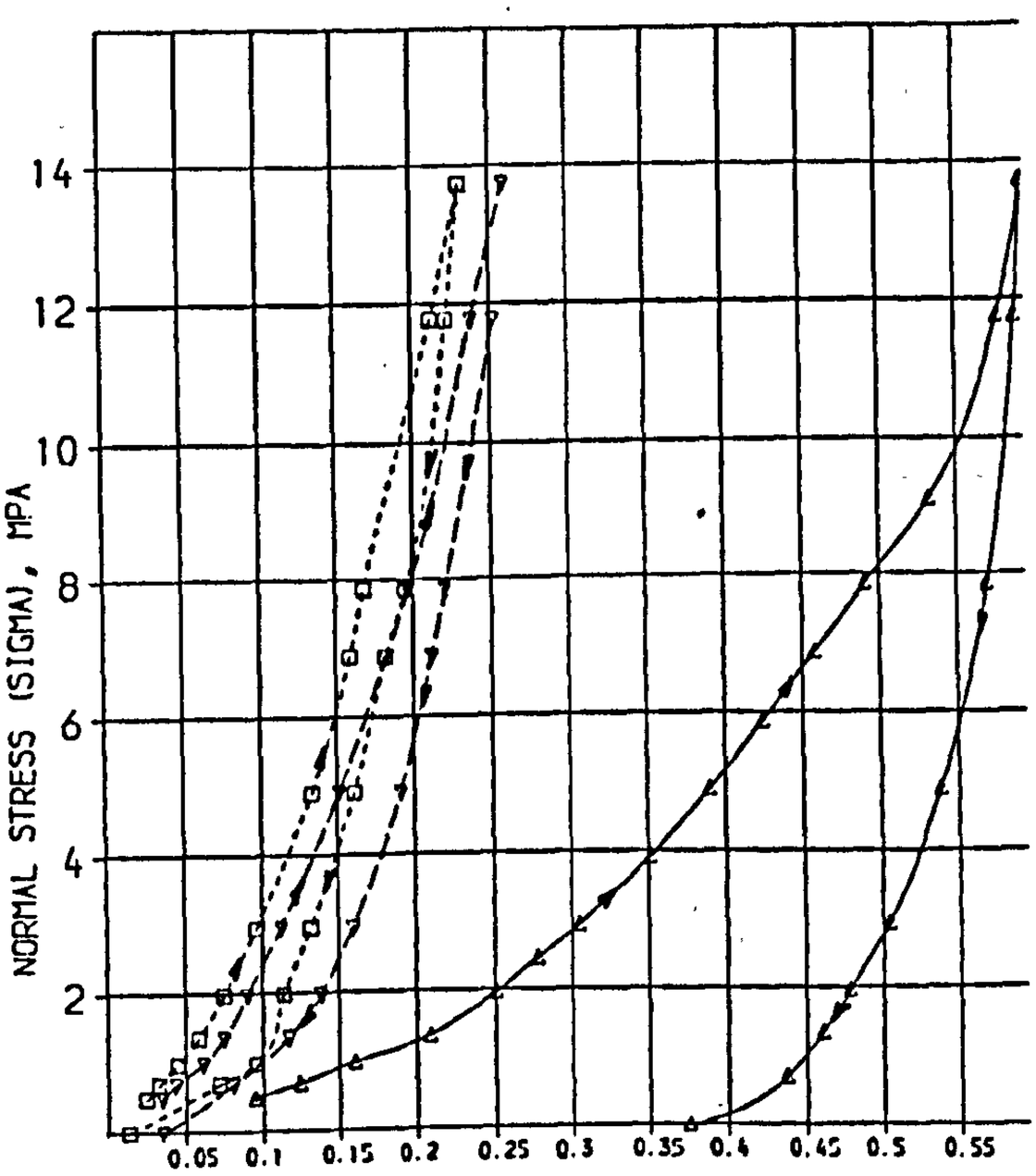

1st loading

SOLUTION:

A=	4,725	SD =	0,2545	% =	5,385
B=	0,4702	SD =	0,03643	% =	7,743
C=	67,36	SD =	9,868	% =	14,66

COMPUTED RESIDUALS

SIGMA	DELTA(V) MEASURED	DELTA(V) CALCULATED	DIFF	% DIFF
0,4900	0,09500	0,09227	0,00273	2,87
0,6860	0,1240	0,1214	0,0026	2,29
0,9810	0,1600	0,1587	0,0013	0,84
1,350	0,2080	0,1979	0,0101	4,88
1,971	0,2510	0,2504	0,0006	0,22
2,452	0,2700	0,2855	-0,0155	1,89
2,942	0,3050	0,3110	-0,0060	2,22
3,923	0,3510	0,3587	-0,0077	2,19
4,904	0,3900	0,3967	-0,0067	1,73
5,884	0,4240	0,4291	-0,0051	1,20
6,865	0,4580	0,4576	0,0004	0,08
7,846	0,4910	0,4835	0,0075	1,54
9,102	0,5330	0,5137	0,0193	3,62
11,77	0,5780	0,5711	0,0069	1,20
13,73	0,5940	0,6075	-0,0135	2,61

2nd loading

SOLUTION

A=	13,67	SD =	0,7253	% =	5,306
B=	0,1510	SD =	0,01160	% =	7,681
C=	100,7	SD =	7,487	% =	7,441

COMPUTED RESIDUALS

SIGMA	DELTA(V) MEASURED	DELTA(V) CALCULATED	DIFF	% DIFF
0,4900	0,03400	0,03356	0,00044	1,29
0,6860	0,04300	0,04410	-0,00110	2,55
0,9810	0,06100	0,05784	0,00316	5,17
1,350	0,07500	0,07297	0,00203	2,71
1,971	0,09900	0,09224	0,00676	6,83
2,942	0,1120	0,1163	-0,0043	3,87
4,904	0,1510	0,1523	-0,0013	0,83
6,865	0,1820	0,1805	0,0015	0,84
7,846	0,1970	0,1931	0,0039	1,97
11,77	0,2330	0,2338	-0,0008	0,35
13,73	0,2500	0,2510	-0,0010	0,39

3rd loading

SOLUTION

A=	19,90	SD =	0,8036	% =	4,036
B=	0,1433	SD =	0,01102	% =	8,221
C=	123,0	SD =	9,495	% =	7,694

COMPUTED RESIDUALS

SIGMA	DELTA(V) MEASURED	DELTA(V) CALCULATED	DIFF	% DIFF
0,4900	0,02400	0,02500	-0,00100	4,19
0,6860	0,03200	0,03338	-0,00138	4,31
0,9810	0,04500	0,04468	0,00032	0,70
1,350	0,05800	0,05706	0,00094	1,61
1,971	0,07500	0,07467	0,00033	0,44
2,942	0,09600	0,09681	-0,00081	0,84
4,904	0,1330	0,1307	0,0023	1,75
6,865	0,1590	0,1573	0,0017	1,07
7,864	0,1650	0,1694	-0,0044	2,64
11,77	0,2120	0,2114	0,0006	0,30
13,73	0,2310	0,2306	0,0004	0,16

SDST : No. 19

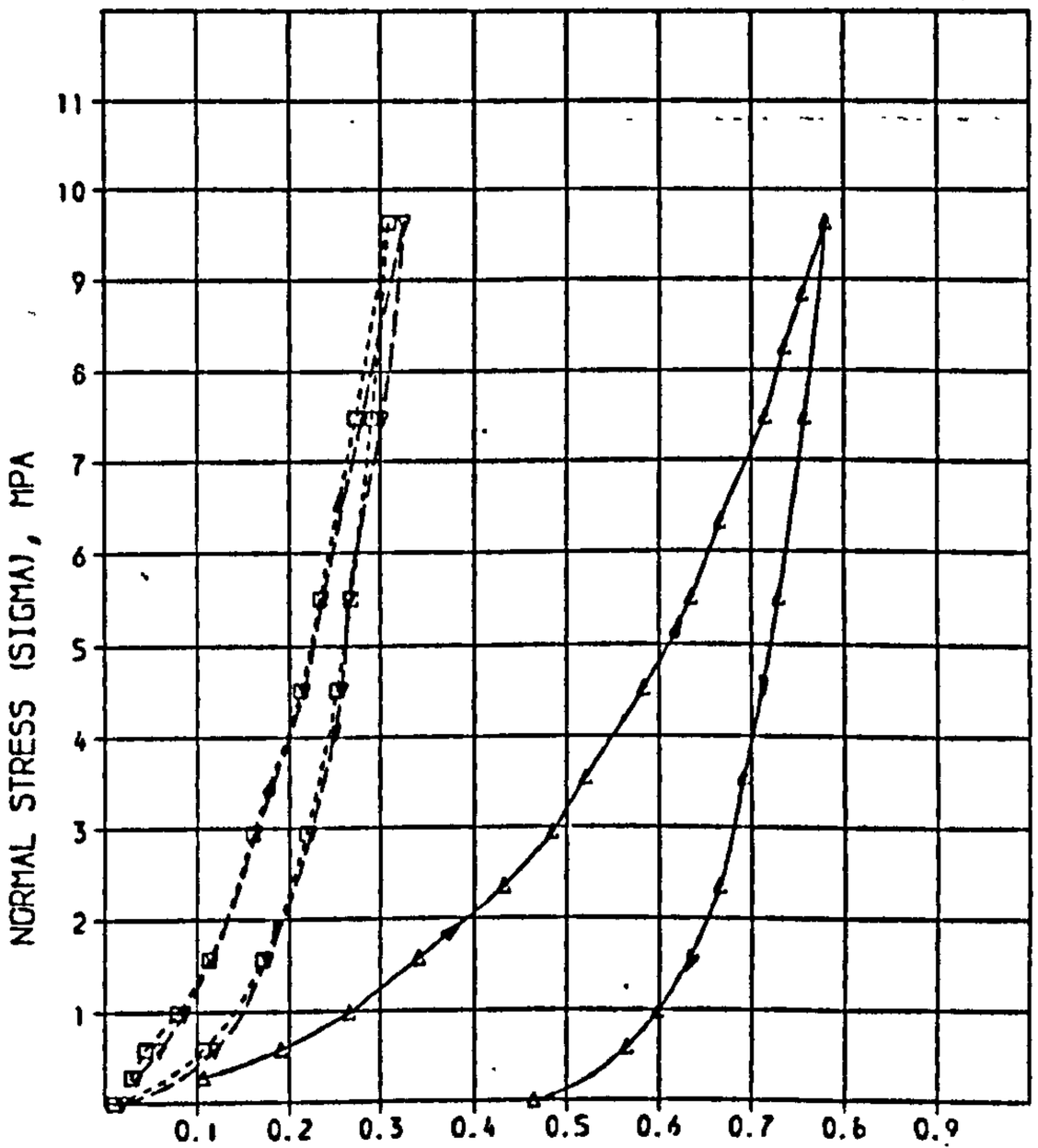

1st loading

SOLUTION

A=	2,002	SD =	0,07020	% =	2,698
B=	0,6517	SD =	0,02483	% =	3,810
C=	42,17	SD =	3,425	% =	8,122

COMPUTED RESIDUALS

SIGMA	DELTA(V) MEASURED	DELTA(V) CALCULATED	DIFF	% DIFF
0,2953	0,1370	0,1036	0,0034	5,22
0,5903	0,1910	0,1822	0,0088	4,61
0,9920	0,2650	0,2640	0,0010	0,36
1,572	0,3410	0,3506	-0,0096	2,86
2,358	0,4320	0,4350	-0,0030	0,69
2,948	0,4840	0,4850	0,0004	0,08
3,538	0,5200	0,5244	-0,0044	0,85
4,520	0,5830	0,5811	0,0019	0,33
5,503	0,6350	0,6287	0,0063	1,00
6,328	0,6060	0,6040	0,0020	0,30
7,478	0,7140	0,7063	0,0077	0,76
8,254	0,7350	0,7363	-0,0013	0,18
8,844	0,7540	0,7560	-0,0020	0,34
9,630	0,7790	0,7825	-0,0035	0,45

2nd loading

SOLUTION

A=	8,946	SD =	0,3700	% =	4,136
B=	0,1745	SD =	0,01045	% =	5,989
C=	55,04	SD =	2,632	% =	4,781

COMPUTED RESIDUALS

SIGMA	DELTA(V) MEASURED	DELTA(V) CALCULATED	DIFF	% DIFF
0,2953	0,03400	0,03309	0,00091	2,66
0,5903	0,05900	0,05858	0,00042	0,71
0,9920	0,08600	0,08583	0,00017	0,20
1,572	0,1160	0,1161	-0,0001	0,10
2,948	0,1640	0,1676	-0,0036	2,22
4,520	0,2150	0,2118	0,0032	1,48
5,503	0,2370	0,2359	0,0011	0,46
7,478	0,2790	0,2802	-0,0012	0,44
9,630	0,3250	0,3251	-0,0001	0,03

3rd loading

SOLUTION

A=	11,33	SD =	0,4855	% =	4,284
B=	0,2807	SD =	0,04151	% =	14,79
C=	99,38	SD =	24,87	% =	25,02

COMPUTED RESIDUALS

SIGMA	DELTA(V) MEASURED	DELTA(V) CALCULATED	DIFF	% DIFF
0,2950	0,02900	0,02679	0,00221	7,61
0,5900	0,04400	0,04986	-0,00586	13,32
0,9920	0,07800	0,07672	0,00128	1,65
1,572	0,1130	0,1087	0,0043	3,84
2,948	0,1610	0,1647	-0,0037	2,29
4,520	0,2120	0,2103	0,0017	0,82
5,503	0,2330	0,2333	-0,0003	0,12
7,478	0,2720	0,2722	-0,0002	0,07
9,630	0,3080	0,3079	0,0001	0,02

SDST : No. 20

1st loading

SOLUTION

A=	2.541	SD =	0.03439	% =	1.354
B=	0.6103	SD =	0.03856	% =	6.384
C=	21.10	SD =	2.226	% =	10.55

COMPUTED RESIDUALS

SIGMA	DELTA(V) MEASURED	DELTA(V) CALCULATED	DIFF	% DIFF
0.3706	0.1320	0.1351	-0.0031	2.35
0.5550	0.1890	0.1872	0.0018	0.98
0.7400	0.2340	0.2322	0.0018	0.76
0.8320	0.2540	0.2525	0.0015	0.58
0.9250	0.2720	0.2719	0.0001	0.05
1.110	0.3070	0.3072	-0.0002	0.06
1.480	0.3690	0.3682	0.0008	0.23
1.850	0.4130	0.4197	-0.0067	1.61
2.591	0.5060	0.5046	0.0014	0.28
3.331	0.5780	0.5743	0.0037	0.65
3.701	0.6060	0.6055	0.0005	0.09
4.459	0.6620	0.6641	-0.0021	0.32

SDST : No. 21

1st loading

SOLUTION

A=	2.685	SD =	0.04367	% =	1.627
B=	0.4427	SD =	0.01545	% =	-3.489
C=	22.89	SD =	1.112	% =	4.857

COMPUTED RESIDUALS

SIGMA	DELTA(V) MEASURED	DELTA(V) CALCULATED	DIFF	% DIFF
0.4520	0.1410	0.1417	-0.0007	0.50
0.9040	0.2300	0.2307	-0.0007	0.32
1.356	0.2980	0.2951	0.0029	0.96
1.808	0.3450	0.3461	-0.0011	0.31
2.260	0.3880	0.3888	-0.0008	0.21
2.825	0.4360	0.4350	0.0010	0.23
3.390	0.4750	0.4758	-0.0008	0.18
3.954	0.5120	0.5131	-0.0011	0.21
4.519	0.5490	0.5478	0.0011	0.20